UNIVERSITY OF BIRMINGHAM

Development of Photobiomodulation (PBM) approaches for the management of oral diseases

By

Hannah Serrage

A thesis submitted to

The University of Birmingham

For the degree of

DOCTOR OF PHILOSOPHY

Oral Biology

School of Dentistry

College of Medical and Dental Sciences

University of Birmingham

May 2019

ABSTRACT

Photobiomodulation (PBM) is a non-invasive phototherapy that has shown promise in the treatment of the chronic oral inflammatory disease, periodontitis. This project aimed to provide evidence of a well characterised system for the evaluation of the effects of PBM on the most abundant cell type in the oral periodontium: primary human gingival fibroblasts (pHGFs).

Two bespoke high throughput light arrays were extensively characterised (2nd generation array: 400-830 nm, 24mW/cm² and LUMOS® array: 405-850 nm, 24mW/cm²) using techniques including beam profilometry and UV-Vis spectrometry. The biological effects of PBM on pHGFs (either single isolates/pooled from 3 individuals) were evaluated following application of media or periodontal disease relevant stimuli.

The effects of PBM were biomodulatory, where application of blue light (400-450 nm, 24mW/cm², 5.76J/cm²) to 'healthy' pHGFs induced increases in markers for inflammation (IL-8, ROS) but application of PBM to 'disease' pHGFs (bacterial stimulus applied) caused decreases in markers for inflammation. PBM also modulated mitochondrial activity, where pHGFs with a higher mitochondrial content exhibited greater maximal and basal respiratory rates.

These data indicate blue light could be an effective modality in the modulation of inflammation in periodontal disease. Results also provide novel evidence that mitochondrial content could be a prerequisite in ensuring a response to PBM *in vivo*.

ACKNOWLEDGEMENTS

I would first like to thank my brilliant supervisors Dr Michael Milward, Professor Paul Cooper and Professor William Palin. The support, guidance and laughs you have provided me with throughout my PhD have truly helped me to develop as a scientist and I could not have asked for a better supervisory team, thank you.

A massive thanks also goes to the team of technicians that have guided me through my PhD journey, in particular I would like to thank Michelle Holder, Gay Smith, Dr Naomi Hubber and Dr Helen Wright. I would also like to extend my thanks to Dr Mohammed Hadis, Dr Sarah Kuehne and Dr Cleo White for all of your help, training and guidance throughout my thesis.

Special thanks also goes to the team at the school of Sport and Exercise for all of their help and support but in particular to Dr Sophie Joanisse, thank you. I would also like to extend my thanks to Nabil Quraishi at the Institute of Biomedical research for undertaking the arduous task of sequencing my biofilm samples. Thank you also to the team at Philips for the discussions we have had and the opportunity to work with such an interesting and passionate group of people. In particular, I would like to thank Dr Owen Darch and Dr Pieter Horstman for enabling me to help develop my research.

I would also like to extend a big shout to the 'office crew' at the School of Dentistry and all those friends I have met around Birmingham (particularly my wonderful quizzing team). Over the past few years I have met some truly incredibly people and I am so grateful to have had the opportunity to get to know you all. Thank you all for the tea, talks, biscuits and burritos. They say people make a place and I certainly believe that after meeting you all.

Thank you also to my wonderful family for supporting me throughout my PhD: Mum, Dad and Olivia, you help me strive to do my best every day, thank you. Finally, a massive thanks goes to the wonderful Eddie Ross. I could not have asked for a better person to share this experience with and your constant encouragement, support and kindness has truly aided me on this journey.

TABLE OF CONTENTS

LIST OF FIGURES

CHAPTER ONE

CHAPTER TWO

CHAPTER THREE

CHAPTER FOUR

CHAPTER FIVE

CHAPTER SIX

CHAPTER SEVEN

APPENDICES

LIST OF TABLES

CHAPTER ONE

CHAPTER TWO

CHAPTER THREE

APPENDICES

ABBREVIATIONS

ANOVA Analysis of variance

ATCC American type culture collection

ATP Adenosine triphosphate

ASV Amplicon sequence variables

B Biopsy number

BCA Bicinchoninic acid protein assay

bFGF basic fibroblast growth factor

BHI Brain heart infusion

BSA Bovine serum albumin

Cu Copper

COX Cyclooxygenase

CCD Charge coupled device

CCO Cytochrome C oxidase/Complex IV

CCTV Closed circuit television

DMEM Dulbecco's modified eagle medium

dsDNA double stranded DNA

ECM Extracellular matrix

ELISA Enzyme-linked Immunosorbent assay

ETC Electron transport chain

FCCP Carbonyl cyanide-p-trifluoromethoxyphenylhydrazone

FBS Foetal bovine serum

FMN	Flavin mononucleotide
GAPDH	Glyceraldehyde 3-phosphate dehydrogenase
GF	Gingival fibroblast
GSH	Glutathione
H_2DCFDA	2', 7'-dichlorodihydrofluorescein diacetate
ICBE	Internal Committee for Biological Ethics
IL	Interleukin
kPa	kilopascal
Laser	Light amplification by stimulated emission of radiation
LED	Light emitting diode
LLLT	Low level light therapy
LPS	Lipopolysaccharide
MAPK	Mitogen activated protein kinase
MeSH	Medical subject heading
mtDNA	mitochondrial DNA
MTT	3-(4,5-dimethylthiazol-2-yl)-2,5-diphenyl-2H-tetrazolium bromide assay
MOI	Multiplicity of infection
NAD	Nicotinamide adenine dinucleotide
nDNA	nuclear DNA
NFκB	nuclear factor kappa-light-chain-enhancer of activated B cells
NIR	Near infrared
NIST	National Institute of Standards and Technology
NO	Nitric oxide

Nrf2	Nuclear factor erythroid 2–related factor 2
ns	non-significant
OCR	Oxygen consumption rate
OM	Oral mucositis
PAGE	Polyacrylamide gel electrophoresis
PBM	Photobiomodulation
PCR	Polymerase chain reaction
PGE	Prostaglandin
pHGF	Primary human gingival fibroblast
PBS	Phosphate buffered saline
PMMA	Poly methyl methacrylate
Qiime	Quantitative Insights into Microbiological Ecology
RFU	Relative fluorescent units
RLU	Relative luminescent unit
ROS	Reactive oxygen species
RT	Reverse transcription
SAB	Sabouraud dextrose broth
SMA	SubMiniature version A
Smad	Small mothers against decentaplegic
SRC	Spare respiratory capacity
TGF	Transforming growth factor
TMRE	Tetramethylrhodamine ethyl ester
TNF	Tumour necrosis factor

TOAC	Total antioxidant capacity
UV	Ultraviolet

1 INTRODUCTION

This chapter contains material contained within a publication by Serrage et al, in which I am the first author and major contributor. This publication has been submitted to the Journal of Photochemistry and Photobiology (see appendices 10.4) and is currently under peer review. Sections included from this review are as follows: 1.4.1.2, 1.4.1.3, 1.4.2.1, 1.4.2.2, 1.4.2.3 and 1.5.2.

1.1 Introduction

The potential application of Photobiomodulation (PBM) was first reported by Endre Mester in 1967 at Semmelweiss University, Budapest (Mester et al., 1968). Mester shaved the backs of mice and exposed the shaved area to the emission of a red laser of wavelength, 694 nm. He found the hair on the backs of the irradiated mice grew back more rapidly compared with that of the non-irradiated control group. He called this phenomenon 'photobiostimulation' and to date (April 2019), over 6000 papers have been published regarding the efficacy of PBM in treating a number of ailments by inducing analgesia (Merigo et al., 2015), promoting wound healing (Kuffler, 2016) and reducing inflammation (da Silveira Campos et al., 2015).

PBM encompasses a wide range of terminologies including low level light therapy (LLLT), cold laser therapy, photobiostimulation and phototherapy. However, PBM is the preferred Medical Subject Heading Term (MeSH) as it encompasses both the biostimulatory and bioinhibitory mechanisms involved. In fact, the number of articles citing the use of PBM has been growing exponentially since the 1980s, with <10 reported in 1980 to >400 in 2018 (PubMed, Dec 2018). To date, PBM has shown clinical efficacy in treating a wide array of diseases ranging from lower back pain (Yousefi-Nooraie et al., 2008) to periodontitis (Ren et al., 2017) to rheumatoid arthritis (Alves et al., 2013).

There is a large body of evidence indicating that electromagnetic radiation spanning the visible to near-infra red spectrum (390-1100 nm) could modulate a broad range of cellular activities including cell proliferation, inflammatory signalling and mitochondrial function. Indeed, these effects have not only been reported in humans but also in many animal species across the animal kingdom (Hamblin et al., 2019). The majority of literature currently reports the beneficial effects of wavelengths spanning the red to NIR spectrum (600-1100 nm). However, the use of blue light has also gathered interest due to its antimicrobial (De Sousa et al., 2015) and anti-inflammatory properties (Alba et al., 2017).

Nonetheless, controversy still surrounds the application of PBM in practice due to the limited knowledge concerning how PBM elicits its molecular effects and also due to a poor understanding of photophysics and radiometric parameters which affect the repeatability and reliability of PBM studies (Hadis et al., 2016a). The importance of reporting treatment parameters in a more consistent and reliable way has been emphasised in several articles and guidance for reporting radiometric properties has previously been published (Jenkins and Carroll, 2011, Hadis et al., 2016a) although this has not necessarily been broadly adopted (Castellano-Pellicena et al., 2018, Fekrazad et al., 2017, Mignon et al., 2018, Tani et al., 2018, Veleska-Stevkoska and Koneski, 2018) (Section 1.3). In addition, the biological mechanisms underpinning PBM are yet to be fully elucidated. It is proposed that PBM can excite a number of cellular chromophores, inducing a cascade of biological effects (Section 1.4). However, the proposed photophysical and biological mechanisms have yet to be confirmed through experimental investigation. Previous research frequently focuses on a mitochondrial dependent mechanism, in which light is proposed to directly upregulate the activities of the mitochondrially located electron transport chain (ETC).

1.2 Controversies surrounding the application of PBM in vivo

1.3 Treatment parameters

It is understood that the parameters employed in PBM can be separated into two discrete categories: the 'medicine' and 'dose' (Huang et al., 2009).

1.3.1 Medicine

The medicine category of PBM is split into four independent variables: wavelength (nm), irradiance (W/cm²), pulse structure and the coherence of the light. These are described in more detail below.

Wavelength

PBM is usually applied at wavelengths from 390-1100 nm (Avci et al., 2013). These wavelengths cover a relatively large part of the electromagnetic spectrum, where ultraviolet is <400 nm, visible light is between 400 – 700 nm and near infra-red light is between 700 – 1400 nm (Hadis et al., 2016a) (*Figure 1.1*). Interestingly, a number of studies indicate that wavelengths between 700 – 750 nm exert little or no biochemical activity and the longer the wavelength, the greater the tissue penetration depth. Wavelengths within the blue-violet

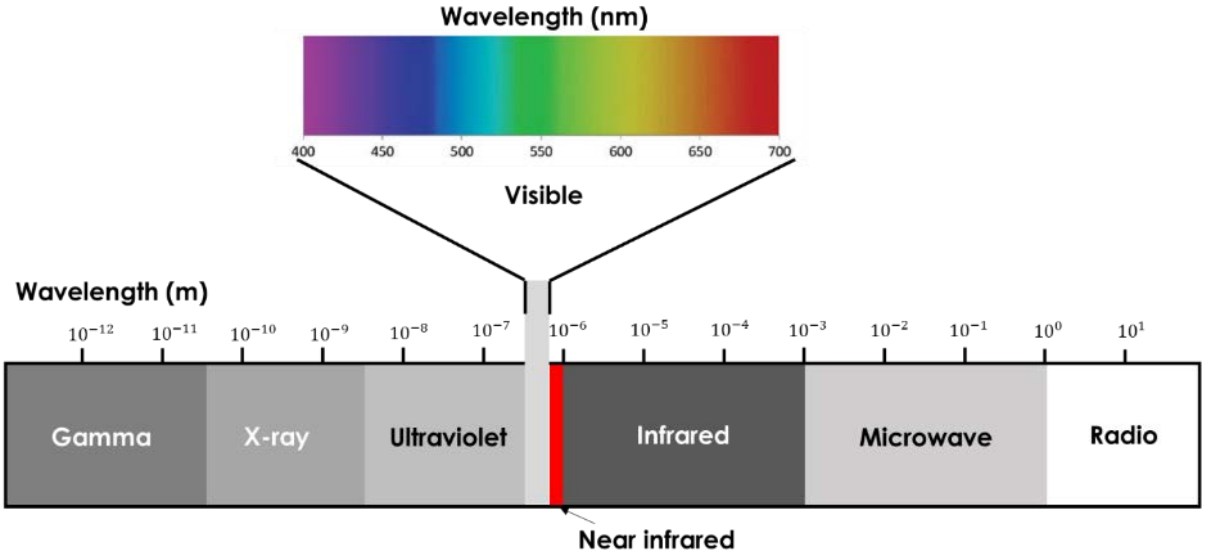

Figure 1.1: The electromagnetic spectrum in which PBM encompasses the visible to NIR part.

section of the electromagnetic spectrum exhibit a penetration depth of ~1mm whilst wavelengths closer to the NIR part of the spectrum have a penetration depth up to 6mm (Barolet, 2008). However, penetration depth of biological tissue can also vary considerably dependent upon factors such as the water content of a biological tissue. Water is cited to possess an absorption peak within the NIR range (980 nm (Pope and Fry, 1997, Pegau et al., 1997)). Indeed, the tissue dependent absorption of NIR light has been documented in the literature (Zhang et al., 2016a). The high absorption of NIR by water may indicate that delivery of light to tissue possessing a high water content may be impaired.

Irradiance

Irradiance is defined as power (or radiant flux, W) per unit area (W/m^2) and is often less appropriately recorded as power density or intensity. This parameter also considers beam area (m^2), a key parameter that is often incorrectly measured and authors will often simply measure the area of the aperture of a light source and not the area illuminated by light at a known distance. Measurement of the beam area using methods such as beam profilometry is fundamental in understanding what proportion of a target tissue is irradiated at a desired irradiance output. Interestingly, authors also assume the beam from a light source will be of uniform distribution (an ideal "top-hat" factor). However, light sources often produce a Gaussian distribution in which light is most intense in the centre and weakens towards the edges of the beam (Yang et al., 2008). Hence, it is vital to measure both the irradiance output and beam area of a light source to fully understand the dose applied to a target.

Pulse Structure

Some researchers choose to use a continuous wave light rather than a single short pulse of light or multiple pulses within a specific time frame. Pulse frequency is defined as the number

of pulses within a specific time frame and is measured in pulses per second (Hz). Current evidence indicates that pulsed light may induce different biological effects to continuous wave light (Hashmi et al., 2010). In which biological response to PBM may relate to the wavelength and set of pulse parameters applied to induce the activities of a specific chromophore. However, further work is required to validate this.

Coherence

PBM utilises lasers, laser emitting diodes (LEDs) and a range of other sources. Lasers are a coherent light source where the emitted light (photons) all have the same frequency and are in phase (with no difference in the wave pattern) (Rubinov and Afanas'ev, 2005). Coherent light will produce a point source narrow beam, and a laser speckle; a random, granular interference pattern produced by the diffuse reflectance of the highly coherent laser source at the target surface. LEDs on the other hand emit non-coherent light, in which light is emitted at different phases and is not monochromatic (Basso et al., 2015). Notably in a review by Heiskanen and Hamblin it was reported that there was no significant benefit to using lasers over LEDs in practice, where both have been identified as having the ability to induce beneficial effects (Heiskanen and Hamblin, 2018a).

Light source

PBM can also utilise an array of light sources. This includes both gas lasers and semi-conductor lasers including Argon (488 nm, 514 nm), Gallium Aluminium Arsenide (GaAlAs, 612 nm – 870 nm), gallium arsenide (GaAs, >760 nm), helium neon (HeNe, 633 nm) and an array of other elements. LED semiconductors can also be used at lower wavelengths. These light sources use elements including Indium and Phosphide (Avci et al., 2013). Some questions surround the application of these varying light sources, including, most importantly whether

coherence of the light source effects the way in which PBM acts *in vivo,* in which current opinion suggest there is no discernible difference in biological outcomes (Hode et al., 2009). However, further evaluation is required to validate this.

1.3.2 Dose

The dose in PBM is separated into four discrete variables: Energy (J), Radiant exposure (J/cm^2), irradiation time (s) and irradiation interval (hours, days or weeks).

Energy

Energy is often disregarded as an important parameter in PBM as it completely ignores the value of irradiance. Energy in PBM is understood to be analogous to photosynthesis as light acts directly to increase energy output (Tafur and Mills, 2008).

Radiant exposure

Radiant exposure or fluence (J/cm2) is deemed unreliable as it makes the assumption that there is an a reciprocal relationship between irradiance and time. A wide range of fluence values are utilised during experimentation. Radiant exposure values utilised during experimentation vary significantly from one publication to the next. For example, Lev Tov et al concluded that application of 830 nm light at radiant exposure values from 80–320J/cm² inhibited gingival fibroblast proliferation (Lev-Tov et al., 2013) while conversely Khadra et al reported that application of 830 nm light at 1.5J/cm^2 and 3J/cm² caused significant increases in fibroblast proliferation (Khadra et al., 2005). These findings are in line with the ideology that PBM elicits its effects in a biphasic manner according to the '*Arndt-Schultz law*.' This law states that a chemical or agent can elicit different effects on a tissue dependent upon the dose applied. For example, increasing radiant exposure values can either cause no effect,

induce biostimulation or indeed cause damage to cells or tissues (Figure 1.2). Hence, each parameter utilised in PBM is understood to cause a response within a narrow therapeutic window and the use of values outside this range can negate the potential positive effects of a specific wavelength (Huang et al., 2011).

Irradiation time

Authors utilise various irradiation times to elicit a range of effects including cell proliferation and reduced inflammation. There is little consistency in the exposure times used between studies making it difficult to compare studies. For example, Lim et al evaluated the effects of irradiation at 635 nm for 60 minutes on Prostaglandin E2 (PGE2, see Section 1.4.2.1) production from fibroblasts (Lim et al., 2015). Conversely, Sakurai et al irradiated cultures for 3-20 minutes at 830 nm (Sakurai et al., 2000). Both authors concluded that light could be used to modulate lipolysaccharide (LPS) induced increases in PGE2. However, due to

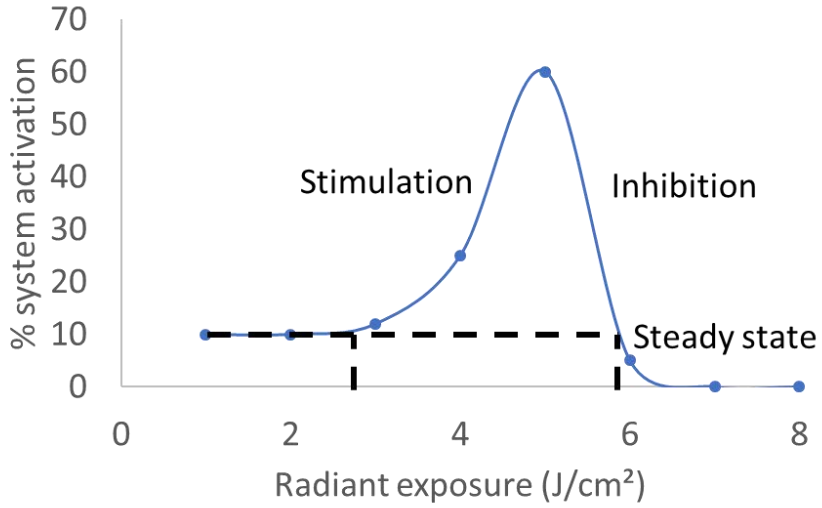

Figure 1.2: The 'Arndt Schulz' curve, where every treatment or substance applied to a system, including PBM, acts in a dose (or fluence/radiant exposure) dependent manner where small doses stimulate, moderate doses may have an inhibitory and larger doses may induce a cytotoxic effect (denoted by either cell activation or cell retardation in the figure above). Hence, PBM is expected to act within in a narrow therapeutic window. However, other variables can be used to induce this effect including wavelength, irradiance and time of exposure (Barolet, 2008).

differences in the parameters employed, it was difficult to draw any firm conclusions as to which parameter combinations could be of greater clinical efficacy.

Irradiation interval

Irradiation interval is also another important parameter. Several authors report a robust response from a single irradiation for a short period of time (Hadis et al., 2015), whilst others propose that a series of separate treatments should be provided to generate the optimum effect (Albuquerque-Pontes et al., 2015, Holder et al., 2012). For example, *Holder et al* reported that application of 635 nm light to dental pulp stem cells 1 day and 4 days post seeding induced a greater increase in cell number when compared to cultures irradiated once.

From the literature it is apparent that there are a set of defined parameters that should be recorded during light delivery. However, these are commonly misreported or not reported at all. In the future, it will be paramount to illustrate the importance of each of these interacting parameters to determine the optimum treatment course to induce an effect *in vitro* and *in vivo*.

1.4 Molecular mechanisms of PBM

The molecular mechanisms of PBM are often cited to be mediated by changes in mitochondrial activity. However, there are a number photosensitive molecules located throughout our body that can each induce a plethora of signalling mechanisms. Hence, this section reports on those currently cited in the literature.

1.4.1 Primary mechanisms of PBM

According to the Grotthuss–Draper law, commonly termed “the First Law of Photochemistry”, photochemical reactions are dependent on the absorption of light by a system (Albini, 2016). Subsequently in this section, a review of the literature of the most frequently proposed

cellular photoacceptors (chromophores) that are reported to mediate the biological effects in PBM is provided.

1.4.1.1 Cytochrome c oxidase

It has been proposed that PBM acts directly on the electron transport chain (ETC) located in the mitochondria, specifically complex IV, also known as cytochrome c oxidase (Bisland and Wilson, 2006). The ETC is comprised of five complexes: complex I (NADH-CoQ reductase), complex II (succinate dehydrogenase), complex III (cytochrome c reductase), complex IV (cytochrome c oxidase (CCO)) and complex V (adenosine triphosphate (ATP) synthase). Electrons are passed systematically down the chain of these complexes in order to generate a proton gradient to provide the activation energy for ATP synthase to catalyse the production of ATP (see Figure 1.3 for diagrammatic illustration of the ETC (Sazanov, 2015)).

CCO is hypothesised to play a particularly important role in PBM due to its structure; it is composed of 14 protein subunits, two heme subunits and two copper chromophores (CuA and CuB). Chromophores are understood to be key in inducing the downstream effects of PBM (Hamblin and Demidova-Rice, 2007). Chromophores or molecular photoacceptors possess the ability to absorb photons and exist in two forms: conjugated pi electron systems and metal complexes (Rogers et al., 2004). CCO is only one example of many chromophores present in the body. Other examples include flavins (see section 1.4.1.2) and myoglobin (Arakaki et al., 2010).

The CCO theory of PBM was first established by Karu et al, as it was observed that CCO exhibited absorption peaks located within the blue (404 nm), red (620-680 nm) and NIR (760-820 nm) spectrum (Karu and Kolyakov, 2005). From this preliminary study, a range of *in vitro*

and *in vivo* studies have demonstrated the effects of PBM on mitochondrial activity (Hamblin, 2018a).

However, despite these finding being published in the early 1980's the mechanism(s) as to how PBM modulates CCO activity are yet to be fully elucidated. Current indications suggest light could either induce CCO activity through inducing the dissociation of nitric oxide (NO, photodissociation theory of light), changes in the CCO redox potential culminate in the acceleration of electron transfer or through superoxide generation (Karu and Kolyakov, 2005). Previous publications also reported that red light could catalyse the activation of CCO (Pastore et al., 2000). However, these findings are yet to be replicated in other studies (Quirk and Whelan, 2016).

The hypothesis that has gathered the most support is the 'photodissociation theory of PBM.' In this case it has been proposed that application of photons of lights induces the excitation of electrons within CCO, causing the transition of electrons from a lower energy orbit to a higher energy orbit (Chung et al., 2012). The residual energy remaining from this process catalyses the release of NO from heme and copper centres within CCO, allowing oxygen to bind in its place and subsequently allowing the progression of the ETC and thus increased ATP synthesis (shown diagrammatically in *Figure 1.4* and *Figure 1.3* shows how the ETC progresses). It is understood that this accounts for the increased levels of circulating NO present following light irradiation (Hamblin, 2008). However, an alternative explanation for the increase in circulating NO has also been proposed suggesting CCO has the potential to act as a nitrite reductase enzyme (see Section 1.4.1.1).

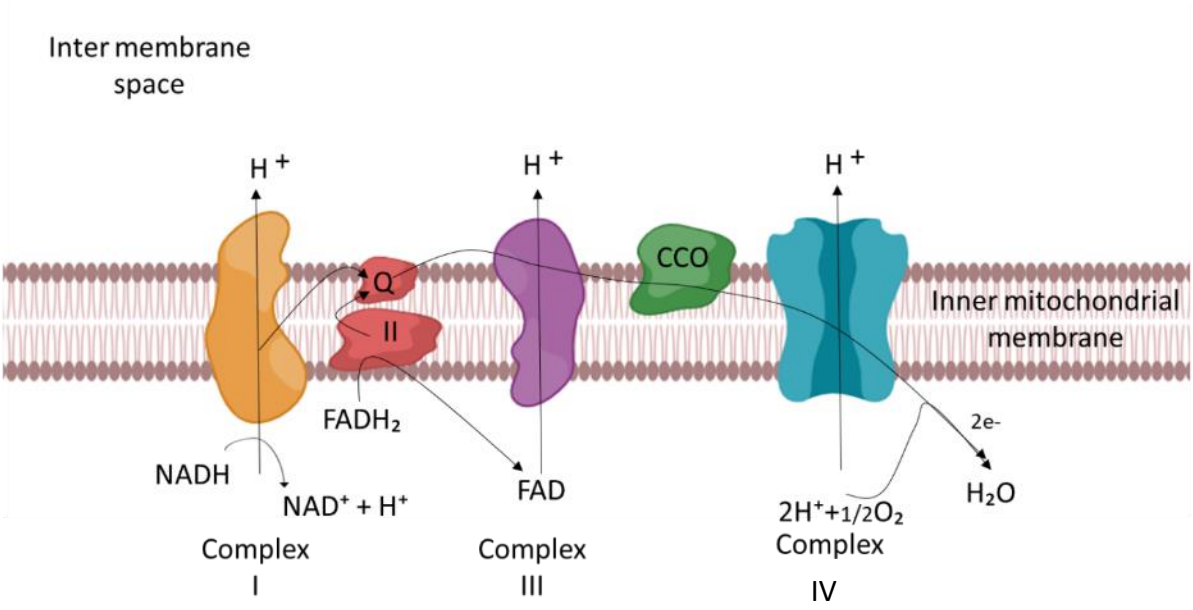

Figure 1.3: The mitochondrial respiratory chain or ETC located within the inner mitochondrial membrane and comprised of 5 complexes: complex I (orange), complex II (red), complex III (purple), complex IV (blue). Electrons are passed down this chain of complexes to provide activation energy for ATP synthase (complex V, not shown on figure) to produce the cells energy source: ATP. However, complex IV is the rate limiting complex of this chain as its activation is dependent upon its association with NO. In which, NO is only displaced when there are sufficient levels of oxygen in the extracellular environment or alternatively, through excitiation of heme and copper centres in complex IV by light, as described in figure 1.4. This subsequently enables the progression of the ETC. Thus, light is proposed to modulate ETC activity through excitation of complex IV.

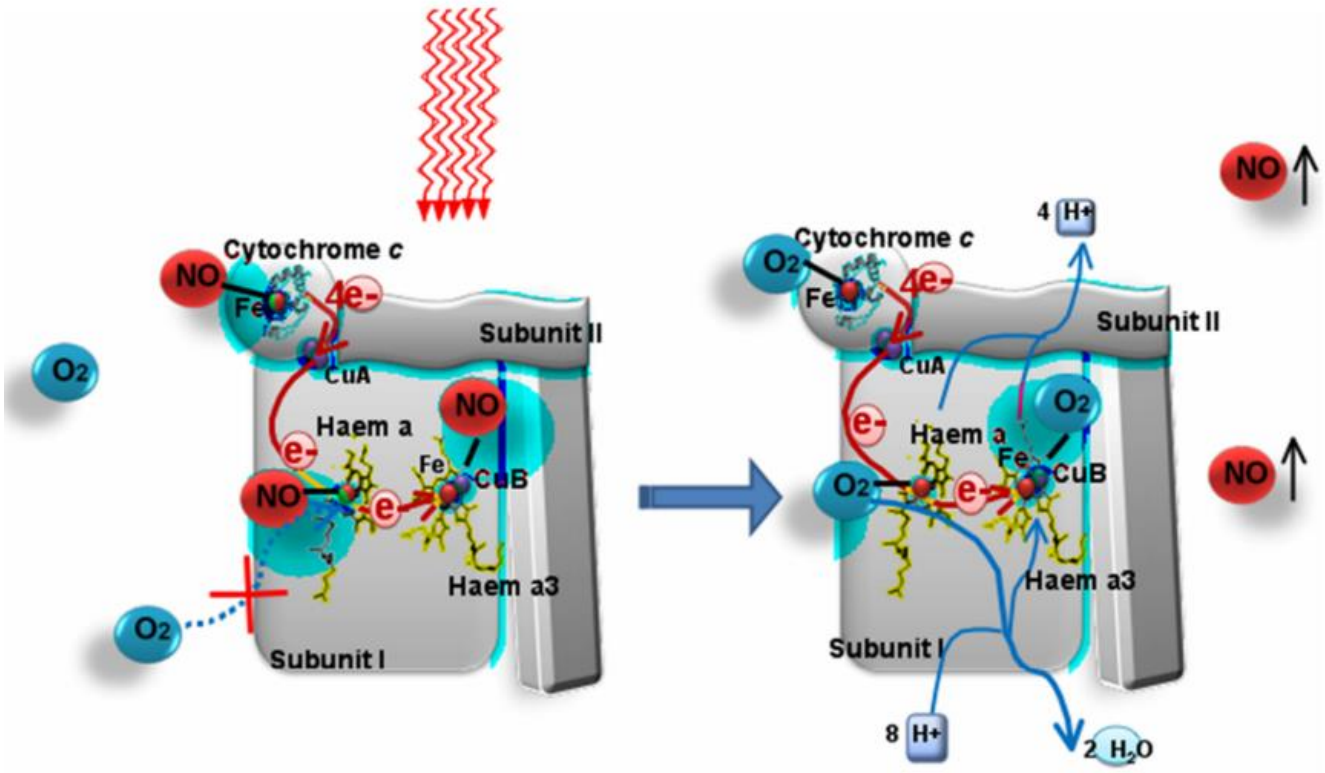

Figure 1.4: 'Photodissociation theory of PBM' in which light acts upon CCO or complex IV enabling the release of NO (red, left image) from its heme and iron centres, allowing oxygen (O_2, blue, right image) to bind in its place. This process induces increases in the circulating levels of NO due to its release from the complex as well as the progression of the ETC (Hamblin et al., 2011)).

1.4.1.2 Flavins and flavoproteins

Blue light (400-500 nm) is known to excite flavins and flavoproteins including flavin mononucleotide (FMN) and flavin adenine dinucleotide (FAD) (Swartz et al., 2001). A well-characterised family of flavin containing complexes are the "cryptochromes" (Yu et al., 2010). Notably, cryptochromes have been widely documented to absorb blue light (Bouly et al., 2007) and are proposed to be involved in the regulation of the circadian rhythm in mammals (Sancar, 2004). Notably, FMN is also found within complex I of the ETC (see Section 1.4.2) and it is proposed that blue light provides the activation energy for FMN to catalyse the reduction of oxygen (O_2) to superoxide ($O_2^{-}\cdot$) (Yang et al., 2017b). Hence, blue light is understood to induce increases in the levels of circulating ROS (Cheon et al., 2013). Complex II is also a flavin containing cytochrome (contains $FADH_2$ (GM., 2000)), and also absorbs blue light (Osborne et al., 2014). Hence, it is plausible that like red and NIR light, blue light could affect mitochondrial activity. Indeed, Serrage et al demonstrated that blue light (400-450 nm, 5.76 J/cm²) was as effective in inducing increases in mitochondrial activity compared with NIR light (810 nm, 5.76 J/cm² (Chapter 7, (Serrage et al., 2019b). Indeed, Buravlev et al also indicate that blue light (442 nm, 3-31J/cm²) modulates the activities of complex I, II and III (Buravlev et al., 2014a). However, further work is required to validate this hypothesis to determine whether blue light can modulate the activity of Flavin containing complexes of the ETC.

1.4.1.3 Porphyrins

Porphyrins, a group of heterocyclic organic compounds found complexed to proteins ranging from haemoglobin (Marengo-Rowe, 2006), to cytochrome p450 enzymes (Ener et al., 2010), to complex IV of the ETC (CCO) (Veerman et al., 1982) are known to possess a typical Soret band at 400-420m and hence possess the ability to absorb blue light (Koren et al., 2011a). Blue light of wavelengths between 400-415 nm induces the π to π* transition in porphyrin

rings (M, 1978). Wavelengths between 400-420 nm could oxidise porphyrin containing heme groups (found within complex IV), whilst a wavelength of 450 nm could induce CuB (a component of complex IV) reduction hence inducing complex IV oxidation or reduction, respectively (Karu, 2010).

When evaluating the influence of PBM on mitochondrial electron transport chain activity, Evgeny et al concluded that blue light application (442 nm, 30 mW/cm², 3 J/cm²) induced significant increases in complex IV activity and cell metabolic activity, compared with NO which inhibited cell responses (Buravlev et al., 2015). Also, Ankiri et al reported that complex IV possesses a maximal absorption at 410 nm and hence this could be due to porphyrins contained within the complex (Ankri et al., 2010b). Similarly, Del Olmo-Aguado et al evaluated the effects of blue light on retinal ganglion cell mitochondrial activity. The authors concluded that blue light upregulated the activities of complexes III, IV and V of the ETC, but also induced significant reduction in cell viability, and induced apoptosis (del Olmo-Aguado et al., 2012). These data indicated a possible role of blue light in affecting porphyrin-containing complexes of the ETC.

Cytochrome p450s (CYPs) are also porphyrin-containing complexes that have gained interest in phototherapy research, as their activation by blue light has been reported (Muller-Enoch, 1997). CYPs are a family of proteins that contain heme and are vital for drug metabolism. The p450 element of the cytochrome refers to the protein absorption spectra, since CYPs exhibit a maximal absorption peak at 450 nm when bound to carbon monoxide (Werck-Reichhart and Feyereisen, 2000). CYPs are membrane bound proteins that can be located either in the endoplasmic reticulum or the inner mitochondrial membrane. Mitochondrially-located CYPs including cytochrome P450 reductase, transfer electrons from

nicotinamide adenine dinucleotide phosphate (NAPDH) and thus could play a role in ETC activity (Hannemann et al., 2007).

Interestingly, Becker et al evaluated the effects of blue LED irradiation (453 nm, 23 mW/cm², 41.4 J/cm²) on the proliferation and gene expression of keratinocytes and found that irradiation induced a decrease in cell proliferation. However, the authors also reported that blue light induced significant increases in the transcription of ETC-related genes, cytochrome P450-related genes and also genes relevant to steroid hormone synthesis (Becker et al., 2015). Becker and colleagues also reported that genes relevant to inflammation were significantly down-regulated due to this exposure, and proposed that this may be due to the induction of steroid hormone biosynthesis via the CYPs pathway. Hence, these data provide an additional hypothesis as to how blue light PBM could affect cellular signalling.

1.4.1.4 Nitric Oxide (NO) containing complexes, related enzymes and compounds

It is hypothesised that alongside the photodissociation theory of PBM described in Section 1.4.1.1, light may also act to increase the synthesis or indeed release of NO from a variety of cellular sources. For example, PBM has been documented to induce NO release from a range of photolabile sources including S-nitrosothiols (RSNO), nitrosyl haemoglobin (HbNO) and dinitrosyl iron complexes. Indeed, these effects have been reported using blue (Rohringer et al., 2017), green (Sexton et al., 1994) and red light (Lohr et al., 2009, Keszler et al., 2018). Whilst, comparably NIR light is understood to have no significant effect. Indeed, Oplander et al reported that blue light at a wavelength range between 420-453 nm induced NO release through photodecomposition of S-nitrosalbumin (Oplander et al., 2013). Similarly, Mittermayr et al also showed that blue light exposure at 470 nm improved local tissue perfusion by inducing NO release from NO-haemoglobin complexes (Mittermayr et al., 2007).

A second hypothesis is that CCO has the potential to act as a nitrite reductase enzyme. This enzymatic reaction involves the reduction of nitrite to NO and water, catalysed by CCO, thus inducing increases in circulating levels of NO (Ball et al., 2011a). Usually, CCO acts as a nitrite reductase enzyme only in hypoxic conditions to mediate cytoprotection (Dungel et al., 2014). However, Ball et al demonstrated green light exposure at 590 nm could induce the activation of nitrite reductase (Ball et al., 2011b). Hence, further research is required to validate the exact mechanism by which PBM is increasing levels of circulating NO.

1.4.2 ROS induced secondary mechanisms of PBM

Reactive oxygen species are derived from oxygen and include hydrogen peroxide (H_2O_2) and superoxide ($\bullet O_2^-$). The accumulation of ROS induces a condition known as oxidative stress which involves an imbalance between the generation of ROS and antioxidants. Antioxidants including glutathione act to catalyse the conversion of volatile oxygen species to less damaging by-products including water. There are two forms of oxidative stress; exogenous oxidative stress induced by health and lifestyle (such as overexposure to UV light) and endogenous oxidative stress, produced intracellularly. Endogenous oxidative stress is caused by the generation of ROS as a by-product of internal processes. Aside from causing oxidative damage to tissue, ROS also play a key role in maintaining redox homeostasis and in cell signalling. There are a number of intracellular sources of ROS including the mitochondrion, the endoplasmic reticulum, the peroxisome and various enzymes (Holmstrom and Finkel, 2014).

The mitochondrion is regarded as the greatest contributor to endogenous ROS production. In particular, ROS are generated through the progression of the ETC (see Section 1.4.1.1), in which complexes I and III produce ROS as a by-product of ETC activity (Chen et al.,

2003). As discussed in section 1.4.1, the ETC is a fundamental target for PBM and a number of authors have described the absorption of light at a range of wavelengths by complexes I, III and IV.

Complex I is the largest complex in the respiratory chain (Zhu et al., 2016, Lenaz et al., 2006) and accepts electrons from nicotinamide adenine dinucleotide (NADH) and passes them through a FMN and iron-sulphur (Fe-S) clusters to ubiquinone (Ohnishi, 1998). In order for complex I to accept electrons from NADH, oxygen catalyses the reduction of NADH to NAD^+ to enable a proton gradient to be established. This reaction then produces superoxide, a highly reactive radical. Mitochondrially located manganese superoxide dismutase then catalyses the conversion of superoxide to hydrogen peroxide (Buettner, 2011). It is proposed that superoxide is generated at the FMN and potentially the ubiquinone binding site (Ohnishi et al., 2005).

Complex III functions as a dimer and each monomer possesses three heme groups bound to cytochromes and an Fe-S cluster (Zhang et al., 1998). Complex III forms its proton gradient in a process known as the 'Q cycle' (Bleier and Dröse, 2013). The Q cycle occurs through a net movement of two protons and two electrons through a series of processes at both ubiquinol-oxidation and ubiquinone-reduction sites and the movement of electrons through cytochrome b. Electrons can then be transferred to cytochrome c to enable the ETC to progress. Superoxide is generated at the Q_o ubiquinone reduction site as the Q cycle progresses.

It is hypothesised that whilst complex I releases superoxide into the mitochondrial matrix, complex III releases it into the intermembrane space (Muller et al., 2004). It has been shown that 50% of the superoxide produced at Q_o of complex III is released into the

intermembrane space, the other 50% is released into the matrix. It is thought that there is a lower peroxidase capacity in the intermembrane space and therefore superoxide may more effectively diffuse into the cytoplasm through porins. Whilst, superoxide that has diffused into the matrix may be more readily converted into hydrogen peroxide.

Hence, it is apparent that mitochondria are a key source of ROS and thus it is important to evaluate the production of ROS when investigating the effects of PBM on mitochondrial activity *in vitro*. Indeed, the majority of pathways induced by PBM are reported to be regulated by ROS production and thus are further described below.

1.4.2.1 Nuclear factor kappa-light-chain-enhancer of activated B cells (NFκB)

ROS production instigates a signalling cascade ultimately leading to the phosphorylation of IκB, an inhibitor of the pro-inflammatory transcription factor NFκB. In its inactive state IκB is bound to NFκB in the cytoplasm, however, once phosphorylated, IκB dissociates from NFκB and is targeted to the proteasome for degradation. This then allows the translocation of free NFκB to the nucleus binding to DNA, and initiation of a series of gene transcription changes, mRNA production and downstream expression of key cytokines, chemokines and growth factors including interleukin-8 (IL-8), IL-6 and vascular endothelial growth factor (VEGF (Elliott et al., 2001, das Neves et al., 2017, Cury et al., 2013, Choi et al., 2012)).

A number of authors report the modulation of NFκB by light irradiation. For example, Chen et al reported that irradiation at 810 nm and radiant exposure of 0.003 J/cm² induced the activation of NFκB through increased ROS production (Chen et al., 2011a). Similarly, Curra et al evaluated the effects of a 660 nm diode laser on NFκB protein levels using an *in vivo* hamster model of oral mucositis (Curra et al., 2015). The authors concluded that PBM reduced disease severity through the activation of the NFκB pathway. Conversely, PBM reportedly may

reduce NFκB activation and subsequently reduces the expression of pro-inflammatory mediators in several diseases (Hamblin, 2017). Interestingly, de Farias Gabriel also reported that application of 660 nm (4J/cm²) modulated NFκB activation leading to keratinocyte migration, resulting in improved wound healing in a rat model of oral epithelial wound healing (de Farias Gabriel et al., 2019). Hence, modulation of NFκB not only affects pathways related to inflammation but also those influencing wound healing.

Another gene directly regulated by NFκB activation is cyclooxygenase-2 (COX-2). Its main role is to catalyse the conversion of arachidonic acid to prostaglandins including prostaglandin E2 (PGE2 (Stack and DuBois, 2001)). PGE2 has been reported to be involved in the activation of a variety of pathways including cyclic adenosine monophosphate/protein kinase A (cAMP/PKA) signalling (Greenhough et al., 2009, Namkoong et al., 2005). To stimulate activity of the cAMP pathway, PGE2 binds to prostaglandin E_2 receptor 4 (EP4). EP4 is a G protein coupled receptor (GPCR) associated with a stimulatory G protein (Gs). On binding, PGE_2 induces a conformational change activating Gs, which then activate adenylyl cyclase to catalyse the conversion of ATP (a second molecule whose production is increased by PBM) to cAMP (Diaz-Munoz et al., 2012). cAMP then induces the activation of protein kinase A (PKA) leading to the phosphorylation of transcription factors including cAMP response element-binding protein (CREB (Delghandi et al., 2005)). Several authors have reported the effects of PBM on NFκB induced signalling. Lim et al reported that irradiation at 635 nm modulated both COX2 and PGE_2 protein expression (Lim et al., 2015). Current literature also indicates the effects of PBM on a series of signalling proteins/molecules implicated in this pathway, including CREB (Lan et al., 2009).

Another key molecule modulated by NFκB signalling is VEGF, a growth factor central to the promotion of angiogenic events (Toomey et al., 2009, Kiriakidis et al., 2003). Literature reports indicate that activation of PGE2 receptor 4 (EP4) induces the upregulation of the expression of VEGF and several authors have reported the effects of PBM on VEGF expression and activity. Tim et al concluded that 830 nm irradiation of male Wistar rats with induced bone defects exhibited significant increases in COX2 and VEGF expression (Tim et al., 2015), and das Neves et al also reported an increase in VEGF expression following irradiation of male Wistar rats with transverse *rectus abdominis* musculocutaneous flap at 660 nm or 830 nm (das Neves et al., 2017). Cheng et al also reported application of 450 nm light induced significant increases in COX2 and VEGF in a dose dependent manner (0.001-0.1J/cm^2) relative to LPS treated microglial cells (Cheng et al., 2016). Hence, the effects of blue, red and NIR light on NFκB associated pathways have been reported in several studies. However, no studies to date have evaluated the effects of green light on these pathways. Hence, it will be of future interest to evaluate the wavelength and dose dependent effects of light on downstream targets of PBM.

1.4.2.2 Transforming growth factor-β (TGFβ) signalling

Transforming growth factor-β (TGF-β) molecules represent a family of growth factors in which there are three mammalian isoforms: TGF-β1, TGF-β2 and TGF-β3. They have been extensively documented for their crucial role in wound healing processes (Penn et al., 2012) and in promoting angiogenesis and fibrosis (Ferrari et al., 2009). They are secreted by a variety of cell types in inactive form as latent-TGF-β in which a TGF-β dimer is linked by disulphide bonds and is non-covalently bound to a pro-domain known as latency associated peptide (LAP). This complex is also commonly referred to as small latent complex (SLC). The dissociation of this complex to enable activation of free TGF-β can be induced by a range of

activation stimuli including heat and pH changes (Liu and Desai, 2015, Horimoto et al., 1995). Notably, one mechanism of particular interest here is that PBM could induce activation of TGF-β signalling (Luo et al., 2013, Pamuk et al., 2017, Pyo et al., 2013). In a recent study Arany et al employed a laser emitting a wavelength of 904 nm with radiant exposure outputs ranging from 0.1-6 J/cm² and concluded that PBM was able to activate latent-TGF-β1 (Arany et al., 2007). It has subsequently been hypothesised that light induces an increase in levels of ROS including superoxide (O_2^-) ˙(de Freitas and Hamblin, 2016) which interacts with the methionine 253 amino acid residue on LAP (Jobling et al., 2006). This, in turn, then induces a conformational change in LAP, enabling its dissociation from TGF-β1 enabling it to bind with high affinity to its cell-surface receptors, including TGF-β receptors (TGFβRI, TGFβRII and TGFβRIII). Notably, TGFβRIII binds TGF-β1 and then transfers it to TGFβRI and TGFβRII, which are both serine/threonine kinases. In turn, these receptors phosphorylate transcription factors including "small mothers against decentaplegic" (Smad). Once phosphorylated Smad2 and Smad3 bind Smad4, the complex then translocates to the nucleus and interacts with transcriptional coactivators including p300, a nuclear scaffolding protein. This signalling then enables the binding of the complex with the Smad binding element, leading to the transcription of multiple target genes (Jain et al., 2013).

Interestingly, several authors have also provided evidence for an increase in the activity of Smad proteins following irradiation. The Smad family is comprised of the receptor Smads (Smad-1, -2, -3, -5 and -8/-9), the inhibitory Smads (Smad-6 and -7) and the co-Smad, Smad-4. Hirata et al found that irradiation at 805 nm induced increases in phosphorylation of Smad-1/-5/-8 (Hirata et al., 2010). Interestingly, Dang et al also found an increase in phosphorylated Smad proteins, specifically Smad-2 and Smad-4 following irradiation at 800 nm (Dang et al., 2011). Similarly, Yuchao et al reported application of 475 nm light induced significant

increases in Smad2 phosphorylation. Providing evidence that blue light may also show efficacy in modulating TGFβ signalling (Li et al., 2018). Hence, these data indicate the possible involvement of TGF-β signalling through Smad proteins during the transduction of the molecular effects of PBM. However, other pathways are also induced by TGF-β signalling including the mitogen associated protein kinase pathway (MAPK (Derynck et al., 2014)). Subsequently, it will be interesting to determine how PBM modulates TGF-β signalling through these interlinked pathways, and which wavelengths of light can induce them.

1.4.2.3 Nuclear factor erythroid 2–related factor 2 (Nrf2) signalling

Nrf2 is a protein in the "basic leucine zipper protein" (bZIP) family and is implicated in regulation of the expression of antioxidant proteins (Shelton and Jaiswal, 2013). Increases in ROS production lead to the dissociation of Nrf2 from its inhibitor, Keap1, targeting it for degradation. This enables Nrf2 to translocate into the nucleus and induce the transcription of antioxidant genes, due to the binding of Nrf2 to antioxidant response elements (AREs). To date, only a handful of studies have evaluated the effects of PBM on Nrf2 expression and activity. Interestingly, Sohn et al reported an increase in Nrf2 gene expression following irradiation at 635 nm (Sohn et al., 2015). Similarly, Trotter et al also found that application of blue light induced significant increases in Nrf2 expression *in vitro* (Trotter et al., 2017). This acts as a feedback mechanism following NFkB activation so the interaction of these two pathways may be important in PBM modulation of chronic inflammatory diseases. Indeed a differential upregulation of Nrf2 may be important in such diseases. However, further work will be required to fully dissect the effects of light irradiation on Nrf2 signalling.

1.5 Wavelength dependent response to PBM

It is proposed that the effects of PBM are wavelength and dose dependent. Wavelengths employed in PBM span the electromagnetic spectrum (Figure 1.1). However, wavelengths spanning the red to NIR spectrum are the subject of the highest proportion of literature reports due to their high penetration depth and their non-cytoxic effects, even at high doses (Huang et al., 2009). However, blue light effects are also gathering considerable interest. Hence, this section below aims to evaluate the effects of blue, red and NIR light, with particular focus on blue light.

1.5.1 Red and NIR light

The biological effects of red and NIR light have been widely reported. It is proposed that red and NIR light modulates mitochondrial activity inducing a series of downstream effects including decreases in oxidative stress and inflammation (see Section 1.4.1 (Hamblin, 2018a)). A recent study using aged *Drosophila melanogaster* (fruit flies) provided evidence that irradiation with red light increased mitochondrial function whilst also decreasing oxidative stress. The exposure to red light was accompanied by improved mobility, memory and retinal function in aged flies (Weinrich et al., 2017).

Indeed, the potential use of red and NIR light to manage disease is rapidly growing, with 87 clinical trials being reported across the world currently (clinicaltrials.gov database accessed: April 2019). In fact, a Scopus search revealed 4170 articles citing the use of red and NIR light PBM both *in vitro* and *in vivo* to date (April 2019, Figure 10.1). Further evaluation of recent reviews (systematic and meta-analysis published from the 30/4/2018-19) revealed 19 articles citing the use of red and NIR light PBM in the management of a wide array diseases ranging from symptoms of Parkinson's disease (Hamilton et al., 2018) to traumatic brain Injury (TBI) (Hamblin, 2018b, Rocha et al., 2018, Salehpour et al., 2018b). These articles were

reviewed systematically using the Scopus database and are summarised in Table 10.1 (see appendix).

Hence, current indications suggest that whilst red and NIR light may prove an effective modality in the management of disease it is clear further work is required to elucidate not only the molecular mechanisms of PBM but also the treatment parameters that will prove efficacious for clinical translation. This may be undertaken through high-throughput assessment of an array of wavelengths and doses (radiant exposures) of light on markers for mitochondrial activity.

1.5.2 Blue light

The majority of literature surrounding the use of PBM cites the use of wavelengths spanning the visible to NIR spectrum (600-1100 nm). In comparison the use of violet-blue light (400-495 nm) is less commonly reported and this may be due to the issue that the margin between 'biocompatible' blue light and damaging ultraviolet light (UV) is not yet fully defined.

UV light spans wavelengths of 100-400 nm and can be subdivided into three discrete categories: UVA (long-wave, 315-400 nm), UVB (medium-wave, 280-315 nm) and UVC (100-280 nm). The effects elicited by UV radiation are wavelength and dose dependent, and UVB and UVC wavelengths are most commonly associated with DNA damage and mutagenesis (Sage et al., 2012). Where, DNA has a peak absorption at 254 nm and subsequent UV irradiation leads to the formation of covalent linkages between adjacent pyrimidine bases in DNA to form a thymine dimer (B Alberts, 2002). If these dimers remain uncorrected, during DNA replication these mutant dimers are either deleted or substituted. However, these deletions or substitutions can lead to changes in gene sequence, and for example, can alter

expression and function of genes regulating cell division such as p53, which subsequently leads to uncontrolled cell division and therefore cancer (Kuluncsics et al., 1999).

Comparatively, UVA radiation has a poor efficiency in inducing DNA damage but can cause the generation of singlet oxygen through excitation of a photosensitiser that consequently reacts with molecular oxygen (ROS (Baier et al., 2006, Rastogi et al., 2010)). Whilst, increases in the generation of ROS have been associated with the pathogenesis of diseases such as periodontitis (Dahiya et al., 2013), small increases in ROS have also been associated with maintaining cellular function by modulating activities such as cell proliferation (Day and Suzuki, 2006). Indeed, the induction of ROS production by PBM has been cited to be pivotal in inducing the biological effects of light both *in vitro* and *in vivo* (1.4.2 (Hamblin, 2018a). Nevertheless, it is apparent that further work is required to evaluate the dose dependent effects of blue light PBM, in which biostimulatory and cytotoxic doses can be identified.

Indeed another key caveat of the use of blue light is its relatively low tissue penetration depth, as discussed in Section 1.3. However, despite this there is a growing body evidence supporting the use of blue light to reduce inflammation (Alba et al., 2017) and promote wound healing (Masson-Meyers et al., 2016a), as well as being able to limit bacterial growth (Veleska-Stevkoska and Koneski, 2018). Hence, a literature review was undergone to evaluate the effects of blue light PBM.

1.5.2.1 Evaluating the effects of blue light PBM

Review of the literature using the Scopus database revealed 68 articles citing the use of blue light (25/01/2008-25/01/2019, Figure 10.5) for a range of applications, including accelerated wound healing (Kim et al., 2017a), inhibition of cancer cell proliferation (Choe et al., 2017),

prevention of keloid formation (Lee et al., 2017b) and bacterial cell death (Bumah et al., 2015, Masson-Meyers et al., 2015, Schafer and McNeely, 2015) (see Appendix, section 10.1 for all articles reviewed).

Analysis of publications citing the effects of blue light PBM revealed 7% (5/68) inhibitory or cytotoxic effects, 21% (14/68) reported no significant biological response whilst, 72%(49/68) reported stimulatory effects on cultures including modulation of inflammation and markers for wound healing. However, information regarding the reporting and recording of treatment parameters in the articles reviewed remains lacking. Indeed key parameters were not reported in full by authors including exposure time (34%, 23/68), beam area (82%, 56/68), irradiance (29%, 20/68) and radiant exposure (38%, 26/68). Notably, 68% (46/68) articles reviewed disclosed no information regarding light characterisation methodology. The information reported by the other 22 articles were minimal, and the majority of studies only reported the power or irradiance output of an LED/laser light source (12/22 (Priglinger et al., 2018, Rohringer et al., 2017, Ashworth et al., 2016, Takhtfooladi and Sharifi, 2015, Niu et al., 2015, Teuschl et al., 2015a, Buravlev et al., 2014a, Dungel et al., 2014, Buravlev et al., 2014b, Buravlev et al., 2013, Fushimi et al., 2012, Adamskaya et al., 2011)). These findings fall in line with those reported by Hadis et al, in which the authors reported 76% of articles reviewed failed to report any light irradiation characterisation methods (Hadis et al., 2016b). Hence, future studies must prioritise the reliable measurement and reporting of treatment parameters to ensure the reproducibility of studies. This approach will enable robust studies to determine the efficacy of blue light for therapeutic application.

To determine potential treatment parameters for *in vitro* application, median radiant exposure values could be calculated from publications reporting parameters. In fact, a median

radiant exposure of 7.8J/cm² (range 1.5-90J/cm²) was calculated for those articles citing the biomodulatory effects of blue light in which 63% (17/27) reported the use of radiant exposure values <10J/cm². Potentially the application of doses of blue light within this range could be applied *in vitro* to evaluate the molecular mechanisms of PBM.

Review of the literature has revealed blue light PBM is effective in treating a wide array of diseases and ailments from reduction of symptoms in acne (Jung et al., 2015, Alba et al., 2017) to reduced bleeding time following tooth extraction (Veleska-Stevkoska and Koneski, 2018). However, the reporting of treatment parameters was minimal and only a handful of authors reported the biphasic dose response to PBM. In their article Masson-Meyers et al investigated the effect of blue light on wound healing using human dermal fibroblast (Masson-Meyers et al., 2016b). The authors reported irradiating cell cultures at 470 nm (30mW/cm², 3-55J/cm²) and evaluated the effects of light on markers for wound healing. It was concluded that radiant exposure values with the range of 3-10J/cm² reduced the secretion of IL-6, increased general protein production (which correlates with changes in gene expression), induced mean increases in basic fibroblast growth factor (bFGF) but had no significant impact on wound healing. Conversely, when utilising a fluency value of 55J/cm², the authors reported that irradiation did significantly reduce the rate of wound healing. These data suggest whilst low doses of blue light may modulate cellular activity whilst high doses may be cytotoxic. However, comparatively a publication also reported that doses of blue light (453 nm) up to 500J/cm² induced no cytotoxic effects on human skin cells (Liebmann et al., 2010). Hence, it is apparent further work is required to not only to evaluate the dose and wavelength dependent effects of PBM but also the differential response of cells isolated from different locations in the body to blue light.

Similarly, Mamalis et al investigated the effect of a blue light LED emitting a wavelength of 415 nm at fluency values between 5-80J/cm² on cell viability, proliferation, migration speed and ROS production utilising primary human skin fibroblasts (Mamalis et al., 2015). They found that irradiation at any fluency value had no effect on cell viability but induced significant increases in ROS production at every fluency value studied. Conversely, at fluency values greater than 10J/cm², there were significant reductions in cell proliferation and relative cell migration. Suggesting doses >10J/cm² may be cytotoxic. This may potentially be due to increases in ROS production inducing the activation of NFκB pathway and increases in the production of pro-inflammatory cytokines such as IL-8 and the activation of p21, a cyclin kinase inhibitor protein (He et al., 2005). Ultimately this may divert the cell into a cell survival state and arrested state, therefore preventing re-entry into the cell cycle and hence exhibits a decreased proliferation capacity (Hwang et al., 2017). Comparatively, application of a dose of 5J/cm² induced increases in ROS production but had no significant changes in cell proliferation compared with the non-irradiated controls. The current literature indicates that small increases in ROS production can promote increases in cell proliferation through the activation of NFκB which promote increases in production of growth factors such as basic fibroblast growth factor (bFGF) (Boonstra and Post, 2004, Sullivan and Chandel, 2014, Groeger et al., 2012).

Cheon et al also explored the use of blue light irradiation on proliferation of cells extracted from Sprague-Dawley rats (Cheon et al., 2013). Rats were shaved and consequently two circular excision wounds were created on the rat's dorsum. Subsequently the wound was irradiated with a blue LED emitting a wavelength of 470 nm at an irradiance of 3.55mW/cm² for 1 hour a day for 9 days (providing a total dose over nine days of 1.92J/cm²). Consequently,

the effects of PBM on cell proliferation as a marker for wound healing was assessed histologically. It was found that blue light irradiation induced significant improvements in wound healing compared with non-irradiated controls. These data could also indicate that low doses of blue light could increases cell proliferation, potentially due to relatively small increases in ROS production.

1.6 Periodontal disease

In the UK periodontitis is the most common chronic inflammatory disease, affecting 60% of those over the age of 65 (Chapple, 2014). In addition, oral disease treatment is estimated to cost the NHS £2.8 billion per annum for patient treatment (White et al., 2012). Periodontitis significantly impacts adversely on patients quality of life and is associated with a number of systemic diseases including type two diabetes mellitus (Preshaw et al., 2007, Taylor et al., 2013), rheumatoid arthritis (Persson, 2012) and coronary heart disease (H. Bokhari et al., 2012). Chronic levels of pro-inflammatory mediators including IL-1β and tumour necrosis factor-α play a role in mediating systemic disease induced periodontitis, amongst other possible molecular mediators including lipids and bacterial virulence factors (Nagpal et al., 2015, Koshy and Mahendra, 2017, Dominy et al., 2019).

Periodontal diseases can be subdivided into gingivitis and periodontitis. Gingivitis is inflammation of the gums and is also known as non-destructive periodontal disease as it doesn't result in any soft or hard tissue loss or destruction and is reversible. Gingivitis is treatable by ensuring good oral hygiene regimes. Although not inevitable, gingivitis is often a precursor to periodontitis in susceptible patients. Gingivitis develops in response to plaque formation and is initially associated with Gram positive aerobic bacteria, in contrast periodontitis is associated with an established subgingival biofilm mainly consisting of Gram

negative anaerobic bacteria (White, 1997). Periodontitis is characterised by a non-resolving chronic inflammatory lesion associated with excess inflammation which causes local tissue loss (connective tissue and bone). If allowed to progress the associated tissue loss results in tooth mobility and ultimately tooth loss.

1.6.1 Periodontal tissue anatomy

The main purpose of the periodontal tissues is to provide protection for the tooth from both masticatory forces and colonisation by periopathogenic bacteria (Chapple, 2002a). Healthy periodontal tissues comprise the gingivae, alveolar bone, periodontal ligament and root cementum (Hassell, 1993). The alveolar bone is covered by a muscosal tissue known as the gingiva (also known as the lamina propria), which is composed of a type I and III collagen rich extracellular matrix. The gingival tissue is separated by a basal lamina, rich in type IV collagen which connects to an epithelial layer. Collagen fibrils within the lamina propria attach directly to the alveolar bone (Lamont RJ, 2006). The predominant cell type within the gingiva are fibroblasts which function to remodel and produce various ECM components. Fibroblasts are also capable of responding to various pro-inflammatory stimuli ranging from bacterial stimuli to damage to the gingiva (Bartold and Narayanan, 2006). Immune cells are also present including macrophages, endothelial cells and neurons.

The external surface of the gingiva is covered by three distinct types of epithelium; the gingival, sulcular and junctional epithelium (Mah et al., 2014). In which the gingival epithelium is ketatinised and covers the external surface of the gingiva. The gingival epithelium aids in protecting the gingiva from damage during mastication and acts as a barrier to oral microbes. The sucular epithelium is not keratinised and covers the surface from the free gingival margin to the gingival sulcus. The junctional epithelium is non-keratinised, thin (which makes it

permeable to fluid and cells) and is found between the sulcular epithelium and tooth surface (Shimono et al., 2003).

The cementum and periodontal ligament are tissues that surround and provide support for the tooth. The periodontal ligament comprises a dense extracellular matrix (ECM), consisting primarily of types I, III and V collagen, that form fibres facilitating the attachment of the root cementum to the alveolar bone. The periodontal ligament suspends the tooth in the socket and protects both the teeth and bone from forces occurring during mastication. This thin layer of connective tissue comprises primarily of fibroblasts. However, neurons and epithelial cells are also present (Bartold and Narayanan, 2006). Periodontal tissue anatomy is indicated diagrammatically in Figure 1.5.

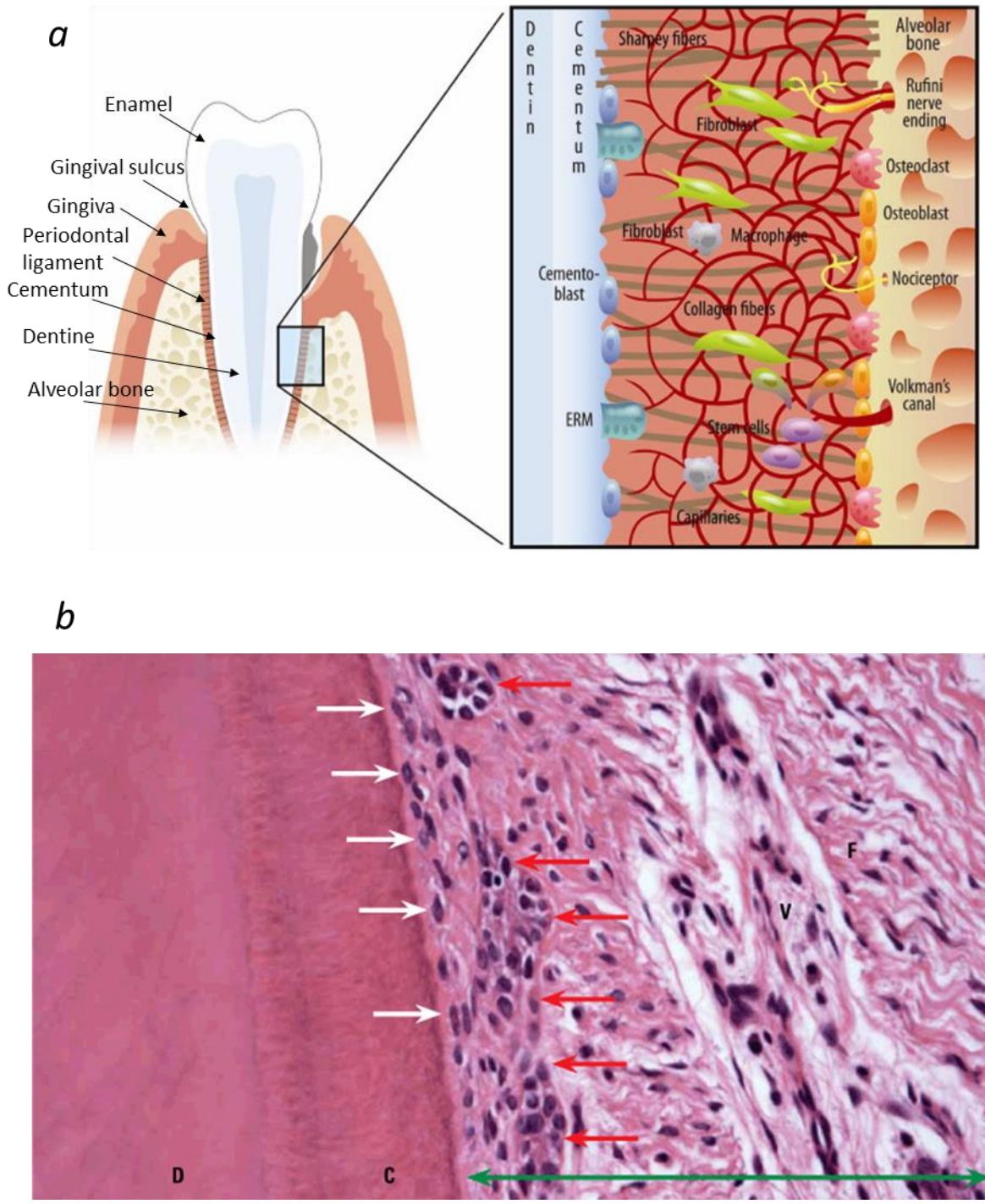

Figure 1.5 Periodontal tissue anatomy a) schematic of the periodontal tissue in which the a longitudinal section is labelled to demonstrate the location of various components of this complex tissue including the alveolar bone and dentine. The schematic also indicates the cells comprising the cementum, periodontal ligament and alveolar bone. In which fibroblasts in green predominate within the periodontal ligament. The periodontal ligament is also abundant in a complex network of collagen fibres as shown in red (adapted from (Marchesan et al., 2011)). Histological analysis is employed to evaluate tissue structure in vitro as indicated in b). The tissue was stained with 4-hydroxynoneal. D indicates dentin and C denotes the cementum, in which white arrows denote cementoblasts at the root surface. The green arrow denotes the periodontal ligament. The Epithelial Rests of Malassez are a network of epithelial cells and are indicated by red arrows. Blood vessels are also labelled as V and fibroblasts as F (from (CONSOLARO, 2010))

1.6.2 Gingivitis

Clinically, gingivitis is characterised by redness of the gingiva, bleeding, swelling and increased flow of inflammatory exudate, also known as gingival crevicular fluid (GCF). The initial development of gingivitis is caused by the accumulation of supragingival plaque. Whilst, gingivitis is not characterised by host tissue invasion by microbes, it is established that bacterial components derived from the plaque can induce an acute inflammatory response (How et al., 2016). These bacterial components include molecules such as LPS and bacterial DNA, also known as pathogen associated molecular patterns (PAMP).

These PAMPs are subsequently recognised by pathogen recognition receptors (PRR), including the cell surface receptors Toll like Receptors (TLRs). There are 10 functional human TLRs, in which Table 1.1 indicates the cells they are expressed by and what they recognise. TLRs are a crucial element of the innate immune system enabling the recognition of pathogens. Oral cell types including gingival fibroblasts (GFs) express TLR1, TLR2, TLR3, TLR4, TLR5, TLR6, TLR7, TLR8 and TLR9 (Di Benedetto et al., 2013, Uehara and Takada, 2007). LPS or endotoxin is composed of lipid and polysaccharide and is found on the outer membrane of gram negative bacteria and is recognised by TLR4. TLR4 stimulates a cascade of events that culminate in the activation of NFκB via the phosphorylation of its inhibitor IκB. NFκB then translocates into the nucleus to induce the expression of interleukin-8 (IL-8) and various other inflammatory mediators. IL-8 is a potent chemokine associated with periodontal disease, involved in the recruitment of neutrophils to the site of infection, binding to the chemokine receptors CXCR1 and CXCR2 on the neutrophils cell surface (Hazeldine et al., 2014, Sahingur and Yeudall, 2015). Indeed cytokines are responsible for the recruitment, differentiation, activation and growth of lymphocytes including T-cells (Taubman and Kawai, 2001). In turn, this leads to further increases in cytokine secretion, inducing increases in local tissue

inflammation, characteristic of gingivitis. However, this inflammation can be resolved, as discussed in Section 1.6, through thorough removal of the bacterial plaque inducing inflammation.

Table 1.1: Human leukocytes expressed by the human body (Murphy, 2012)

Toll Like Receptor	Examples of ligands	Cellular distribution
TLR1:TLR2 heterodimer	Lipomannans (mycobacteria), lipoproteins (diacyl lipoproteins, triacyl lipopeptides)	Monocytes, dendritic cells, mast cells, eosinophils, basophils
TLR2:TLR-6 heterodimer	Lipomannans (mycobacteria), lipoproteins (diacyl lipoproteins, triacyl lipopeptides)	Monocytes, dendritic cells, mast cells, eosinophils, basophils
TLR-3	Double-stranded RNA (viruses)	Natural killer (NK) cells
TLR-4 (plus MD-2 and CD14)	LPS (gram-negative bacteria), Lipoteichoic acid (gram-positive bacteria)	Macrophages, dendritic cells, mast cells, eosinophils
TLR-5	Flaggellin (bacteria)	Intestinal epithelium
TLR-7	Single-stranded RNA (viruses)	Plasmacytoid dendritic cells, NK cells, eosinophils, B cells
TLR-8	Single-stranded RNA (viruses)	NK cells
TLR-9	DNA with unmethylated CpG (bacteria and herpesviruses)	Plasmacytoid dendritic cells, eosinophils, B cells, basophils
TLR-10	Unknown	Plasmacytoid dendritic cells, eosinophils, B cells, basophils

1.6.3 Periodontitis

The clinical manifestation of periodontitis is that of soft and hard tissue loss resulting in tooth mobility , a probing pocket depth >4mm and possible gingival recession as can be seen in *Figure 1.6* (Chapple, 2002b)). Whilst, the aetiology of periodontitis, as with gingivitis, is plaque accumulation, periodontitis is associated with an agressive host inflammatory response in susceptible patients. This aberrant response is driven by recruitment of neutrophils to the site of inflammation where they release excess free radicals and ROS which cause the local tissue damage (discussed in Section 1.6.2). The onset and progression of periodontitis can also be influenced by a number of risk factors including systemic disease, smoking and diet (Najeeb et al., 2016, da Silva et al., 2017).

The bacterial species found in subgingival plaque are often considered more periopathogenic than those found in supragingival plaque (Listgarten, 1988). Indeed, species colonising both subgingival and supragingival have been grouped into what are known as 'Socransky complexes' (Socransky et al., 1998, Haffajee et al., 2008). These complexes are categorised by how strongly associated they are with periodontitis. Bacteria such as *Porphyromonas gingivalis* and *Treponema denticola* found in the red complex and are deemed as having a strong association with periodontitis. Comparatively, the early colonisers (Streptococci species) form the yellow complex and are deemed least pathogenic. Socransky complexes comprising subgingival plaque are described in Figure 1.7. *P. gingivalis* is a Gram negative bacterial species whose presence in the oral cavity has been correlated with increases in the severity of periodontal disease (Rafiei et al., 2017). *P. gingivalis* not only possesses the ability to produce proteases to lyse cells to extract nutrients but also produce proteases that degrade cytokines, enabling evasion from the host immune response (Lamont and Jenkinson, 1998).

Figure 1.6: Clinical manifestation of periodontitis, characterised by the loss of structures surrounding and supporting the tooth. In which, this image shows there is evidence of generalised inflammation, abnormal gingival anatomy due to tissue destruction, gingival recession, swelling and inflammation and abundant plaque and tartare build up (brown deposits on tooth). This is indicative of a poor oral health regime.

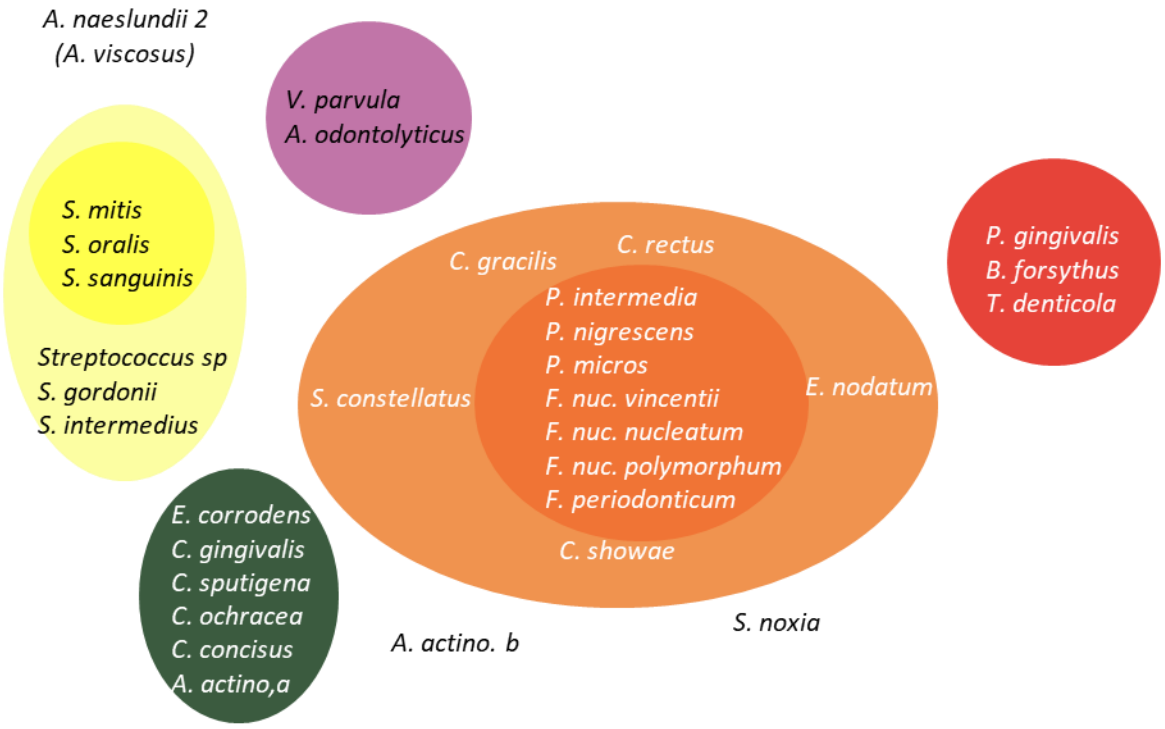

Figure 1.7: Complexes comprising subgingival plaque, also known as Sockransky complexes in which bacterial species colonising the oral cavity are divided into groups (indicated by different colours above) based on virulence. Where species comprising the 'yellow' complex are primary colonisers and are all Streptococcus species including Streptococcus gordonii (S. gordonii). In turn, the vicinity of the yellow complex to the green, purple and orange complexes indicates the association of streptococcus species with various species including Veilonella parvula (V. parvula, purple complex), Capnocytophaga species (C. gingivalis, C. sputigena, green complex) and Fusobacterium species (F. nucleatum subsp, F. periodonticum, orange complex). Those species comprising the purple complex are also early colonisers with a low to moderate pathogenicity whilst those within the green complex are facultative anaerobes exhibiting moderate pathogenicity. In comparison, species comprising the orange complex exhibit the ability to produce exotoxins and are also known as bridging species, exhibiting the ability to coaggregate with more pathogenic species comprising the red complex including Porphyromonas gingivalis (P. gingivalis). The red complex comprises species commonly associated with periodontal disease. This is described in further detail by Socransky et al (Socransky et al., 1998).

1.6.4 Oral biofilm and the onset of disease

Plaque is characterised by the coaggregation of several bacterial species to form a complex bacterial biofilm. Bacterial colonisation can vary greatly from one individual to the next and can also vary considerably depending on the regularity and efficiency of oral hygiene procedures and the variety of bacteria within the biofilm. Plaque can form either supragingival or subgingival, with subgingival plaque more strongly associated with periodontitis.

Oral biofilms are formed through complex interactions between bacteria colonising the oral cavity. Their formation involves a series of environmental shifts including pH changes to facilitate the colonisation of an array of microbes ultimately leading to formation of a diverse ecosystem protected from insult via the production of the extracellular polysaccharide (EPS) matrix from species such as *Streptococcus mutans (S. mutan*s) (Jakubovics and Kolenbrander, 2010, Koo et al., 2010). Oral pH is generally maintained at 6 but consumption of food or drink can lower pH to 5. Oral pH can be regulated by a range of factors including host immune response, plaque biofilm composition and levels of ions including phosphate, calcium and hydroxide (PO_4^{3-}, Ca^{2+} and OH-). The initial step in the formation of an oral biofilm is the adhesion of primary colonisers including *Streptococcus* and *Actinomyces* species to the salivary pellicle through salivary receptors such as proline-rich protein and α-amylase (O'Toole et al., 2000, Zhou et al., 2016). Primary colonisers can then interact through adhesins to enable coaggregation with late colonisers (Kolenbrander et al., 2010). For example, the primary coloniser *Streptococcus gordonii* (*S. gordonii*) possesses a cell surface receptor containing a serine rich repeat enabling its adhesion to the salivary pellicle. In turn, *P. gingivalis* expresses short fimbriae known as *Mfa1* that enables its interaction and hence coaggregation with *S. gordonii* (Nobbs et al., 2011, Gerits et al., 2017). Interestingly

other species also mediate the colonisation of *P. gingivalis* including *Fusobacterium nucleatum* (*F. nucleatum*) through expression of the outer membrane protein *FomA* (Jakubovics and Kolenbrander, 2010). Thus, *F. nucleatum* plays a pivotal role in inducing oral biofilm maturation. Interactions between these bacterial species are displayed in *Figure 1.8.*

Other bacterial species prevent colonisation by periopathogenic bacteria such as *F. nucleatum* and *P. gingivalis.* For example, *Streptococcus intermedius* can downregulate the expression of *Mfa1*, hence preventing the coaggregation of *S. gordonii* with *P. gingivalis* (Christopher et al., 2010a). It is understood that the oral microbiome is comprised of over 600 species (Dewhirst et al., 2010b, Sulyanto et al., 2019) and these species interact under given conditions to aid the progression of the oral biofilm formation. The disruption of this progression is important in the prevention of the onset of several oral diseases, including periodontitis (Chandki et al., 2011).

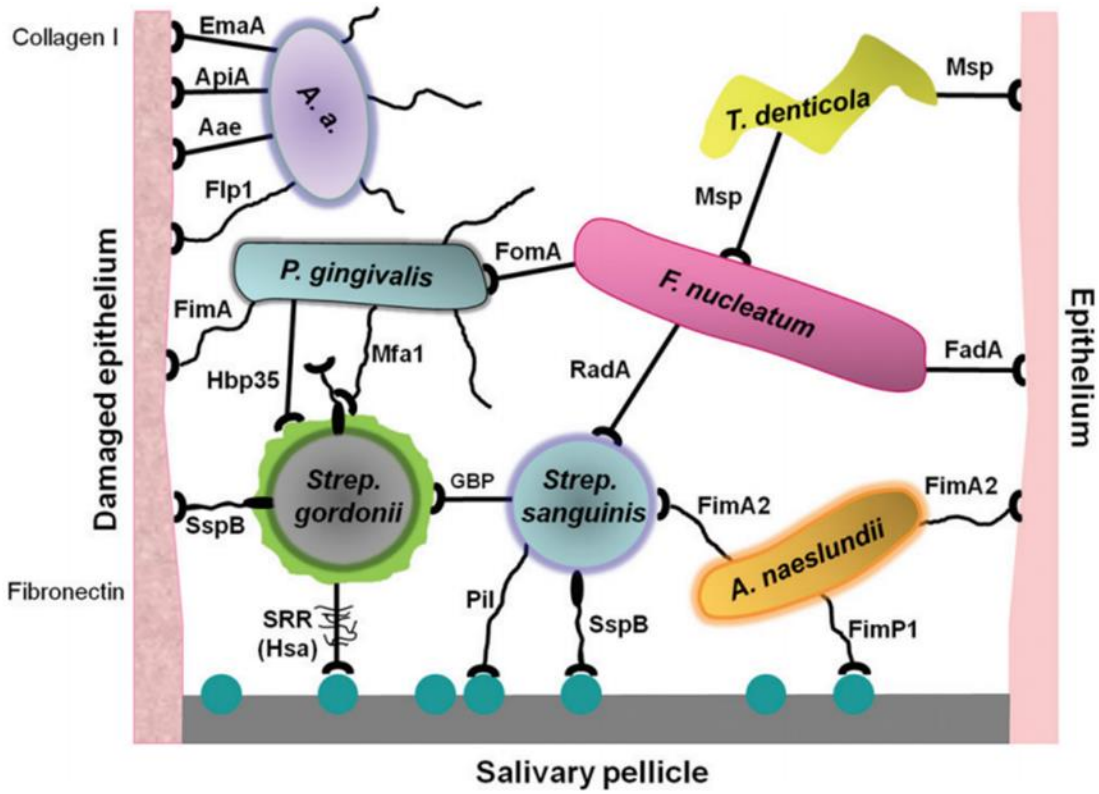

Figure 1.8 Illustration of the interactions of several bacterial species colonising the oral cavity using the medium of outer membrane proteins, pili and fimbrae. Bacterial species included are Streptococcus gordonii (Strep. gordonii), Streptococcus sanguinis (Strep. Sanguinis), Actinomyces Naeslundii (A. naeslundii), Fusobacterium. Nucleatum (F. nucleatum), Porphyromonas gingivalis (P. gingivalis), Treponem denticola (T. denticola) and Aggregatibacter. Actinomycetemcomitans (A.a). (from Nobbs et al (Nobbs et al., 2011)).

1.6.5 The role of gingival fibroblasts in periodontal disease

Gingival fibroblasts (GFs) are mesenchymally derived cells that are the most abundant cell type in the periodontium (Ara et al., 2009a). GFs are characteristically spindle shaped in morphology and exhibit the ability to remodel extracellular matrix (ECM) components through upregulation of ECM remodelling enzymes including matrix metalloproteinases (MMPs) and upregulating the production of ECM components (Williams et al., 2016). The ECM is a network predominantly composed of collagen (Yoshizaki and Yamada, 2013). GFs are a fundamental cell type used in the study of oral diseases due to their abundance and their ability to modulate the oral immune response (Bartold and Narayanan, 2006). GFs also exhibit the ability to recognise fluctuations in inflammation in the gingival microenvironment for example, due to the presence of bacterial cells or damage to the gingival ECM (Scragg et al., 1999). Indeed, studies have shown that healthy GFs exhibit different responses to stimuli when compared to inflamed GFs. In which the response of GFs to pro-inflammatory stimuli including *Porphyromonas gingivalis* lipopolysaccharide (*P. gingivalis* LPS) are time and dose dependent (Kang et al., 2016). In response to pro-inflammatory stimuli GFs produce cytokines including IL-6 and IL-8 and hence GFs are termed immunocompetent (Belibasakis et al., 2005). Hence, GFs are reported to be a key source of pro-inflammatory cytokines including prostaglandin-E_2 (PGE_2) and IL-6 within the oral cavity and thus play a fundamental role in modulating the oral immune response (Sakaki et al., 2004, Imatani et al., 2001). One unique characteristic displayed by GFs is the fact that this cell type does not develop tolerance to pro-inflammatory stimuli including LPS, whilst comparatively cell types such as monocytes do exhibit tolerance (Ara et al., 2009a). Which may suggest that GFs could play a crucial role in driving the persistent chronic inflammation, characteristic of periodontal disease (Naylor et al., 2013).

Fibroblasts isolated from different locations display differential responses to stimuli. For example, in 3D culture it has been shown that gingival and breast skin fibroblasts are phenotypically distinct. Where, GFs exhibit elevated levels of molecules crucial in ECM remodelling and regulation of inflammation compared to dermal fibroblasts and thus are hypothesised to be conducive in the quick resolution of inflammation and ECM remodelling (Mah et al., 2014). This phenomenon is known as fibroblast heterogeneity and it has also been shown that fibroblast sub-populations derived from different locations in the oral cavity exhibit distinct phenotypes (Smith et al., 2019). In which fibroblasts such as gingival and periodontal ligament fibroblasts exhibit differential surface marker expression and also have different morphologies (Phipps et al., 1997). Additionally, a number of authors have reported the differential response of GFs isolated from different individual's to stimuli (Tipton et al., 1991), including when evaluating the effects of PBM *in vitro* (Basso et al., 2015). Hence, GFs are not only an excellent model cell type for the study of periodontal disease pathogenesis but also for use in dissecting the individual dependent response to stimuli. This property could prove useful when exploring possible tailored treatments for periodontal disease using PBM, in which, inter-individual differences in response to PBM have been reported (Qamruddin et al., 2018).

1.6.6 Use of PBM in oral disease management

The use of PBM has been widely documented in the management of oral disease. In fact, a Scopus search identified 999 articles which cite the use of PBM in dental applications (30/4/2019-30/4/2013). However, in order to succinctly evaluate the utility of PBM in dentistry, reviews (systematic reviews and meta-analysis) reporting the use of PBM in management of oral disease were evaluated. A Scopus search employing the key words and exclusion criteria described in Figure 10.2 was undertaken.

The search revealed 42 relevant reviews, in which a high proportion reported the use of PBM for the management of oral mucositis (OM, 12/42, (Anschau et al., 2019, Bensadoun, 2018, de Pauli Paglioni et al., 2019, Fekrazad and Chiniforush, 2014, He et al., 2018b, Peralta-Mamani et al., 2019, Robijns et al., 2017, Sonis et al., 2016, Spanemberg et al., 2016, Sung et al., 2017, Zecha et al., 2016a, Zecha et al., 2016b)) or for orthodontic applications (17/42, see Appendix, Table 10.2 (Carvalho-Lobato et al., 2014, Ge et al., 2015, Kacprzak and Strzecki, 2018, Meng et al., 2017, Seifi and Vahid-Dastjerdi, 2015, Swidi et al., 2018, Yi et al., 2017, Eslamipour et al., 2017, Fleming et al., 2016, Li et al., 2015, Srivastava and Mahajan, 2014, Tania et al., 2015, Amid et al., 2014, Skondra et al., 2018, Kamel et al., 2014, Mathews et al., 2015, Prados-Frutos et al., 2016)) including accelerated orthodontic tooth movement. OM is a debilitating side effect of chemotherapy treatment, characterised by the development of ulcerative lesions in the oral mucosa. OM affects 29-66% of chemotherapy patients and is frequently painful, with few therapies proving efficacious in the management of this disease (Lalla et al., 2008). However, whilst these reviews do highlight the biomodulatory effects of PBM, many authors do still address the current ongoing issues reported in the literature. Indeed, there remains poor experimental design where parameters are not measured or reported, rendering it difficult to compare studies and draw conclusions regarding possible parameters to have an effect on cellular activity for application *in vivo*.

A similar issue is apparent in reviews reporting the use of PBM in the management of periodontal disease (Ren et al., 2017, Porteous and Rowe, 2014), gingival healing following surgery (Akram et al., 2018), dentine hypersensitivity (Moraschini et al., 2018) and burning mouth syndrome (Pandeshwar et al., 2016). Carroll et al also evaluated the use of PBM in dentistry and concluded that whilst there is evidence supporting the its use, there still remains

a lack of consistency in the reporting and recording of treatment parameters and also a lack of knowledge as to how PBM elicits its cellular and tissue effects (Carroll et al., 2014).

Hence it is apparent further *in vitro* and *in vivo* evaluation of PBM are required. Not only providing clear guideline as to how to report and measure treatment parameters but also in further dissecting the molecular mechanisms of PBM. This will then ensure clarity as to which possible parameters could induce effects clinically.

1.6.7 The biomodulatory effects of PBM on GFs.

As discussed in Section 1.6.5, GFs are a key cell type in the pathogenesis of oral disease and subsequently have commonly been used to study the use of PBM in its management. Indeed, a systematic review of relevant literature using the Scopus database and key words illustrated in Figure 10.3 identified 40 articles (see appendix, Table 10.3) that have been published detailing the effects of PBM on GFs (Almeida-Lopes et al., 2001b, Azevedo et al., 2006, Basso et al., 2013a, Basso et al., 2015, Basso et al., 2012b, Basso et al., 2013b, Basso et al., 2016a, Basso et al., 2016b, Chen et al., 2011a, Choi et al., 2012, Damante et al., 2009, Frozanfar et al., 2013, Gkogkos et al., 2015, Hakki and Bozkurt, 2012, Khadra et al., 2005, Kreisler et al., 2002, Kreisler et al., 2003, Kreisler et al., 2001, Kreisler et al., 2005, Liang et al., 2015, Lim et al., 2015, Lim et al., 2013, Lim et al., 2007, Marques et al., 2004, Nomura et al., 2001, Ogita et al., 2014, Pansani et al., 2014, Pansani et al., 2017, Park and Hong, 2014, Pourzarandian et al., 2005, Sakurai et al., 2000, Saygun et al., 2008, Schartinger et al., 2012, Takema et al., 2000, Wang et al., 2015, Yoshida et al., 2013, Yeh et al., 2017, Eslami et al., 2017). Notably 73% (29/40) of the articles reviewed reported the use of primary human GFs (pHGFs).

Of these 40 articles, 80% reported the use of a laser for light application (32/40) and 70% (28/40) reported the use of NIR laser light at wavelengths ranging between 780-2940

nm. High power lasers are frequently used in dentistry for a range of applications including tooth whitening, treatment of gum disease (by photodynamic therapy) or ablating decay in teeth affected by cavities (Verma et al., 2012). However, as discussed in Section 1.3 there are limitations to the use of lasers in PBM which includes their cost and their being no discernible difference in biological outcomes following application of either light source.

Interestingly, the most commonly applied wavelength for the study of PBM on GFs was 780 nm which was reported by 22% (9/40) of the articles reviewed. Only 1 article reported the use of blue light (460 nm (Yoshida et al., 2013)) and 13 reported the use of red light (Almeida-Lopes et al., 2001b, Azevedo et al., 2006, Choi et al., 2012, Damante et al., 2009, Lim et al., 2015, Lim et al., 2013, Lim et al., 2007, Park and Hong, 2014, Saygun et al., 2008, Schartinger et al., 2012, Wang et al., 2015, Yeh et al., 2017, Eslami et al., 2017). Evaluation of the reporting of treatment parameters revealed the majority of parameters were not reported in full including beam area (25%,10/40), power (75% 29/40), irradiance (25% 10/40) and radiant exposure/fluence (83% 33/40).

Review of the literature citing the effects of PBM on GFs identified 83% (33/40) reporting the significant biological effects of PBM, whilst 8% (3/40) cited cell toxicity and 10% (4/40) reported no significant effect on GF cellular activity. The majority of articles reporting biological effects provided evidence that light application either induced significant increases in cell proliferation (Park and Hong, 2014, Almeida-Lopes et al., 2001b, Azevedo et al., 2006, Basso et al., 2012b, Basso et al., 2016b, Khadra et al., 2005, Kreisler et al., 2002, Pansani et al., 2014, Pourzarandian et al., 2005) or reductions in markers for inflammation, including IL-1β (Basso et al., 2013a, Basso et al., 2015, Lim et al., 2015, Lim et al., 2013, Lim et al., 2007, Nomura et al., 2001). Notably the highest proportion of authors either cultured cells in low

serum (0-5% foetal bovine serum, FBS) or applied a pro-inflammatory stimulus such as LPS to induce conditions to mimic those exhibited in disease (57%, 19/33). Interestingly, for those articles reporting positive effects, a median radiant exposure of 3J/cm² was calculated (range: 1.5-155J/cm²).

When evaluating articles reporting no significant effect, all articles determined the effects of NIR light (780-904 nm) on cell proliferation at a median radiant exposure of 4J/cm² (range: 0.5-60J/cm²) of GFs cultured in 10% FBS (Frozanfar et al., 2013, Marques et al., 2004, Pansani et al., 2014, Liang et al., 2015). Hence, it may be hypothesised that application of a stimulus to induce stress to cell cultures may be a prerequisite for induction of cell proliferation by NIR PBM *in vitro*. Alternatively those doses used in the studies reported above may not have been within the narrow therapeutic window of PBM and thus no effect was induced. Hence, it will be important to evaluate the dose dependent effects of NIR PBM in a reproducible model, where all parameters are accurately measured and disclosed by the author.

Of the three articles reporting negative effects, only one reported the radiant exposure used. The authors concluded that application of 810 nm light was dose dependent where increases in radiant exposure output to cultures (24.6-792.8J/cm²) correlated with significant reductions in cell viability (Kreisler et al., 2001). Whilst radiant exposure was not disclosed for the other two articles, one used pulsed light, in which higher doses can be delivered within shorter irradiation periods and the other used blue light, which is reported to induce cell cytoxicity at doses >55J/cm² (see Section 1.5.2, (Kreisler et al., 2001, Yoshida et al., 2013)).

This systematic review therefore provides evidence that the literature supports the use of GFs as an appropriate model for the evaluation of effects of PBM *in vitro*. Indeed, the majority of authors report a response from cultures, either biostimulatory or bioinhibitory. However, it is apparent that further work is required to ensure the reproducibility of these studies as the majority of authors still fail to report key irradiation parameters. Interestingly, Ren et al also conducted a systematic review evaluating the effects of PBM on oral fibroblasts (Ren et al., 2016). The author concluded that better experimental design and more appropriate study models are required to validate current findings.

1.7 Evaluation of the effects of PBM in vitro

Whilst the effects of PBM have been widely documented to promote tissue healing (Adamskaya et al., 2011, Ankri et al., 2010b, Avci et al., 2013) and reduce inflammation (Chung et al., 2012) through modulation of ROS production (Hamblin, 2018a) *in vivo,* the cellular mechanisms induced by light to cause these modulatory effects are yet to be fully elucidated. Often, authors employ assays cited to act as markers for tissue healing, such as cell metabolic, viability and proliferation assays (Czekanska, 2011). Hence, this section aimed to explore assays commonly used to evaluate these markers, to determine their reliability for *in vitro* assessment of the effects of light.

1.7.1 The use of cell viability assays in PBM studies

The 3-(4,5-dimethylthiazol-2-yl)-2,5-diphenyl-2H-tetrazolium bromide (MTT) assay is regarded as a good indicator of cytoxicity due to its sensitivity and its applications in high-throughput screening of an array of different parameters. MTT is a monotetrazolium salt which are heterocyclic organic compounds and were first prepared in 1894 for their use in

biological redox systems and viability assays. Unlike other assays, MTT has a positive charge and readily penetrates eukaryotic cells (Riss et al., 2004).

In 1963, Slater et al indicated that MTT was metabolised by a succinate-dependent reduction by rat liver homogenates at two sites along the mitochondrially located electron transport chain, namely coenzyme Q and cytochrome c (Mosmann, 1983, Slater et al., 1963). However, other studies including one by Berridge et al have contradicted this hypothesis, suggesting that MTT is a glycolytic rate dependent reaction that requires ATP and NADH for its metabolism (Berridge and Tan, 1993). Evidence for this is presented by the inability of the cell to metabolise MTT without the presence of d-glucose and is supported by the sensitivity of MTT responses to cytochlasin B, an inhibitor of glucose transport in cells. Other support for this comes from the fact that cells without mitochondria are readily able to metabolise MTT. However, this occurs at a much slower rate than in wild-type mitochondria containing cells. Also, inhibitors of the mitochondrially located electron transport chain: azide and rotenone have little or no effect on the metabolism of MTT (Shearman et al., 1995). However, MTT can also be reduced by non-mitochondrial dehydrogenases or flavin oxidases. These data indicate that the reduction of MTT is not isolated to the mitochondria. However, this evidence does not rule out the possibility that complex II of the ETC (succinate dehydrogenase), contributes in some way to MTT metabolism (Liu et al., 1997).

The current literature however indicates that MTT is taken up by cells through endocytosis and is reduced by N-ethylmaleimide (NEM)-sensitive flavin oxidase. MTT then requires ATP and NADH to be metabolised in the cell, to form the insoluble precipitate, formazan, a crystal that is deposited granularly predominantly in a perinuclear localisation. Formazan accumulates in cells but is also deposited near the cell surface and in culture

medium. It is proposed that formazan formation directly correlates with cell metabolic activity as the more MTT metabolised, the more NADH is reduced and therefore the more formazan is produced. Interestingly, formazan is not formed in the mitochondria (Berridge et al., 2005). The chemical reduction of MTT to formazan is shown in Figure 1.9.

Current indications suggest that MTT is reduced by microsomal enzymes that require reduced pyridine nucleotides. Although, previously it was proposed that succinate dehydrogenase metabolises MTT, it is now recognised that although this complex can contribute to MTT metabolism alone, this reduction is low and contributes minimally to total cellular MTT reduction. Hence, the molecular mechanism of MTT is yet to be fully understood. However, the assay is regarded as a suitable method for screening an array of variable parameters in a high-throughput format.

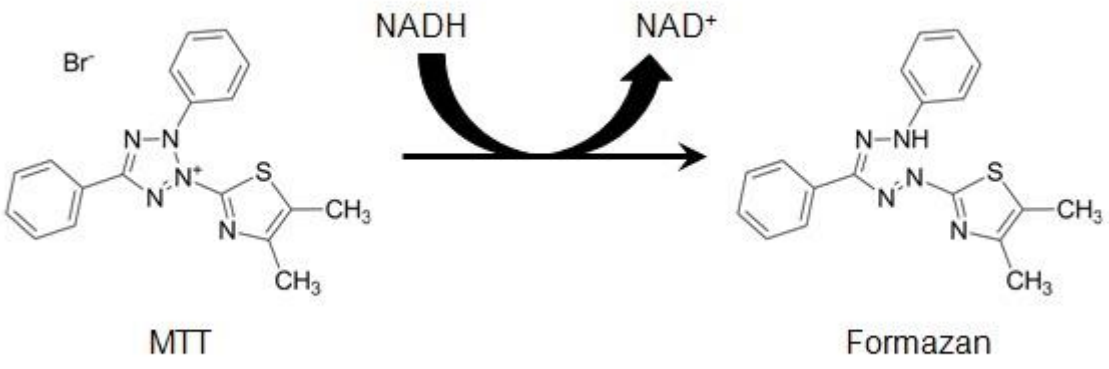

Figure 1.9: Structures of MTT and the coloured formazan product produced due to the reaction (Riss et al., 2004).

1.7.1.1 The use of MTT in photobiomodulation studies

One application of particular interest here is the use of MTT in assessing the effects of photobiomodulation *in vitro.* MTT is used widely to assess these effects, indeed when inputting the key words *'MTT'* and *'PBM'* or '*Low Level Light therapy'* or *'PBM'* or *'Photobiomodulation'*, into the Scopus database, 106 documents use these terms in combination (April 2019).

To evaluate the use of MTT in PBM studies, a systematic review of publications describing the use of light to modulate gingival fibroblast activity was undertaken (as described in section 1.6.7). Of the 42 publications reviewed investigating the effect of light on gingival fibroblasts 21 reported the use of cell proliferation assays (see Appendix Table 10.3 (Basso et al., 2015, Basso et al., 2012b, Basso et al., 2013b, Basso et al., 2016a, Basso et al., 2016b, Chen et al., 2000a, Damante et al., 2009, Frozanfar et al., 2013, Khadra et al., 2005, Kreisler et al., 2002, Kreisler et al., 2001, Kreisler et al., 2005, Liang et al., 2015, Lim et al., 2015, Ogita et al., 2014, Pansani et al., 2014, Pansani et al., 2017, Park and Hong, 2014, Pourzarandian et al., 2005, Schartinger et al., 2012, Wang et al., 2015, Yoshida et al., 2013)). Of these, 57% (12/21) indicated the use of an MTT assay (Basso et al., 2013a, Basso et al., 2012b, Basso et al., 2013b, Chen et al., 2000a, Damante et al., 2009, Frozanfar et al., 2013, Khadra et al., 2005, Lim et al., 2015, Pansani et al., 2017, Park and Hong, 2014, Schartinger et al., 2012, Wang et al., 2015). Other analyses applied included the Alamar blue, WST-8, BrdU and Cell-titer 96 assays. In the other 21 publications reviewed, a high proportion also assayed the effect of light on 'cell proliferation', however these analyses were mainly performed by manual cell counting (12/21 (Almeida-Lopes et al., 2001b, Azevedo et al., 2006, Chen et al., 2011a, Khadra et al., 2005, Kreisler et al., 2001, Pourzarandian et al., 2005, Saygun et al., 2008, Wang et al., 2015)). Other authors reported the effects of light upon the regulation of cell

growth factor and cytokine production (7/21 (Choi et al., 2012, Hakki and Bozkurt, 2012, Lim et al., 2013, Lim et al., 2007, Marques et al., 2004, Nomura et al., 2001, Sakurai et al., 2000, Takema et al., 2000)).

Of the publications identified which cited the use of the MTT assay, authors of these employed a range of irradiation parameters, including different light sources and wavelengths used. For example, Basso et al utilise an InGaAsP laser emitting a wavelength of 780 nm with exposure times of between 40 and 560s (Basso et al., 2013b) whilst, Schartinger et al utilised a GaAlAs laser diode emitting a wavelength of 600 nm with irradiation for 15 minutes, once a day for 3 days (Schartinger et al., 2012). Although different parameters were employed in these studies, both reported that light induced significant increases in cell proliferation.

Conversely, when using an InGaAsP laser emitting a wavelength 780 nm with exposure times between 40 and 240s, *Pansani et al* found that the irradiation exerted no significant effect on cell proliferation compared with untreated gingival fibroblasts (Pansani et al., 2014). Unlike the majority of studies, the authors applied the specific cell proliferation 5-bromo-2'-deoxyuridine (BrdU) assay. BrdU is an analog of the pyrimidine thymidine and is incorporated into the DNA sequence during the synthesis stage of mitosis. The more synthesis that occurs, the more BrdU is incorporated and hence this is deemed a good marker for cell proliferation (Taupin, 2007) .

Hence, it is apparent from this literature review that a large proportion of authors cite the use of MTT when exploring the effects of PBM on GFs. Therefore, it is appropriate to employ this assay to aid comparison with current literature. However, it is also important to note that MTT is not a specific assay for cell proliferation but as described above indicates metabolic and mitochondrial enzyme activity which can be related to cell number. Notably

therefore, MTT may be used alongside other assays including alamar blue, WST1, BrdU or through manual cell counting to further elucidate the effects of PBM on cell activity.

1.7.2 PBM modulation of ROS production

The effects of PBM on ROS production have been widely reported. Hence, the following section aimed to discuss assays commonly used to evaluate the effects of PBM on ROS production.

1.7.2.1 The use of dichlorodihydrofluorescein diacetate (H_2DCFDA) to evaluate ROS production in vitro

There are a range of assays that are reliably reported to measure ROS production, however few have the ability to be applied in a high-throughput microplate format. One assay that is popular for this application is the H_2DCFDA assay due to its relative ease of use. H_2DCFDA is a cell permeable probe that is hydrolysed intracellularly to dichloro-dihydro-fluorescein (DCFH), a carboxylate anion (Kalyanaraman et al., 2012). DCFH is subsequently retained in the cell and oxidised by two electrons to from the fluorescent product dichloroflourescien (DCF), the generation of which can be quantified fluorometrically. Further detail regarding the four-step process in which H_2DCFDA is hydrolysed to DCF is described in Section 2.2.11.3.

However, despite its popularity there are still some issues surrounding the use H_2DCFDA. Whilst, the majority of authors claim that H_2DCFDA can detect intracellular H_2O_2, this has been refuted by several other authors as it is claimed that DCFH does not directly react with H_2O_2 to form DCF. Indeed, the hydrolysis of DCFH to DCF involves a number of free radicals including hydroxyl radicals and peroxynitrite. Furthermore, cytochrome c, a heme protein that enables transfer of electrons from complexes III to IV of the ETC, has also been cited to catalyse the production of DCF (Dikalov and Harrison, 2014). Interestingly, serum in

media has been shown to interfere with the reliability of the assay and therefore it is potentially important to avoid use of media and buffers that may cause false results (Tetz et al., 2013).

While it is apparent that H_2DCFDA comes with its limitations and cannot be used to determine the levels of specific ROS species, it may represent a useful assay for identifying changes in oxidative stress in general.

1.7.2.2 The use of H_2DCFDA in PBM studies

The Scopus database was employed to conduct a systematic review citing the evaluation of ROS production induced by PBM. Evaluation was undertaken for literature published from 30/1/2015-30/1/2019 (see Figure 10.4 for further details regarding article selection criteria). These dates were selected to ensure a manageable but representative number of articles were identified and reviewed. The search revealed 41 publications (see Appendix, Table 10.4) in which the majority of authors employed H_2DCFDA to evaluate ROS production (51%, 21/41 (Djavid et al., 2017, Dong et al., 2015, Engel et al., 2016, Fuma et al., 2015, Giacci et al., 2015, Khan et al., 2015, Lee et al., 2017a, Liang et al., 2015, Lim et al., 2015, Salehpour et al., 2018a, Santos et al., 2017, Serrage et al., 2019b, Spitler et al., 2015, Wang et al., 2017c, Zhu et al., 2017, Migliario et al., 2018b, Ribeiro et al., 2016, Rupel et al., 2018)). Other assays used to evaluate ROS production included thiobarbituric acid reactive substances (2/41 (Tatmatsu-Rocha et al., 2016, Amaroli et al., 2019)), flow cytometry (3/41(Alexsandra da Silva Neto Trajano et al., 2016, Mamalis et al., 2016, Diniz et al., 2018)) and CellROX (3/41 (Mignon et al., 2018, Alves et al., 2016, Bartos et al., 2016)). Further details regarding the use of ROS assays are described in *Table 10.4*.

Of the 21 articles reporting the use of H_2DCFDA, 10 reported an increase in light-induced ROS production whilst the same number reported a decrease. Interestingly, of those 10 reporting a light-induced decrease in ROS production, 70% utilised experimental models with increased oxidative stress prior to light application, and the majority utilised LPS to stimulate the ROS generation (4/7). The use of stimuli to induce oxidative stress was not cited by authors reporting that light induced increases in ROS production.

Interestingly, in their article, Tatmatsu-Rocha et al explored the effects of PBM at 904 nm on ROS production in a models for both 'health' and 'disease' using Swiss male mice (Tatmatsu-Rocha et al., 2016). In their model for disease, the author induced diabetes using streptozotocin injection and subsequently wounds were created on the dorsum of the mice using a surgical blade. The author concluded that light application reduced ROS production relative to non-irradiated mice. Comparatively, when exploring the effects of PBM in a model for 'health', diabetes was not induced nor a wound created, instead the dorsum of the mice was again irradiated at 904 nm. Tatamatsu-Rocha found that application of light to 'healthy' mice induced increases in ROS production. These finding corroborate with current indications, suggesting that light acts in a biomodulatory manner, whereby light application to 'healthy' cells and tissue induces small increases in ROS production (Santos et al., 2017), whilst PBM decreases ROS production in inflamed or diseased tissue (Hamblin, 2017, Huang et al., 2013).

This short review therefore highlights the common use of H_2DCFDA in PBM research. Therefore, future studies may use this assay to aid comparison with current literature whilst also employing other assays to corroborate findings such as antioxidant assays. It will also be important to explore the biomodulatory effects of PBM on both models for disease and health *in vitro*.

1.7.3 Evaluating the mitochondrial dependent effects of PBM in vitro.

The effects of PBM are understood to be mediated through changes in mitochondrial activity whether this is through increases in ETC activity (Section 1.4.1), increases in mitochondrial ROS production (Section 1.4.2) or increases in the release or synthesis of NO from mitochondrial sources (Section 1.4.1.4). However, literature regarding the mitochondrial content dependent effects of PBM remains lacking.

Interestingly, mitochondrial content can vary considerably dependent upon the cell type evaluated (Cole, 2016). Indeed it has been reported that there are approximately 1000 mitochondria per liver cell whilst there are around 300 mitochondria per human lung fibroblast cell (Robin and Wong, 1988). Similarly, mitochondrial number has been cited to vary considerably between individuals (Mengel-From et al., 2014). Hence, this could explain the reported variability in response to PBM both *in vitro* and *in vivo*.

One way to explore this hypothesis *in vitro* would be to employ cell types that are closely related but commonly cited to possess different mitochondrial numbers. Indeed, the muscle-derived cells, myoblasts and myotubes, fit this criterion. Myoblasts have been reported to be an appropriate model for mimicking the process of skeletal muscle cell differentiation *in vitro* (Rashid et al., 2015) When exposed to appropriate conditions myoblasts differentiate into myotubes *in vitro* (Bentzinger et al., 2012) and mature myotubes are reported to have a significantly higher population of mitochondria than myoblasts (Schoneich et al., 2014, Kraft et al., 2006). Hence, these model cell types could theoretically be employed to evaluate the mitochondrial content dependent effects of PBM.

1.8 Thesis aims

Whilst there is a wealth of evidence supporting the use of PBM to treat disease, controversy still surrounds its application therapeutically due to poor reporting of irradiation parameters and a lack of knowledge as to how PBM elicits it's molecular and cellular mechanisms. This thesis therefore aims to address the key flaws in current literature, firstly providing evidence of a well characterised system for PBM research and secondly to provide indications as to which molecular targets are induced to cause PBM effects *in vitro*.

The objectives which underpin these aims are described in detail below:

Objective 1: To provide evidence of two well characterised systems for exploration of the effects of PBM *in vitro.* The first being a novel LED array in a 96-well plate format, emitting wavelengths from 400-830 nm and an average irradiance of 24mW/cm². This array was developed and designed in house by *Hadis et al* (Hadis et al., 2017a). The second was a bespoke LED array in a 24 well format (designed in collaboration with LUMOS™, Axion Biosystems, US) emitting wavelengths from 405-940 nm and had a variable irradiance output (Chapter 3).

Objective 2: To evaluate whether PBM can modulate markers for mitochondrial activity and which parameters of light prove most effective in doing so using the most abundant cell type in the periodontium: human gingival fibroblasts (Chapter 4).

Objective 3: To investigate the effects of light *in vitro* following the application of periodontal disease relevant stimuli including LPS, *F. nucleatum, P. gingivalis* and salivary biofilm. This will involve evaluation of both markers for mitochondrial activity and inflammation (Chapters 5 and 6).

Objective 4: To further elucidate the mitochondrial dependent mechanism of PBM. To first, characterise an assay to measure changes in mitochondrial activity in real-time (Seahorse cell mito stress assay, Agilent, California, US) and secondly to evaluate whether response to PBM is mitochondrial content dependent (Chapter 7).

2 MATERIALS AND METHODS

2.1 Materials

2.1.1 2nd generation array

The 2nd generation LED array was developed and designed in house as described by *Hadis et al* (Hadis et al., 2017a), utilising CADsoft's EAGLE software, in which 60 centrally located 5mm epoxy encased LEDs (Roithner Laserthek, Vienna, Austria) were designed to be placed within a 96-well microplate. LEDs were located centrally in the 96-well plate format to limit evaporation from wells at the perimeter of the plate *in vitro* due to cell incubation conditions as shown in Figure 2.1. It is understood that this evaporation can alter cell growth rates and responses and is a process known as an "edge effect", hence the array was designed to limit the impact of any confounding variables (Das et al., 2017).

The array contained ten channels, each emitting different wavelengths of light (n=6 per wavelength), which ranged from 400-830 nm (see Figure 2.1) and a standardised irradiance value of 24mW/cm². However, columns five and seven (emitting wavelengths of 605 nm and 670 nm) were not used during experimentation, as it was not possible for these wavelength channels to deliver the required irradiance value of 24mW/cm². Variable resistors were also attached to each wavelength channel to enable independent voltage control to ensure uniform irradiance delivery across the array. A bank of resistors acted to limit current for when the potentiometer was set to zero, this was to ensure the safe operation of the device and limit excessive voltage delivery to the LEDs, therefore preventing damage to diodes. The 2nd generation array also had its own bespoke sleeve which was formed of a black 96-well microplate with the clear bases removed (Corning, Sigma-Aldrich, Missouri, US). This was used as a collimator to limit potential bleed between different wavelength channels. The collimator also allowed accurate concentric alig nment of LEDs to allow optimal irradiation of

cells seeded into the 96-well black clear bottom plate. A bench top power supply (Iso-Tech, IPS-603, UK) was used to power the arrays using appropriate stable voltage and current values (Hadis et al., 2017b, Palin et al., 2015).

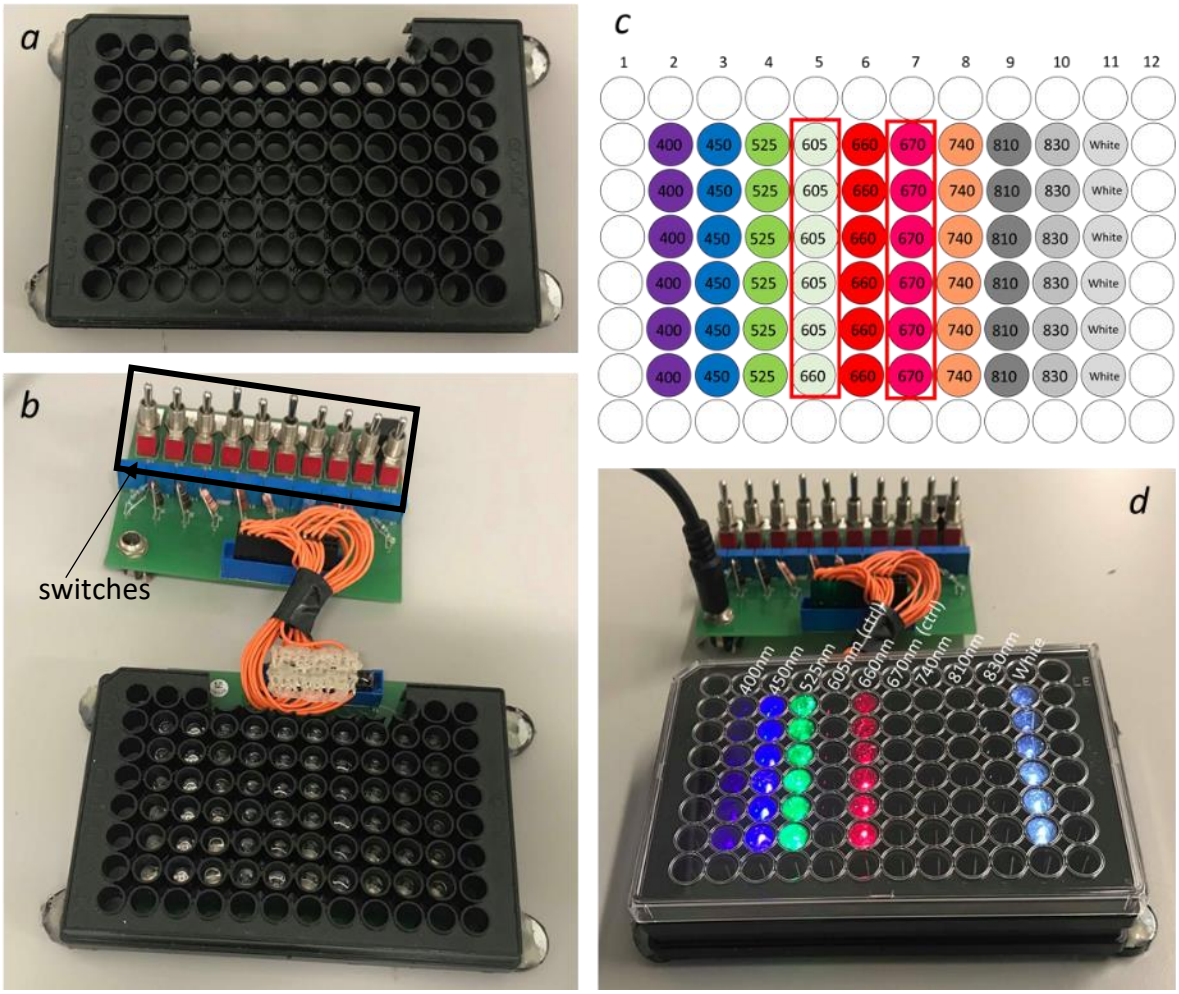

Figure 2.1: LED array layout and experimental setup where a) shows the black clear bottom plate with clear bases removed and b) shows how this plate is placed upon the array and indicates switches where individual wavelength channels can either be switched on or off. c) shows a schematic diagram illustrating the wavelengths used across the array, channels not used during experimentation are highlighted in red and d) shows the experimental setup for the LED array, where a black clear bottom plate is placed upon the array to enable irradiation of cultures from the base of the well in vitro, where all wavelength channels are highlighted for reference.

2.1.2 LUMOS array

A second array, the LUMOS™ optical stimulation system (AXION® biosystems, Atlanta, US) was designed by collaborators to incorporate 96-LEDs into a 24 well format, in which there were 4 LEDs located per well emitting wavelengths of light at 405 nm, 660 nm, 850 nm and 940 nm (as indicated in Figure 2.2). The sources of the individual LEDs and dimensions are displayed below (Table 2.1):

Table 2.1: The wavelengths of light, dimensions of LEDs used and the designation and company they were sourced from input into the LUMOS™ stimulation system.

Wavelength (nm)	Dimensions (mm)	Source
405	1.7x1.3	Lumileds Luxeon Z UV, Philips, Eindhoven, Netherlands
660	1.6x1.6	CREE XQE, Cree Inc, US
850	1.9x1.3	Lumileds Luxeon IR, Philips
940	1.9x1.3	Lumileds Luxeon IR, Philips

The LUMOS™ system comprised a docking station and LUMOS™ head in which the LEDs were incorporated as shown in Figure 2.2. During irradiation, unlike the 2nd generation array described in section 2.1.1, the LUMOS™ head was placed directly above a 24 well culture plate (as shown in Figure 2.2e). A USB cable was then connected to a computer with the programme Axion Integrated Studio (AxIS Navigator 1.40). This software enables the control of the independent stimulation of each well at up to four wavelengths, in which different wavelengths are denoted by different colours (blue: 405 nm, red: 660 nm, green: 850 nm and orange: 940 nm). Other key features include the ability of the software to control the irradiance output of each LED (denoted in the axis programme as % intensity).

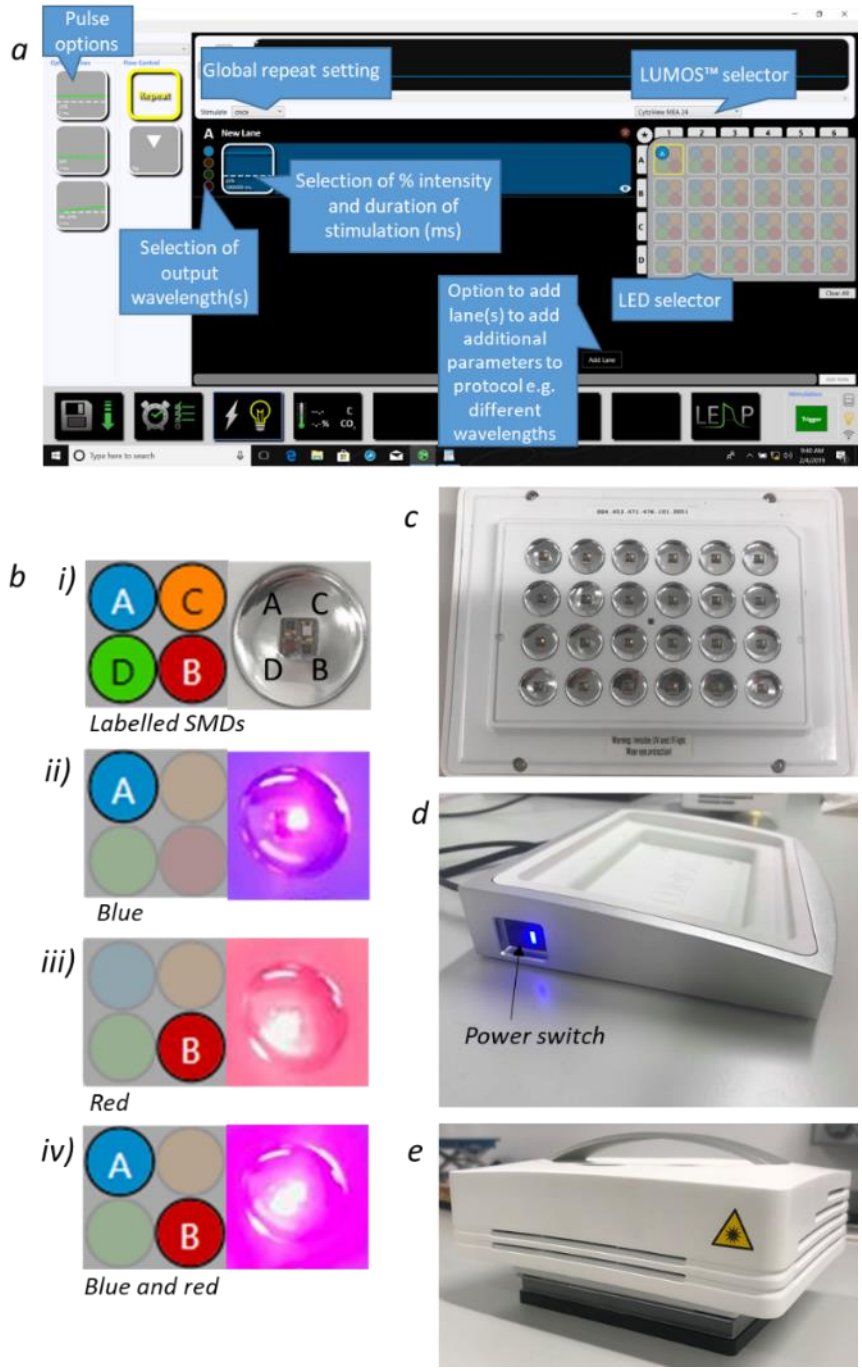

Figure 2.2: The LUMOS LED array system. a) Indicates AxIS navigator software interface where features are labelled including the ability to select LEDs for irradiation and selection of output wavelengths and b) provides evidence of the ability of the AxIS software to either irradiate cultures with a single wavelength or a combination of multiple wavelengths. Where, bi) shows the layout of LEDs on the software and the layout of the four SMDs on the array. Figure bii indicates the selection of blue light and the output of blue light from the array, biii) shows the selection of red light and the output of red light from the array and biv) shows the selection of blue and red light and the output from the array. c) shows the layout of the LUMOS™ head, which allows alignment with a 24 well plate. d) shows the LUMOS™ docking station, where the power switch is labelled and e) indicates experimental setup where the LUMOS™ head is aligned with the lid of a 24 well plate (4titude, US) which enables direct irradiation of cultures in each well from the top.

2.1.3 Light diffuser

To enable beam homogeneity of the LUMOS™ system, diffuser film was acquired (Inventables, Chicago, US). The diffuser film was matte on both sides and was of the dimensions: 0.002inx8.5inx11in. All properties of the diffuser material listed were reported by the manufacturer.

2.1.4 Light collimation device for Seahorse studies

An opaque dental silicone impression material (Impregum™ Penta Soft, 3M, Minnesota, US) mask was created to be fitted onto the bottom of a Seahorse XFe96 microplate to eliminate light bleed at the base of the wells where cells adhere and to ensure cultures were only irradiated at a single desired wavelength (Agilent, California, US). The impression material was injected into the base of the Seahorse XFe96 microplate and moulded. The material was then left for 10 minutes to set and consequently removed until required for experimentation. The distance between the LEDs and cell growth surface was fixed at 3mm in each well. The mask was fitted to a Seahorse XFe96 microplate during irradiation (see sections 2.2.8 and 2.2.11.4 and Figure 2.3 for experimental design).

2.1.5 Reagents

2.1.5.1 Dulbecco's modified eagle medium (DMEM)

DMEM high glucose with phenol red (BioSera, Nuaillé, France) was employed for cell culture which was supplemented to a final concentration of 1% w/v glutamine (L-glut), 1% v/v penicillin-streptomycin (P/S), 1% v/v Amphotericin B and 10-2% v/v foetal bovine serum dependent upon the specific experimental protocol (FBS, all Sigma-Aldrich). Growth medium was checked for sterility by placing an aliquot of the solution overnight in a tissue culture incubator (37^{o}C, 5% CO_2) and subsequently inspected for turbidity. Phenol red-free DMEM

medium (Gibco, Massachusettes, US) supplemented with sodium pyruvate (1% v/v, Sigma-Aldrich) and 4-(2-hydroxyethyl)-1-piperazineethanesulfonic acid (HEPES, 25mM, Sigma-Aldrich) was used to culture cells in appropriate plasticware (see Table 2.4 for details of plasticware employed during experimentation). All media was supplemented to a final concentration of 10% v/v with FBS directly before application to cells. All media was stored at 4°C and warmed to 37°C in a water bath prior to use (Sub Aqua Pro, Grant, Cambridge, UK).

2.1.5.2 Phosphate Buffered Saline solution (PBS)

Phosphate buffered saline was prepared to wash cells prior to application of ROS assay, to dilute reagents and to make wash buffer to wash plates during the ELISA procedure (2.2.10.2). PBS comprised of 0.775% w/v NaCl (Sigma-Aldrich), 0.02% w/v KH_2PO_4 (Sigma-Aldrich), 0.15% w/v K_2HPO_4, Sigma-Aldrich). Components were then dissolved in 1L of distilled water and pH was adjusted to 7.4 using 1M NaOH. Following this the PBS was autoclaved (121°C , 100kPa, 1 hour) to ensure sterility for use in tissue culture experiments and stored at room temperature until required for experimentation.

2.1.5.3 Trypsin ethylenediaminetetraacetic acid (Trypsin-EDTA)

Trypsin-EDTA was used to detach adherent cells from tissue culture plasticware in order to produce a single cell suspension for cell counting, archiving and passaging (see sections 2.2.6.2, 2.2.6.3, 2.2.6.4). Trypsin-EDTA comprised a final concentration of 0.25 % w/v sterile filtered porcine trypsin and 0.02% w/v EDTA·4Na solution in Hanks' balanced salt solution with phenol red (Sigma-Aldrich). Aliquots (20ml) were stored at -20°C and warmed to 37°C prior to use.

2.1.5.4 Escherichia coli Lipopolysaccharide (E. coli LPS)

E. coli LPS (026: B6, Sigma-Aldrich) was used to stimulate cells to produce a pro-inflammatory response via NF-kB activation prior to analysis using ELISA, MTT, NO and ROS assays (Kent et al., 1998, Andreakos et al., 2004). 1mg/ml of Lyophilised *E. coli* LPS was resuspended in 1ml of PBS and vortexed until completely dissolved (Vortex Genie, UK). The solution was then further diluted in PBS to 100μg/ml and aliquoted (1ml/aliquot) into 1.5ml siliconized Eppendorf tubes (to minimise LPS attachment to the plasticware, Eppendorf, Hamburg, Germany). Aliquots were frozen at -20^{o}C until required.

2.1.5.5 Cryogenic cell storage solution

Cryogenic storage of cells was performed by resuspension of cell pellets (generation of cell pellets described in section 2.2.6.2) in DMEM containing 10% FBS. The solution was then aliquoted (1ml/aliquot) into a 1.5ml Eppendorf (Eppendorf), followed by the careful addition of 100µl of 10% v/v dimethyl sulfoxide (DMSO, Sigma-Aldrich), cell cultures were then stored immediately as described in section 2.2.6.7.

2.1.6 Bacterial culture

2.1.6.1 Stocks

Bacterial stocks of *Porphyromonas gingivalis* (*P. gingivalis*, ATCC 33277) and *Fusobacterium nucleatum sp. Polymorphum* (*F. nucleatum*, ATCC 10953) were originally purchased from the American Type Culture Collection (ATCC, USA) and stored at -20^{o}C until required for use. Following growth of bacteria on fastidious anaerobe agar as described in sections 2.1.6.4 and 2.1.6.3, a sterile loop was used to collect colonies grown on plates and placed in a cryogenic

storage vials containing 25 cryogenic storage beads and cryogenic storage fluid (Thermo fisher, Massachusettes, US). Following inoculation, the cultures were mixed in the vial through inversion and subsequently incubated at room temperature for 15 minutes. This enabled adherence of microorganisms to the porous beads. Cryopreserving fluid was then poured away and samples were stored at -80°C until required.

2.1.6.2 Fastidious anaerobe agar

Fastidious anaerobe agar plates were purchased containing neomycin, 5% v/v horse blood, proteose peptone, liver digest, yeast extract and NaCl (OXOID, Thermo Fisher) were stored at 4°C. At least two hours prior to inoculation with bacterial colonies, plates were placed in an anaerobic cabinet to normalise temperature and deoxygenate plates (Don Whitley Scientific Ltd, UK) to provide conditions for anaerobic bacterial growth (37°C, humidified atmosphere).

2.1.6.3 Brain heart infusion (BHI) broth

Brain heart infusion (BHI) broth was prepared at 2.65% w/v in distilled water and was comprised of 10% horse serum, brain infusion solids, beef heart infusion solids, proteose peptone, glucose, NaCl and Na_2HPO_4 (OXOID). The solution was then autoclaved (121°C, 100kPa, 1 hour) and stored at 4°C until required. Sterility of broths was determined by eye, in which an increase in turbidity prior to inoculation of bacteria suggested contamination.

2.1.6.4 Sabouraud dextrose broth (SAB)

SAB, (3.7% w/v, OXOID) was prepared in distilled water and autoclaved (121°C , 100kPa, 1 hour). SAB comprised 1% w/v mycological peptone, 2% w/v dextrose and was stored at 4°C until required for use.

2.1.6.5 Artificial saliva media

An artificial saliva medium was produced (also known as McBain media (McBain et al., 2005), containing mucin (0.5%w/v), Bacto Peptone (0.2%w/v), BBL-Trypitcase Peptone (0.2%w/v), Bacto yeast extract (0.1%w/v), sodium chloride (0.035%w/v), potassium chloride (0.02%w/v), calcium chloride (0.02%w/v), PIPES (50mM), HEPES (50mM) and sucrose (1%w/v) (Sigma-Aldrich), dissolved in deionised water. Following this, 1%v/v of hemin (final concentration, Sigma-Aldrich) was added and the pH adjusted to 7.8 utilising NaOH. The media was then autoclaved for 20 minutes at 121°C . Vitamin K was then added to a final concentration of 0.0002% v/v (Sigma-Aldrich). Media was then stored at 4°C until required for use.

2.2 Methods

2.2.1 Array characterisation

2.2.1.1 Experimental setup for array characterisation

2.2.1.1.1 Second generation LED array

For LED array characterisation, a black clear bottom 96-well plate (Corning, Sigma-Aldrich) or Seahorse XFe96 microplate fitted with mask (see section 2.1.4) was used to overlay the surface of the bespoke 96-well LED array described in section 2.1.1. Each well was concentrically aligned with the LED inset beneath through the application of a sleeve developed through removal of the clear bases of a 96-well black clear bottom plate (Corning, UK) and the consequent application of either plate format on top of this (see Figure 2.3 for experimental design). Spectral characteristics (2.2.1.2), beam profiles (2.2.1.4) and thermal output (2.2.1.5) of the array were then assessed.

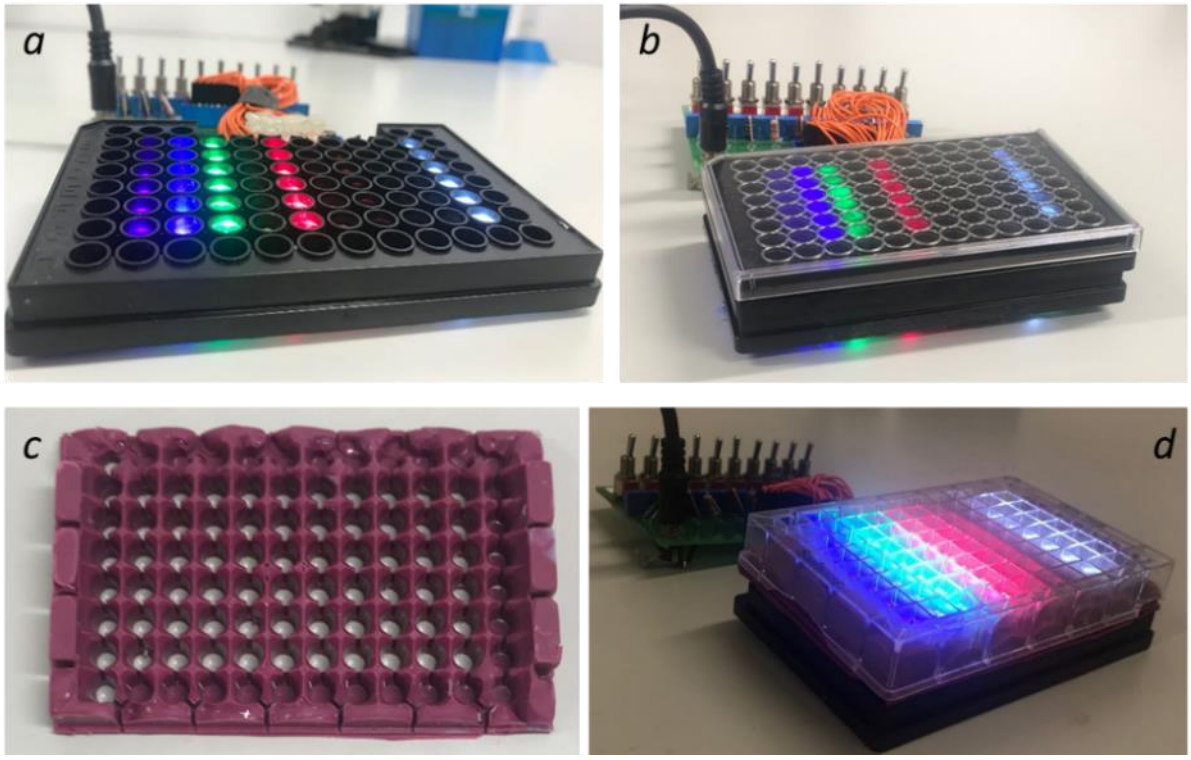

Figure 2.3: Experimental setup for LED array characterisation where a) shows LED array without plate-overlaid b) array overlaid with 96-well black clear bottom plate c) mask constructed from opaque dental silicone impression material described in section 2.1.3 and d) seahorse plate fitted with mask and placed upon LED array. Further detail describing array design can be found in section 2.1.1.

2.2.1.1.2 LUMOS™ optical stimulation suite

During *in vitro* experimentation, the LUMOS™ head is designed to be placed directly upon the lid of a 24 well plate (see Figure 2.2, 4titude, US). However, evaluation of beam profiles and spectral characterisation (see section 2.2.1.4 and 2.2.1.2) could not be performed when LEDs could not be visualised, where *in vitro* the LUMOS™ head would be placed upon the lid of a 24 well plate (see Figure 2.2 for experimental setup *in vitro*). Hence, the LUMOS™ head and plate were inverted to ensure various optical parameters from the LUMOS™ array including irradiance and average beam area could be assessed. Following inversion, two discrete experimental setups were applied in which an inverted 24 well plate with or without the addition of a diffuser material (see section 2.1.3) was placed upon the array. The experimental setup can be seen in Figure 2.4. These experimental setups were applied to determine whether the addition of a diffuser would improve beam homogeneity (2.2.1.4), whilst also evaluating to what extent the addition of this material affects irradiance output (2.2.1.2).

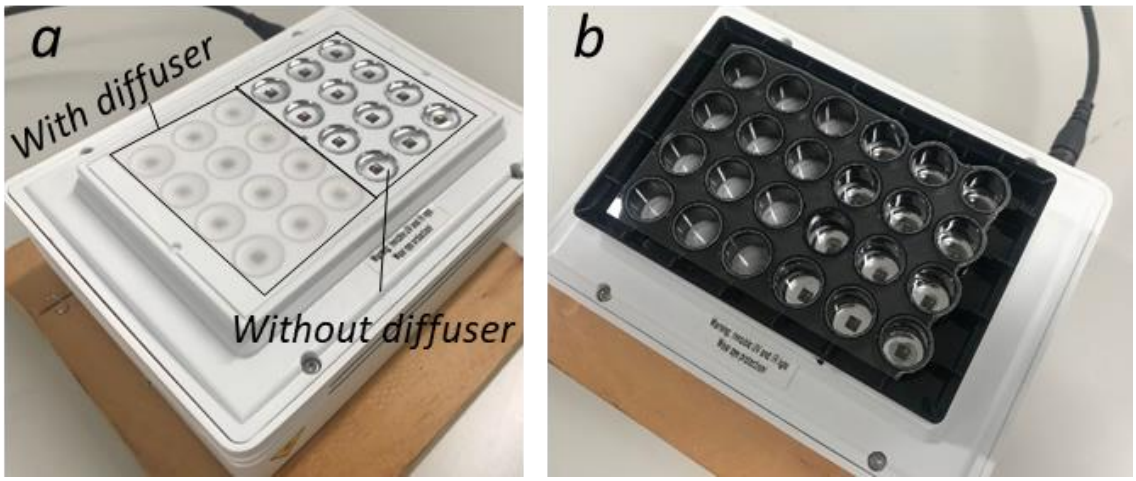

Figure 2.4 Experimental setup for evaluation of spectral properties and beam profiles output from the LUMOS™ array where a) indicates inverted LUMOS™ head with the application of a diffuser material on half of the array and the other half possesses no diffuser material. Figure 4b shows the setup with the addition of an inverted 24 well plate (4titude, US).

2.2.1.2 Spectral characterisation

A UV-Vis spectrometer (USB4000, Ocean Optics, UK) was used to assess emitted spectral irradiance and wavelength values from each individual well on the 2nd generation array (n=6 LEDs per wavelength channel measured) or LUMOS™ array (n=24 LEDs per wavelength/percentage intensity output measured).

The UV-Vis spectrometer was coupled to a 200μm optical fibre and an opaline glass CC3 cosine corrector (see Figure 2.5, 3.9mm diameter of collection area; 6mm outer diameter; Ocean Optics, UK). The spectrometer was calibrated to a National Institute of Standards and Technology (NIST) traceable light source (Micropack DH200/Ocean Optics, UK). Spectral irradiance measurements from each individual LED were recorded utilising OceanView software (Ocean Optics, UK). For each LED within the array, absolute irradiance was recorded through integration of spectral irradiance within the LED emission region. In order to maintain an average emitted spectral irradiance (~24mW/cm²), the array could be calibrated utilising potentiometers to regulate voltage emitted from each channel emitting a single wavelength as described in section 2.1.1. This was done by monitoring irradiance in real time employing OceanView software whilst adjusting screws controlling voltage output. These were adjusted until the highest common spectral irradiance value was output across the array. Figure 2.5 shows how emitted irradiance and wavelengths were recorded.

To ensure irradiance values comparable to the 2nd generation array were outputted from the LUMOS™ array (24mW/cm²), the unit of power output (% intensity) utilised by the software coupled to the array (see section 2.2.1.1.2) were correlated against irradiance. This involved manual input of % intensity values into the software ranging from 5-100%. The

irradiance output of all 24 LEDs at various % intensity outputs and wavelengths were then monitored using OceanView Software.

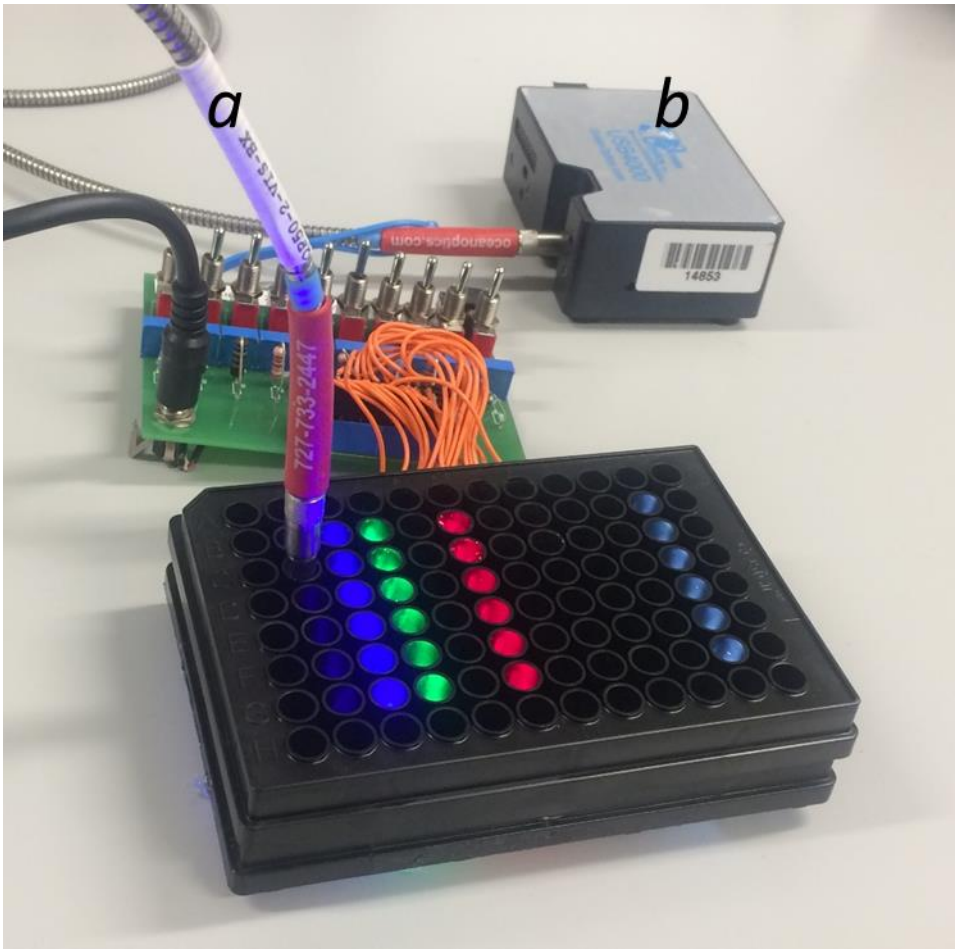

Figure 2.5: Experimental set up used to measure wavelength and irradiance values. A 96-well clear bottom plate was placed over the surface of the array. There was concentric alignment of each LED with the lower surface of the overlaid 96-well plate. A 200µm optical fibre and an opaline glass CC3 cosine corrector (a) coupled to a UV-Vis spectrometer (b, Ocean optics, UK) was placed in each well of the LED array and OceanView software (Ocean Optics, UK) recorded spectral irradiance and wavelength output.

2.2.1.3 Real time irradiance measurements

Real time irradiance was assessed to determine whether there were any fluctuations in LED irradiance output over longer periods of irradiation as previously reported in the literature (up to 240s, (Pansani et al., 2017, Kreisler et al., 2001, Khadra et al., 2005)) that could potentially alter radiant exposure values emitted from each LED (the product of irradiance and irradiation time (J/cm^2)). To assess this, a UV-Vis Spectrometer (Ocean Optics, UK) was coupled to an optical fibre and a cosine corrector, as previously described in section 2.2.1.2. The spectrometer was set to measure changes in irradiance utilising OceanView software by integrating peak areas of each LED (e.g. where integration occurred over a range between 380 nm and 420 nm for an LED emitting a peak wavelength of 400 nm). Using the 'strip-chart' element of OceanView software, real time measurement of changes in intensity emitted from LEDs were determined. The measured intensity counts could then be converted into irradiance values. Percentage change in absolute irradiance values could then be calculated and analysed in Excel software (Microsoft, US).

2.2.1.4 Beam profile

A charge coupled device (CCD) camera beam profiler (SP620, Ophir, Spiricon, Jerusalem, Israel) was employed to measure spatial distribution of irradiance. Wavelengths between 400 nm – 940 nm were measured through a target screen (N-BK7 ground glass diffuser, Thorlabs, New Jersey, US) to ensure reliable indication of the spatial distribution of irradiance at the plane of the adherent cells (n=3) (Palin et al., 2015). The orientation of the 2nd generation array meant the target screen could not be incorporated with either plate format. Hence, the target screen was placed at the same distance from the light source as the bottom surface of either 96-well plate (~3mm), to enable reliable evaluation of the beam profiles at the plane of the adherent cell cultures. For reference, images were also taken with either plate format but without the target screen. These images provide an indication of light delivered to the whole well and not just at the plane of the adherent cells and hence are not a reliable indication of the distribution of light delivered to cells in monolayer.

A camera was used with a 50mm CCTV lens (Ophir, Spiricon) and focused directly upon the point at which cells would adhere to the well culture surface, in which the corresponding LED below was directly emitted through. A maximum CCD sensor area was used, this involved the enlargement of the beam image projected on the sensor by using spacer rings (Ophir, Spiricon; 20mm) between the sensor and lens. A series of calibration steps were also undertaken to ensure accurate measurements of the spatial distribution of irradiance and to enable definition of the beam area emitted from each LED. The first calibration step undertaken was that of optical scaling to record precise measurements of beam. This utilised a ruler of known dimensions to calculate a scaling factor to enable pixel dimension calibration. This step enabled accurate measurements and therefore determination of values including beam diameter. Before imaging in each measurement, the UltraCal function in the Beam Gage

Software (Ophir, Spiricon) was used to correct for any background light or pixel response. A neutral density filter was also applied to enable real time visualisation of variations in irradiance values across each well. Previously determined power values (PD300 photodiode, Ophir Spiricion) were used for power calibration. The diameter of the light beam (D4omega or second moment, ISO reference 11145 3.5.2) was determined automatically by the Beam Gage software and was used to calculate the irradiance based on the inputted power values Figure 2.6 shows the experimental set up of the beam profiling equipment.

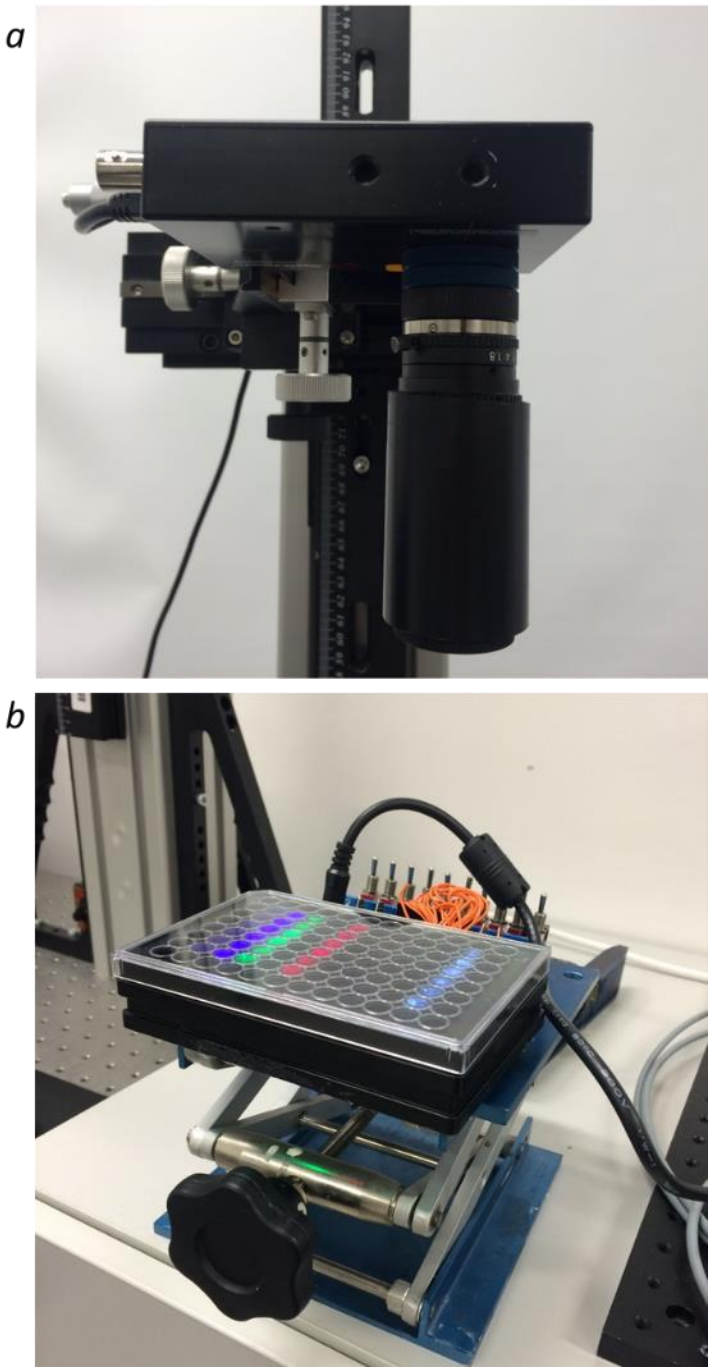

Figure 2.6: Beam profiling experimental set up in which CCD camera beam profile (6a) was placed 33mm from the culture plate. The culture plate was placed on a platform of known height (6b) to enable alignment of the camera with each LED. Data from each LED was captured individually, whilst surrounding LEDs were covered by opaque tape. This therefore enabled accurate capture of an image and hence enabling reliable calculation of beam area and power.

2.2.1.5 Thermal analysis

The effect of light irradiation on media temperature was assessed to ensure that changes in temperature would not affect the biological outcomes from the experimental studies. Phenol red free DMEM media (Thermo fisher) was aliquoted into a 96-well clear bottom plate (200µl/well), Seahorse XFe96 microplate (100µl/well) or 24 well clear bottom plate (500µl/well). The media was warmed to 37^{o}C to mimic experimental conditions *in vitro* and subsequently each plate was irradiated with the specific array and temperature changes measured in real time. All measurements were obtained in triplicate.

A K-type thermocouple (Maplin, UK; diameter 1.21mm) was fixed into a SubMiniature version A (SMA) adapter (6mm outer diameter, 4mm diameter). Access holes were made in the lid of an identical plate at the centre of each well to enable direct insertion of the thermocouple into media containing wells. Measurement of changes in temperature induced by irradiation were monitored at room temperature (~25^{o}C) and irradiated for up to 240s (24mW/cm^2, 5.76J/cm^2). Real-time measurement of changes in temperature were then assessed continuously at an acquisition rate of 2Hz for 240s using a multimeter (Iso-Tech, IDM 207, UK) and logged through data capture software (Virtual DMM, UK). Figure 2.7 shows the experimental set up used for the thermal analysis instruments for the 2nd generation array.

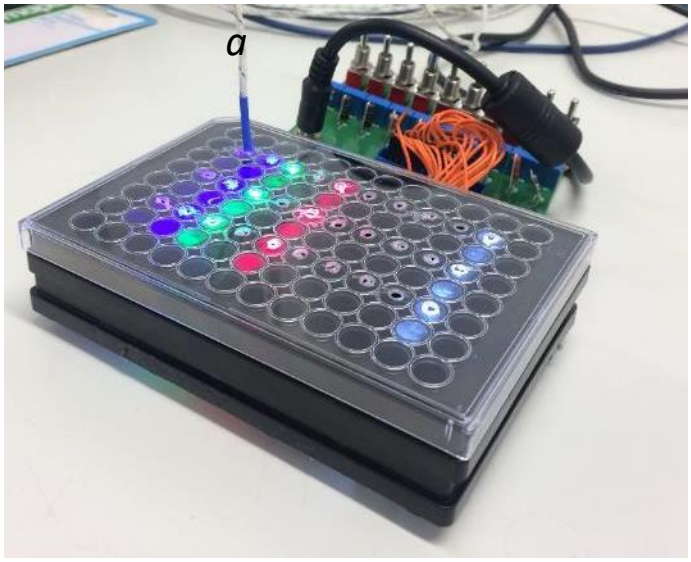

Figure 2.7: Set up used for thermal analysis experiment in which holes were generated in the lid of a 96-wells plate to enable input of a thermistor (a) to allow measurement of changes in temperature throughout irradiation for time periods of up to 4 minutes (24mW/cm², 5.76J/cm²).

2.2.1.6 Absorption measurements

To assess media and plasticware characteristics, a broadband deuterium-tungsten NIST traceable light sources (Micropack DH2000) was employed. Media containing phenol red +/- FBS or media without phenol red +/- FBS was assessed (DMEM, Thermo fisher). The base of a single well of a 96-well black clear bottom plate was also investigated for its absorption characteristics. Light was guided through a 600μm optical fibre and passed through air, an empty well of a 96-well plate, a cuvette containing distilled water (1000μl) or a cuvette containing media. The system was calibrated to enable the storage of a 'light spectrum' of an equivalent volume of distilled water for media measurements and the equivalent amount of air for plasticware measurements. For further calibration, a 'dark spectrum' was stored with the light source switched off. This then enabled the system to normalise with the effects of surrounding ambient light.

2.2.2 Bacterial growth and preparation

2.2.2.1 F. nucleatum growth

F. nucleatum polymorphum (2.1.6.1) was inoculated onto an fastidious anaerobe agar plate with neomycin (see section 2.1.6.2) and incubated for 5 days in an anaerobic chamber (Whitley anaerobic workstation, Don Whitley Scientific Ltd, UK). BHI was prepared as described in section 2.1.6.3. Prior to inoculation, the broth was placed in an anaerobic chamber to acclimatise to oxygen deprived conditions to ensure reduction of oxygen tension in media to prevent toxicity to strict anaerobes for 24h. The broth was then inoculated with representative colonies of *F. nucleatum*, incubated for up to 10 days, aliquoted into 50ml Falcon tubes (Thermo fisher) and centrifuged at 3000rpm for ten minutes (Durafuge 100, Precision, Expotech, Texas, US). Confirmation of *F. nucleatum* in samples is described in sections 2.2.3 and 2.2.4. The supernatant was discarded, and pellet re-suspended in PBS and centrifuged again. This step was repeated twice. Bacterial concentration was then determined using a spectrophotometer at 600 nm (Jenway 6300, Bibby Scientific Ltd, Stone, UK), this gave an optical density (OD) reading. Bacterial concentration was then determined and diluted to desired volumes in PBS and heat killed as described in section 2.2.2.4.

2.2.2.2 *P. gingivalis* growth

P. gingivalis (2.1.6.1) was plated using a sterile loop on Fastidious anaerobe agar with neomycin (see section 2.1.6.2). Prior to inoculation the plate was then pre-incubated in an anaerobic chamber (Whitley anaerobic workstation, Don Whitley Scientific Ltd, UK) for 2 hours. The plate was then incubated for 7 days and monitored daily to determine colour changes in colonies (where colonies developed from a light grey phenotype at days 3-4 to a dark brown phenotype 2 days, characteristic of *P. gingivalis*). SAB was prepared (see section 2.1.6.4) and subsequently placed in the anaerobic chamber for 24h prior, following this, the broth was inoculated with identical colonies. The cultures were then incubated in the anaerobic chamber for up to 10 days. Over this time-course, drops of the broth were tested on an agar plate to ensure there was no contamination in broth cultures. Once the broth was turbid, it was aliquoted and centrifuged (Durafuge 100, Precision, Expotech, USA) at 3000rpm for ten minutes. The supernatant was then discarded and the pellet was resuspended in PBS. The solution was then centrifuged a further two times. The pellet was then resuspended once more in PBS and bacterial concentration was determined by reading OD values at 600 nm using a spectrophotometer (Jenway 6300, Bibby Scientific Ltd, UK). Bacterial species in solution were confirmed using methods described in sections 2.2.4 and 2.2.5. Bacteria were then diluted to desired concentrations and heat killed for in vitro study as described in section2.2.2.4

2.2.2.3 Biofilm culture methods

2.2.2.3.1 Saliva Collection

To culture saliva, at least 5 to a maximum of 20 internal periodontally healthy (a dentist was recruited prior to the start of the trial to ascertain periodontal health of employees) Philips employees were recruited (Ethics approved by internal committee for biological ethics (ICBE-2-18519,), Philips research, Cambridge, UK). Prior to saliva collection, employees were asked to use a toothpaste (standard fluoride, non-antimicrobial toothpaste, no brand specified to avoid differences in marketed brands between countries) provided to them for a week and participants were asked not to utilise any antimicrobial mouthwashes. Volunteers were also instructed not to perform any oral hygiene measures 24h before saliva collection. For saliva collection, participants were asked to brush their teeth without toothpaste and subsequently saliva was collected from volunteers through passive drool into a universal up to a maximal volume of 20ml. The samples were then pooled in a laminar type II flow hood on ice (Thermo fisher). DMSO was subsequently added to a final concentration of 7% v/v and pooled saliva was aliquoted into 1ml cryovials. The samples were then stored at -80°C until required for use.

2.2.2.3.2 Preparation of poly (methyl methacrylate) (PMMA) substrates

PMMA is a substrate used commonly in dentistry to fabricate dental restorations. PMMA is also a useful substrate in biofilm culture (Spicer et al., 2013, Bertazzoni Minelli et al., 2011). PMMA chips or substrates were employed in this study to culture a mixed species biofilm. Substrates were cleaned with 1.2% Extran (Millipore, US), followed by 10 minutes ultra-sonication. Substrates were subsequently rinsed with deionised water; excess deionised water was then drained away (repeated three times). The substrates were then rinsed in

methanol and excess liquid was removed (step repeated twice). Substrates were then allowed to dry in laminar air flow hood.

2.2.2.3.3 Salivary Biofilm Culture

Approximately 10 PMMA substrates were added to an empty Petri dish (Sigma-Aldrich). Following this 20ml of artificial saliva media (see section 2.1.6.5) and 500µl of pooled saliva were added to each dish. Dishes were placed in an anaerobic chamber (Whitley DG250 anaerobic workstation, Don Whitley Scientific, West Yorkshire, UK) on a plate rocker at a speed of 50 cycles/min (Stuart Scientific, UK). Following this, media was replaced twice a day for seven days. Bacterial composition, height of the biofilm and ratio of live to dead bacteria was investigated using confocal microscopy (TCS SP5 X, Leica Microsystems, Milton Keynes, UK) (see section 2.2.2.3.4) every other day. Following seven days of growth, the biofilm was removed from PMMA chips (see section 2.2.2.3.5) and heat-killed (see section 2.2.2.4). Protein content was subsequently quantified to enable application of the biofilm at relevant concentrations to cell cultures (2.2.2.5).

2.2.2.3.4 Biofilm imaging

A live-dead stain was utilised to image bacteria and investigate biofilm composition in which two stains, each exhibiting fluorescence at different wavelengths enabled differentiation between live and dead bacteria, where a green stain was used to image live bacteria whilst the red stain was used to image dead bacteria (Life Technologies, UK). The stain was composed of SYTO 9 green nuclei acid stain (1.67mM, ex/em: 485 nm, 498 nm) and propiduim iodide red nucleic acid stain (1.67mM, ex/em: 535 nm, 617 nm). The stain was consequently added to a PMMA chip, in which biofilm was growing upon (300µl) and incubated for 30mins at 37°C and 5% CO_2 (Galaxy 48R CO_2 incubator, Eppendorf). Imaging was undertaken using a

confocal microscope (Leica Microsystems, Milton Keynes, UK) at magnifications of 10x and 100x. An argon laser was utilised at 25% of its maximum emittance excite photons in the biofilm, enabling fluorescence. Images were analysed utilising LAS software (Leica Microsystems, UK). LAS software could also be utilised to form Z stack images to formulate 3D images. IMARIS software was then utilised to formulate 3D images of the biofilm (Bitplane, Zurich, Switzerland). This then allowed investigation into the changes in the biofilm from day-to-day.

2.2.2.3.5 Preparation of biofilm for assays

The biofilms were removed from PMMA chips by placing the chips in 1.5ml Eppendorf tubes (Eppendorf, UK) and adding 1ml of PBS to each sample. The substrates were sonicated for 30 minutes (In-ceram, Vitasonic, VITA Zahnfabrik, Bad Säckingen, Germany). Following sonication, the PMMA chips were manually scraped with cell scrapers (CytoOne®, STARLAB group, Germany) and the suspension was pooled in a 50ml Falcon tube (Thermo fisher). The suspension was then centrifuged (10,000rpm, 10 min, 4°C, centrifuge 5804R, Eppendorf) and washed with PBS three times.

2.2.2.4 Heat-killing of bacteria

Following preparation of bacterial suspensions in PBS, the samples were placed in a water bath (Sub Aqua Pro, Grant, UK) at 80°C for 1 hour. Once heat killed, a small sample of the culture was inoculated onto a blood agar plate (section 2.1.6.2) for 24h to determine viability. Aliquots of dead bacteria at known concentrations were then stored at -20°C prior to use.

2.2.2.5 Bicinchoninic acid (BCA) protein assay

The BCA assay was used to assess protein content in the heat-killed biofilm and *F. nucleatum* in suspension (Thermo fisher) to subsequently determine optimal and standardised protein

concentrations to stimulate inflammation in tissue culture *in vitro*. This method quantifies the amount of Cu^{2+} reduced to Cu^{1+} by protein in alkaline solution, commonly known as the biuret reaction. The formation of Cu^{1+} (or the cuprous cation) is then detected colourmetrically at 562 nm utilising the reagent bicinchoninic acid (BCA). The purple colour of this assay is formed by the chelation of two BCA molecules with one Cu^{1+} ion. In order to quantify protein concentration, initially a standard curve was formulated utilising bovine serum albumin (BSA) as a standard and producing a range of dilutions in PBS (stock from 20-2000µg/ml diluted in PBS. PBS was used a negative control. BCA reagents A and B were mixed at a ratio of 50:1 respectively. 25µl of the standards and unknowns were then added to a 96-well plate followed by the addition of 200µl of the BCA reagent mixture to each well. The plate was then mixed thoroughly and incubated for 30 minutes at 37°C. After this, the plate was cooled to room temperature and absorbance read at 562nm using a spectrophotometer (ELx800 absorbance microplate reader, Biotek, Swindon, UK).

2.2.3 Identification of Bacteria

Bacteria was identified by streaking colonies onto a blood agar plate and investigating colony morphology as described in section 6.2. Bacterial identity was also validated using Gram staining and PCR analysis.

2.2.3.1 Gram Staining

Gram staining is utilised to distinguish Gram positive bacteria from Gram negative bacteria (Silhavy et al., 2010) based on different bacterial wall characteristics. Gram positive bacteria are stained purple with crystal violet due to the presence of their outer peptidoglycan layer whilst Gram negative bacteria only possess a lipid membrane which is removed by acetone

along with the purple crystal violet stain. Hence, in order to distinguish between the two, Gram negative bacteria are counter stained pink with carbol fuschin.

2.2.3.1.1 Crystal Violet Solution

Crystal Violet (C0775 Sigma-Aldrich) was dissolved to a concentration of 10% w/v in 95% v/v Ethanol. 20ml of this solution was then mixed with 80ml of 1% v/v solution of ammonium oxalate (A8545 Sigma-Aldrich).

2.2.3.1.2 Carbol fuschin

Carbol fuschin (351874U BDH, Sigma-Aldrich) was diluted in distilled water to a final concentration of 10% v/v.

2.2.3.1.3 Gram staining method

Using an inoculating loop, a few colonies were transferred from an agar plate to a microscope slide. A drop of saline solution was then pipetted onto the slide and spread around, this caused the emulsification of bacterial colonies. This suspension was then dried by passing the slide though a flame three times, this allowed fixation of the bacteria onto the slide. The slide was then covered with crystal violet for 30s and rinsed with tap water. Following this, iodine (diluted to 20%v/v in distilled water, L6146 Sigma-Aldrich) was applied for 15s, then rinsed, acetone was then briefly applied and washed immediately. Carbol fuschin was then applied for 15s and once again rinsed. The slide was then dried and viewed using a light microscope (Zeiss Primotech, Zeiss, Germany). Images were then captured using the Zeiss Labscope app (Zeiss, Germany) which was coupled to the microscope using an IPad (Apple, US).

2.2.4 PCR identification

Bacterial species-specific DNA was amplified using PCR.

2.2.4.1 Bacterial PCR

A volume of 1µl of bacterial suspension in nuclease-free molecular grade water was mixed with 12.5µl of Biomix red (Taq polymerase) (Bioline, Meridian bioscience, Ohio, US), 10.5µl molecular grade water, 0.5µl forward primer and 0.5µl reverse primer. *P. gingivalis* and *F. nucleatum* DNA was amplified using this method, where *F. nucleatum* primers were employed as negative controls for *P. gingivalis* amplification, whilst the converse was used for *F. nucleatum* amplification. Water was also used as a negative control, whilst a 16s universal primer was used as a positive control as all bacteria possess a 16s rRNA gene with highly conserved sequences and hence would confirm bacterial DNA presence in samples. Primer sequences are provided in *Table 2.2*. Amplification was undertaken in an Eppendorf thermocycler (Eppendorf). This process consisted of a denaturing step at 98°c for five minutes which lysed the bacteria followed by a number of repeated steps including denaturation at 98°c for 15s, primer annealing at 55°C for 30s and extension at 72°c for 20s. These three steps were repeated for 30 cycles. A final extension was then undergone at 72°c for 5 min, the samples were then cooled to 15°C. PCR products were then analysed using a 1.5% agarose gel electrophoresis, where 10µl of each product PCR product were loaded onto the gel alongside a 1Kb ladder (Bioline, 2.2.13.2.1).

Table 2.2: Primer sequences used for identification of bacterial species are these derived from the 16S gene region

Bacterial species	Symbol	Primer Sequence	PCR product (bp)	Reference
F. nucleatum	FN	F:5'-CTAAATACGTGCCAGCAGCC-3' R: 3'-CGACCCCCAACACCTAGTAA-5'	334	(Takeshita et al., 2017)
P. gingivalis	PG	F: 5'-ATAATGGACAACAGCAGGAA-3' R: 3'-TCTTGCCAACCAGTTCCATTGC-5'	414	(Takeshita et al., 2017)
16s rRNA gene	16suni-bact	F: 5'-AGAGTTTGATCATGGCTCAG-3' R: 5'-ACCGCGACTGCTGCTGGCAC-3'	~1350	(Srinivasan et al., 2015)

2.2.5 16s rRNA sequencing

2.2.5.1 Single Bacteria

Following amplification of the 16s gene isolated from individual bacterial sources as described in section 2.2.4, the band containing 16s DNA was visualised using a UV light source and excised from the agarose gel. Samples were then processed and analysed by Source Bioscience (Nottingham, UK), and bacterial species present in samples were confirmed. Sequences were then analysed using the blast nucleotide portal (blastn, https://blast.ncbi.nlm.nih.gov/Blast.cgi?PAGE_TYPE=BlastSearch&BLAST_SPEC=TargLociBlast) to determine the presence of *P. gingivalis* in PCR rRNA gene products.

2.2.5.2 Multispecies biofilm

2.2.5.2.1 DNA extraction

To assess the composition of species within the biofilm, three samples of DNA were extracted from salivary biofilm suspension (see section 2.2.2.3 for details). A masterpure Gram positive DNA extraction kit (Lucigen, US) was used. Firstly, 2ml of the suspension was centrifuged at

3000rpm for 10 minutes (Durafuge 100, Precision, Expotech, USA). Following this the supernatant was discarded and the pellet resuspended in 150µl of TE buffer (10mM Tris-HCl solution containing 1mM EDTA, provided by manufacturer) and mixed by vortex (Vortex genie). 1µl of Ready Lyse solution (lysozyme) was then added to the suspension and incubated at 37°c overnight. A 1:150 solution of proteinase K diluted in 150µl of gram positive lysis solution was then added to the suspension and incubated at 70°c for 15 minutes, cooled to 37°c and subsequently cooled on ice for five minutes. 175µl of MPC (abbreviation not defined by manufacturer) protein precipitation reagent was then added to the solution and vortexed for 10s. Debris was then pelleted through centrifugation at 4°c for 10 minutes at 10000g in a micro centrifuge (Eppendorf). The supernatant was transferred to a further Eppendorf and 1µl of RNase A was added to the solution and incubated at 37°C for 30 minutes. 500µl of isopropanol (Sigma-Aldrich) was then added to the solution and inverted 40 times, DNA was the pelleted for 10 minutes (4°C at 10000g) and isopropanol removed leaving the pellet. The pellet was then washed three times with 70% ethanol and the DNA was consequently resuspended in 35µl of TE buffer. For 16s sequencing, the samples DNA concentration was measured spectrophotometrically (Eppendorf Biophotometer Plus, Eppendorf) and diluted to 2ng/µl accordingly.

2.2.5.3 DNA sequencing

Library preparation and sequencing was kindly undertaken by Nabil Quraishi at Andrew Beggs Laboratory (Institute of Biomedical Research, University of Birmingham, UK). Paired-end 16S community sequencing was undertaken using the Illumina platform (Caporaso et al., 2012), in which primers targeted the variable 4 (V4) region of 16s small subunit ribosomal ribonucleic acid (SSU rRNA) for amplification (spanning 16s gene regions 515F-806R). Primers were in the 5'-3' direction and are indicated as follows:

- *Forward:* GTGCCAGCMGCCGCGGTAA
- *Reverse:* GGACTACHVGGGTWTCTAAT

For amplification, a series of sequences were added to the 515F forward primer, including a 5' Illumina adapter (a short DNA sequence that 'fishes' for an unknown DNA sequence), a Golay barcode (added for error prevention and recognition of sequences computationally), a forward primer pad and a forward primer linker (both of which used to link the adapter to the primer sequence). Similarly, for the 806R reverse primer, a reverse complement of the 3' Illumina adapter, a reverse primer pad and a reverse primer linker were included in the mixture.

Samples were added to a PCR mixture as follows: PCR-grade water (13µl, Sigma-Aldrich), PCR master mix (2X, 10µl, Platinum Hot Start PCR master mix (2x), ThermoFischer, UK), Forward primer mixture (10µM, 0.5µl), reverse primer mixture (10µM, 0.5µl), DNA sample of interest (1µl). Following this, PCR samples were placed in a thermocycler (Eppendorf) under conditions described in Table 2.3. Samples were amplified in triplicate and pooled (75µl). Amplicons from each sample were then ran on an agarose gel as described in section 2.2.13.2, in which the amplicon size was between 300-350bp. 16s amplicons were then quantified utilising the Quant-iT PicoGreen dsDNA reagent and kit according to the manufacturers protocol (Invitrogen, UK). Equal concentrations of amplicon from each sample (240ng) were pooled. The amplicon pool was then cleaned using the MolBio UltraClean PCR Clean-Up kit (Qiagen, Netherlands) according to the manufacturer's instructions. Concentration of DNA was measured as per section 2.2.12.2. Equimolar concentrations of each amplicon were subsequently pooled and sequenced on the Miseq platform (Illumina).

Paired-end DNA sequencing was then used to align DNA sequences containing repeated regions of sequence to produce a set of overlapping DNA fragments (contigs) and hence enabled de novo sequencing. This method also enabled detection of DNA rearrangements including deletions and insertions. A total of 497,176 sequences were identified in the 3 samples sequences, with a median number of 165,725 sequences per sample.

Table 2.3: Conditions used for PCR amplification of bacterial DNA

Temperature	Time	Repeat
94°c	3 min	
94°c	45s	x35
50°c	60s	x35
72°c	90s	x35
72°c	10 min	
4°c	hold	

2.2.5.3.1 Sequence processing

Nabil Quraishi (Institute of Biomedical Research, University of Birmingham, UK) undertook all sequence processing, in which raw sequencing (fastaq) files were input into Quantitative Insights into Microbiological Ecology (Qiime) version 2 pipelines. A data pipeline consists of a series of processing elements arranged to enable the output of each element to be the input of the next, analogous to a physical pipeline. These bioinformatic pipelines were employed to pre-process sequences to ensure there were no errors in the sequences and thus analyse sequences. Sequences were scored for quality and those that did not achieve a score of 99% were discarded. Sequences of less than 300bp were also discarded. Following pre-processing of samples, sequences were mapped to the SILVA rRNA database (Max Planck Institute for Marine Microbiology and Jacobs University, Bremen, Germany). Following mapping, an Excel file (Microsoft, US) providing data indicating the relative abundance of different bacteria at different taxonomic levels was produced and thus analysed.

2.2.6 Cell Culture

2.2.6.1 Tissue Culture Techniques

All tissue culture experiments were performed in a type II laminar air flow hood (Guardian MSC T1200, Monmouth Scientific Ltd, Somerset, UK) using aseptic techniques. All materials and reagents used were sterilised using either using an autoclave (121°C, 100kPa, 1 hour, MLS-3781L, Sanyo, Japan) or 0.22µM filter (Millipore, US). Cells were incubated at 37°c in 5% CO_2 unless otherwise indicated. In order to maintain the viability of cells, DMEM high glucose media (Biosera, Lab Tech International Ltd, Uckfield, UK) was utilised. For irradiation experiments supplemented DMEM without phenol red was used (Fischer Scientific, Loughborough, UK) (see section 2.1.5.1).

2.2.6.2 Primary human gingival fibroblast (pHGF) isolation and subculture

Primary pHGFs were obtained from gingival tissue withdrawn during surgical extraction of impacted third molars in adult subjects and grown from explants (prepared and characterised by Cleo White, School of Dentistry, University of Birmingham). Detail regarding age, sex and ethnicity of gingival fibroblast donors was not disclosed during this study. Ethical approval for this study was granted by the University of Birmingham Ethics Committee (RG_12-020). The pHGFs were frozen at -80°c until required. For the majority of studies, pHGFs isolated from three individuals which were relatively high responders to irradiation were pooled (B16, B19, B13) and used at p5-p8 unless otherwise indicated where a pHGF B15 isolate was also evaluated.

pHGFs were grown in a monolayer using DMEM growth media supplemented with FBS, P/S and L-glutamine to aid growth (see sections 2.1.5.1 and 2.2.6.1). Growth media was changed every 2-3 days. Once cultures reached ~80% confluence (7-10 days post seeding),

they were passaged. Confluence levels were estimated visually under light microscopy (Zeiss Axiocam erc 5s, Carl Zeiss Microscopy Ltd, Cambridge, UK). In order to passage cultures, existing media was aspirated, unsupplemented DMEM media was then added to wash cells. Following this, media was removed and 5mL 0.25% w/v trypsin-EDTA added to the monolayer and incubated for 5 minutes at 37ºC in order to detach cells from the plasticware surface (see section 2.1.5.3). Once detachment was determined by microscopic examination an equal volume of warmed supplemented DMEM media was added to stop the action of the trypsin. The solution was then transferred to a 50ml Falcon tube (Thermo fisher). The cells were then pelleted for 6 minutes at 850rpm, at 4ºC using a centrifuge (Durafuge 100, Precision, Expotech, USA). The resulting supernatant was then aspirated and discarded and the pellet resuspended in 1ml of DMEM media. Cells were counted and checked for viability (>99%) using a hemocytometer, as described in section 2.2.6.5. Cells either were then re-seeded into specific cultureware for subsequent studies or cryopreserved dependent on requirements.

2.2.6.3 Myoblast subculture

A mouse myoblast cell line was purchased (C2C12 (ATCC® CRL-1772™), ATCC, LGC standards, UK) and grown in monolayer utilising DMEM supplemented with FBS, P/S and L-glut from passage 4 (p4). Growth media was changed every 2-3 days. Three days post-seeding, cells reached 80-90% confluency and were passaged. Cells were initially washed with PBS and trypsin-EDTA was subsequently applied as described in section 2.2.6.2. Five minutes post-application, the trypsinised cells were mixed with an equal volume of media supplemented with 10% FBS and centrifuged at 900rpm for 5 minutes (B4i, Jouan, US). The supernatant was discarded, and pellet resuspended in an appropriate volume of supplemented media. Cells were counted and viability assessed (see section 2.2.6.4). Myoblasts either were then re-seeded into cultureware or cryopreserved dependent upon requirements.

2.2.6.4 Myotube differentiation

Following myoblast subculture, myotube differentiation was undertaken. Initially, myoblasts were cultured as normal between passages 6-11. Once cells had reached ~70% confluency,

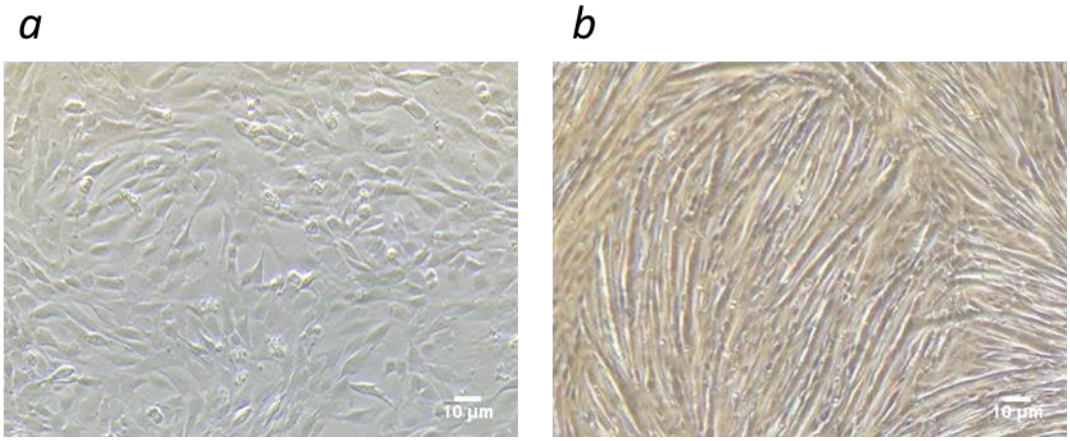

Figure 2.8: a) representative image of single nucleated myoblasts, exhibiting typical morphology and b) shows the multinucleated fibres of myotubes in which it is apparent there are significant differences in the morphology of these two cell types and thus can be evaluated using light microscopy. Images were taken using an iPhone 7 (Apple, California, US), in which the camera lens was porinted directly down the lens of a light microscope at a magnification of 10x (Zeiss Axiocam erc 5s, Carl Zeiss Microscopy Ltd, Cambridge, UK).

differentiation media was applied to cells containing DMEM supplemented with 2% v/v horse serum (Sigma-Aldrich) and 1% v/v P/S (2.1.5.1). Media was replaced every 2-3 days to aid growth. The differentiation of myotubes was determined using light microscopy (Zeiss Axiocam erc 5s, Carl Zeiss Microscopy Ltd, Cambridge, UK). Myoblasts and myotubes exhibit significant morphological differences, myoblasts are single nucleated cells with a radial branching, whilst myotubes are formed through the fusion of myoblasts to form multinucleated fibres ((Ali, 1979) Figure 2.8). Following 6 days of differentiation, the myotubes were utilised in experiments.

2.2.6.5 Cell counting and viability assessment

Following trypsinisation, an equal volume of cell suspension was added to trypan blue (0.4%, Sigma-Aldrich) diluted in deionised water. Assessment of cell numbers and viability was then

undertaken using light microscopy at 10 x magnification (Axiovert 25, Zeiss, Cambridge, UK). The application of trypan blue enabled differentiation between live and dead cells, where dead cells appeared blue under the microscope. A hemocytometer (improved Neubauer, Sigma-Aldrich) was used to determine the number of cells per ml of media using the following calculation (n=4 per cell suspension):

$$\text{Number of cells per ml} = \text{number of cells counted in } 1\text{mm}^2 \text{ x } 2 \text{ (dilution factor)x } 10^4$$

Cells were then distributed at a range of densities into appropriate cultureware dependent upon the subsequent studies to be performed. Table 2.4 shows the cell densities used for experimental application based on the results of cell growth curve studies. In all experiments, cells were incubated overnight (37°C, 5% CO_2) prior to the application of any stimulus.

Table 2.4: Cell seeding densities used dependent upon the plasticware selected for experimentation.

Plasticware	cell seeding density (cells/well)
96 well clear bottom plate (Sigma-Aldrich, UK)	7000
96 well clear plate (Sigma-Aldrich, UK)	7000
Seahorse XFe96 microplate (Agilent, UK)	10000
24 well plate (4titude, US)	17500

2.2.6.6 Automated cell counting

2.2.6.6.1 Tecan Spark® cell counting chip

To evaluate the effects of PBM on pHGFs over a time-course, Spark® (Tecan, Switzerland) cell chips™ were employed to enable high-throughput analysis of cell number in 96-well plates. Cell chips™ are designed to enable automated counting of cells using the Spark® and dashboard method editor interface. The Spark® employs bright-field imaging technology in which cell number can be quantified due to the contrast in the absorption spectra of cells compared with the surrounding media. Once cells were extracted from respective plates as described in section 2.2.6.2, an equal volume of cell suspension and trypan blue was aliquoted onto a cell chip™ (20µl of each and 10µl of the subsequent suspension was loaded onto the

cell chip™). A maximum of 4 cell counting chips were then counted systematically through placement in the Spark® cell chip™ adapter (Figure 2.9). The cassette was then placed in the Spark® microplate reader. Following this, Spark® dashboard software was utilised to automatically quantify cell numbers in chips. Reliability of automated cell counts using the Spark® were assessed compared to manual cell counting described in section 2.2.6.5. Results are displayed in Figure 2.10.

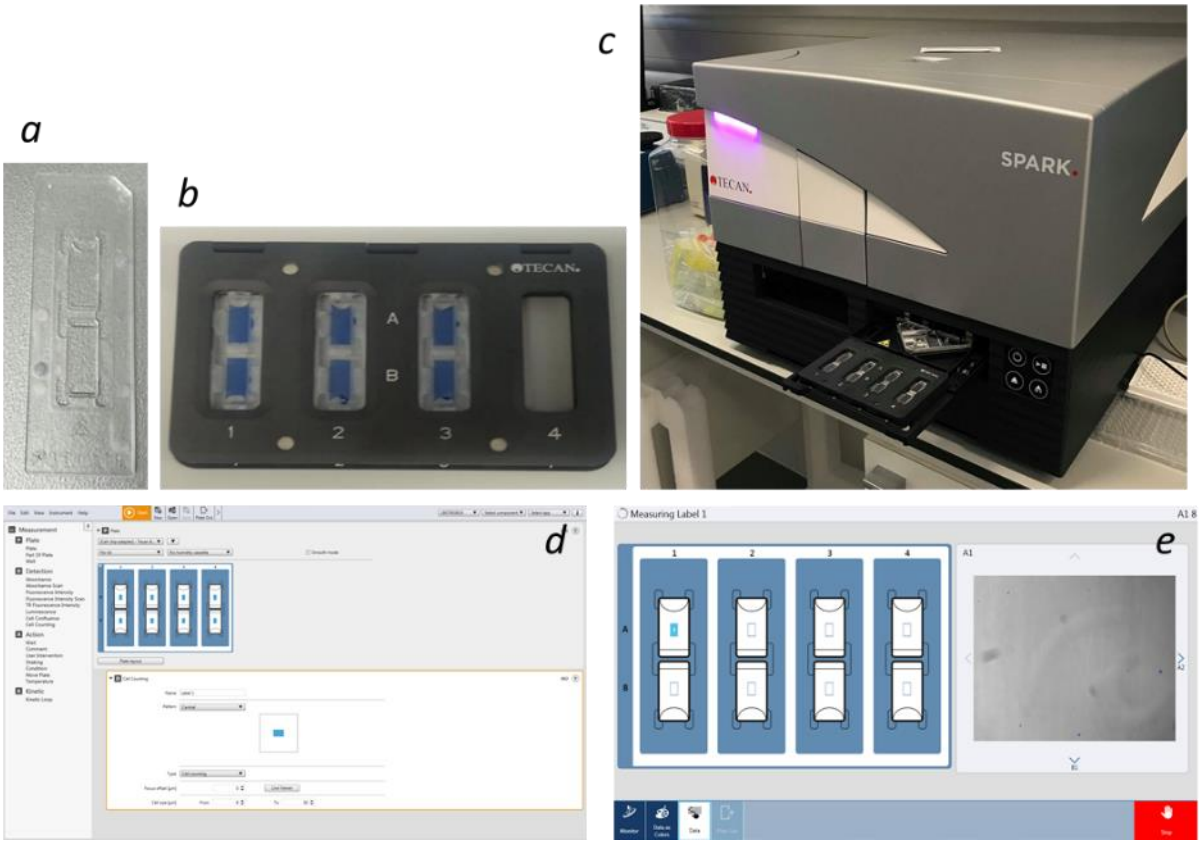

Figure 2.9: Experimental setup for automated cell counting using cell chip™, where a) shows a single cell chip with two loading chamber for cell suspensions and b) shows three cell chips™ placed in a cell chip™ adapter loaded with cell suspension mixed with trypan blue. This then allows the cell chip adapter to be placed in the microplate holder of the Spark® (c). Subsequently, a protocol can be setup using the Spark® control dashboard method editor, which is coupled to the Spark® machine. The cell chip™ adapter can be selected on the plate setting and the number of chambers containing cell suspensions can be selected (up to 8). A cell counting protocol is then selected where settings can be changed to view specific cell sizes and to adapt the focus of the live cell viewer, to ensure the Spark® is reliably reading cell number (d). Subsequently the Spark® reads the number of cells in a defined area and records live images of cells within a suspension (e).

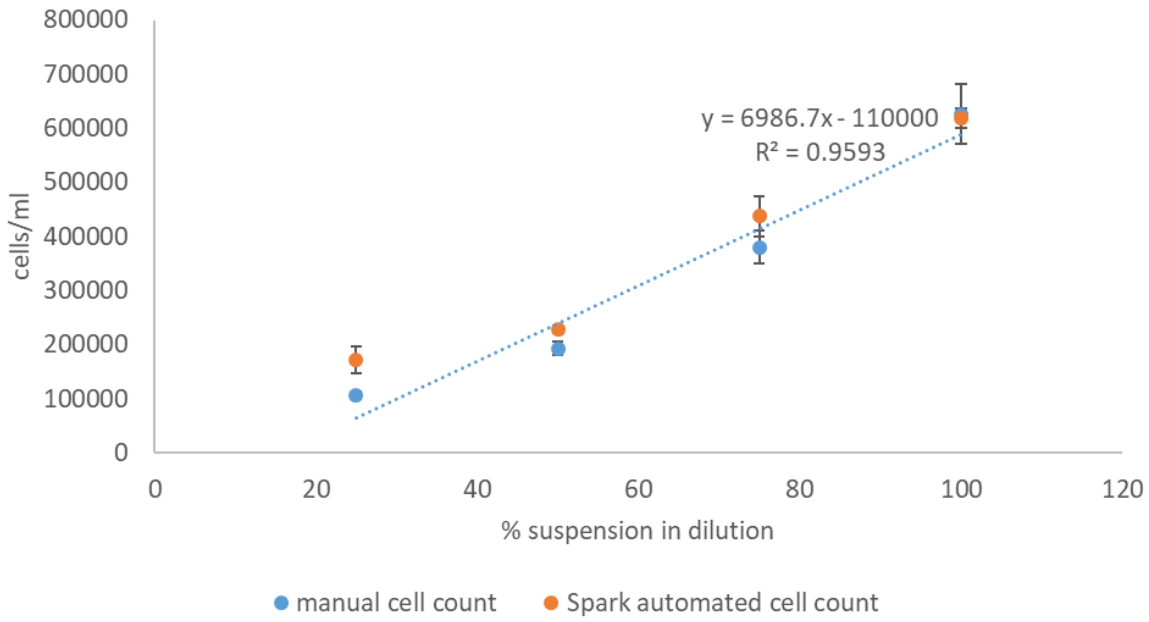

Figure 2.10 Cell counts when using manual counting vs Spark® automated cell counting. A suspension of cells (pHGF pool p6) were isolated from two confluent flasks. The suspension was then diluted in media containing 10% FBS to achieve a four point dilution series (100% v/v: undiluted suspension, 75% v/v: the suspension is diluted with an equivalent 25% media, 50% v/v: 50% dilution and 25% v/v: 25% suspension, 75% media). All points were measured in triplicate and correlation analysis revealed a Pearson correlation coefficient of 0.980.

2.2.6.7 Cryopreservation and recovery of cells

Cryopreservation of cells for future experimentation was achieved by first producing a pellet of the desired cell type (see sections 2.2.6.2 and 2.2.6.3). Following this, supplemented DMEM media was added to the resuspended pellet, followed by the addition of DMSO (10% v/v, Sigma-Aldrich). Aliquots were then dispensed into cryovials (Eppendorf) and stored in Nalgene® Mr. Frosty overnight (Sigma-Aldrich). Nalgene® Mr Frosty is used to provide a freezing gradient to prevent formation of intracellular ice crystals and therefore cell death. This technique therefore implements optimal conditions for cell preservation. The following day the frozen cells were transferred to liquid nitrogen for long-term storage.

Cells were revived from cryopreservation by rapid warming of cryovials to 37ºC in a water bath (Sub Aqua Pro, Grant, UK). Cells were then resuspended in an additional 9ml of supplemented DMEM media and centrifuged as described previously to pellet the cells (2.2.6.2 and 2.2.6.3). The supernatant was then discarded and pellet resuspended in an appropriate volume (dependent of culture ware utilised) of supplemented DMEM media (Table 2.4). The resulting cell suspension was then distributed into cell culture flasks. The cells were then monitored for adherence using a light microscope (Axiovert 25, Zeiss, Cambridge, UK) following incubation overnight. Once adherent, media was changed to remove any residual cryopreservant and non-viable cells.

2.2.7 Dose response experiments

Dose response experiments were used to determine the minimum concentration of a given pro- inflammatory stimulus (described in Table 2.5) required to induce reactive oxygen species (ROS) production (see section 2.2.11.3) and promote interleukin-8 (IL-8) secretion detectable by these assays at an appropriate range of sensitivity (see section 2.2.10.2.1). Following, seeding of pooled pHGFs (as described in section 2.2.6.2) into 96-well plates (see seeding densities in Table 2.4) and incubation overnight (37°C , 5% CO_2), pHGFs were washed with PBS once (room temperature, see section 2.1.5.2 for PBS composition). Media was subsequently replaced with DMEM media containing 10% FBS (negative control) or media containing 10% FBS plus an inflammatory stimulus. The following inflammatory stimuli were individually applied: *Escherichia coli* lipopolysaccharide (*E. coli* LPS, 026:B6, see section 2.1.5.4), whole heated-inactivated *Fusobacterium nucleatum* (*F. nucleatum*, see section 2.2.2.1) or *Porphyromonas gingivalis (P. gingivalis,* see section 2.2.2.2) or a mixed species biofilm (MSB, see section 2.2.2.3). A range of stimuli concentrations were used to challenge the pooled fibroblasts and the pro-inflammatory response determined at 24h post stimulation. Following

examination of the minimum concentration required to induce a significant increase in the inflammatory response measured, a single concentration was then selected for future analysis as indicated in Table 2.5.

2.2.8 Experimental protocol for irradiation of cultures in vitro.

Following fibroblast sub culturing (2.2.6) and the application of the appropriate media treatment (with/without a pro-inflammatory stimulus (2.2.7)), either the 2nd generation array or LUMOS™ array was used to irradiate cultures dependent upon the experimental application (2nd generation was used for high-throughput analysis of parameters whilst the LUMOS™ array was used to determine the effects of combining wavelengths *in vitro*). 96-well plates were placed directly above the 2nd generation array (as described in sections 2.1.1 and 2.2.1), with concentric alignment between the well and LED directly beneath. Cultures were irradiated for up to 480s at wavelengths between 400-830 nm (24mW/cm², 0.72-11.52J/cm², see Figure 2.1 for details regarding wavelength range of LED array). For irradiation with the LUMOS™, the LED array head was placed upon the lid of a 24 well culture plate and irradiated for 240s at either 405 nm, 850 nm or both (24mW/cm², 5.76J/cm², see Figure 2.2).

Table 2.5: Pro-inflammatory stimuli applied to cell cultures, the concentration range applied in preliminary studies and the final concentration applied when evaluating the effects of PBM following inflammatory stimulus application.

Inflammatory stimulus	Concentration range	Concentration applied in vitro
E. coli LPS	0.1-20µg/ml	1µg/ml
F. nucleatum	10-500:1 MOI	100:1MOI
P. gingivalis	10-500:1 MOI	500:1MOI
MSB	64-1451µg/ml	1451µg/ml

2.2.9 Cell proliferation and metabolic activity assays

2.2.9.1 Automated confluency assay

To assess cell confluency a Tecan Spark® (Tecan Group Ltd, Switzerland) multimode microplate reader was employed as described in section 2.2.6.6.1.

Pooled pHGFs were seeded as described in section 2.2.6.2. A standard curve was created through seeding of a range of cell concentrations from 3000-10000 cells/well (n=3 per plate). Plates were then incubated overnight (37°C, 5% CO_2). Following overnight incubation to enable cells to adhere, the bacterial stimulation or negative media control was applied (Table 2.5) and subsequently cultures were irradiated at wavelengths of 400 nm, 450 nm and 810 nm as described in section 2.2.8. Cultures were then incubated for a further 8-168 h. Following these intervals levels of confluence were assessed through development of a method using Spark® dashboard method editor. This involved selection of the appropriate plasticware (96-well black clear bottom plate, Sigma-Aldrich). Following this, a plate layout was formulated to include a (i) a standard curve of cells seeded at decreasing densities, (ii) samples ordered by treatment (+/- inflammatory stimulus and +/- irradiation) (iii) a series of blank wells as a negative control. This plate layout is depicted in Figure 2.11. Levels of cell confluence were then assessed through selection of a pre-set algorithm to measure cell confluence on the Spark® dashboard. The Tecan employs bright field imaging in which light emitted from an LED is guided through aperture to illuminate samples from the top of the plate. Adherent cells can then be imaged due to variations in levels of light absorption of cells compared to the surrounding media. This allows determination of the well area populated with cells in comparison to no cell thereby allowing % confluence to be calculated. Levels of confluence were measured across the whole well. Cells were maintained at a temperature of

37°C during the experiment (Figure 2.11). Once levels of confluence were assessed, the wells used to produce a standard curve were washed and trypsinised using Trypsin-EDTA as described in section 2.1.5.3 (20µl/well). After 5 minutes incubation at 37°C, cells were mixed with an equal volume of media containing FBS and cell counts were performed using Tecan cell chips as described in section 2.2.6.6.1. This approach was undertaken in order to enable calibration of levels of cell confluence with cell number to produce a standard curve. This allows determination of number of cells per well of the standard curve as described in 4.2**.**

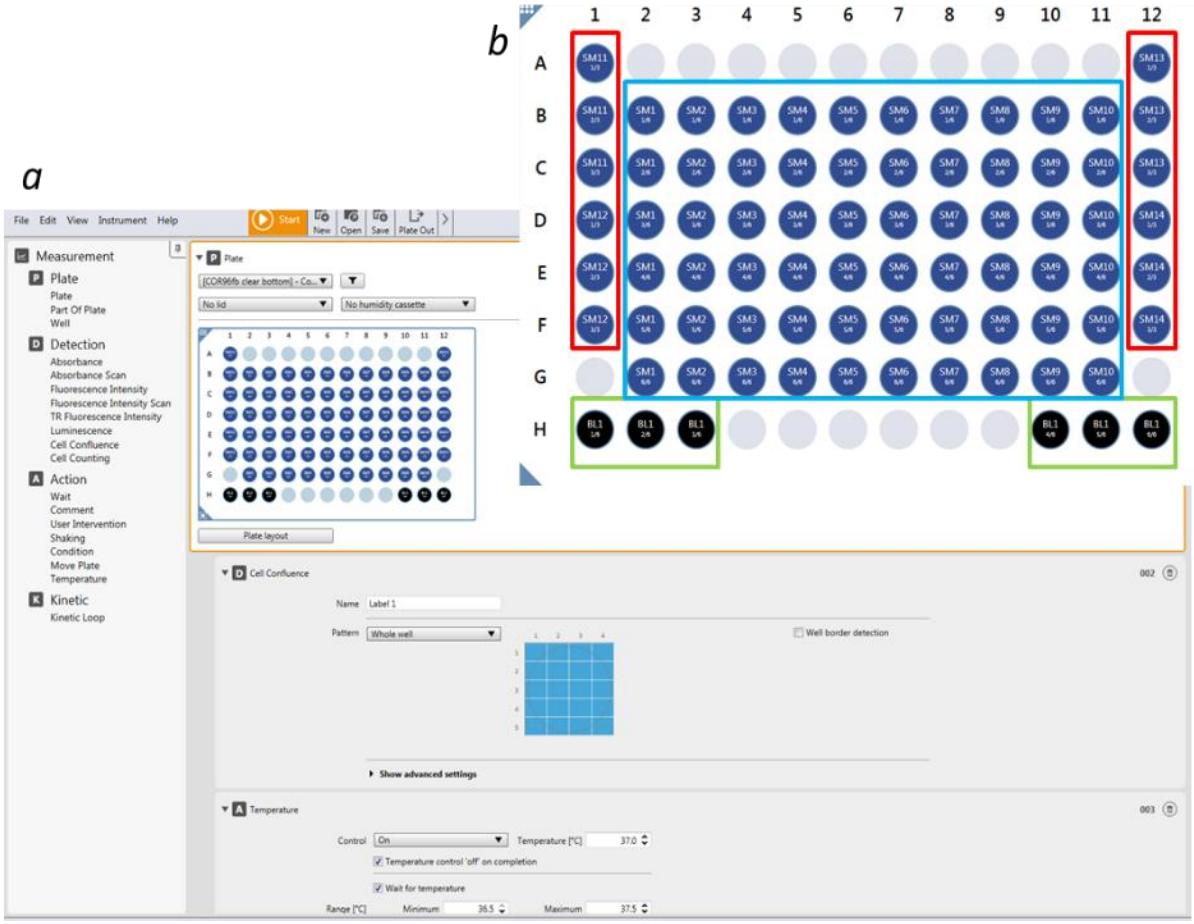

Figure 2.11: Spark® dashboard method editor interface where a) shows how specific parameters were selected for analysis including the plate type used, the plate layout, the selection of the cell confluence detection and application of this detection method to evaluate cell confluency across the whole well. Temperature was also set to 37°C to ensure cell cultures were in physiological conditions, to ensure fluctuations in enviro nmental temperature did not induce stress. b) indicates plate layout, where wells outlined in red were those seeded with decreasing densities of cells (n=3), green outlined wells were set as blanks and the central 60 wells were denoted as samples, where all cells were seeded at 7000cells/well.

2.2.9.2 3-(4, 5-dimethylthiazol-2-yl)-2, 5-diphenyltetrazolium bromide (MTT) assay

To assess cell metabolic activity, an MTT (3-(4, 5-dimethylthiazol-2-yl)-2, 5-diphenyltetrazolium bromide) (Sigma-Aldrich) assay was utilised. MTT is regarded as a good indicator of cell metabolic activity and viability due to its sensitivity and is routinely applied in high-throughput screening as described in section 1.7.1.1.

2.2.9.2.1 Assay procedure

Following preparation of cells as described in sections 2.2.7 and 2.2.8, the MTT solution at 0.05g/ml was aliquoted at 20μl/well 8/24h post-irradiation. Cells were subsequently incubated for 4h (37ºC, 5% CO_2). MTT solution was removed from wells and 50μl of dimethyl sulphoxide (DMSO, Sigma-Aldrich) was added per well. Formazan crystals were dissolved for 10 minutes at room temperature on a plate rocker. Absorbance was then read at 570 nm using a colorimetric micro-plate reader (ELx800 Universal Micro-plate reader, Bio-Tek Instruments, Vermont, US).

2.2.10 Cell Supernatant assays

2.2.10.1 Cell supernatant preparation

Following sub culturing (see section 2.2.6) and the application of the appropriate stimuli (see sections 2.2.7, 2.2.8), supernatants were collected 8/24hrs post-irradiation based on initial experimentation in which the optimum time points to review the effects of PBM on ROS production were assessed (see section 2.2.11.3). Supernatants were transferred to a 96-well plate (Sigma-Aldrich) and centrifuged at 1500rpm for 10 minutes (Universal 320R, Hettich, Germany). Supernatants were consequently stored at -20°C until required for analysis.

2.2.10.2 Enzyme-linked Immunosorbent assay (ELISA)

2.2.10.2.1 Interleukin-8 (IL-8) and basic fibroblast growth factor (bFGF)

pHGF supernatants (prepared as described in section 2.2.10) were assayed for human total IL-8 and bFGF by ELISA according to the manufacturer's protocol (Human IL-8/CXCL8 Duoset ELISA and human bFGF Duoset ELISA, both R and D systems, Biotechne, Minnesota, US). Prior to use, reagents were diluted to specified working concentrations as described in Table 2.6.

Plates for ELISA were initially coated with capture antibody diluted in PBS at 100µl/well and incubated at room temperature (RT) overnight. Subsequently, the plates were aspirated and washed three times with 0.05% v/v Tween 20 (Sigma-Aldrich) in PBS (wash buffer) utilising a plate washer (Biotek). Individual plate wells were then blocked with 300µl 1% v/v Bovine Serum Albumin (BSA) in PBS for 1 hour at room temperature. Wells were then washed three times. Following this, two fold serial dilutions of the standards were performed using reagent diluent (1% v/v BSA in PBS, used as a buffer in this assay). This then enabled the construction of a seven point standard curve at ranges described in Table 2.6*a* (bFGF) and Table 2.6*b* (IL-8). Cell culture supernatants were also diluted as necessary to ensure

concentrations of IL-8 or bFGF in samples were in the range of the standard curve. 100µl of standards, samples and blanks were then aliquoted onto the plate in duplicate and incubated for 2 hours at RT. Subsequently, the wash step was repeated. The biotinylated detection antibody was diluted in reagent diluent and 100µl/well aliquoted. Plates were incubated for 2 hours at RT. Plates were then washed/aspirated as previously described. Streptavidin-horseradish peroxidase (HRP) solution was diluted in reagent diluent and 100µl/well applied before incubation for 20 mins at RT in the dark. A final wash step was performed and a 1:1 mixture of H_2O_2 (Colour reagent A) and tetramethylbenzidine (Colour reagent B) was added to wells for 20 mins at RT in the dark. Further colour development was halted through the addition of 2N H_2SO_4. (R and D systems, UK). A deep yellow colour was produced by this reaction and secretion of IL-8 and bFGF into supernatants could be quantified utilising a spectrometer (ELx800 Universal Micro-plate reader, Bio-Tek Instruments, UK) at 450 nm and 570 nm. The readings at 570 nm were subtracted from readings at 450 nm to eliminate any background variances.

Mean readings for each standard concentration and blank were employed to generate a line of best fit. Concentrations in samples could then be calculated based on the equation of this line and were multiplied by any dilution factor employed during experimentation.

2.2.10.2.2 Tumour Growth Factor-β 1 (TGF-β1)

pHGF supernatants (prepared as described in section 2.2.10.1) were assessed for total TGFβ by ELISA as per the manufacturer's instructions (Human TGF-β1 Duoset ELISA, R and D systems). Reagents were diluted as indicated in Table 2.6*c*.

Initially, capture antibody was applied at 2µg/ml, diluted in PBS and incubated overnight. Subsequently the plates were washed (2.2.10.2.1). Blocking buffer was then

applied (5% Tween 20 in PBS, R and D Systems, UK) for one hour. Prior to application of standards, supernatants were activated in order to catalyse the conversion of latent-TGFβ1 to immunoreactive TGFβ1. This was process firstly involved addition of 1N HCL (20% v/v, R and D systems, UK) for 10 minutes at room temperature. Samples were then mixed thoroughly and 0.5M HEPES (14% v/v, R and D systems, UK) was added. Once activated the plate was washed as described previously. Standards were applied at concentrations between 2000-31.3pg/ml, diluted in reagent diluent 1 (1.4% v/v in 1 x wash buffer). Samples were subsequently aliquoted at 100µl/well. The plate was then incubated for two hours at room temperature before being washed three times. The detection antibody was then applied at 50ng/ml per well and incubated for two hours at room temperature. The plate was then washed as before and Streptavidin HRP was applied (1:40 dilution with reagent diluent 1) and incubated for 20 minutes in the dark at room temperature. Following this, plates were washed and colour developing reagent was applied (100µl/well, Colour Reagent A: Colour Reagent B at 1:1 ratio as per section 2.2.10.2.1). After 20 minutes incubation in the dark at room temperature, the stop solution applied and absorbance read using a colorimetric plate reader at 450 nm and 570 nm (ELx800 Universal Micro-plate reader, Bio-Tek Instruments, UK).

Table 2.6 Presents the dilutions of reagents to working concentrations where a) shows dilutions for bFGF ELISA, b) IL-8 ELISA and c) TGF-β1 ELISA.

a

Reagent	Amount per vial	Working concentration	Preparation
Capture	120µg	2µg/ml	Reconstitute with 0.5ml PBS
Detection	15.0µg	250ng/ml	Reconstitute with 1.0ml of Reagent diluent.
Standard	75.0ng	15.6-1000pg/ml	Reconstitute with 0.5ml of Reagent Diluent.

b

Reagent	Amount per vial	Working concentration	Preparation
Capture	240µg	4µg/ml	Reconstitute with 0.5ml PBS
Detection	1.2µg	20ng/ml	Reconstitute with 1.0ml of Reagent diluent.
Standard	40ng	2000-31.3pg/ml	Reconstitute with 0.5ml of Reagent Diluent.

c

Reagent	Amount per vial	Working concentration	Preparation
Capture	120µg	2µg/ml	Reconstitute with 0.5ml PBS
Detection	3µg	50ng/ml	Reconstitute with 1.0ml of Reagent diluent.
Standard	95ng	2000-31.3pg/ml	Reconstitute with 0.5ml of Reagent Diluent.

2.2.10.3 Nitric oxide (NO) assay

To assess the secretion of NO from pHGFs, a nitrate/nitrite colorimetric assay kit was employed (Cayman Chemical, USA). The assay quantifies relative concentrations of nitrite and nitrate in cell supernatants. *In vivo* NO undergoes a series of reactions to be metabolised to the final biproducts of nitrite (NO_2^-) and nitrate (NO_3^-) as the equations below illustrate:

$$NO + O_2^- + H^+ = ONO_2^- + H^+ = NO_3^- + H^+$$

$$2NO + O_2 = N_2O_4 + H_2O = NO_2^- + NO_3^- + 2H^+$$

$$NO + NO_2 = N_2O_3 + H_2O = 2NO_2^- + 2H^+$$

Hence, it is reported that the sum of both NO_2^- and NO_3^- secretion is an appropriate measure of total NO production.

The nitrite/nitrate assay procedure involves a two-step process in which first NO_3^- is converted into NO_2^- utilising nitrate reductase. The second step involves addition of Griess Reagent 1 (sulphanilamide) and Griess Reagent 2 (N-(1-naphthyl) ethylene diamine). The addition of these compounds produce a deep purple azo-compound, the formation of which can be quantified photometrically. The Griess reaction is illustrated in Figure 2.12. Further detail regarding experimental protocol are illustrated in sections 2.2.10.3.1 and 2.2.10.3.2.

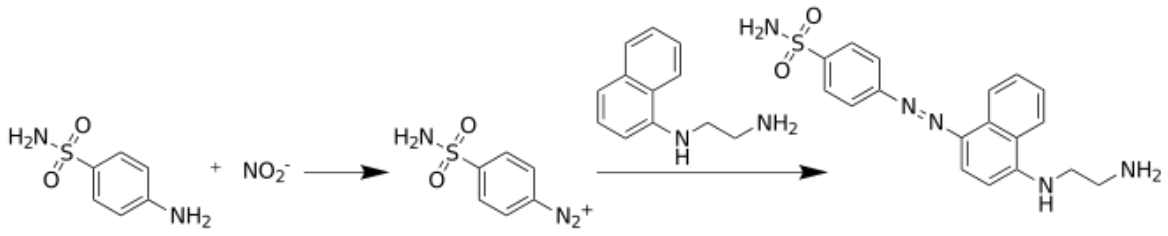

Figure 2.12: Chemical reaction of the Griess reagents in which Griess reagent 1 reacts with nitrite to form a diazonium salt and Griess reagent 2 catalyses the conversion of the diazonium salt to a purple azo product that can be quantified using a spectrophotometer at 540 nm or 550 nm.

2.2.10.3.1 Total Nitrate and Nitrite quantification

For quantification of total nitrate and nitrite in cell supernatants, first cell supernatants were prepared as described in section 2.2.10.1. Prior to application of cell supernatants, a nitrate standard curve was prepared, in which a stock of lyophilised nitrate standard is first reconstituted in 1ml of nitrate/nitrite assay buffer (assay buffer stock diluted in 100ml of deionised water prior to use in assays). Consequently, the reconstituted standard is diluted at 10% v/v in assay buffer to achieve a concentration of 200µM. The nitrate standard is then diluted further to achieve a 7 point standard curve at a concentration range between 0-35µM (in the final 200µl assay volume, following application of Griess reagents). Following preparation of standards, 200µl of assay buffer was added to blank wells (where no further reagents were added to these wells) and 80µl of cell supernatants were added to all other wells. Subsequently, 10µl of enzyme cofactor (nitrate reductase cofactor reconstituted in 1.2ml assay buffer prior to use) and 10µl of nitrate reductase mixture (reconstituted in 1.2ml assay buffer) was added to wells containing samples/standards. Cofactors were added to enable recycling of nicotinamide dinucleotide diphosphate (NADP+) to NADPH, to prevent the interference of NADP+ with Griess reagents. The plate was consequently incubated for two hours at room temperature and following this Griess Reagent 1 was added at 50µl/well to wells containing samples/standards. Griess reagent 2 was then added directly after at the same volume. The plate was then incubated for ten minutes at room temperature to enable colour development and absorbance was subsequently read using a plate reader at 550 nm (ELx800 Universal Micro-plate reader, Bio-Tek Instruments, UK).

2.2.10.3.2 Nitrite quantification

For nitrite quantification, cell supernatants and assay buffer were prepared as described in section 2.2.10.3.1. Prior to application of cell supernatants, nitrite standards were prepared

in which firstly, the lyophilised nitrite standard was reconstituted in 1ml of nitrite/nitrate assay buffer and a 7 point standard curve was prepared as described in section 2.2.10.3.1 to achieve concentrations between 0-35µM in a final assay volume of 200µl (following application of Griess reagents). Following preparation of standards, 200µl of assay buffer were loaded into blank wells and 100µl of samples into chosen wells. Subsequently after this, 50µl of Griess Reagent 1 followed by 50µl of Griess reagent 2 were added to sample/standard containing wells. The plate was then incubated for 10 minutes to allow colour to develop and absorbance was then read at 550 nm using a plate reader (ELx800 Universal Micro-plate reader, Bio-Tek Instruments, UK).

2.2.10.3.3 Total Nitrite and Nitrate measurements

Following measurement of absorbance from samples and standards described in sections 2.2.10.3.1 and 2.2.10.3.2, data was exported to excel (Microsoft, US) and standard curves were created to enable quantification of either nitrate, nitrite or total nitrite and nitrate in samples. Equation 1 illustrates formulae used to calculate concentrates of nitrite/nitrate/nitrite and nitrate in samples.

Equation 1: Formulae employed to calculate nitrite, nitrate or total nitrite and nitrate concentrations in samples.

$$(Nitrate + Nitrite)(\mu M) = \left(\frac{A^{540} - y\ intercept}{slope}\right)\left(\frac{200\mu l}{volume\ of\ sample\ used\ (\mu l)}\right)xdilution$$

$$(Nitrite)(\mu M) = \left(\frac{A^{540} - y\ intercept}{slope}\right)\left(\frac{200\mu l}{volume\ of\ sample\ used\ (\mu l)}\right)xdilution$$

$$(Nitrate)(\mu M) = (Nitrate + Nitrite) - (Nitrite).$$

2.2.10.4 Antioxidant assay

A total antioxidant assay (TOAC) was utilised to measure the relative levels of antioxidants in cell supernatants compared with the analog of Vitamin E, Trolox. When applied to a mixture containing horseradish peroxidase (HRP), Trolox quenches the signal through neutralisation of free radicals in solution. The longer this quenching occurs for, the greater the antioxidant capacity of a given substance.

2.2.10.4.1 Assay procedure

Running buffer (PBS containing Bovine serum Albumin (BSA, 0.005% w/v, Sigma-Aldrich) and Signal reagent (signal reagent buffer ((Potassium Chloride (0.75%w/v), Boric acid (0.62% w/v), Trisodium citrate dihydrate (0.1% w/v) and Sodium hydroxide (0.08% w/v) (Sigma-Aldrich), reagent A (0.006% w/v (sodium chloride (0.556% w/v), sodium benzoate (0.02% w/v), Trisodium citrate dehydrate (0.009% w/v), 4-iodophenol sodium salt (0.00762% w/v), sodium Luminol (0.0075% w/v) and reagent B (sodium chloride (0.523% w/v), sodium perborate tetra hydrate (0.048% w/v), sodium benzoate (0.02% w/v), Trisodium citrate dehydrate (0.009% w/v)) (Sigma-Aldrich) were warmed to 19^{o}C using a heat block. A 1:200 solution of horseradish peroxidase (HRP) in running buffer was also prepared and warmed to 19^{o}C. Once at temperature, 100µl of signal reagent and 8µl of HRP were added to 1ml of running buffer. The mixture was briefly vortexed (vortex genie, scientific industries Inc, US) and subsequently placed in a tube luminometer (Berthold, Berthold Ltd, UK). Luminescence was read using ICE software (Berthold, Berthold Ltd, UK). Following luminescence measurements, 20µl of standards or samples (cell supernatants, for supernatant preparation see section 2.2.10.1) were loaded into the reaction mixture and vortexed briefly. The tube was again placed in a tube luminometer and luminescence was measured for up to 400s. A standard curve was

created utilising Trolox at concentrations between 80-20µM to enable calculation of the antioxidant capacity of cell supernatants.

2.2.11 Mitochondrial activity assays

2.2.11.1 Adenosine triphosphate (ATP) assay

A luminescent ATP detection assay (Abcam, UK) was utilised to detect total levels of cellular ATP. The ATP assay is based on the production of light due to luciferase and luciferin. The light emitted during this reaction is proportional to ATP concentration intracellularly. This reaction is summarised in the following equation:

ATP + D-Luciferin + O2 → Oxyluciferin + AMP + PPi + CO2 + Light

2.2.11.1.1 Assay procedure

At 24h post-irradiation an ATP assay was conducted, cells were prepared using protocol described in section 2.2.8. Initially, an ATP standard was diluted in ultra-pure water (ddH_2O, Sigma-Aldrich) to produce a 20mM stock, which was stored at -20^{o}C until required. This was used to generate a standard curve. This involved diluting the ATP standard in substrate buffer (lyophilised substrate resuspended in 5ml of substrate buffer, no details provided regarding composition) to produce a 100µM standard. The standard was diluted in phenol red free DMEM (see section 2.1.5.1) to produce an 8 point standard curve at concentrations of between 10µM-0.01pM. Subsequently, detergent (used to lyse cells, provided in 20ml aliquots, no details regarding composition provided, Abcam, UK) was added to cell cultures at 50µl/well and plates were placed on an orbital shaker at 600-700rpm for 5mins. Following this, substrate solution was added at 50µl/well and the microplate placed on a shaker at 600-700rpm for 5mins. The plate was incubated in the dark for 10 minutes, to prevent absorption of ambient light, which can be emitted during luminescence experiments. Luminescence was

then measured using a Luminometer (Microlumat plus, Microplate Luminometer LB96V, EG&G Berthold, Berthold Ltd, UK).

2.2.11.2 Tetramethylrhodamine, ethyl ester (TMRE) assay

A TMRE assay was utilised to measure changes in mitochondrial membrane potential (Cayman Chemical, Michigan, US). TMRE is a cell permanent, positively charged red-orange dye that readily accumulate in mitochondrion due to its relative negative charge. Through the progression of electron transport chain (due to increased mitochondrial activity), protons with a positive charge (H^+) move across the mitochondrial membrane, inducing membrane depolarisation, causing the mitochondrion to possess a relative positive charge. This therefore prevents the accumulation of TMRE, producing a decrease in relative fluorescence and hence TMRE is a good indicator of membrane depolarisation.

2.2.11.2.1 Assay procedure

Initially, Carbonyl cyanide-p-trifluoromethoxyphenylhydrazone (FCCP) was applied to a single column of wells on the plate at 10µM, diluted in phenol red free DMEM media to act as a positive control. Concentration of FCCP required to induce membrane depolarisation was determined through the construction of a standard curve at concentrations between 40-2.5µM FCCP (6 point standard curve). The plate was then incubated for 45 minutes (37°C, 5% CO_2). TMRE was then applied to cell cultures (see sections 2.2.6.2 and 2.2.8 for cell preparation) at 500 nm. Concentration of TMRE utilised during experimentation was determined through construction of a standard curve at concentrations between 15.6-500 nm. The plate was then incubated for 30 minutes, washed 3 times with assay buffer and subsequently incubated at room temperature for 10 minutes. Consequently, fluorescence

was read at excitation/emission: 530/580 nm utilising a fluorimeter (Clariostar, BMG Labtech, UK).

2.2.11.3 ROS assay

Total ROS production was assessed using the cell diffusible fluorescent probe 2', 7'-dichlorodihydrofluorescein diacetate (H_2DCFDA, Thermo fisher). H_2DCFDA is generalised ROS marker but has the greatest affinity for the free radicals CO_3^- and NO_2^- and reduced glutathione. In turn these radicals aid the reduction of H_2DCFDA to 2', 7'-dichlorodihydrofluorescein ($DCFH_2$) which leads to the generation of Dichlorofluorescin (DCFH). The generation of superoxide catalyses the reduction of DCFH to DCF. DCF in turn reacts with light to fluoresce allowing the production of ROS to be quantified. Figure 2.13 indicates the four-step process in which H_2DCFDA is hydrolysed *in vitro*.

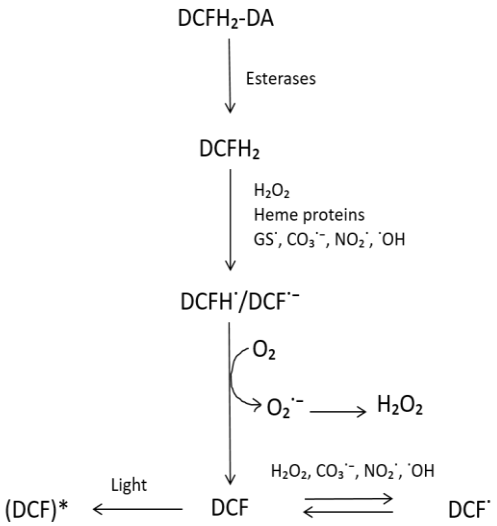

Figure 2.13: The 4 step process in which H_2DCFDA is hydrolysed in the cell to form a fluorescent product (indicated here by (DCF)). DCF is a secondary marker for ROS production due to the fact that its hydrolysis is firstly dependent upon intracellular and extracellular esterase's. However, the final three steps are dependent upon reactive oxygen species (ROS) produced by the cell.*

2.2.11.3.1 Assay procedure

Following irradiation and subsequent incubation of pHGFs for 8/24h (37°C , 5% CO_2, as described in sections 2.2.6.2 and 2.2.8), media was aspirated from wells and cultures were

washed three times with PBS (room temperature). This was to remove any excess media that may interfere with the activity of the ROS probe. H_2DCFDA florescent probe was applied at 50µl/well (10µm) and incubated for 30 minutes (37°C, 5% CO_2) in the dark. A fluorimeter was utilised to quantify the production of ROS (Twinkle LB 970, Berthold Industries Ltd, and UK). The fluorimeter had an excitation wavelength of 485 nm and emission wavelength of 535 nm. Microwin software (Siemens, Germany) was used to the read the plate, raw data was then saved and analysed in Excel software (Microsoft, US).

2.2.11.4 Seahorse assay

To assess the effect of light on real-time mitochondrial activity, a Seahorse XFe96 Analyser was employed. The Seahorse analyser measures the cells oxygen consumption rate (OCR) as a marker of mitochondrial activity (and therefore respiration). This is undertaken through the sequential injection of compounds to determine a series of key parameters including basal respiration, ATP production, proton leak, maximal respiration, spare respiratory capacity and non-mitochondrial respiration.

2.2.11.4.1 Cell Preparation

Cells were seeded at 10,000 cells/well in phenol red free medium and incubated overnight. Subsequently myoblasts and myotubes were irradiated for 30s (24mW/cm², 0.72J/cm²) whilst pHGFs were irradiated for 240s (24mW/cm², 5.76J/cm²). Prior to irradiation, a mask was placed beneath the plate to prevent bleed of light between columns of wells. Figure 2.3 shows the mask design (see section 2.1.4) and experimental set up. A Seahorse assay was then performed 1, 8 or 24h post-irradiation.

2.2.11.4.2 Mitochondrial stress assay

One-hour prior to undertaking the assay, culture media was aspirated, cells washed with phosphate buffered saline (PBS) three times and Seahorse XF assay media (25mM glucose, 1mM pyruvate and 2mM glutamine) was applied and equilibrated in a CO_2 free incubator (INCU-line®, VWR, UK). Compounds altering mitochondrial activity were then applied to the system including: Oligomycin (inhibits complex V of the ETC, 1µM), carbonyl cyanide-4(triflouromethoxy) phenylhydrazone (FCCP, uncoupling agent induces respiration to be undergone at maximal rates, 2µM), antimycin and rotenone A (inhibit complexes I and III respectively, inhibiting ETC activity, 0.5µM). Subsequently the plate was placed in a Seahorse XFe96 analyser and compounds were sequentially injected into the system to induce changes in ETC activity.

The Seahorse analyser then determined changes via assessment of oxygen consumption rate in real-time (OCR, pmol/min). OCR values were subsequently normalised for protein content in individual wells. Protein concentration was determined using DC protein assay (Bio-rad, USA). This enabled calculation of individual parameters including basal respiration, maximal respiration, ATP production, spare respiratory capacity and non-mitochondrial respiration (Tan et al., 2015). During analysis, values for non-mitochondrial activity were subtracted from values evaluating the effects of PBM directly on mitochondrial activity. This provided a further control step ensuring results would reflect the effects of PBM on mitochondrial activity only.

2.2.12 DNA and RNA extraction techniques for PCR analysis

2.2.12.1 Total RNA purification

For Reverse Transcription-Polymerase Chain Reaction (RT-PCR) experiments, in which the assessment of the yield and quality of RNA was required, pHGFs were lysed and RNA extracted from the lysate utilising an RNeasy mini kit (Qiagen, Manchester, UK), according to the manufacturer's protocol. pHGFs were seeded into 96-well plates at 7000 cells/well and incubated overnight. The cultures were irradiated the following morning (240s, 24mW/cm², 5.76J/cm²) and consequently incubated for a further 24h post-irradiation. Subsequently cultures were washed three times with ice cold PBS. Following this, 20µl of ice-cold lysis buffer was applied to each well and cells were agitated on a plate rocker at 50 cycles/minute for 5 minutes. Cells were harvested by scraping wells using a 200µl pipette tip to ensure cells were fully dissociated. Lysates were then collected and stored in 1.5ml tubes at -80°C as necessary.

An equal volume of 70% v/v ethanol was added to defrosted lysates and the mixture was added to an RNeasy spin column in a 2ml collection tube. The solution was then centrifuged at 10,000rpm for 30s (Micro centrifuge, Eppendorf). The flow through was then discarded and 350µl of Buffer RW1 was added to the column, the column was then centrifuged at 10,000rpm for 30s. Flow through was discarded and 80µl of DNase I diluted in buffer RDD (1:7 ratio of reagents) was added to the column and incubated at room temperature for 15minutes. The column was then washed three times to improve RNA purity. The column was then placed in a 1.5ml Eppendorf and 30µl of RNase free water was added and spun at 10,000rpm for 1minute.

1.1.1.1 DNA isolation

pHGFs were grown to 80-90% confluency in T75 flasks and then washed three times with PBS, trypsinised and centrifuged (as described in sections 2.2.6.2 and 2.2.6.3). Following this, the pellet was washed with PBS and resuspended in 200µl PBS. Subsequently, a Purelink Genomic DNA mini kit (Invitrogen, UK) was utilised to isolate DNA. Firstly, 20µl of proteinase K was added to each sample followed by 20µl of RNase A. The solution was then mixed by vortexing and incubated at room temperature for 2 minutes. 200µl of genomic lysis buffer was then added to each sample, mixed by vortexing and subsequently incubated at 55^{o}C for 10 minutes using a water bath (Sub Aqua Pro, Grant, UK). Next, 200µl of Ethanol was added and mixed by vortexing. The lysate was then transferred to a spin column (approximately 640µl) and centrifuged at 13000rpm for 1 minute at room temperature. Waste was then discarded and the column was washed twice with buffer to improve DNA purity and quality. Following these wash steps, 50µl of genomic elution buffer was added to the column and centrifuged at 16000g for 1 minute.

2.2.12.2 Assessment of RNA/DNA quality

To assess RNA and DNA quality and yield the sample was diluted in RNA free water (1:35 ratio) and absorbance of ssRNA/dsDNA was assessed at 260/280 nm using a spectrophotometer (Eppendorf biophotometer, Eppendorf). Pure nucleic acid samples typically yield a 260/280 ratio of between 1.8-2.2, where values lower than this could be contaminated with compounds such as phenol (Desjardins and Conklin, 2010) . Hence, samples with a ratio outside this range were discarded. RNA was subsequently stored at -80^{o}C until required. DNA was stored at -20^{o}C prior to use.

2.2.13 Reverse Transcription-Polymerase chain reaction

2.2.13.1 RT method

Reverse Transcription (RT) of RNA samples was performed with the aim of producing high quality cDNA samples by utilising a Bioline Tetro cDNA kit (Bioline, UK) according to the manufacturer's guidelines using an Eppendorf thermocycler (Eppendorf). RNA was diluted in ddH_2O to enable a uniform RNA solution concentration of 2µg. The RNA was then mixed with $oligo(dT)_{18}$ (1µL), 5 x reverse transcriptase buffer (4µl), reverse transcriptase (1µl), RNase inhibitor (1µl) and a mixture of nucleotides (dNTPs, 1µl). The mixture was then made up to 20µl utilising diethyl pyro carbonate (DEPC) treated water. Samples were incubated at 45ºC for 30 minutes, followed by a further incubation at 85ºC for 5 minutes to terminate the reaction. Samples were then chilled on ice and subsequently stored at -20ºC to be used in future experimentation.

2.2.13.2 Conventional RT-PCR

2.2.13.2.1 Evaluation of gene expression

Prior to the evaluation of light on gene expression, cDNA required normalisation to enable reliable evaluation of differential gene expression when comparing controls to experimental samples. The housekeeping gene glyceraldehyde-3-phosphate dehydrogenase (GAPDH) was used to normalise all samples. Optimal number of cycles required to evaluate gene expression were also undertaken during this process.

A primer mix was prepared containing up to 2µl of cDNA, 2µl of primer, 8.5µl of RNase free water (Qiagen, UK) and 12.5µl of Biomix red (Bioline, UK). Prior to application of primers into this solution 10µl of forward primer and 10µl of reverse primer were diluted in 60µl of

RNase free water and then applied to the reaction mixture. All reagents were stored individually at -20ºC prior to use. Samples of cDNA were amplified in a thermocycler (Eppendorf) utilising the following conditions:

- Denaturation: 94ºC 5 minutes
- 60°C , 1 min for annealing, 72°C , 1 min for extension, 94°C , 1 min for denaturation (20-40 cycles to yield sufficient quantities of DNA to be analysed using densitometry)
- Final extension: 72°C , 10 min

Confirmation of PCR products was undertaken using SYBR red (0.01%v/v, Invitrogen, UK) containing agarose gel electrophoresis (1.5% w/w agarose). Hyperladder IV (5µL, Invitrogen, UK) was ran alongside cDNA samples (5µl) to confirm PCR product size. Gels were electrophoresed at 120V for 30 minutes. Images were then captured under Ultraviolet trans-illumination utilising Genesnap software on the G:box imaging system (Syngene, UK). Once images had been obtained, semi-quantification of PCR bands was undertaken using Genetools software (Syngene, UK). Values obtained from densitometry were subsequently used to identify quantities of cDNA required for gene expression studies and were calculated as follows:

$$\frac{intensity\ of\ sample\ band}{intensity\ of\ band\ required\ to\ normalise}\ x\ volume\ of\ sample = volume\ of\ cDNA\ required\ to\ normalise$$

2.2.13.2.2 PCR primers

PCR primers were designed utilising primer-BLAST (NCBI, USA) according to published gene ascension number. The primers employed are listed in Table 2.7.

Table 2.7: List of primers employed when evaluating the effects of PBM on gene expression

Gene	Symbol	Primer Sequence	PCR product (bp)	Relevance	Reference
NADH dehydrogenase (ubiquinone) Fe-S protein 7	NDUFS7	F: 5'-GGATGACCTCGTCAACTGGG-3' R: 3'-ACAACCTCACGGGACACAAG-5'	519	Subunit of complex I of ETC, target for PBM	(Masha et al., 2013)
cytochrome c oxidase subunit IV isoform 1	COX4I1	F:5'-CCGGCCCGGCATTTTACGAC-3' R: 5'-GGGGTGGTCACGCCGATCCA-3'	315	Subunit of complex IV of ETC, target for PBM	(Huttemann et al., 2001, Barolet, 2008)
ATP synthase, H +transporting, mitochondrial Fo complex, subunit B1	ATP5F1	F: 5'-GCATTGCGGACCTAAAGCTG-3' R: 3'-ATCAGCCAGAAACAGTTCACCA-5'	519	Subunit of complex V of ETC, target for PBM	(Houreld, 2014)
NF-KappaB subunit 1 (NFkB1), transcript variant 3	NFKB	F: 5'-CCTGGATGACTCTTGGGAAA-3' R: 3'-CTTCGGTGTAGCCCATTTGT-5'	366	Downstream target for PBM	(Chen and Greene, 2004, Zhang et al., 2014)
Glutathione synthetase	GSH-S	F: 5'-TCACTGGATGTGGGTGAAGA-3' R: 5'-CGTGCTTGTTCATCACGAGT-3'	315	Antioxidant enzyme, hypothesised to be activated by PBM	(Gunduz et al., 2016)
Transforming growth factor beta receptor-1	TGFBR1	F: 5'-CGTTACAGTGTTTCTGCCACCT-3' R: 5'-AGACGAAGCACACTGGTCCAGC-3'	314	Proposed to be induced by PBM.	(Luo et al., 2013, Fang et al., 2013)
Interleukin-8	IL8	F: 5'-CGCCTTAGCGCCCACTGCTCCTGT-3' R: 5'-GGGGCGGGACCTCAGCTGCAC-3'	533	Marker for inflammation and NFκB activation	(Basso et al., 2015)

2.2.14 Mitochondrial DNA amplification and quantification

2.2.14.1 mtDNA amplification

A REPLI-g® Mitochondrial DNA Kit (Qiagen, UK) was utilised to amplify mtDNA in DNA samples isolated from pHGFs (n=3). Firstly, DNA concentration in samples was measured utilising a spectrophotometer (Eppendorf biophotometer, Eppendorf) and samples were diluted to contain 10ng/µl of DNA each. Subsequently, 29µl of REPLI-g mt reaction buffer (containing 27µl of reaction buffer and 2µl of mt primer mix) was added to each sample. Samples were then centrifuged briefly and incubated at 75°C for 5 minutes. Samples were then cooled to room temperature and 1µl of REPLI-g Midi polymerase was added to each of the reaction mixtures. Samples were then centrifuged briefly and were then incubated at 33°C for 8 hours. The polymerase was then inactivated by heating at 65°C for 3 minutes. Samples were then stored at -20°C until required for further experimentation.

2.2.14.2 mtDNA quantification

To assess the varying quantities of mtDNA in cell lysates, initially a 6 point standard curve was generated using calf thymus DNA (Invitrogen, UK) between 10-0.625ng/µl to enable quantification of sample DNA concentrations. The method for quantification was adapted from a previously published article (Leggate et al., 2006). Standards were diluted in 1x TAE buffer (40mM Tris, 20mM acetic acid, 1mM EDTA, fermentas life sciences, Lithuania). Nuclear DNA (nDNA) samples were diluted to 10ng/µl in PBS, as per previous dilutions made to amplify mtDNA. 2µl of samples and standards were aliquoted in triplicate in a black clear bottom 96-well plate. SYBR® safe DNA gel stain (10,000x concentrate, Invitrogen, UK) was diluted 1:1250 in 1xTAE buffer and briefly mixed by vortexing. 98µl of the solution was applied to the standards and samples. The plate was then incubated for 10 minutes at room temperature in

the dark. Relative fluorescence was then measured using a fluorimeter (ex/em: 485/535 nm, Twinkle LB 970, Berthold Industries Ltd, UK). Microwin software (Siemens, US) was then utilised to record fluorescence data and was then exported to an Excel spreadsheet for further analysis (Microsoft, US). A standard was created to calculate concentrations of DNA in samples. Ratios of DNA content in nDNA and corresponding mtDNA were then recorded to enable comparison of DNA content between cell lysate samples.

2.2.15 Statistical analysis

Data were processed utilising Excel software (Microsoft) and analysis was performed using SigmaPlot software (Systat Software Inc, UK) and Minitab (Minitab, US). All data was analysed using a general linear model (GLM) followed by one-way ANOVA test and a Tukey test to determine significant differences between non-irradiated controls, stimulated controls and light treated groups (with or without the application of an inflammatory stimulus*, $p<0.05$)*. For data analysed using minitab software significant differences between treatment groups were denoted by letters, where means that did not share the same letter were significantly different. For example, if the control group is denoted A but the treated group is denoted C, there is a significant different between these groups with a P value of least 0.05.

3 LED ARRAY CHARACTERISATION

3.1 Introduction

This chapter aimed to demonstrate a well characterised and reproducible system for delivery of light for *in vitro* PBM analyses. A novel LED array developed in-house (2nd generation array) and previously reported was employed for *in vitro* application (Hadis et al., 2017a) as described in section 2.1.1.

A further array (LUMOS™) was designed by a collaborating company as described in section 2.1.2. Firstly, each array was thoroughly characterised using a series of techniques described in 2.2.1. These techniques were used to evaluate the output of different parameters across each array including wavelength, spectral irradiance output, thermal output of each array and beam profiles of LEDs.

Beam profiles were evaluated using a CCD camera beam profiler and analysed using Beam Gage software (Section 3.3). The effects of PBM on media temperature were also evaluated as current literature surrounding this variable remains lacking and could have a confounding effect when investigating biological response to light (Kim and Kim, 2016). Finally, the effect of plasticware and media on light absorption were evaluated as described in section 3.5. Often, this parameter is not evaluated. However, media such as DMEM exhibits an absorption spectrum at specific wavelengths and this could therefore alter biological response to PBM (Zhao et al., 2004). Also, light has been cited to induce photo degradation of components of cell culture media, altering conditions for cell growth (Nielsen and Bertheussen, 1991, Neutsch et al., 2018). Thus, preventing evaluation of the effects of light on cellular response directly.

These characterisation steps would then enable demonstration of a well characterised system for use in both high-throughput assays employing 96-well black clear bottom plates

and also for use in Seahorse assays, as well as a complimentary array that would allow evaluation of combined wavelengths exposure on cellular and mitochondrial activity.

3.2 Spectral Characterisation

Initially, spectral characterisation was undertaken to determine the emitted spectral irradiance (mW/cm²) and wavelength (nm) values from two LED arrays emitting wavelengths spanning the visible and near infra-red spectrum. The first LED array was designed to emit an average irradiance of 24mW/cm² (termed 2nd Generation 96-well array) at all wavelengths whilst the irradiance output of the second array (LUMOS™ array, Axion Biosystems, US) was variable and to be determined through spectral characterisation. The second array could also be employed to assess the effects of simultaneous irradiation of cultures with multiple wavelengths of light. An irradiance output of 24mW/cm² was selected based on a review of the current literature that evaluated the effects of PBM both *in vitro* and *in vivo* (Chen et al., 2009a, Sharma et al., 2011c, Huang et al., 2013, Yoshimoto et al., 2018, Becker et al., 2016a). These characterisations were undertaken to ensure that the same irradiation conditions were applied in both array systems.

3.2.1 Analysis of irradiance delivered to the black clear bottom 96-well plate

Emitted irradiance values, peak wavelengths and fluency values were first evaluated using a 96-well black clear bottom plate. A 96-well black clear bottom plates was selected based on primary experiments conducted by *Hadis et al* (Hadis et al., 2017a), in which it was revealed that the black colour of the plate minimised light bleed between different wavelength channels, whilst the clear bottom of the plate ensured concentric alignment with the LED inset beneath to ensure light penetrated the cell monolayer.

3.2.1.1 Results

Figure 3.1*b* reports average irradiance output from each group of LEDs emitting the same wavelength (n=6), where there was no significant different in irradiance output across the

array. Table 3.1*b* describes variance in irradiance output from each LED. This varied from 16.75mW/cm² at a wavelength of 830 nm to 33.66mW/cm² at a wavelength of 525 nm. From the irradiance values recorded by the spectrometer, fluency values (J/cm²) could be calculated using the following equation:

$$Fluency\ \left(\frac{J}{cm^2}\right) = Irradiance\ \left(\frac{mW}{cm^2}\right)\ x\ Time\ (s)$$

Differences in delivered fluency values at various exposure times are displayed in Table 3.1.

Variation in irradiance output from the 2nd generation array over extended periods of irradiation (up to 240s) was also explored. There was an average change in irradiance of 0.105±0.076 mW/cm² across the array. However, this was only 0.4% of the total irradiance output and could merely be due to experimental error. Subsequently, after statistical analysis it was concluded that there was no significant change in irradiance output between wavelengths over a 240s irradiation period (Figure 3.2*).*

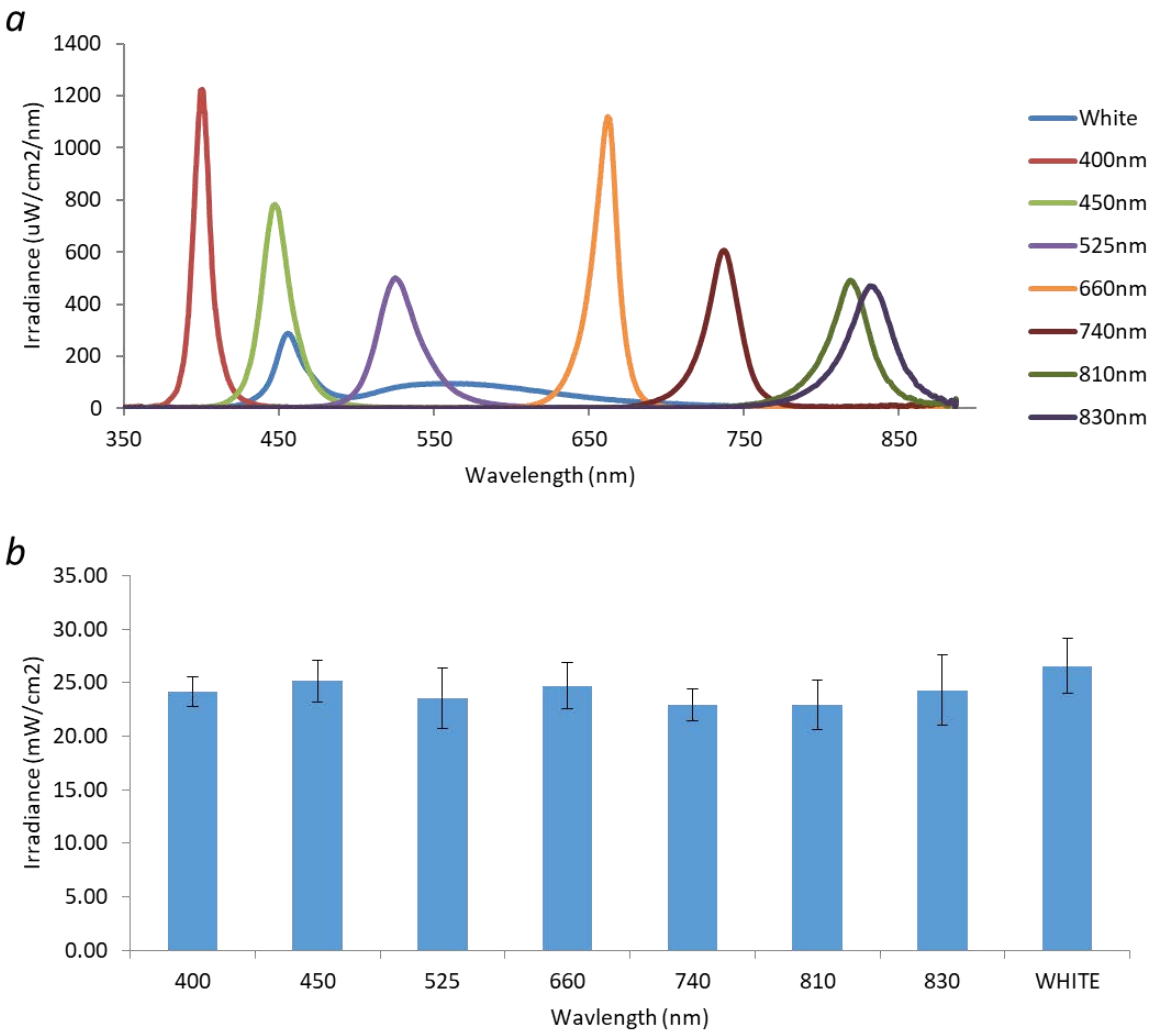

Figure 3.1: a) Average peak wavelengths (n=6) emitted across the LED array at wavelengths varying from 400 nm-830 nm and b) Spectral irradiance values of the LEDs utilised in this study (400 nm – 830 nm) showing peak wavelength values emitted from LEDs. 6 LEDs were measured per wavelength employed in the array. Differences in emitted spectral irradiances from one wavelength to the next were analysed using one way ANOVA following by Tukey test, where no significant differences between wavelength channels were observed.

Table 3.1a Wavelengths emitted from each individual LED across the array. The top row of the tables (in white text) indicates wavelength values claimed by the manufacturer, whilst values below show the actual emitted wavelengths across the array, and vary from 398.18-835.77 nm. Table 1b shows variance in emitted spectral irradiance from each individual LED from the whole array (n=60) from LEDs emitting wavelengths ranging from 400-830 nm with an average emitted irradiance of 24.26mW/cm². Where, numbers in rows indicate LED positioning. Table 1c provides fluency values emitted across the array at a series of time points between 30s-480s and at wavelengths from 400-830 nm. Data indicate emitted energy per unit area delivered to cell cultures.

a

Wavelength (nm)	400	450	525	660	740	810	830	White
1	399.41	447.16	521.86	661.65	735.78	818.60	827.81	455.43
2	398.18	445.34	523.64	662.21	736.87	817.38	828.85	455.43
3	399.41	445.34	524.23	661.84	733.60	817.38	829.20	455.43
4	399.41	446.75	525.61	662.40	735.78	819.12	829.20	456.03
5	400.84	451.19	524.23	662.02	735.24	817.38	835.77	456.03
6	400.84	445.34	523.44	663.32	735.78	817.38	829.37	456.03
AVG (mW/cm²)	*399.68*	*446.85*	*523.83*	*662.24*	*735.51*	*817.87*	*830.03*	*455.73*
STD DEV	*1.02*	*2.27*	*1.23*	*0.60*	*1.08*	*0.78*	*2.87*	*0.33*

b

Wavelength (nm)	400	450	525	660	740	810	830	White
1	21.83	21.00	24.61	21.98	24.31	26.10	22.15	24.96
2	20.44	21.14	24.54	22.30	22.05	23.45	21.79	25.15
3	22.26	23.27	25.05	26.81	24.61	25.60	16.75	24.03
4	24.23	22.13	26.94	24.75	23.79	23.16	22.03	25.03
5	24.12	23.63	23.55	25.62	18.35	21.86	32.03	26.17
6	24.17	22.69	33.66	26.80	21.67	21.82	23.18	26.00
AVG (mW/cm²)	*22.84*	*22.31*	*26.39*	*24.71*	*22.46*	*23.67*	*22.99*	*25.23*
STD DEV	*1.58*	*1.09*	*3.73*	*2.14*	*2.34*	*1.82*	*4.97*	*0.78*

c

Wavelength (nm)	Irradiance (mW/cm²)	Radiant exposure at 30s (J/cm²)	Radiant exposure at 60s (J/cm²)	Radiant exposure at 120s (J/cm²)	Radiant exposure at 240s (J/cm²)	Radiant exposure at 480s (J/cm²)
400	24.14±1.42	0.72	1.45	2.90	5.79	11.59
450	25.16±1.97	0.75	1.51	3.02	6.04	12.08
525	23.52±2.81	0.71	1.41	2.82	5.64	11.29
660	24.56±1.40	0.74	1.47	2.95	5.89	11.79
740	22.90±1.46	0.69	1.37	2.75	5.50	10.99
810	22.93±2.35	0.69	1.38	2.75	5.50	11.01
830	24.29±3.26	0.73	1.46	2.92	5.83	11.66
White	26.57±2.53	0.80	1.59	3.19	6.38	12.75
AVERAGE:	*24.25±1.22*	*0.73±0.04*	*1.46±0.07*	*2.91±0.15*	*5.82±0.29*	*11.65±0.58*

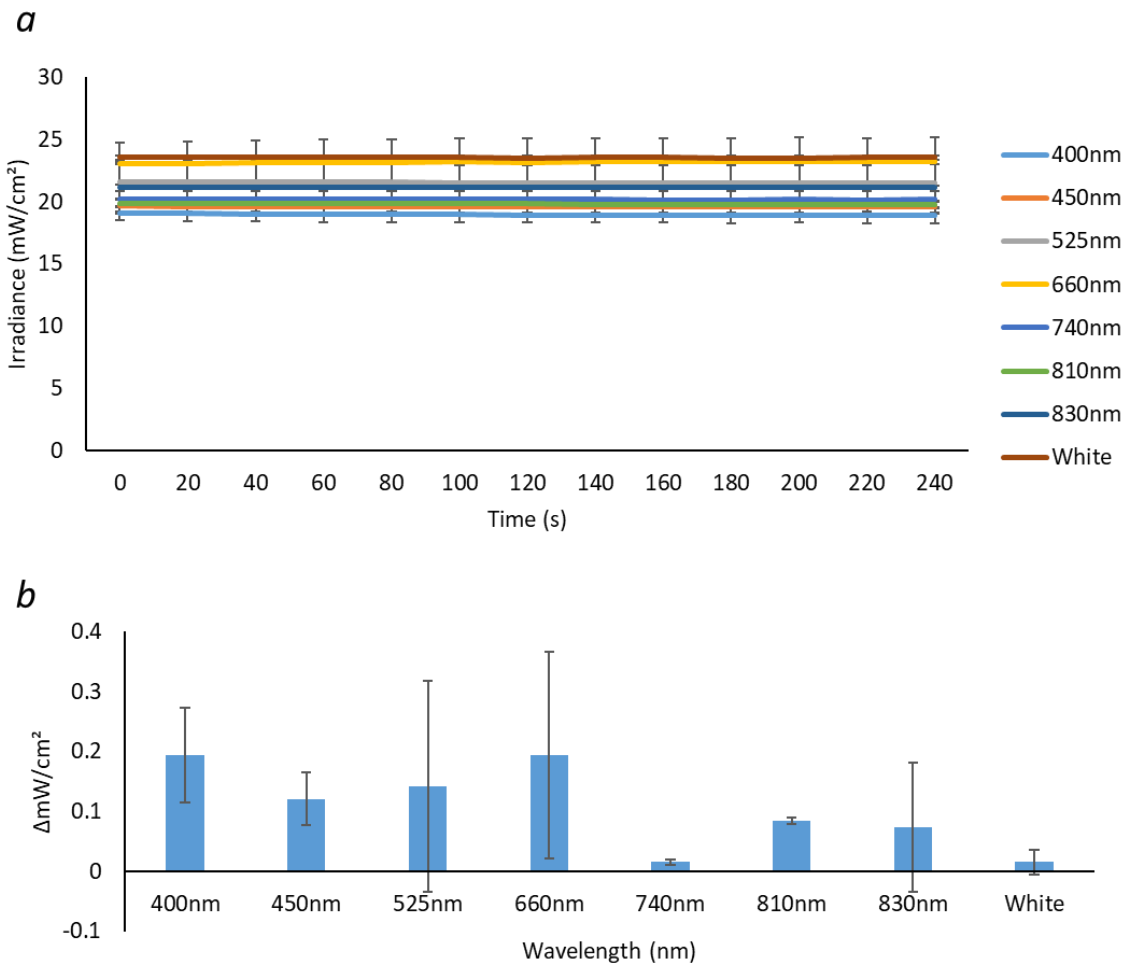

Figure 3.2a: Changes in irradiance in real-time over a period of 240s taken from an average (n=3) of the irradiance emitted at each time point assessed using each wavelength channel (400-830 nm).b) Shows average change in irradiance over a 240s period (n=3). Data was analysed using one-way ANOVA followed by Tukey test where no significance difference was found between wavelength channels.

3.2.2 Analysis of irradiance delivered to the Seahorse XFe96 microplate

The spectral characteristics of the 96-well array fitted with a Seahorse XFe96 microplate (and mask constructed from dental impression material to prevent bleed between LEDs was then assessed to determine whether emitted wavelengths and spectral irradiance were similar to those delivered to the 96-well black clear bottom plate (Sigma-Aldrich).

3.2.2.1 Results

Data indicate spectral characteristics similar to those described in section 3.2.1.1 in which there was no significant difference in peak wavelength output when employing either a black clear bottom 96-well plate (Table 3.1*a)* or a Seahorse XFe96 plate (Table 3.2*a*). Indeed, there was an average emitted spectral irradiance of 24.26mW/cm² *(*Table 3.1*c)* across the array with the placement of a black clear bottom plate and 23.04mW/cm² emitted with a Seahorse XFe96 plate employed *(*Table 3.2*c).* Where, statistical analysis revealed there was no significant difference in the irradiance output across the array when employing either type of plasticware. Table 3.2*c* also indicates there was no significant difference in fluency values employed *in vitro* when using both the Seahorse XFe96 microplate and black clear bottom 96-well plate (average emitted fluency values outlined in Table 3.2*c)*.

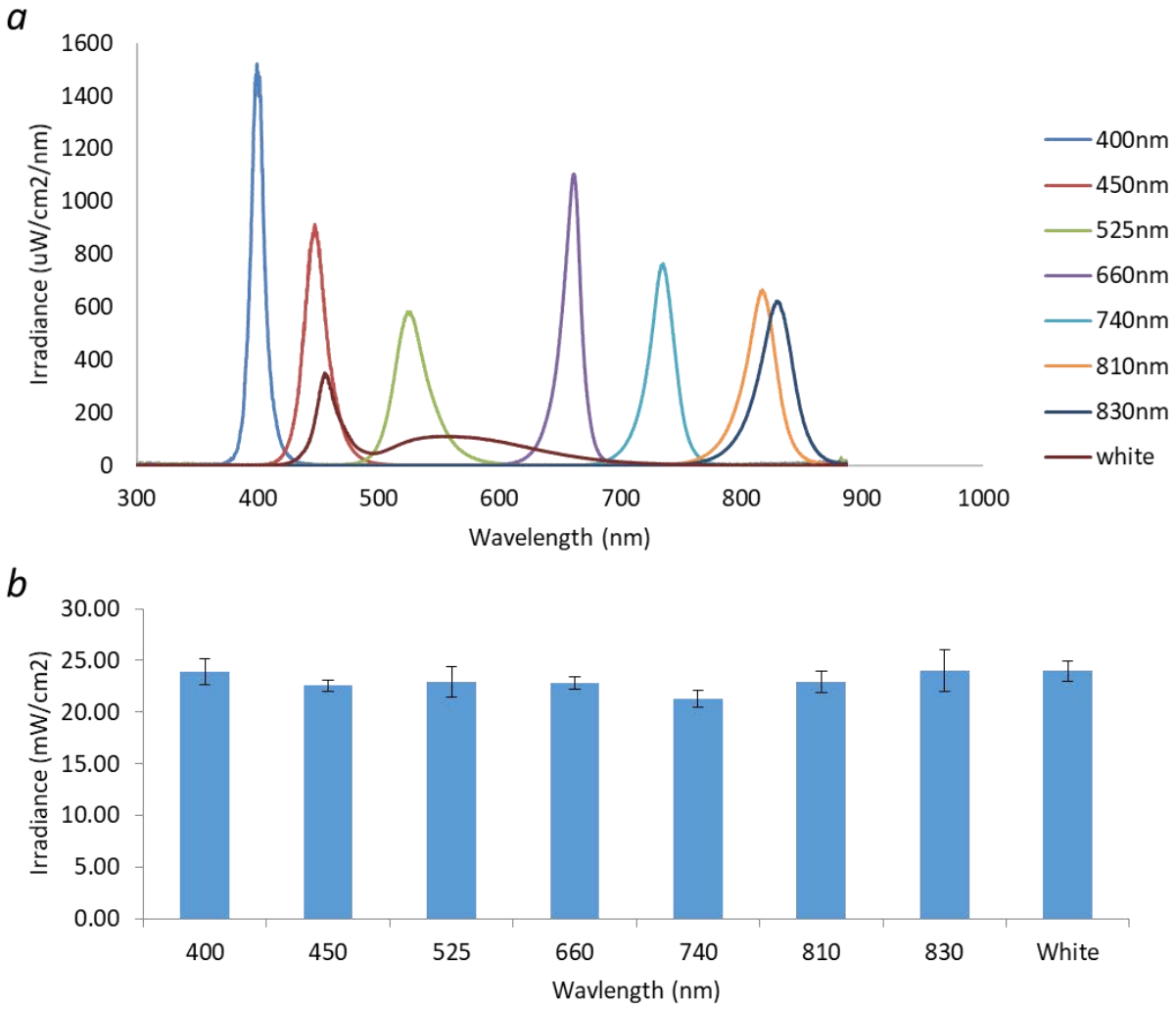

Figure 3.3a) Average peak wavelengths and b) spectral irradiance values of the LEDs utilised in this study (400 nm – 830 nm) emitted across the array. 6 LEDs were measured per wavelength employed in the array. Differences in emitted spectral irradiances from one wavelength to the next were analysed using one-way ANOVA followed by Tukey test where no significant difference was found between wavelength channels.

Table 3.2a Wavelengths emitted from each individual LED across the array. Where, the top line of the tables (in white text) indicates wavelength values stated by the manufacturer, whilst those below show the actual emitted wavelengths across the array, varying from 397.44-834.905 nm, b) shows variance in emitted spectral irradiance from each individual LED from the array (n=60) and c) depicts fluency values emitted across the array at a irradiation times ranging from 30-480s at wavelengths across the array (n=6).

a

Wavelength (nm)	400	450	525	660	740	810	830	White
1	399.41	447.157	524.229	660.708	735.238	817.379	828.851	455.426
2	399.41	447.157	523.835	660.708	733.419	817.379	827.465	455.224
3	401.658	451.193	526.4	660.896	735.238	817.379	834.905	455.426
4	397.774	446.753	525.808	661.648	736.693	817.379	828.851	455.224
5	399.41	447.157	526.4	661.835	733.783	817.379	828.851	455.224
6	401.658	447.157	523.835	661.835	735.602	815.809	828.851	455.426
AVG (mW/cm²)	*399.8867*	*447.7623*	*525.0845*	*661.2717*	*734.9955*	*817.1173*	*829.629*	*455.325*
STD DEV	*1.511307*	*1.688428*	*1.252111*	*0.557294*	*1.210163*	*0.64095*	*2.64349*	*0.11064*

b

Wavelength (nm)	400	450	525	660	740	810	830	White
1	23.889	24.279	28.077	24.171	23.371	25.065	24.805	25.686
2	23.296	22.545	25.138	24.550	23.955	26.230	17.673	25.269
3	24.506	23.884	21.068	23.579	19.278	20.507	32.751	21.573
4	18.436	22.243	19.797	20.323	19.266	22.896	22.610	20.481
5	25.970	21.539	18.656	22.073	21.890	23.162	22.608	24.208
6	27.152	20.756	24.657	22.209	19.916	19.564	23.633	26.531
AVG (mW/cm²)	*23.875*	*22.541*	*22.899*	*22.818*	*21.279*	*22.904*	*24.013*	*23.958*
STD DEV	*3.015*	*1.349*	*3.630*	*1.585*	*2.089*	*2.557*	*4.925*	*2.415*

c

Wavelength (nm)	Irradiance (mW/cm²)	Radiant exposure at 30s (J/cm²)	Radiant exposure at 60s (J/cm²)	Radiant exposure at 120s (J/cm²)	Radiant exposure at 240s (J/cm²)	Radiant exposure at 480s (J/cm²)
400	23.87±3.01	0.72	1.43	2.86	5.73	11.45
450	22.54±1.35	0.68	1.35	2.70	5.41	10.82
525	22.90±3.63	0.69	1.37	2.75	5.50	10.99
660	22.82±1.58	0.68	1.37	2.74	5.48	10.95
740	21.28±2.09	0.64	1.28	2.55	5.11	10.21
810	22.90±2.56	0.69	1.37	2.75	5.50	10.99
830	24.01±4.92	0.72	1.44	2.88	5.76	11.52
White	23.96±2.42	0.72	1.44	2.87	5.75	11.50
AVERAGE:	*23.04±1.16*	*0.69±0.03*	*1.38±0.06*	*2.76±0.11*	*5.53±0.22*	*11.05±0.44*

3.2.3 LUMOS array

3.2.3.1 Introduction

The LUMOS™ optical stimulation suite was employed to evaluate the effects of simultaneous multi-wavelength *in vitro* irradiation of cell cultures. The array was initially spectrally characterised to demonstrate average peak wavelengths emitted from each LED and also to determine the range of emitted spectral irradiance values when delivering different relative (%) intensities of light. These were then used to calculate spectral irradiance parameters to enable comparison with the 2nd Generation LED array described previously (3.2.1 and 3.2.2). These parameters were also evaluated to determine the difference in wavelength and spectral irradiance output from one LED to the next.

3.2.3.2 Results

The following data report on an LED array system calibrated to output parameters similar to those described in sections 3.2.1 and 3.2.2. However, this system also displays the capability of evaluating the effects of several wavelengths simultaneously *in vitro.*

These data indicated that whilst the manufacturer's proposed outputs of the LEDs were 405 nm and 850 nm, it was found the array had an average output of 407.57±1.04 nm and 857.60±0.85 nm for all 24 LEDs incorporated.

Evaluation of peak wavelength outputs, Figure 3.5*,* indicates the spectral irradiance output of the array at % intensities ranging from 100-5%. Irradiance varied significantly dependent upon the wavelength and experimental setup applied. At 100% intensity, irradiance exhibited by the 405 nm and 850 nm emitting LEDs were 100.00±7.81 mW/cm² and 66.36±5.85 mW/cm² respectively. Irradiance with the addition of a diffuser was also

evaluated in which 405 nm LEDs at 100% intensity emitted an average irradiance of 26.16±0.93 mW/cm².

Evaluation of irradiance output at various % intensities of the LUMOS™ enabled production of a standard curve, which then allowed prediction of the % intensity that equated to an average irradiance output of 24mW/cm². These were calculated for 405 nm (24.74%), 850 nm (34.55%) and 405 nm with diffuser (91.53%). However, the % intensity required to emit an average irradiance of 24mW/cm² when applying the diffuser material to LEDs emitting a wavelength of 850 nm was outside the range emitted by the LUMOS™ array. Hence, a diffuser material could not be used in this model to compare the effects of application of multiple wavelengths simultaneously or single wavelengths. Figure 3.6 indicates wavelength and spectral irradiance output at selected parameters, where Figure 3.6*b* describes spectral irradiance output at 12mW/cm² at 405 nm and 850 nm, to be used when evaluating whether combined wavelengths could improve response to PBM *in vitro*. However, % intensity could only be entered into Axis Navigator as whole numbers, hence numbers calculated above were rounded where appropriate. Therefore, this meant the average irradiance utilising both single and combined wavelengths was 23.14±1.85 mW/cm² *(*Table 3.3*),* less than the anticipated value of 24mW/cm².

Nevertheless, one way ANOVA was used followed by Tukey test to determine whether there was any significant difference in irradiance output utilising both the 2nd Generation LED array with black clear bottom plate (24.26±1.22 mW/cm²) or Seahorse XFe96 microplate (23.04±1.16 mW/cm²) and the LUMOS™ array fitted with 4titude 24 well plate, where no significant difference was detected. It was also demonstrated that the LUMOS™ array exhibited comparable radiant exposures following 240s irradiation (5.56±0.12 J/cm², Table

3.3*c*) compared with either the LED array with black clear bottom plates (5.82±0.29 mW/cm²) or with the Seahorse XFe96 plate (5.53±0.22 mW/cm²), where statistical analysis showed there was no significant difference between either array format.

Therefore, it was validated that the LUMOS provides a well characterised system emitting parameters comparable with those emitted by the 2nd Generation array.

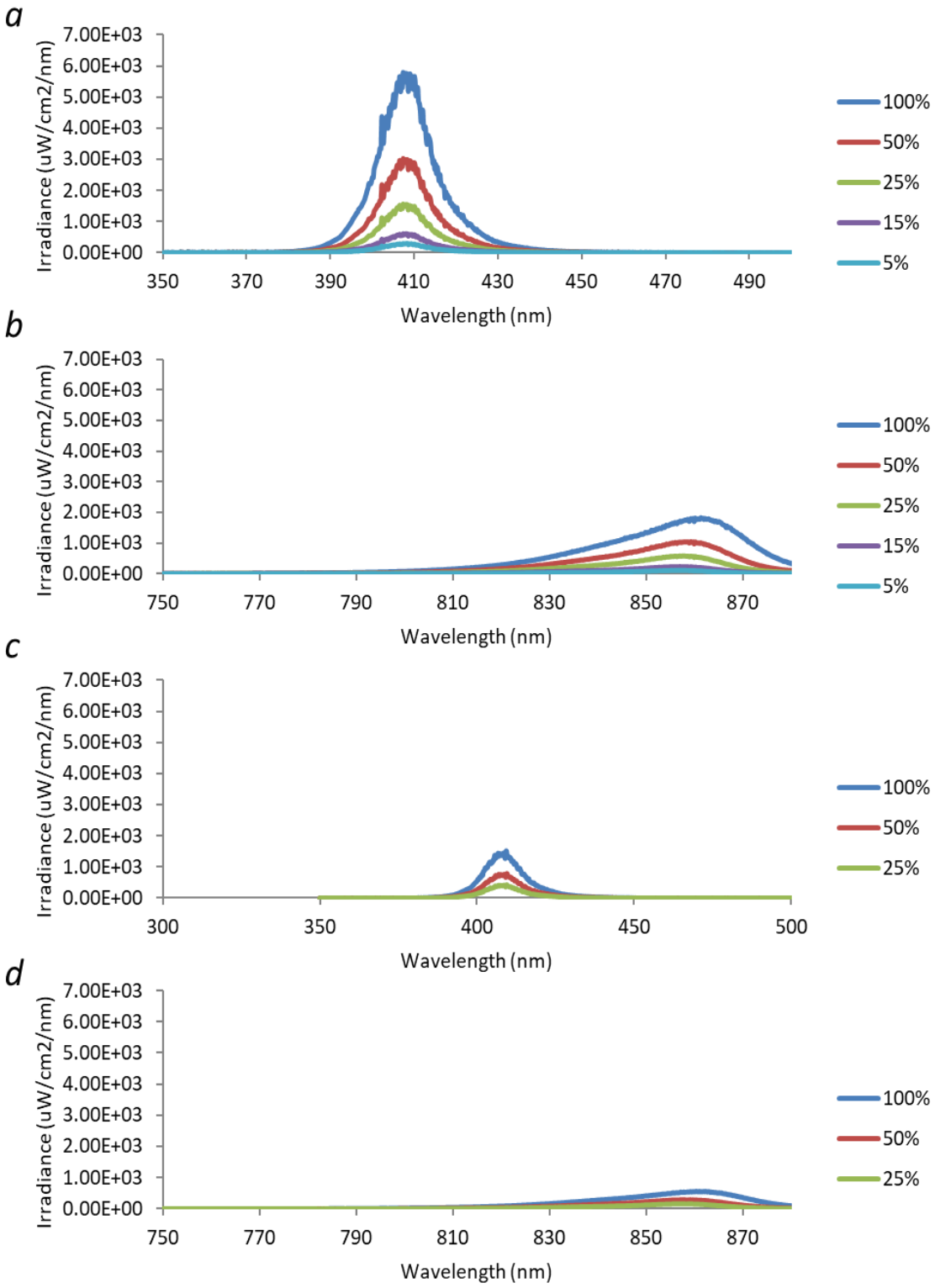

Figure 3.4: Average peak wavelengths (n=24) at 100%, 50%, 25%, 10% and 5% average intensity when altering the output of the LUMOS™ optical stimulation system on the adjoining Axis Navigator software at wavelengths of a) 405 nm, b) 850 nm, c) 405 nm with a diffuser and d) 850 nm with the addition of a diffuser.

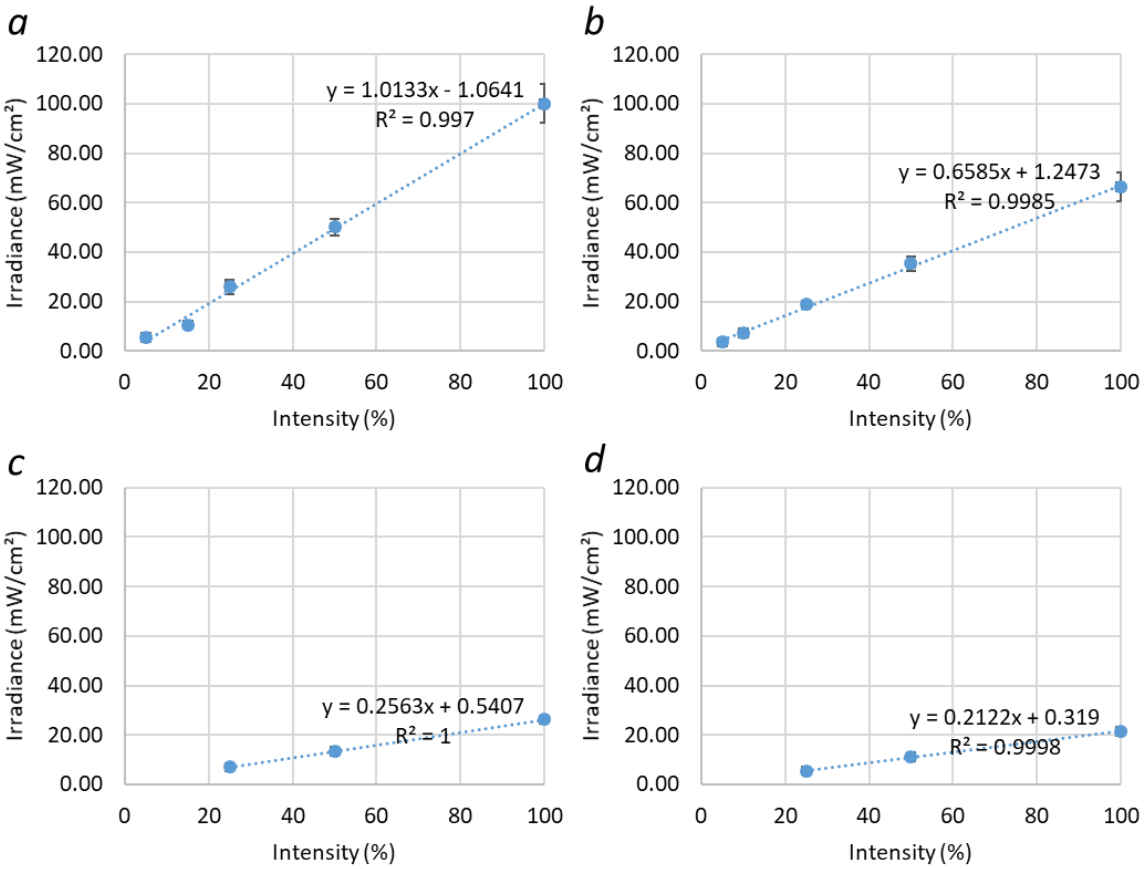

Figure 3.5: % intensity output of the LUMOS™ system calibrated against irradiance output using ocean optics software to record data to produce a standard curve. These analyses then enabled prediction of % intensity output to set on Axis navigator software to provide an output of 24mW/cm² from the array and hence mimicking the output of the 2nd generation LED array described in section 3.2.1. The figure above provides the different standard curves utilising different experimental setups and wavelengths where a) indicates 405 nm, b) 850 nm, c) 405 nm with diffuser and d)850 nm diffuser (where each point indicates the average irradiance taken from all LEDs on the array, n=24).

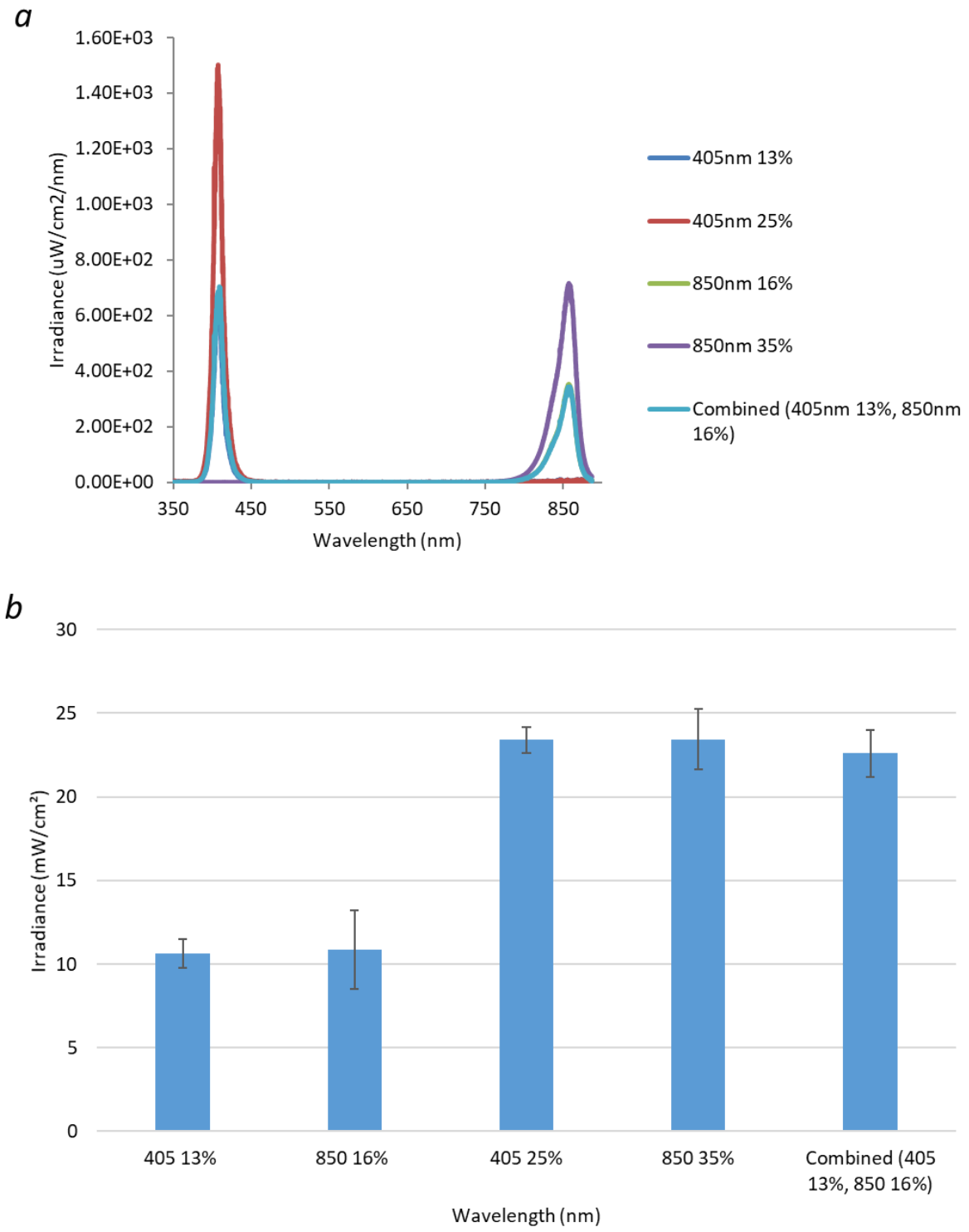

Figure 3.6a) Average peak wavelengths output when parameters calculated from Figure 3.5 are inputted into axis navigator software where an average irradiance output of 24mW/cm² was required for in vitro study. b) Spectral irradiance output when using calculated parameters where there is no significant difference between parameters to be used experimentally (405 nm 25%, 850 35%, combined). Outputs with a diffuser were not assessed as the application of diffuser meant parameters required were out of range using data calculated in figure 3.5. Significance was evaluated using one way ANOVA followed by post-hoc Tukey test.

Table 3.3: Output of a) wavelengths and b) irradiance output from each LED across the array when specific parameters were applied to Axis Navigator software at 405 nm, 850 nm and combining both at the same calculated irradiance output (24mW/cm², n=24). Table 7c indicates calculated radiant exposure (J/cm²) at selected irradiation periods to be used in vitro and corresponding average irradiance output.

a

	Wavelength (nm)		
LED	405	850	405 + 850
1	406.56	857.03	413.90
2	407.38	858.57	886.58
3	410.03	857.03	416.14
4	407.38	856.01	415.73
5	407.38	859.25	415.53
6	407.38	857.03	415.12
7	407.38	857.03	413.90
8	406.56	858.57	860.27
9	407.38	858.57	860.78
10	408.40	857.03	415.73
11	408.40	857.03	860.78
12	406.56	858.05	415.53
13	407.38	857.03	860.27
14	406.56	857.03	413.70
15	410.03	858.05	860.27
16	406.56	857.03	412.68
17	408.40	857.03	860.78
18	406.56	857.03	860.61
19	406.56	859.25	860.10
20	407.38	857.03	860.27
21	407.38	858.05	416.14
22	407.38	858.05	860.78
23	407.38	858.57	860.10
24	409.42	857.03	413.90
AVG (mW/cm²)	407.57	857.60	638.73
STD DEV	1.04	0.85	228.78

b

	Irradiance (mW/cm²)		
LED	405	850	405 + 850
1	26.18	25.15	21.82
2	26.86	22.92	21.09
3	23.56	22.69	21.50
4	20.75	22.48	21.14
5	22.28	23.63	21.05
6	26.25	21.20	21.19
7	22.59	21.20	22.42
8	24.56	22.92	23.29
9	21.51	22.92	24.14
10	22.29	26.58	22.62
11	23.53	23.46	24.14
12	22.01	22.49	21.05
13	22.49	21.20	20.11
14	21.11	26.19	21.33
15	20.44	25.74	22.09
16	26.00	21.20	22.18
17	20.95	21.20	24.24
18	26.03	23.13	23.38
19	27.44	24.21	24.86
20	23.99	22.53	23.92
21	22.87	26.20	23.20
22	26.86	26.89	24.14
23	20.93	22.92	24.86
24	20.03	23.46	22.42
AVG (mW/cm²)	23.40	23.44	22.59
STD DEV	2.34	1.81	1.39

c

Wavelength (nm)	Irradiance (mW/cm²)	Radiant exposure at 240s (J/cm²)	Radiant exposure at 480s (J/cm²)
405	23.40±2.34	5.62	11.23
850	23.44±1.81	5.63	11.25
405 + 850	22.59±1.39	5.42	10.84
AVERAGE:	*23.14±1.85*	*5.56±0.12*	*11.11±0.23*

3.3 Beam Profile

In the present study, a CCD beam profiler was utilised to demonstrate the spatial distribution of irradiance emitted from each light source. Using beam gage software (Ophir, Spiricon, Israel) average beam area (cm^2) and average power output (mW) were also evaluated. These analyses would then not only provide information on distribution of light but would also indicate whether the light source is suitable to irradiate the area of cultureware employed in PBM *in vitro* studies.

3.3.1 2nd Generation array

Beam profiles of each individual LED on the array were obtained when either a 96-well black clear bottom plate or Seahorse plate was fitted to the LED array to mimic the PBM studies, this therefore enabled demonstration of the spatial distribution of irradiance in a 3D plane. Images were also obtained using a target screen (N-BK7 ground glass diffuser, Thorlabs, US) to enable visualisation of the spatial distribution of light in the plane at which adherent cells would be irradiated. Use of a target screen was incorporated at the same distance from the array (3mm) as cultureware used during experimentation. Hence, whilst the images obtained with a target screen did not incorporate a plate, this model is reliable as it provides detail of how light will be delivered directly to cell cultures.

3.3.1.1 Results

Data obtained indicate that LEDs across the array emit a Gaussian distribution of light at the plane of adherent cells through the addition of a target screen, hence enabling precise calculation of beam diameter *(*Table 3.4*a* (Palin et al., 2015)). Figure 3.7*a* shows a representative image of a beam profile where different colours on the profile indicate

differing levels of irradiance. White demarcation shows high irradiance and grey shows low irradiance. Figure 3.8 and Figure 3.9 describe the beam profiles exhibited when the black clear bottom plate or Seahorse XFe96 microplate are placed above the array without the use of a target screen. Hence, these images are only provided for reference as they were not obtained in the focal plane of the light source. These images are also used to demonstrate whether there is any difference in beam area dependent upon the plate type used.

Table 3.4 provides detail of the beam areas exhibited dependent upon the wavelength channel evaluated and/or experimental setup applied to the LED array. The results show that the LED array fitted with the Seahorse plate exhibited the smallest beam areas (0.24±0.02 cm^2) compared with the black clear bottom plate (0.28±0.04 cm^2) or target screen (0.32 ±0.04 cm^2). This is simply due to the difference in well area, where the Seahorse plate has a well area of 0.11cm^2 (bottom diameter 0.38mm and top diameter of 0.81cm, hence allowing the beam area to expand, (see Figure 3.7*b*) and the black clear bottom plate has a well area of 0.32cm^2. The target screen beam area is also larger due to the plane at which the image was taken. There is also a significant difference in the average beam area between wavelength channels, hence these differences should be considered when evaluating cellular effects observed in the subsequent *in vitro* studies.

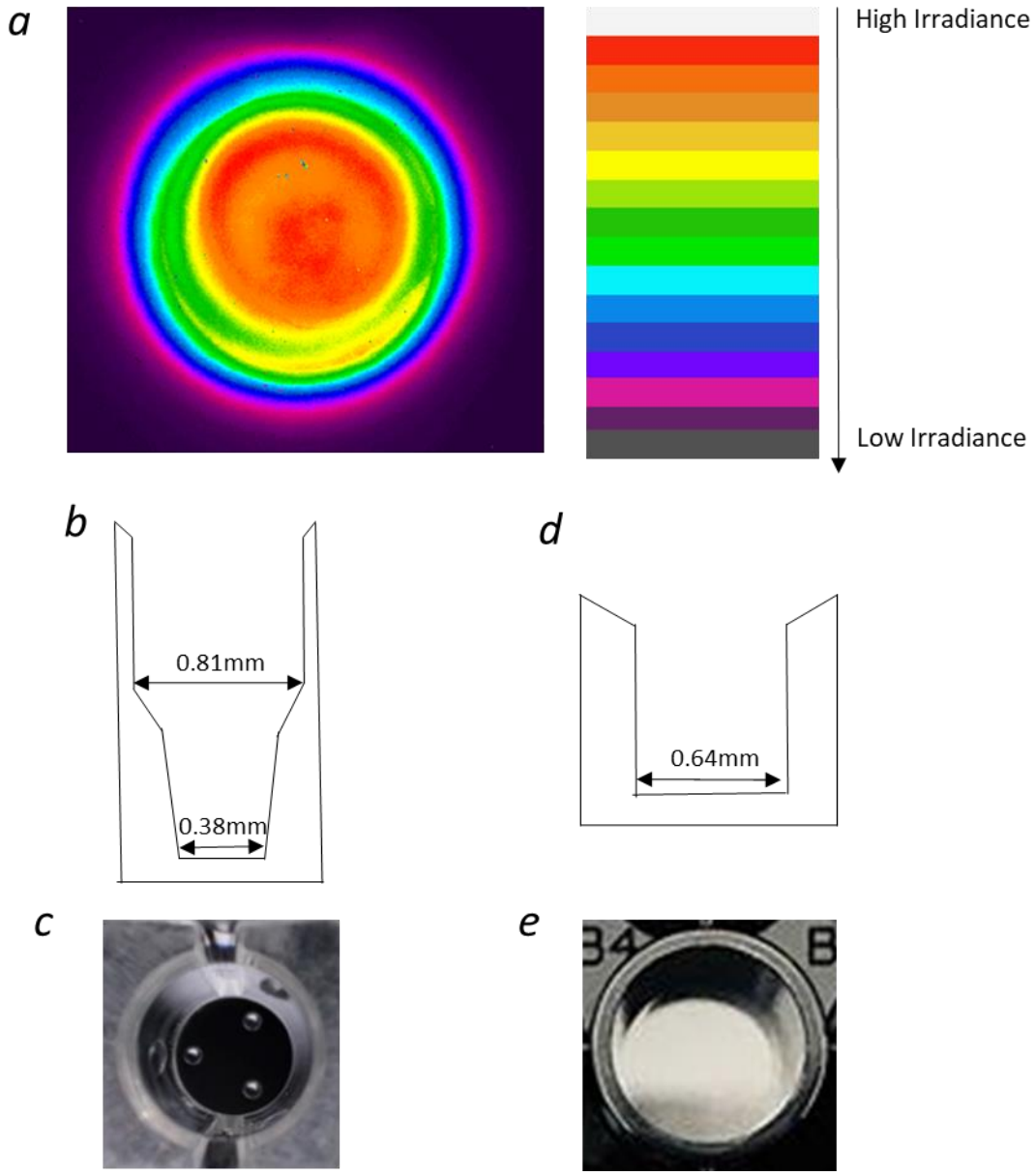

Figure 3.7: Example of beam profile adjacent to a colour scale depicting changes in irradiance where white and red show high spectral irradiance and purple indicates lower irradiance outputs (mW/cm²). b) Depicts top and bottom well diameters of the Seahorse XFe96 plate, indicating beam area could widen if an image is obtained not at the plane where the cells would be adhered (no target screen and c) shows a birds eye view of a well of the Seahorse XFe96 microplate, in which there are three circular indentations enabling reliable insertion of injection ports into the centre of each well (image from https://www.agilent.com/cs/library/brochures/5991-8657EN_seahorse_plastics_brochure.pdf). c) Shows well diameter of the 96-well black clear bottom plate, for reference and e) shows an image of a well of a 96-well black clear bottom

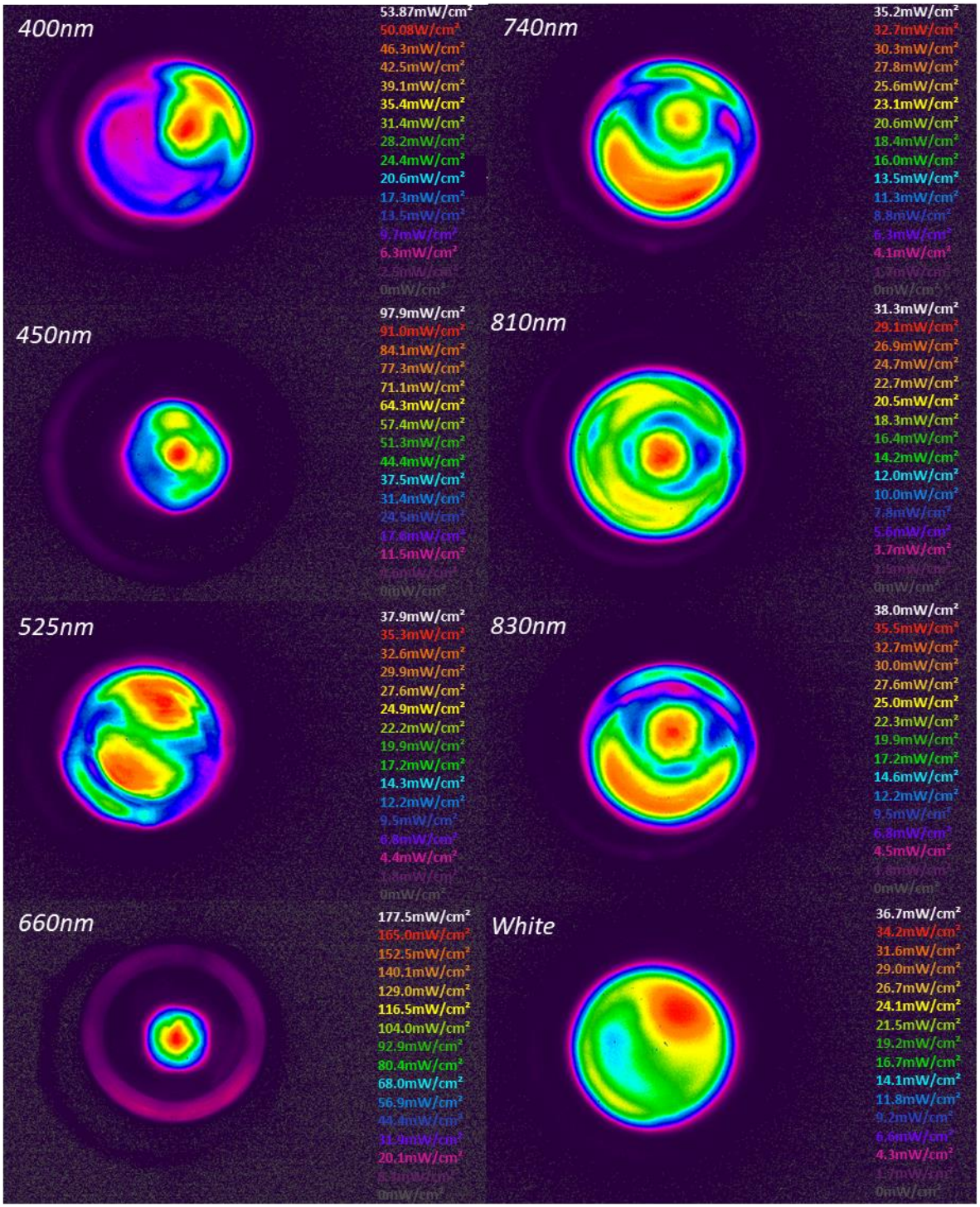

Figure 3.8 Representative images of the spatial distribution of irradiance from each wavelength channel when a black clear bottom plate is placed directly above the 2nd generation LED array. These images show the 3D profile of irradiance, which indicates the light delivered outside of the plate. Representative images showing the spectral irradiance which would be delivered directly to adherent cells in 2D can be seen in Figure 3.10.

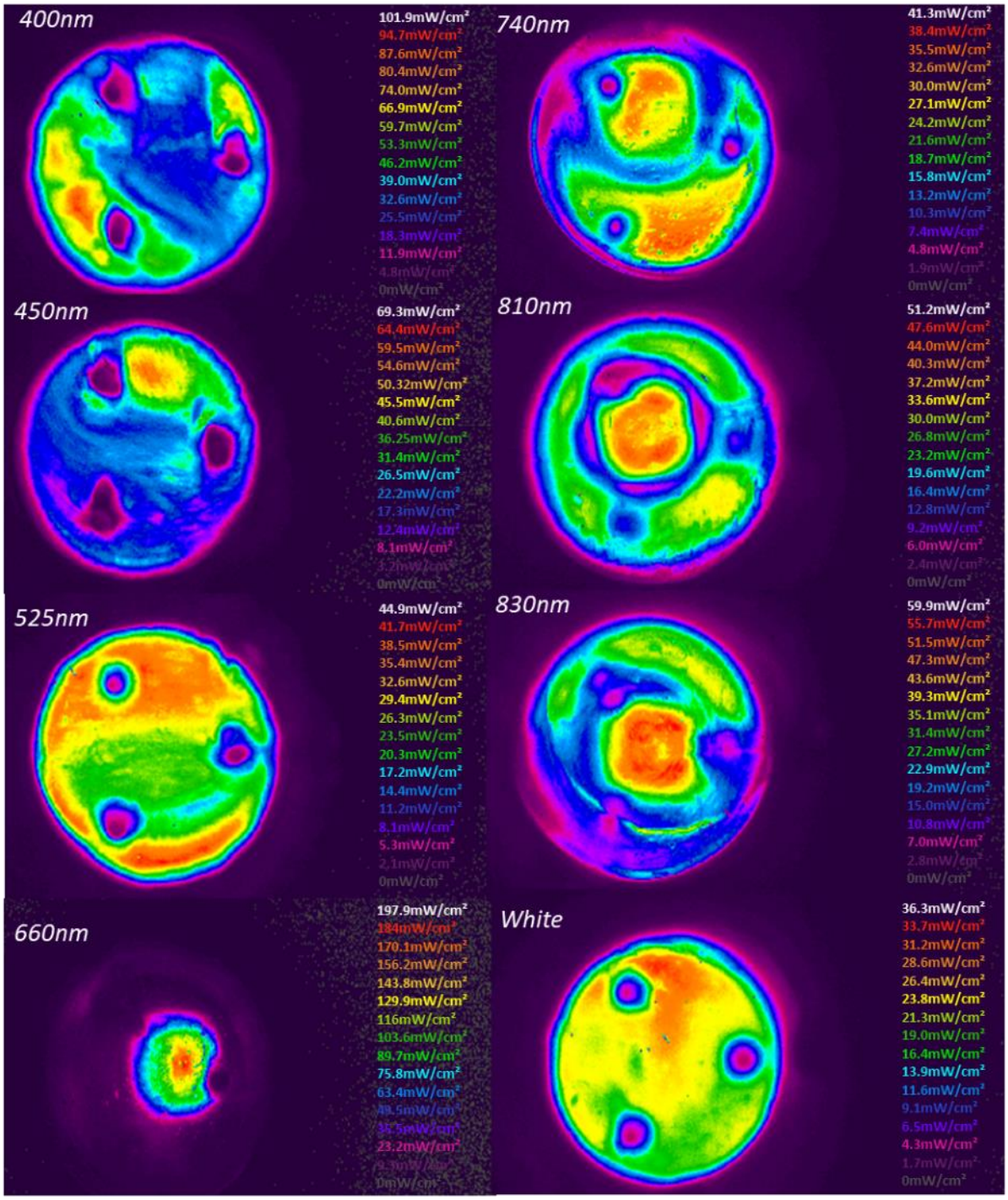

Figure 3.9 Spatial distribution of irradiance of LEDs emitting each wavelength on the array (representative image from each wavelength channel) when a Seahorse XFe96 microplate is placed upon the second generation array. Images were obtained without the presence of a target screen, therefore the image above provides the profiles delivered in 3D. Hence, they provide information on the light delivered to the whole well and that emitted outside of the well. Hence, this is not a reliable indication of light delivered to adherent cells in culture and whilst it would have been beneficial to visualise light delivery with the seahorse XFe96 microplate and target screen in place, this was not feasible in the case of this model. The three distinct areas of each well are indicative of the Seahorse XFe96 microplate design as described *Figure 3.7.*

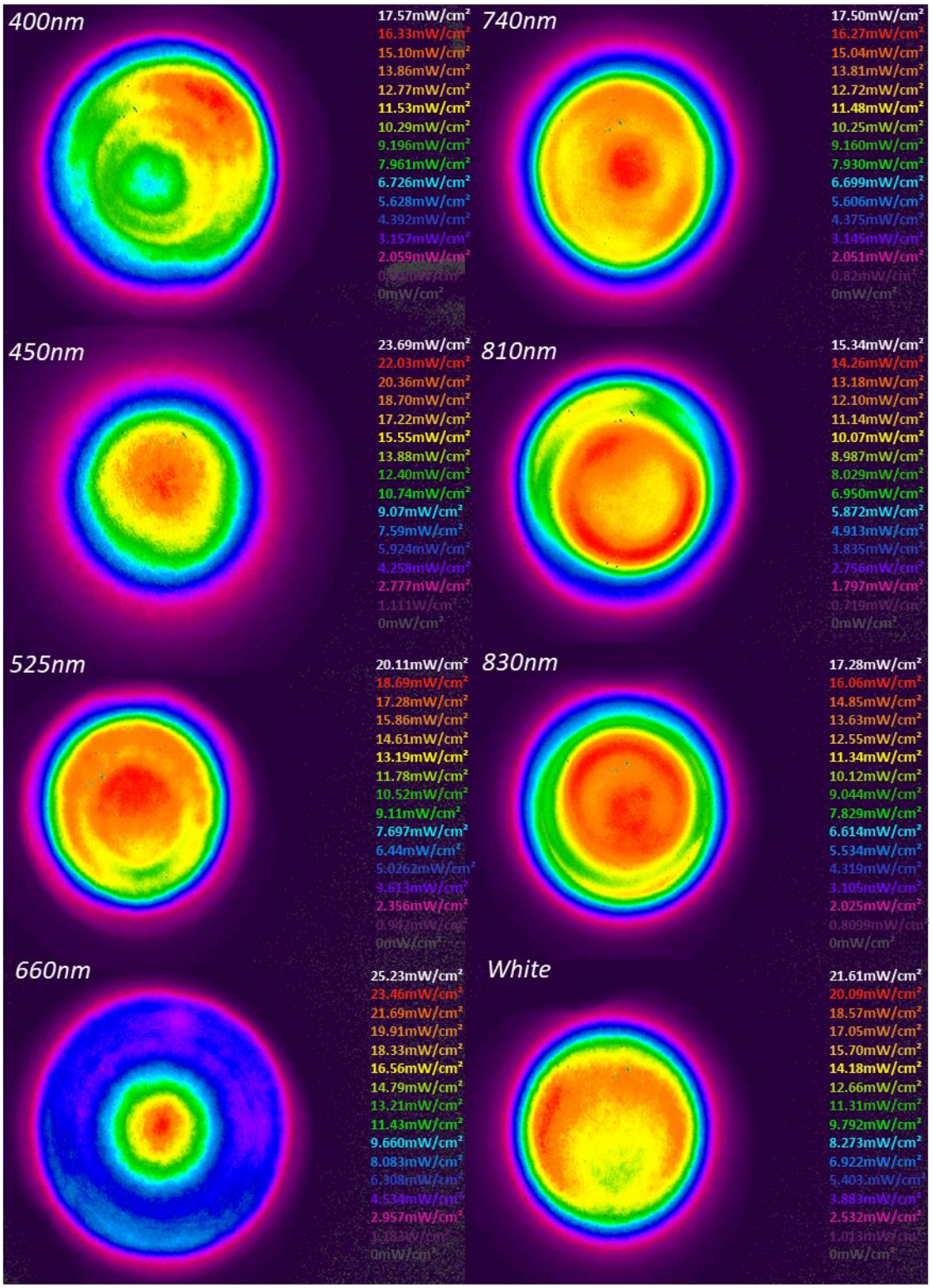

Figure 3.10: Spatial distribution of irradiance of LEDs emitting each wavelength on the array. Images were obtained in the plane of a target screen placed over the array surface to enable accurate measurement of beam diameter using BeamGage software. The target screen was placed at the same distance away from the array as a Seahorse XFe96 plate and a black clear bottom plate. Whilst the target screen could not be incorporated with either plate in place representative images are indicated in Figure 3.8 and Figure 3.9.

Table 3.4: a) Average beam area and b) power output from each wavelength channels when using either a Seahorse XFe96 microplate, black clear bottom plate or target screen. Significance was analysed using one way ANOVA followed by Tukey test. Significant differences between outputs of wavelength channels using different plate format are indicated where means do not share the same capital letter (A/B/C). Significance between use of different plate formats and the target screen are indicated where means do not share the same lower case letter (bold and italic: a/b/c).

a

	Beam area (cm²)		
Wavelength (nm)	Seahorse	Black clear	Target screen
400	0.250±0.009 AB	0.315±0.037 ABC	0.370±0.008 A
450	0.242±0.010 B	0.239±0.023 ABC	0.337±0.003 AB
525	0.211±0.182 AB	0.255±0.019 C	0.257±0.007 B
660	0.215±0.002 A	0.316±0.035 BC	0.364±0.003 A
740	0.258±0.011 AB	0.275±0.040 A	0.298±0.007 AB
810	0.256±0.021 AB	0.284±0.022 AB	0.335±0.007 AB
830	0.248±0.026 AB	0.270±0.0159 ABC	0.307±0.01 AB
White	0.249±0.002 AB	0.249±0.007 ABC	0.291±0.009 AB
AVERAGE	*0.24±0.02* ***c***	*0.28±0.04* ***b***	*0.32±0.04* ***a***

b

	Power (mW)		
Wavelength (nm)	Seahorse	Black clear	Target screen
400	5.96±0.21 A	7.60±0.89 A	8.93±0.18 A
450	5.45±0.22 AB	6.00±0.58 A	8.48±0.06 AB
525	4.83±0.42 B	6.00±0.46 A	6.04±0.16 B
660	4.90±0.05 B	7.81±0.87 A	9.01±0.07 A
740	5.48±0.24 AB	6.29±0.91 A	6.83±0.16 AB
810	5.87±0.48 A	6.52±0.50 A	7.69±0.16 AB
830	5.94±0.62 A	6.55±0.39 A	7.45±0.23 AB
White	5.97±0.05 A	6.63±0.18 A	7.72±0.24 AB
AVERAGE	*5.55±0.53* ***c***	*6.68±0.84* ***b***	*7.77±0.99* ***a***

3.3.2 LUMOS™ array

Beam profiles of the LUMOS™ optical stimulation suite were imaged to determine the spatial distribution of irradiance. A diffuser material was also placed upon the array to investigate whether this would improve the homogeneity of the arrays beam profiles. All images were taken with the target screen in place as in this experimental setup, the screen could be positioned at the base of the cell culture plate.

3.3.2.1 Results

Data indicated that the addition of a diffuser material dramatically improved homogeneity of beam profiles (Figure 3.11) and also increased beam area by an average of 56.7±2.34 % whilst also ensuring there was no significant difference in beam area between wavelengths (Table 3.5*a*). Evidence indicated that addition of a diffuser material ensures there is no significant difference in power output at each wavelength (Table 3.5*b*).

However, despite providing evidence that the addition of a diffuser material improves beam homogeneity, unfortunately this could not be incorporated in future *in vitro* studies. This is due to a number of reasons, including the fact that the addition of a diffuser meant greater % intensities of the light source were required to enable the emission of equivalent irradiance outputs (24mW/cm²) using all experimental setups. In the case of the delivery of 850 nm, the % intensity required to emit this irradiance was outside the range of the light source. Hence, this approach could therefore not be applied, and is discussed further in section 3.4.

Another key reason why this approach could not be undertaken was that employing such high light intensities (due to diffuser application) meant that the light source would have a significant effect on media temperature, which would likely dramatically influence the

biological outcomes of cell analysis studies, as discussed in section 3.4.1. Hence, the array without the addition of a diffuser was selected for further evaluation.

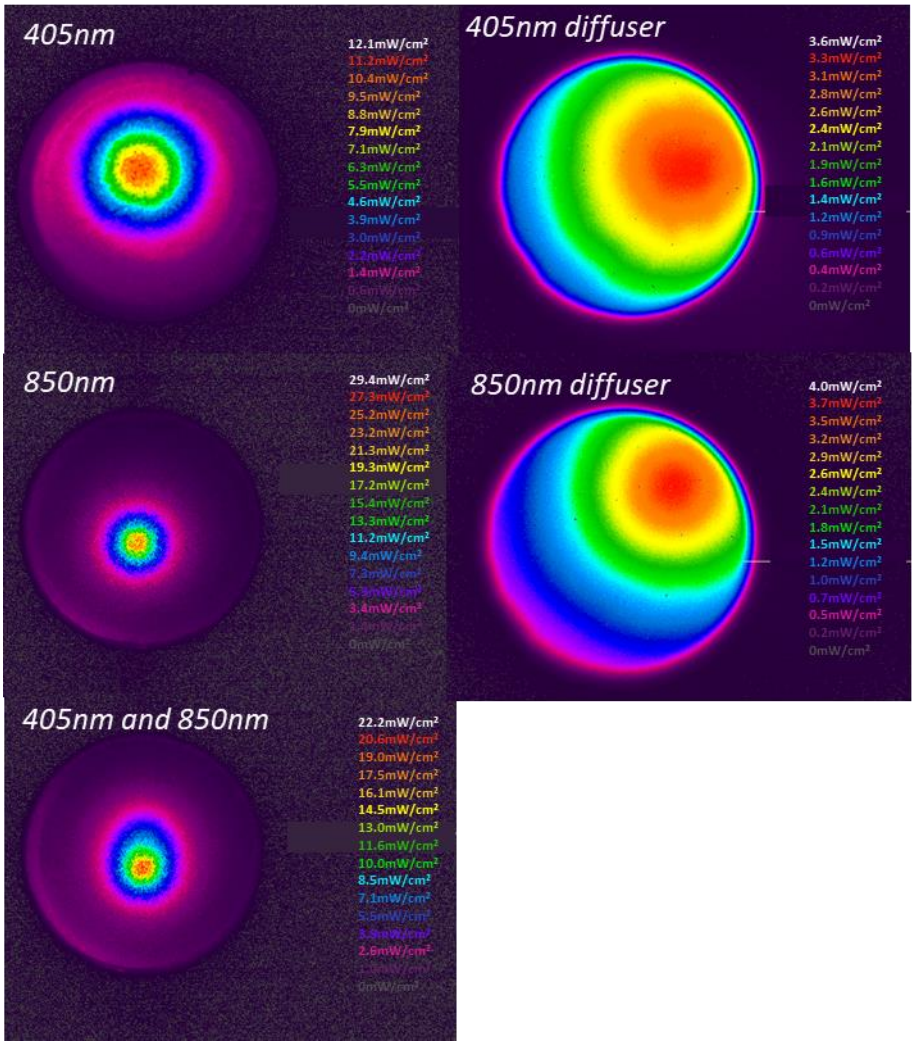

Figure 3.11 Representative images of spatial distribution of irradiance emitted from LEDs using different experimental setups (with or without diffuser) to determine whether user of a diffuser could homogenise the beam profile. Images were taken in the plane of a target screen placed over the array surface to enable accurate measurement of beam diameter using BeamGage software. The target screen was placed on the bottom of the plate where cells would adhere to enable accurate representation of delivery of spectral irradiance in vitro. All images were taken of the same single well of the LUMOS™ array, to enable direct comparison of profiles.

Table 3.5 a) Average beam area and b) power output when placing a 24 well 4titude plate with or without a diffuser atop the LUMOS array. Significance was analysed using one way ANOVA followed by Tukey test. Significant differences between outputs of different wavelengths/wavelength combinations are indicated where means do not share the same capital letter (A/B/C).

a

	Beam area (cm²)	
Wavelength (nm)	4titude	4titude + diffuser
405	0.99±0.04 A	1.61±0.01 A
850	0.90±0.01 B	1.66±0.03 A
405 + 850	0.92±0.01 AB	

b

	Power (mW)	
Wavelength (nm)	4titude	4titude + diffuser
405	24.05±3.33 A	38.54±1.15 A
850	20.82±0.57 B	39.94±2.32 A
405 + 850	20.69±0.68 B	

3.4 Thermal analysis

Changes in temperature during light irradiation were evaluated to determine whether light exposure could alter media temperature and hence biological outcomes of cell analysis. Changes in temperature were measured in real-time up to maximum irradiation periods employed in subsequent biological experiments. Conditions employed in these experiments were selected to mimic those used *in vitro* in which media was warmed to 37^{o}C and then irradiated on the bench surface for up to 4 minutes. The effects of both of the 2nd Generation LED array (fitted either with the 96-well black clear bottom plate or Seahorse XFe96 microplate) and LUMOS™ array were evaluated.

3.4.1 2nd Generation LED array analysis

Changes in media temperature and thermal output of the 2nd Generation LED array were assessed with the placement of either a 96 black clear bottom plate or a Seahorse XFe96 microplate fitted with a silicon mask.

3.4.1.1 Results

The data outlined below demonstrated the 2nd Generation LED array induces no significant effect on media temperature when compared with the non-irradiated control where Figure 3.12 shows mean changes in temperature. The data also shows there was no significant difference in media temperature change when comparing either experimental setup used. Where, when the 2nd Generation LED array was fitted with a black clear bottom plate it exhibited a mean decrease in media temperature of on average 2.50±0.19 °C and when the Seahorse XFe96 microplate was fitted with the mask and placed upon the array there was a decrease in media temperature on average of 2.44±0.17 °C .

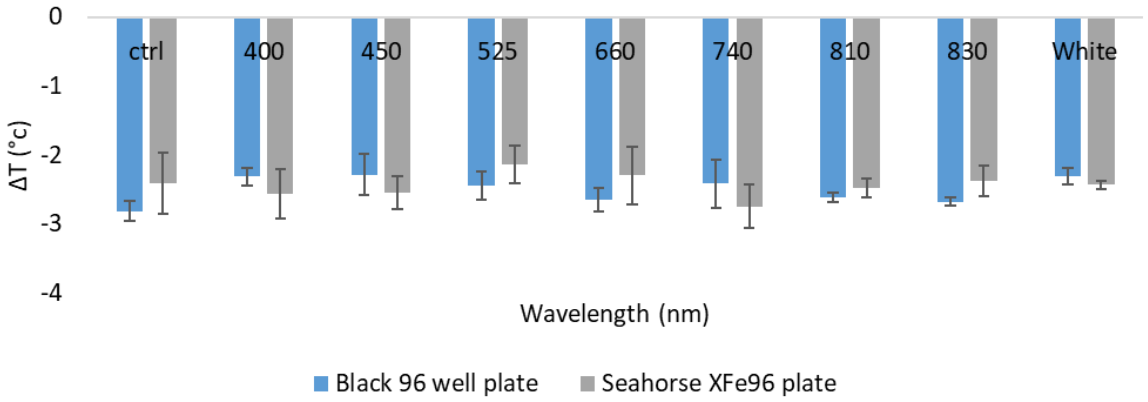

Figure 3.12: Change in media temperature following irradiation at room temperature where mean changes in temperature (ΔT) over a 250s period (24mW/cm², n=4) are described, comparing changes when either plate format is placed upon the array. One-way ANOVA followed by Tukey test was used to evaluate statistical significance, where no significant difference between means was detected in either experimental setup.

3.4.2 LUMOS™ array

3.4.2.1 Introduction

Assessment of changes in media temperature and thermal output of the LUMOS™ were assessed with the placement of either a 4titude plate +/- a diffuser material above the array. Changes were assessed over a 250s period at 24mW/cm².

3.4.2.2 Results

Data indicated that irradiation using the LUMOS™ optical stimulation system could induce an effect on media temperature dependent upon the experimental setup applied (with or without the addition of a diffuser, Figure 3.13). The experimental setup with the 4titude plate resulted in relatively small increases in media temperature when irradiating at 405 nm (0.15±0.42°C), 850 nm (0.20±0.04 °C) or both wavelengths (0.53±0.20 °C). However, these increases were significant when compared with the non-irradiated control, where an average decrease in media temperature of 2.67±0.15 °C was observed. However, the application of a diffuser material and 4titude plate on the LUMOS™ array induced the greatest increases in temperature, particularly after irradiation at 405 nm where an average increase in temperature of 4.67±0.47 °C was observed. This may be due to the addition of the diffuser where a higher intensity output of the array (91.53%) was required to enable an average irradiance output of 24mW/cm². Hence, through the addition of a diffuser a higher intensity output is required to generate a uniform irradiance of 24mW/cm², which in turn means the LUMOS™ array generates more heat at higher percentage intensity outputs. Comparably, an intensity output of 24.74% was a prerequisite to allow the same irradiance output when irradiating at 405 nm without the addition of a diffuser.

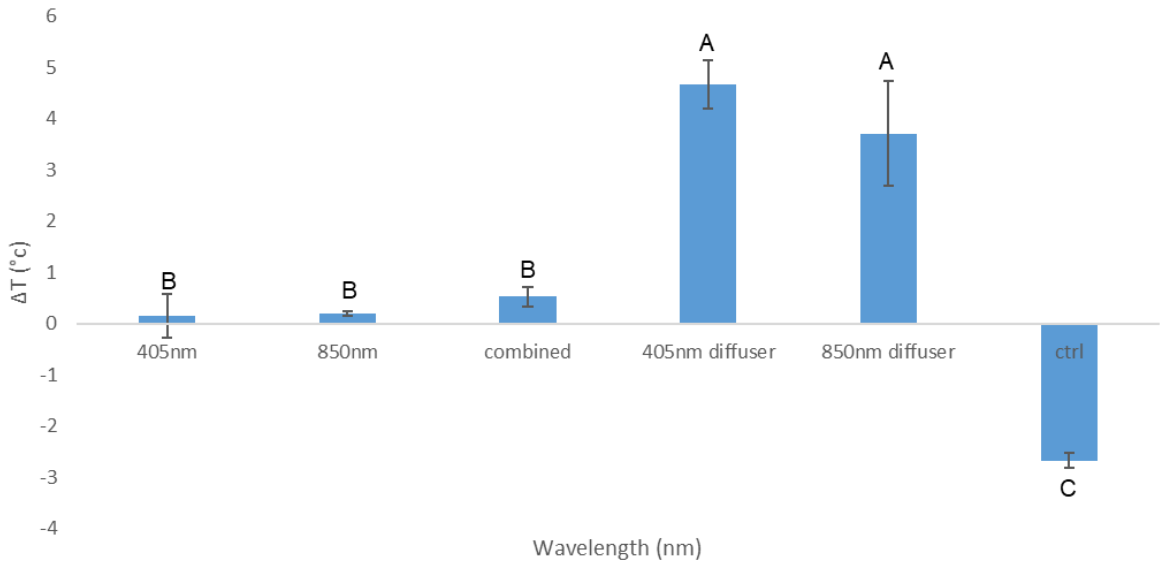

Figure 3.13 The mean change in temperature over a period of 240s with LUMOS fitted with 4titude plate and irradiated at 405 nm, 850 nm, both 405 nm and 850 nm (combined) or LUMOS fitted with diffuser and 4titude plate and irradiated at 405 nm, 850 nm or left untreated with light at 24mW/cm² (n=4 per setup). Statistical analysis was undertaken using one-way ANOVA followed by Tukey test where means that do not share the same letter are significantly different ($p<0.05$).

3.5 Absorption Measurements

3.5.1 Introduction

The properties of both media and plasticware were analysed to determine whether they exhibited absorbance spectra at wavelengths emitted by either the 2nd Generation array or LUMOS™ optical stimulation suite (400-850 nm). This study was undertaken to determine whether absorbance properties of either media or plasticware could influence the biological effects observed *in vitro* by limiting the irradiance delivered at a cellular level.

3.5.2 Results

Data indicated that phenol red containing DMEM exhibited an absorbance spectrum ranging from approximately 280-660 nm, with peaks at 292.6 nm and 558.4 nm with media containing no FBS, with the peak at 558.4 nm being the highest. Comparatively, media containing FBS exhibited similar peaks (295.8 nm and 559.5 nm), however the peak at 295.8 nm was higher *(*Figure 3.14*a).* These data thus provide evidence that red media exhibited absorption characteristics at wavelengths emitted from either array, hence this could potentially influence biological outputs of future experiments. Therefore, absorption characteristics of phenol red free DMEM (clear media) were subsequently investigated.

Clear media containing no FBS exhibited a peak at 288 nm whilst media containing 10% FBS exhibited a significant peak at 294 nm (absorbance 0.88) and a smaller peak at 406.6 nm (absorbance 0.19, Figure 3.14*b*). Hence, it was aimed to determine as to what extent FBS concentration influences this smaller peak. Figure 3.15*a* shows that reducing the concentration of FBS in media to 5%, resulted in the removal of this peak. However, as both arrays emit wavelengths ~400 nm, it was then evaluated whether irradiation of media containing 10% FBS at either 400 nm or 450 nm for 240s at 24mW/cm² altered this peak

output. Figure 3.15*b* provides evidence that at 24hrs post irradiation, there was no discernible difference in the absorbance spectra exhibited by either non-irradiated or irradiated media containing FBS.

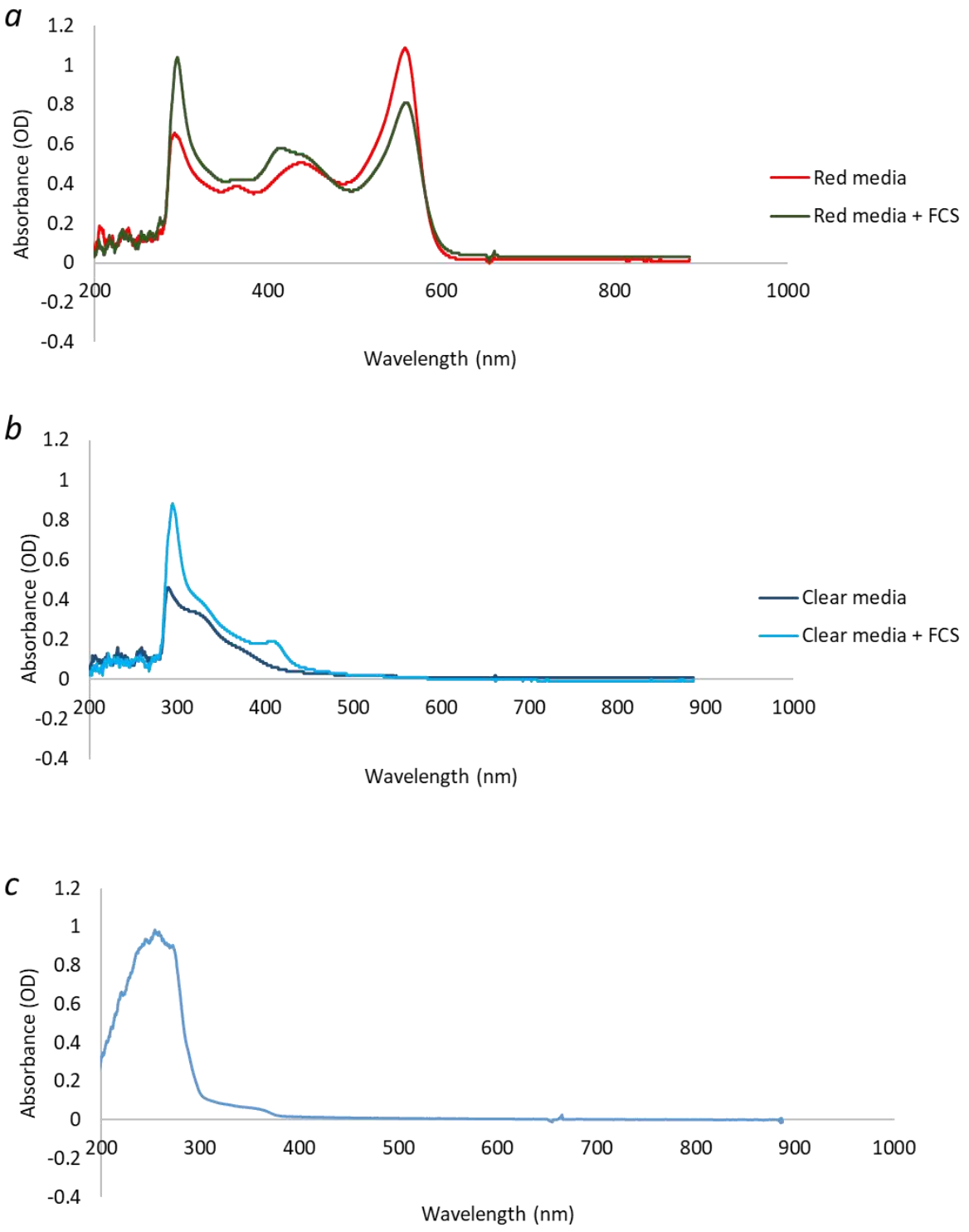

Figure 3.14: Absorbance of a) phenol red media with or without the addition of foetal bovine serum (FBS, n=6). b) Phenol red free media (clear) with or without FBS (n=6) and, c) cultureware absorbance (n=3). This was used to determine whether media colour or cultureware could affect the biological output of an experiment.

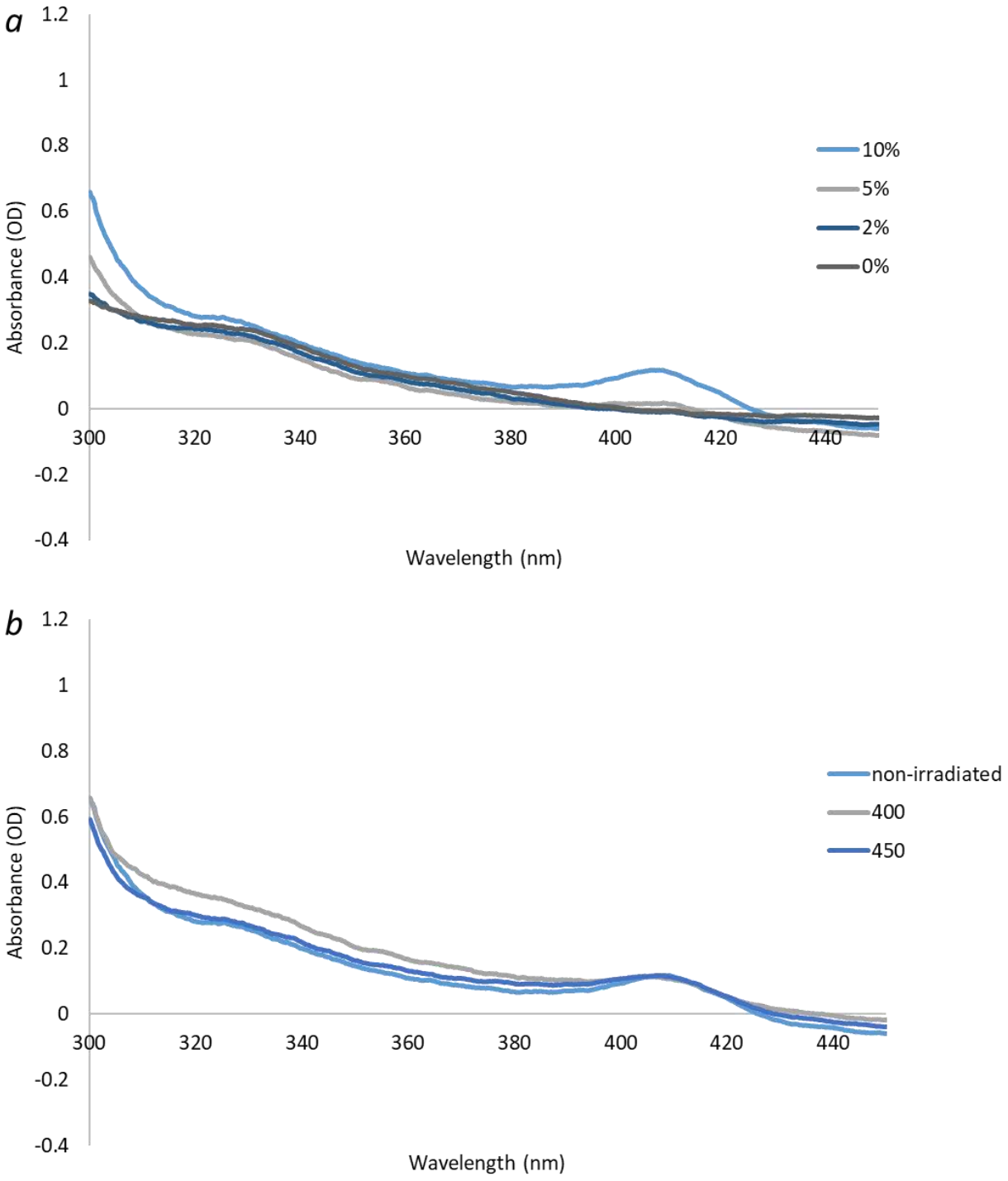

Figure 3.15: The effects of a) FBS concentration (2-10% concentration) on the absorption spectra exhibited by clear media (n=6) and, b) the effects of irradiation on the absorption spectra of media supplemented with 10% FBS 24hrs post-irradiation (as per experimental conditions) to determine whether this would potentially influence biological output (n=6). Media was irradiated using the 2nd generation array (400-450 nm, 24mW/cm², and 5.76J/cm²).

3.6 Discussion

3.6.1 Spectral Characterisation

Data demonstrate two well characterised systems, emitting comparable irradiance (~24mW/cm²) and radiant exposure (~5.76J/cm²) values, key parameters commonly used in PBM studies (Basso et al., 2013a, Basso et al., 2015, Pourzarandian et al., 2005). It was also shown that the 2nd Generation array ensures the capability of high-throughput screening of wavelengths from 400-830 nm at a single irradiance output, where there was no significant difference in the irradiance output between wavelength channels.

It is shown that the AxIS navigator software included in the LUMOS™ optical stimulation suite can be used to modulate the irradiance output of the system. In this case, calibration curves were created to correlate % intensity output with irradiance (mW/cm²), to ensure light delivered to *in vitro* cultures would be comparable to that delivered by the 2nd Generation array. This would then allow us to evaluate whether combining wavelengths (405 nm and 850 nm) would influence the biological output of an experiment.

Therefore, these data provide evidence for two novel arrays emitting parameters comparable with those utilised in many PBM studies both *in vitro* and *in vivo*.

3.6.2 Beam Profiles

Beam profiles of LEDs on each array were determined to demonstrate the spatial distribution of irradiance and also to enable calculation of average beam area (cm²) and power output (mW).

LEDs employed in the 2nd Generation array exhibited a typical Gaussian distribution of light (Figure 3.8*,* indicates a single representative from each wavelength channel) in which

spectral irradiance is most intense in the central area and becomes more diffuse towards the edges of the beam area (Yang et al., 2008). Table 3.4*a* (target screen column) indicates LEDs emitting a wavelength of 525 nm exhibited a significantly smaller ($p<0.05$) beam area and power output compared with LEDs emitting wavelengths of 400 nm and 660 nm, whilst there was no significant difference at all other wavelengths. In this particular experimental set-up, the LED array was designed to enable alignment of LEDs with the plate directly above them at a specific irradiance value. As described by *Hadis et al* (Hadis et al., 2017a) that whilst there is variability in the homogeneity of each LED, the effects of this have been minimised through ensuring there is no significant difference in the output of a series of parameters including irradiance (mW/cm^2) and radiant exposure (J/cm^2). However, despite this it will be important to take into account the effects this may have on the biological output of subsequent studies.

When evaluating the beam profiles emitted from the LUMOS™ array, the addition of a diffuser material dramatically improved average beam area by 58%. However, the use of a diffuser could not be incorporated due to the greater % intensity required to output uniform irradiance across the array of $24mW/cm^2$ as described in section 3.2.3.2.

Therefore, in subsequent studies, to account for the smaller beam profiles output from the LUMOS™ array, cell cultures will be seeded into the centre of the well, to ensure uniform irradiation. However, further work with alternative diffuser materials may also be important to determine whether irradiance output can be maximised whilst also ensuring homogenous beam profiles.

3.6.3 Thermal analysis

The effects of irradiation on media temperature were evaluated to attempt to determine whether changes in media temperature could contribute to any biological effects observed rather than light irradiation alone.

Irradiation using the 2nd Generation array had no significant effect on media temperature compared with non-irradiated controls (Figure 3.12). Notably the majority of studies currently do not report whether their light source has an effect on media temperature and hence, negative or indeed positive effects detected at a given wavelength could be due to the heating effect of the light (Kim and Kim, 2016). However, routinely studies utilise low irradiance values hence irradiation is deemed unlikely to have a heating effect. However, this is not always the case, for example, Chen et al reported that irradiating gingival fibroblasts at 1064 nm using an Nd:YAG laser source induced severe damage and loss of cell viability, while irradiance values were not reported it was noted that energy of up to 150mJ was utilised during irradiation (Chen et al., 2000b). This outcome could indeed be due to the thermal output of the laser utilised during experimentation as reported by Kim et al (Kim and Kim, 2016). Hence, we provide evidence for the importance of measuring changes in temperature induced by irradiation. However, in our experimental setup, no significant change in media temperature was observed.

In contrast, irradiation of media using the LUMOS™ system did significantly increase media temperature, particularly in the experimental setup in which a diffuser material was used (Figure 3.13). However, the increase in media temperature induced by irradiation in the setup without the addition of a diffuser, whilst significant, was minimal (average increase of 0.29±0.20 °C). Current literature indicates that small changes in temperature are not

detrimental to cell survival, where only increases past 42.5°C have been documented to induce large effects on oxidative stress (Nielsen and Overgaard, 1982, Ibtisham et al., 2018). Hence, as only a small change in temperature has been documented, in this case it is unlikely to exert any effect and ought to be within the limits of normal temperature fluctuations when culturing cells.

3.6.4 Absorption measurements

From our data, it is apparent that phenol red containing growth media exhibits an absorption spectra spanning wavelengths utilised in either array and is therefore unsuitable for our applications. Comparatively, clear media exhibits a large peak outside the range of either array but also a small peak at 405 nm when supplemented with 10% FBS, a wavelength emitted by both arrays. However, Figure 3.15 provides evidence that absorbance at 405 nm was reduced following a decrease in FBS concentration in media from 2-10%.

It may be argued that it would seem prudent to reduce FBS concentration simply to ensure that all light would be delivered to adherent cells and not absorbed by media. However, reducing FBS concentrations to 5% may induce stress in cell cultures or reduce proliferative capacity of cells(Urban et al., 2012). Almeida Lopes et al explored this and found cells grown in a lower FBS concentration (5%) had a lower proliferative rate than those grown in 10% FBS. However, light application (670-786 nm, 2J/cm^2) induced a significantly greater increase in cell proliferative rate from serum starved cells (Almeida-Lopes et al., 2001a). However, as the aim of this project was to compare the response to PBM from cultures treated with a pro-inflammatory stimuli (to induce stress) or left untreated (to mimic a healthy control), it was paramount to minimise the risk that any stress could be induced by application of lower FBS concentrations. Therefore, we wanted to first explore whether

irradiation of media containing 10% FBS with blue light would alter the absorption spectrum of media, suggesting irradiation could be exerting an effect on media composition. It has been shown that blue light can generate ROS, regardless of whether cells are present (Omata et al., 2006). It has also been documented that FBS possesses a high antioxidant component (Mun et al., 2017, Bump and Reed, 1977), in which it could be hypothesised that ROS generated by blue light could be converted to non-toxic biproducts such as water by antioxidants (Lázaro et al., 2013), hence components of FBS could exert a protective effect. Therefore, we provide evidence that in this experimental setup, irradiation with blue light has no significant effect on the absorbance spectra exhibited by media containing 10% FBS. Hence, as we wanted to evaluate the effects of PBM in a model comparable to current publications, an FBS concentration of 10% was selected for in vitro experimentation (Basso et al., 2016c, Hadis et al., 2015, Marques et al., 2017, Milward et al., 2015, Montoro et al., 2014, Pansani et al., 2017, Yang et al., 2012, Zaccara et al., 2018).

4 THE EFFECTS OF PBM ON MARKERS FOR MITOCHONDRIAL ACTIVITY

4.1 Introduction

Current literature indicates PBM modulates mitochondrial activity (Hamblin, 2018a). Hence, this chapter aimed to explore the effects of PBM on mitochondrial activity. Firstly, the objective of this chapter was to identify parameters that could modulate cell metabolic activity using a high-throughput assay whose output has been cited to correlate with mitochondrial activity (MTT assay, 1.6.1 (Liu et al., 1997)).

Following identification of these key parameters, the subsequent aim of this work was to establish whether cell confluency and foetal bovine serum (FBS) concentration influenced cellular responses. This would therefore determine whether cell confluency and culture conditions could influence response to PBM (Mignon et al., 2017) and hence may provide some insight as to why there is controversy in the field with regards to both positive effects (Avci et al., 2013), negative effects (Rohringer et al., 2017) or no effect (Takhtfooladi et al., 2014) being reported for PBM *in vitro*.

Subsequently, evaluation of PBM on a series of markers for mitochondrial activity was performed. This included the assessment of the effects of PBM on mitochondrial associated gene expression. Genes evaluated included a series of subunits of complexes comprising the mitochondrially located ETC as well as genes encoding molecules involved in the regulation of reactive oxygen species (ROS) production as a result of increases in ETC activity. A series of surrogate markers for determining mitochondrial activity were also employed including NO, ATP and ROS assays. These analyses would enable comparisons with the current literature as studies have assessed levels of ROS (Migliario et al., 2014) and ATP (Rhee et al., 2014) to evaluate the effects of PBM *in vitro*.

The effects of PBM on markers of downstream PBM-associated signalling were also explored including the effects on interleukin-8 (IL-8) and TGF-β1 gene expression and protein secretion. IL-8 was selected as its expression and secretion correlate with the activation of NFκB (Matsusaka et al., 1993), a key transcription factor whose activity has been cited to be modulated by light (Chen et al., 2011a). Increases in ROS have also been cited to modulate the activity of NFκB (Morgan and Liu, 2011), a key bi-product generated through increases in mitochondrial activity (Hoffmann et al., 2018, Liu and Desai, 2015).

The final aim of this chapter was to explore whether combining irradiation conditions could enhance the effect of PBM *in vitro.* A number of studies have reported that various wavelength combinations can induce biological effects i*n vitro* and *in vivo* (Askhadulin et al., 2018, Garlet, 2010, Moskvin et al., 2017, Niu et al., 2015). However, the majority of these reports do not compare the use of single wavelengths to the effects of combining wavelengths (Alba et al., 2017, Figurová et al., 2016) or do not match spectral irradiance outputs for all treatments, therefore variables other than wavelength could be influencing experimental outcome (Fekrazad et al., 2018). Hence, the effects of combinations of wavelengths versus single wavelength application (whilst ensuring irradiance output and radiant exposure was standardised across the experimental setup, 3.2.3) on a series of markers for mitochondrial activity could be compared.

The data generated could then be used to determine whether PBM affects mitochondrial activity and to what extent does this effect markers for downstream signalling.

4.2 Determining seeding densities for in vitro studies

To standardise the experimental protocol, a single seeding density was selected for in *vitro* application. This was performed using a series of assays applied throughout this project including MTT (2.2.9.3), ROS (2.2.11) and a cell confluency assay (2.2.9.1). The purpose of this was to ensure cultures were within a standardised confluency range (~70-80%) following application of stimuli (assessment occurred 24h post irradiation (Wright Muelas et al., 2018)).

4.2.1 Results

The following data provide evidence for the selection of a cell seeding density to be used *in vitro.* Firstly, a protocol was established to correlate cell number with percentage confluence using the Tecan Spark® platform. Figure 4.1*a* demonstrates the linear relationship between cell confluence and cell number. These analyses also enabled identification of a cell seeding density that achieved a cell confluency, cited to be within the optimal proliferative range ((Abo-Aziza and A, 2017, Aumailley et al., 1982) 70-80%) at the point of analysis (24h post application of light)). Hence, a cell seeding density of 7000 cells/well in a 96-well plate was selected for future study.

Following selection of a cell seeding density, cell growth was also evaluated 120h post application of a potential stimulus to determine whether this cell seeding density could be used to demonstrate the effects of PBM over a longer time-course. Figure 4.2 provides evidence that cell growth does not plateau after 120h using a seeding density of 7000 cells/well. So, cell growth did not reach confluence and there is therefore potential for additional cell growth, possibly induced by light. Hence this seeding density was appropriate to evaluate the long term effects of PBM on cell growth *in vitro.*

Figure 4.3 shows a cell seeding density of 7000cells/well was appropriate for use in assays measuring changes in both cell metabolic activity (MTT) and mitochondrial activity (ROS). Where, relative ROS production and MTT absorbance is only significantly higher than the media control at cell seeding densities >5000cells/well indicating that at this seeding density changes in cell metabolic activity induced by stimuli can be reliably evaluated and background interference from media will not influence experimental output.

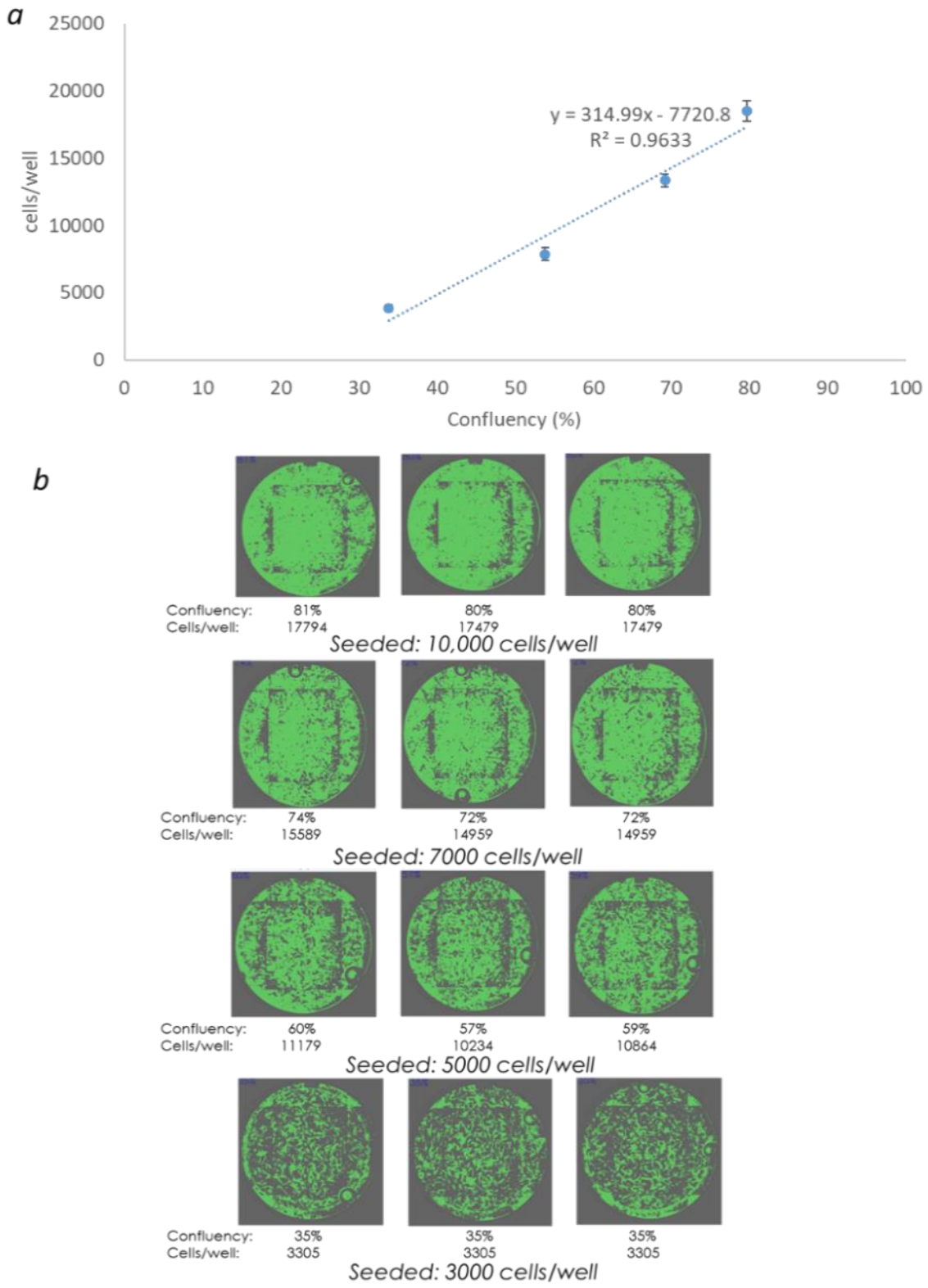

Figure 4.1a Calibration curve in which a range of concentrations of cells were seeded (10,000-3000 cells/well, n=6 per seeding density, pooled pHGF, p6) to determine whether cell seeding density correlated with cell confluency detected by the Tecan Spark® platform. Correlation analysis using the Pearson correlation coefficient was performed to confirm the linear relationship between correlation and confluency, $p<0.05$, Pearson correlation=0.961. Figure 1b shows representative images of well scans on the Tecan Spark® platform in which relative confluency of each well across a 96-well black clear bottom plate was determined, three representative images of each cell seeding density are shown.

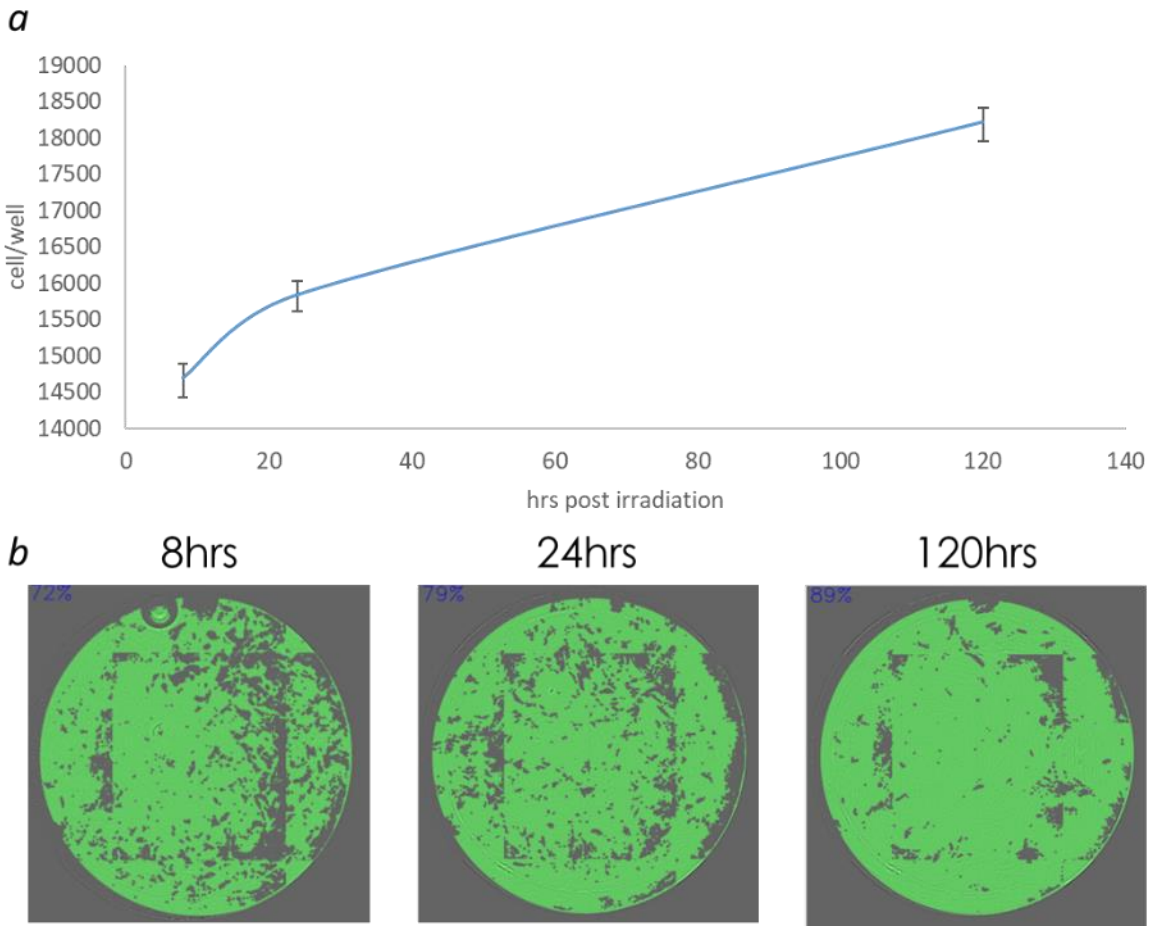

Figure 4.2a Growth curves for cells seeded at 7000 cells/well (pooled pHGFs, p6, n=18 (3 plates, 6 replicates per plate), incubated overnight and assessed 8, 24 and 120h post-application of a theoretical stimulus, no plateau in growth is evident at these time-points. Figure 2b shows representative images of well scans indicating cell confluency 8, 24, 120h post-application, from which cell number/well could be calculated.

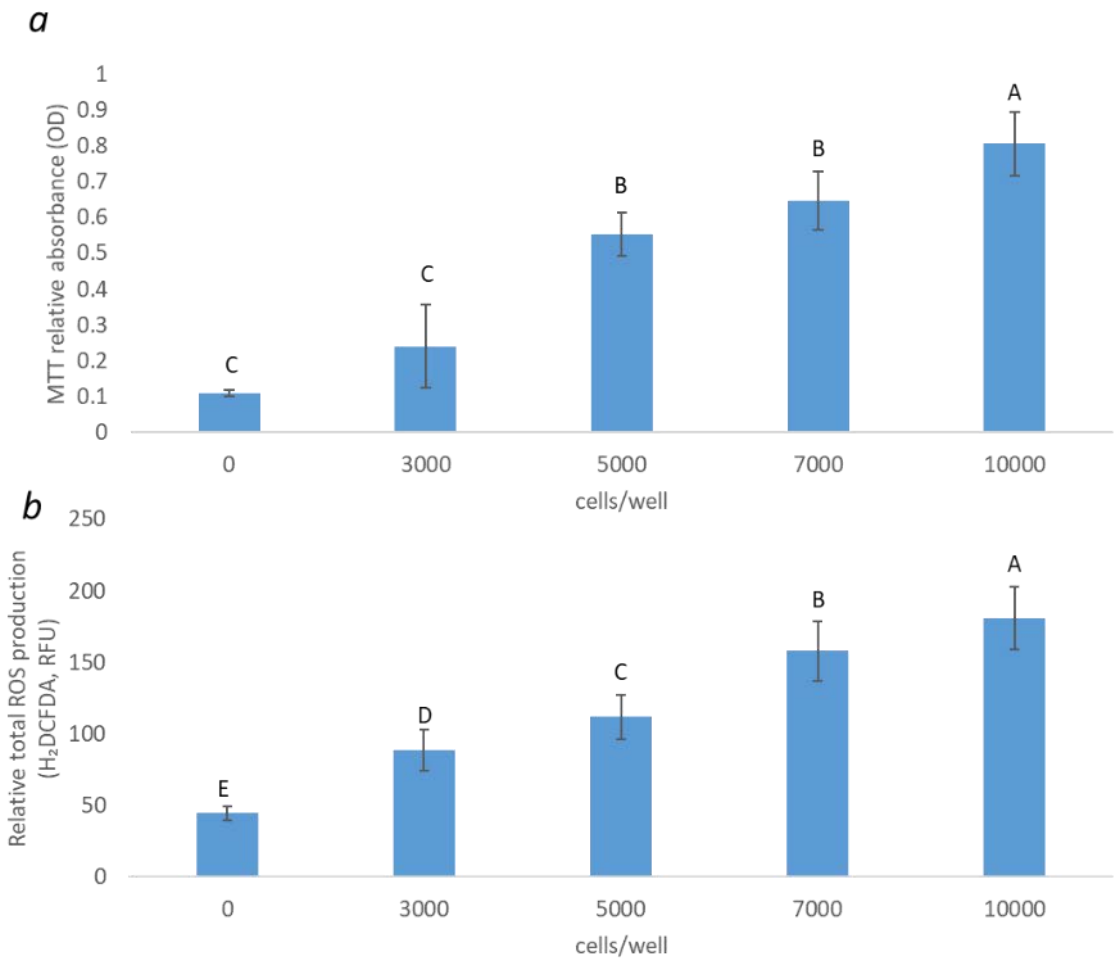

Figure 4.3a Relative absorbance values for MTT analysis at cell seeding densities ranging from 3000-10000 cells/well 24h post application of a theoretical stimulus (pHGF pool, p7, n=6 replicates per seeding density). 3b shows relative ROS production using H_2DCFDA probe analysis, where ROS production was evaluated at cell seeding densities ranging from 3000-10000cells/well 24h post application of stimulus (changed media, pHGF, pool p7, n=6 replicates per seeding density). Significance was assessed using one-way ANOVA followed by post-hoc Tukey test, where significant differences in means is indicated by different letters ($p<0.05$).

4.3 High-throughput assessment of PBM treatment parameters and cell culture conditions

Following selection of an appropriate cell seeding density, the effects of PBM *in vitro* were evaluated. This initially involved high-throughput screening of potential stimulatory treatment parameters at a range of wavelengths (400-830 nm) and irradiation periods (30s-240s, 0.72-5.76J/cm², 24mW/cm²). Parameters were selected based on review of the literature indicating therapeutic efficacy of PBM on pHGFs *in vitro* (Almeida-Lopes et al., 2001a, Azevedo et al., 2006, Basso et al., 2011, Basso et al., 2013a, Basso et al., 2015, Ogita et al., 2014). The influence of cell culture conditions on response to PBM was also evaluated in which the effects of cell seeding density and FBS concentration were assessed.

4.3.1 Results

Data provided evidence of the effects of PBM on cell metabolic activity and cell number. Results showed that irradiation at 400 nm and 450 nm for 240s induced the greatest (14.6% and 9.2% respectively) increases in MTT levels relative to the untreated control ($p<0.05$, see Figure 4.4). Hence, an irradiation period of 240s (24mW/cm², 5.76J/cm²) and wavelengths of 400 nm and 450 nm were selected for further study. A wavelength of 810 nm was also selected for further study, as although no significant increase in MTT was detected, this wavelength is commonly used when evaluating the effects of PBM *in vitro* and hence, this would enable comparison with the literature (Kharkwal et al., 2011, Sharma et al., 2011c, Usumez et al., 2014, Wang et al., 2017c, Wang et al., 2017b).

Following selection of exposure parameters, the effects of cell culture conditions on response to PBM were also evaluated. Figure 4.5 provides evidence that cells seeded at 7000 cells/well exhibited the greatest mean response to PBM where irradiation at 400 nm and 450

nm induced 16.6% and 9.6% increases in MTT relative to the untreated control ($p<0.001$). This supports the selection of the cell seeding density of 7000 cells/well as described in section 4.2.

To determine whether the parameters selected induced a significant increase in cell number as well as MTT levels, the Tecan Spark® platform was employed. Figure 4.6*b,* shows that whilst wavelengths of 450 nm and 810 nm induced mean increases in cell number relative to the control at all-time points, a significant increase was only induced by a wavelength of 450 nm 8h post irradiation ($p<0.05$). Further evaluation was then performed to determine to what extent FBS media concentrations influenced response to PBM *in vitro*.

Data presented in Figure 4.8 indicates that FBS concentration influenced responses to PBM, where the greatest mean response to PBM was exhibited by cells cultured in 5% FBS. This was evident at 24h post application for all wavelengths of light applied. However, Figure 4.8*c* shows data for culture of cells in 2% FBS and application of 400 nm light, where a 14.1% decrease in cell growth 8h post-irradiation relative to the non-irradiated control ($p<0.05$) was induced. These, effects were not significant following further incubation. Figure 4.7*b* also highlights the inhibitory effect of long term culture of cells in media containing no FBS due to lack of nutrition, where an average decrease in cell number of ~40% was observed at 24-144hr post-irradiation.

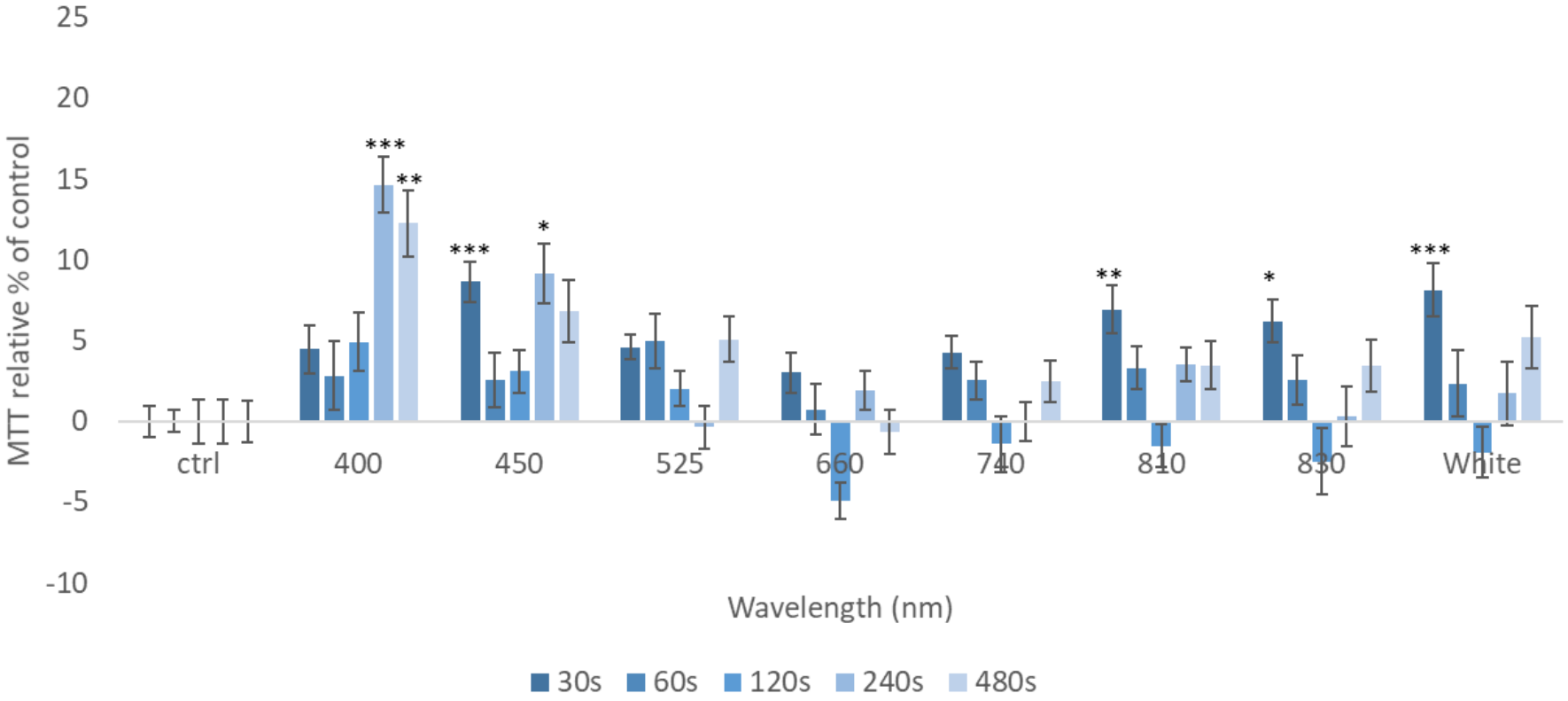

*Figure 4.4: High-throughput analysis of various wavelengths (400-830 nm) and irradiation periods (30-240s) on cell metabolic activity of pHGFs (pool p6-7, n=18 replicates, 6 replicates per plate) (24mW/cm², 0.72-5.76J/cm², 30-240s). Significance is indicated by ***=p<0.001, **=p<0.01, *=p<0.05 relative to the non-irradiated control, where all data is shown as a percentage of the non-irradiated control, where the non-irradiated control was normalised to 0%.*

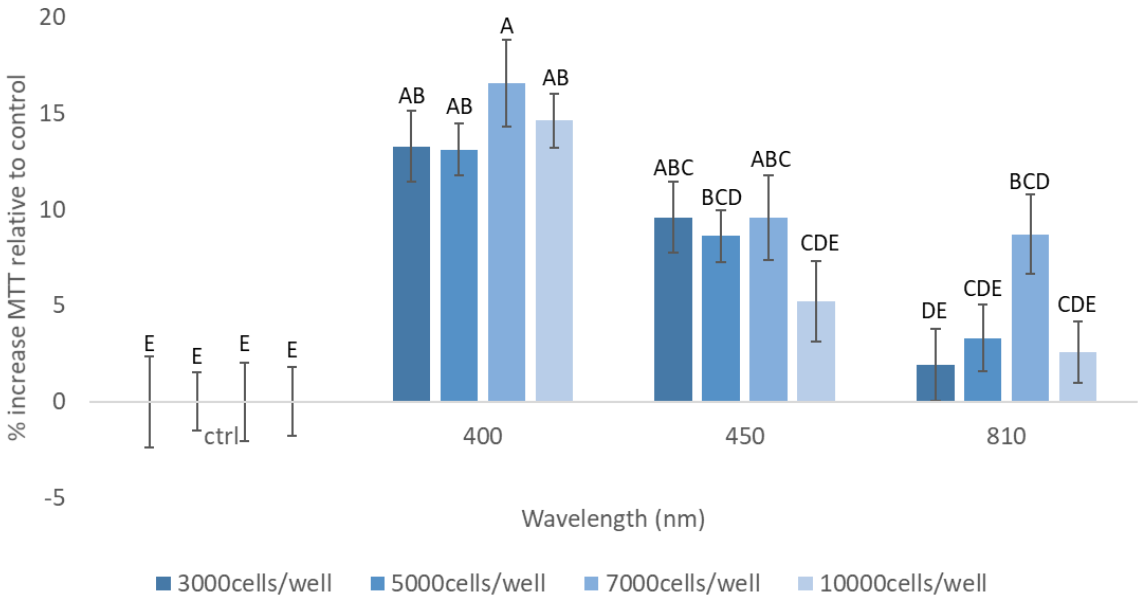

Figure 4.5 Cell seeding density effects on the response of cultures to PBM in which cells were seeded at 3000-10000 cells/well and incubated overnight (pool pHGFs, p7, n=18 per treatment condition and seeding density, 6 replicates per plate) subsequently cells were irradiated (240s, 24mW/cm², 5.76J/cm²) and incubated for a further 24h. Changes in metabolic activity were assessed using MTT and significance was evaluated using one way ANOVA followed by Tukey test. Means that do not share the same letter are significantly different ($p<0.05$).

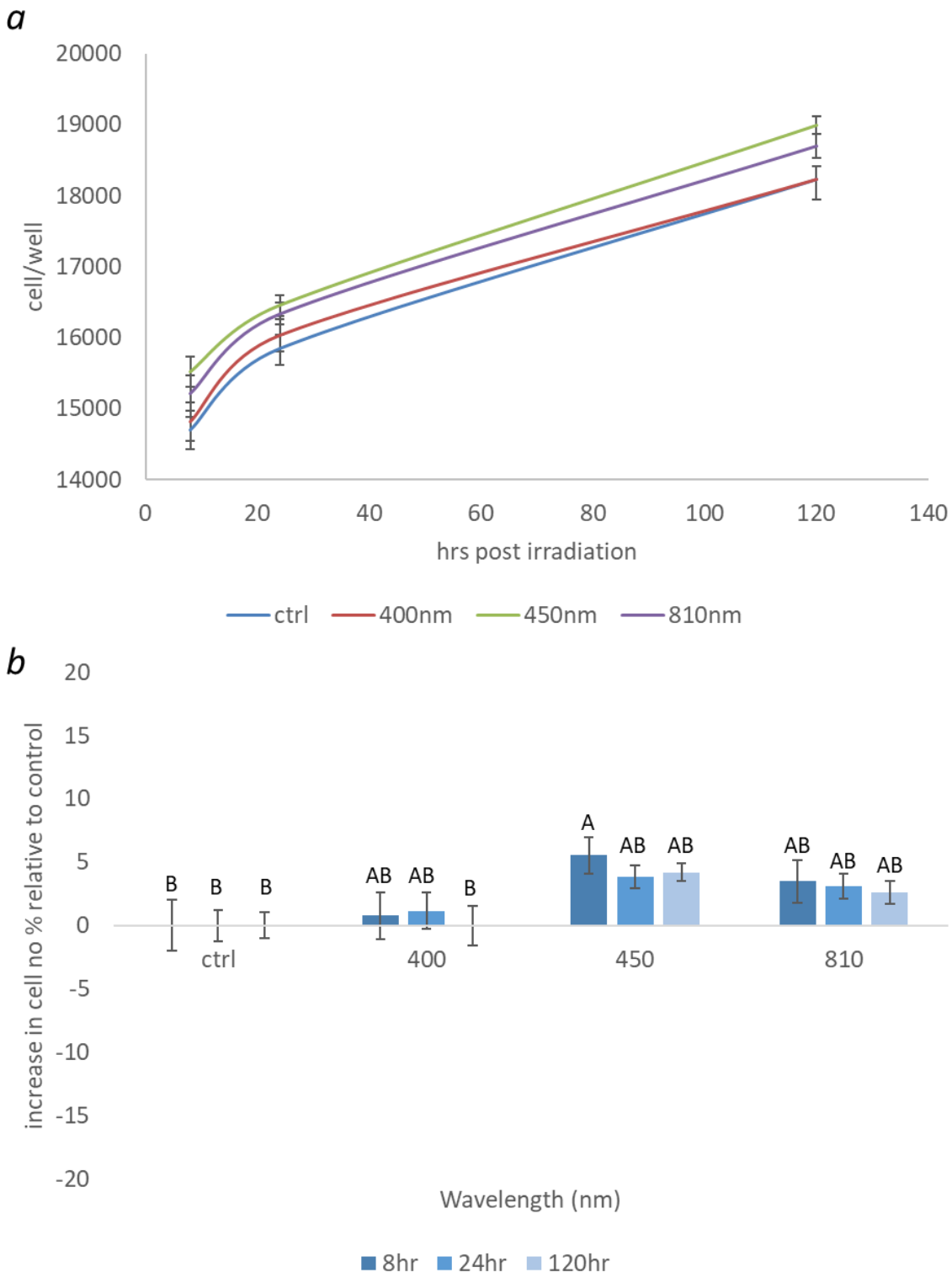

Figure 4.6 The effects of PBM on cell number, 8, 24 and 120h post-irradiation (24mW/cm², 240s, 5.76J/cm²). pHGFs were seeded at 7000 cells/well (pool, p7, n=18 per treatment condition, 6 replicates per plate), incubated overnight and subsequently irradiated the following morning. Changes in cell number were then analysed using the Tecan Spark® platform. Figure 6a shows cell growth curves over a 120h period for each treatment condition whilst b) shows % changes in cell number relative to the respective untreated control at each time point. Significance was measured using one-way ANOVA followed by Tukey test where means not sharing the same letter are significantly different ($p<0.05$).

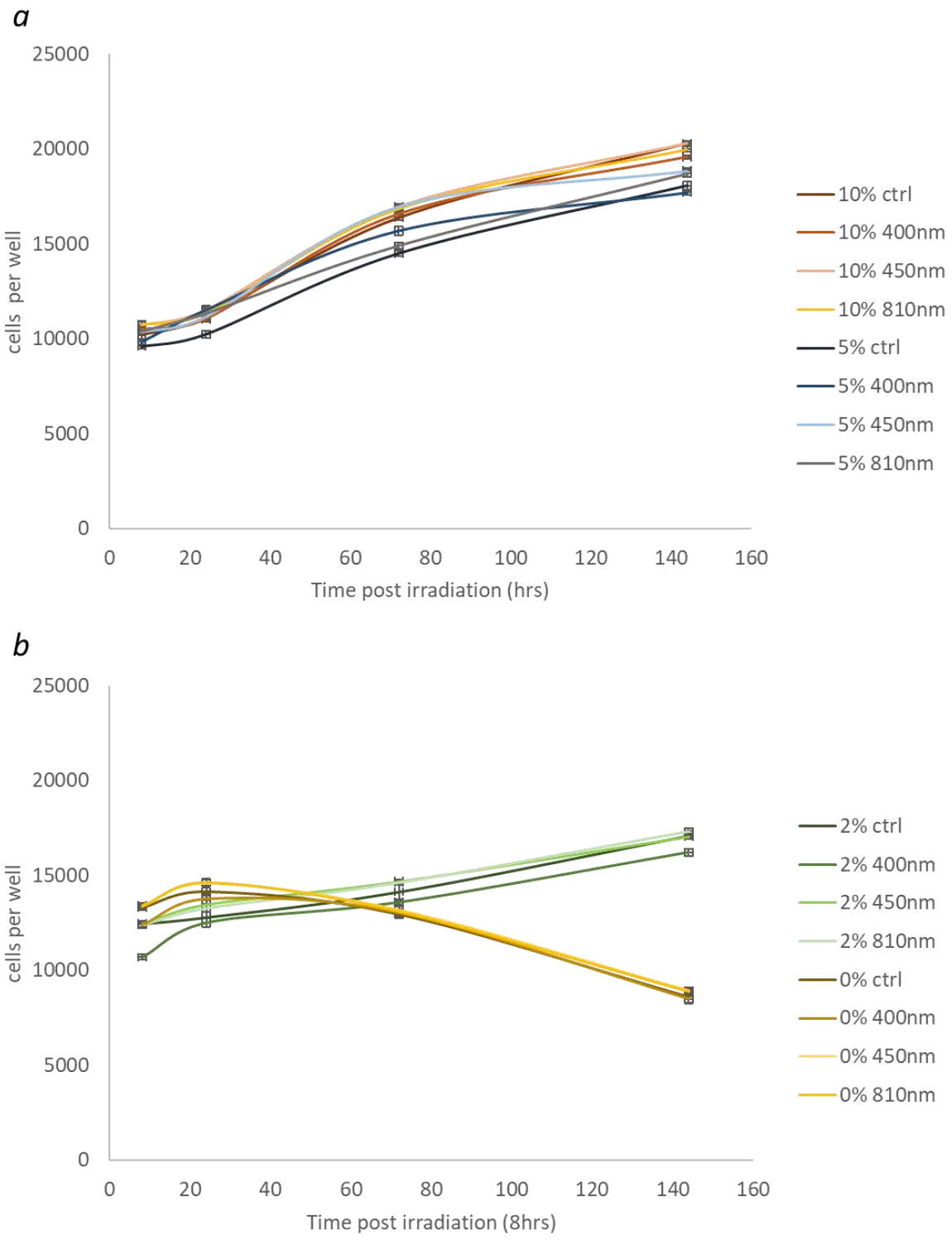

Figure 4.7 Cell growth curves for pHGFs seeded at 7000 cells/well (pool p7, n=18 replicates per treatment condition) and cultured in phenol red free media supplemented with 0-10% FBS, all cultures were incubated overnight and subsequently irradiated (400-810 nm, 240s, 24mW/cm², 5.76J/cm²). Changes in cell number were then assessed, 8, 24, 72 and 144hr post-irradiation. Figure 7a indicates changes in cell growth with cells treated with 10% or 5% FBS and 7b indicates changes in cell number when cultures were grown in 2% or 0% FBS.

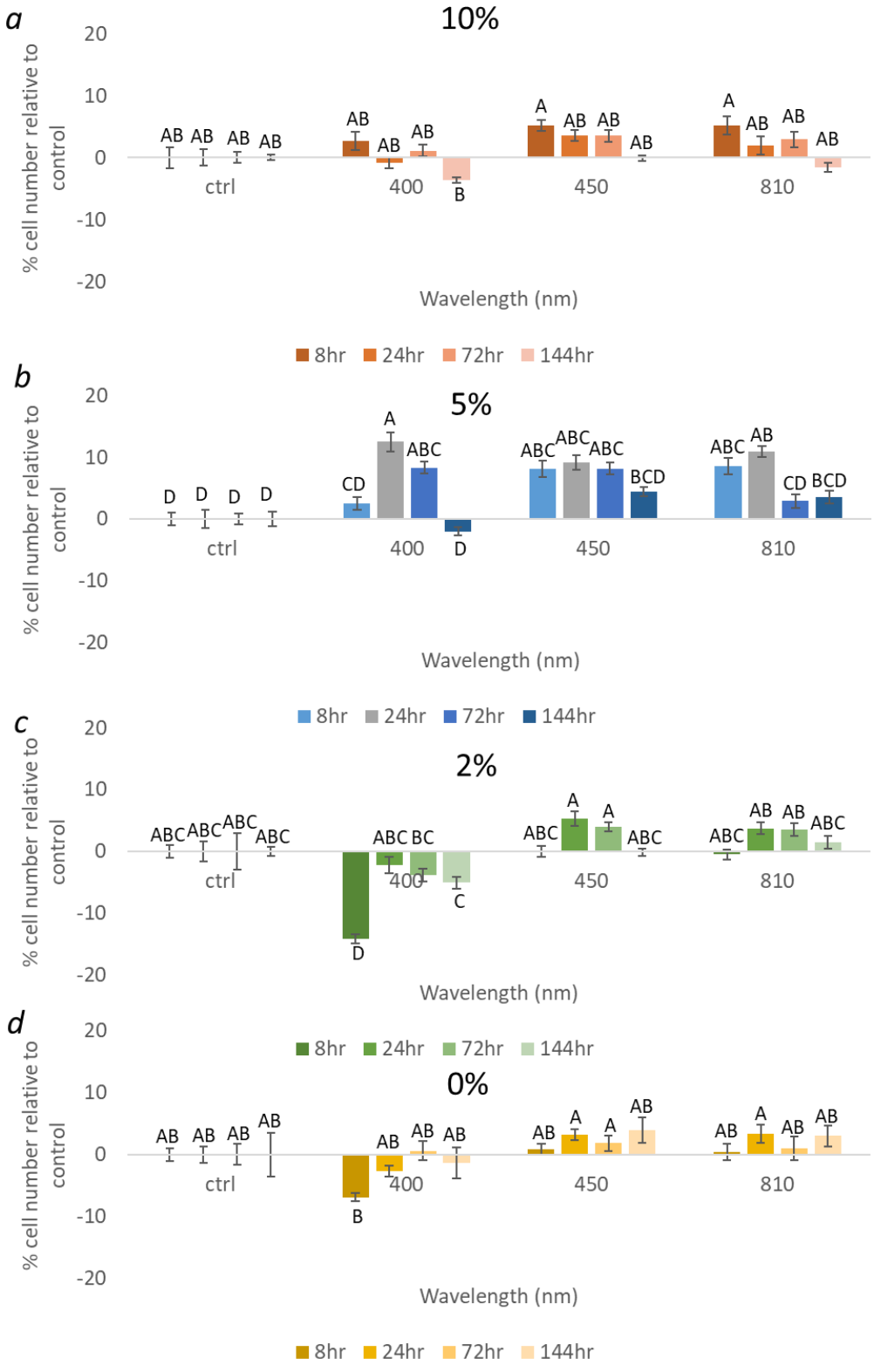

Figure 4.8 Percentage changes in cell number relative to each of the respective controls. Culture techniques are described in Figure 4.7 legend. Each figure indicates the effects of light on cultures grown in DMEM at concentrations of FBS varying from 0-10% where a) cultures were grown in 10% FBS, b) 5% FBS, c) 2% FBS and d) 0% FBS. Significance was assessed using one way ANOVA followed by Tukey test where means that do not the share the same letter are significantly different in each figure ($p<0.05$).

4.4 Effects of PBM on mitochondrial activity

Current indications suggest that PBM can modulate mitochondrial activity and this is the proposed mechanism by which PBM exerts its effects (Hamblin, 2018a, Karu, 2008). However, to date few studies have explored the possible effects of blue light PBM on mitochondrial activity (Buravlev et al., 2014a, Buravlev et al., 2015, Wang et al., 2017c). Hence, this section aimed to explore the effects of blue and NIR light on mitochondrial gene expression and assays evaluating the effects of PBM on markers of mitochondrial activity.

4.4.1 Results

Data captured provided evidence of the effects of PBM on mitochondrial activity. Firstly, the effects of PBM on the gene expression of subunits of complex IV and V (ATP synthase) of the ETC were examined. Irradiation at 810 nm induced 12.5% increases in complex IV subunit expression (Figure 4.9*a,* $p<0.001$) but significant decreases in complex V subunit expression (Figure 4.9*b, p<0.05*).

Subsequently, the effects of PBM on markers for mitochondrial relevant gene expression were evaluated. Blue light induced the greatest changes in markers of mitochondrial activity. Where, 400 nm light application induced 21.0% and 27.2% increases in ATP levels *(*Figure 4.10) and ROS *(*Figure 4.13*a)* production respectively ($p<0.05$) compared with the controls. Blue light application also induced significant increases in Nitrite production (Figure 4.12*a*, $p<0.05$). Irradiation at 400 nm also induced the greatest mean change in mitochondrial membrane potential (Figure 4.11*b*). However, this was not statistically significant relative to the untreated control.

Interestingly, application of 400 nm and 450 nm light induced 32.6% and 43.1% decreases in antioxidant capacity (Figure 4.13*b*, $p<0.05$) respectively. Whilst 810 nm light

application induced mean increases in markers for mitochondrial activity, these were not significant. These data are in agreement with those reported in section 4.3.1, where application of 810 nm for 240s induced no statistically significant effect on MTT activity.

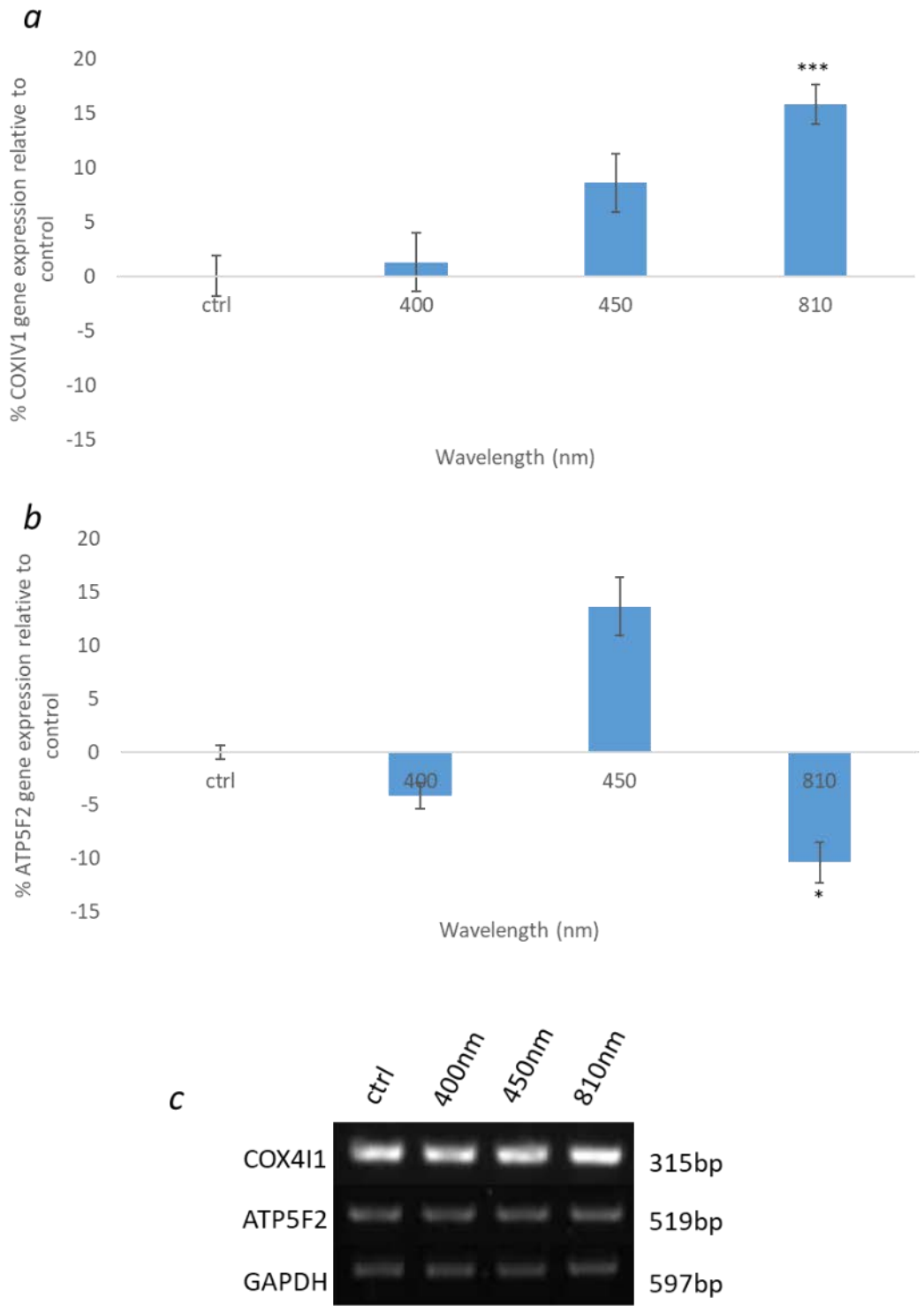

*Figure 4.9 The effects of PBM (400-810 nm, 5.76J/cm², and 24mW/cm²) on the gene expression of components of the electron transport chain 24h post-irradiation. RNA was collected (n=30 wells) for each treatment condition (5 plates, pHGF pool p6) studies were repeated in triplicate. a) illustrates the effects of PBM on cytochrome c oxidase subunit IV expression (COX4I1) and b) evaluates the effects on ATP synthase subunit F2. c) provides representative images of gels for gene expression analysis. All results were normalised to GAPDH expression. Significance relative to the untreated control was evaluated using one was ANOVA followed by Tukey test where significance is indicated by ***=p<0.001, **=p<0.01 and *=p<0.05.*

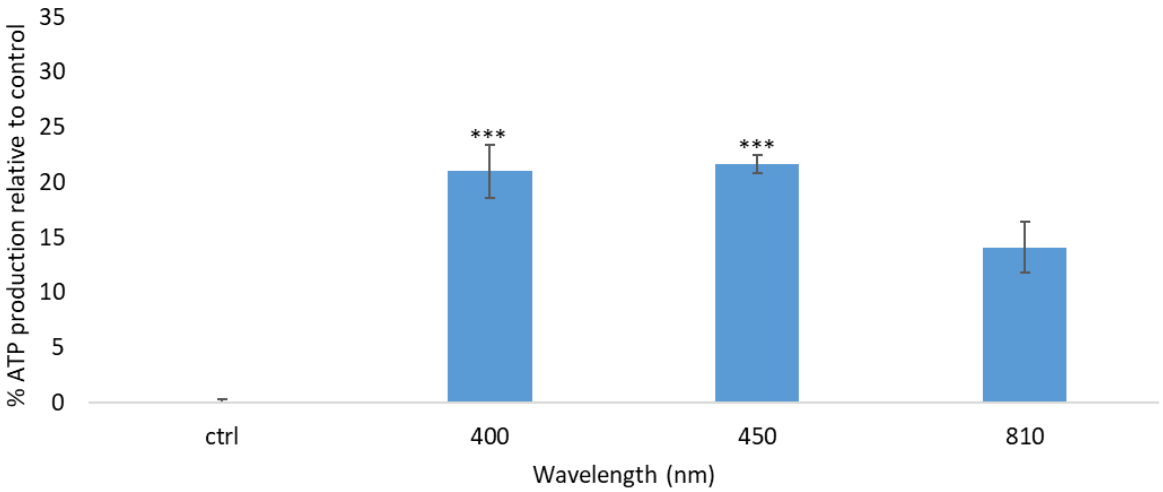

*Figure 4.10 Percentage changes in ATP production induced by light (400-810 nm, 5.76J/cm², 24mW/cm²), 24h post- irradiation for pHGFs (pool p6-7, n=12, 4 replicates per repeat). Significance was determined using one way ANOVA followed by Tukey test where significance is indicated by ***=p<0.001 relative to the untreated control.*

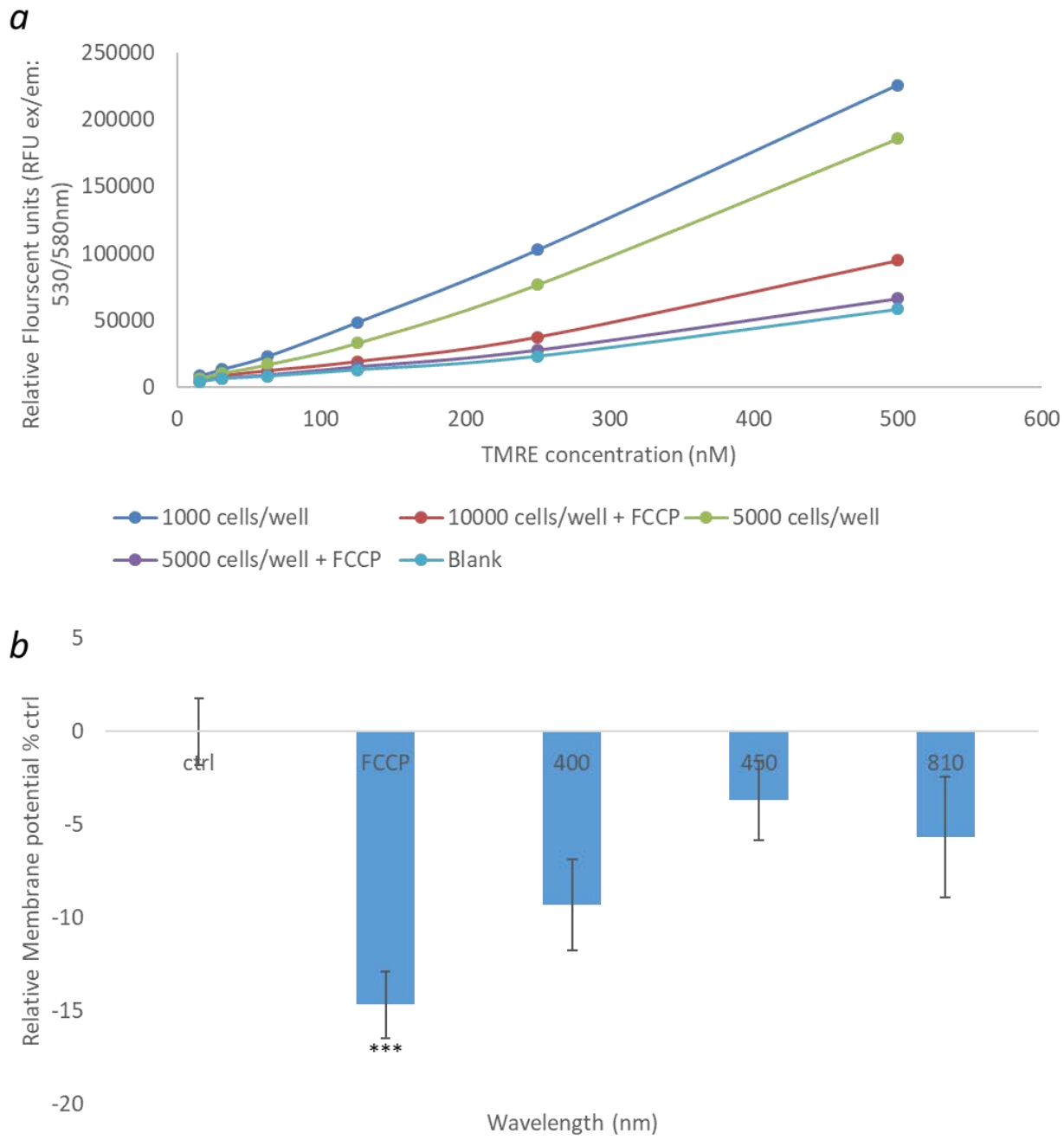

*Figure 4.11a Assay evaluating mitochondrial membrane potential (see section 2.2.11.2 for assay details) involving analysis of cell seeding density, TMRE concentration and FCCP concentration (an uncoupling agent that enables oxidative phosphorylation and therefore allowing membrane depolarisation to occur at a maximal rate, acted as a positive control). These analyses therefore provided evidence that a seeding density between 10000 to 5000 cells/well was sufficient to demonstrate the effects of PBM on mitochondrial membrane potential. Hence a seeding density of 7000 cells/well was selected. Figure 11b demonstrates the effects of FCCP (10µM) or light application (400-810 nm, 24mW/cm², 5.76J/cm²) on mitochondrial membrane potential (pHGF pool p7, n=12) 24h post-irradiation. Significance was assessed using one-way ANOVA followed by Tukey test where significance is indicated by ***=p<0.001 relative to the non-irradiated control.*

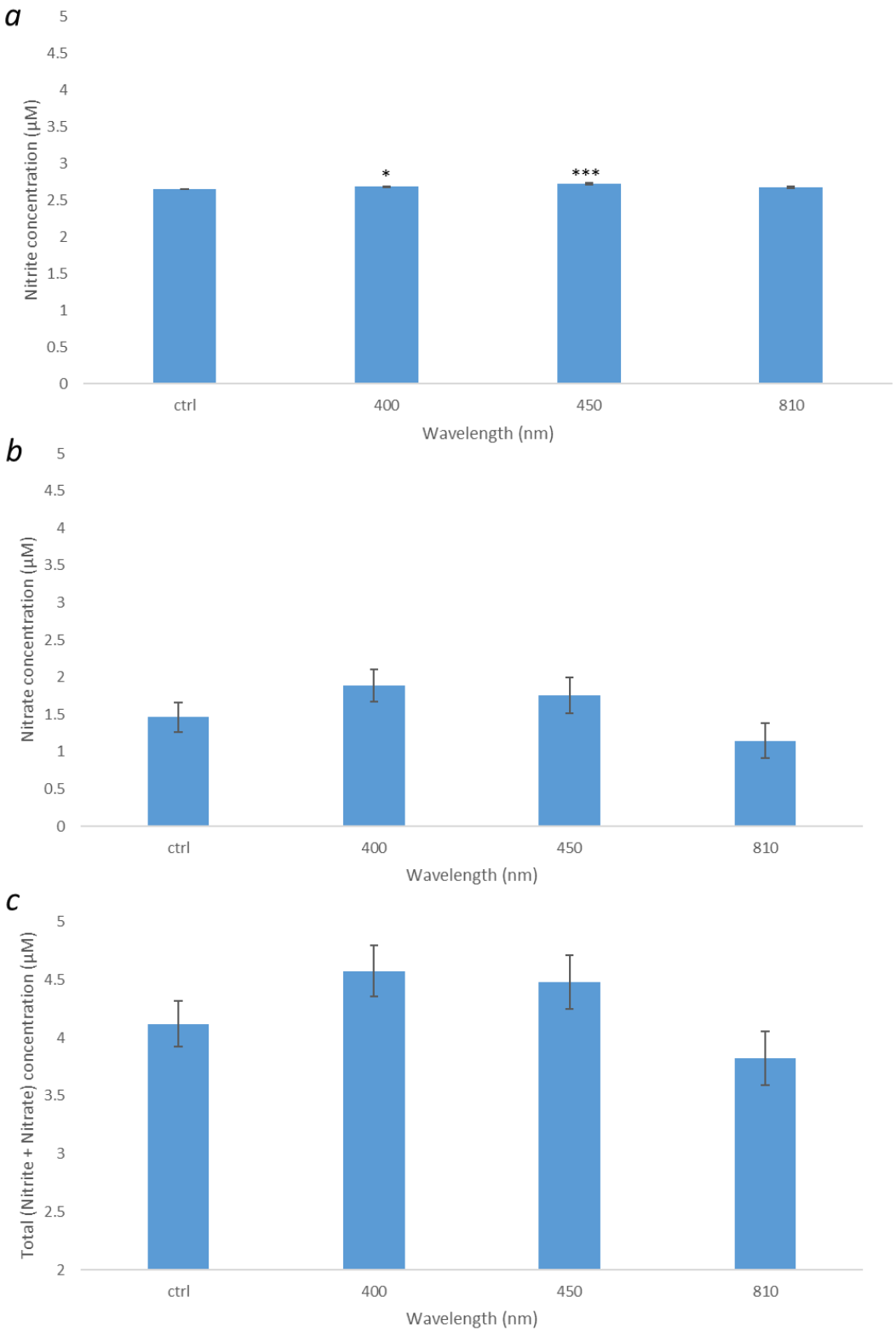

*Figure 4.12 The effects of PBM on a) nitrite secretion, b) nitrate secretion and c) total nitrate and nitrite production. Effects were assessed 24h post-irradiation (400-810 nm, 240s, 5.76J/cm², pHGF pool p7, n=4 per treatment condition, where each replicate was the result of pooling 3 supernatant samples). Significance was assessed using one-way ANOVA followed by Tukey test where significance is indicated by ***=p<0.001, *=p<0.05 relative to the non-irradiated control. See section 9.3 for nitrite/nitrate standard curves.*

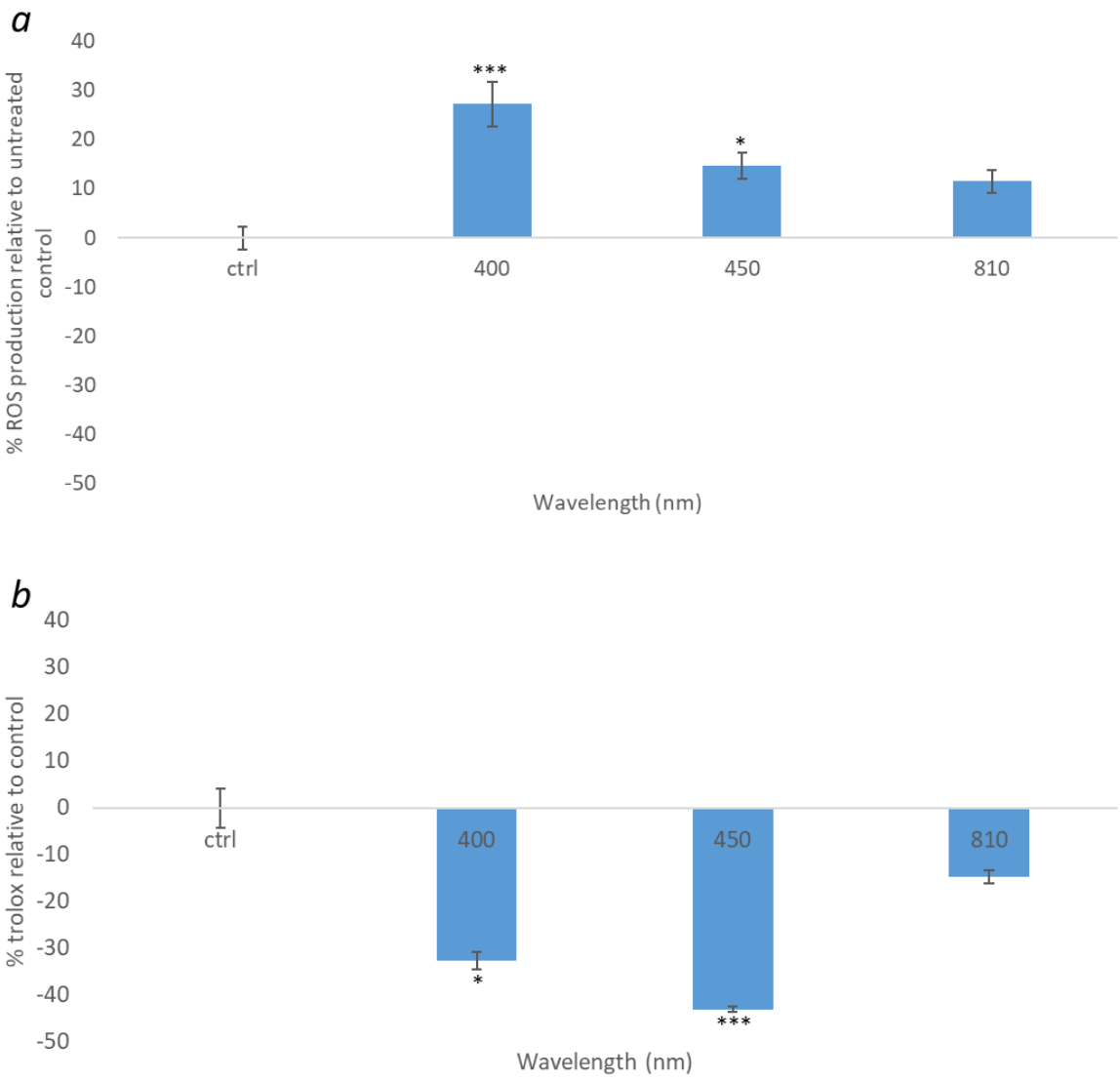

*Figure 4.13a the effects of PBM on ROS production 24h post-irradiation (pHGF pool, p5-7, n=18, 400-810n nm, 24mW/cm², 5.76J/cm²). Figure 13b indicates the effects of light irradiation on antioxidant capacity (pHGF pool p6-7, n=4 where each replicate is produced from pooling 6 cell supernatant samples, 400-810 nm, 24mW/cm², 5.76J/cm²) using the Trolox assay. Significance was assessed using one-way ANOVA followed by Tukey test where significance is indicated by ***=p<0.001, **=p<0.01 and *=p<0.05 relative to the untreated control.*

4.5 Effects of PBM on gene expression and downstream signalling markers

Following examination of the effects of PBM on mitochondrial activity (4.4), the effects of light on downstream signalling markers were assessed. In particular, those pathways modulated by ROS production were explored, where it is hypothesised that changes in ROS production are fundamental to inducing the effects of PBM exhibited *in vivo* (Hamblin, 2017, Hamblin, 2018a).

4.5.1 Results

Application of 450 nm light induced 12.5% increases in NFkB gene expression (Figure 4.14*a,* $p<0.001$) but 15.2% decreases in Glutathione Synthetase expression (GSH-S, Figure 4.14*b,* $p<0.01$*).* Interestingly these data are in agreement with those discussed in section 4.4.1. Where, it was reported that blue light induced significant increases in ROS production and that NFkB expression is modulated by cellular ROS levels (Morgan and Liu, 2011). Similarly, Figure 4.14*b* shows that 450 nm light application significantly reduced antioxidant capacity in cell supernatants and these data suggest that PBM could also alter antioxidant relevant gene expression (GSH-S). However, assays of a higher sensitivity may be required to evaluate this further.

The application of 400 nm light also induced 15.5% increases in cyclooxygenase-2 (COX2) gene expression relative to the untreated control. COX2 is a signalling molecule whose expression has been cited to be upregulated by mitochondrial ROS generation ($p<0.05$, Figure 4.14*c* (Kiritoshi et al., 2003)).

Another key signalling pathway regulated by ROS is the TGFβ pathway. Application of 400 nm or 450 nm light induced 24.3% and 59.9% decreases in TGFβR1 gene expression respectively ($p<0.001$, Figure 4.15*a*). Irradiation at 400 nm or 450 nm also resulted in 13.6%

and 14.0% decreases in TGFβ1 secretion ($p<0.01$, Figure 4.15*b*). Hence, data indicates that application of blue light can modulate both TGFβR1 gene expression and TGFß1 secretion.

The effects of PBM on IL-8 expression and secretion were subsequently evaluated, a cytokine whose expression is directly regulated by NFkB activation (Yoshida et al., 1998). Figure 4.16 provides evidence that application of 450 nm light induced 75.6% increases in IL-8 gene expression and 7.9% increases in IL-8 secretion ($p<0.001$).

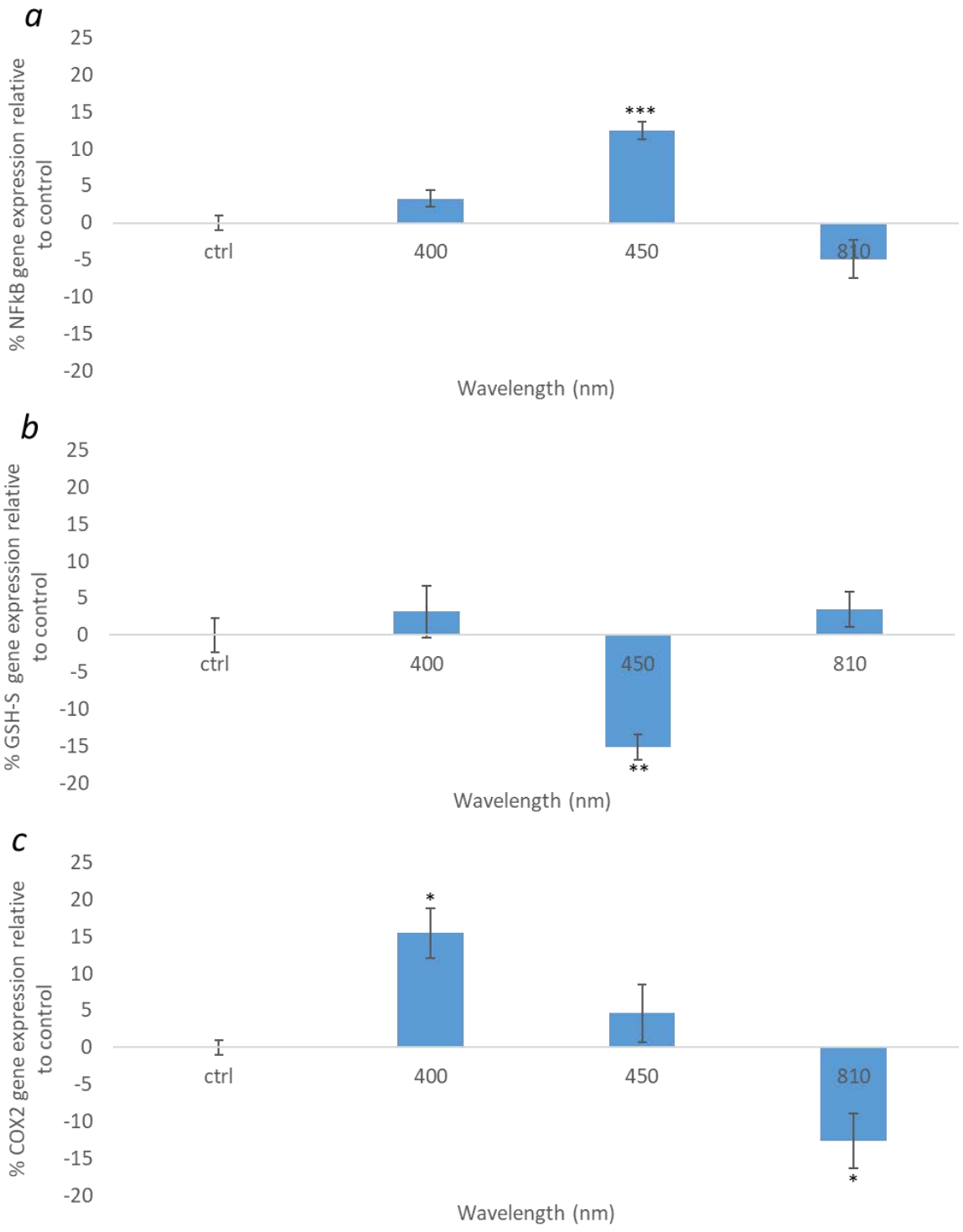

*Figure 4.14 Effects of PBM on gene expression of a) NFkB, b) Glutathione Synthetase (GSH-S) and c) Cycloxygenase-2(COX2) where gene expression from pHGFs (pool p7, n=6) was evaluated 24h post-irradiation. One-way ANOVA followed by Tukey test was used to measure statistical significance. Where, significance is indicated by ***=p<0.001, **=p<0.01 and *=p<0.05 relative to the non-irradiated control.*

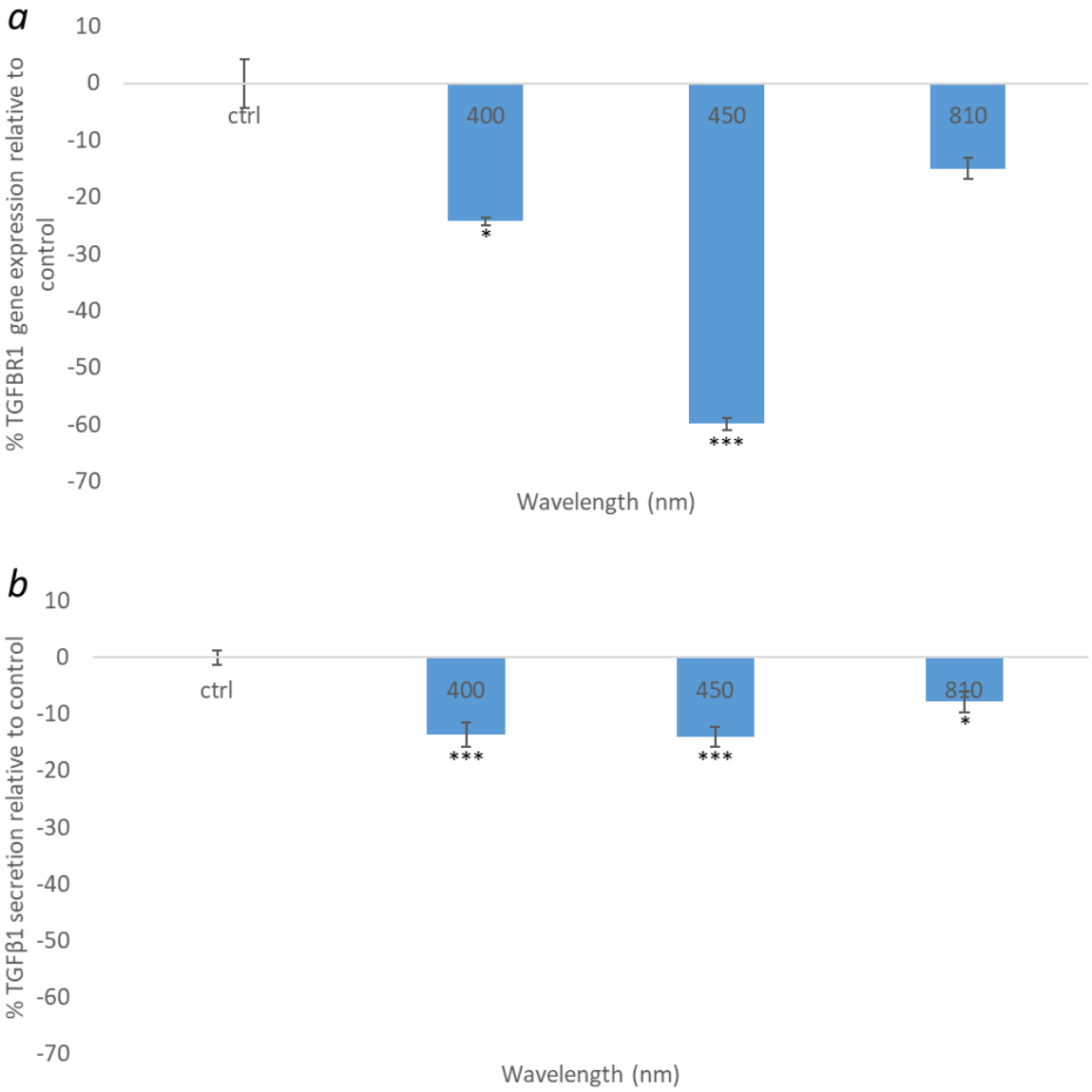

*Figure 4.15 Effects of PBM on a) TGFβR1 gene expression (n=6) and b) TGFβ secretion (n=12). Where, the effects of PBM on pHGFs (pool p7, 400-810 nm, 24mW/cm², and 5.76J/cm²) were assessed 24h post-irradiation. Significance was measured using one-way ANOVA followed by Tukey test where significance is indicated by ***=p<0.001, **=p<0.01, *=p<0.05 relative to the non-irradiated control.*

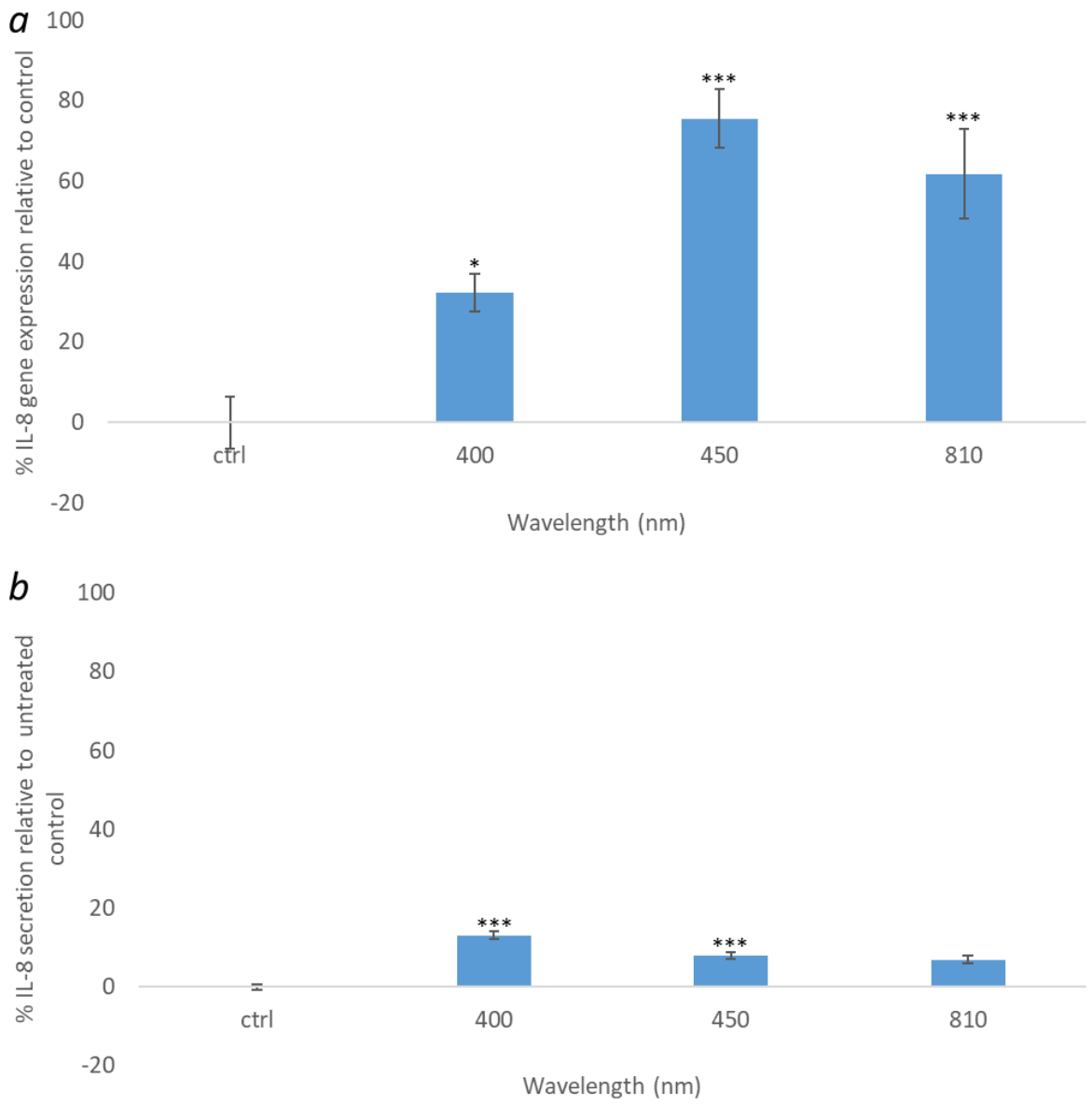

*Figure 4.16 The effects of PBM on IL-8 a) gene expression (n=6) and b) secretion (n=12). Where, the effects of PBM on pHGFs (pool p6/7, 400-810 nm, 24mW/cm², and 5.76J/cm²) were assessed 24h post irradiation. Significance was measured using one-way ANOVA followed by Tukey test where significance is indicated by ***=p<0.001, **=p<0.01, *=p<0.05 relative to the non-irradiated control.*

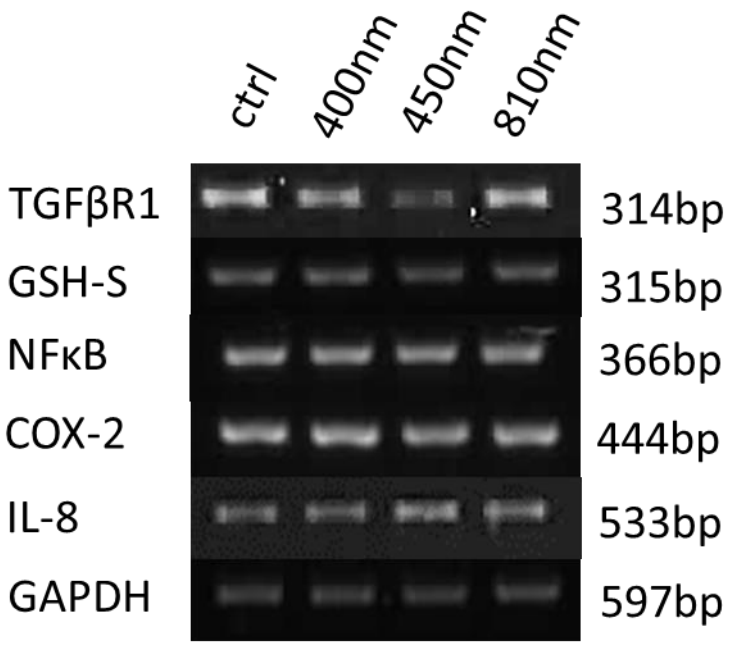

Figure 4.17: Representative PCR images of TGFβR1, GSH-S, NFkB, COX-2, IL-8 and GAPDH (control) expression from pool pHGFs either untreated or treated with 400-810 nm irradiation. All gene expression was normalised against GAPDH expression.

4.6 The effects of simultaneous application of multiple wavelengths on markers of mitochondrial activity

Studies were performed to determine the effects of combining multiple wavelengths on PBM of oral fibroblasts. The LUMOS™ stimulation suite was employed to determine whether combining both blue and NIR light could influence markers for mitochondrial activity *in vitro*. These parameters were selected for combination as data outlined in sections 4.4.1 and 4.5.1 suggests application of either blue or NIR light are capable of modulating cellular activity *in vitro*. However, blue light has been shown to have a much lower tissue penetration depth than NIR light *in vivo* (Ash et al., 2017). Hence, it is hypothesised that combination of these parameters may improve tissular response to PBM, by improving the total surface area of tissue exposed to light (Avci et al., 2013). However, prior to application *in vivo* this project aimed to establish to what extent the combination of these parameters at the same average irradiance output (24mW/cm^2), could modulate cellular activity.

4.6.1 Results

Results show that combining blue and NIR light had no significant effect on experimental outcomes relative to irradiation at 405 nm or 850 nm alone. Only application of 405 nm light induced significant increases in MTT levels (Figure 4.18a) but with no significant effect on ROS production (Figure 4.18b).

Interestingly, application of both 405 nm and 850 nm light or just 850 nm induced 42.6% and 43.9% increases in IL-8 secretion respectively ($p<0.001$). These data may suggest application of multiple wavelengths simultaneously may induce significant effects on markers

for inflammation. However, these are not significantly different to those induced by single wavelength application.

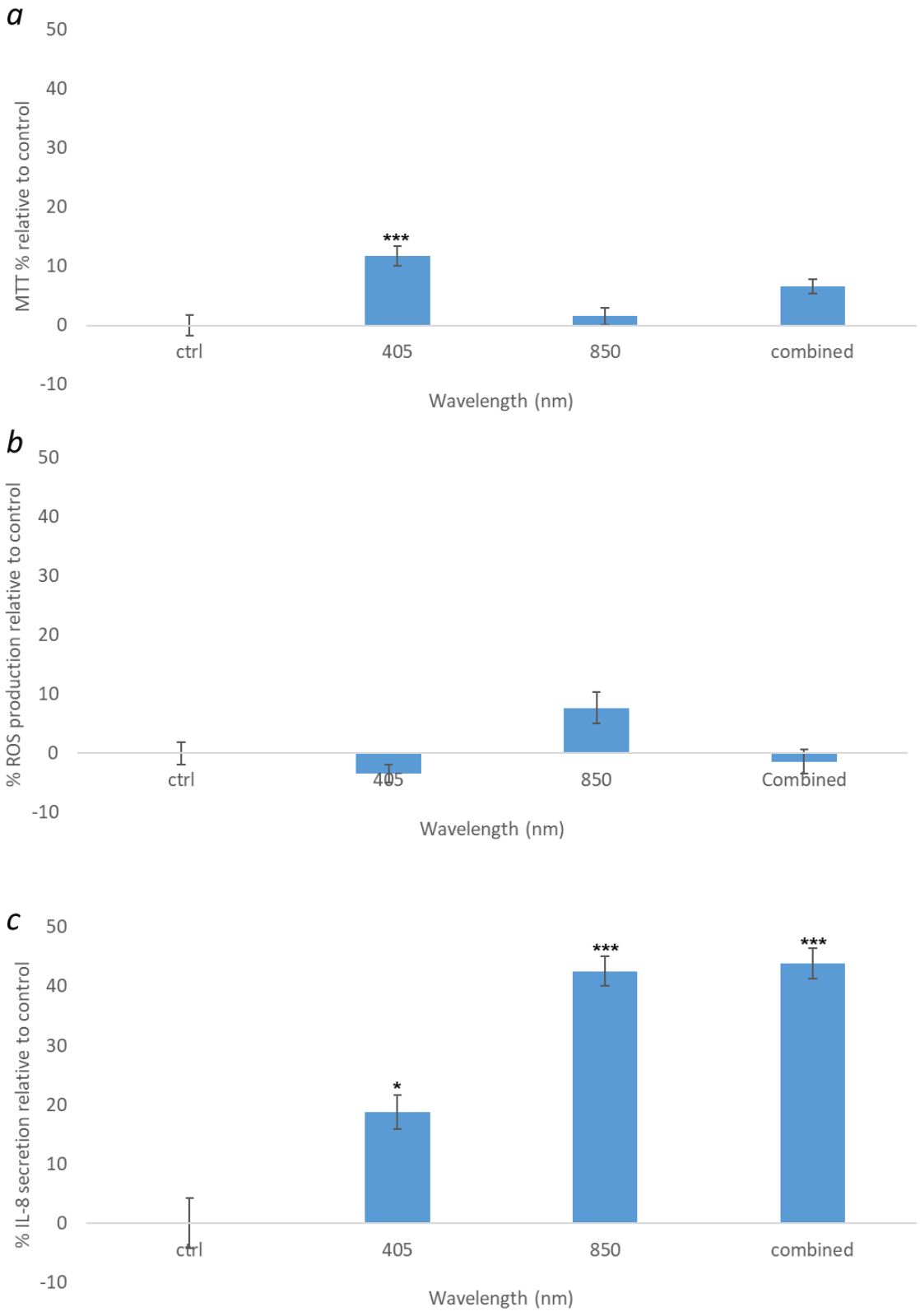

*Figure 4.18 The effects of 405 nm or 850 nm or both (24mW/cm², 5.76J/cm²) on a) MTT (n=18), b) ROS (n=18) production and c) IL-8 secretion (n=12) from pHGFs (pool p7) 24h post-irradiation. Significance was assessed using one-way ANOVA followed by Tukey test where significance is indicated by ***=p<0.001, **=p<0.01 and *=p<0.05 relative to the untreated control.*

4.7 Discussion

4.7.1 Determining seeding densities for in vitro application

Data demonstrates a cell seeding density of 7000 cells/well was appropriate for the evaluation of PBM *in vitro*. It is shown that the selected seeding density enables evaluation of the effects of PBM at cell confluency levels relevant to current publications (70-90% (Cheon et al., 2013, Amid et al., 2014, Chen et al., 2009a, Rohringer et al., 2017)). High levels of confluency (90-100%) may cause contact inhibition between fibroblasts, inducing different signalling pathways to those activated by PBM and thus masking the potential effects of light *in vitro* (Wayne et al., 2006). Higher seeding densities may also increase competition for nutrients and limit the potential for expansion of cell numbers. Interestingly, Figure 4.2 provides evidence that pHGFs did not reach confluence following 120h incubation. Hence, a seeding density of 7000 cells/well was appropriate for evaluating the long term response of pHGFs to PBM *in vitro*.

Data generated also provided evidence that a cell seeding density of 7000 cells/well was suitable for use in biological assays employed throughout this thesis (Figure 4.3). Notably, a cell seeding density of 7000 cells/well was also used by *Gomez-Florit et al* to explore the effects of ROS production from pHGFs following application of pro-inflammatory stimuli (Gomez-Florit et al., 2014).

4.7.2 High-throughput assessment of PBM parameters and cell culture conditions

Following selection of an appropriate cell seeding density, high-throughput assessment of PBM parameters were performed. Figure 4.4 demonstrates application of 400 nm or 450 nm light for 240s induced the greatest increases in cell metabolic activity relative to the untreated control ($p<0.05$). Therefore, these parameters were selected for further analyses. Interestingly, wavelengths commonly used in PBM studies within the red spectra (660-740 nm) induced little or no significant effect on cell metabolic activity relative to the untreated control in the present study (Azevedo et al., 2006, Damante et al., 2009, Almeida-Lopes et al., 2001a, Basso et al., 2011, Basso et al., 2013a). This may reflect a differential biphasic dose response exhibited by different wavelengths of light whereby shorter or longer periods of irradiation could induce significant biological responses dependent upon the wavelength applied (Hamblin et al., 2011). Hence, future work will endeavour to evaluate the effects of red light over a wider range of irradiation periods.

Application of NIR light (810-830 nm) for 30s also induced significant increases in cell metabolic activity. Interestingly, irradiation of fibroblast cultures with NIR light at 5-7J/cm² have been shown to modulate cellular signalling *in vitro* (Kreisler et al., 2002, Kreisler et al., 2003, Sakurai et al., 2000, Takema et al., 2000). Therefore, a wavelength of 810 nm and irradiation period of 240s (5.76J/cm²) was also selected for further evaluation and to enable comparison with current literature. Subsequent to selection of treatment parameters, the influence of cell culture conditions on response to PBM were evaluated. Data demonstrated mean responses to light application was greatest at a cell seeding density of 7000cells/well (Figure 4.5), however, application of 400-450 nm light induced significant increases in cell metabolic activity at all cell seeding densities studied (3000-10000 cells/well, $p<0.05$). Hence,

whilst a seeding density of 7000 cells/well exhibits the optimal response to PBM, other cell seeding densities could be employed to evaluate the effects of PBM *in vitro*.

In addition, it was found that FBS concentration could influence response to PBM whereby irradiation at 400 nm induced decreases in cells cultured in 2-0% FBS *(*Figure 4.7*).* Similarly, *Mignon et al* reported that serum concentration could dramatically influence the inhibitory effects of blue light (450 nm, 60J/cm²) on cell proliferation. Notably, the inhibitory effects of blue light were significantly higher in cells cultured in 2% FBS compared with 10% FBS (60% reduction low serum vs 40% reduction high serum (Mignon et al., 2017)). Interestingly, PBM induced the greatest increases in cell number from cells cultured in 5% FBS compared with those cultured in 10% FBS. These data are in agreement with current literature which report the effects of PBM on stressed tissue, where cell growth is restricted (Adamskaya et al., 2011, Al-Watban et al., 2009, Basso et al., 2012b, Basso et al., 2016b). Notably culture of fibroblasts in 5% FBS has been shown to induce reductions in cell proliferation relative to cells cultured in 10% FBS (Urban et al., 2012).

The results presented indicate the parameters for cell culture and the PBM dependent response *in vitro*. These data may provide some clarity as to the variability in response to PBM, where a number of variables can interact to influence biological response to light.

4.7.3 The effects of PBM on markers for mitochondrial activity

Studies have illustrated the effects of PBM on markers for mitochondrial activity including ROS (Alexsandra da Silva Neto Trajano et al., 2016) and ATP (Ferraresi et al., 2015a). However, few studies have reported the effects of blue light PBM on markers for mitochondrial activity. Data presented here provides evidence that blue light (400-450 nm) modulates markers for mitochondrial activity including ROS, ATP and nitrite levels ($p<0.05$). Whilst application of 810 nm light, a wavelength commonly used in PBM studies exerted no significant effect on markers of mitochondrial activity.

Kushibiki et al also explored the effects of both blue light (405 nm) and NIR light (808 nm) on ROS production from a range of cell types and found only blue light induced significant increases in ROS production (Kushibiki et al., 2013). Hence, these data support findings illustrated here where only blue light induced significant increases in ROS production (Figure 4.13*a*). *Sharma et al* also explored the dose dependent effect of 810 nm light application on ROS production from primary cortical neurons (Sharma et al., 2011a). The author concluded that whilst a dose of 3J/cm² induced significant increase in ROS production, a dose of 10J/cm² resulted in no significant change in ROS production. Hence, the dose used in the present study (5.76J/cm²) may be outside the therapeutic range for induction of ROS production using NIR light.

Furthermore, *Burvalev et al* evaluated the effects of blue laser light (442 nm) compared with green laser (532 nm) or red LED (650 nm) on photo activation of ETC complexes inhibited by NO (Buravlev et al., 2015). The authors concluded that only blue light was capable of partial recovery of complex IV activity. Data demonstrated here indicated that only application of 810 nm light induced significant increases in gene expression of a subunit

of complex IV *(*Figure 4.9*).* Hence, future work will be required to determine to what extent blue light application modulates mitochondrial gene expression.

The application of blue light PBM also induced significant increases in nitrite secretion ($P<0.05$) and mean increases in nitrate secretion *(*Figure 4.12*).* Interestingly, whilst the photodissociation theory of PBM has considerable support (4.1), a growing body of evidence has been accumulating indicating that complex IV can act as a nitrate reductase, providing a second pathway to induce increases in circulating levels of NO (Ball et al., 2011a). Blue light has also been cited to induce the release of NO from photo liable sources of NO including S-nitrosthiols (RSNO) and nitrosyl myoglobin (Oplander et al., 2013). However, whilst data reported in Figure 4.12 indicates blue light significantly increases nitrite secretion, the percentage increase is marginal (~2%). This may be due to the relatively poor sensitivity of the Griess assay used to evaluate this (Hunter et al., 2013). Hence, alternative assays such as fluorometric assays may be required as they exhibit a sensitivity lower than 500 nm hence enabling significant differences between treatment conditions to be detected (Csonka et al., 2015).

Therefore, combined these data provide evidence that blue light is an effective modality in modulating markers for mitochondrial activity.

4.7.4 Downstream signalling effects of PBM

The downstream effects of PBM are cited to be modulated by ROS production (Chen et al., 2009b, Hamblin, 2017). Therefore, a series of signalling molecules modulated by both ROS and PBM were evaluated including NFkB (Gloire et al., 2006, Chen et al., 2011c), GSH-S (Aquilano et al., 2014, Asghari et al., 2016), COX2 (Onodera et al., 2015, Prianti Jr et al., 2014) and TGFβ (Liu and Desai, 2015, Arany et al., 2007).

Gene expression studies revealed application of 450 nm light induced significant increases in NFkB expression ($p<0.05$, Figure 4.14*a*). Interestingly, the effects of PBM on NFkB activity have only been studied utilising either red or NIR light (Curra et al., 2015, Chen et al., 2011a). In previous reports, *Chen et al* explored the effects of 810 nm light application on NFkB activation and concluded that a dose of 0.3J/cm² was sufficient to induce maximal increases in activation (Chen et al., 2011a). Similar to the findings presented here, the authors concluded that there was no significant change in NFkB activation 24h post application of PBM. Indeed the peak at which changes were detected was 6h post application. Hence, future studies may endeavour to evaluate the effects of 810 nm light at lower doses, notably it has been found that a dose of 0.72J/cm² induced significant increases in MTT levels (Figure 4.4). It may also be prudent to evaluate the effects of PBM on NFkB expression at a broader selection of time-points, investigating the expression of NFkB at both the transcriptional (PCR) and secretory levels using IL-8 as a surrogate marker for NFκB activation (ELISA).

The application of 400 nm light also induced significant increases in COX2 expression whilst 810 nm light induced significant decreases ($p<0.05$, Figure 4.14*b*). COX2 is an enzyme that plays a key role in prostanoid formation and whose expression has been shown to be a biomarker for periodontitis progression (Schaefer et al., 2010). Interestingly, a selection of

studies have found that PBM induces significant decreases in COX2 (Lim et al., 2013, Lim et al., 2007, Choi et al., 2012, Sakurai et al., 2000). However, all of these studies evaluated the effects of PBM following the application of a pro-inflammatory stimulus. The literature has shown that PBM has a biomodulatory effect whereby in chronically inflamed tissue PBM has an anti-inflammatory effect whereas in healthy tissue PBM induces a relatively small and acute increase in inflammation which may be crucial in modulating cellular homeostasis (Hamblin, 2017).

PBM also reduced TGFβR1 gene expression and downstream TGFβ1 secretion ($p<0.05$, Figure 4.15). In a recent study *Arany et al* employed a laser emitting a wavelength of 904 nm with radiant exposure outputs ranging from 0.1-6 J/cm² and concluded that PBM was able to activate latent-TGFβ1 (Arany et al., 2007). However, in comparison *Taflinski et al* reported application of 420 nm PBM at up to 30J/cm² inhibited TGFβ1 induced myofibroblast differentiation (Taflinski et al., 2014). Hence, the data demonstrated in this chapter and in the literature provides evidence of the wavelength dependent effects of PBM on TGFβ signalling. Blue light may also offer the potential of a novel application of PBM in inhibiting cell differentiation which can cause fibrosis and thus scar tissue formation (Walton et al., 2017). Further work will be required to validate this hypothesis.

A subsequent aim of this project was to evaluate the effects of PBM on IL-8 levels: a pro-inflammatory cytokine whose production is regulated by NFkB (Elliott et al., 2001). It was found that application of blue or NIR light induced significant increases in IL-8 expression but only blue light induced significant increases in IL-8 secretion. This may be due to the point at which changes in IL-8 secretion were assessed. Where future study may involve evaluation of the time dependent effects of PBM on IL-8 secretion *in vitro*. Interestingly, the increase in IL-

8 induced by light application was approximately 10% of that induced by a bacterial stimulus (~80pg/ml no stimulus applied vs ~1000pg/ml following LPS application, see section 5.2.1). These data suggest that light only induces relatively small increases in inflammatory mediators compared with the application of bacterial components. These increases however could also be deemed beneficial as several studies suggest that small increases in IL-8 are important in upregulating cell proliferation, a key regulator of tissue healing (Li et al., 2007, Spitler and Berns, 2014). *Basso et al* also investigated the effect of light irradiation on IL-8 gene expression from gingival fibroblasts and found that there was an increases detected after irradiation at a wavelength of 780 nm for between 1.5 and 3J/cm² (Basso et al., 2015). Hence, we provide evidence that PBM application can induce small increases in pro-inflammatory mediators such as IL-8 which could prove useful in 'priming' the host immune response for any future insult.

4.7.5 The effects of simultaneous application of multiple wavelengths on markers for mitochondrial activity

Several studies have provided evidence that simultaneous application of various wavelengths are capable of regulating cellular proliferation and promoting tissue healing (Fekrazad et al., 2018, Montazeri et al., 2017, Niu et al., 2015, Figurová et al., 2016). Data presented in section 4.6 here indicates there is no significant difference in the effects induced by the application of 405 nm, 850 nm or both at the same dose (24mW/cm², 5.76J/cm²).

However, one key caveat of this experimental model are the beam profiles exhibited by LEDs across the LUMOS™ array. In fact, the LEDs used by this array were only capable of irradiating 57% of the total well area (see section 3.3.2). Whilst cells were seeded in the centre of the well to ensure good irradiation coverage of adherent cells, inspection of wells by light microscopy revealed some cell adherence at the periphery of the well. Therefore, the effects of PBM on markers for mitochondrial activity may have been masked by the response of cells not receiving light exposure. Subsequently, further work is required to ensure uniform irradiation of cultures *in vitro* to enable reliable comparison of the application of either single or multiple wavelengths of light.

5 PBM MODULATES ROS PRODUCTION AND CYTOKINE SECRETION INDUCED BY LPS

5.1 Introduction

The effects of PBM in modulating symptoms of disease including inflammation and pain have been widely documented (Doeuk et al., 2015, Garcia et al., 2013, Ismaili and Bokonjic, 2014). However, way in which PBM modulates these symptoms *in vivo* remains poorly understood. One way researchers have attempted to dissect the signalling mechanisms induced by PBM has been through development of *in vitro* models to mimic the 'disease state' (Weinreb and Nemcovsky, 2015). This often involves the application of pro-inflammatory stimuli to induce oxidative stress and thus causing increases in markers for inflammation and apoptosis, key hallmarks for pathogenesis of diseases including periodontitis (Listyarifah et al., 2017, Dabiri et al., 2016). One pro-inflammatory stimulus commonly used *in vitro* to model disease is by treatment with the bacterial component, lipopolysaccharide (LPS), due to its ability to induce oxidative stress and promote increases in markers for inflammation, such as IL-8 (Bozkurt et al., 2017).

In fact, a number of authors have employed LPS in PBM studies using gingival fibroblasts to induce inflammation levels relevant to those found in oral disease (Choi et al., 2012, Sakurai et al., 2000, Takema et al., 2000, Pansani et al., 2017, Lim et al., 2013, Lim et al., 2015, Nomura et al., 2001). However, despite there being a wealth of evidence suggesting red and NIR light is useful in the modulation of inflammation induced by LPS, to date no studies have evaluated the effects of blue light using these disease models (Ren et al., 2017). Hence, this chapter aimed to determine how both blue and NIR light could modulate changes in cellular activity induced by LPS.

5.2 Determining the optimal dose of LPS required to induce an inflammatory response in oral fibroblasts.

Prior to assessment of the effects of PBM on changes in cellular signalling induced by LPS, the optimal concentration required to induce ROS production and IL-8 secretion was determined. This involved the application of LPS at a range of concentrations (0.1-5µg/ml) to gingival fibroblasts and assessment of the influence LPS had on markers of inflammation in which concentrations applied were selected based on review of the literature (Wang et al., 2011, Tamura et al., 1992, Bedran et al., 2014, Lee et al., 2006, Napa et al., 2017, Jones et al., 2010). The effects of LPS on ROS production and IL-8 secretion were then assessed: two key biomarkers for periodontitis (Lagdive et al., 2013, Dahiya et al., 2013).

5.2.1 Results

A concentration of 1µg/ml *E. coli* LPS induced a 32.5% increase in ROS production ($p<0.001$, Figure 5.1*a*) and a 1288% increase in IL-8 secretion (69.9pg/ml IL-8 untreated vs 970.6pg/ml 1ug/ml, $p<0.001$, Figure 5.2) relative to the untreated control.

Figure 5.1*b* illustrates the time dependent increase in ROS production induced by LPS stimulation (1µg/ml), where a significant increase in ROS production was only detected 24h post-application of the pro-inflammatory stimulus ($p<0.05$). Therefore, this concentration and incubation time were selected to evaluate the possible effects of PBM on inflammation and mitochondrial activity *in vitro*.

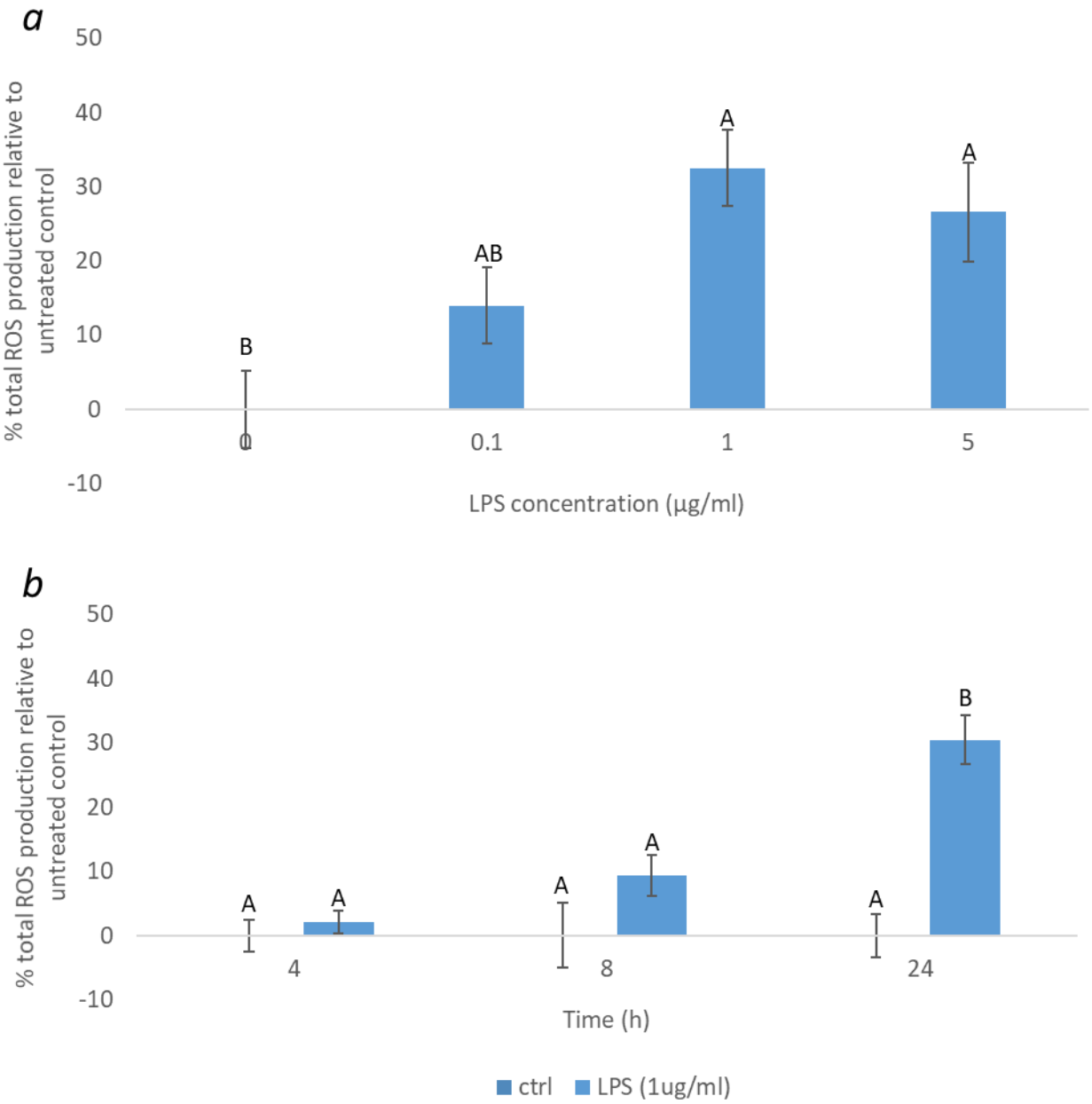

Figure 5.1 Evaluating the optimal a) Escherichia coli LPS concentration (0.1-5µg/ml) required to induce ROS production from pHGFs (pool, p6/7, n=12) 24h post-irradiation and b) the optimal time-point post-LPS application (1µg/ml, 4-24h) required to induce ROS production from pHGFs (pool p7, n=6). Data was analysed using one-way ANOVA followed by Tukey test where significance is indicated by means that do not share the same letter (p<0.05).

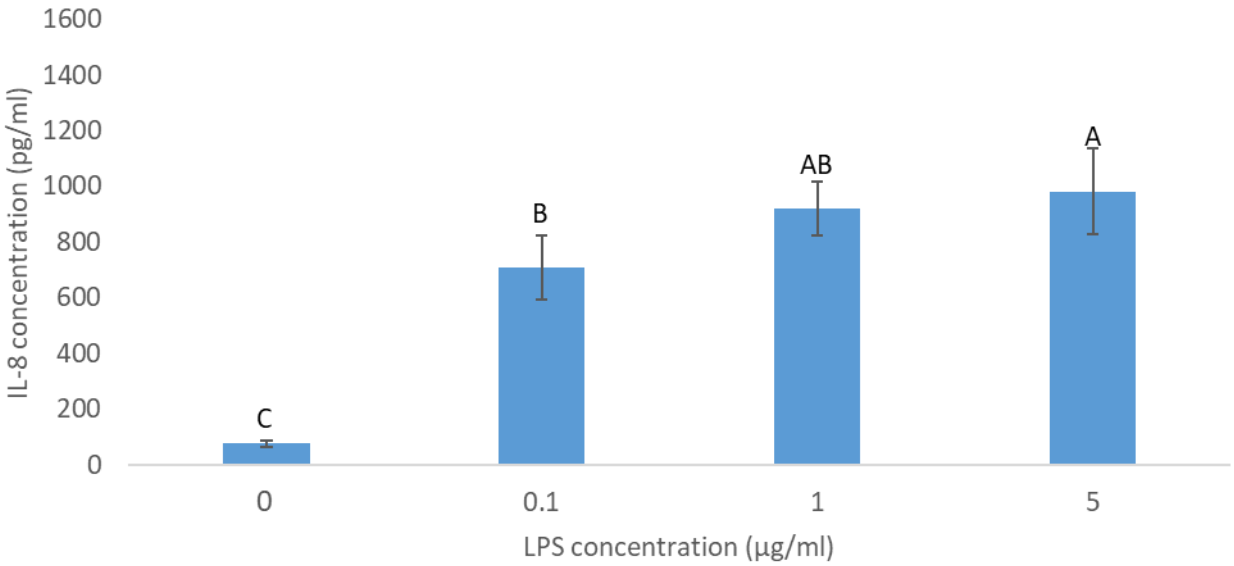

Figure 5.2 The dose dependent effects of E. coli LPS (0.1-5µg/ml) treatment on IL-8 secretion from pHGFs (pool p6/7, n=12) 24h post-application. Significance was measured using one-way ANOVA followed by Tukey test where different letters between means indicates a significant difference ($p<0.05$). In which, LPS at all concentrations (0.1-5µg/ml) induced significantly greater levels of IL-8 secretion relative to the untreated control (0) 24h post application ($p<0.05$), indicating that LPS is an effective stimulus of IL-8 secretion, a key maker for inflammation from pHGFs.

5.3 The effects of PBM on cell number and metabolic activity

Following selection of an appropriate concentration of LPS to stimulate inflammation, the effects of PBM in modulating changes in cell growth and metabolic activity induced by LPS were evaluated. Several authors have reported that red and NIR light increase cell proliferation relative to LPS treated controls, a marker for wound healing (Pansani et al., 2017, Kim et al., 2012). To date, no studies have evaluated the effects of blue light on cell growth of gingival fibroblasts. These studies frequently use the MTT assay to indirectly measure changes in cell responses (see section 1.7.1.1 (Sieuwerts et al., 1995)). Hence this section aimed to not only evaluate the effects of blue light on cell number compared by using cell counts with NIR light but also evaluate the effect of PBM on cell metabolic activity, utilising MTT.

5.3.1 Results

Cell counts revealed LPS significantly reduced cell number relative to the untreated control 8h post-stimulation ($p<0.05$, Figure 5.3*b*). However, this change was not significant following evaluation of cell number 24-120h post irradiation. Application of 450 nm light following LPS stimulation induced 12.1% increases in cell number relative to the pro-inflammatory control 8h post stimulation ($p<0.05$). Irradiation at 400 nm also induced a mean increase in cell number of 8.2% (ns) 24h post-application relative to the LPS treated control.

Comparatively, evaluation of cell metabolic activity using MTT revealed irradiation at 400 nm and 450 nm following LPS stimulation also induced 33.14% and 20.44% increases respectively in MTT response relative to the untreated control 24h post-application ($p<0.001$,Figure 5.4). Application of LPS also induced 13.22% increases in cell metabolic activity relative to the untreated control ($p<0.001$). Similarly, application of PBM at 400 nm also

induced the greatest mean increase in cell number relative to the LPS treated control 24h post-application (Figure 5.3*b*).

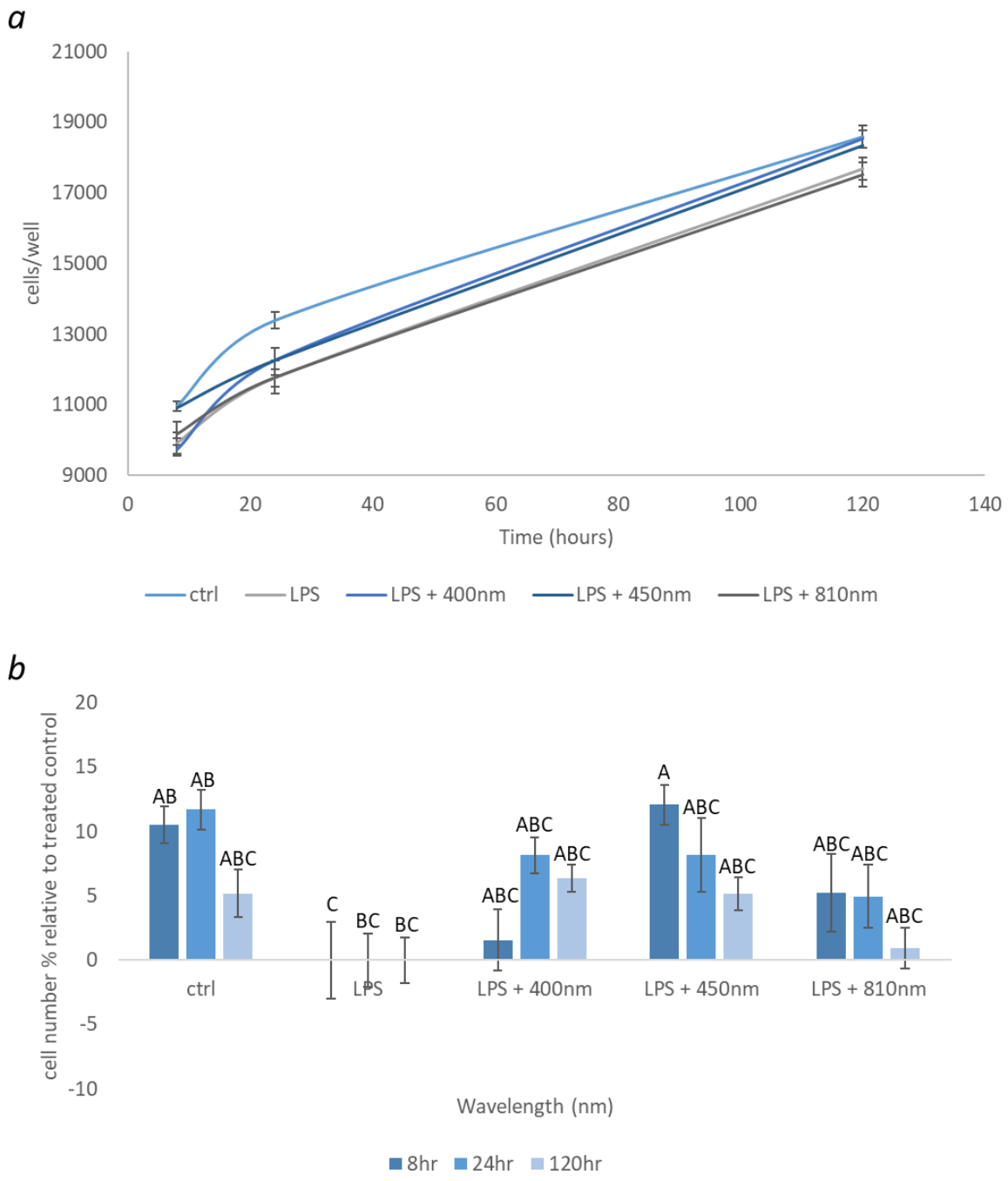

Figure 5.3 Application of light (400-810 nm, 24mW/cm², 5.76J/cm²) following LPS stimulation (1µg/ml) can modulate cell number using cell counting (pHGF pool p7, n=18) 120hr post-application of stimuli and how this compares to cell growth without the application of either light or LPS. Figure 3a shows real time changes in cell number from 8-120hr post-application of a stimulus and b) shows the percentage change in cell number at three time-points (8, 24, 120h) post-application of a stimulus relative to the LPS treated control, where the LPS control was normalised to 0. Significance was measured using one way ANOVA followed by Tukey test in which significance is indicated where means do not share the same letter in which there is at least a difference of $p<0.05$ (see section 4.3 for effects following application of light only).

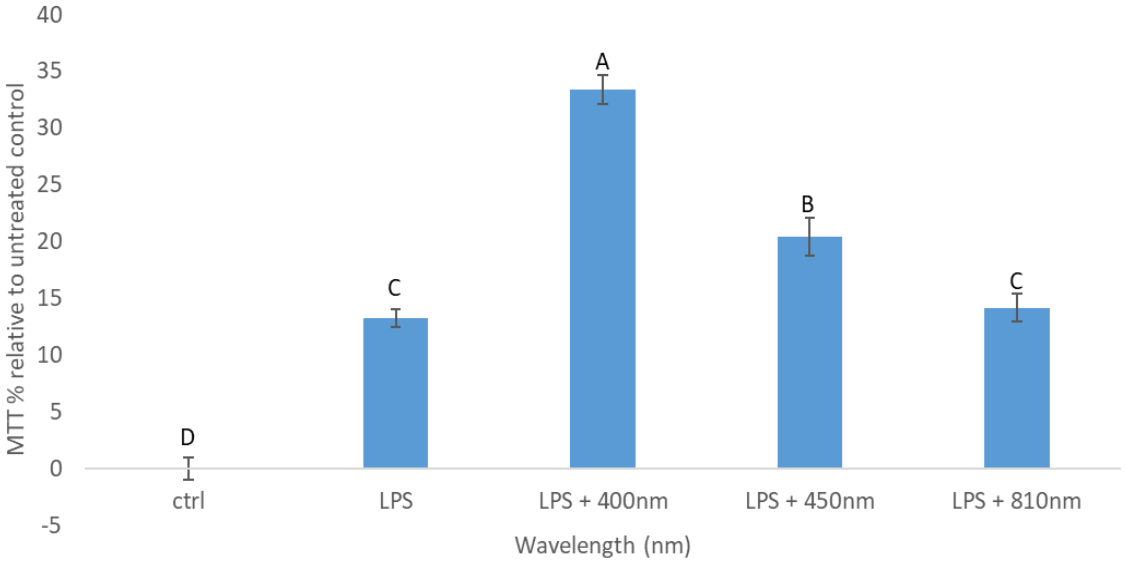

Figure 5.4 The effects of light application following LPS stimulation (1µg/ml) on cell metabolic activity 24h post-irradiation (pHGF pool p7, n=18, 400-810 nm, 24mW/cm², 5.76J/cm²) relative to the unstimulated control (ctrl) in which the control was normalised to 0%. Significance was measured using one way ANOVA followed by Tukey test and significance is indicated where means do not share the same letter in which there is at least a p<0.05 (see Figure 4.4 for effects of light on pHGFs cultured in media only).

5.4 The effects of PBM on LPS induced changes in gene expression

The effects of red and NIR light on mitochondrial activity have been widely documented (Hadis et al., 2015, Hadis et al., 2017a, Milward et al., 2015, Hamblin, 2018a). However, the effects of blue light following application of LPS on mitochondrial activity of gingival fibroblasts are yet be explored. This section therefore aimed to evaluate the effects of both blue and NIR light on mitochondrial related gene expression and a series of markers for mitochondrial activity including ROS and ATP.

5.4.1 Results

Data indicated the modulatory effect of light on mitochondrial activity from pHGFs cultures treated with LPS. Figure 5.5 provides data evidencing that application of LPS induced no significant effect on mitochondrial relevant gene expression compared with untreated cultures. However, following stimulation with LPS, irradiation at 400 nm, 450 nm or 810 nm induced 16.8%, 19.1% and 23.0% decreases in NDUFS7 gene expression. The NDUSF7 gene encodes a subunit of complex I of the ETC, one of the two complexes of the ETC that produces ROS (Lenaz et al., 2006). Interestingly, Figure 5.8*a* also indicates the effects of PBM in inducing decreases in ROS production relative to the LPS treated, where there was a decrease of 9.8% in ROS production following application of 450 nm light ($p<0.05$). Irradiation at 450 nm also induced a 64.6% decrease in antioxidant capacity relative to the LPS treated control, to give levels comparable to that of the control ($p<0.001$).

Similar to results discussed in section 4.4, only application of 810 nm light drove significant increases in COXIV4 gene expression relative to the control ($p<0.05$, Figure 5.6*b*). Comparatively, application of both 450 nm and 810 nm induced 12.0% and 19.1% increases in ATP5F2 gene expression relative to the LPS treated control, respectively. Figure 5.7 also

shows that 400 nm, 450 nm or 810 nm light exposure induced 16.4%, 15.7% and 12.1% increase in ATP production relative to the LPS treated control ($p<0.05$), respectively.

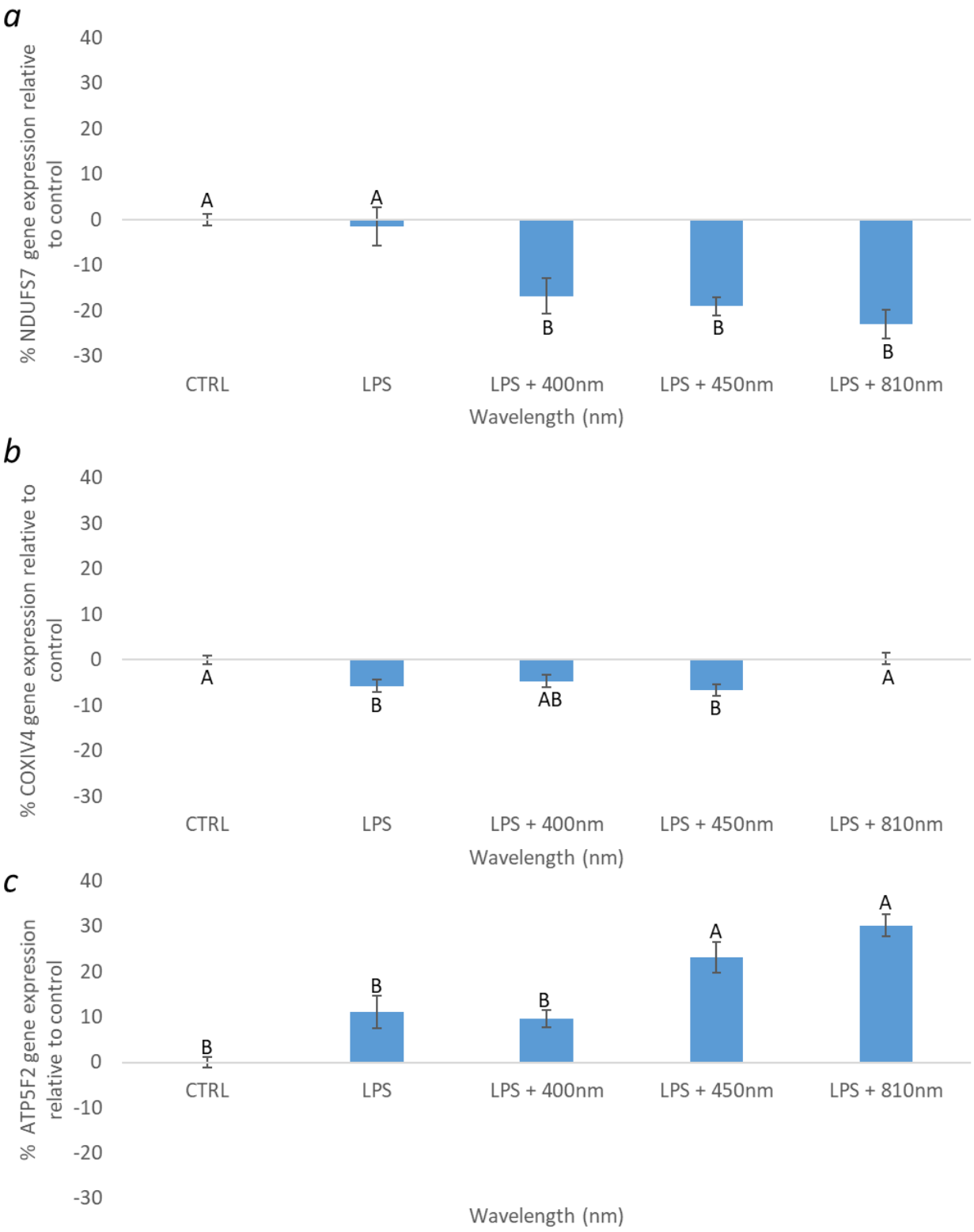

Figure 5.5 The effects of PBM (400-810 nm, 24mW/cm², 5.76J/cm²) on LPS (1µg/ml) induced changes in gene expression relative to expression from transcripts isolated from an untreated control (pHGF pool p7, n=9 per treatment group). Effects of PBM/LPS/both on gene expression of a) NDUFS7, component of mitochondrial ETC complex I, b) COXIV4, subunit of complex of ETC and c) ATP5F2, a subunit of ATP synthase of the ETC 24h post application. Statistical difference was assessed using one-way ANOVA followed by Tukey test where significance is indicated where means do not share the same letter ($p<0.05$).

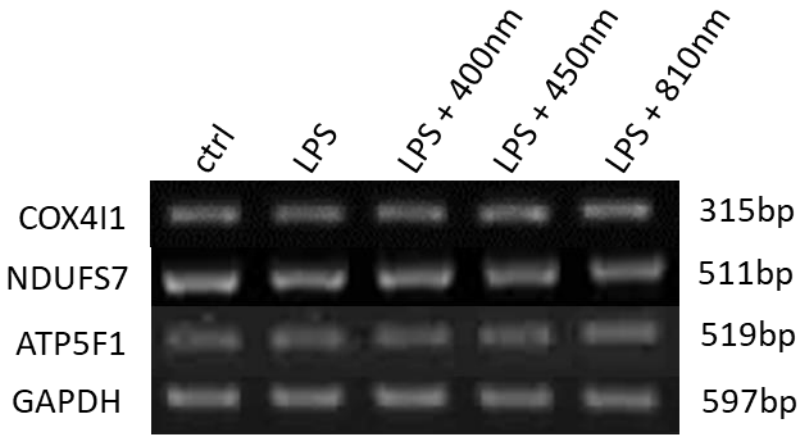

Figure 5.6: Representative gel images of amplified products for the COXIV4, NDUFS7, ATP5F1 and GAPDH (control) transcripts from pooled pHGFs either untreated or treated with LPS (1µg/ml) or LPS and 400-810 nm light. Analyses were performed 24h post-application of light. All gene expression was normalised against GAPDH expression, a gene universally expressed by eukaryotes.

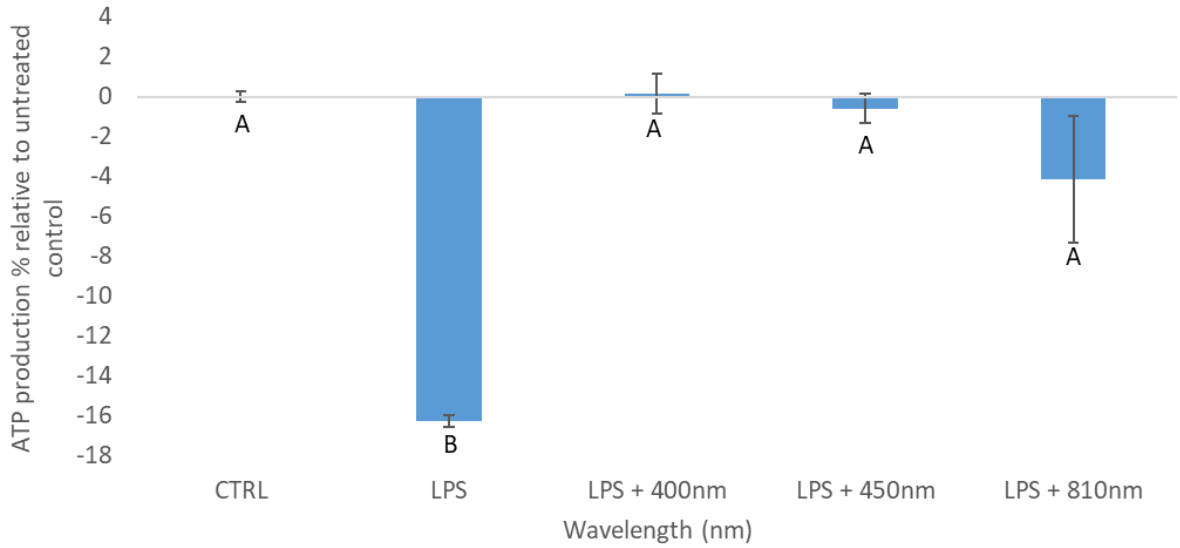

Figure 5.7 The effects of LPS (1µg/ml) application on ATP production and following application of light (400-810 nm) indicating modulation of this effect relative to the untreated control. ATP production was assessed 24h post-application of stimuli on gingival fibroblast cultures (pool p6/7, n=12). Significance was assessed using one way ANOVA followed by Tukey Test and significance is indicated where means do not share the same letter ($p<0.05$, see Figure 4.10 for effects with light only).

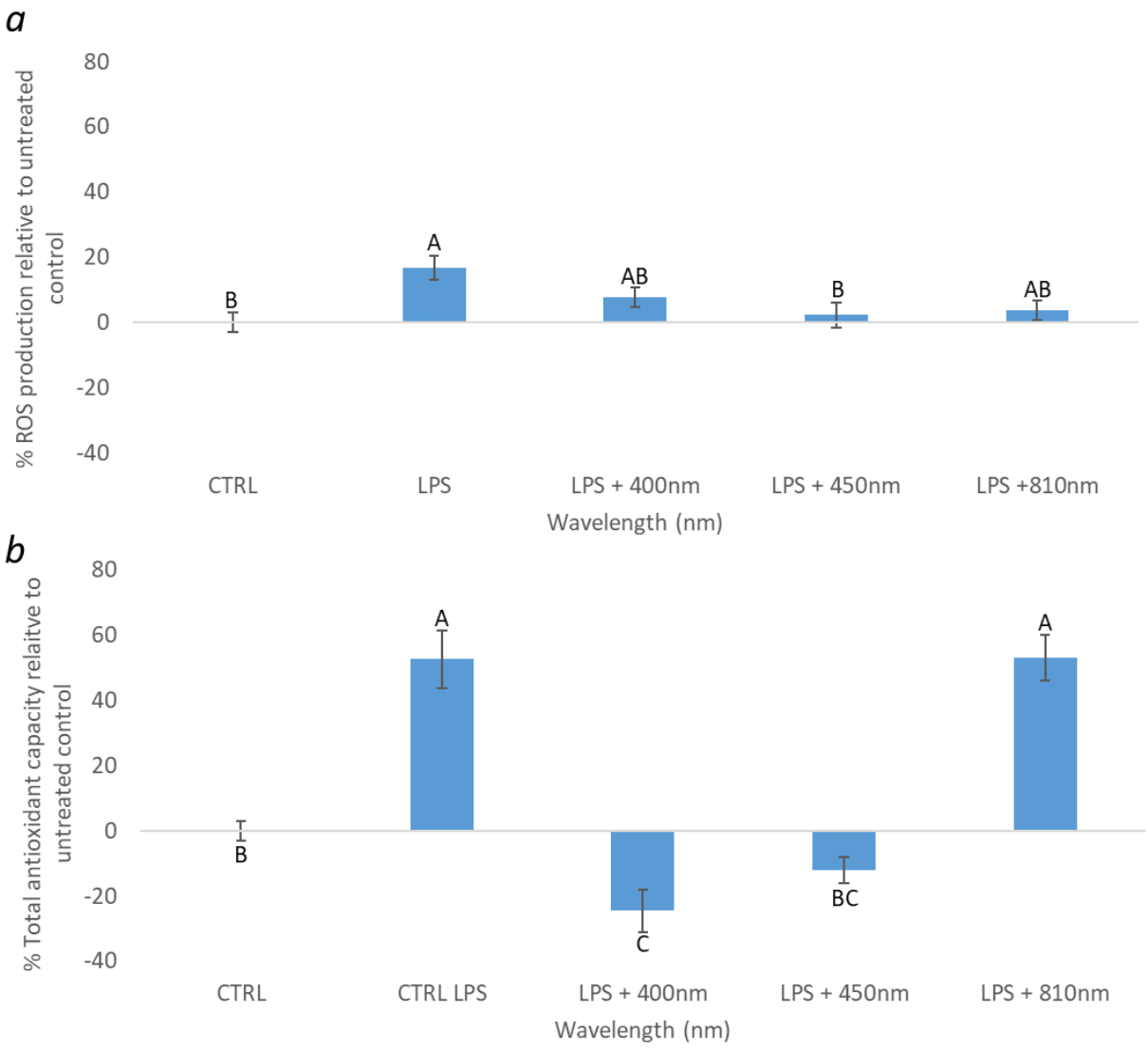

Figure 5.8 The effects of PBM in modulating a) ROS production (pHGF pool p6/7, n=12) and b) antioxidant capacity (pHGF pool p6/7, n=4 where each replicate is the result of pooling 4 cell supernatant samples) of cultures treated with LPS (1µg/ml) or LPS and light (400-810 nm, 24mW/cm², 5.76J/cm²) 24h post-application. Statistical differences were assessed using one way ANOVA followed by Tukey test in which significance is indicated where means do not share the same letter ($p<0.05$, see Figure 4.13 for effects with light only).

5.5 The effects of PBM on LPS induced changes in markers of inflammation in gingival fibroblasts

Several authors have demonstrated the effects of red and NIR light on modulation of inflammation following application of LPS (Aimbire et al., 2005, Wang et al., 2014, Chen et al., 2011b). However, no studies to date have demonstrated the anti-inflammatory potential of blue light. Hence, this section aimed to evaluate the effects of PBM on markers of inflammation in gingival fibroblast cultures.

5.5.1 Results

Results indicate application of LPS and 810 nm light induced a 35.1% increase in NFκB gene expression relative to the LPS treated control ($p<0.05$, Figure 5.9). Interestingly, results also demonstrated that only application of 400 nm or 450 nm light induced 40.2% and 28.3% decreases in IL-8 gene expression relative to the LPS treated control ($p<0.05$, Figure 5.10), whilst application of 810 nm light had no significant effect. These results are also in agreement with data presented in Figure 5.11, where it is demonstrated that irradiation at 400 nm and 450 nm caused a decrease in IL-8 secretion of 40.1% and 39.5% respectively ($p<0.05$).

Furthermore, application of 400 nm or 450 nm light induced 79.7% and 29.1% decreases in TGFßR1 gene expression relative to the LPS treated control ($p<0.05$, Figure 5.12) however 810 nm light exposure exerted no significant effect. However, evaluation of the effects of light on TGFß1 secretion showed that all wavelengths of light utilised (400 nm, 450 nm or 810 nm) induced significant decreases of this pro-inflammatory cytokine relative to the LPS treated control ($p<0.05$, Figure 5.13).

Evaluation of the effects of light on bFGF secretion showed irradiation at 400 nm, 450 nm or 810 nm induced 22.8%, 17.4% and 13.6% increased secretory levels of this growth factor relative to the LPS treated control ($p<0.05$, Figure 5.14).

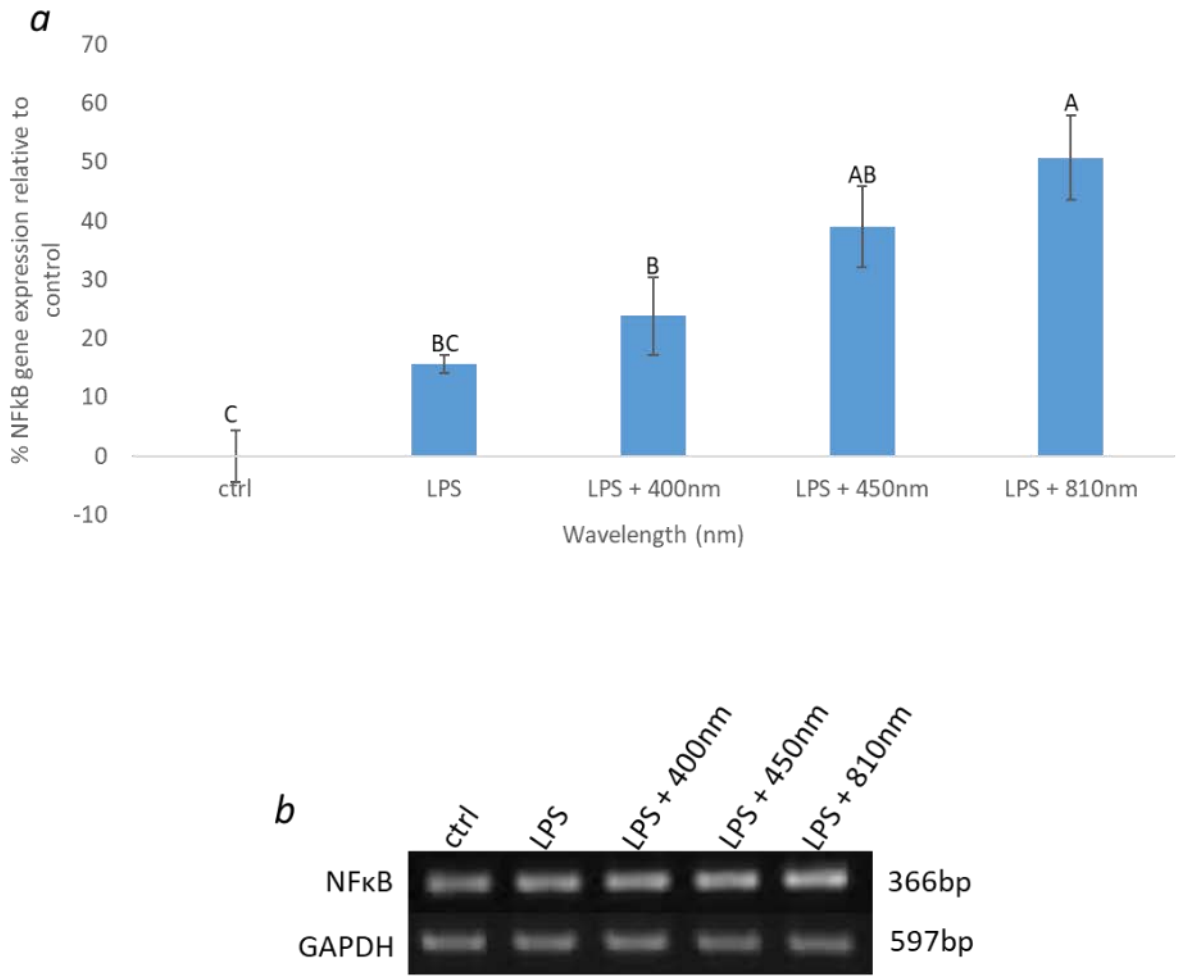

Figure 5.9a the effects of either LPS (1µg/ml) or LPS and light (400-810 nm, 5.76J/cm², 24mW/cm²) on NFκB gene expression from pHGFs (pool p7, n=9) relative to the untreated control (where the untreated control is normalised to 0%). Significance was calculated using one-way ANOVA followed by Tukey test where significance is indicated where means do not share the same letter. 9b) Representative PCR image of NFκB and GAPDH gene expression (p<0.05, see Figure 4.14 for effects with light only).

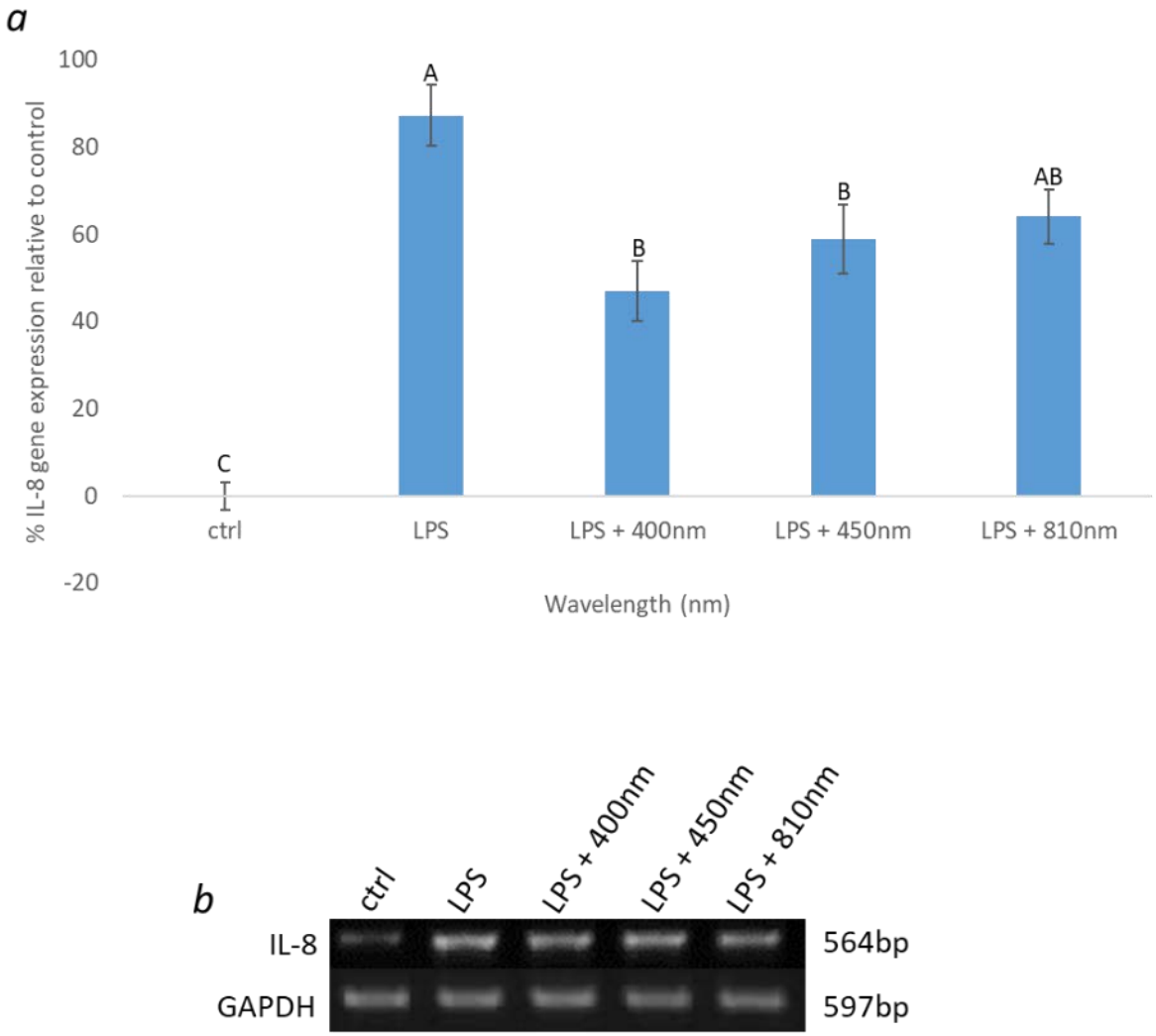

Figure 5.10 The effects of LPS (1µg/ml) or LPS and light (400-810 nm, 5.76J/cm², 24mW/cm²) on IL-8 gene expression (pHGF, pool p7, n=9) relative to the untreated control where a) indicates normalised IL-8 gene expression relative to an untreated control and b) a representative PCR image of IL-8 and GAPDH gene expression. Statistical difference was assessed using one-way ANOVA followed by Tukey test where difference in letters indicates significance differences between means (p<0.05, see Figure 4.16 for light only).

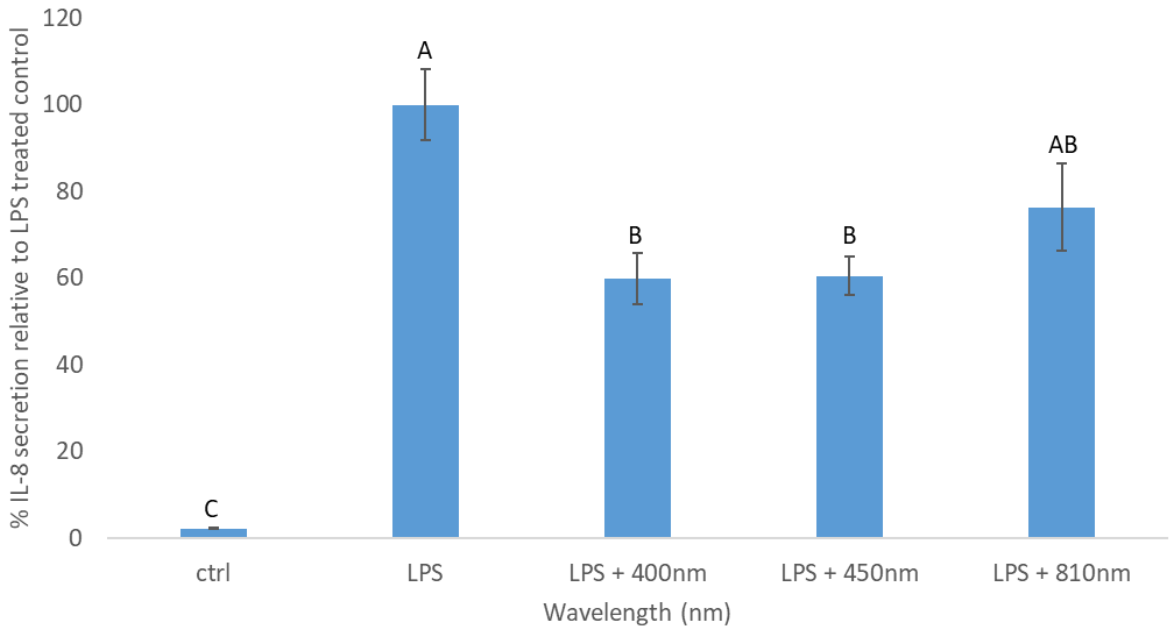

Figure 5.11 The effects of cells treated with media (ctrl), LPS (1µg/ml) or LPS and light (400-810 nm, 5.76J/cm², 24mW/cm²) on IL-8 secretion 24h post-application (pHGF pool p6/7, n=8) relative to the LPS treated positive control (LPS treated control was normalised to 100% to enable comparison between treatment groups). Significant differences were examined using one-way ANOVA followed by Tukey test where significance is indicated by means that do no not share the same letter (p<0.05, see Figure 4.16 for light only).

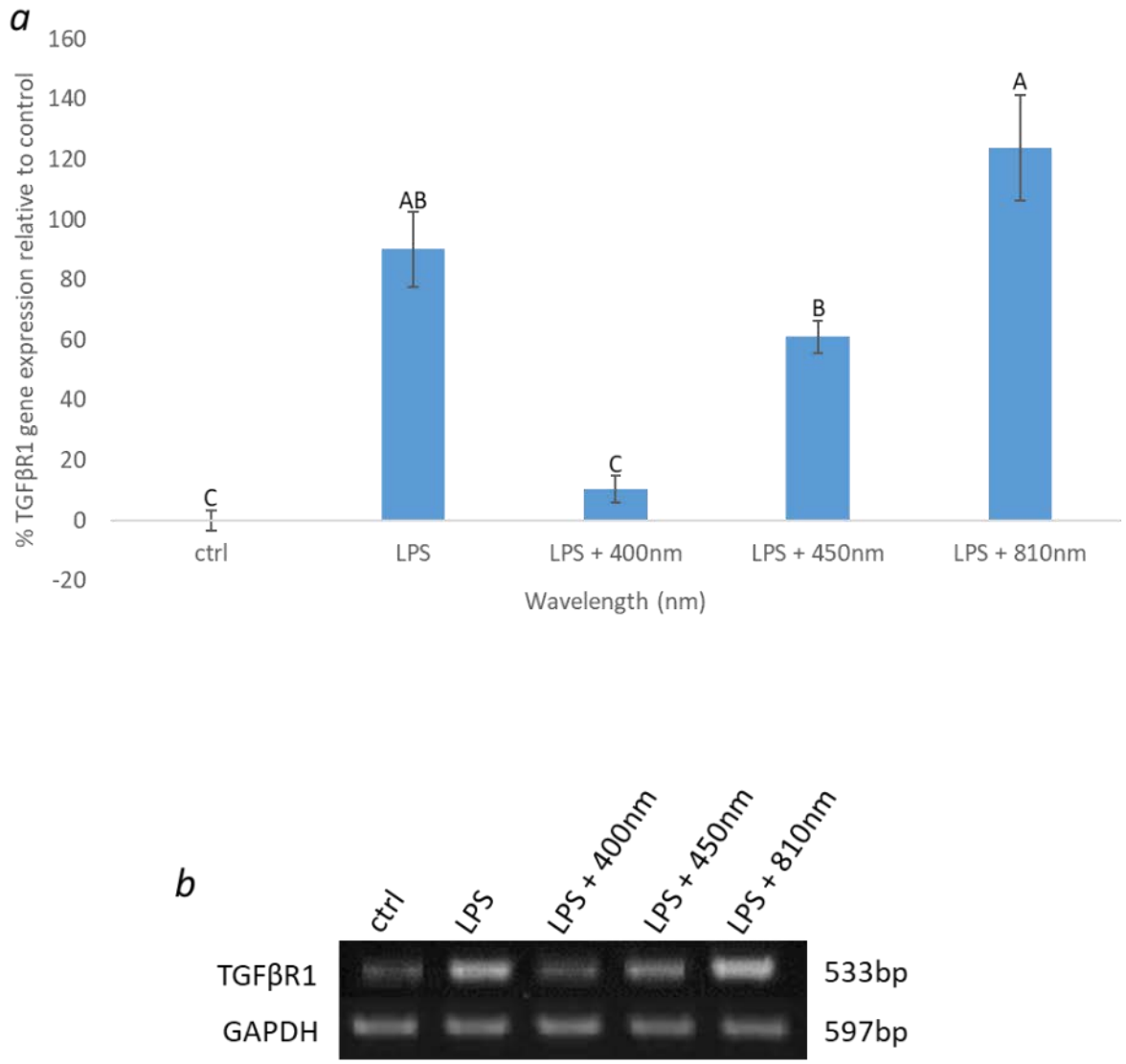

Figure 5.12 The effects of either media (ctrl), LPS (1µg/ml) or LPS and light (400-810 nm, 5.76J/cm², 24mW/cm²) on TGFβR1 gene expression (pHGF pool p7, n=8) where a) shows % TGFβR1 gene expression relative to the untreated control (ctrl) normalised to 0% and b) shows a representative PCR image of TGFβR1 and GAPDH gene expression. Significance was analysed using one-way ANOVA followed by Tukey test where different letters indicate significance differences between means (p<0.05, see Figure 4.15 for light only).

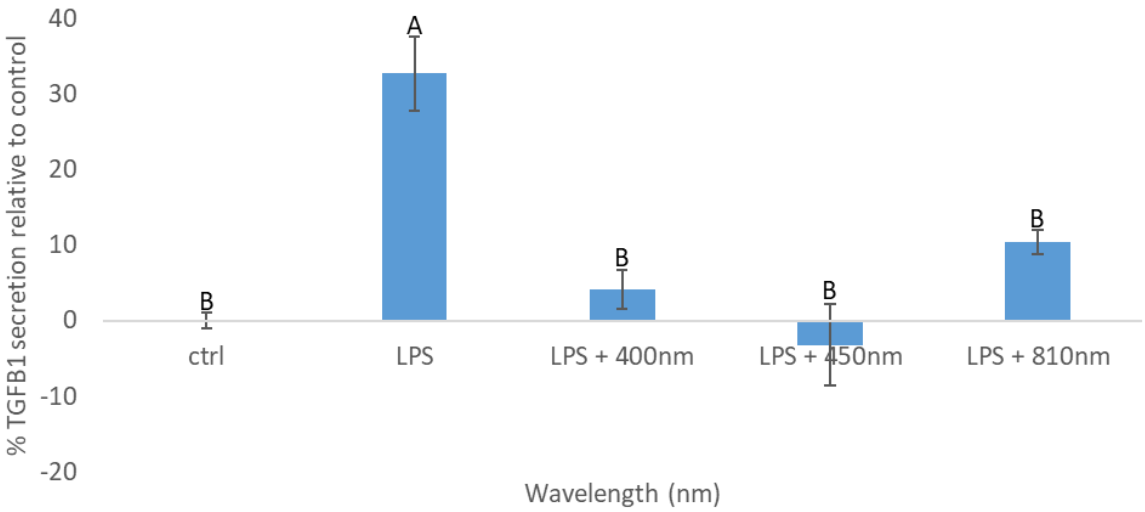

Figure 5.13 The effects of media, LPS (1µg/ml) or LPS and light (400-810 nm, 24mW/cm², 5.76J/cm²) on gene expression of TGFß1 secretion as determined by ELISA at 24h post-application of stimuli (pHGFs, pool p6/7, n=12). Significance was analysed using one-way ANOVA followed by Tukey test where difference in letters indicates significance differences between means (p<0.05, see Figure 4.15 for light only).

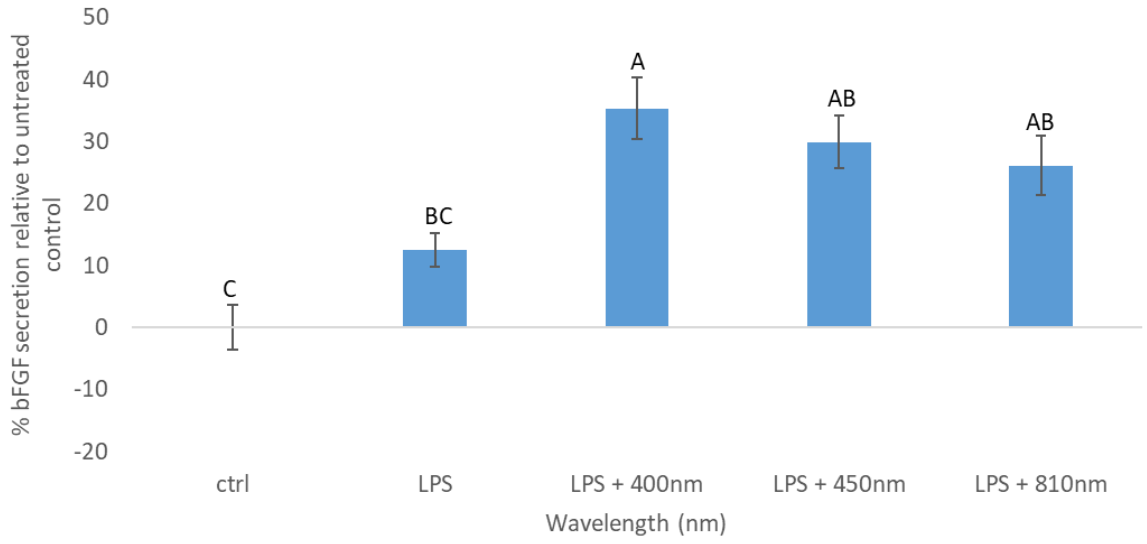

Figure 5.14 The effects of media, LPS (1µg/ml) or LPS and light (400-810 nm, 24mW/cm², 5.76J/cm²) on bFGF secretion as determined by ELISA from pHGFs (pool p6, n=6) 24h post-application. Significance was analysed using one-way ANOVA followed by Tukey test where difference in letter indicates significance difference between means (p<0.05).

5.6 Discussion

5.6.1 Determining optimal dose of LPS to induce inflammation

Data demonstrates that application of 1µg/ml of LPS and incubation for 24h was sufficient to induce significant increases in IL-8 secretion (Figure 5.2, $p<0.05$) and ROS production (Figure 5.1, $p<0.05$) and hence these conditions were selected for use in future studies. Interestingly, *Kang et al* also demonstrated the dose and time dependent response of gingival fibroblasts to LPS and concluded that a concentration of LPS of 1µg/ml induced significant increases in both IL-8 gene expression and secretion 24h post-application (Kang et al., 2016). Similarly, *Cheng et al* also demonstrate a concentration of 1µg/ml of LPS induced significant increases in ROS production from gingival fibroblasts 24h post-application (Cheng et al., 2015).

5.6.2 The effects of PBM on cell metabolic activity and cell number.

PBM has been widely documented to induce increases in cellular proliferation (Aleksic et al., 2010, Almeida-Lopes et al., 2001b, Amid et al., 2014, Fekrazad et al., 2018, Gao and Xing, 2009, Hadis et al., 2015). However, whist there are a number of publications reporting the anti-inflammatory effects of PBM both *in vitro* and *in vivo* (Oton-Leite et al., 2015, Prianti Jr et al., 2014, Sobouti et al., 2015, Song et al., 2012, Yamaura et al., 2009), few report the effects of PBM on cell growth and proliferation following application of a pro-inflammatory stimuli. Data displayed here indicates 8h post-irradiation, 450 nm light induced significant increases in cell number relative to the LPS treated control ($p<0.05$, Figure 5.3).

It was also demonstrated that application of 400 nm or 450 nm (24mW/cm², 5.76J/cm²) induced significant increases in cell metabolic activity relative to the LPS treated control, whilst 810 nm light application alone induced no significant effect (Figure 5.4). Interestingly, LPS also induced a significant increase in cell metabolic activity 24h post-

application, whilst no significant effect on cell number was seen at this time point. The MTT assay used in these studies has been cited to be affected by mitochondrial activity, amongst other changes in cellular activity (Sieuwerts et al., 1995). Indeed, LPS has been reported to induce mitochondrial biogenesis (Suliman et al., 2003) and increase mitochondrial related gene expression (Bauerfeld et al., 2012). Hence, results described in section 5.3.1 may be reflective of the effects of LPS on mitochondrial activity.

Furthermore, the effects of PBM induced both *in vitro* and *in vivo* have been reported to be induced by changes in mitochondrial activity (Belletti et al., 2014, Buravlev et al., 2014a, Buravlev et al., 2013, Chung et al., 2012, Hamblin, 2018a). Therefore, increases in mitochondrial biogenesis induced by compounds such as LPS may be important in improving response to PBM, where it has been reported in a study published our group that the cellular response to PBM is mitochondrial number dependent (Serrage et al., 2019a). Where cell types reported to possess a higher mitochondrial population prior to irradiation (myotubes), respond significantly more to PBM when compared to cell types with a lower mitochondrial population (myoblasts (Schoneich et al., 2014)). Further detail regarding this study is described in chapter 7. Data described in section 4.3 indicated application of 400 nm light induced 14.6% increases in metabolic activity relative to the control, whilst data described here shows irradiation at the same parameters induced 33.1% increases in cell metabolic activity relative to the LPS treated control. Hence, these data provide evidence that increased response of cultures treated with LPS to PBM may be due to changes in mitochondrial activity. However, further work will be required to validate this hypothesis.

Interestingly, *Pansani et al* also explored the effects of PBM on cell proliferation following application of LPS. The author showed that application of 780 nm light at 3J/cm^2 to

LPS stimulated cultures induced significant increases in gingival fibroblast cell number relative to the LPS stimulated control 48-72h post-application of the first stimulus (Pansani et al., 2018). Whilst, application of light to unstimulated cultures induced no significant effect on cell proliferation relative to the unstimulated control. Interestingly, this study utilised the Alamar® blue assay: a cell metabolic activity assay whose activity has also been associated with changes in mitochondrial activity (Springer et al., 1998). Hence, this is not a reliable indicator of cellular proliferation but does corroborate with data described here suggesting response of LPS stimulated cultures to light is greater than the response of cells cultured in media alone.

Data therefore indicate that PBM may influence both cell proliferation and cell metabolic activity. However, whilst assays such as MTT are commonly used as a marker for a cell proliferation (Koyanagi et al., 2016), particularly for use in PBM studies (Basso et al., 2013a, Basso et al., 2016b, Pansani et al., 2014, Damante et al., 2009, Frozanfar et al., 2013, Kreisler et al., 2003, Kreisler et al., 2005), data here demonstrates the unreliability of this method as results evaluating changes in cell number do not corroborate with those investigating the effects of PBM on cell metabolic activity using MTT. For example, LPS causes mean decreases in cell number but induces increases in cell metabolic activity relative to the untreated control (Figure 5.3, Figure 5.4). Hence, this demonstrates the importance of the employment of reliable indicators for cell growth and/or proliferation including cell counts or assays that directly measures changes in cell proliferation including the BrdU assay (Madhavan, 2007).

5.6.3 The effects of PBM on LPS induced changes in mitochondrial relevant gene expression

As discussed in section 5.6.2, it has been claimed that application of both LPS and light induce changes in mitochondrial activity. Data demonstrated here indicates application of either LPS or light and LPS can modulate mitochondrial relevant gene expression *(*Figure 5.5). Where, application of 810 nm light induced significant increases in cytochrome c oxidase subunit expression and ATP synthase subunit gene expression relative to the LPS treated control: two key components of the ETC.

Interestingly, the CCO hypothesis of PBM is one of the most widely accepted theories for the effects of PBM, in which *Karu et al* provided evidence that NIR light could excite CCO whilst blue light modulates the activity of Flavin or porphyrin containing complexes (see section 1.3.1.1 (Karu and Kolyakov, 2005)). Hence, the data presented here are in agreement with this as only NIR light (810 nm) induced significant increases in CCO subunit gene expression. However, LPS induced significant decreases in CCO subunit expression. *Quolin et al* also demonstrated application of LPS at 1µg/ml significantly reduced CCO release and ATP production (Quoilin et al., 2014). Data presented here also demonstrate that application of LPS induced significant decreases in ATP production (Figure 5.7) but application of 400 nm, 450 nm or 810 nm application following LPS treatment induced significant increases in ATP production relative to the LPS treated control ($p<0.05$). *Sharma et al* also reported 810 nm irradiation induced significant increases in ATP production (Sharma et al., 2011b). However, to date this is the only study to evaluate the effects of PBM on ATP production following application of LPS. It was also demonstrated that application of 400 nm, 450 nm or 810 nm light induced significant decreases in complex I subunit gene expression (Figure 5.6*a*). Complex I is a Flavin containing complex of the ETC (Hirst, 2013) reported to absorb blue light (Yang et

al., 2017b). Complex I is also one of the two complexes in the ETC to produce ROS (Murphy, 2009). Interestingly, studies have shown that modulators of complex I such as coenzyme Q_2 reduce oxidative stress through inhibition of ROS production from complex I (Fato et al., 2009). This could prove an interesting hypothesis as to how PBM modulates oxidative stress through downregulation of complex I activity. However, changes in gene expression may also be indicative of changes in mitochondrial number, where a series of authors have reported the efficacy of PBM in inducing mitochondrial biogenesis (Chen et al., 2014, Nguyen et al., 2014, Yang et al., 2016, Yang et al., 2017a, Yin et al., 2017, Zhang et al., 2016b).

Zhang et al also explored the effects of light on complex I and found that irradiation at 628 nm at 0.88J/cm² induced significant increases in complex I subunit gene expression from human fibroblasts (Zhang et al., 2003). However, the fibroblasts were not treated with pro-inflammatory stimuli prior to light application. Current indications suggests PBM elicits different effects dependent upon the inflammatory state of the tissue, where for example PBM can induce decreases in ROS production in inflamed tissue (Lim et al., 2013) and increases in ROS from untreated 'healthy' tissue (Kushibiki et al., 2013). This thinking is in agreement with data shown here where Figure 5.8*a* shows application of 450 nm light induced significant decreases in ROS production relative to the LPS stimulated cells. Comparatively data described in section 4.4 shows application of 450 nm light induced significant increases in ROS production in non-stimulated cells. This therefore provides evidence for the biomodulatory effects of PBM.

However, the data also suggest that whilst LPS induced a 52.6% increase in total antioxidant capacity (TAOC) relative to the untreated control ($p<0.05$), application of 400 nm or 450 nm light caused a decrease in TAOC of 24.44% and 12.01% respectively relative to the

untreated control (ns, Figure 5.8). This may suggest blue light inhibited antioxidant production induced by LPS application due to the resolution of inflammation, allowing antioxidant concentration in supernatants to return to control levels. Indeed, current literature indicates LPS induces significant increases in antioxidant activity through upregulation of Nrf2 signalling (Yin and Cao, 2015), which ultimately leads to increases in glutathione production (Spolarics and Wu, 1997) and increased manganese superoxide dismutase (MnSOD) gene expression (Del Vecchio and Shaffer, 1991). Hence, blue light may also be important in modulating not only ROS levels but also antioxidant levels, inhibiting LPS induced changes in signalling and thus restoring normal cellular function.

In conclusion the data indicate that light can modulate LPS induced changes in mitochondrial activity which could be key in the modulation of chronic inflammatory diseases including periodontitis.

5.6.4 The effects of PBM on LPS induced changes in ROS production and IL-8 secretion.

Several authors have demonstrated the anti-inflammatory properties of PBM following bacterial challenge (Fornaini et al., 2013, Kim et al., 2012, Lima et al., 2014, Wang et al., 2014, Yamaura et al., 2009). However, none to date have compared the effects of blue and NIR light on inflammation induced by LPS. Data indicated that blue light is an effective modality in significantly reducing the gene expression (Figure 5.10, $p<0.05$) and secretion (Figure 5.11, $p<0.05$) of IL-8 relative to the LPS treated control, whilst NIR light had no significant effect. *Basso et al*, also showed application of 780 nm at 1.5-3J/cm² induced significant decreases in IL-8 gene expression from gingival fibroblasts relative to the LPS treated control. Interestingly the author used much lower doses of NIR light than the 5.76J/cm² used in this study, which provides further indication that doses of 810 nm light <5J/cm² may have been more

efficacious in modulating inflammation *in vitro*. IL-8 is a key pro-inflammatory cytokine whose expression is not only regulated by NFκB (Matsusaka et al., 1993) but is also a biomarker for inflammatory diseases including periodontitis (Lagdive et al., 2013). Hence, modulation of this pro-inflammatory cytokine could prove useful in disease modulation.

Despite evidence suggesting NFκB activation modulates levels of IL-8 in gingival fibroblasts, data presented in Figure 5.9 suggests only application of 810 nm light induces significant increases in NFκB gene expression relative to the LPS treated control, whilst only blue light induced significant changes in IL-8 gene expression and secretion. However these changes could occur due to a number of reasons including the time at which NFκB gene expression was evaluated. Where, a series of authors indicate changes in NFκB expression induced by LPS are most significant 0.5-6h post-application, with no significant effect observed at 24h post-application (Sharif et al., 2007). These findings corroborate with data presented here, where LPS exposure exerted no significant effect on NFκB gene expression relative to the untreated control. Interestingly, Chen et al also demonstrated the effects of PBM on NFκB gene expression were most significant 6-10h post irradiation, with no significant effect being seen 24h post-irradiation (Chen et al., 2009a). Hence further work is required to evaluate the effects of PBM on NFκB gene expression at a wider array of time points post-irradiation or indeed the direct effect of PBM on translocation of NFκB into the nucleus using immunofluorescence staining (Noursadeghi et al., 2008). Such studies may enable establishment of a clearer picture as to how PBM elicits its anti-inflammatory effects post application of LPS.

However, one other hypothesis addressing the differential response of pHGFs to blue or NIR light is the idea that different wavelengths may also modulate different signalling

pathways such as the Nrf2 pathway. Interestingly, *Trotter et al* provided evidence that application of violet/blue light (45J/cm²) to LPS (1µg/ml) treated human monocyte cells induced significant increases in Nrf2 protein expression which in turn led to decreases in IL-8 secretion (Trotter et al., 2017). However, to date no studies have reported the effects of NIR PBM on Nrf2 expression.

Data also demonstrate that application of 400 nm light induced significant reductions in TGFβR1 gene expression (Figure 5.12) and TGFβ1 secretion (Figure 5.13) relative to the LPS treated control. Increases in TGFβ1 have been shown to correlate with increases in severity of periodontitis (Mize et al., 2015). Hence, modulation of this cytokine could be important in moderating the progression of disease. Interestingly, *Keskiner et al* also demonstrated that PBM at 1064 nm on palatal wounds induced significant reductions in TGFβ1 secretion (Keskiner et al., 2016).

However, data also demonstrates that whilst 810 nm light application induces significant decreases in TGFβ1 secretion (Figure 5.13), it has no significant effect on TGFβR1 gene expression (Figure 5.12). This may be reflective of the wavelength dependent response to PBM, where levels of different TGFβR's have proven crucial in determining signalling pathway activation, regardless of the relative levels of TGFβ1 (Rojas et al., 2009). Hence, it will be important to evaluate the effects of PBM on all three TGFβ receptors and subsequently investigate the effects of PBM on downstream targets for TGFβ signalling.

Data also demonstrated that irradiation at 400 nm induced significant increases in bFGF relative to the LPS treated control (Figure 5.14). bFGF is a growth factor, key to promoting wound healing (McGee et al., 1988) and is also proven efficacy in regeneration of periodontal tissues (Murakami et al., 1999). Basso et al, also reported application of 780 nm light induced

significant increases in bFGF in a model for wound healing using gingival fibroblasts (Basso et al., 2012a). Therefore, these findings support the premise that PBM can induce not only anti-inflammatory effects but also promote the secretion of growth factors, fundamental in stimulating cellular growth, proliferation and thus healing.

6 PBM MODULATES THE CELLULAR RESPONSE INDUCED BY PERIODONTAL DISEASE RELEVANT STIMULI

6.1 Introduction

The modulatory effects of PBM on the inflammatory response induced by LPS have been described in detail both in chapter 5 and by a number of authors (Aimbire et al., 2005, Chen et al., 2011b, Kim et al., 2012, Wang et al., 2014, Yamaura et al., 2009). However, whilst *E.coli* LPS is a robust stimulus of inflammation both *in vitro* and *in vivo*, the oral cavity is home to a diverse range of bacterial species each possessing factors to enable interspecies communication, coaggregation and stimulation of inflammation. Factors inducing changes in range of signalling pathways including inflammation are known as virulence factors and whilst LPS is a key virulence factor, periopathogenic bacteria possess multiple virulence factors to induce inflammation and promote tissue destruction (Graves et al., 2000).

However, whilst these bacterial stimuli are more representative of the oral inflammation induced *in vitro* compared with LPS, they were still not comparable to the inflammation induced by a multispecies bacterial biofilm. Therefore, a biofilm derived from human saliva was generated, characterised and heat inactivated to enable comparison between the inflammatory response induced by LPS, *F. nucleatum* or *P. gingivalis* from pHGFs. Subsequently, the effects of light on inflammatory response induced by these pro-inflammatory stimuli was evaluated. These studies would then provide data on how PBM could be potentially used to modulate inflammation induced by stimuli relevant to the pathogenesis of periodontitis.

6.2 Growth and characterisation of periodontal disease-relevant bacterial species

6.2.1 Fusobacterium nucleatum and Porphyromonas gingivalis

Prior to assessment of the effects PBM on *in vitro* inflammatory response following the application of either *F. nucleatum* or *P. gingivalis*, bacterial cultures were characterised. This work was performed using various techniques including PCR and 16s sequencing to ensure bacterial stimuli were appropriate for application to HGF cultures *in vitro*.

6.2.1.1 Results

Initial experiments aimed to confirm presence of *P. gingivalis* and *F. nucleatum* in bacterial suspensions. Figure 6.1*b* provides evidence of the spindle-shaped morphology characteristic of *F. nucleatum* (Uitto et al., 2005). The pink colour of this image also indicates the Gram negative staining characteristic of this bacterium. Figure 6.1*c* also provides evidence of the presence of *F. nucleatum polymorphum* using bacterial PCR, where a band at 334bp denotes the presence of this bacterial species and also provides evidence of the purity of the culture.

Figure 6.2*a* provides evidence of the characteristic black colonies of *P. gingivalis* grown on blood agar (How et al., 2016). However, *P. gingivalis* could not be identified using traditional bacterial PCR techniques as shown in Figure 6.2*b*, possibly due to the specificity of the primers used in this study. Where, the primers employed have only shown specificity to ATCC strains W83 and FDC381 of *P. gingivalis* (Kasuga et al., 2000). Hence, the 16s band shown in Figure 6.2*b* was excised from the gel and sequenced to determine the identity of the bacterial species in the sample. Figure 6.2*c* shows 16s sequencing revealed *P. gingivalis* was solely present in the sample with a 99% match to ATCC strain 33277 (Hahnke et al., 2016). Hence, these data provided confirmation of the expected species in bacterial samples and that they could therefore be used for further study.

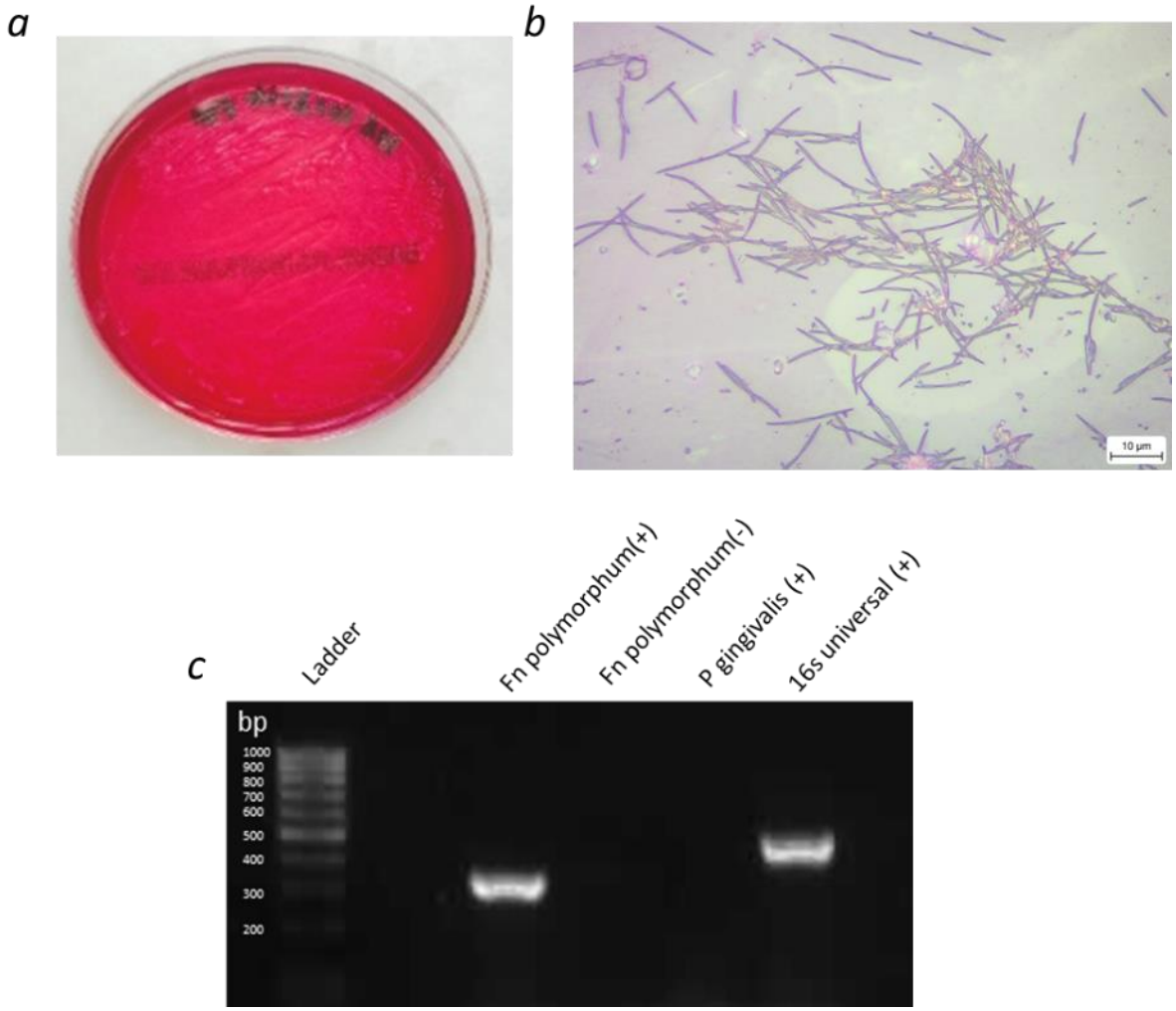

Figure 6.1 Characterisation of F. nucleatum where a) shows colonies upon a blood agar plate, b) shows a Gram staining image and c) indicates the presence of F. nucleatum polymorphum in the bacterial sample where a + indicates the presence of the bacterial sample with either an F. nucleatum, P. gingivalis or 16s universal primer. The F. nucleatum polymorphum primer was also tested without a bacterial sample (with water, indicated by – on image) to ensure the primer was bacterial specific.

a

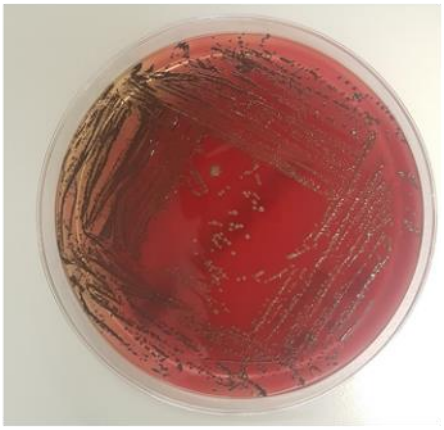

b

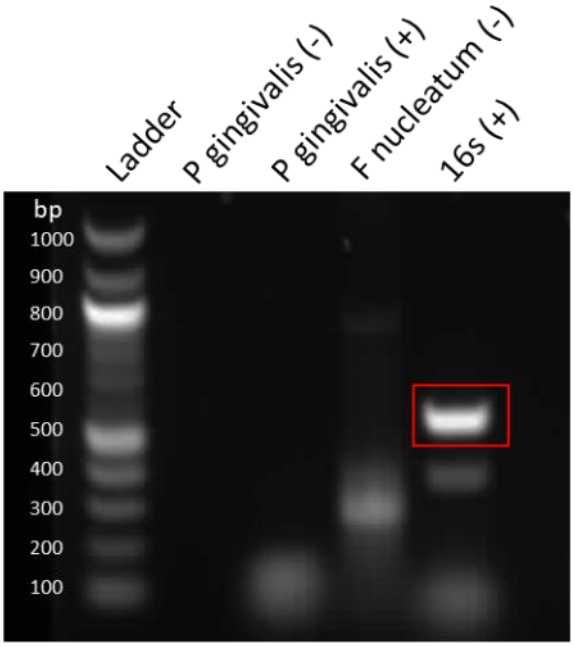

c

Porphyromonas gingivalis strain ATCC 33277 16S ribosomal RNA gene, complete sequence

Sequence ID: NR_074234.1 Length: 1475 Number of Matches: 1

Range 1: 47 to 517 GenBank Graphics Next Match Previous Match

Score	Expect	Identities	Gaps	Strand
843 bits(456)	0.0	466/471(99%)	2/471(0%)	Plus/Plus

```
Query  13   CTT-ACNCATGC-AGTCGAGGGGCAGCATGATCTTAGCTTGCTAAGGTTGATGGCGACCG  70
Sbjct  47   CTTAACACATGCAAGTCGAGGGGCAGCATGATCTTAGCTTGCTAAGGTTGATGGCGACCG  106
Query  71   GCGCACGGGTGCGTAACGCGTATGCAACTTGCCTTACAGAGGGGGATAACCCGTTGAAAG  130
Sbjct  107  GCGCACGGGTGCGTAACGCGTATGCAACTTGCCTTACAGAGGGGGATAACCCGTTGAAAG  166
Query  131  ACGGACTAAAACCGCATACACTTGTATTATTGCATGATATTACAAGGAAATATTTATAGC  190
Sbjct  167  ACGGACTAAAACCGCATACACTTGTATTATTGCATGATATTACAAGGAAATATTTATAGC  226
Query  191  TGTAAGATAGGCATGCGTCCCATTAGCTTGTTGGTGAGGTAACGGCTCACCAAGGCGACG  250
Sbjct  227  TGTAAGATAGGCATGCGTCCCATTAGCTAGTTGGTGAGGTAACGGCTCACCAAGGCGACG  286
Query  251  ATGGGTAGGGGAACTGAGAGGTTTATCCCCCACACTGGTACTGAGACACGGACCAGACTC  310
Sbjct  287  ATGGGTAGGGGAACTGAGAGGTTTATCCCCCACACTGGTACTGAGACACGGACCAGACTC  346
Query  311  CTACGGGAGGCAGCAGTGAGGAATATTGGTCAATGGGCGAGAGCCTGAACCAGCCAAGTC  370
Sbjct  347  CTACGGGAGGCAGCAGTGAGGAATATTGGTCAATGGGCGAGAGCCTGAACCAGCCAAGTC  406
Query  371  GCGTGAAGGAAGACAGTCCTAAGGATTGTAAACTTCTTTTATACGGGAATAACGGGCGAT  430
Sbjct  407  GCGTGAAGGAAGACTGTCCTAAGGATTGTAAACTTCTTTTATACGGGAATAACGGGCGAT  466
Query  431  ACGAGTATTGCATTGAATGTACCGTAAGAATAAGCATCGGCTAACTCCGTG  481
Sbjct  467  ACGAGTATTGCATTGAATGTACCGTAAGAATAAGCATCGGCTAACTCCGTG  517
```

Figure 6.2 Confirmation of P. gingivalis in bacterial samples where a) shows an example of P. gingivalis growing upon a blood agar plate. Figure 16b indicates PCR identification of P. gingivalis where water was used as a negative control for the P. gingivalis primer and the F. nucleatum primer was used as a negative control for the bacterial sample and a 16s universal primer was used to ensure the presence of bacteria in the sample (key: +=bacterial sample present in sample, -=water used as a negative control). However, the presence of P. gingivalis could not be identified using standard PCR techniques. Hence the 16s band was excised from the gel and sequenced. Figure 16c indicates comparative sequencing alignment data where a 99% match to the presence of P. gingivalis was obtained. Hence, this confirmed the presence of P. gingivalis in the culture samples.

6.2.2 Salivary Biofilm

Subsequent to growth and characterisation of the species described in section 6.2, a salivary biofilm was grown and characterised to ensure its relevance to the human oral microbiome.

6.2.2.1 Results

Data indicated the generation of a well characterised 7 day biofilm model derived from saliva extracted from 20 individuals (ethics described in section 2.2.2.3.1). Biofilm growth was monitored utilising live/dead staining where Figure 6.4 shows depth of the biofilm increased from 34.2µm to 60.5µm and relative ratios of live/dead bacteria declined over the 7 day culture period from 86.2% viability on day 1 to 75.1% viability on day 7 as displayed in Figure 6.3.

Following monitoring of growth, DNA was harvested from the salivary biofilm and 16s sequencing was used to determine its composition. Sequencing output information regarding the relative abundance of organisms at different taxonomic levels, where the most abundant phyla was the Gram positive Firmicutes (97.4%) followed by Gram negative Proteobacteria (2.2%, Figure 6.5). Figure 6.6 shows the composition of the biofilm at the class and order taxonomic levels, where 96.37% and 2.2% of the sample are comprised of the bacilli (part of the Firmicutes family) and gammaproteobacteria (part of the Proteobacteria family) classes respectively. The most abundant organisms at the order level were lactobacilli, comprising 79.1% of the sample.

Genus-level sequences that comprised at least 0.1% of the amplicon sequence variables (ASV) were as follows (comprising at least 0.1% of the total biofilm population): *Streptococcus* (75.16%), *Staphylococcus* (19.35%), *Aggregibacter* (2.13%), *Lactobacillus* (1.19%), *Veilonella* (0.70%), *Granulicatella* (0.53%), *Prevotella* (0.17%) and *Bacteroides*

(0.17%). Interestingly, 0.89% of the total sequences were not classifiable under the genus level and were derived from family levels including Rikenellcae (<0.01%), Lactobacillaceae (0.14%), Christensenellaceae (<0.01%), Lachnospiraceae (0.10%) and Gemellaceae (<0.01%).

Figure 6.7 provides information regarding the composition of the salivary biofilm at the species level where, the specific species within each genus was not identified for 98.94% of the biofilm. Of the remaining 2.3%, 12 species of bacteria were identified. Species-level sequences identified by 16s sequencing were as follows: *Bacteroides caccae* (0.05%), *Bacteroides uniformis* (<0.01%), *Prevotella corpi* (0.17%), *Lactobacillus zeae* (1.19%), *Streptococcus anginosus* (0.01%), *Ruminococcus gnavus* (0.03%), *Faecalibacterium prausnitz* (0.09%), *Veillonella dispar* (0.55%), *Veillonella parvula* (0.15%), *Bulleidia moorei* (<0.01%), *Escherichia coli* (0.03%) and *Haemophilus parainfluenzae* (0.04%).

Figure 6.8 also demonstrates the wide variety of organisms comprising the salivary biofilm at different taxonomic levels. Where, branching indicates how organisms evolved from a common ancestor.

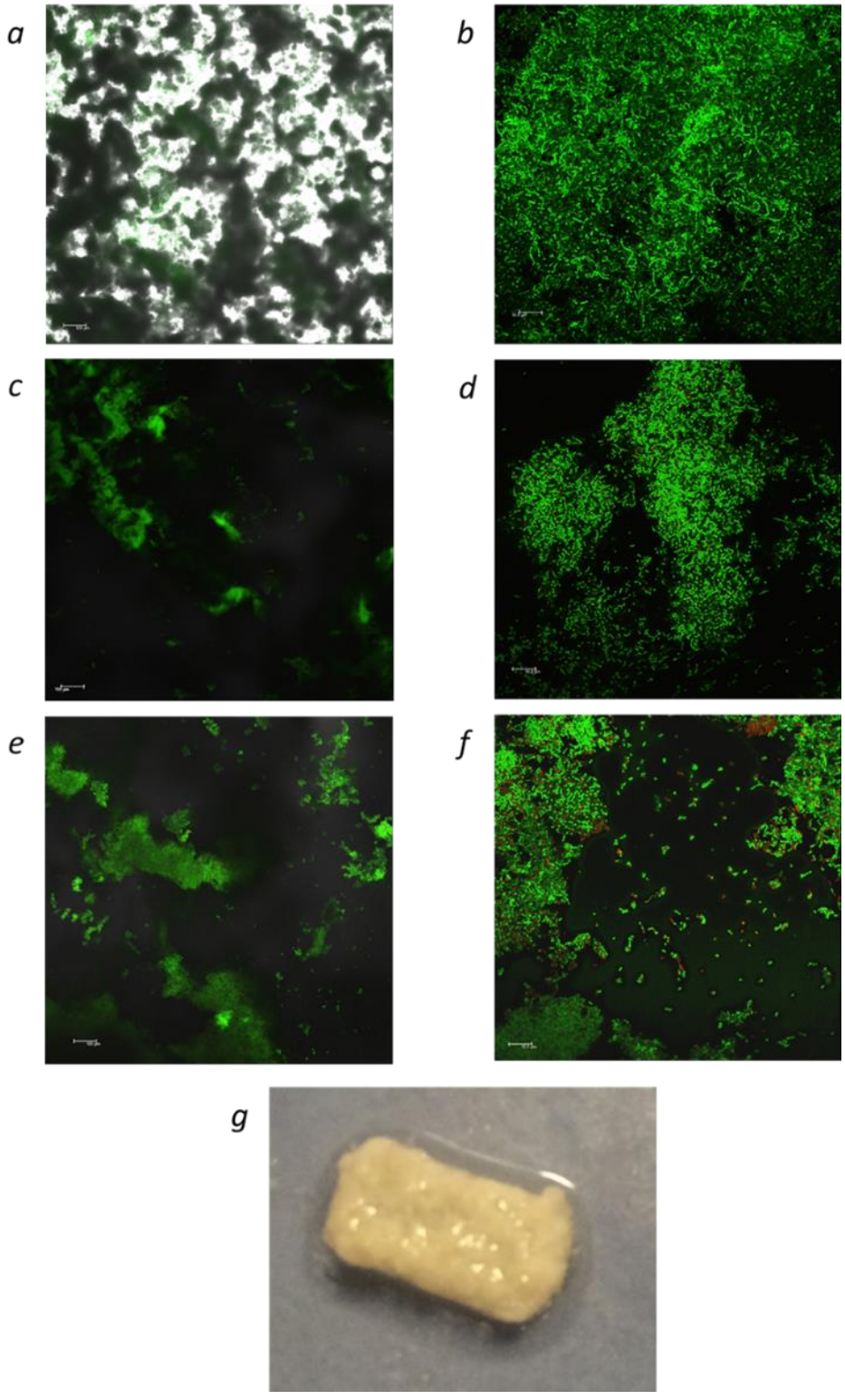

Figure 6.3a-f Representative confocal images of biofilm growth over a 7 day period at either 10x magnification (a, c, e, scale bar: 100µm) or 100x magnification (b, d, f, scale bar: 10µm). Images horizontal to each other indicate a single time point where figures 17a and b show biofilm growth following 24h incubation, figures 17c and d show growth following 4 days incubation and figures 17e and f show growth following 7 days incubation. Figure 17g shows a representative image of biofilm growth upon a PMMA substrate following 7 days incubation.

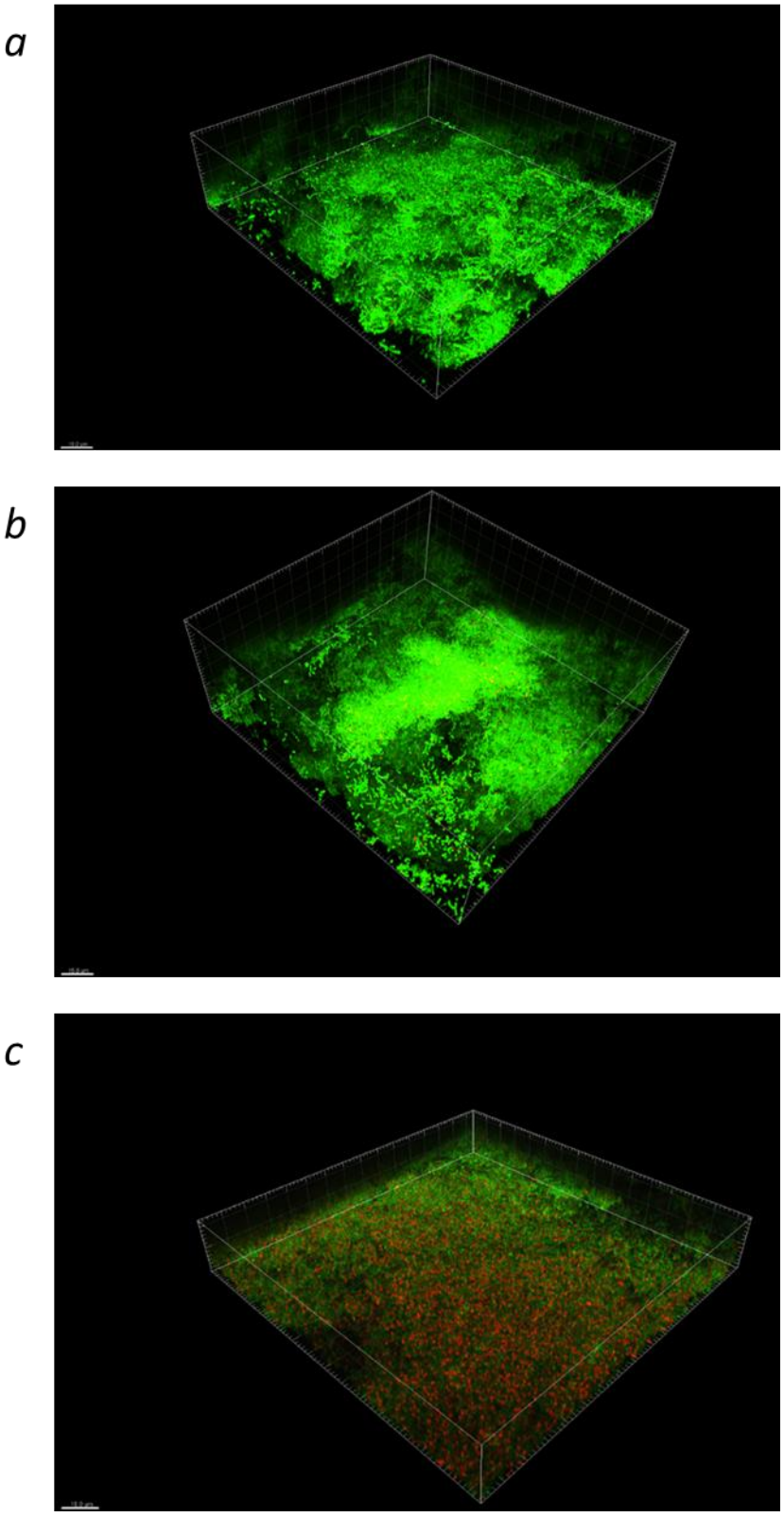

Figure 6.4 Z stack images of biofilm growth to identify changes in biofilm thickness and relative ratio of live to dead bacteria (green=live, red=dead) over a 7 day period where a) image captured following 24h incubation (depth 34.2µm), b) image captured following 4 days incubation (depth 58.1µm) and c) image captured following 7 days incubation (60.5µm). All scale bars on images are 15µm.

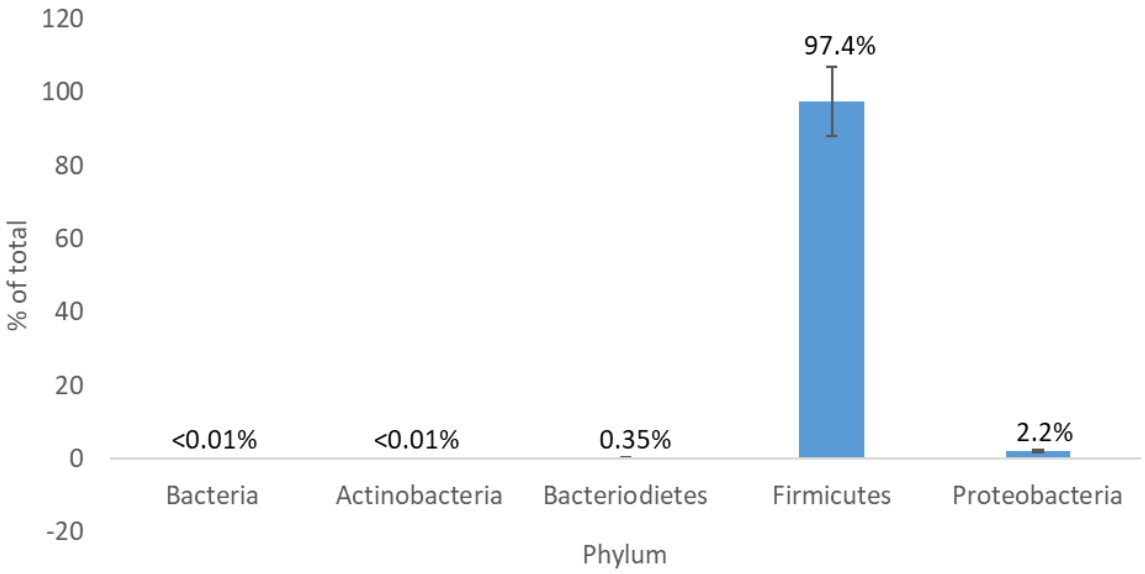

Figure 6.5 Relative levels of each bacterial phylum in DNA extracted from salivary biofilm following 7 days incubation. Samples were assayed in triplicate and the "Bacteria" category denotes bacterial phyla that could not be identified using 16s sequencing.

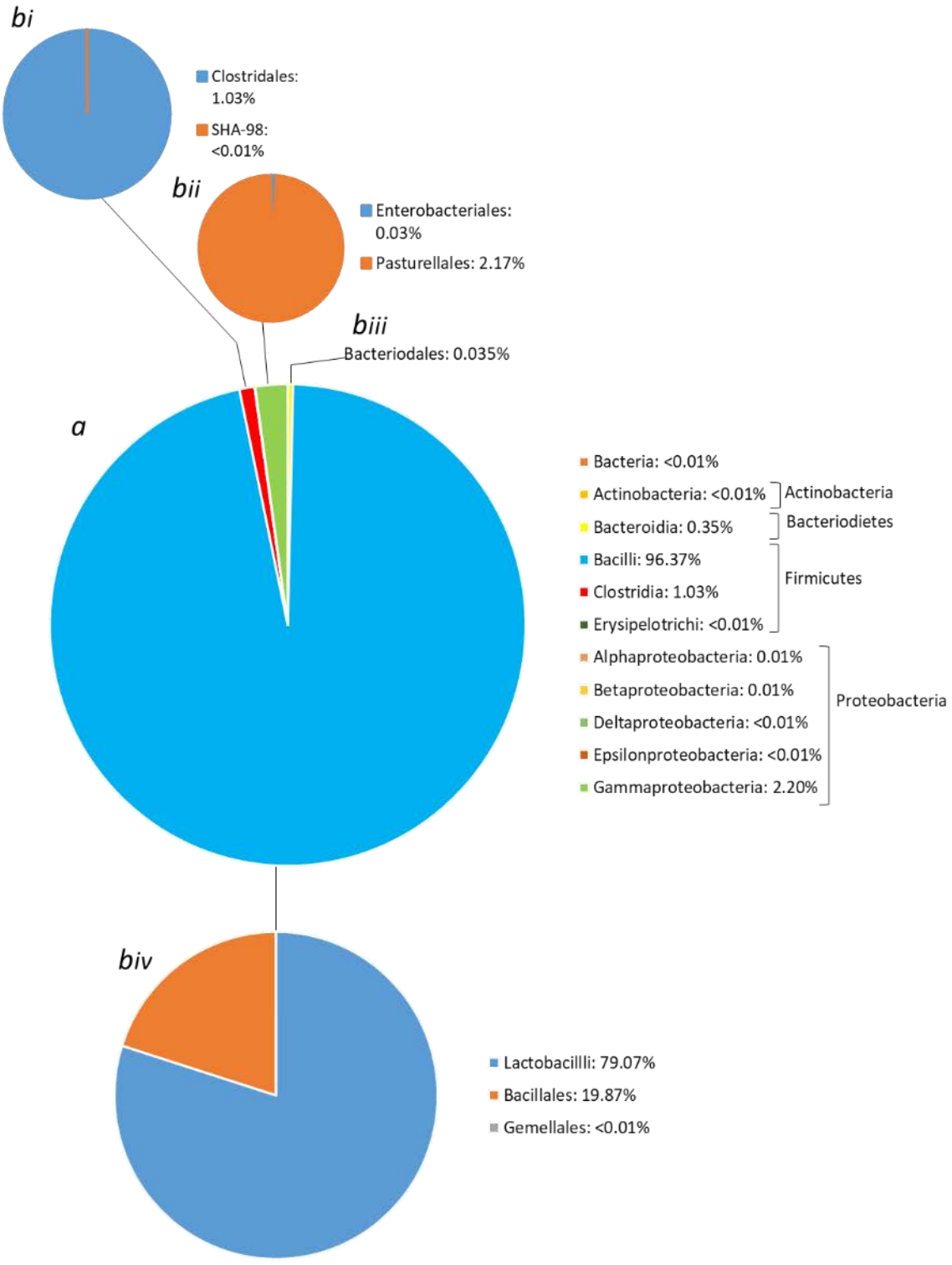

Figure 6.6 Assessment of the composition of the salivary biofilm at increasingly specific taxonomic levels where a) shows designation of bacterial class, where the bacilli bacterial class under the Firmicutes phylum is most abundant. Figure 20b indicates further analysis evaluating salivary biofilm composition at the order taxonomic level where bi) shows bacterial orders under the clostridia class, bii) bacterial orders under the gammaproteobacteria class, biii) the single order: bacteriodales in the salivary biofilm sample under the bacteroidia class and biv) indicates bacterial orders including lactobacillus under the bacilli class.

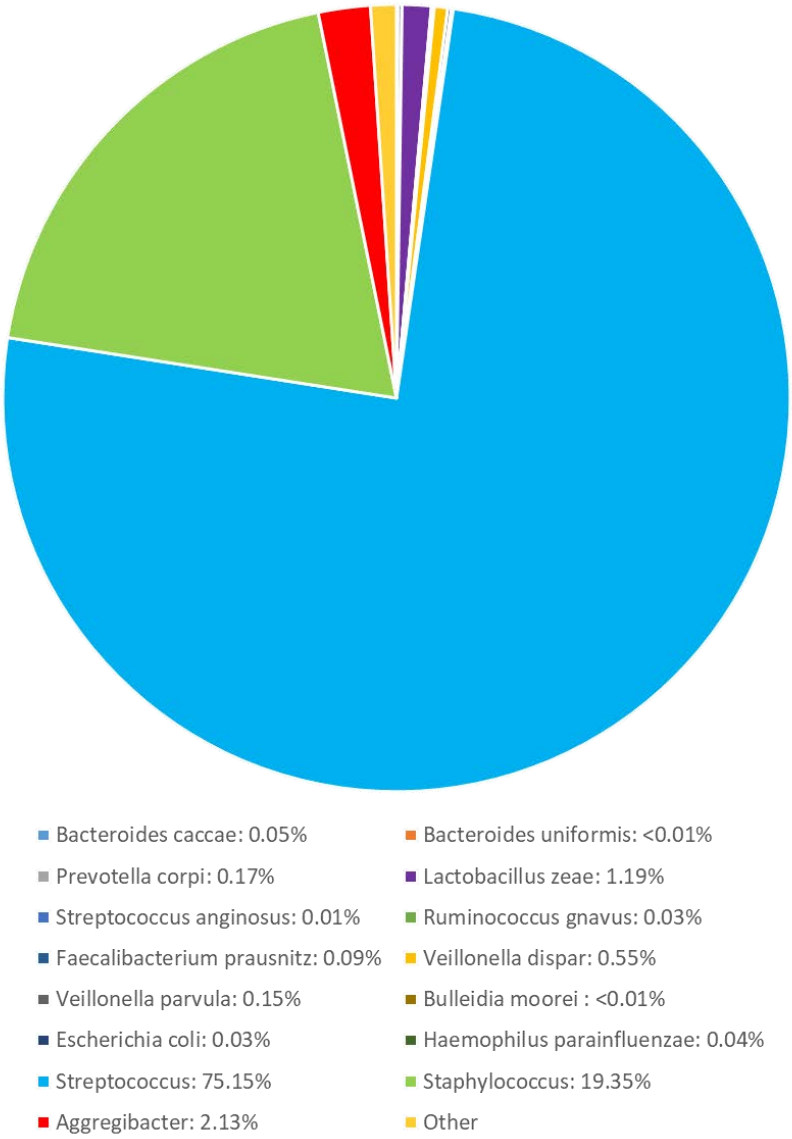

Figure 6.7 Pie chart showing genus and species and their relative abundance within the salivary biofilm where each value was taken as an average of the relative % abundance of each species within each biofilm samples (n=3).

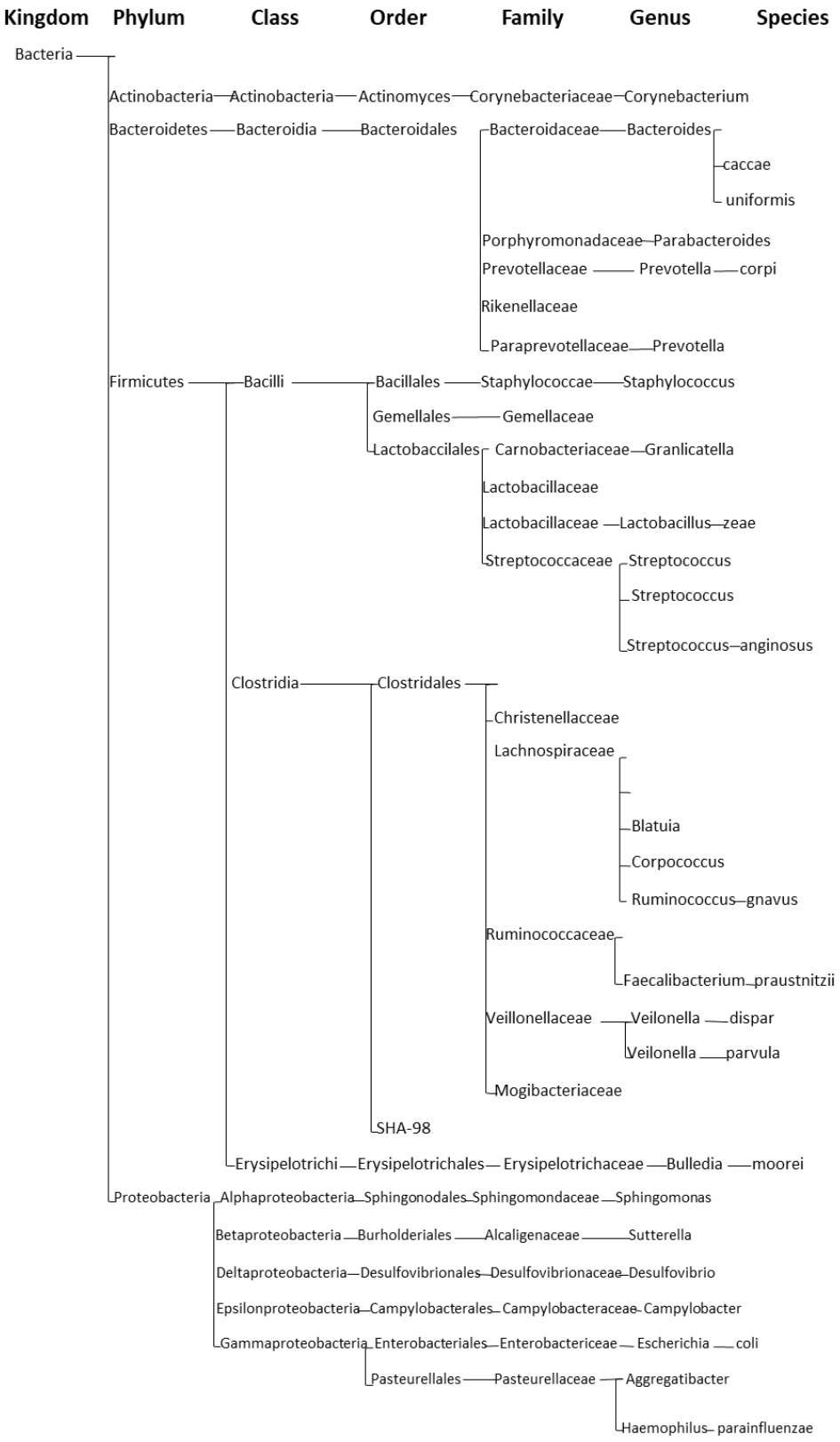

Figure 6.8 Phylogenetic tree showing all of the groups comprising the salivary biofilm. The diagrams show the relationship between organisms where the pattern of branching is indicative of how groups evolved from a common ancestor. It also provides some clarity of the diversity of organisms within the salivary biofilm. Branches are not drawn to scale of evolutionary distance due to lack of information from final excel file, which could therefore not be input into a Phylogenetic tree builder such as iTOL.

6.3 Determining optimal dose of pro-inflammatory stimuli required to induce increases in ROS production and IL-8 secretion.

6.3.1 F. nucleatum and P. gingivalis

Prior to the assessment of the effects of PBM on *in vitro* inflammation induced by periodontal disease relevant stimuli, the optimal dose for each bacterial stimulus required to induce an inflammatory response from HGFs was assessed. Studies involved assessment of the effect of heat inactivated *F. nucleatum* or *P. gingivalis* on two key markers of inflammation: ROS and IL-8, 24h post-application as is described in section 5.2.

6.3.1.1 Results

Results indicate *F. nucleatum* and *P. gingivalis* induced increases in markers for inflammation in a dose dependent manner 24h post-application. Where, application of a MOI 100:1 of *F. nucleatum* induced a 29.74% increase in ROS production (Figure 6.9, $p<0.001$) and a 1422.03% increase in IL-8 secretion (Figure 6.10, $p<0.001$). Comparatively, a MOI of 500:1 of *P. gingivalis* was required to induce significant increases ($p<0.05$) in ROS production (14.95%,Figure 6.9) and IL-8 secretion (176.45%, Figure 6.10). Hence, these concentrations of each bacterial stimuli were selected to evaluate the effects of PBM on inflammation induced by periodontally relevant bacteria.

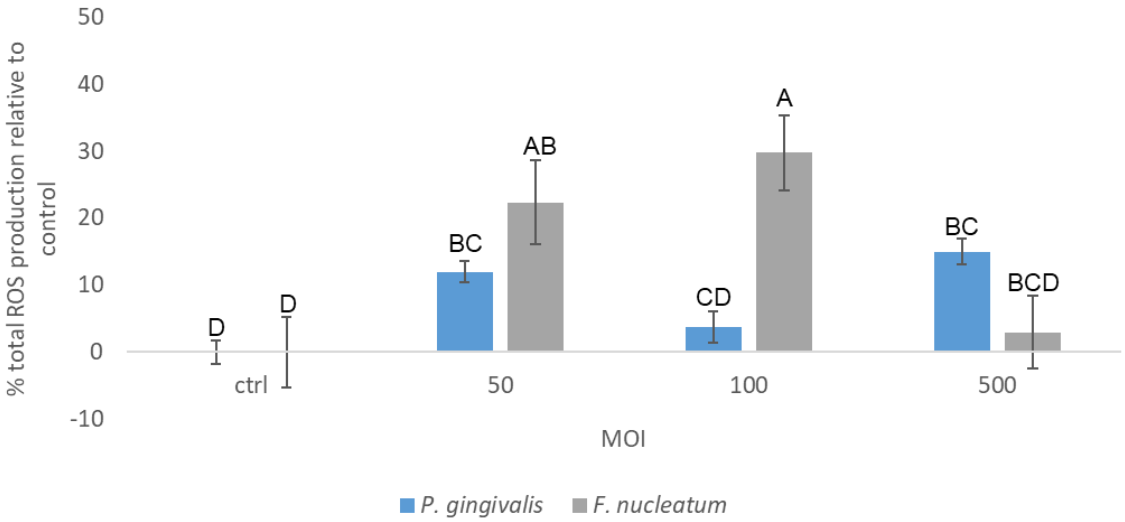

Figure 6.9 Relative % ROS production from HGFs (pool p6/7, n=18) 24h post-application of either P. gingivalis (50-500:1 MOI) or F. nucleatum (50-500:1 MOI) relative to the untreated control, where the untreated control was normalised to 0%. Significance was assessed using one-way ANOVA followed by Tukey test where significance is indicated where means do not share the same letter (p<0.05).

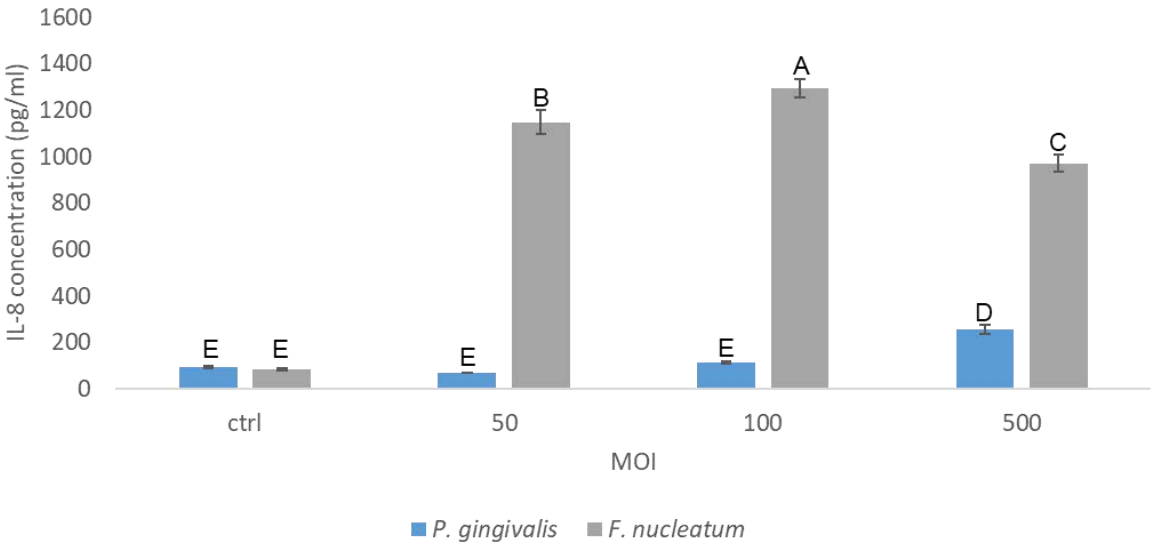

Figure 6.10 Secretion of IL-8 from HGFs (pool p6/7, n=18) 24h post-application of either P. gingivalis (50-500:1 MOI) or F. nucleatum (50-500:1 MOI). Significance was assessed using one way ANOVA followed by Tukey test where significance is indicated by means that do not share the same letter ($p<0.05$).

6.3.2 Salivary Biofilm

As described in section 6.3.1, prior to the application of PBM the optimal dose of bacterial stimuli required to induce *in vitro* inflammation was investigated. However, as the salivary biofilm was composed of a plethora of bacterial species the MOI could not be calculated based on a single OD reading. Hence, a BCA assay to assess protein concentration in both *F. nucleatum* samples and salivary biofilm samples was employed. This would then enable establishment of the relative protein concentration of *F. nucleatum* required to induce an inflammatory response as described in section 6.4.1.1 and hence evaluate the effects of salivary biofilm at a comparable concentration range on ROS production and IL-8 secretion.

6.3.2.1 Results

Results provide evidence of the pro-inflammatory effect of 'heat inactivated' salivary biofilm on pHGFs 24h post-application. Firstly, an appropriate range of concentrations to evaluate the optimal dose of biofilm required to induce a pro-inflammatory response were selected. This involved the use of a BCA protein assay to determine the protein concentrations of suspensions of both *F. nucleatum* and salivary biofilm, in which a standard curve using bovine serum albumin (BSA) at a concentration range of 2000-25µg/ml was used to predict protein concentration of samples. The protein concentration in a suspension *F. nucleatum* was evaluated to act as a standard, in which known volumes of this stimulus had been applied previously to induce inflammation, as described in section 6.3.1. Protein concentrations of a 1µg/ml sample of LPS and a suspension of heat inactivated *P. gingivalis* were also evaluated. However, the protein levels in these samples were negligible (data not shown) and hence *F. nucleatum* was the only viable option to provide a standard for this model.

Hence, the protein content of 25, 12.5 or 6.25µl of a suspension of $3.8x10^9$ bacterial cells/ml of *F. nucleatum* was assessed, enabling the production of a standard curve as shown in Figure 6.11*a*. Similarly, the same volumes of salivary biofilm with unknown MOI were used to create a standard curve as described in Figure 6.11*b*. From these data, the equations of either standard curve were used to establish an appropriate range of concentrations to assess the pro-inflammatory effects of salivary biofilm *in vitro.* As described in section 6.3.1.1, a concentration of 100:1 MOI of *F. nucleatum* was sufficient to induce significant increases in IL-8 secretion and ROS production *in vitro*. Therefore, protein concentrations of suspensions of *F. nucleatum* with MOIs of 300-50:1 were selected for evaluation and calculated as follows:

A. Calculation of the volume of suspension in which there will be 300-50 *F. nucleatum*

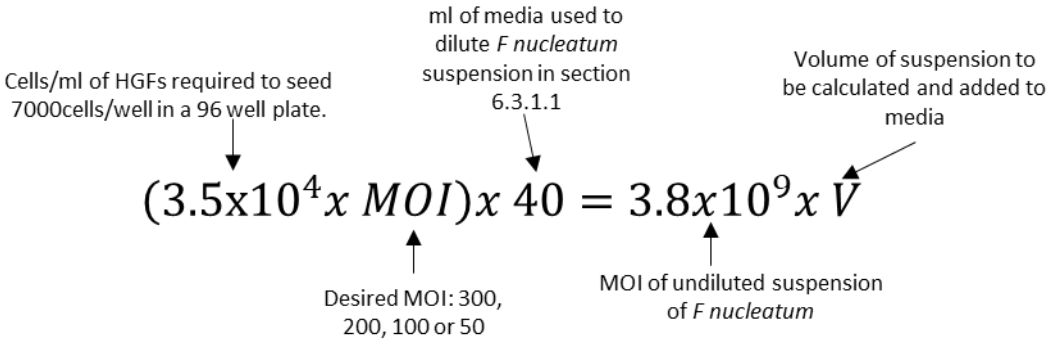

cells per gingival fibroblast:

B. The equation of the *F. nucleatum* standard curve (Figure 6.11*a*) was then used to calculate the protein concentration in bacterial suspensions of the desired MOI.

C. The salivary biofilm trend line equation was then used to calculate the volume of suspension required to possess comparable levels of protein of *F. nucleatum* at the desired MOI. This volume could then be applied *in vitro* in a defined volume of media. Figure 6.11*c* describes the final volumes of salivary biofilm suspension selected to be applied to pHGFs.

Following selection of these concentrations, it was found that the salivary biofilm induced an inflammatory response in gingival fibroblasts in a dose dependent manner 24h post-stimulation. Where, application of the salivary biofilm at 4.2µl/ml induced 969.90% (Figure 6.12, $p<0.001$) and 18.58% (Figure 6.13, $p<0.001$) increases in IL-8 secretion and ROS production respectively relative to the unstimulated control. Hence, this concentration was selected to assess the effects of PBM in modulating inflammation induced by salivary biofilm application.

Interestingly, Figure 6.14 also provides data indicating the effects of pro-inflammatory stimuli on IL-8 secretion were bacterial dependent where application of LPS, *F. nucleatum* or salivary biofilm induced 1102.13%, 1422.03% and 969.99% increases in IL-8 secretion relative to an untreated control ($p<0.001$). Comparatively, application of *P. gingivalis* induced a 176.4% increase in IL-8 secretion, which was significantly lower than levels induced by the other pro-inflammatory stimuli ($p<0.001$).

a

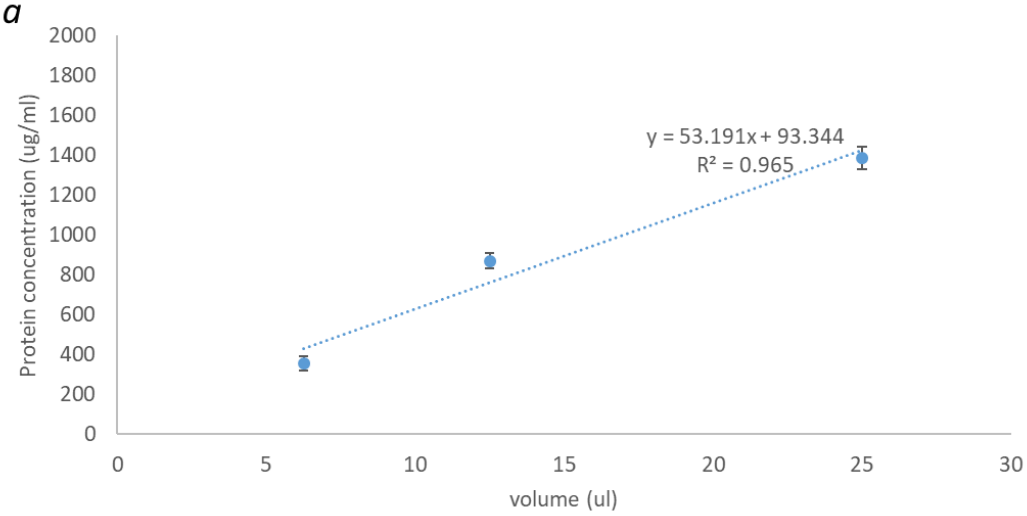

b

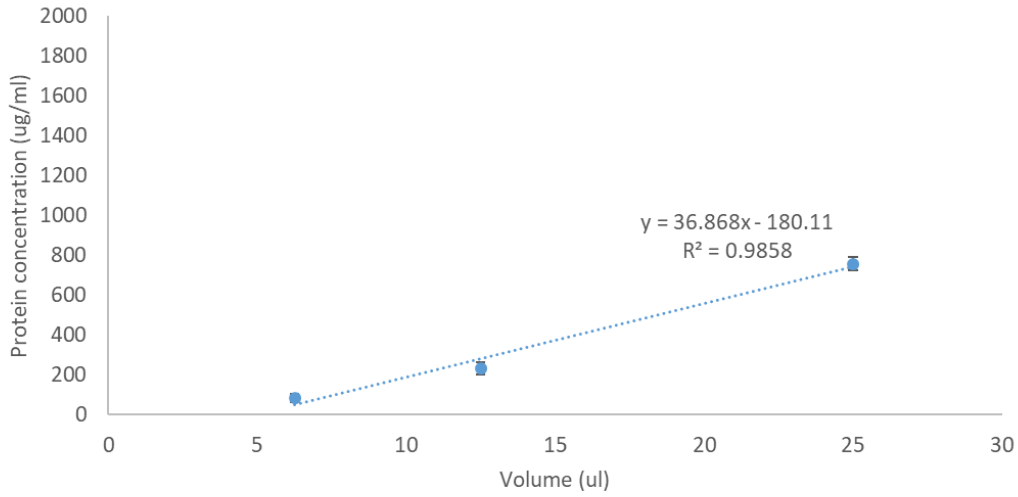

c

MOI	Heat inactivated *F nucleatum* Volume of supension (µl/40ml)	Heat inactivated *F nucleatum* Protein concentration (µg/40ml)	Salivary Biofilm Volume of suspension (µl/40ml)	Salivary Biofilm Volume of suspension (µl/ml)
300	111	4012.5	167	*4.2*
200	74	3032.7	87	*2.8*
100	36	2008.2	59	*1.5*
50	18	1050.8	33	*0.8*

Figure 6.11 The methodology used to calculate protein concentrations of salivary biofilm comparable to those applied to induce inflammation using a suspension of F. nucleatum in vitro. In which firstly, a 3 point serial dilution of each bacterial stimulus was created using 25, 12.5 and 6.25µl (n=3). Volumes were selected based on experimental protocol of the Pierce BCA protein assay. A standard curve (see appendix) was then used to calculate protein content at each volume of the suspension where a) indicates protein concentration in a serial dilution of heat inactivated F. nucleatum polymorphum ($3.8x10^9$:1 MOI suspension) and b) indicates protein concentration in a serial dilution of heat inactivated salivary biofilm. From this, volumes of the biofilm suspension could be selected for experimentation based upon volumes and thus protein concentrations used to stimulate inflammation by F. nucleatum in vitro as described in section 6.3.1. These were calculated from the equations of the standard curves depicted in a) and b) and results are described in c).

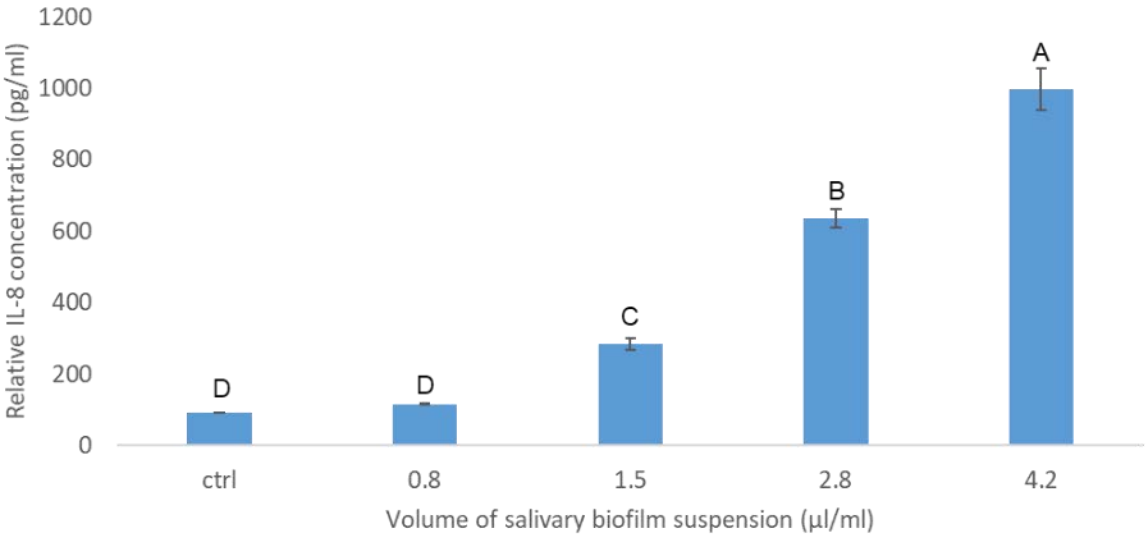

Figure 6.12 The effects of increasing concentrations ('heat inactivated' salivary suspension was added to phenol red free media containing 10% FBS to produce a final volume of 10ml) of salivary biofilm suspension on IL-8 secretion from pHGFs (p7, n=10) 24h post-application. Significance was analysed using one-way ANOVA followed by Tukey test where different letters indicate significant differences between means.

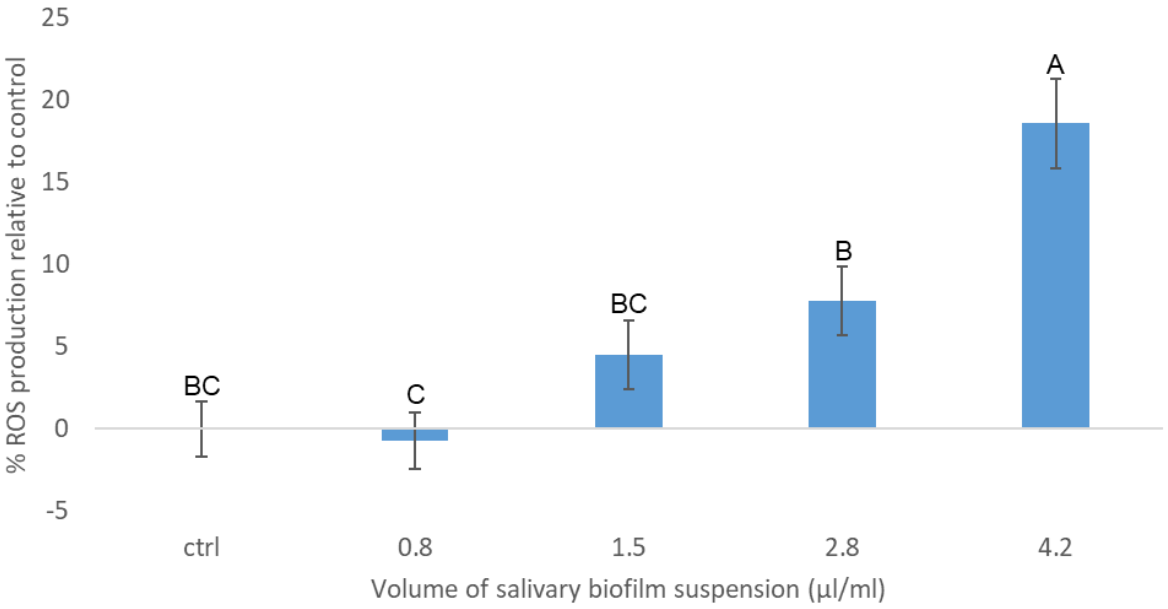

Figure 6.13 The effects of increasing concentrations of salivary biofilm (salivary suspension was added to phenol red free media containing 10% FBS to produce a final volume of 10ml) on ROS production 24h post-application, where ROS production was measured as a % of the unstimulated control (unstimulated control was normalised to 0%). Significance was assessed using one way ANOVA followed by Tukey test where different letters indicate significant differences between means.

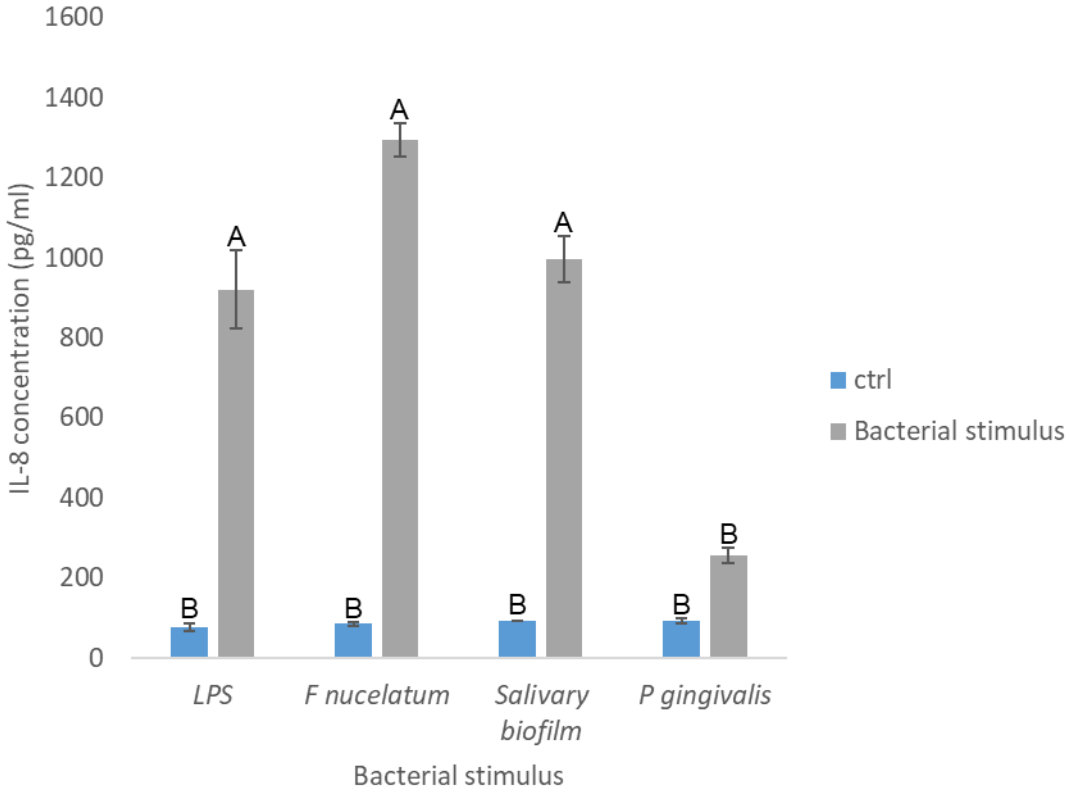

Figure 6.14 The effects of LPS (1µg/ml, n=10, pool p6/7), F. nucleatum (100:1 MOI, n=10, pool p7), Salivary biofilm (4.2µl/ml = 300:1 MOI, n=12, pool p7) and P. gingivalis (500:1 MOI, n=12, pool p7) on IL-8 secretion 24h post-application, relative to respective untreated controls. Significance was assessed using one way ANOVA followed by Tukey test in which significance is indicated where means do not share the same letter.

6.4 The effects of PBM on cell number and metabolic activity

To aid comparison with data evaluating the effects of PBM following application of LPS (see section 5.3.1), the effects of PBM following application of *F. nucleatum*, *P. gingivalis* or salivary biofilm on cell number and metabolic activity were evaluated.

6.4.1.1 Results

Results indicate the effects of pro-inflammatory stimuli on cell number. Where, application of *F. nucleatum*, *P. gingivalis* or salivary biofilm induced 2.29% (ns, Figure 6.15), 10.83% (ns, Figure 6.16) and 23.08% ($p<0.05$, Figure 6.17) decreases in cell number respectively relative to the corresponding untreated control. However, whilst irradiation at 450 nm induced 14.96% (Figure 6.16b) and 7.15% (Figure 6.17b) increases in cell number relative to the *P. gingivalis* or salivary biofilm treated control 24h post-application respectively, these increases were not significant. Indeed, light application induced no significant changes in cell number relative to any respective bacterially stimulated control. The greatest mean changes in cell number induced by light however, were those induced by irradiation at 450 nm following application of salivary biofilm (Figure 6.17). Interestingly, salivary biofilm was also the only pro-inflammatory stimulus to cause significant reductions ($p<0.05$) in cell number relative to the untreated control at all-time points assessed (8, 24, 120 and 144h post-application of a stimulus, Figure 6.17).

Comparatively however, PBM did induce significant changes in cell metabolic activity relative to stimulated controls. Where, following application of *F. nucleatum,* irradiation at 400 nm or 450 nm induced 9.36% and 8.19% increases in cell metabolic activity relative to the *F. nucleatum* treated control ($p<0.05$, Figure 6.18), respectively. Similarly, application of 450 nm light to *P. gingivalis* or salivary biofilm treated cultures induced 9.04% (Figure 6.19, $p<0.05$)

and 5.40% (Figure 6.20, $p<0.05$) increases in cell metabolic activity respectively relative to their particular bacterially stimulated control.

Interestingly, similar to LPS treated cultures (5.3.1), *F. nucleatum* induced significant increases in cell metabolic activity relative to the untreated control (5.34%, $p<0.05$, Figure 6.18). In comparison, however application *of P. gingivalis* or salivary biofilm induced 29.27% ($p<0.05$, Figure 6.19) and 2.56% ($p<0.05$, Figure 6.20) decreases in cell metabolic activity relative to the untreated control. However, despite this blue light (400-450 nm) induced significant increases in cell metabolic activity following application of either of the three bacterial stimuli. Indeed, 810 nm light application only induced significant increases in MTT following application of salivary biofilm ($p<0.05$, Figure 6.20). However, application of NIR light only induced increases in cell metabolic activity of 1.99% relative to the salivary biofilm treated control.

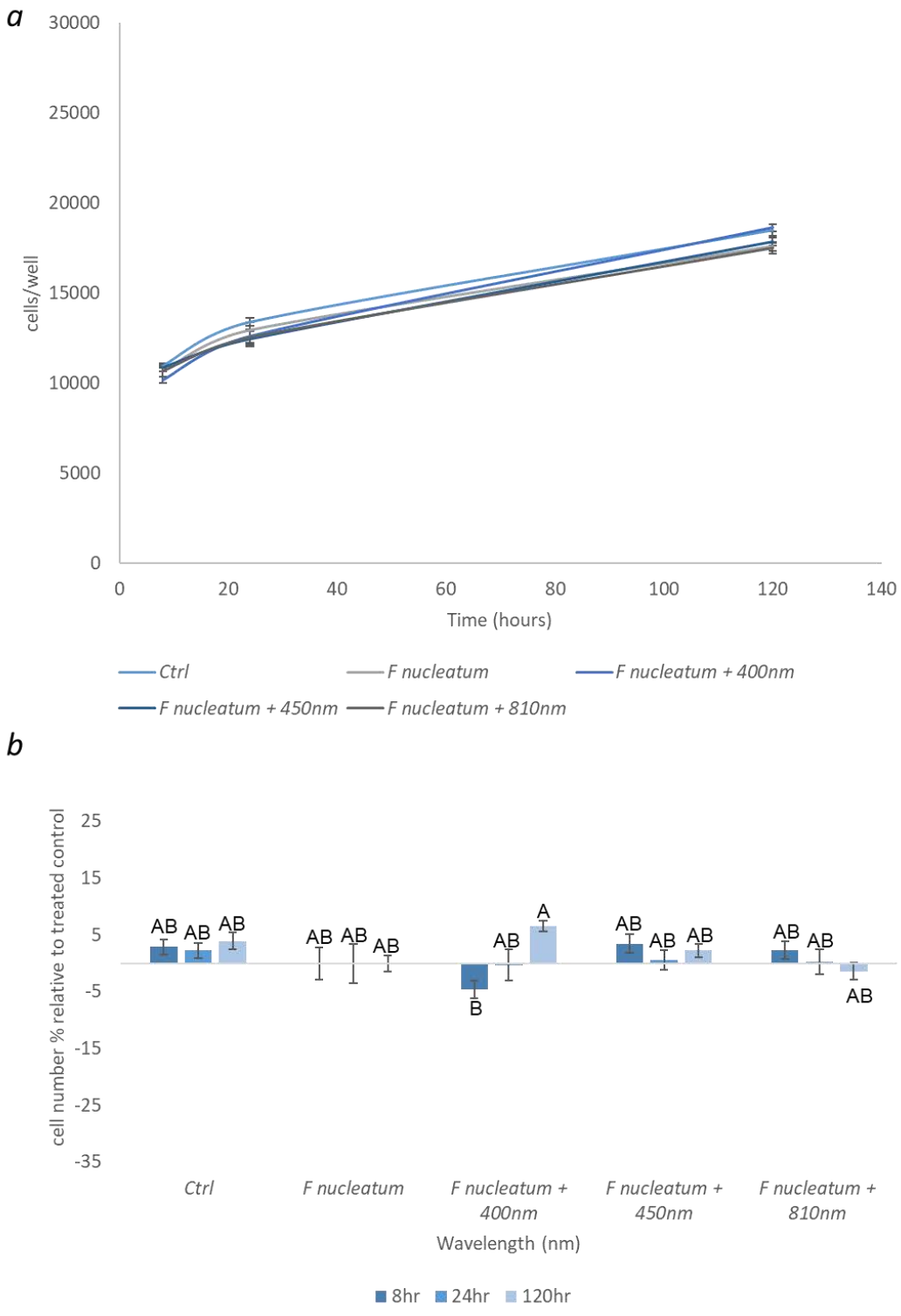

Figure 6.15 PBM modulates (400-810 nm, 24mW/cm², 5.76J/cm²) F. nucleatum (MOI 100:1) induced changes in cell growth (pHGF pool p7, n=12, 4 replicates per plate) 8-120hr post-application of stimuli. a) Shows real time changes in growth from 8-120hr post application of a stimulus and b) shows the percentage change in cell number at three time points (8, 24, 120h) post application of a stimulus relative to the F. nucleatum treated control, where the F. nucleatum control was normalised to 0. Significance was measured using one way ANOVA followed by Tukey test in which significance is indicated where means do not share the same letter($p<0.05$).

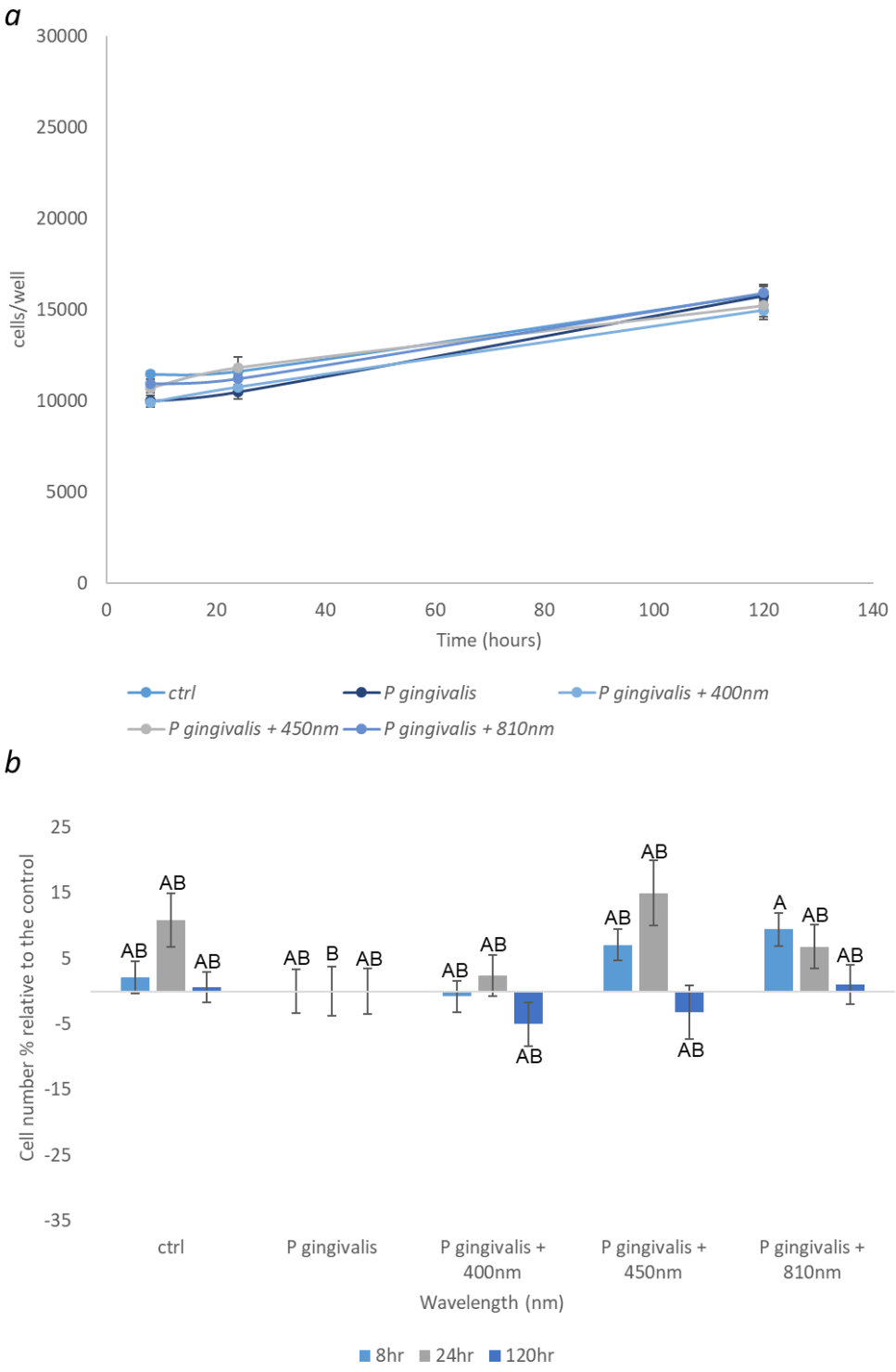

Figure 6.16 Application of light (400-810 nm, 24mW/cm², 5.76J/cm²) following P. gingivalis (MOI 500:1) can modulate cell growth (pHGF pool p7, n=12, 4 replicates per plate) 120hr post-application of stimuli and how this compares to cell growth without the application of either light or P. gingivalis. a) Shows real time changes in growth from 8-120hr post-application of a stimulus and b) shows the percentage change in cell number at three time points (8, 24, 120h) post-application of a stimulus relative to the P. gingivalis treated control, where the P. gingivalis control was normalised to 0. Significance was measured using one way ANOVA followed by Tukey test in which significance is indicated where means do not share the same letter (p<0.05).

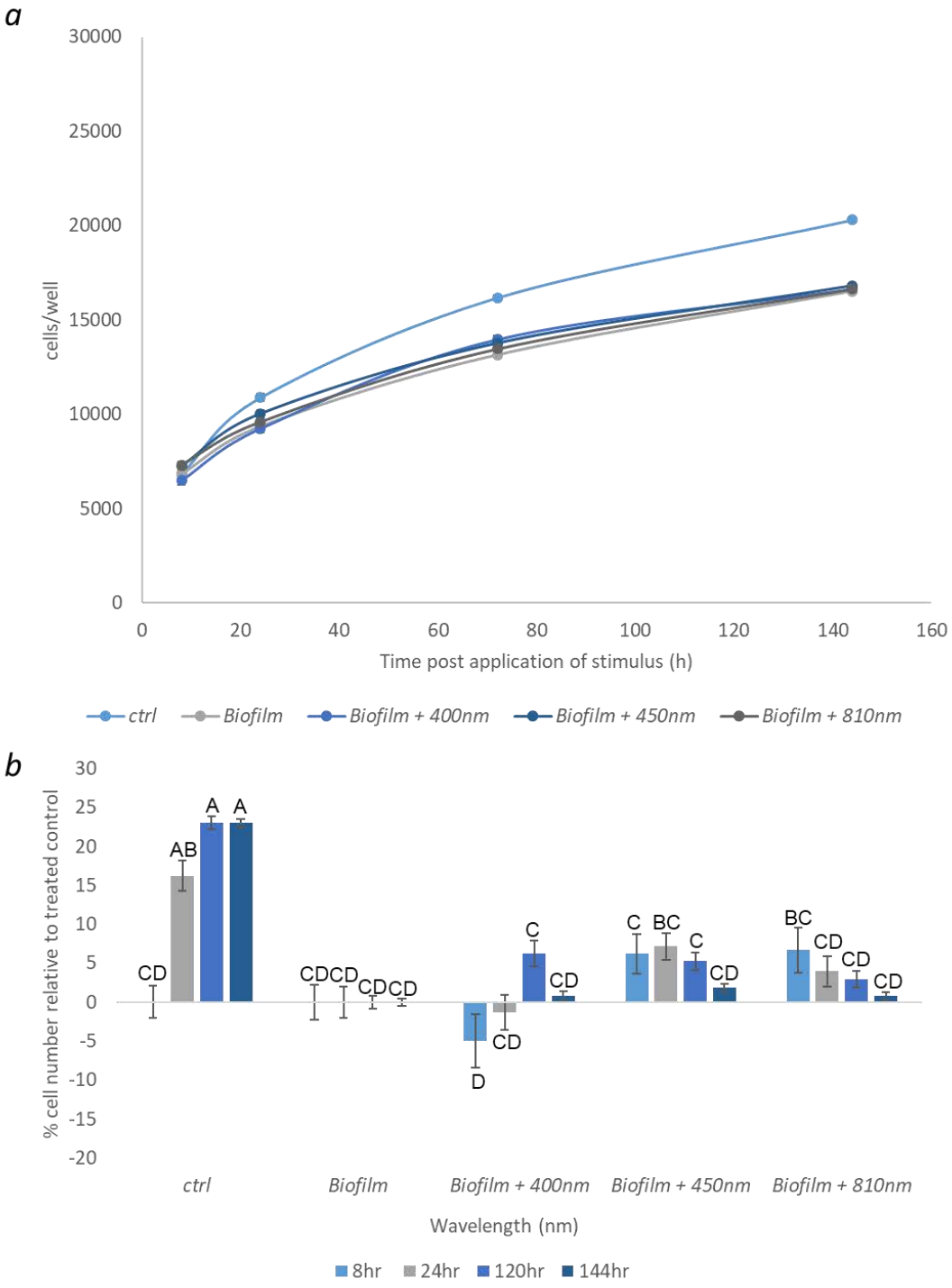

Figure 6.17 Application of light (400-810 nm, 24mW/cm², 5.76J/cm²) following salivary biofilm treatment (4.2µl/ml) can modulate cell growth (pHGF pool p7, n=30, 10 replicates per plate) 120hr post application of stimuli and how this compares to cell growth without the application of either light or salivary biofilm. a) shows real time changes in growth from 8-120hr post application of a stimulus and b) shows the percentage change in cell number at three time points (8, 24, 120h) post application of a stimulus relative to the salivary biofilm treated control, where the salivary biofilm control was normalised to 0. Significance was measured using one way ANOVA followed by Tukey test in which significance is indicated where means do not share the same letter ($p<0.05$).

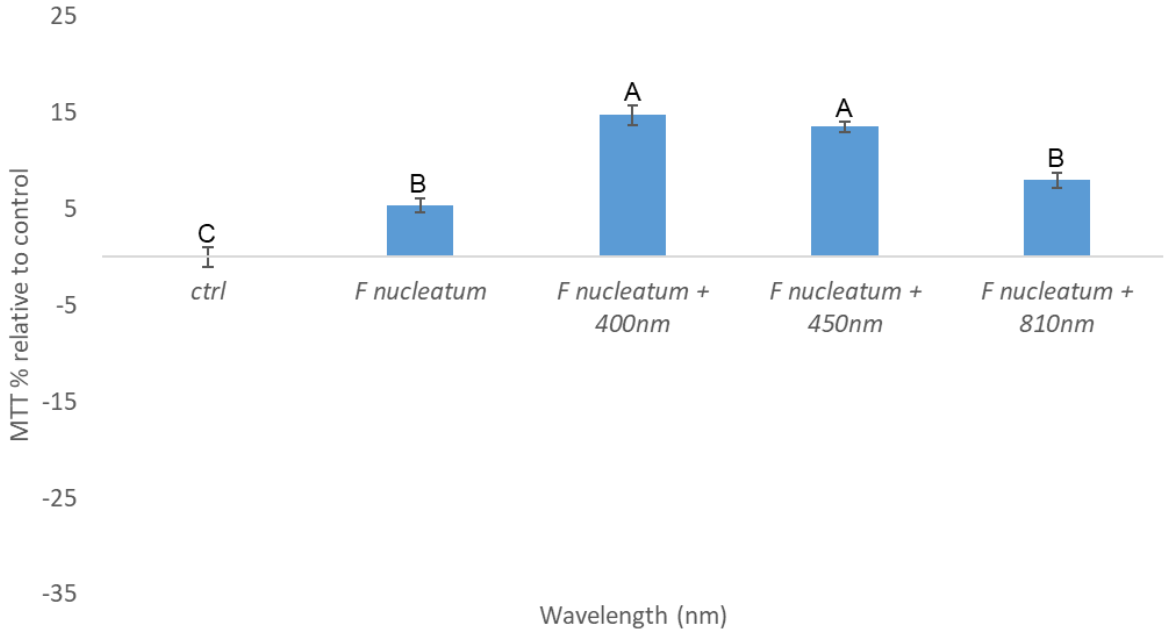

Figure 6.18 The effects of F. nucleatum (MOI 100:1) or F. nucleatum and light (400-810 nm, 5.76J/cm², 24mW/cm², 240s) on cell metabolic activity from pHGFs (pool p7, n=18, 6 replicates per plate) relative to an untreated control 24h post application. Where, significance was measured using one way ANOVA followed by Tukey test in which significance is indicated where means do not share the same letter ($p<0.05$).

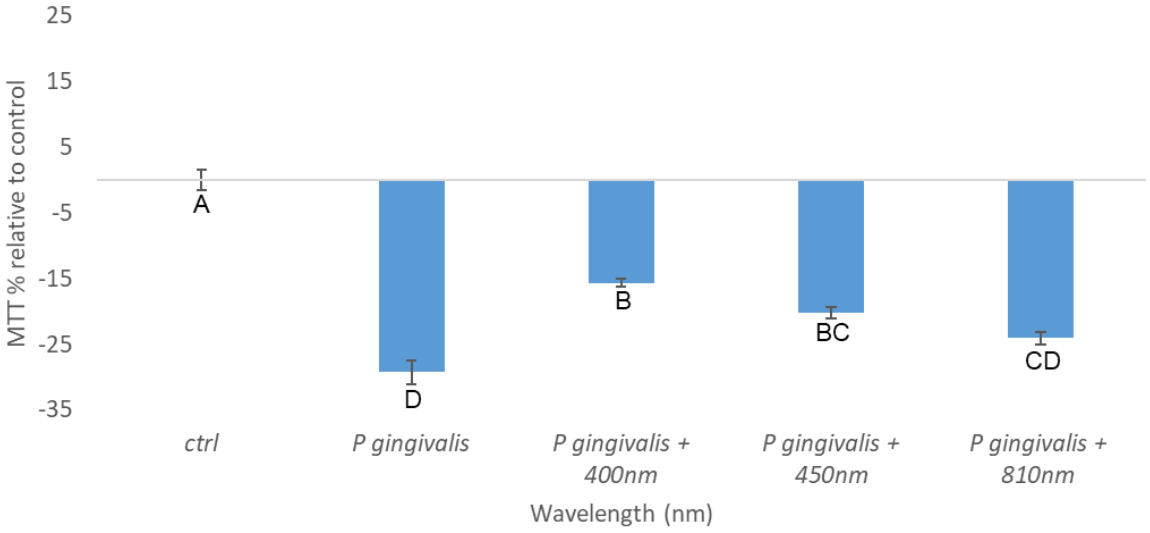

Figure 6.19 The effects of P. gingivalis (MOI 500:1) or P. gingivalis and light (400-810 nm, 24mW/cm², 5.76J/cm², 240s) on cell metabolic from pHGFs (pool p7, n=18, 6 replicates per plate) relative to an untreated control (ctrl), where the control was normalised to 0%. Significance was assessed using one way ANOVA followed by Tukey test where means that do not share the same letter are significantly different (p<0.05).

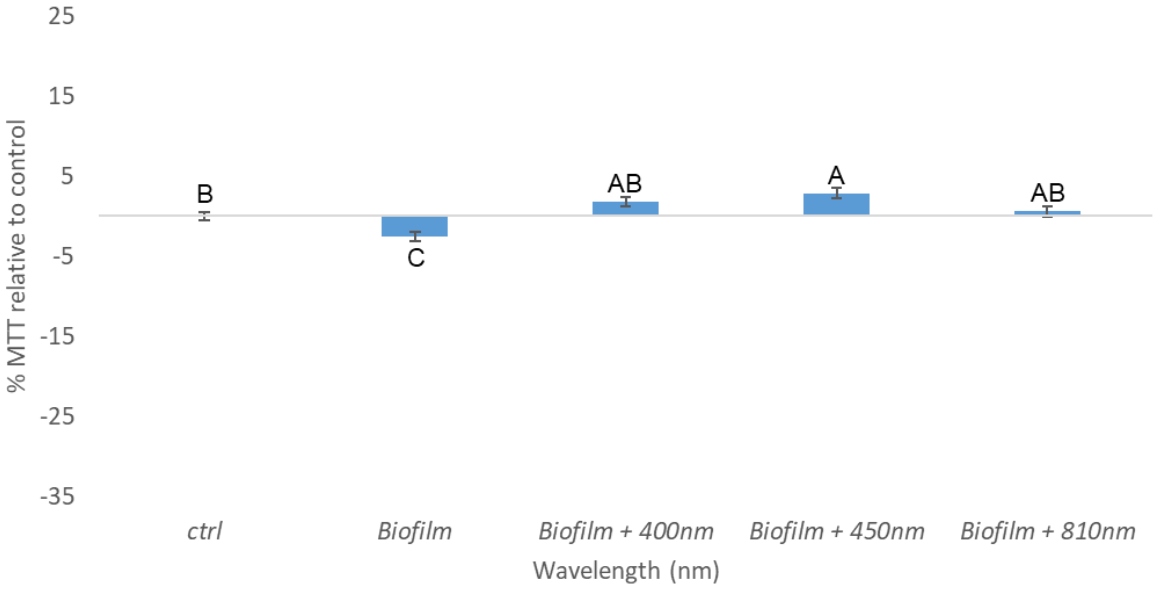

Figure 6.20 The effects of salivary biofilm (4.2µl/ml) or salivary biofilm and light (400-810 nm, 24mW/cm², 5.76J/cm², 240s) on cell metabolic from pHGFs (pool p7, n=30, 10 replicates per plate) relative to an untreated control (ctrl), where the control was normalised to 0%. Significance was assessed using one way ANOVA followed by Tukey test where means that do not share the same letter are significantly different (p<0.05).

6.5 The effects of PBM on markers for inflammation in gingival fibroblast cultures

Following assessment of the effects of PBM in modulating changes in cell growth and metabolic activity induced by bacterial stimuli, the effects on markers for inflammation were investigated. These studies involved assessment of the effects of PBM in modulating changes in IL-8 and TGFβ1 secretion induced by the application of *F. nucleatum, P. gingivalis* or salivary biofilm. Data obtained would then also enable comparison with results presented in section 5.5.

6.5.1 Results

Results demonstrate the effects of PBM in modulating changes in inflammation induced by bacterial stimuli. Where, application of 400 nm light induced 11.29% reduction in ROS production relative to the *F. nucleatum* treated control ($p<0.05$, Figure 6.21a). Similarly, irradiation at 400 nm induced 10.4% and 9.29% decreases in ROS production relative to the salivary biofilm treated control ($p<0.05$, Figure 6.21b) and *P. gingivalis* treated control respectively ($p<0.05$, Figure 6.21c). Interestingly, application of 450 nm light also induced 16.26% and 5.43% decreases in ROS production relative to the salivary biofilm and *P. gingivalis* treated controls, respectively ($p<0.05$). However, application of 810 nm light only induced significant decreases in ROS production relative to the *F. nucleatum* or *P. gingivalis* treated controls ($p<0.05$) but not the salivary biofilm treated control.

Application of 400 nm light also induced 32.12%, 7.29% and 21.33% decreases in TGFβ1 secretion relative to the *F. nucleatum* ($p<0.05$, Figure 6.22a), salivary biofilm ($p<0.05$, Figure 6.22b) or *P. gingivalis* ($p<0.05$, Figure 6.22c) treated controls respectively. Irradiation at 450 nm also induced 18.03% and 24.95% decreases in TGFβ1 secretion relative to the *F. nucleatum* ($p<0.05$) or *P. gingivalis* ($p<0.05$) treated controls respectively.

Data also demonstrated that 400 nm light induced 9.89% and 13.63% decreases in IL-8 secretion relative to the *F. nucleatum* ($p<0.05$, Figure 6.23a) or salivary biofilm ($p<0.05$, Figure 6.23b) treated control. Figure 6.23b also shows that irradiation at 450 nm or 810 nm light induced 14.17% and 14.77% decreases in IL-8 secretion relative to the salivary biofilm treated control ($p<0.05$). Comparatively, Figure 6.24 shows application of 400 nm, 450 nm or 810 nm light induced 36.45%, 28.43% and 29.15% increases in IL-8 relative to the *P. gingivalis* treated control ($p<0.05$).

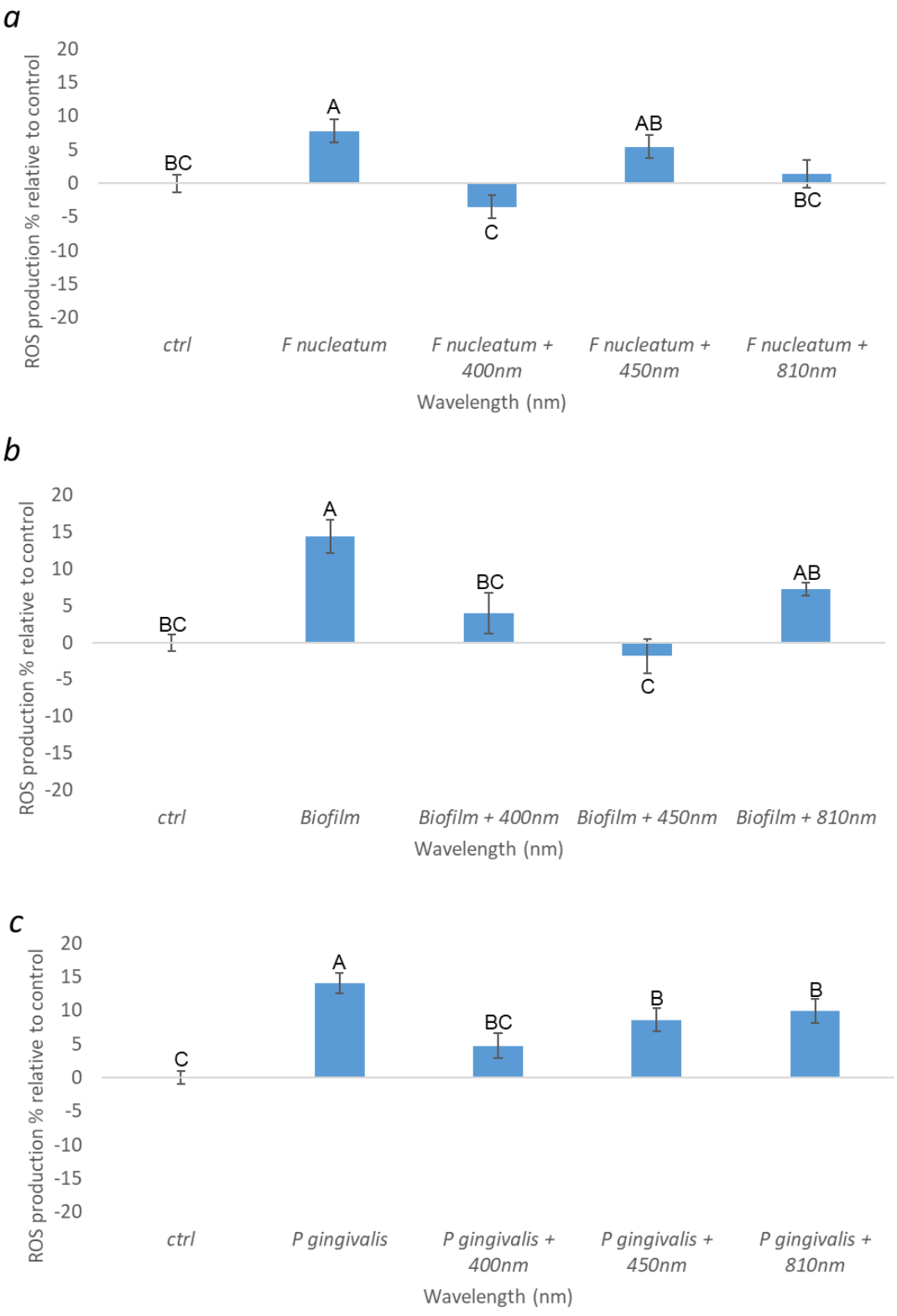

Figure 6.21 The effects of a) F. nucleatum (MOI 100:1), b) salivary biofilm (4.2µg/ml), c) P. gingivalis (MOI 500:1) or PBM and the respective bacterial stimulus (400-810 nm, 24mW/cm², 5.76J/cm²) on ROS production 24h post application relative to an untreated control, where the control was normalised to 0% (pHGF pool p6/7, n=18 per treatment group, 6 replicates per plate). Significance was assessed using one way ANOVA followed by Tukey test in which significance is indicated where means do not share the same letter (p<0.05).

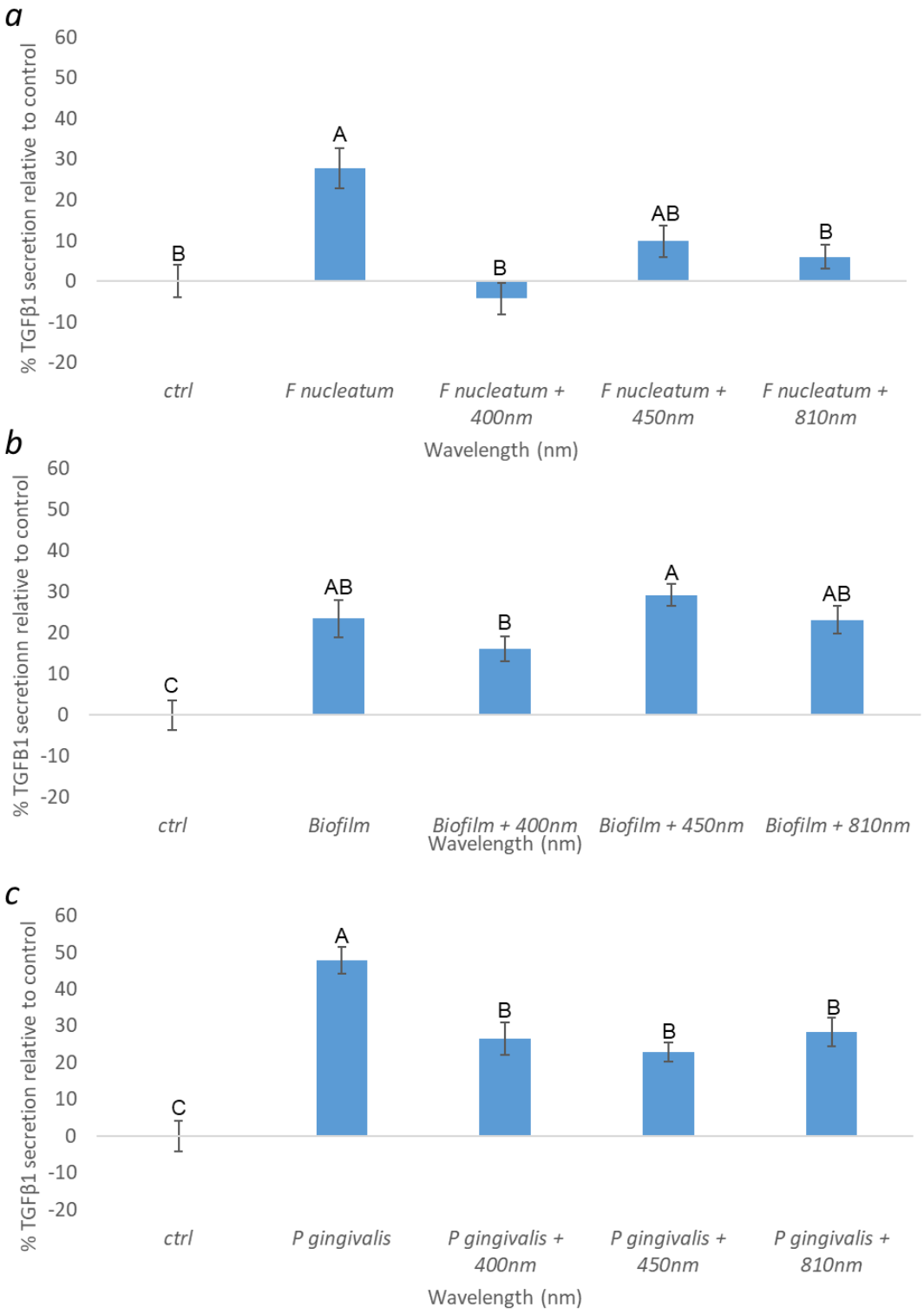

Figure 6.22 The effects of a) F. nucleatum (MOI 100:1), b) salivary biofilm (4.2µg/ml), c) P. gingivalis (MOI 500:1) or the respective bacterial stimulus and light (400-810 nm, 24mW/cm², 5.76J/cm²) on TGFβ1 secretion 24h post application, relative to an untreated control, where the untreated control was normalised to 0% (pHGF pool p7, n=12 per treatment group). Significance was analysed using one way ANOVA followed by Tukey test in which significance is indicated where means do not share the same letter.

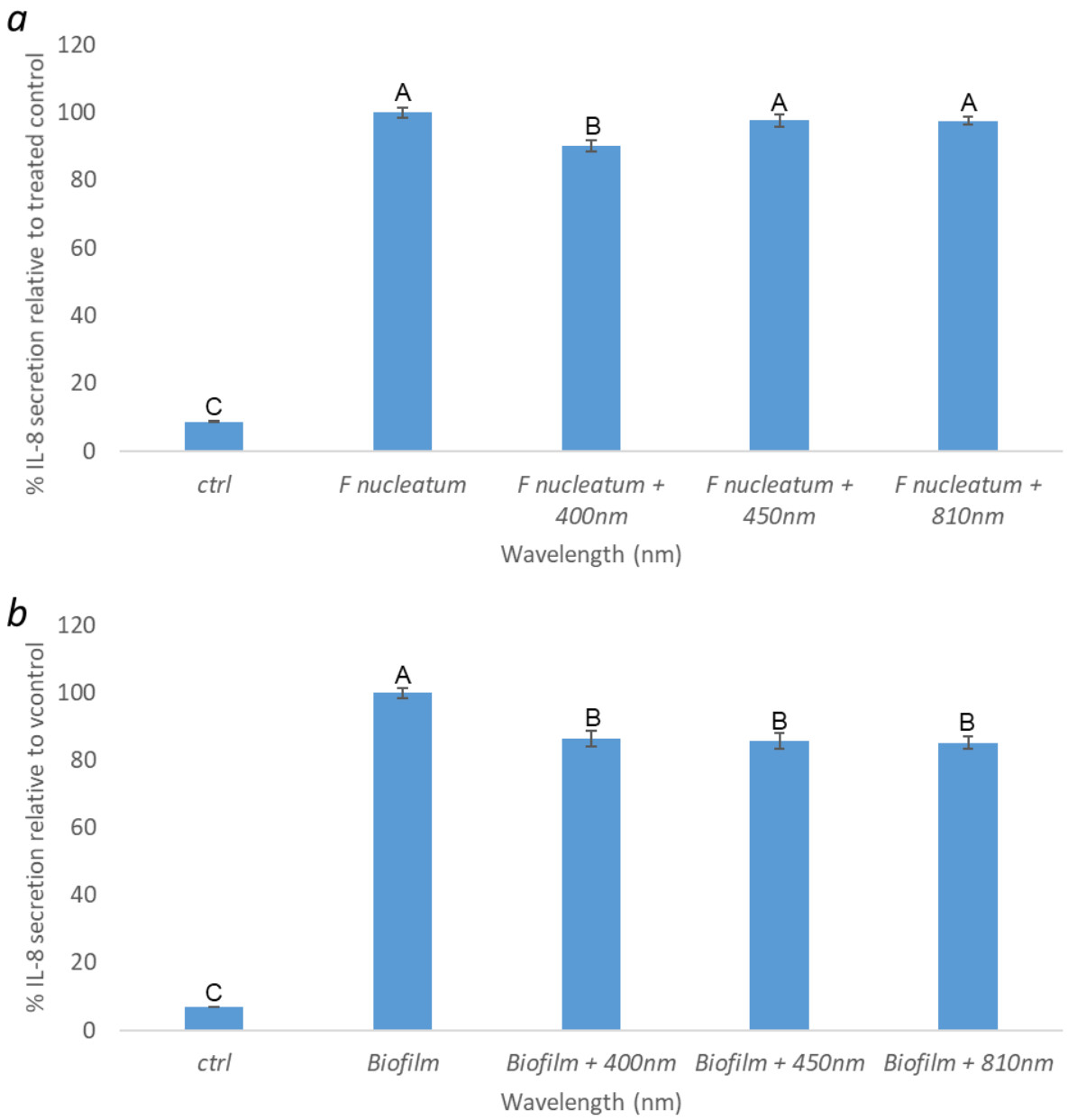

Figure 6.23 The effects of a) F. nucleatum (MOI 100:1), b) salivary biofilm (4.2µg/ml) or light (400-810 nm, 24mW/cm², 5.76J/cm²) and the respective bacterial stimulus on IL-8 secretion 24h post application from pHGFs (pool p7, n=12 replicates per treatment group) relative to an untreated control, where the treated control was normalised to 100%. Significance was analysed using one way ANOVA followed by Tukey test in which means that do not share the same letter are significantly different.

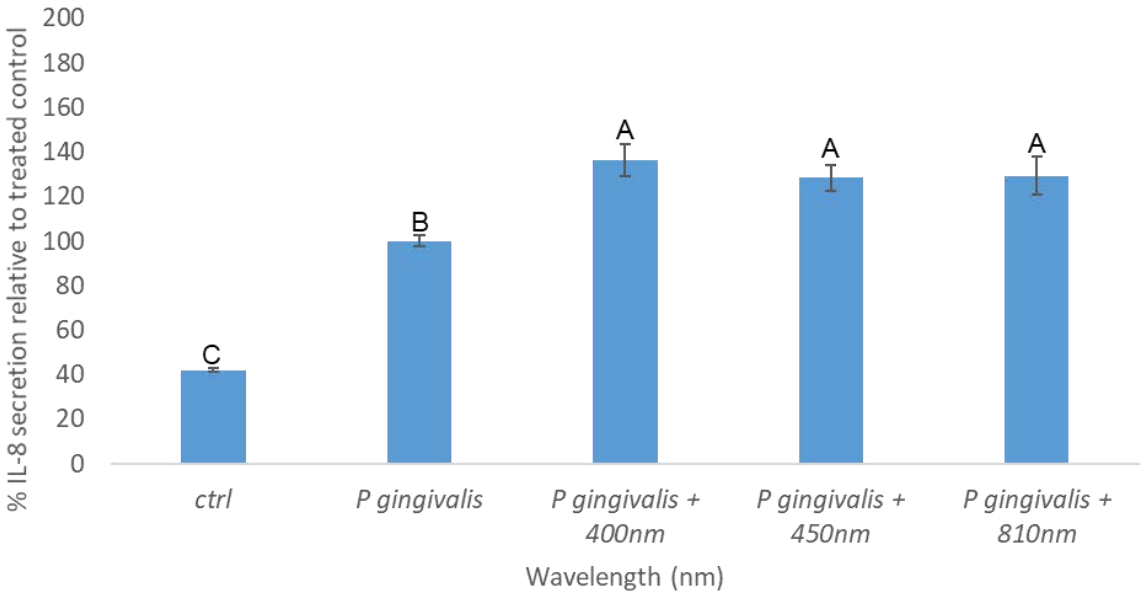

Figure 6.24 The effects of P. gingivalis (MOI 500:1) or P. gingivalis and light (400-810 nm, 24mW/cm², 5.76J/cm²) on IL-8 secretion from pHGFs (pool p7, n=12 replicates per treatment group), relative to the stimulated control, where the P. gingivalis treated control was normalised to 100%. Significance was assessed using one way ANOVA followed by Tukey test in which significance is indicated where means do not share the same letter.

6.6 Discussion

6.6.1 Growth and characterisation of orally relevant stimuli

The results demonstrated confirmation of the presence of two key pathogens associated with periodontitis in bacterial samples: *F. nucleatum* and *P. gingivalis* (6.2.1). *F. nucleatum* plays a key role in periodontal disease due to its ability to coaggregate with not only key periopathogenic species such as *P. gingivalis* but also early colonisers including *Streptococcus gordonii* through expression of various membrane proteins, such as FomA (Nobbs et al., 2011). Hence, *F. nucleatum* is vital in enabling the shift of species colonising the oral cavity, causing dysbiosis and therefore disease. Interestingly, increases in *P. gingivalis* have also been associated with increases in the severity of periodontal diseases (How et al., 2016, Rafiei et al., 2017). Hence, these data provide evidence of two stimuli for application *in vitro*, more relevant to periodontal disease pathogenesis than LPS (as described in chapter 5).

However, whilst these bacterial stimuli have been cited to play key roles in periodontal diseases, a possible 600 different species have been reported to colonise the oral cavity, with approximately 100 or more species identified per individual (Dewhirst et al., 2010a). Hence, to provide a more relevant model for bacteria colonising the oral cavity, saliva was harvested from periodontally healthy individuals, pooled and biofilm was grown for 7 days and characterised. Figure 6.5 indicates the most abundant phyla in the biofilm was Firmicutes, followed by Proteobacteria. Interestingly, a number of studies have also reported the most abundant phyla in the human oral microbiome is Firmicutes. However, the relative abundance of this phyla can vary greatly from 36.7% (Dewhirst et al., 2010b) to >60% (Mok et al., 2017, Koren et al., 2011b) dependent upon the study and subjects examined. This may be

dependent upon a number of factors including the patient from which the biofilm was extracted from or indeed biofilm culture methodologies.

The most abundant genus within the biofilm was *Streptococcus* (75.16%, Figure 6.7) which is in line with current literature suggesting *Streptococci* are the predominant genus of the oral microbiome (Klug et al., 2016a), particularly in biofilm derived from saliva (Eriksson et al., 2017). However, data also demonstrated the second most abundant genus within the biofilm was *Staphylococci* (19.39%). Whilst *Staphylococci* are not generally considered as part of the normal oral flora, current data indicates 94% of healthy adults exhibit oral colonisation of *Staphylococcus* species (Jackson et al., 2000). *Staphylococci* species have also been isolated from both subgingival and supragingival plaque (Smith et al., 2001). Hence, these data provide further evidence of the relevance of this biofilm model to species cited to be abundant within the oral cavity.

Other genus abundant in the biofilm included *Aggregatibacter* and *Veillonella*. Whilst species within the *Aggregatibacter* genus were not defined within this biofilm, one particular species has been shown to play a crucial role in periodontitis: *Aggregatibacter actinomycetemcomitans* (Herbert et al., 2016). Hence, further sequencing and optimisation of DNA extraction techniques may have revealed more information regarding the species colonising this biofilm. Where, 97.69% of the species within the biofilm were not defined. Interestingly, two species of particular interest were defined and these included *Veillonella dispar* (0.15%) and *Veillonella parvula* (0.55%). *Veillonella* species are common oral commensals, whose presence in the oral cavity have been cited to correlate with decreased oral hygiene (Mashima et al., 2016).

However, despite a broad range of relevant oral bacterial species colonising this model biofilm, no *Fusobacterium* or *Porphyromonas* species were identified as being present. The lack of abundance of *Porphyromonas* sp within the biofilm may have been due to the method of sampling or indeed, due to the negative reciprocal regulation between *Streptococcus* and *Porphyromonas* sp (Wang et al., 2009). In which, *Streptococcu*s sp including *Streptococcus intermedius* produce an extracellular arginine deaminase which signals the downregulation of Mfa1 (Christopher et al., 2010b). Mfa1 is a short fimbrae protein expressed by *P. gingivalis* to enable coaggregation with *Streptococcus* species including *Streptococcus gordonii* (Chawla et al., 2010). Hence, downregulation of Mfa1 inhibits coaggregation and therefore *P. gingivalis* colonisation within the biofilm. Interestingly, *Langefdt et al* also reported no *Porphyromona*s sp were detected within human oral biofilm samples cultured *in vivo* for up to 14 days (Langfeldt et al., 2014).

Undetectable levels of *Fusobacterium* sp may have been due to biofilm culture methods, DNA extraction technique or the individual's saliva the biofilm was isolated from. Indeed, authors have reported the relative abundance of *Fusobacterium* sp can vary dependent upon the individual the biofilm was isolated or grown from (Klug et al., 2016b).

Hence, data demonstrate a biofilm model more relevant to health, in which the genus most commonly associated with health, *Streptococcu*s, predominates. However, some *Streptococcus* species are also associated with disease including *Streptococcus mutans*, whose presence in oral biofilm is linked to the onset of dental caries (Loesche, 1986). Whilst, this species was not detected within the biofilm, *Streptococcus anginosus* was identified, another *Streptococcus* sp associated with the onset of dental caries (Kianoush et al., 2014). Some species relevant to gingivitis including *Campylobacter* (<0.01%) and *Prevotella* (0.17%)

were also present in low abundance (Palmer, 2014). Therefore, future work may involve growth of biofilms more relevant to oral disease and evaluation of how these stimuli influence inflammation *in vitro*.

Therefore, these data indicate bacterial stimuli relevant to those found in the oral cavity. Two of which are commonly associated with disease (*F. nucleatum* and *P. gingivalis*) and a salivary biofilm mainly containing species more relevant to health.

6.6.2 Determining the optimal dose of pro-inflammatory stimuli required to induce in vitro inflammation

Following confirmation of bacterial species within bacterial samples as described in section 6.6.1, the concentrations of *F. nucleatum*, *P. gingivalis* and salivary biofilm required to induce increases in ROS production and IL-8 secretion were assessed.

It was determined that a MOI of 100:1 of *F. nucleatum* was able to induce 29.74% and 1422.03% increases in ROS production and IL-8 secretion, respectively ($p<0.001$, 6.3.1). Interestingly a series of publications also report the use of a MOI of 100:1 to induce significant increases in IL-8 secretion (Tang et al., 2016, Huang et al., 2001). Therefore, this concentration was selected for application in vitro.

Comparatively, a MOI of 500:1 of *P. gingivalis* was required to induce significant increases in ROS production (14.95%, $p<0.001$) and IL-8 secretion (176.45%, $p<0.05$). Interestingly, the levels of IL-8 secretion induced by *P. gingivalis* were significantly lower than those induced by *F. nucleatum* (Figure 6.10). *Stathopoulou et al* also reported similar results, where application of heat inactivated *P. gingivalis* at a MOI:100 induced IL-8 secretion only a

fraction of that induced by heat inactivated *F. nucleatum* at the same concentration (Sahingur and Yeudall, 2015). Interestingly, *Milward et al* also reported similar findings where application of heat inactivated *F. nucleatum* (MOI 100:1) induced significantly higher levels of IL-8 gene expression from epithelial cells when compared to *P. gingivalis* (MOI 100:1) treated cultures (Milward et al., 2007). This may be due to the 'immunoevasive phenotype' *P. gingivalis* exhibits. In which this periopathogen produces cysteine proteases known as gingipains, key virulence factors that cleave chemokines including IL-8 (Yamatake et al., 2007). This enables *P. gingivalis* to evade the host immune response and induce tissue destruction (Hajishengallis, 2011). However, further work will be required to determine whether gingipains are denatured at temperatures used to heat-inactivate bacteria. Indeed current indications suggest IL-8 secretion induced by heat killed *P. gingivalis* is significantly higher than that induced by live *P. gingivalis* (Palm et al., 2013). Subsequently a MOI of 500:1 was selected to evaluate the effects of *P. gingivalis* on gingival fibroblasts *in vitro*.

Following selection of concentrations of *F. nucleatum* and *P. gingivalis* to be applied *in vitro*, the effects of salivary biofilm on inflammation were assessed. However, to enable comparable studies a concentration range to assess the dose dependent effects of salivary biofilms on markers for inflammation was performed. This involved assessing protein concentrations in both *F. nucleatum* and salivary biofilm samples. Subsequently, a protein concentration range comparable to that used to induce inflammation by heat inactivated *F. nucleatum in vitro* was selected (4.2-0.8µl/ml, Figure 6.11c).

Whilst other assays including the LAL assay, which measure relative levels of LPS in samples (Schwarz et al., 2017), may have been more reliable to enable the selection of a concentration range used to induce inflammation by LPS, *P. gingivalis* and also *F. nucleatum*,

data demonstrates the method used was sufficient to provide evidence of the dose dependent effects of salivary biofilm on markers for inflammation. Subsequently a concentration of 4.2µg/ml of salivary biofilm induced 18.58% and 969.98% increases in ROS production and IL-8 secretion respectively ($p<0.001$, Figure 6.12 and Figure 6.13). Hence this concentration was selected for application *in vitro*.

Therefore, these data demonstrate heat-inactivated *F. nucleatum, P. gingivalis* and salivary biofilm were effective in inducing significant increases in ROS production and IL-8 secretion in a dose dependent manner. Hence, the effects of PBM in modulating inflammation induced by these bacterial stimuli were evaluated.

6.6.3 The use of PBM for modulating cell number and metabolic activity

Data demonstrated that PBM induced no significant effect on cell number following application of *F. nucleatum, P. gingivalis* or salivary biofilm (6.4.1.1). Interestingly, however application of salivary biofilm did induce significant decreases in cell number relative to the untreated control. These data are in agreement with current publications suggesting biofilm constituents can impede wound healing and thus cellular growth (Jeffery Marano et al., 2015). However, whilst PBM did induce mean increases in cell number 24h post application of 450 nm light and salivary biofilm, these changes were not significant. Several authors have reported application of multiple doses of light could effects including increased cell growth, the induction of which is crucial in inducing tissue healing (Holder et al., 2012, Santos et al., 2014, Soleimani et al., 2012). Hence, future work may involve application of double doses of blue or NIR light to provide some clarity as to what extent dose of light influences markers for cellular activity *in vitro*.

However, comparatively PBM did induce significant changes in cell metabolic activity. Indeed, application of 400 nm or 450 nm light resulted in significant increases in cell metabolic activity of *F. nucleatum, P. gingivalis* and salivary biofilm treated controls. Interestingly, whilst *F. nucleatum* and salivary biofilm induced significant increases in cell metabolic activity, *P. gingivalis* induced significant decreases. Whilst, *Kang et al* reported that *F. nucleatum* induced no cytotoxic effects on oral epithelial cell cultures (Kang et al., 2011), these data are the first to report *F. nucleatum* could drive increases in metabolic activity from gingival fibroblast. However, comparatively *Le et al* also reported application of heat inactivated *P. gingivalis* to cultures induced significant decreases in cell metabolic activity (Le et al., 2009). Interestingly, *P. gingivalis* has been reported to perturb mitochondrial function and hence, as MTT assay provides a marker for mitochondrial activity, this may explain the decrease in metabolic activity induced by this periopathogen (Bullon et al., 2011). Currently there are no publications reporting the effects of *F. nucleatum* or salivary biofilm on mitochondrial activity. It may therefore, be prudent to evaluate the effects of various periopathogen on mitochondrial function in the future. Hence, the data presented here show the bacterial stimuli dependent effects on cell metabolic activity and also corroborate with data described in section 5.6.2.

In conclusion, whilst these data suggest PBM has no significant effect on cell number, they do suggest blue light in particular can modulate changes in cell metabolic activity induced by application of bacterial stimuli.

6.6.4 The utility of PBM in modulating markers for inflammation in vitro.

Results indicate that PBM could be an effective modality in modulating inflammation induced by bacterial stimuli. Figure 6.21 provides evidence that PBM can induce decreases in ROS

production, particularly at a wavelength of 400 nm relative to *F. nucleatum, P. gingivalis* or salivary biofilm treated controls. A series of authors have reported the modulatory effects of PBM on ROS production both *in vitro* and *in vivo* (Tatmatsu-Rocha et al., 2016, Erthal et al., 2016, Bartos et al., 2016). Interestingly, *Huang et al* also reported that 810 nm light induced significant reductions in ROS production following application of pro-inflammatory stimuli such as hydrogen peroxide (H_2O_2) to primary cortical neurones (Huang et al., 2013). Similarly, *Lim et al* also reported that application of 635 nm light to LPS treated gingival fibroblasts, significantly reduced ROS production (Lim et al., 2015). However, data presented here are the first reports to demonstrate that blue light could be as effective as NIR light in inducing decreases in inflammation induced by periodontally relevant stimuli. *Song et al* also reported that application of light at 456 nm and a dose of 7.5J/cm² induced significant reductions in both *P. gingivalis* and *F. nucleatum* biofilm formation (Song et al., 2013). These data therefore provide evidence that blue light could not only be an efficacious in modulating ROS production induced by periodontal pathogens. In addition as blue light has bactericidal effects then this wavelength could be important in the management of periodontal disease (Song et al., 2013, Felix Gomez et al., 2018, Schnedeker et al., 2017).

These data also provide evidence that PBM is effective in reducing TGFβ1 secretion, particularly following application of 400 nm light to *F. nucleatum* or *P. gingivalis* treated cultures (Figure 6.22). Indeed only application of 400 nm light induced mean decreases in TGFβ1 secretion from salivary biofilm treated cultures. Despite this, these results corroborate with those described in section 6.5.1 where blue light induced significant decreases in TGFβ1 secretion from LPS treated HGFs. Results also demonstrate application of pro-inflammatory stimuli induce increases in TGFβ1 secretion. Previous studies have also shown that application of *P. gingivalis* (Zhang et al., 2013) and *F. nucleatum* (Bolstad et al., 1996) induce significant

increases in TGFβ1 secretion, increases of which have been associated with the progression of oral disease (Wahl et al., 1993). Hence, data is suggestive that blue light could be used to modulate TGFβ1 secretion induced by *P. gingivalis, F. nucleatum* and LPS (5.5). However, further work will be required to determine the effects of PBM on TGFβ1 secretion from cultures treated with a salivary biofilm model which may be more relevant to oral disease.

Whilst, application of PBM has been shown to modulate both ROS production and TGFβ1 secretion, results presented here demonstrated that effects of PBM on IL-8 secretion were pro-inflammatory stimulus dependent. Indeed, irradiation of salivary biofilm and *F. nucleatum* treated cultures at 400 nm induced significant decreases in IL-8 secretion relative to the treated control (Figure 6.23). As discussed in section 5.6.4, this could prove beneficial in modulation of disease as IL-8 is a key periodontal biomarker and driver of disease pathogenesis (Lagdive et al., 2013).

Comparatively, whilst application of *P. gingivalis* induced significant increases in IL-8 secretion, irradiation at 400 nm, 450 nm or 810 nm further exacerbated this increase (Figure 6.24). However, the levels of IL-8 secretion induced by *P. gingivalis* were relatively small compared with those induced by *F. nucleatum*, salivary biofilm or indeed LPS, as is discussed in section 6.6.2. Current studies suggest that light acts in a biomodulatory manner, whereby application of light to chronically inflamed tissues induces significant decreases in inflammation but, irradiation of 'healthy' tissue induces significant increases in inflammation (Tatmatsu-Rocha et al., 2016, Milward et al., 2015, Huang et al., 2013), see section 5.7.4). Hence, application of *P. gingivalis* may not have induced inflammation to this hypothetical 'chronic inflammation' threshold and thus light induces further increases in inflammation. This increase in IL-8 secretion induced by light application may alert the immune system of

the presence of a bacterial stimulus, ensuring effective management of infection. However, further work will be required to validate this hypothesis.

These data provide evidence that PBM could be useful in not only modulating inflammation induced by LPS but also stimuli more relevant to periodontal disease pathogenesis.

7 DISSECTING THE MITOCHONDRIAL DEPENDENT EFFECTS OF PBM

Parts of this chapter comprise part of a publication by Serrage et al (Serrage et al., 2019b), in which I am the first author and major contributor. All work described in this chapter was undergone by myself and sections included as part of the publication are as follows: 2.2.11.4, 7.2 and 7.3. See appendices section 10.4 for full article.

7.1 Introduction

The effects of PBM on mitochondrial activity have been widely documented both in this project (Chapters 4-6) and in the literature (Belletti et al., 2014, Buravlev et al., 2014a, Buravlev et al., 2013, Buravlev et al., 2014b, Hamblin, 2018a). However, whilst the effects of PBM on markers of mitochondrial activity including ATP (Ferraresi et al., 2015a, Rhee et al., 2014, Sharma et al., 2011b, Wang et al., 2017b) and ROS (Lim et al., 2007, Sharma et al., 2011b, Silveira et al., 2013, Yuan et al., 2017) have been reported, the effects of PBM on real-time changes in mitochondrial activity have not yet been widely assessed. Hence, this Chapter aimed to develop a system to measure changes in mitochondrial activity in real-time using the Seahorse XFe96 analyser platform (see 2.2.11.4 for further detail). The system was first optimised using a cell type commonly used in Seahorse assays: myoblasts (C2C12 cells (Patton et al., 2018, Guo et al., 2017, Frisard et al., 2015, Krajcova et al., 2015, Mookerjee et al., 2015)). Notably, it has also been reported that PBM can modulate cellular and mitochondrial activity of this cell type (Alexsandra da Silva Neto Trajano et al., 2016, da Silva Neto Trajano et al., 2016, Serrage et al., 2019a, Silva et al., 2016, Teuschl et al., 2015b), however, to date no studies have evaluated the effects of blue light on C2C12 cells.

Another key question remaining to be asked is as to whether mitochondrial content could influence the cellular response to PBM. This section aimed to evaluate this using cell types commonly cited to possess different mitochondrial contents: myoblasts and myotubes

(Schoneich et al., 2014, Kraft et al., 2006). Therefore an assay to measure mtDNA was developed, to confirm myotubes contain a higher mitochondrial DNA content when compared with myoblasts. The effects of PBM on both markers and real-time changes in mitochondrial activity using both myoblasts and myotubes were then assessed.

The current literature has provided evidence that response to PBM can be variable dependent upon the individual the treatment is applied to. Reports evaluating the effects of PBM have shown that the effects of light seen *in vivo* are due to changes in mitochondrial activity. Interestingly, the literature has also shown that the mitochondrial genome can vary significantly from one individual to the next (Carter, 2007). Hence, this Chapter aimed to address whether mitochondrial content could influence response to PBM *in vitro*. This involved evaluation of the mitochondrial content of pHGFs derived from different individuals and subsequent investigation into the individual dependent response to light. Data obtained may indicate as to why there is significant variability in response to PBM reported in the literature between individuals and different cell types.

7.2 Optimisation of a method to determine real-time changes in mitochondrial activity.

In order to assess the effects of PBM on real-time mitochondrial activity of myoblasts, initially a high throughput assay (MTT) was employed to assess possible treatment parameters required to induce significant changes in markers for mitochondrial activity. Following selection of these parameters the effects of PBM on real-time mitochondrial activity were assessed at a number of time-points. These data were then used to determine at which point PBM induced the most significant changes in real-time mitochondrial activity, relative to an untreated control.

7.2.1 The effects of PBM on myoblast metabolic activity

The effects of PBM at wavelengths spanning the visible to NIR spectrum and doses relevant to those used in the literature (Andreo et al., 2018, Santos et al., 2018, Silva et al., 2016, Kushibiki et al., 2013) were employed to evaluate the modulatory effects of light on mitochondrial activity of myoblasts.

7.2.1.1 Results

Data indicated a dose and wavelength dependent effect of PBM on the mitochondrial activity of myoblasts 24h post-application. Where, irradiation for 30s at a wavelengths of 400 nm, 525 nm, 810 nm or 830 nm induced 18.46%, 16.47%, 14.40% and 12.12% increases in cell metabolic activity, respectively (Figure 7.1, $p<0.05$). Interestingly, 240s irradiation with white light also induced 12.99% increases in MTT relative to the untreated control ($p<0.05$). However, no significant increases in MTT following irradiation for 240s with any other wavelengths were observed.

To enable comparison with results described in Chapters 4, 5 and 6, an irradiation period of 30s and wavelengths of 400 nm, 450 nm and 810 nm were selected for *in vitro*

application. This would then enable further clarification as to what extent blue light modulates mitochondrial activity when compared with NIR light.

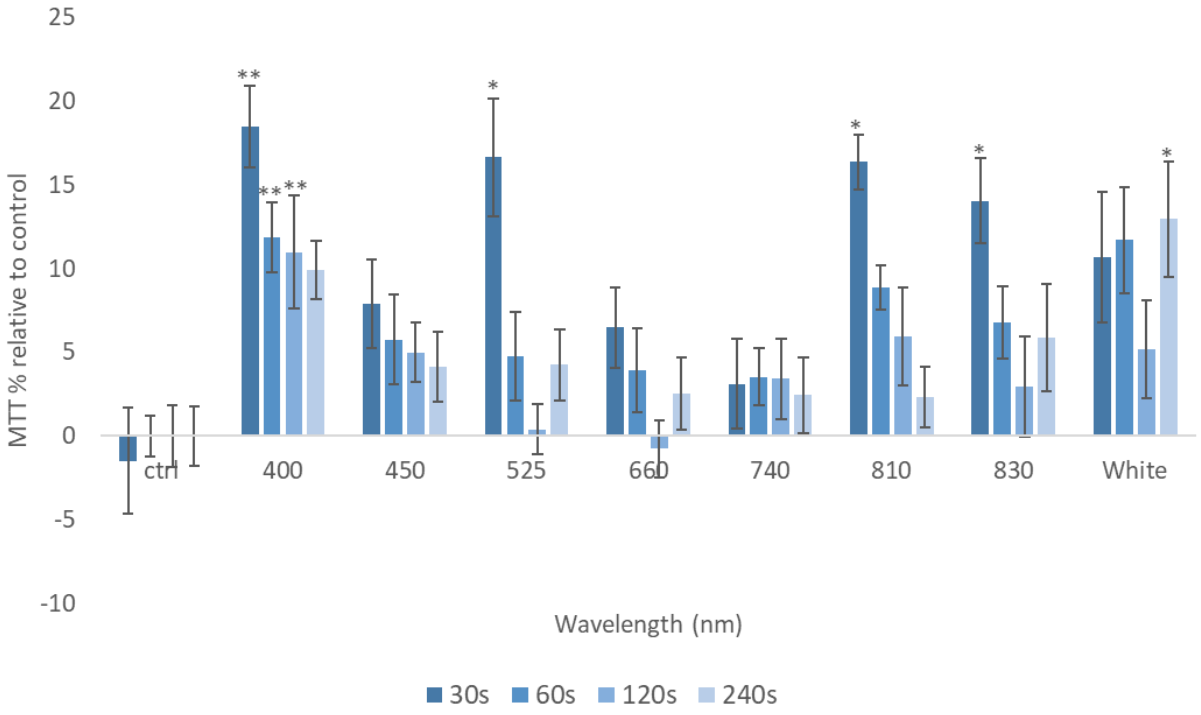

*Figure 7.1 High throughput analysis data for specific wavelengths (400-830 nm) and irradiation periods (30-240s) on cell metabolic activity of mouse myoblast cells (C2C12, n=12 replicates) (24mW/cm², 0.72-5.76J/cm², 30-240s). Significance is indicated by ***=p<0.001, **=p<0.01, *=p<0.05 relative to the non-irradiated control, where all data is shown as a percentage of the non-irradiated control, where the non-irradiated control was normalised to 0%. Significance was assessed using one way ANOVA followed by Tukey test.*

7.2.2 Time dependent effects of PBM on real-time mitochondrial activity

Initially a Seahorse XFe96 analyser was used to assess the optimal time-point post-irradiation to evaluate real-time changes in mitochondrial activity induced by PBM. The Seahorse XF Cell Mito stress assay evaluates changes in mitochondrial activity through the sequential injection of compounds that directly alter the activities of the mitochondrial electron transfer chain (ETC) as described in Section 2.2.11.4.

7.2.2.1 Results

The results presented show the time dependent effects of PBM. Figure 7.2 shows a representative image of the trace produced through the duration of the Seahorse cell mito stress assay. Application of compounds either induced inhibitory (Oligomycin, antimycin A and rotenone, inhibit the activities of complexes IV, III or I of the ETC respectively) or stimulatory (FCCP, uncoupling agent enabling ETC activities to occur at maximal rates) effects on ETC activity causing fluctuations in the oxygen consumption rate (OCR) of the studied cell type. Subsequently, traces produced showed data for 1, 8 and 24h post application of PBM.

Figure 7.3c provides evidence that changes in mitochondrial activity 24h post application of PBM could not be reliably measured. Indeed, the trace generated at this time-point was not comparable with the example described in Figure 7.2 in which Oligomycin induced significant decreases in OCR. Comparatively, the trace produced 1h post-irradiation was similar to that displayed in the example (Figure 7.3a). However, OCR was variable between replicates and therefore there was a high standard deviation around the mean, particularly following application of FCCP. Hence, the effects of PBM 8h post-irradiation were also assessed. It was found that relative OCR was lower when assessing the effects of PBM 8h post-irradiation (max: 267.30pmol/min) compared with 1h post-irradiation (max:

556.95pmol/min). However, the trace was similar to that described in Figure 7.2 and the variability between replicates was relatively low. Hence, the effects of PBM on real-time mitochondrial activity were assessed at 8h post-irradiation.

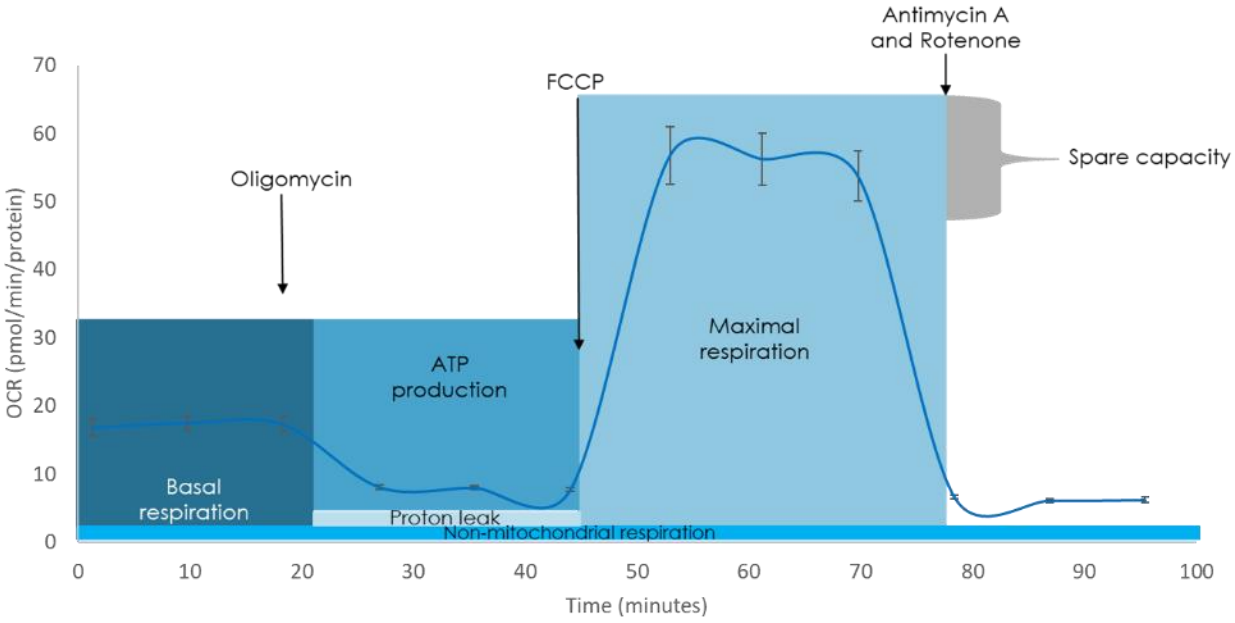

Figure 7.2 Representative image of the points at which compounds were sequentially injected to modulate mitochondrial activity. This image provides an example of how a trace should appear following employment of the Seahorse XFe96 cell mito stress assay. In which, firstly oligomycin is applied to the system which inhibits complex V of the ETC thus causing a decrease in oxygen consumption rate (OCR, y axis) and enabling calculation of ATP production, which is calculated as the difference between basal respiration and proton leak. In which, proton leak is the movement of protons across the mitochondrial membrane, independent of ATP synthase activity (complex V). Subsequently FCCP is added to the system, an uncoupling agent which enables respiration to occur at maximal rates, inducing increases in OCR and enabling calculation of maximal respiration. Finally, Antimycin A and rotenone are added to the system, complex III and I inhibitors respectively. These directly inhibit ETC activity thus causing OCR to decrease and enabling non-mitochondrial respiration calculation.

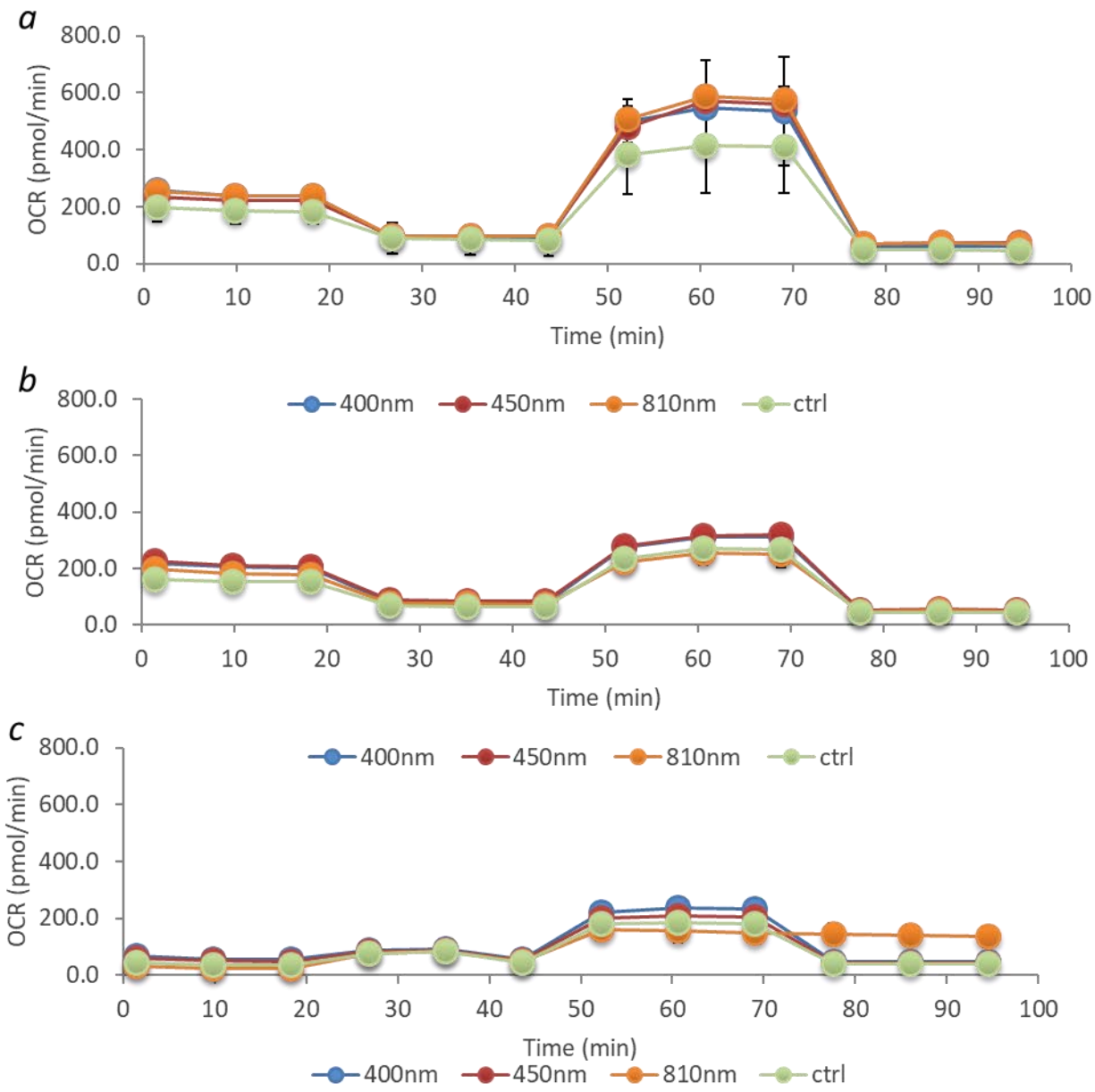

Figure 7.3a) Changes in mitochondrial 1hr post-irradiation in which statistical analysis using one way ANOVA followed by Tukey test revealed there was no significant difference between control and light treated groups when assessing basal and maximal respiration and ATP production. This could possibly be due to the degree of standard deviation about means within discrete groups, b) Changes in mitochondrial activity 8hr post-irradiation where there is much less deviation in outcome and the trend in data is much more similar to the figure depicted by figure 2. c) Changes in mitochondrial activity 24hrs post-irradiation where deviation is again larger and there is an error in the loading of antimycin and rotenone in 810 nm treated wells. Hence, with these data considered a time-point 8h post-irradiation was selected due to reliability. Cells (C2C12, p6, n=6) were treated for 30s, 24mW/cm², 0.72J/cm² at wavelengths of 400 nm, 450 nm or 810 nm and evaluated 1, 8 and 24hrs post-irradiation.

7.3 Determining whether the effects of PBM may be mitochondrial content dependent

No studies to date have investigated whether mitochondrial cellular content influences biological response to light. Hence, myoblasts and myotubes were employed to determine to what extent mitochondrial content influences response to PBM *in vitro*.

7.3.1 Developing and characterising a method to measure mtDNA content

Differences in mitochondrial content in both myoblast and myotube cultures were confirmed through the optimisation of an assay measuring relative ratios of mitochondrial DNA (mtDNA) to nuclear DNA (nDNA) and quantified using a calf thymus DNA standard curve (2.2.14).

7.3.1.1 Results

Figure 7.4 demonstrates application of the dsDNA binding dye SYBR® safe stain (Invitrogen, UK) was the most effective in measuring changes in DNA concentration compared with other dsDNA stains including Sytox green and SYBR green I (both Thermo fisher). A Pearson correlation coefficient of 0.999 was obtained following application of SYBR® safe stain to serially diluted calf thymus DNA samples. Hence, this stain was selected for further study application.

Subsequently, DNA was isolated from myoblast and myotube cultures, mtDNA was amplified and relative ratios of mtDNA:nDNA in samples were quantified. Figure 7.5 provides evidence that myotubes possessed a 46.49% greater ratio of mtDNA:nDNA compared with myoblasts *($p<0.05$)*. Hence, these data were consistent with literature indicating myotubes possess greater mitochondrial levels than myoblasts (Hoffmann et al., 2018). Therefore, the mitochondrial content dependent effects of PBM were subsequently evaluated.

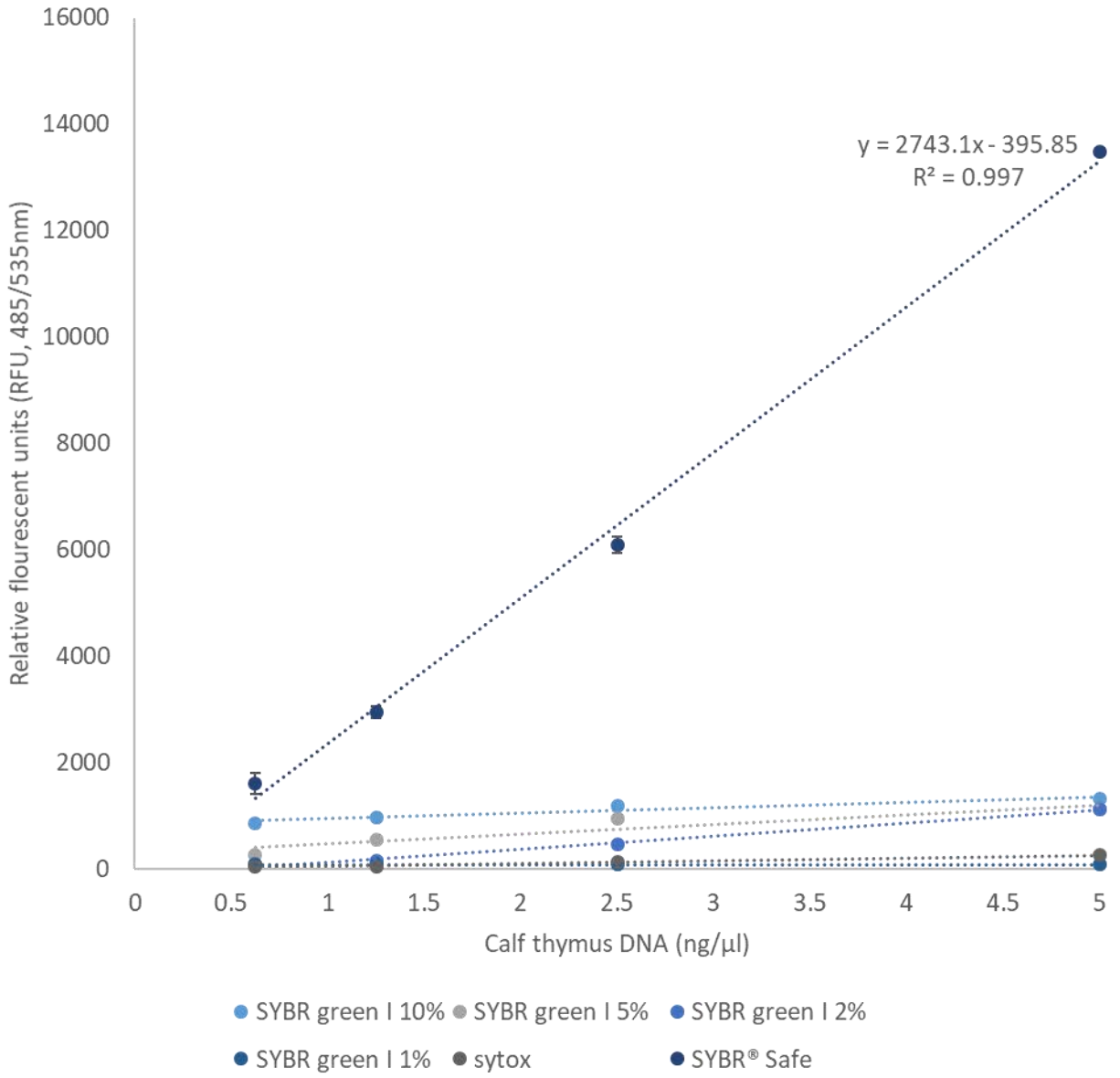

Figure 7.4 Standard curves produced following serial dilution of calf thymus DNA (5-0.625ng/µl, n=3) and relative fluorescence following application of several fluorescent dsDNA stains including: 10% v/v, 5% v/v. 2% v/v or 1% v/v dilutions of SYBR green I (Thermo fisher), Sytox green (1mM, Thermo fisher) or SYBR® safe dye (2% v/v, Invitrogen, UK). All dsDNA stains were diluted in TAE buffer at the concentrations described. These data indicated which dye would prove most effective in demonstrating decreases in relative fluorescence as DNA concentration decreases and to ascertain concentrations of DNA in samples using the equation of the line.

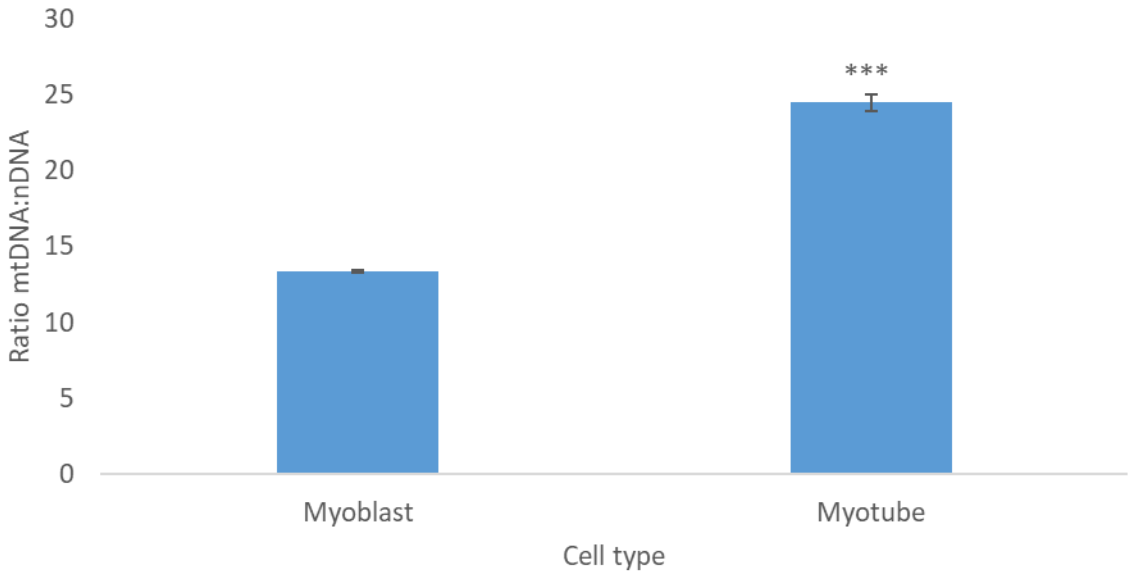

*Figure 7.5: Relative differences in the ratio of mtDNA:nDNA between myoblasts and myotubes (n=4, p8). Significance was assessed using t-test where ***=p<0.001.*

7.3.2 The effects of PBM on myoblasts vs myotubes

Following validation of an assay measuring mitochondrial content, the effects of PBM on both markers for mitochondrial activity (MTT and ROS) in real-time were assessed. These data were therefore used to determine the reliability of assays cited to act as a markers for mitochondrial activity.

7.3.2.1 Results

Data generated provided evidence of the mitochondrial content dependent effects of PBM. Figure 7.6 indicates that whilst a wavelength of 400 nm and irradiation period of 30s induced significant increases in cell metabolic activity and ROS production from myoblasts and myotubes, increases in the activities of both these mitochondrial markers following irradiation at 400 nm, 450 nm or 810 nm were only observed in myotube cultures ($p<0.05$). Interestingly, application of 450 nm light to myotubes induced 8.13% and 2.60% greater increases in ROS and MTT respectively relative to 450 nm treated myoblast cultures.

These results are also comparable with those describing the effects of PBM on real-time mitochondrial activity. Where the application of 400 nm light to myotube cultures induced 41.98%, 39.78%, 53.22% and 58.85% increases in basal respiration, ATP production, maximal respiration and spare respiratory capacity (SRC, the amount of extra ATP produced through oxidative phosphorylation available in the case of an increase in energy demand (Desler et al., 2012)) relative to the untreated control ($p<0.05$,Figure 7.7). Comparatively, application of 400 nm light to myoblast cells induced no significant changes in basal or maximal respiration, ATP production or SRC. Interestingly, only NIR light was able to modulate myoblast mitochondrial activity, where application of 810 nm light induced significant

increases in ATP production (17.74%, $p<0.05$, Figure 7.7d) and maximal respiration (21.67%, $p<0.05$, Figure 7.7c). However, application of NIR light to myotubes induced ATP production levels 26.83% greater than that caused by irradiation of myoblast cultures at 810 nm (Figure 7.7d).

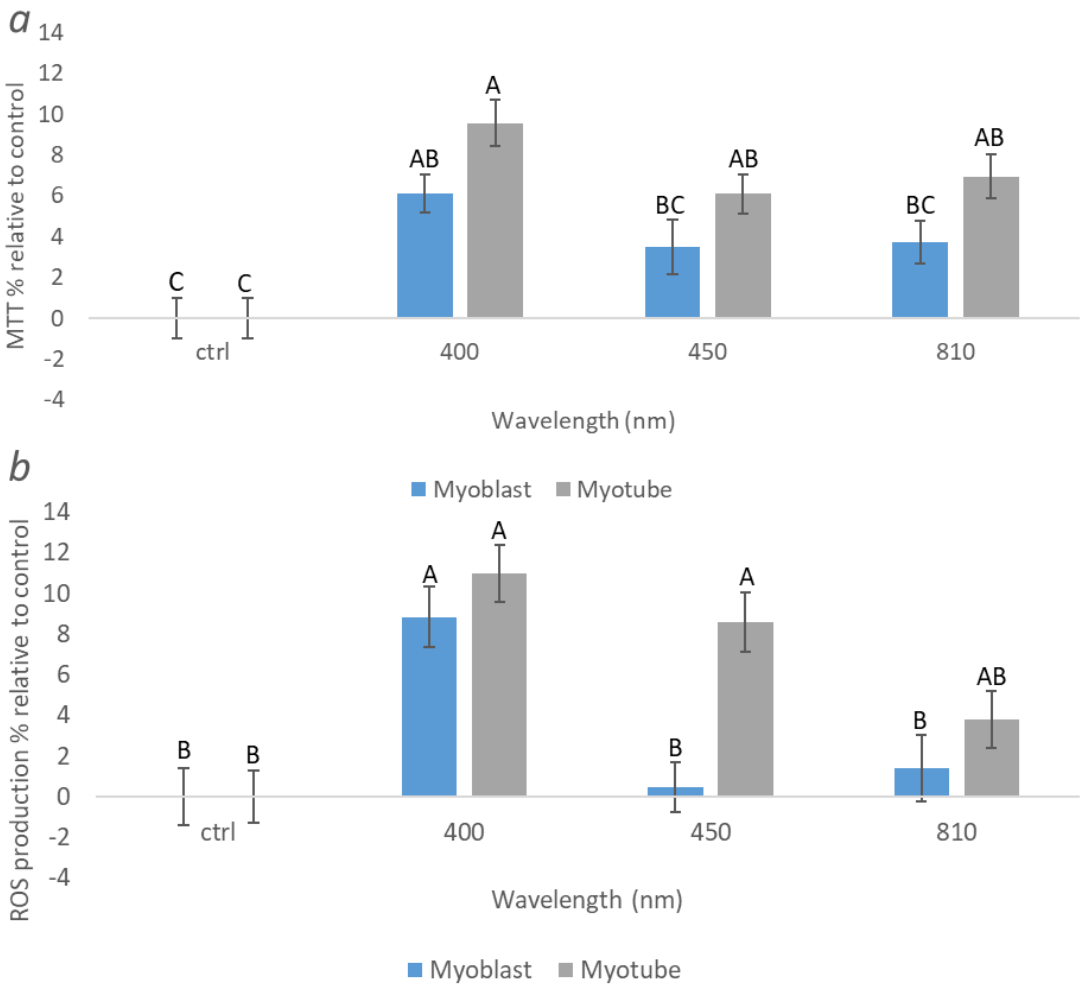

Figure 7.6 a) The effect of PBM on cell metabolic activity in myoblasts and myotubes (30s, 0.72J/cm², n=18) to wavelengths of 400, 450 and 810 nm. b) Indicates the effects of PBM on ROS production from myoblasts and myotubes (30s, 0.72J/cm², n=18) relative to the control (ctrl) which was normalised to 0%. The effects of PBM were evaluated 8h post-irradiation. Mean values that do not share the same letter are significantly different (p<0.05). Significance was analysed using one way ANOVA followed by a post-hoc Tukey test.

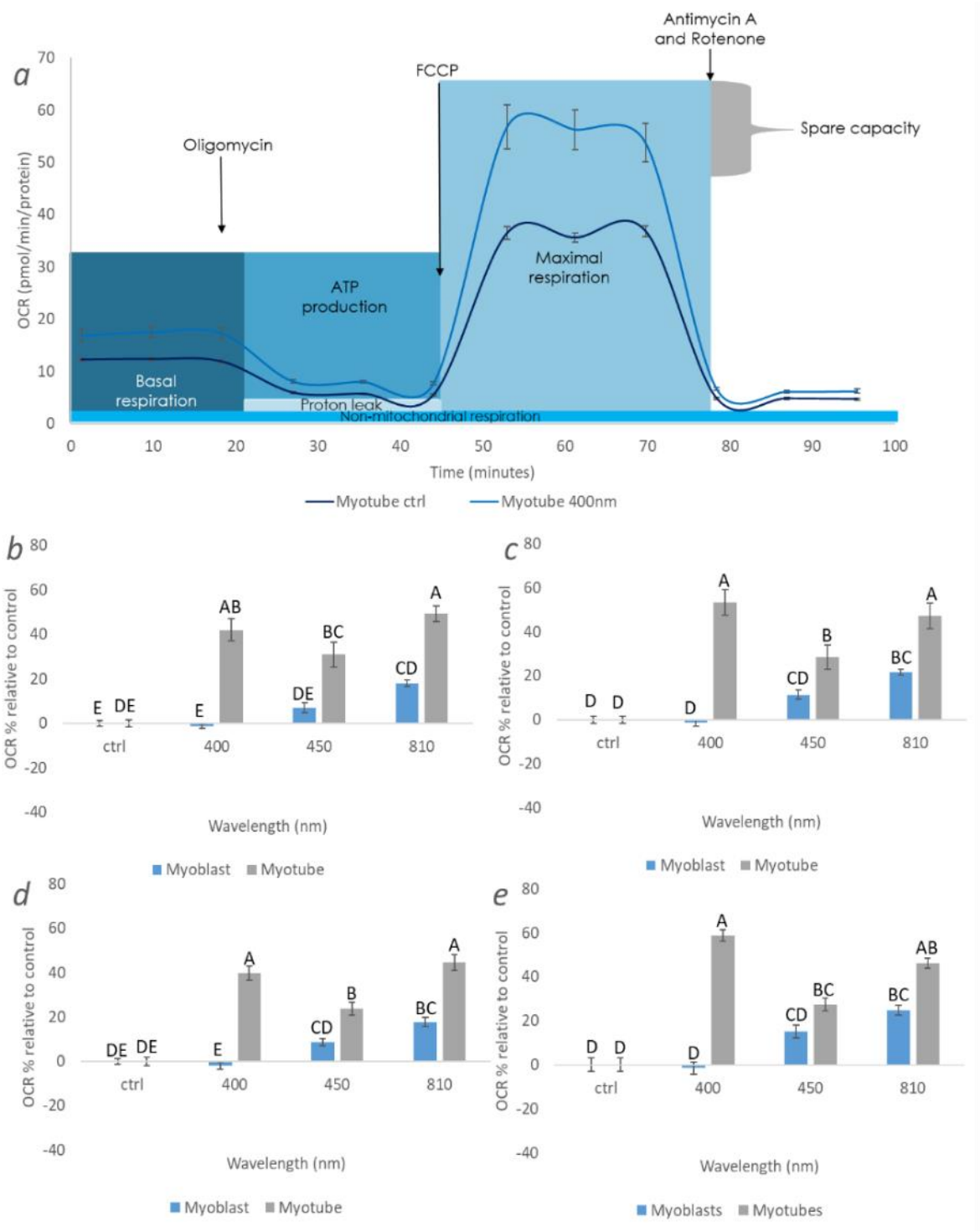

Figure 7.7 The effects of PBM on markers for changes in real-time mitochondrial activity utilising the Seahorse assay from myoblasts and myotubes (myotubes, p7, myoblasts p13, n=6, effects evaluated 8h post-irradiation). a) Presents a trace comparing response of untreated myotubes and myotubes treated with 400 nm light in which compounds were sequentially applied to the system to alter elements of oxidative phosphorylation. Data enabled calculation of specific parameters of oxidative phosphorylation including b) basal respiration, c) maximal respiration, d) ATP production and e) Spare respiratory capacity. Means that do not share the same letter are significantly different ($p<0.05$).

7.4 Assessment as to whether mitochondrial content of pHGFs may influence the cellular response to PBM

The data described in Section 7 and in the publication presenting these data (Serrage et al., 2019a), provides evidence that response to PBM could be mitochondrial content dependent. Potentially PBM could theoretically induce a greater response from cell types with a higher mitochondrial content. This may be responsible for the variability in response frequently observed in PBM research. Hence, to assess this premise further, mitochondrial content of pHGFs isolated from different individuals was quantified and the response of these different cell isolates to PBM was evaluated. Studies investigated the effects of PBM on both markers for mitochondrial activity and changes in real-time mitochondrial activity from these different pHGF isolates.

7.4.1 Individual-dependent effects of PBM on cell metabolic activity.

Prior to investigation as to whether responses to PBM could be mitochondrial content dependent, a high throughput assay was used to determine the individual dependent response to PBM *in vitro*. Subsequently pHGFs isolated from four individuals (B13, B15, B16 and B19) were irradiated at specific wavelengths (400-830 nm) and doses (2.88-5.76J/cm^2) and the effects of light on cell metabolic activity were subsequently evaluated 24h post-irradiation. The effects of PBM on cell metabolic activity of a pool of three pHGF isolates (B13, B16 and B19) were also evaluated. This was to aid comparison with studies described in Chapters 4-6, in which pooled pHGFs comprising the same isolates were assayed.

7.4.1.1 Results

Data indicated the individual dependent response to PBM *in vitro*, where irradiation at specific wavelengths and doses induced no significant change in cell metabolic activity from

B15 pHGFs (Figure 7.8b) but light application did induce changes in metabolic activity from B13 (Figure 7.8a), B16 (Figure 7.8c) and B19 (Figure 7.8d) pHGF isolates. Particularly following application of blue light, where irradiation at 400 nm for 240s induced increases in cell metabolic activity from B13 (6.22%, $p<0.05$), B16 (10.23%, ns) and B19 (12.16%, $p<0.05$) pHGF isolates relative to unstimulated controls.

Interestingly application of 450 nm or 525 nm for 120s also induced 6.86% and 9.90% increases in cell metabolic activity respectively from the B13 pHGF culture relative to the non-irradiated control ($p<0.05$). Whilst comparable, no significant changes in metabolic activity following irradiation for 120s at wavelengths between 400-830 nm were detected from the B15, B16 or B19 cultures. Application of 450 nm for 240s also induced a 7.37% increase in cell metabolic activity of the B13 pHGF isolate ($p<0.05$).

When comparing the response of individual isolates of pHGFs (B13, B15, B16 and B19) to PBM to that of the response elicited from a pool of three pHGF isolates (B13, B16, B19,Figure 7.8e), it was also found that pooled pHGFs exhibited the greatest mean response to blue light. Indeed application of 400 nm or 450 nm light for 240s induced 14.63% and 9.17% increases in cell metabolic activity relative to the untreated control ($p<0.05$). Interestingly, irradiation at 400 nm also induced mean increases in the cell metabolic activity of all three individual pHGF isolates, however application of 450 nm light for 240s only induced significant increases in cell metabolic activity from the B13 isolate. Mean increases in cell metabolic activity induced by 400 nm light were also greater when applied to pooled pHGFs compared with individual cell isolates.

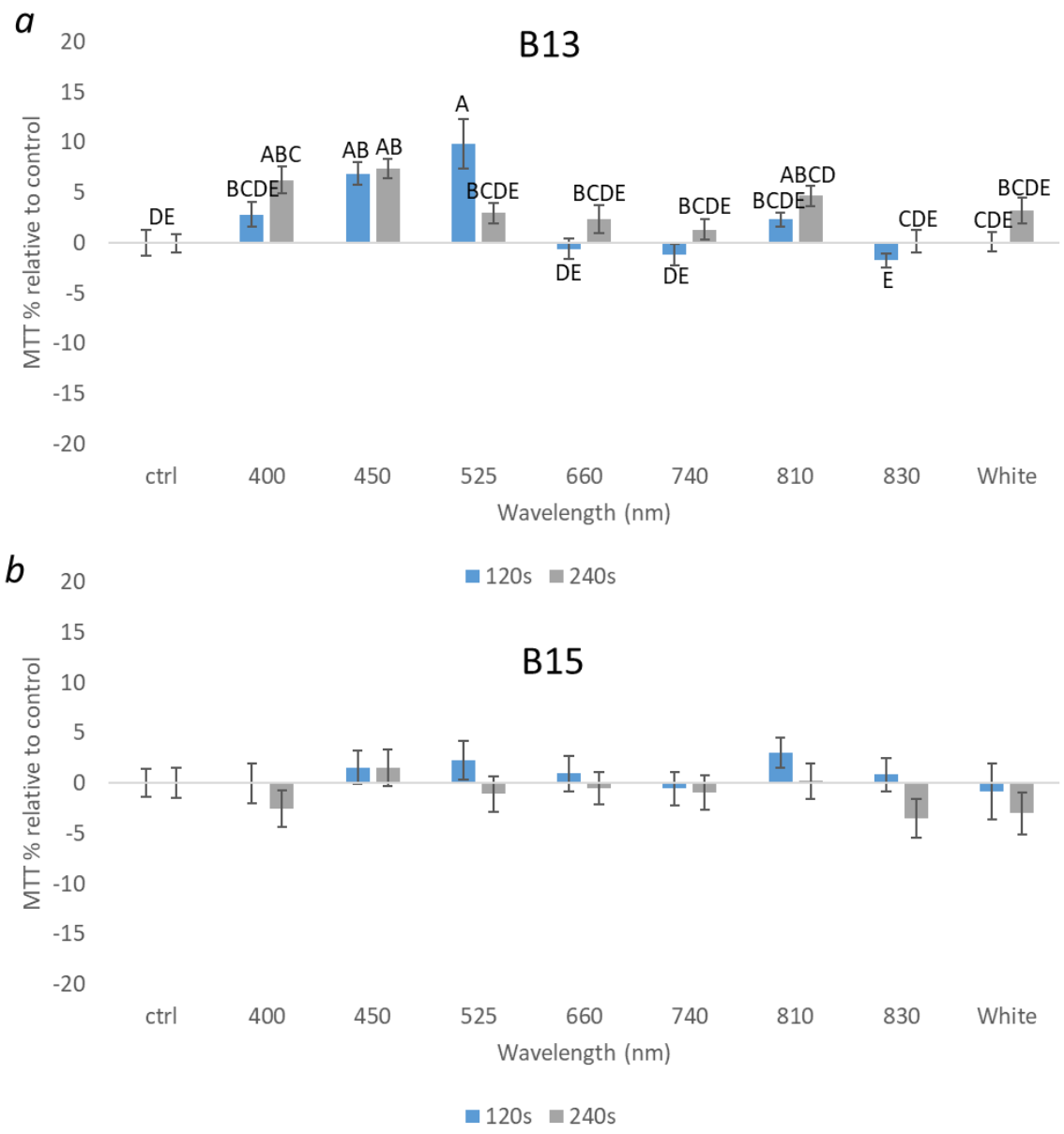

Figure 7.8: High-throughput analysis at specific wavelengths (400-830 nm) and doses (120-240s, 24mW/cm², 2.88-5.76J/cm²) for cell metabolic activity 24h post-irradiation of a) B13 pHGF isolate (p5-7, n=18 replicates, 6 replicates per plate).b) B15 pHGF cell isolate (p5-7, n=24) c) B16 cell isolate (n=24, p5-7), d) B19 cell isolate (n=24, p5-7) and e) on pooled pHGFs (p5-7, n=18) relative to the normalised untreated control (normalised to 0%) 24h post-irradiation. Significance was assessed using one way ANOVA followed by Tukey test, where means that do not share the same letter are significantly different (p<0.05).

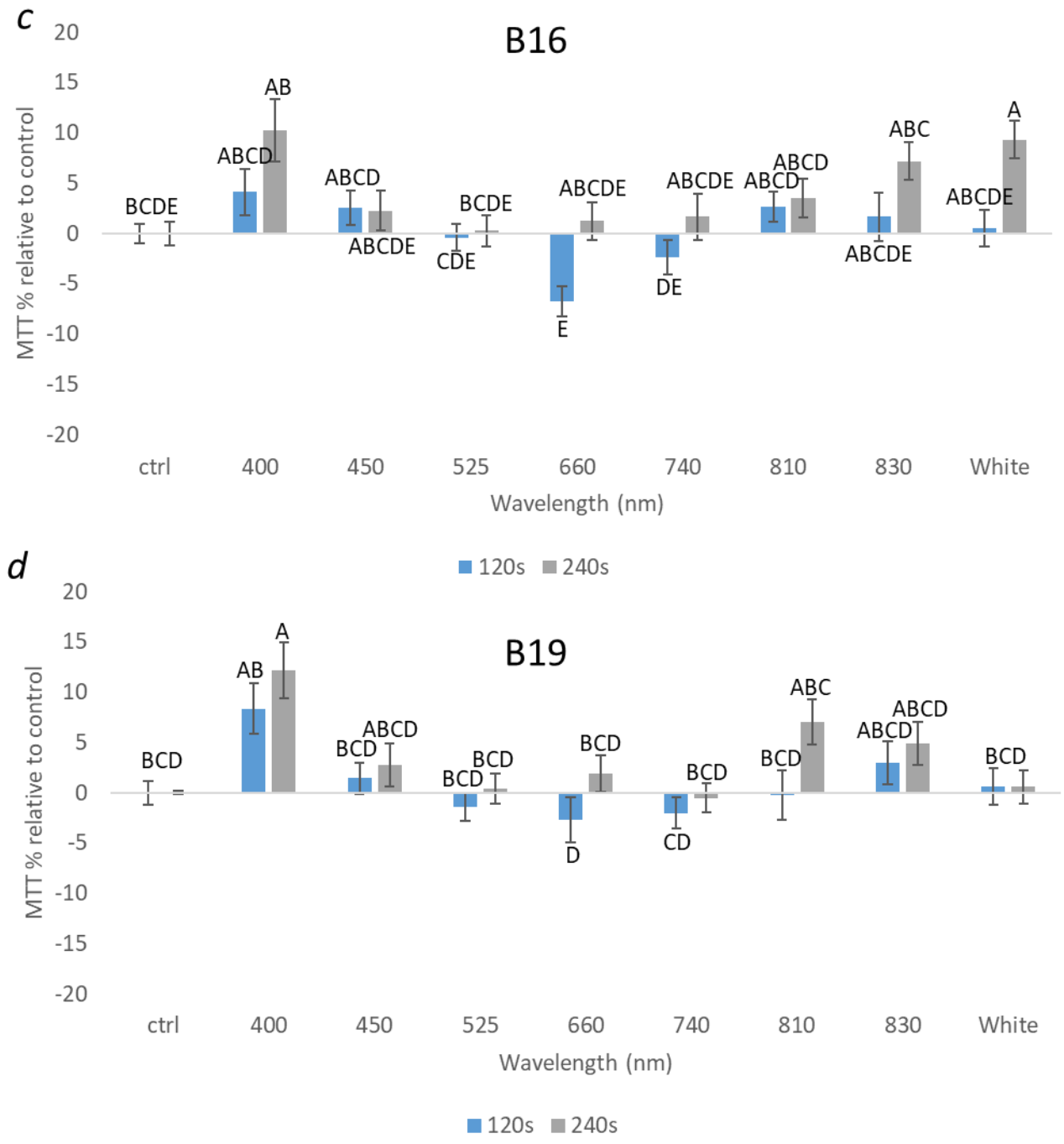
c
B16
MTT % relative to control
20
15
10
5
0
-5
-10
-15
-20
BCDE
ABCD
AB
ABCD
ABCDE
BCDE
CDE
ABCDE
E
ABCDE
DE
ABCD
ABCD
ABC
ABCDE
ABCDE
A
ctrl
400
450
525
660
740
810
830
White
Wavelength (nm)
d
120s
240s
B19
MTT % relative to control
BCD
AB
A
BCD
ABCD
BCD
BCD
BCD
D
BCD
CD
BCD
ABC
BCD
ABCD
ABCD
BCD
ctrl
400
450
525
660
740
810
830
White
Wavelength (nm)
120s
240s

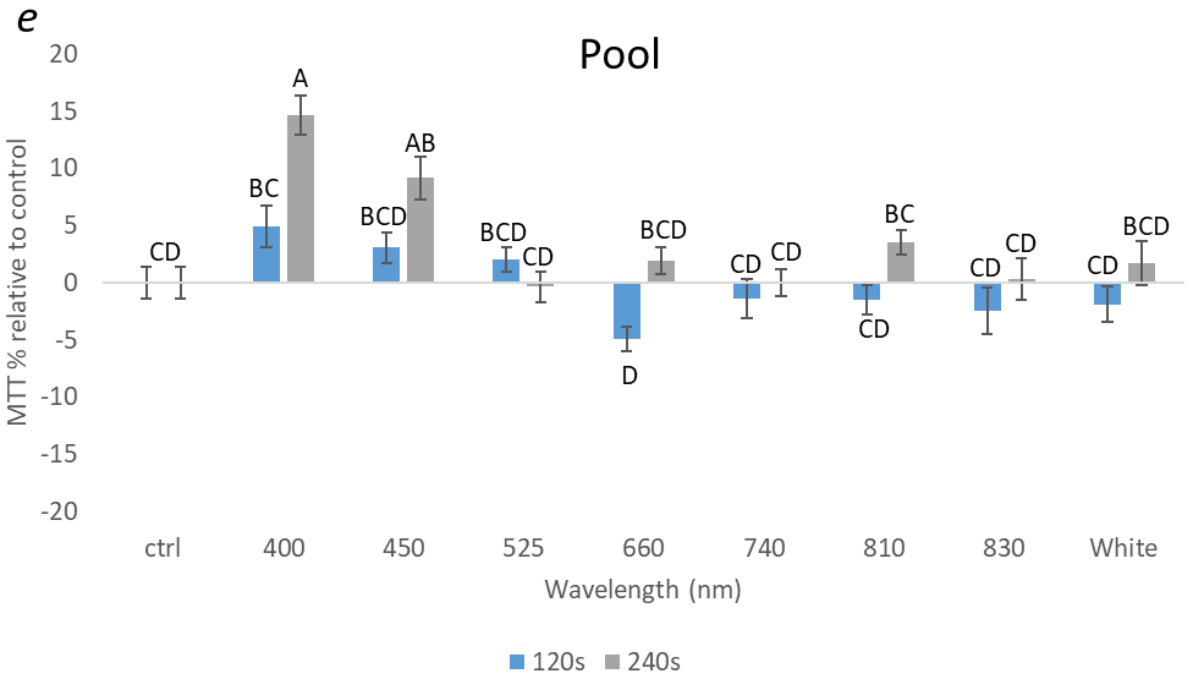
e
Pool
MTT % relative to control
20
15
10
5
0
-5
-10
-15
-20
CD
BC
A
BCD
AB
BCD
CD
BCD
D
CD
CD
CD
BC
CD
CD
CD
BCD
ctrl
400
450
525
660
740
810
830
White
Wavelength (nm)
120s
240s

7.4.2 The effects of PBM could be mitochondrial content dependent.

Results presented in Section 7.4.1 indicate that responses to PBM could be individual dependent. Hence, the next step in this project was to determine whether the differential response to PBM between pHGF isolates could be due to mitochondrial content. Hence, in order to evaluate this, mitochondrial content of three pHGFs isolates (B15, B16 and B19) and a pool of three pHGF isolates (B13, B16, B19) was quantified. The effects of PBM on mitochondrial activity were assessed at the same passages (p6-7) for all cell isolates. The same passage number was used for each isolate as literature indicates passage number of pHGFs can influence both cell growth rate and cytokine release (Kent et al., 1996). The effect of PBM on both markers of mitochondrial activity and changes in mitochondrial activity were then assessed 8h post-irradiation as previously described and this enabled comparison with results described in Section 7.3.2.

7.4.2.1 Results

The results presented here provide evidence that pHGFs isolated from different individuals elicit a response to PBM dependent upon their mitochondrial content. Results revealed mitochondrial content of B19 and pool pHGFs was significantly higher than B15 and B16 cell isolates ($p<0.05$, Figure 7.9). Where B19 and pooled pHGFs exhibited mtDNA:nDNA ratios 54.01% and 64.13% greater than the B16 isolate respectively ($p<0.05$).

Interestingly, application of 400 nm light for 240s induced 14.90% and 16.17% increases in cell metabolic activity of B19 and pooled pHGF isolates (high mitochondrial content) respectively relative to the unstimulated control 8h post-irradiation ($p<0.05$, Figure 7.10). Whilst, irradiation of B15 and B16 (low mitochondrial content) isolates at the same parameters induced no significant increase in cell metabolic activity relative to the untreated

control. Similarly, irradiation at 400 nm for 240s also induced 17.9% and 36.89% increases in IL-8 secretion from B19 and pool isolates 8h post-irradiation ($p<0.05$, Figure 7.12) but there was no significant increase in IL-8 secretion following application of 400 nm light to B15 and B16 pHGF cultures. Hence, these data indicate cell isolates with a higher mitochondrial content may respond more significantly in particular, to 400 nm light.

However, this same trend was not seen when evaluating the effects of PBM on ROS production. Where, irradiation at 400 nm induced 9.32%, 16.92% and 10.36% increases in ROS production from B16, B19 and pooled pHGFs respectively relative to the non-irradiated control ($p<0.05$, Figure 7.11). Comparatively, application of 450 nm light induced significant increases in ROS production from the B15, B16 and B19 isolates but not from the pooled pHGF cultures: the cell isolate with the highest mitochondrial content. Also, irradiation of B15 and B19 isolates at 810 nm for 240s induced 13.75% and 8.16% increases in ROS production respectively relative to the non-irradiated control.

To further evaluate the mitochondrial content dependent effects of PBM *in vitro*, two individual pHGF isolates with the highest (B19) and lowest (B16) mitochondrial contents were used to investigate the effects of irradiation on real-time mitochondrial activity. It was found that mitochondrial content does influence response to blue light in this study. Where, application of 400 nm light to B19 (high mitochondrial content) cultures induced 29.30%, 64.50%, 31.66% and 57.72% increases in basal respiration, maximal respiration, ATP production and SRC respectively 8h post-irradiation relative to the unstimulated control ($p<0.05$, Figure 7.14). Comparatively, application of 400 nm or 450 nm light to B16 (low mitochondrial content) pHGFs induced no significant changes in basal or maximal respiration, ATP production or SRC. However, irradiation at 810 nm for 240s did induce 29.46% increases

in basal respiration from B16 cultures relative to the non-irradiated controls ($p<0.05$) but this was the only significant change in mitochondrial activity caused by light application to B16 cultures.

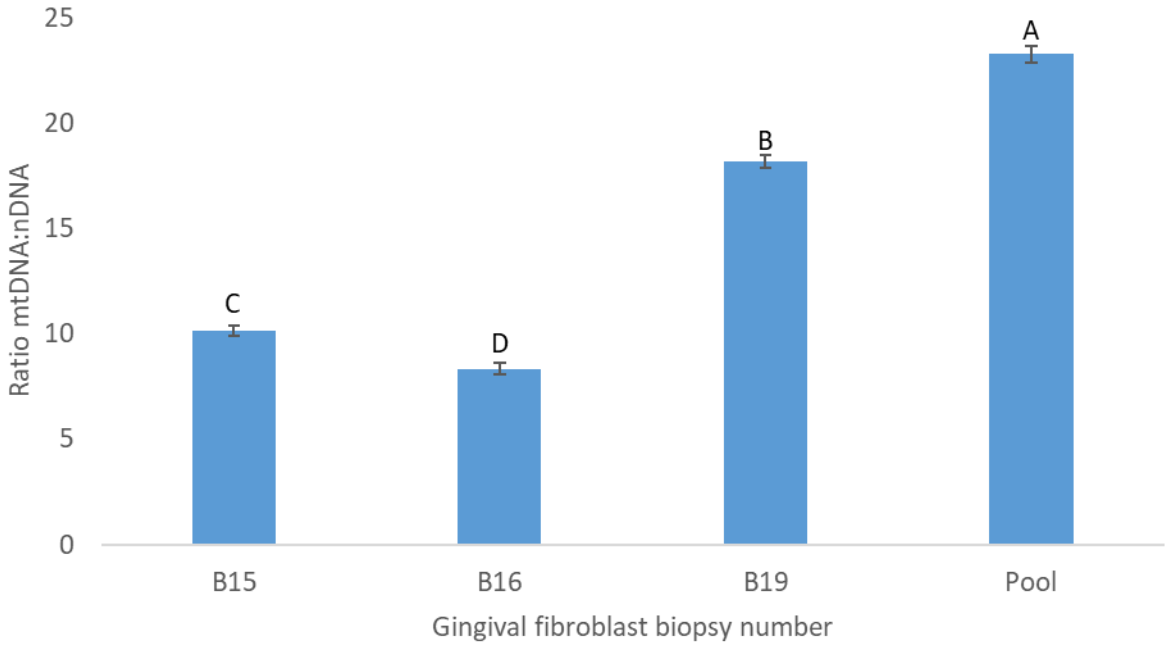

Figure 7.9 Relative differences in ratios of mtDNA:nDNA quantified from fibroblasts isolated from three individuals (n=4, p7, B15, B16, B19) or the mtDNA:nDNA when three patient isolates were pooled and grown together (pool, n=4, B13, B16, B19, p7). Significance is indicated where means do not share the same letter. Significance was analysed using one way ANOVA followed by Tukey test ($p<0.05$).

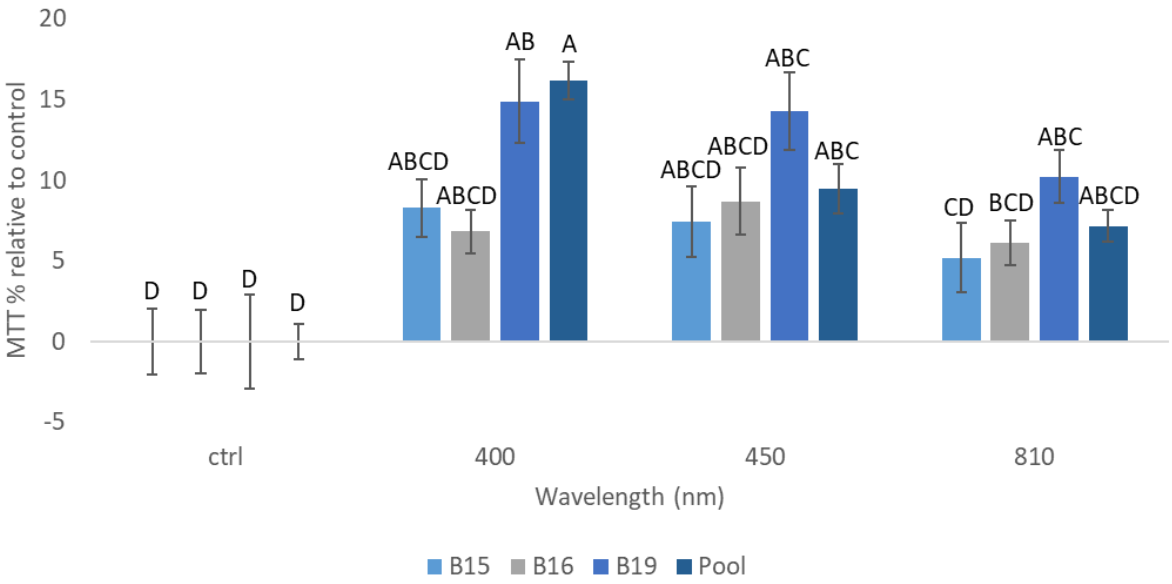

Figure 7.10 The effects of PBM (400-810 nm, 24mW/cm², 5.76J/cm²) on the cell metabolic activity of B15, B16, B19 and pool (B13, B16, B19) pHGF isolates (all p6/7, n=18) 8h post-irradiation relative to the non-irradiated control. The non-irradiated control was normalised to 0% and % change in cell metabolic activity induced by light is presented relative to the control. Significance was assessed using one-way ANOVA followed by Tukey test. Means that do not share the same letter are significantly different (p<0.05).

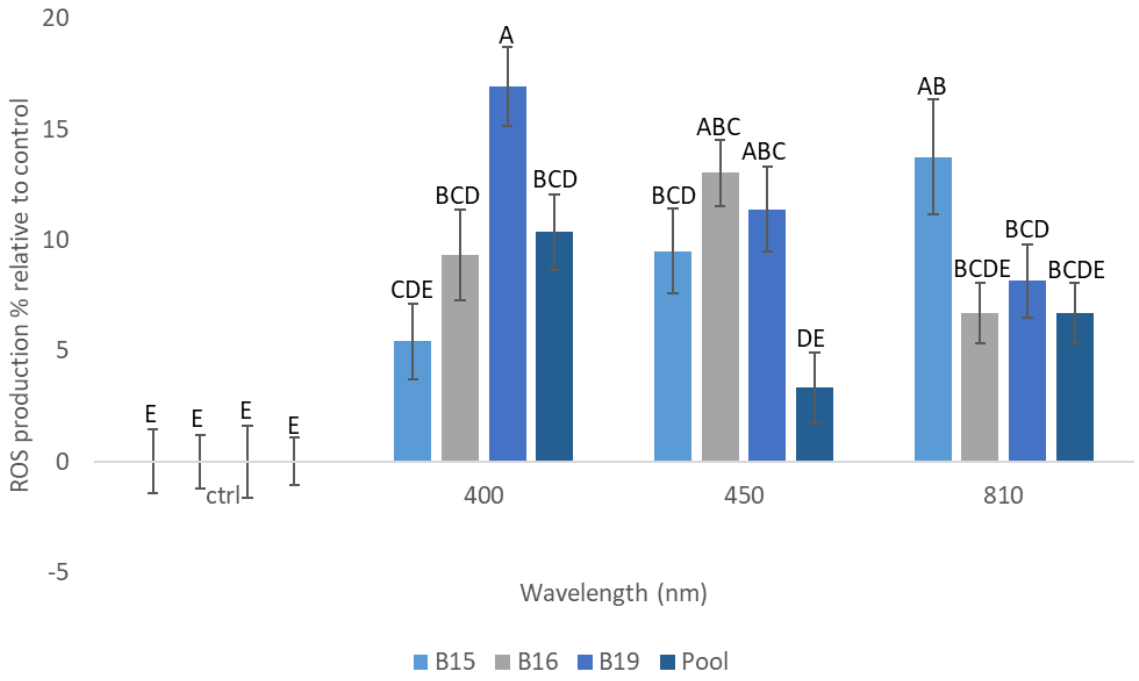

Figure 7.11 The effects of PBM (400-810 nm, 24mW/cm², 5.76J/cm²) on ROS production from B15, B16, B19 and pool (B13, B16, B19) pHGF isolates (all p6/7, n=18) 8h post-irradiation relative to the non-irradiated control, which was normalised to 0%. Significance was assessed using one-way ANOVA followed by Tukey test. Means that do not share the same letter are significantly different ($p<0.05$).

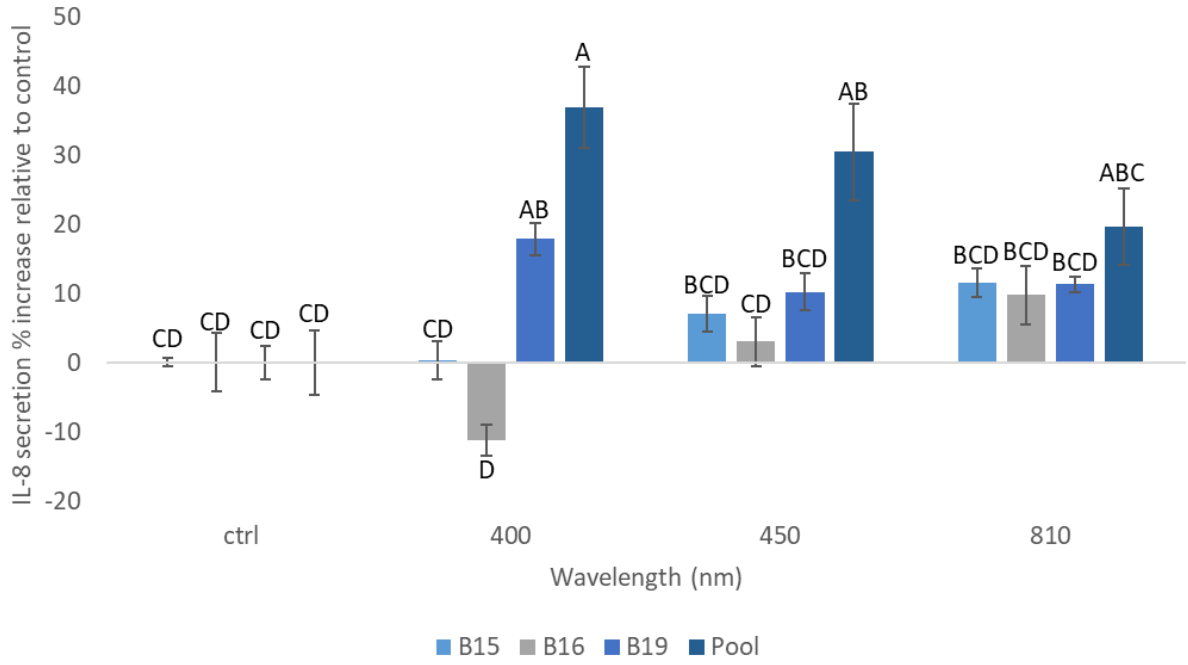

Figure 7.12 The effects of PBM (400-810 nm, 24mW/cm², 5.76J/cm²) on IL-8 secretion from B15 (n=8, p7), B16 (n=8, p7), B19 (n=8, p7) and pooled (B13, B16, B19, n=13, p7) pHGF isolates 8h post-irradiation relative to the non-irradiated control which was normalised to 0%. Significance was assessed using one-way ANOVA followed by Tukey test. Means that do not share the same letter are significantly different ($p<0.05$).

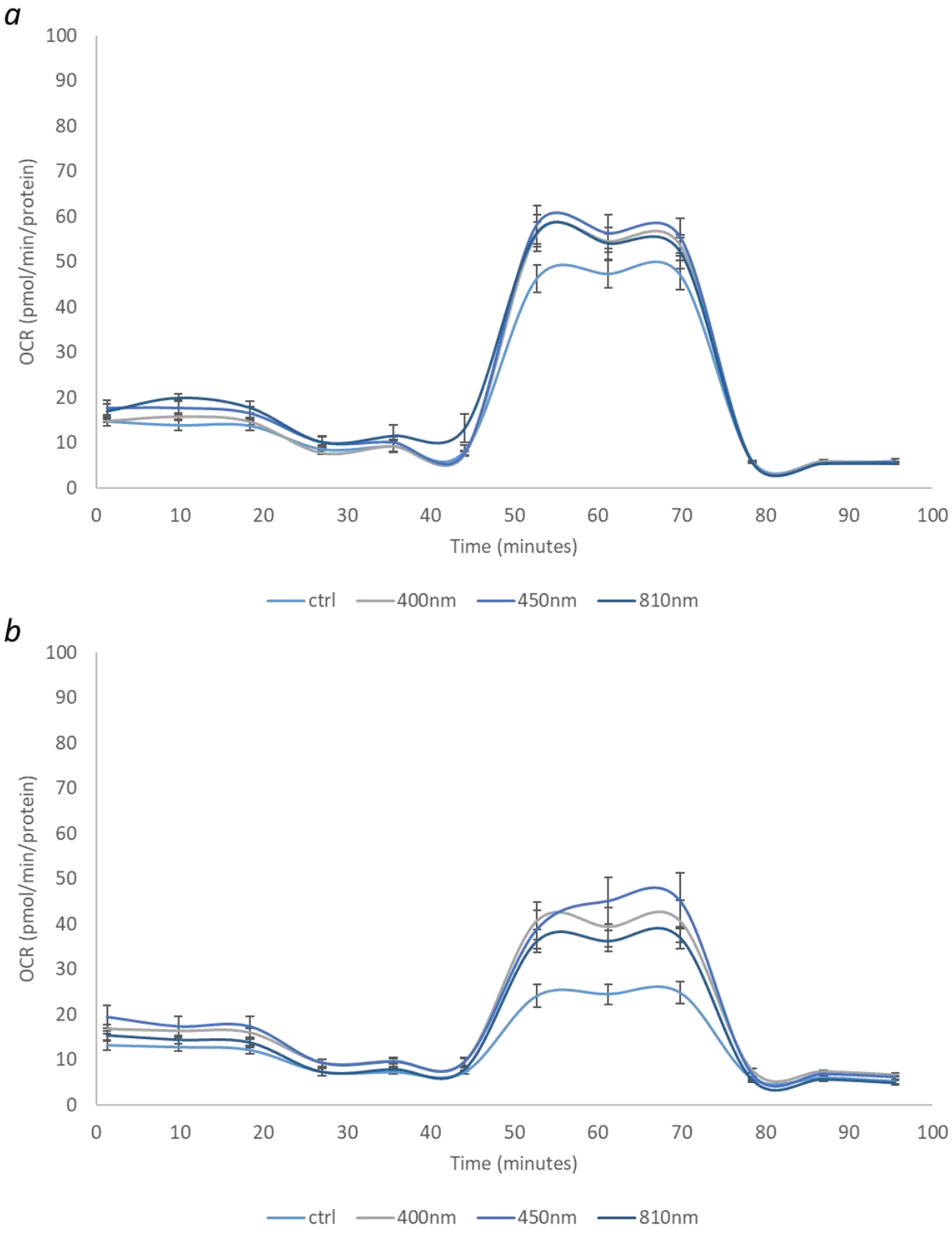

Figure 7.13 Changes in mitochondrial activity induced by PBM (400-810 nm, 5.76J/cm², 24mW/cm²), 8h post application to a) B16 pHGF isolate (p7, n=6) and b) B19 pHGF isolate (p7, n=6) analysed using the Seahorse cell mito stress assay. Abrupt changes in the traces above indicate the injection of compounds altering ETC activity. OCR values were also normalised for protein content.

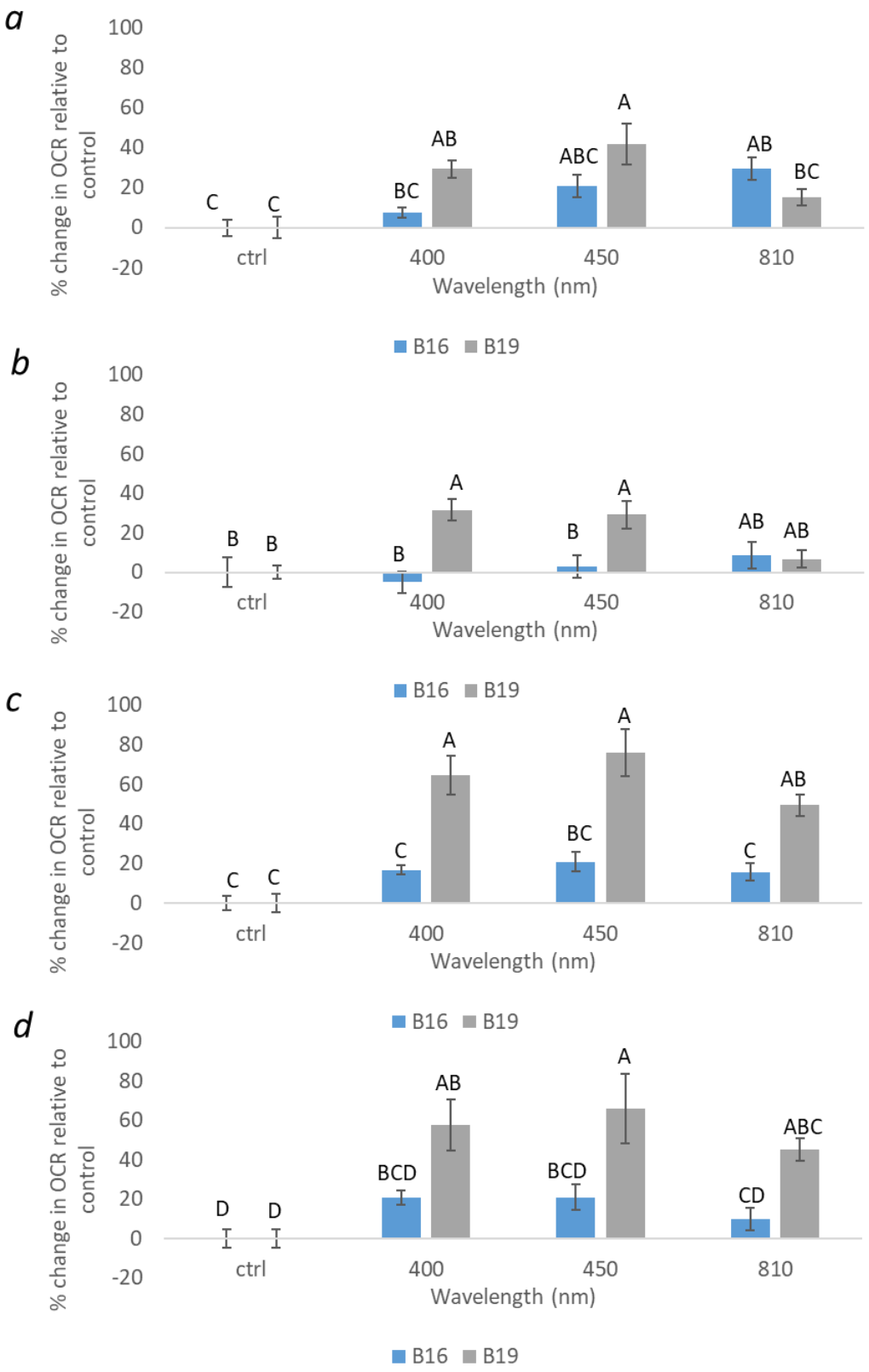

Figure 7.14 The effect of PBM 8 hours post-irradiation on a) basal respiration, b) ATP production, c) Maximal respiration, d) Spare respiratory capacity from B16 (p7, n=6) or B19 (p7, n=6) pHGF isolates irradiated for 240s at wavelengths between 400-810 nm. Significance was assessed using one-way ANOVA followed by Tukey test. Means that do not share the same letter are significantly different ($p<0.05$).

7.5 Discussion

7.5.1 Assessment of the mitochondrial dependent effects of PBM.

The data presented in this Chapter provide evidence of a well characterised system for exploration of the mitochondrial content dependent effects of PBM using cell types commonly reported to possess different mitochondrial numbers: namely myoblasts and myotubes (Wagatsuma and Sakuma, 2013). Initially, to evaluate the dose and wavelength dependent effects of PBM on myoblasts, an MTT assay was employed. The MTT assay revealed a dose of 0.72J/cm² and wavelengths of 400 nm and 810 nm were sufficient to induce significant increases in cell metabolic activity from myoblasts and hence these parameters were selected for further application (Figure 7.1). Notably, the response reported in the MTT assay have been correlated with changes in mitochondrial activity (Basoah et al., 2005, Liu et al., 1997, Rai et al., 2018). Hence, these data indicate violet-blue and NIR light could modulate mitochondrial activity.

Interestingly, *Xu et al* reported that irradiation at 810 nm and doses between 0.33-1.34J/cm² induced increases in mitochondrial function (Xu et al., 2008). However, this is the first study to date to describe the effects of blue light on cell metabolic activity of myoblasts at the doses described (0.72-5.76J/cm²). To aid comparison with experimental data described throughout this thesis (Chapters 4-6), wavelengths of 400 nm, 450 nm and 810 nm and a dose of 0.72J/cm² were selected to evaluate the effects of PBM on real-time mitochondrial activity.

In order to assess the effects of PBM on real-time mitochondrial activity, the time-point at which to employ the use of the Seahorse XF cell mito stress assay post-irradiation was determined. Where, it was concluded that the effects of PBM on real-time mitochondrial activity would be evaluated 8h post-irradiation (Figure 7.3) as the trace produced at 8h post-

irradiation was most representative of that expected of the assay (see Figure 7.2). Similarly, *Ferreria et al* explored the optimal time-point post-irradiation to evaluate the effects of irradiation at 850 nm and 2.5J/cm² on mitochondrial membrane potential and ATP production (Ferraresi et al., 2015b). The authors evaluated the effects of PBM 15min, 3h, 6h and 24h post-irradiation and concluded that mitochondrial activity peaked 6h post-irradiation. Whilst a time-point 8h post-irradiation was not evaluated in that study, the results corroborate with those stated here in which changes in mitochondrial activity could not be reliably evaluated <1h and >24h post-irradiation.

Myotubes have been cited to possess a higher mitochondrial number when compared with myoblasts (Wagatsuma and Sakuma, 2013). However, to confirm current reports an assay was developed to demonstrate differences in mitochondrial content of these two cell types. Commonly, mtDNA content is measured as a marker for mitochondrial number as the mitochondrial number per cell cannot be directly measured due to the dynamic nature of mitochondria and the reported poor reproducibility of current isolation methods (Picard et al., 2011). Importantly, mtDNA copy number has been correlated to mitochondrial content in previous studies (Larsen et al., 2012).

Hence, to perform these studies mtDNA and nuclear DNA was isolated and amplified in samples and quantified using a microplate assay. Reportedly, most commonly, the dsDNA binding dye PicoGreen® (Thermo fisher) is used in these studies (He et al., 2018a). However, whilst this dye reliably indicates DNA concentrations of samples the relative expense of this reagent is high (Abiodun et al., 2010).Hence, cost effective alternatives were evaluated including Sytox green (1mM), SYBR green I (10-1% v/v) and SYBR® safe dye (2% v/v). Using a protocol adapted from one described by *Leggate et al,* the data displayed in Figure 7.4

provides evidence that SYBR® safe dye was effective in demonstrating changes in fluorescence due to changes in calf thymus DNA concentration (Leggate et al., 2006). Therefore, using this dsDNA dye, Figure 7.5 provides evidence that myotubes possess a higher mitochondrial content than myoblasts, corroborating with current literature. Therefore, the next objective of this project could be addressed: does mitochondrial content influence response to PBM?

7.5.2 Does mitochondrial content influence response to PBM?

Following optimisation of assays to reliably measure mitochondrial content and changes in mitochondrial activity, the influence of mitochondrial content on mitochondrial associated response to PBM was evaluated. Results suggest mitochondrial content could influence response to PBM. Figure 7.6 indicated that whilst a wavelength of 400 nm (0.72J/cm²) induced significant increases in markers for mitochondrial activity (ROS and cell metabolic activity) from myoblasts and myotubes, increases in the activities of these mitochondrial markers at all wavelengths were only observed in myotube cultures *($p<0.05$).* This may indicate that cells with a higher mitochondrial content exhibit an increased responsivity to light. *Kushibiki et al* also evaluated the effects of irradiation at 405 nm and 808 nm on ROS production from myoblast cells. The authors reported that only irradiation at 405 nm (100mW/cm², 6J/cm²) significantly increased ROS production whilst NIR exerted no significant effect (Kushibiki et al., 2013). The lack of effect exerted by NIR light on ROS production from myoblasts may be due to the difference in photon energy of blue light compared to NIR light (Tsai and Hamblin, 2017). In which, shorter wavelengths possess a higher photon energy when compared to longer wavelengths and thus can exert greater effects on tissue (Liebel et al., 2012). Hence, further work may be required to determine the photon energy dependent effects of PBM on

ROS production. Data described in this thesis also provides evidence that only violet-blue, and not NIR, light induced significant increases in ROS production from myoblasts.

Interestingly, *Mesquita-Ferrari et al* also used the MTT assay to demonstrate that application of NIR light (780 nm, 5J/cm²) induced significant increases in cell metabolic activity of myoblasts cultured in 2% v/v horse serum (to induce the differentiation process of myoblasts to myotubes (Kubo, 1991)) 24-72h post-irradiation (Mesquita-Ferrari et al., 2015). However, in another study published by the same group it was concluded that application of NIR light to myoblasts cultured in 10% FBS induced no significant change in cell metabolic activity 24-72h post-irradiation (Mesquita-Ferrari et al., 2011). Hence, results previously reported corroborate with findings outlined in this project suggesting irradiation of myotubes with NIR light induces significant increases in MTT but has no significant effect on the same parameters in myoblasts. However, one limitation of these studies is the fact that the parameters used may be outside of the therapeutic range for myoblasts. Where, data described in Figure 7.1 provides evidence that application of NIR light (740-830 nm) at doses >1.44J/cm² induced no significant changes in cell metabolic activity of myoblasts 24h post-irradiation. Nevertheless, these studies demonstrate the differential response of myoblasts and myotubes to PBM. In which, myotubes appear more responsive to light when compared with myoblasts.

Subsequent to the evaluation of the effects of PBM on markers for mitochondrial activity, the Seahorse platform was used to evaluate the effects of PBM on mitochondrial-respiration directly. Results corroborated with those described above in which the effects of PBM correlated with mitochondrial content. Where, application of 400 nm, 450 nm or 810 nm light to myotube cultures (high mitochondrial content) induced significant increases basal

and maximal respiration, ATP production and SRC (Figure 7.7, $p<0.05$). Whilst comparatively, irradiation at 810 nm only induced significant increases in maximal respiration, ATP production and SRC from myoblasts (low mitochondrial content, $p<0.05$). However, mean changes in respiration induced by light were higher from myotubes when compared with myoblasts. To date, only a handful of studies have evaluated the effects of PBM using the Seahorse platform (Chu-Tan et al., 2016, Wigle and Castellanos, 2016). Previously, the effects of red light on mitochondrial activity have been investigated and only *Chu-Tan et al* provided evidence that PBM could modulate mitochondrial activity (Chu-Tan et al., 2016).

Hence, for the first time, these data provide evidence for the utility of the Seahorse platform in measuring changes in mitochondrial activity induced by blue and NIR light. This is also the first study to demonstrate the mitochondrial content dependent effects of PBM, in which cultures with a higher mitochondrial content are more responsive to PBM, particularly blue light PBM.

7.5.3 The effects of PBM on pHGFs are mitochondrial dependent.

The potential effects of PBM in the management of oral diseases have been widely documented (Milward et al., 2014). However, despite the large majority of authors reporting the clinical efficacy of PBM, a small yet substantial number still cite that PBM has no significant effect in relieving disease symptoms. In a review on the use of PBM in dentistry, *Carroll et al* reported that of the 153 articles reviewed, 15% reported negative or inconclusive outcomes (Carroll et al., 2014). The authors concluded that this lack of effect may be due to the irradiation parameters employed being outside the therapeutic range. However, one other hypothesis discussed in this thesis is the idea that mitochondrial content could influence

response to PBM *in vivo.* Thus providing some explanation as to the variability of patient outcomes in response to PBM.

In order to address this hypothesis, firstly high throughput assessment of the effects of a range of treatment parameters (400-830 nm, 2.88-5.76J/cm², 24mW/cm²) on cell metabolic activity of pHGF cultures isolated from four individuals (B13, B15, B16 and B19, p5-7) were assessed. Responses were then compared to those elicited from a pool of three pHGF isolates (B13, B16 and B19, p5-7) to aid comparison with data described throughout this thesis (where pool pHGFs only have been used in Chapters 4-6). Data indicated that the response to PBM *in vitro* is individual dependent where the B15 isolate elicited no significant response to PBM, whilst B13, B19 and pool isolates exhibited significant increases in cell metabolic activity following application of 400 nm light for 240s (24h post-irradiation, Figure 7.8-10, $p<0.05$). However, mean increases in cell metabolic activity induced by blue light were variable ranging from 6.22-14.63% dependent upon the pHGF isolate irradiated. Notably, B19 and pool isolates exhibited the greatest increases in cell metabolic activity induced by blue light. Interestingly, *Basso et al* also reported the variability in response of pHGFs isolated from different individuals to PBM (Basso et al., 2015). Hence, these data provide evidence that response to PBM *in vitro* is individual dependent. Therefore, the next step in this project was to assess whether these difference were due to mitochondrial content.

Results indicated that there were significant differences in the mitochondrial content of pHGFs isolated from different individuals (Figure 7.9) and the B19 and pool isolates had the highest mitochondrial content. However, to further evaluate whether mitochondrial content could influence response to PBM, the effects of PBM on cell metabolic activity, ROS production and IL-8 were evaluated 8h post-irradiation. IL-8 was evaluated as a downstream

marker for NFkB, a gene transcription factor whose activities are modulated by mitochondrial activity (Formentini et al., 2017, Biswas et al., 2003). It was found that irradiation of pHGFs with a high mitochondrial content (B19 and pool) induced significant increases in both ROS production and IL-8 secretion ($p<0.05$, Figure 7.10 and Figure 7.12). Whilst, comparably violet-blue light had no significant effect on pHGFs with a relatively low mitochondrial content (B15 and B16). Individual differences in mitochondrial content may be reflective of a number of factors including diet, exercise and age. Key factors that have been cited to dictate mitochondrial biogenesis and thus mitochondrial number (Pizzorno, 2014, López-Lluch et al., 2008). Whilst information regarding pHGF donors was not provided in this study, it will be prudent in future studies to take these factors into consideration.

However, the same trend was not seen when evaluating the effects of PBM on ROS production. Where, response to PBM was more variable and did not appear to be dependent on mitochondrial content (Figure 7.11). However, the ROS assay used in this project (H_2DCFDA) is not associated with mitochondrial ROS production and is primarily used as a general marker for oxidative stress (Forkink et al., 2010). Hence, changes in ROS production induced by PBM measured in this assay may not be directly related to changes in mitochondrial activity and hence due to differences in mitochondrial content. This outcome may also be due to the time-point at which ROS production was assessed, as it was reported in this project (Chapters 4, 5 and 6) that PBM could modulate ROS production 24h post application whilst in comparison ROS production was measured 8h post application in this Chapter. Hence, future work may involve evaluation of the time dependent response of pHGF isolates to PBM in terms of ROS production.

Subsequently, mitochondrial content dependent response of pHGFs to PBM using the Seahorse cell Mito stress assay were evaluated. The B16 and B19 isolates were selected for analysis due to the fact that they exhibited significantly different mitochondrial contents (Figure 7.9). Results corroborated with those described above, in which mitochondrial content reportedly influenced the response to PBM *in vitro.* Where, application of 400 nm or 450 nm light induced significant changes in mitochondrial activity from B19 pHGFs but not in B16 pHGFs.

These data provide evidence that the response to PBM could be mitochondrial content dependent. This may prove useful in understanding the inconsistency in response to PBM clinically as it is well reported there is variability in the mitochondrial content between individuals (Carter, 2007). Where mitochondrial function and number declines with age (Chistiakov et al., 2014a), whilst in comparison, on average athletes are cited to possess higher mitochondrial numbers (Menshikova et al., 2006). Hence, this may enable development of strategies for successful application of PBM *in vivo*. Where, individuals with lower mitochondrial contents may require a greater dose of light to ensure stimulation of mitochondria, or alternatively supplements could be added to a patients diet to induce mitochondrial biogenesis prior to treatment with light such as resveratrol or curcumin (Gibellini et al., 2015).

Data has also shown that PBM induces increased mitochondrial function regardless of mitochondrial content. In a study using *Drosophila Melanogaster* (fruit flies), Weinrich et al found that application of 670nm light reduced metabolic, visual and cognitive decline in the flies due to an increase in mitochondrial activity (Weinrich et al., 2017). Hence, it is apparent from these studies that the mitochondria are instrumental in orchestrating a response to PBM

and that the number of mitochondria could be pivotal in determining the level of response. To further evaluate this, it will be fundamental to investigate response to PBM using fibroblasts from not only a range of patients but also from a range of locations within the oral cavity for example through employment of both gingival and periodontal ligament fibroblasts. This may give some idea as to how fibroblast heterogeneity influences response to PBM as studies currently indicate differences in cell surface marker expression and also mitochondrial heterogeneity between different cell types which could mediate response to PBM (Palaiologou et al., 2001, Kuznetsov and Margreiter, 2009).

8 CONCLUSIONS AND FUTURE PERSPECTIVES

8.1 Summary of main findings.

Despite best efforts to improve oral health across the UK, the prevalence of chronic periodontitis remains at 45% (Ahmed, 2017). Indeed, a plethora of authors have reported the adverse effects of poor oral health on quality of life (Ferreira et al., 2017) and systemic disease (Najafipour et al., 2013). Even with these findings indicating the importance of oral health there still remains no novel non-invasive devices to aid in the treatment of periodontal disease besides traditional methods. In which, 20-30% of patients exhibit little response to conventional periodontal treatment (Shaddox and Walker, 2010).

As discussed throughout this thesis, one treatment modality, cited to prove efficacious in both the treatment of oral disease and maintenance of oral health is PBM (Milward et al., 2014). However, despite ~1000 articles citing the application of PBM in treating oral disease (April 2019, Figure 9.2), controversy still surrounds the use of PBM clinically. Due to a lack of consistency in the reporting and recording of treatment parameters and also a lack of knowledge as to how PBM induces its cellular effects (Hadis et al., 2016a). Hence, this thesis aimed to address these two issues firstly by providing clear guidelines on how authors should measure and report key treatment parameters for PBM applications and secondly, by further elucidating the biological effects of PBM.

Firstly, data provides evidence of two well characterised systems for evaluation of the effects of PBM. Corroborating with current publications citing the importance of the measurement of parameters such as beam area (cm^2), irradiance (mW/cm^2), wavelength (nm) and radiant exposure (J/cm^2) to ensure reliable measurement of biological response to light (Hadis et al., 2016a, Jenkins and Carroll, 2011, Tunér and Hode, 1998). For example, had the assumption been made that average beam area correlated to the area of the aperture

used in light studies with the LUMOS™ array (section 3.3.2), cultures would have been seeded to cover the entire well area whereas beam profilometry revealed that only a small percentage of the well area was illuminated on irradiation and hence a smaller proportion of cells irradiated. Meaning the biological response to light may have been masked by those cells receiving no light. Indeed, review of the literature revealed that 82% of authors citing the effects of blue light failed to report beam area (1.4.2). I hypothesise that this may account for variability in results currently published in which a large proportion of authors report that PBM has no significant effect both *in vitro* and *in vivo*. It also demonstrates the reproducibility of our work, in which authors can directly compare treatment parameters used in our studies to those used for example, in clinical applications. The data presented here therefore may assist in the translation of PBM to use in practice.

Subsequent to characterisation of light sources, the biological effects of PBM were evaluated using the most abundant cell type in the oral periodontium: pHGFs (Ara et al., 2009b). Results provided novel evidence of the biomodulatory effects of blue light PBM in which, application of blue light (400-450 nm, 5.76J/cm², 24mW/cm²) to a model for 'health' modulated markers for mitochondrial activity (ATP, basal and maximal respiration rates chapters 4 and 7) whilst also inducing small increases in markers for inflammation (ROS and IL-8, chapter 4). Small, acute increases in markers for inflammation such as cytokines are associated with the modulation of cellular proliferation and differentiation, thus they are crucial in ensuring cellular homeostasis (Itoh et al., 2005, Turner et al., 2014). It could also be hypothesised that promotion of cellular activities in response to light could prove beneficial in priming the host to appropriately respond to any future bacterial insult.

Comparatively, in a model for 'periodontal disease', whilst blue light also modulated mitochondrial relevant gene expression (complex I and V gene expression, ATP, chapter 5), irradiation of bacterially challenged cultures induced significant decreases in markers for inflammation (ROS, IL-8 and TGFβ1 chapters 5 and 6). Whilst authors have previously illustrated similar findings in which PBM induced biomodulatory effects on pHGF cultures (Basso et al., 2015), this is the first to report the effects of blue light PBM on inflammation induced by four periodontal disease relevant stimuli: LPS, *F. nucleatum, P. gingivalis* and salivary biofilm. The importance of pathogens used in this thesis have been demonstrated throughout the literature where it has been shown that *P. gingivalis* could be instrumental in inducing neurodegeneration in Alzheimer's disease (Dominy et al., 2019) and *F. nucleatum* has been cited to contribute to the progression of colorectal cancer (Wu et al., 2019). Interestingly, blue light has also been shown to have a bactericidal effect on both *P. gingivalis* and *F. nucleatum* (Song et al., 2013). Therefore, it could be hypothesised that blue light could be an effective modality in modulating inflammation in disease whilst also inducing bacterial cell death.

Hence, these novel data provide evidence of the potential benefits of blue light for use in both health and disease. However, one other key issue reported was the variability in response to PBM. In which it was shown that pHGFs isolated from different individuals either elicited a positive, negative or no response to PBM (7.4.1). Whilst there are several factors that drive response to PBM including the wavelength and dose of light applied *in vitro* or indeed the inflammatory status of cultures (see section 1.5.4) there may be other factors contributing to this response. Observed for the first time in this thesis was that mitochondrial content could drive response to blue and NIR PBM. In which pHGFs isolated from different individuals exhibited different mitochondrial content (7.3). Where, individuals with a higher

mitochondrial content elicited a significantly greater biological response to both blue and NIR light when compared to those with a lower mitochondrial level. These data may therefore provide some clarity as to the reason why there is variability in individual patient response to PBM. This may also provide reasoning as to why PBM treatments may needed to be specifically tailored to each individual, where patients with a lower mitochondrial content may require greater light dose to induce an effect. Indeed, decreasing mitochondrial function and numbers are associated with the aging process and light has not only been shown to stimulate mitochondrial activity but also induce mitochondrial biogenesis (Chistiakov et al., 2014b, Ferraresi et al., 2012). Which, could prove beneficial to the aging population, where decreased mitochondrial function is associated with increased oxidative stress and thus a greater pre-disposition to diseases such as periodontitis (Bhatti et al., 2017, Tóthová and Celec, 2017).

However, despite these novel findings indicating the plausible efficacy of blue light in modulating cellular response, it is prudent to highlight limitations of the translation of studies to patients. In which, current literature indicates pHGF response to stimuli is driven by a number of key factors including the surface cells are cultured upon (Smith et al., 2009) and whether pHGFs are cultured in 2D or 3D models (Cukierman et al., 2001). Hence, whilst this work provides fundamental detail of the effects of PBM *in vitro*, future work will endeavour to develop models more closely related to those found in the oral cavity to evaluate the effects of PBM.

Nonetheless, this thesis provides not only evidence of a well characterised system for evaluation of PBM but also novel evidence that blue light could prove as effective as NIR light in modulating pHGF inflammatory and mitochondrial response. This could therefore prove

beneficial in the management of inflammation in chronic inflammatory diseases such as periodontitis.

8.2 Future work

Whilst this thesis provides fundamental evidence for the effects of PBM *in vitro* using a novel reproducible system, there still remains some limitations to the research and questions yet to be asked:

- Notably, while the salivary biofilm induced significant increases in markers for inflammation in cell cultures, it was not particularly relevant to periodontal disease as it mainly comprised of *Streptococcal* species, a species more commonly related to oral health. Hence, future studies may endeavour to evaluate the effects of PBM in modulating inflammation induced by a biofilm more relevant to periodontal disease. Comprising species including *Fusobacterium* and *Porphyromonas*. This may therefore involve the use of biofilm models similar to those developed by *Millhouse et al* (Millhouse et al., 2014), in which models relevant to health, gingivitis and periodontitis have been established.
- A further limitation of this study was that clinical and demographic data of the source patients that donated pHGFs isolates used in this study were not available. Hence, future work would aim to evaluate the effects of PBM on pHGF isolates from a well characterised origin. This may include evaluation of the effects PBM on pHGFs isolated from individuals representing a range of periodontal disease severities as well as non-periodontitis patients to further elucidate the effects of PBM. This would also involve examination of the mitochondrial content of these isolates to determine whether mitochondrial number is influenced by the onset of disease. Notably periopathogenic

bacteria, such as *P. gingivalis,* have been reported to promote mitochondrial dysfunction and thus decreased mitochondrial DNA copy number (Sun et al., 2017). Similarly, the mitochondrial content dependent effects of PBM could be further evaluated by applying compounds to cell cultures that induce mitochondrial biogenesis such as resveratrol (Dominy and Puigserver, 2013).

- This thesis also provided novel evidence as to how PBM modulates mitochondrial relevant gene expression. Specifically the effects of PBM on the expression of subunits of complexes I and IV (CCO) of the ETC were evaluated. However, only a single subunit comprising each complex was studied. Future work could therefore aim to evaluate not only the effects of blue light PBM on a number of subunit of complexes I and IV but also of complexes II, III and V. This work may provide an indication as to how PBM modulates ETC activity.
- Other signalling molecules shown to be modulated by blue light included TGFβ1. This is a key cytokine that has been shown to not only be a target for PBM (Arany et al., 2007) but it's presence in the oral cavity has been correlated with increased severity of periodontal disease (Skaleric et al., 1997). Hence, future work may involve evaluation of the effects of PBM on TGFβ related signalling, such as determining the effects of PBM on Smad protein expression and also TGFβR expression. This work may then provide further elucidation as to the downstream effects of PBM.
- A further limitation of this study was the lack of beam homogeneity across the LUMOS array, indeed the entire well area was not uniformly irradiated. It will therefore be prudent to evaluate the application of other diffuser materials to improve homogeneity whilst also preventing significant increases in media temperature.

- Finally, the effects of PBM have been cited both on eukaryotic cells and bacterial cells. This thesis provides evidence that blue light could prove an effective modality in modulating pHGF cellular response. However, the bactericidal effects of PBM utilising the same treatment parameters on periodontopathogens are yet to be evaluated. Hence, future work will endeavour to evaluate both either separately or combined, through the development of oral cavity relevant 3D models.

8.3 Concluding remarks

In conclusion, this thesis provides evidence of two well characterised light sources for reliable evaluation of the effects of PBM *in vitro*. It also provides novel evidence of the biomodulatory effects of PBM in which four periodontally relevant stimuli were employed to evaluate the effects of irradiation in a 'disease' model. Results also show fundamentally that the effects of PBM are mitochondrial dependent, where mitochondrial content can dramatically influence response to PBM. These findings may therefore aid in providing evidence of possible treatment parameters for application *in vivo*. In turn, this may enable effective translation of these parameters to a novel device utilising blue light to promote tissue healing and modulate inflammation in prevalent diseases including periodontitis.

9 REFERENCES

Abiodun, O. O., Gbotosho, G. O., Ajaiyeoba, E. O., Happi, C. T., Hofer, S., Wittlin, S., Sowunmi, A., Brun, R. and Oduola, A. M. (2010) 'Comparison of SYBR Green I-, PicoGreen-, and [3H]-hypoxanthine-based assays for in vitro antimalarial screening of plants from Nigerian ethnomedicine', *Parasitol Res,* 106(4), pp. 933-9.

Abo-Aziza, F. A. M. and A, A. Z. (2017) 'The Impact of Confluence on Bone Marrow Mesenchymal Stem (BMMSC) Proliferation and Osteogenic Differentiation', *Int J Hematol Oncol Stem Cell Res,* 11(2), pp. 121-132.

Adamskaya, N., Dungel, P., Mittermayr, R., Hartinger, J., Feichtinger, G., Wassermann, K., Redl, H. and van Griensven, M. (2011) 'Light therapy by blue LED improves wound healing in an excision model in rats', *Injury,* 42(9), pp. 917-21.

Ahmed, H. (2017) 'Oral health: What is gum disease?', *Bdj,* 222, pp. 323.

Aimbire, F., Albertine, R., de Magalhaes, R. G., Lopes-Martins, R. A., Castro-Faria-Neto, H. C., Zangaro, R. A., Chavantes, M. C. and Pacheco, M. T. (2005) 'Effect of LLLT Ga-Al-As (685 nm) on LPS-induced inflammation of the airway and lung in the rat', *Lasers Med Sci,* 20(1), pp. 11-20.

Akram, Z., Vohra, F. and Javed, F. (2018) 'Low-level laser therapy as an adjunct to connective tissue graft procedure in the treatment of gingival recession defects: A systematic review and meta-analysis', *Journal of Esthetic and Restorative Dentistry,* 30(4), pp. 299-306.

Al-Watban, F. A. H., Zhang, X. Y., Andres, B. L. and Al-Anize, A. (2009) 'Visible lasers were better than invisible lasers in accelerating burn healing on diabetic rats', *Photomedicine and Laser Surgery,* 27(2), pp. 269-272.

Alba, M. N., Gerenutti, M., Yoshida, V. M. H. and Grotto, D. (2017) 'Clinical comparison of salicylic acid peel and LED-Laser phototherapy for the treatment of Acne vulgaris in teenagers', *Journal of Cosmetic and Laser Therapy,* 19(1), pp. 49-53.

Albini, A. (2016) 'Some remarks on the first law of photochemistry', *Photochem Photobiol Sci,* 15(3), pp. 319-24.

Albuquerque-Pontes, G. M., Vieira, R. P., Tomazoni, S. S., Caires, C. O., Nemeth, V., Vanin, A. A., Santos, L. A., Pinto, H. D., Marcos, R. L., Bjordal, J. M., de Carvalho Pde, T. and Leal-Junior, E. C. (2015) 'Effect of pre-irradiation with different doses, wavelengths, and application intervals of low-level laser therapy on cytochrome c oxidase activity in intact skeletal muscle of rats', *Lasers Med Sci,* 30(1), pp. 59-66.

Aleksic, V., Aoki, A., Iwasaki, K., Takasaki, A. A., Wang, C. Y., Abiko, Y., Ishikawa, I. and Izumi, Y. (2010) 'Low-level Er: YAG laser irradiation enhances osteoblast proliferation through activation of MAPK/ERK', *Lasers in Medical Science,* 25(4), pp. 559-569.

Alexsandra da Silva Neto Trajano, L., da Silva, C. L., de Carvalho, S. N., Cortez, E., Mencalha, A. L., de Souza da Fonseca, A. and Stumbo, A. C. (2016) 'Cell viability, reactive oxygen species, apoptosis, and necrosis in myoblast cultures exposed to low-level infrared laser', *Lasers in Medical Science,* 31(5), pp. 841-848.

AlGhamdi, K. M., Kumar, A., A Al-ghamdi, A., Al-Rikabi, A. C., Mubarek, M. and Ashour, A. E. (2016) 'Ultra-structural effects of different low-level lasers on normal cultured human melanocytes: an in vitro comparative study', *Lasers in Medical Science,* 31(9), pp. 1819-1825.

AlGhamdi, K. M., Kumar, A., Ashour, A. E. and AlGhamdi, A. A. (2015) 'A comparative study of the effects of different low-level lasers on the proliferation, viability, and migration of human melanocytes in vitro', *Lasers in Medical Science,* 30(5), pp. 1541-1551.

Ali, M. A. (1979) 'Myotube formation in skeletal muscle regeneration', *Journal of anatomy,* 128(Pt 3), pp. 553-562.

Almeida-Lopes, L., Rigau, J., Zangaro, R. A., Guidugli-Neto, J. and Jaeger, M. M. (2001a) 'Comparison of the low level laser therapy effects on cultured human gingival fibroblasts proliferation using different irradiance and same fluence', *Lasers Surg Med,* 29(2), pp. 179-84.

Almeida-Lopes, L., Rigau, J., Zângaro, R. A., Guidugli-Neto, J. and Jaeger, M. M. M. (2001b) 'Comparison of the low level laser therapy effects on cultured human gingival fibroblasts

proliferation using different irradiance and same fluence', *Lasers in Surgery and Medicine,* 29(2), pp. 179-184.

Alves, A. C. A., De Carvalho, P. D. T. C., Parente, M., Xavier, M., Frigo, L., Aimbire, F., Leal Junior, E. C. P. and Albertini, R. (2013) 'Low-level laser therapy in different stages of rheumatoid arthritis: A histological study', *Lasers in Medical Science,* 28(2), pp. 529-536.

Alves, M. B., de Arruda, R. P., Batissaco, L., Florez-Rodriguez, S. A., de Oliveira, B. M., Torres, M. A., Ravagnani, G. M., Lanconi, R., de Almeida, T. G., Storillo, V. M., Vellone, V. S., Franci, C. R., Thome, H. E., Canella, C. L., De Andrade, A. F. and Celeghini, E. C. (2016) 'Low-level laser therapy to recovery testicular degeneration in rams: effects on seminal characteristics, scrotal temperature, plasma testosterone concentration, and testes histopathology', *Lasers Med Sci,* 31(4), pp. 695-704.

Amaroli, A., Ravera, S., Baldini, F., Benedicenti, S., Panfoli, I. and Vergani, L. (2019) 'Photobiomodulation with 808-nm diode laser light promotes wound healing of human endothelial cells through increased reactive oxygen species production stimulating mitochondrial oxidative phosphorylation', *Lasers in Medical Science,* 34(3), pp. 495-504.

Amid, R., Kadkhodazadeh, M., Ahsaie, M. G. and Hakakzadeh, A. (2014) 'Effect of low level laser therapy on proliferation and differentiation of the cells contributing in bone regeneration', *Journal of Lasers in Medical Sciences,* 5(4), pp. 163-170.

Andreakos, E., Sacre, S. M., Smith, C., Lundberg, A., Kiriakidis, S., Stonehouse, T., Monaco, C., Feldmann, M. and Foxwell, B. M. (2004) 'Distinct pathways of LPS-induced NF-kappa B activation and cytokine production in human myeloid and nonmyeloid cells defined by selective utilization of MyD88 and Mal/TIRAP', *Blood,* 103(6), pp. 2229-37.

Andreo, L., Mesquita-Ferrari, R. A., Ribeiro, B. G., Benitte, A., de Fátima Nogueira, T., França, C. M., Silva, D. F. T., Bussadori, S. K., Fernandes, K. P. S., Corrêa, F. I. and Corrêa, J. C. F. (2018) 'Effects of myogenic precursor cells (C2C12) transplantation and low-level laser therapy on muscle repair', *Lasers in Surgery and Medicine,* 50(7), pp. 781-791.

Ankri, R., Friedman, H., Savion, N., Kotev-Emeth, S., Breitbart, H. and Lubart, R. (2010a) 'Visible light induces nitric oxide (NO) formation in sperm and endothelial cells', *Lasers Surg Med,* 42(4), pp. 348-52.

Ankri, R., Lubart, R. and Taitelbaum, H. (2010b) 'Estimation of the optimal wavelengths for laser-induced wound healing', *Lasers Surg Med,* 42(8), pp. 760-4.

Anschau, F., Webster, J., Capra, M. E. Z., de Azeredo da Silva, A. L. F. and Stein, A. T. (2019) 'Efficacy of low-level laser for treatment of cancer oral mucositis: a systematic review and meta-analysis', *Lasers in Medical Science*.

Ao, J., Wood, J. P. M., Chidlow, G., Gillies, M. C. and Casson, R. J. (2018) 'Retinal pigment epithelium in the pathogenesis of age-related macular degeneration and photobiomodulation as a potential therapy?', *Clinical and Experimental Ophthalmology,* 46(6), pp. 670-686.

Aquilano, K., Baldelli, S. and Ciriolo, M. R. (2014) 'Glutathione: new roles in redox signaling for an old antioxidant', *Frontiers in pharmacology,* 5, pp. 196-196.

Ara, T., Kurata, K., Hirai, K., Uchihashi, T., Uematsu, T., Imamura, Y., Furusawa, K., Kurihara, S. and Wang, P. L. (2009a) 'Human gingival fibroblasts are critical in sustaining inflammation in periodontal disease', *Journal of Periodontal Research,* 44(1), pp. 21-27.

Ara, T., Kurata, K., Hirai, K., Uchihashi, T., Uematsu, T., Imamura, Y., Furusawa, K., Kurihara, S. and Wang, P. L. (2009b) 'Human gingival fibroblasts are critical in sustaining inflammation in periodontal disease', *J Periodontal Res,* 44(1), pp. 21-7.

Arakaki, L. S., Ciesielski, W. A., Thackray, B. D., Feigl, E. O. and Schenkman, K. A. (2010) 'Simultaneous optical spectroscopic measurement of hemoglobin and myoglobin saturations and cytochrome aa3 oxidation in vivo', *Appl Spectrosc,* 64(9), pp. 973-9.

Arany, P. R., Nayak, R. S., Hallikerimath, S., Limaye, A. M., Kale, A. D. and Kondaiah, P. (2007) 'Activation of latent TGF-beta1 by low-power laser in vitro correlates with increased TGF-beta1 levels in laser-enhanced oral wound healing', *Wound Repair Regen,* 15(6), pp. 866-74.

Asghari, A., Takhtfooladi, M. A. and Hoseinzadeh, H. A. (2016) 'Effect of photobiomodulation on ischemia/reperfusion-induced renal damage in diabetic rats', *Lasers Med Sci,* 31(9), pp. 1943-1948.

Ash, C., Dubec, M., Donne, K. and Bashford, T. (2017) 'Effect of wavelength and beam width on penetration in light-tissue interaction using computational methods', *Lasers in Medical Science,* 32(8), pp. 1909-1918.

Ashworth, B. E., Stephens, E., Bartlett, C. A., Serghiou, S., Giacci, M. K., Williams, A., Hart, N. S. and Fitzgerald, M. (2016) 'Comparative assessment of phototherapy protocols for reduction of oxidative stress in partially transected spinal cord slices undergoing secondary degeneration', *BMC Neuroscience,* 17(1).

Askhadulin, E. V., Konchugova, T. V. and Moskvin, S. V. (2018) '[The application of combined low-intensity laser therapy for the treatment of the patients presenting with trophic ulcers associated with chronic venous insufficiency of the lower extremities]', *Vopr Kurortol Fizioter Lech Fiz Kult,* 95(6), pp. 27-33.

Aumailley, M., Krieg, T., Razaka, G., Müller, P. K. and Bricaud, H. (1982) 'Influence of cell density on collagen biosynthesis in fibroblast cultures', *The Biochemical journal,* 206(3), pp. 505-510.

Avci, P., Gupta, A., Sadasivam, M., Vecchio, D., Pam, Z., Pam, N. and Hamblin, M. R. (2013) 'Low-level laser (light) therapy (LLLT) in skin: stimulating, healing, restoring', *Seminars in cutaneous medicine and surgery,* 32(1), pp. 41-52.

Azevedo, L. H., De Paula Eduardo, F., Moreira, M. S., De Paula Eduardo, C. and Marques, M. M. (2006) 'Influence of different power densities of LILT on cultured human fibroblast growth: A pilot study', *Lasers in Medical Science,* 21(2), pp. 86-89.

B Alberts, A. J., J Lewis, M Raff, K Roberts, P Walter (2002) 'Molecular Biology of the cell', *Molecular Biology of the cell*: Garland Science, pp. 296.

Baier, J., Maisch, T., Maier, M., Engel, E., Landthaler, M. and Bäumler, W. (2006) 'Singlet oxygen generation by UVA light exposure of endogenous photosensitizers', *Biophysical journal,* 91(4), pp. 1452-1459.

Ball, K. A., Castello, P. R. and Poyton, R. O. (2011a) 'Low intensity light stimulates nitrite-dependent nitric oxide synthesis but not oxygen consumption by cytochrome c oxidase: Implications for phototherapy', *J Photochem Photobiol B,* 102(3), pp. 182-91.

Ball, K. A., Castello, P. R. and Poyton, R. O. (2011b) 'Low intensity light stimulates nitrite-dependent nitric oxide synthesis but not oxygen consumption by cytochrome c oxidase: Implications for phototherapy', *Journal of Photochemistry and Photobiology B: Biology,* 102(3), pp. 182-191.

Barolet, D. (2008) 'Light-Emitting Diodes (LEDs) in Dermatology', *Seminars in Cutaneous Medicine and Surgery,* 27(4), pp. 227-238.

Bartold, P. M. and Narayanan, A. S. (2006) 'Molecular and cell biology of healthy and diseased periodontal tissues', *Periodontol 2000,* 40, pp. 29-49.

Bartos, A., Grondin, Y., Bortoni, M. E., Ghelfi, E., Sepulveda, R., Carroll, J. and Rogers, R. A. (2016) 'Pre-conditioning with near infrared photobiomodulation reduces inflammatory cytokines and markers of oxidative stress in cochlear hair cells', *J Biophotonics,* 9(11-12), pp. 1125-1135.

Basoah, A., Matthews, P. M. and Morten, K. J. (2005) 'Rapid rates of newly synthesized mitochondrial protein degradation are significantly affected by the generation of mitochondrial free radicals', *FEBS Lett,* 579(28), pp. 6511-7.

Basso, F. G., Oliveira, C. F., Fontana, A., Kurachi, C., Bagnato, V. S., Spolidório, D. M. P., Hebling, J. and de Souza Costa, C. A. (2011) 'In vitro effect of low-level laser therapy on typical oral microbial biofilms', *Brazilian Dental Journal,* 22(6), pp. 502-510.

Basso, F. G., Oliveira, C. F., Kurachi, C., Hebling, J. and Costa, C. A. D. S. (2013a) 'Biostimulatory effect of low-level laser therapy on keratinocytes in vitro', *Lasers in Medical Science,* 28(2), pp. 367-374.

Basso, F. G., Pansani, T. N., Soares, D. G., Scheffel, D. L., Bagnato, V. S., De Souza Costa, C. A. and Hebling, J. (2015) 'Biomodulation of Inflammatory Cytokines Related to Oral Mucositis by Low-Level Laser Therapy', *Photochemistry and Photobiology,* 91(4), pp. 952-956.

Basso, F. G., Pansani, T. N., Turrioni, A. P., Bagnato, V. S., Hebling, J. and de Souza Costa, C. A. (2012a) 'In vitro wound healing improvement by low-level laser therapy application in cultured gingival fibroblasts', *Int J Dent,* 2012, pp. 719452.

Basso, F. G., Pansani, T. N., Turrioni, A. P. S., Bagnato, V. S., Hebling, J. and De Souza Costa, C. A. (2012b) 'In vitro wound healing improvement by low-level laser therapy application in cultured gingival fibroblasts', *International Journal of Dentistry*.

Basso, F. G., Pansani, T. N., Turrioni, A. P. S., Kurachi, C., Bagnato, V. S., Hebling, J. and De Souza Costa, C. A. (2013b) 'Biostimulatory effects of low-level laser therapy on epithelial cells and gingival fibroblasts treated with zoledronic acid', *Laser Physics,* 23(5).

Basso, F. G., Soares, D. G., de Souza Costa, C. A. and Hebling, J. (2016a) 'Low-level laser therapy in 3D cell culture model using gingival fibroblasts', *Lasers in Medical Science,* 31(5), pp. 973-978.

Basso, F. G., Soares, D. G., Pansani, T. N., Cardoso, L. M., Scheffel, D. L., de Souza Costa, C. A. and Hebling, J. (2016b) 'Proliferation, migration, and expression of oral-mucosal-healing-related genes by oral fibroblasts receiving low-level laser therapy after inflammatory cytokines challenge', *Lasers in Surgery and Medicine*.

Basso, F. G., Soares, D. G., Pansani, T. N., Cardoso, L. M., Scheffel, D. L., de Souza Costa, C. A. and Hebling, J. (2016c) 'Proliferation, migration, and expression of oral-mucosal-healing-related genes by oral fibroblasts receiving low-level laser therapy after inflammatory cytokines challenge', *Lasers in Surgery and Medicine,* 48(10), pp. 1006-1014.

Bath, A. S. and Gupta, V. (2019) 'Cardio-light: nitric oxide uncaged', *Lasers in Medical Science,* 34(2), pp. 405-409.

Bauerfeld, C. P., Rastogi, R., Pirockinaite, G., Lee, I., Huttemann, M., Monks, B., Birnbaum, M. J., Franchi, L., Nunez, G. and Samavati, L. (2012) 'TLR4-mediated AKT activation is MyD88/TRIF dependent and critical for induction of oxidative phosphorylation and mitochondrial transcription factor A in murine macrophages', *J Immunol,* 188(6), pp. 2847-57.

Becker, A., Distler, E., Klapczynski, A., Arpino, F., Kuch, N., Simon-Keller, K., Sticht, C., Van Abeelen, F. A., Gretz, N. and Oversluizen, G. 'Blue light inhibits proliferation of melanoma cells'. *Progress in Biomedical Optics and Imaging - Proceedings of SPIE*.

Becker, A., Klapczynski, A., Kuch, N., Arpino, F., Simon-Keller, K., De La Torre, C., Sticht, C., Van Abeelen, F. A., Oversluizen, G. and Gretz, N. (2016b) 'Gene expression profiling reveals aryl hydrocarbon receptor as a possible target for photobiomodulation when using blue light', *Scientific Reports,* 6.

Becker, A., Sticht, C., Dweep, H., Van Abeelen, F. A., Gretz, N. and Oversluizen, G. 'Impact of blue LED irradiation on proliferation and gene expression of cultured human keratinocytes'. *Progress in Biomedical Optics and Imaging - Proceedings of SPIE*.

Bedran, T. B., Mayer, M. P., Spolidorio, D. P. and Grenier, D. (2014) 'Synergistic anti-inflammatory activity of the antimicrobial peptides human beta-defensin-3 (hBD-3) and cathelicidin (LL-37) in a three-dimensional co-culture model of gingival epithelial cells and fibroblasts', *PLoS One,* 9(9), pp. e106766.

Belibasakis, G. N., Johansson, A., Wang, Y., Chen, C., Lagergård, T., Kalfas, S. and Lerner, U. H. (2005) 'Cytokine responses of human gingival fibroblasts to Actinobacillus actinomycetemcomitans cytolethal distending toxin', *Cytokine,* 30(2), pp. 56-63.

Belletti, S., Uggeri, J., Mergoni, G., Vescovi, P., Merigo, E., Fornaini, C., Nammour, S., Manfredi, M. and Gatti, R. (2014) 'Effects of 915 nm GaAs diode laser on mitochondria of human dermal fibroblasts: analysis with confocal microscopy', *Lasers in Medical Science,* 30(1), pp. 375-381.

Bensadoun, R. J. (2018) 'Photobiomodulation or low-level laser therapy in the management of cancer therapy-induced mucositis, dermatitis and lymphedema', *Current Opinion in Oncology,* 30(4), pp. 226-232.

Bentzinger, C. F., Wang, Y. X. and Rudnicki, M. A. (2012) 'Building Muscle: Molecular Regulation of Myogenesis', *Cold Spring Harbor Perspectives in Biology,* 4(2), pp. a008342.

Berridge, M. V., Herst, P. M. and Tan, A. S. 2005. Tetrazolium dyes as tools in cell biology: New insights into their cellular reduction. *Biotechnology Annual Review.*

Berridge, M. V. and Tan, A. S. (1993) 'Characterization of the Cellular Reduction of 3-(4,5-dimethylthiazol-2-yl)-2,5-diphenyltetrazolium bromide (MTT): Subcellular Localization, Substrate Dependence, and Involvement of Mitochondrial Electron Transport in MTT Reduction', *Archives of Biochemistry and Biophysics,* 303(2), pp. 474-482.

Bertazzoni Minelli, E., Della Bora, T. and Benini, A. (2011) 'Different microbial biofilm formation on polymethylmethacrylate (PMMA) bone cement loaded with gentamicin and vancomycin', *Anaerobe,* 17(6), pp. 380-3.

Bhatti, J. S., Bhatti, G. K. and Reddy, P. H. (2017) 'Mitochondrial dysfunction and oxidative stress in metabolic disorders — A step towards mitochondria based therapeutic strategies', *Biochimica et Biophysica Acta (BBA) - Molecular Basis of Disease,* 1863(5), pp. 1066-1077.

Bisland, S. K. and Wilson, B. C. 'To begin at the beginning: The science of bio-stimulation in cells and tissues'. *Progress in Biomedical Optics and Imaging - Proceedings of SPIE*.

Biswas, G., Anandatheerthavarada, H. K., Zaidi, M. and Avadhani, N. G. (2003) 'Mitochondria to nucleus stress signaling: a distinctive mechanism of NFkappaB/Rel activation through calcineurin-mediated inactivation of IkappaBbeta', *J Cell Biol,* 161(3), pp. 507-19.

Bleier, L. and Dröse, S. (2013) 'Superoxide generation by complex III: From mechanistic rationales to functional consequences', *Biochimica et Biophysica Acta (BBA) - Bioenergetics,* 1827(11–12), pp. 1320-1331.

Bolstad, A. I., Jensen, H. B. and Bakken, V. (1996) 'Taxonomy, biology, and periodontal aspects of Fusobacterium nucleatum', *Clinical microbiology reviews,* 9(1), pp. 55-71.

Bonatti, S., Hochman, B., Tucci-Viegas, V. M., Furtado, F., Pinfildi, C. E., Pedro, A. C. and Ferreira, L. M. (2011) 'In vitro effect of 470 nm LED (Light Emitting Diode) in keloid fibroblasts', *Acta Cir Bras,* 26(1), pp. 25-30.

Boonstra, J. and Post, J. A. (2004) 'Molecular events associated with reactive oxygen species and cell cycle progression in mammalian cells', *Gene,* 337, pp. 1-13.

Bouly, J. P., Schleicher, E., Dionisio-Sese, M., Vandenbussche, F., Van Der Straeten, D., Bakrim, N., Meier, S., Batschauer, A., Galland, P., Bittl, R. and Ahmad, M. (2007) 'Cryptochrome blue light photoreceptors are activated through interconversion of flavin redox states', *J Biol Chem,* 282(13), pp. 9383-91.

Bozkurt, S. B., Hakki, S. S., Hakki, E. E., Durak, Y. and Kantarci, A. (2017) 'Porphyromonas gingivalis Lipopolysaccharide Induces a Pro-inflammatory Human Gingival Fibroblast Phenotype', *Inflammation,* 40(1), pp. 144-153.

Brassolatti, P., de Andrade, A. L. M., Bossini, P. S., Orth, D. L., Duarte, F. O., dos Anjos Souza, A. B., Parizotto, N. A. and de Freitas Anibal, F. (2018) 'Photobiomodulation on critical bone defects of rat calvaria: a systematic review', *Lasers in Medical Science,* 33(9), pp. 1841-1848.

Buettner, G. R. (2011) 'Superoxide Dismutase in Redox Biology: The roles of superoxide and hydrogen peroxide', *Anti-cancer agents in medicinal chemistry,* 11(4), pp. 341-346.

Bullon, P., Cordero, M. D., Quiles, J. L., Morillo, J. M., del Carmen Ramirez-Tortosa, M. and Battino, M. (2011) 'Mitochondrial dysfunction promoted by Porphyromonas gingivalis lipopolysaccharide as a possible link between cardiovascular disease and periodontitis', *Free Radic Biol Med,* 50(10), pp. 1336-43.

Bumah, V. V., Whelan, H. T., Masson-Meyers, D. S., Quirk, B., Buchmann, E. and Enwemeka, C. S. (2015) 'The bactericidal effect of 470-nm light and hyperbaric oxygen on methicillin-resistant Staphylococcus aureus (MRSA)', *Lasers in Medical Science,* 30(3), pp. 1153-1159.

Bump, E. A. and Reed, D. J. (1977) 'A unique property of fetal bovine serum: high levels of protein-glutathione mixed disulfides', *In Vitro,* 13(2), pp. 115-8.

Buravlev, E. A., Zhidkova, T. V., Osipov, A. N. and Vladimirov, Y. A. (2014a) 'Are the mitochondrial respiratory complexes blocked by NO the targets for the laser and LED therapy?', *Lasers in Medical Science,* 30(1), pp. 173-180.

Buravlev, E. A., Zhidkova, T. V., Osipov, A. N. and Vladimirov, Y. A. (2015) 'Are the mitochondrial respiratory complexes blocked by NO the targets for the laser and LED therapy?', *Lasers Med Sci,* 30(1), pp. 173-80.

Buravlev, E. A., Zhidkova, T. V., Vladimirov, Y. A. and Osipov, A. N. (2013) 'Effects of laser and LED radiation on mitochondrial respiration in experimental endotoxic shock', *Lasers in Medical Science,* 28(3), pp. 785-790.

Buravlev, E. A., Zhidkova, T. V., Vladimirov, Y. A. and Osipov, A. N. (2014b) 'Effects of low-level laser therapy on mitochondrial respiration and nitrosyl complex content', *Lasers in Medical Science,* 29(6), pp. 1861-1866.

Buscone, S., Mardaryev, A. N., Raafs, B., Bikker, J. W., Sticht, C., Gretz, N., Farjo, N., Uzunbajakava, N. E. and Botchkareva, N. V. (2017) 'A new path in defining light parameters for hair growth: Discovery and modulation of photoreceptors in human hair follicle', *Lasers Surg Med,* 49(7), pp. 705-718.

Caldieraro, M. A. and Cassano, P. (2019) 'Transcranial and systemic photobiomodulation for major depressive disorder: A systematic review of efficacy, tolerability and biological mechanisms', *Journal of Affective Disorders,* 243, pp. 262-273.

Caporaso, J. G., Lauber, C. L., Walters, W. A., Berg-Lyons, D., Huntley, J., Fierer, N., Owens, S. M., Betley, J., Fraser, L., Bauer, M., Gormley, N., Gilbert, J. A., Smith, G. and Knight, R. (2012) 'Ultra-high-throughput microbial community analysis on the Illumina HiSeq and MiSeq platforms', *Isme j,* 6(8), pp. 1621-4.

Carroll, J. D., Milward, M. R., Cooper, P. R., Hadis, M. and Palin, W. M. (2014) 'Developments in low level light therapy (LLLT) for dentistry', *Dental Materials,* 30(5), pp. 465-475.

Carter, R. W. (2007) 'Mitochondrial diversity within modern human populations', *Nucleic Acids Research,* 35(9), pp. 3039-3045.

Carvalho-Lobato, P., Garcia, V. J., Kasem, K., Ustrell-Torrent, J. M., Tallón-Walton, V. and Manzanares-Céspedes, M. C. (2014) 'Tooth movement in orthodontic treatment with low-level laser therapy: A systematic review of human and animal studies', *Photomedicine and Laser Surgery,* 32(5), pp. 302-309.

Castellano-Pellicena, I., Uzunbajakava, N. E., Mignon, C., Raafs, B., Botchkarev, V. A. and Thornton, M. J. (2018) 'Does blue light restore human epidermal barrier function via activation of Opsin during cutaneous wound healing?', *Lasers in Surgery and Medicine*.

Cavalcanti, M. F. X. B., Maria, D. A., De Isla, N., Leal-Junior, E. C. P., Joensen, J., Bjordal, J. M., Lopes-Martins, R. A. M. B., Diomede, F., Trubiani, O. and Frigo, L. (2015) 'Evaluation of the Proliferative Effects Induced by Low-Level Laser Therapy in Bone Marrow Stem Cell Culture', *Photomedicine and Laser Surgery,* 33(12), pp. 610-616.

Cerdeira, C. D., Lima Brigagão, M. R. P., Carli, M. L., de Souza Ferreira, C., de Oliveira Isac Moraes, G., Hadad, H., Costa Hanemann, J. A., Hamblin, M. R. and Sperandio, F. F. (2016) 'Low-level laser therapy stimulates the oxidative burst in human neutrophils and increases their fungicidal capacity', *Journal of Biophotonics,* 9(11-12), pp. 1180-1188.

Chan, I. L., Cohen, S., da Cunha, M. G. and Maluf, L. C. (2019) 'Characteristics and management of Asian skin', *International Journal of Dermatology,* 58(2), pp. 131-143.

Chandki, R., Banthia, P. and Banthia, R. (2011) 'Biofilms: A microbial home', *Journal of Indian Society of Periodontology,* 15(2), pp. 111-114.

Chapple, I. L., Gilbert A,D (2002a) *Understanding Periodontal Diseases Assement and Diagnostic Procedures in Practice.* Quintesscence Publishing Co, Ltd, p. 1-13.

Chapple, I. L., Gilbert A,D (2002b) *Understanding Periodontal Diseases Assement and Diagnostic Procedures in Practice.* Quintesscence Publishing Co, Ltd, p. 77.

Chawla, A., Hirano, T., Bainbridge, B. W., Demuth, D. R., Xie, H. and Lamont, R. J. (2010) 'Community signalling between Streptococcus gordonii and Porphyromonas gingivalis is controlled by the transcriptional regulator CdhR', *Molecular microbiology,* 78(6), pp. 1510-1522.

Chen, A. C., Arany, P. R., Huang, Y. Y., Tomkinson, E. M., Sharma, S. K., Kharkwal, G. B., Saleem, T., Mooney, D., Yull, F. E., Blackwell, T. S. and Hamblin, M. R. (2011a) 'Low-level laser therapy activates NF-kB via generation of reactive oxygen species in mouse embryonic fibroblasts', *PLoS One,* 6(7), pp. e22453.

Chen, A. C., Huang, Y. Y., Sharma, S. K. and Hamblin, M. R. (2011b) 'Effects of 810-nm laser on murine bone-marrow-derived dendritic cells', *Photomed Laser Surg,* 29(6), pp. 383-9.

Chen, A. C. H., Arany, P. R., Huang, Y. Y., Tomkinson, E. M., Saleem, T., Yull, F. E., Blackwell, T. S. and Hamblm, M. R. 'Low level laser therapy activates NF-kB via generation of reactive oxygen species in mouse embryonic fibroblasts'. *Progress in Biomedical Optics and Imaging - Proceedings of SPIE*.

Chen, A. C. H., Arany, P. R., Huang, Y. Y., Tomkinson, E. M., Sharma, S. K., Kharkwal, G. B., Saleem, T., Mooney, D., Yull, F. E., Blackwell, T. S. and Hamblin, M. R. (2011c) 'Low-Level laser therapy activates NF-kB via generation of reactive oxygen species in mouse embryonic fibroblasts', *PLoS ONE,* 6(7).

Chen, A. C. H., Huang, Y. Y., Arany, P. R. and Hamblin, M. R. 'Role of reactive oxygen species in low level light therapy'. *Progress in Biomedical Optics and Imaging - Proceedings of SPIE*.

Chen, C. H., Wang, C. Z., Wang, Y. H., Liao, W. T., Chen, Y. J., Kuo, C. H., Kuo, H. F. and Hung, C. H. (2014) 'Effects of low-level laser therapy on M1-related cytokine expression in monocytes via histone modification', *Mediators of Inflammation,* 2014.

Chen, L.-F. and Greene, W. C. (2004) 'Shaping the nuclear action of NF-[kappa]B', *Nat Rev Mol Cell Biol,* 5(5), pp. 392-401.

Chen, Q., Vazquez, E. J., Moghaddas, S., Hoppel, C. L. and Lesnefsky, E. J. (2003) 'Production of reactive oxygen species by mitochondria: central role of complex III', *J Biol Chem,* 278(38), pp. 36027-31.

Chen, Y. J., Jeng, J. H., Lee, B. S., Chang, H. F., Chen, K. C. and Lan, W. H. (2000a) 'Effects of Nd:YAG laser irradiation on cultured human gingival fibroblasts', *Lasers Surg Med,* 27(5), pp. 471-8.

Chen, Y. J., Jeng, J. H., Lee, B. S., Chang, H. F., Chen, K. C. and Lan, W. H. (2000b) 'Effects of Nd:YAG laser irradiation on cultured human gingival fibroblasts', *Lasers in Surgery and Medicine,* 27(5), pp. 471-478.

Cheng, K. P., Kiernan, E. A., Eliceiri, K. W., Williams, J. C. and Watters, J. J. (2016) 'Blue Light Modulates Murine Microglial Gene Expression in the Absence of Optogenetic Protein Expression', *Scientific reports,* 6, pp. 21172-21172.

Cheng, R., Choudhury, D., Liu, C., Billet, S., Hu, T. and Bhowmick, N. A. (2015) 'Gingival fibroblasts resist apoptosis in response to oxidative stress in a model of periodontal diseases', *Cell death discovery,* 1, pp. 15046-15046.

Cheon, M. W., Kim, T. G., Lee, Y. S. and Kim, S. H. (2013) 'Low level light therapy by Red-Green-Blue LEDs improves healing in an excision model of Sprague-Dawley rats', *Personal and Ubiquitous Computing,* 17(7), pp. 1421-1428.

Chi, C. C., Wang, S. H., Delamere, F. M., Wojnarowska, F., Peters, M. C. and Kanjirath, P. P. (2015) 'Interventions for prevention of herpes simplex labialis (cold sores on the lips)', *Cochrane Database of Systematic Reviews,* 2015(8).

Chistiakov, D. A., Sobenin, I. A., Revin, V. V., Orekhov, A. N. and Bobryshev, Y. V. (2014a) 'Mitochondrial aging and age-related dysfunction of mitochondria', *BioMed research international,* 2014, pp. 238463-238463.

Chistiakov, D. A., Sobenin, I. A., Revin, V. V., Orekhov, A. N. and Bobryshev, Y. V. (2014b) 'Mitochondrial Aging and Age-Related Dysfunction of Mitochondria %J BioMed Research International', 2014, pp. 7.

Choe, S. W., Park, K., Park, C., Ryu, J. and Choi, H. (2017) 'Combinational light emitting diode-high frequency focused ultrasound treatment for HeLa cell', *Computer Assisted Surgery,* 22, pp. 79-85.

Choi, H., Lim, W., Kim, I., Kim, J., Ko, Y., Kwon, H., Kim, S., Kabir, K. M., Li, X., Kim, O., Lee, Y., Kim, S. and Kim, O. (2012) 'Inflammatory cytokines are suppressed by light-emitting diode irradiation of P. gingivalis LPS-treated human gingival fibroblasts: inflammatory cytokine changes by LED irradiation', *Lasers Med Sci,* 27(2), pp. 459-67.

Christopher, A. B., Arndt, A., Cugini, C. and Davey, M. E. (2010a) 'A streptococcal effector protein that inhibits Porphyromonas gingivalis biofilm development', *Microbiology,* 156(11), pp. 3469-3477.

Christopher, A. B., Arndt, A., Cugini, C. and Davey, M. E. (2010b) 'A streptococcal effector protein that inhibits Porphyromonas gingivalis biofilm development', *Microbiology,* 156(Pt 11), pp. 3469-77.

Chu-Tan, J. A., Rutar, M., Saxena, K., Wu, Y., Howitt, L., Valter, K., Provis, J. and Natoli, R. (2016) 'Efficacy of 670 nm Light Therapy to Protect against Photoreceptor Cell Death Is Dependent on the Severity of Damage', *International Journal of Photoenergy,* 2016.

Chung, H., Dai, T., Sharma, S. K., Huang, Y. Y., Carroll, J. D. and Hamblin, M. R. (2012) 'The nuts and bolts of low-level laser (Light) therapy', *Annals of Biomedical Engineering,* 40(2), pp. 516-533.

Cole, L. W. (2016) 'The Evolution of Per-cell Organelle Number', *Frontiers in Cell and Developmental Biology,* 4, pp. 85.

CONSOLARO, A. e. C., Maria Fernanda MO (2010) 'The functions of Malassez Epithelial Rest, EGF and orthodontic movement or Why does orthodontic movement not promote alveolodental ankylosis ?', *Dental Press J. Orthod.,* 15(2), pp. 8.

Costa Carvalho, J. L., de Brito, A. A., de Oliveira, A. P. L., de Castro Faria Neto, H. C., Pereira, T. M., de Carvalho, R. A., Anatriello, E. and Aimbire, F. (2016) 'The chemokines secretion and the oxidative stress are targets of low-level laser therapy in allergic lung inflammation', *Journal of Biophotonics,* 9(11-12), pp. 1208-1221.

Csonka, C., Páli, T., Bencsik, P., Görbe, A., Ferdinandy, P. and Csont, T. (2015) 'Measurement of NO in biological samples', *British journal of pharmacology,* 172(6), pp. 1620-1632.

Cukierman, E., Pankov, R., Stevens, D. R. and Yamada, K. M. (2001) 'Taking cell-matrix adhesions to the third dimension', *Science,* 294(5547), pp. 1708-12.

Curra, M., Pellicioli, A. C., Filho, N. A., Ochs, G., Matte, U., Filho, M. S., Martins, M. A. and Martins, M. D. (2015) 'Photobiomodulation reduces oral mucositis by modulating NF-kB', *J Biomed Opt,* 20(12), pp. 125008.

Cury, V., Moretti, A. I. S., Assis, L., Bossini, P., De Souza Crusca, J., Neto, C. B., Fangel, R., De Souza, H. P., Hamblin, M. R. and Parizotto, N. A. (2013) 'Low level laser therapy increases angiogenesis in a model of ischemic skin flap in rats mediated by VEGF, HIF-1α and MMP-2', *Journal of Photochemistry and Photobiology B: Biology,* 125, pp. 164-170.

Czekanska, E. M. (2011) 'Assessment of cell proliferation with resazurin-based fluorescent dye', *Methods Mol Biol,* 740, pp. 27-32.

da Silva, M. K., de Carvalho, A. C. G., Alves, E. H. P., da Silva, F. R. P., Pessoa, L. D. S. and Vasconcelos, D. F. P. (2017) 'Genetic Factors and the Risk of Periodontitis Development: Findings from a Systematic Review Composed of 13 Studies of Meta-Analysis with 71,531 Participants', *International journal of dentistry,* 2017, pp. 1914073-1914073.

da Silva Neto Trajano, L. A., Stumbo, A. C., da Silva, C. L., Mencalha, A. L. and Fonseca, A. S. (2016) 'Low-level infrared laser modulates muscle repair and chromosome stabilization genes in myoblasts', *Lasers in Medical Science,* 31(6), pp. 1161-1167.

da Silveira Campos, R. M., Dâmaso, A. R., Masquio, D. C. L., Aquino, A. E., Jr., Sene-Fiorese, M., Duarte, F. O., Tock, L., Parizotto, N. A. and Bagnato, V. S. (2015) 'Low-level laser therapy

(LLLT) associated with aerobic plus resistance training to improve inflammatory biomarkers in obese adults', *Lasers in Medical Science,* 30(5), pp. 1553-1563.

Dabiri, D., Halubai, S., Layher, M., Klausner, C., Makhoul, H., Lin, G. H., Eckert, G., Abuhussein, H., Kamarajan, P. and Kapila, Y. (2016) 'The Role of Apoptotic Factors in Assessing Progression of Periodontal Disease', *International journal of dentistry and oral science,* 3(9), pp. 318-325.

Dahiya, P., Kamal, R., Gupta, R., Bhardwaj, R., Chaudhary, K. and Kaur, S. (2013) 'Reactive oxygen species in periodontitis', *Journal of Indian Society of Periodontology,* 17(4), pp. 411-416.

Damante, C. A., De Micheli, G., Miyagi, S. P. H., Feist, I. S. and Marques, M. M. (2009) 'Effect of laser phototherapy on the release of fibroblast growth factors by human gingival fibroblasts', *Lasers in Medical Science,* 24(6), pp. 885-891.

Dang, Y., Liu, B., Liu, L., Ye, X., Bi, X., Zhang, Y. and Gu, J. (2011) 'The 800-nm diode laser irradiation induces skin collagen synthesis by stimulating TGF-beta/Smad signaling pathway', *Lasers Med Sci,* 26(6), pp. 837-43.

das Neves, L. M. S., Leite, G. P. M. F., Marcolino, A. M., Pinfildi, C. E., Garcia, S. B., de Araújo, J. E. and Guirro, E. C. O. (2017) 'Laser photobiomodulation (830 and 660 nm) in mast cells, VEGF, FGF, and CD34 of the musculocutaneous flap in rats submitted to nicotine', *Lasers in Medical Science,* 32(2), pp. 335-341.

Das, V., Fürst, T., Gurská, S., Džubák, P. and Hajdúch, M. (2017) 'Evaporation-reducing culture condition increases the reproducibility of multicellular spheroid formation in microtiter plates', *Journal of Visualized Experiments,* 2017(121).

Day, R. M. and Suzuki, Y. J. (2006) 'Cell proliferation, reactive oxygen and cellular glutathione', *Dose-response : a publication of International Hormesis Society,* 3(3), pp. 425-442.

de Farias Gabriel, A., Wagner, V. P., Correa, C., Webber, L. P., Pilar, E. F. S., Curra, M., Carrard, V. C., Martins, M. A. T. and Martins, M. D. (2019) 'Photobiomodulation therapy modulates epigenetic events and NF-κB expression in oral epithelial wound healing', *Lasers in Medical Science*.

de Freitas, L. F. and Hamblin, M. R. (2016) 'Proposed Mechanisms of Photobiomodulation or Low-Level Light Therapy', *IEEE journal of selected topics in quantum electronics : a publication of the IEEE Lasers and Electro-optics Society,* 22(3), pp. 7000417.

de Pauli Paglioni, M., Araújo, A. L. D., Arboleda, L. P. A., Palmier, N. R., Fonsêca, J. M., Gomes-Silva, W., Madrid-Troconis, C. C., Silveira, F. M., Martins, M. D., Faria, K. M., Ribeiro, A. C. P., Brandão, T. B., Lopes, M. A., Leme, A. F. P., Migliorati, C. A. and Santos-Silva, A. R. (2019) 'Tumor safety and side effects of photobiomodulation therapy used for prevention and management of cancer treatment toxicities. A systematic review', *Oral Oncology,* 93, pp. 21-28.

de Sousa, A. P., Santos, J. N., Dos Reis, J. A., Jr., Ramos, T. A., de Souza, J., Cangussu, M. C. and Pinheiro, A. L. (2010) 'Effect of LED phototherapy of three distinct wavelengths on fibroblasts on wound healing: a histological study in a rodent model', *Photomed Laser Surg,* 28(4), pp. 547-52.

De Sousa, N. T. A., Santos, M. F., Gomes, R. C., Brandino, H. E., Martinez, R. and De Jesus Guirro, R. R. (2015) 'Blue laser inhibits bacterial growth of staphylococcus aureus, escherichia coli, and pseudomonas aeruginosa', *Photomedicine and Laser Surgery,* 33(5), pp. 278-282.

Del Fabbro, M., Corbella, S., Sequeira-Byron, P., Tsesis, I., Rosen, E., Lolato, A. and Taschieri, S. (2016) 'Endodontic procedures for retreatment of periapical lesions', *Cochrane Database of Systematic Reviews,* 2016(10).

del Olmo-Aguado, S., Manso, A. G. and Osborne, N. N. (2012) 'Light might directly affect retinal ganglion cell mitochondria to potentially influence function', *Photochem Photobiol,* 88(6), pp. 1346-55.

Del Vecchio, P. J. and Shaffer, J. B. (1991) 'Regulation of antioxidant enzyme expression in LPS-treated bovine retinal pigment epithelial and corneal endothelial cells', *Curr Eye Res,* 10(10), pp. 919-25.

Delghandi, M. P., Johannessen, M. and Moens, U. (2005) 'The cAMP signalling pathway activates CREB through PKA, p38 and MSK1 in NIH 3T3 cells', *Cell Signal,* 17(11), pp. 1343-51.

Denadai, A. S., Aydos, R. D., Silva, I. S., Olmedo, L., De Senna Cardoso, B. M., Da Silva, B. A. K. and De Tarso Camillo De Carvalho, P. (2015) 'Acute effects of low-level laser therapy (660 nm) on oxidative stress levels in diabetic rats with skin wounds', *Journal of Experimental Therapeutics and Oncology,* 11(2), pp. 85-89.

Dereci, Ö., Sindel, A., Serap, H., Yüce, E., Ay, S. and Tozoglu, S. (2016) 'The Comparison of the Efficacy of Blue Light-Emitting Diode Light and 980-nm Low-Level Laser Light on Bone Regeneration', *Journal of Craniofacial Surgery,* 27(8), pp. 2185-2189.

Derynck, R., Muthusamy, B. P. and Saeteurn, K. Y. (2014) 'Signaling pathway cooperation in TGF-β-induced epithelial-mesenchymal transition', *Current opinion in cell biology,* 31, pp. 56-66.

Desjardins, P. and Conklin, D. (2010) 'NanoDrop microvolume quantitation of nucleic acids', *Journal of visualized experiments : JoVE,* (45), pp. 2565.

Desler, C., Hansen, T. L., Frederiksen, J. B., Marcker, M. L., Singh, K. K. and Juel Rasmussen, L. (2012) 'Is There a Link between Mitochondrial Reserve Respiratory Capacity and Aging?', *Journal of Aging Research,* 2012, pp. 192503.

Dewhirst, F. E., Chen, T., Izard, J., Paster, B. J., Tanner, A. C. R., Yu, W.-H., Lakshmanan, A. and Wade, W. G. (2010a) 'The human oral microbiome', *Journal of bacteriology,* 192(19), pp. 5002-5017.

Dewhirst, F. E., Chen, T., Izard, J., Paster, B. J., Tanner, A. C. R., Yu, W. H., Lakshmanan, A. and Wade, W. G. (2010b) 'The human oral microbiome', *Journal of Bacteriology,* 192(19), pp. 5002-5017.

Di Benedetto, A., Gigante, I., Colucci, S. and Grano, M. (2013) 'Periodontal Disease: Linking the Primary Inflammation to Bone Loss', *Clinical and Developmental Immunology,* 2013, pp. 7.

Diaz-Munoz, M. D., Osma-Garcia, I. C., Fresno, M. and Iniguez, M. A. (2012) 'Involvement of PGE2 and the cAMP signalling pathway in the up-regulation of COX-2 and mPGES-1 expression in LPS-activated macrophages', *Biochem J,* 443(2), pp. 451-61.

Dikalov, S. I. and Harrison, D. G. (2014) 'Methods for detection of mitochondrial and cellular reactive oxygen species', *Antioxidants & redox signaling,* 20(2), pp. 372-382.

Diniz, I. M. A., Carreira, A. C. O., Sipert, C. R., Uehara, C. M., Moreira, M. S. N., Freire, L., Pelissari, C., Kossugue, P. M., de Araújo, D. R., Sogayar, M. C. and Marques, M. M. (2018) 'Photobiomodulation of mesenchymal stem cells encapsulated in an injectable rhBMP4-loaded hydrogel directs hard tissue bioengineering', *Journal of Cellular Physiology,* 233(6), pp. 4907-4918.

Djavid, G. E., Bigdeli, B., Goliaei, B., Nikoofar, A. and Hamblin, M. R. (2017) 'Photobiomodulation leads to enhanced radiosensitivity through induction of apoptosis and autophagy in human cervical cancer cells', *Journal of Biophotonics,* 10(12), pp. 1732-1742.

Doeuk, C., Hersant, B., Bosc, R., Lange, F., SidAhmed-Mezi, M., Bouhassira, J. and Meningaud, J. P. (2015) 'Current indications for low level laser treatment in maxillofacial surgery: A review', *British Journal of Oral and Maxillofacial Surgery,* 53(4), pp. 309-315.

Dominy, J. E. and Puigserver, P. (2013) 'Mitochondrial biogenesis through activation of nuclear signaling proteins', *Cold Spring Harb Perspect Biol,* 5(7).

Dominy, S. S., Lynch, C., Ermini, F., Benedyk, M., Marczyk, A., Konradi, A., Nguyen, M., Haditsch, U., Raha, D., Griffin, C., Holsinger, L. J., Arastu-Kapur, S., Kaba, S., Lee, A., Ryder, M. I., Potempa, B., Mydel, P., Hellvard, A., Adamowicz, K., Hasturk, H., Walker, G. D., Reynolds, E. C., Faull, R. L. M., Curtis, M. A., Dragunow, M. and Potempa, J. (2019) 'Porphyromonas gingivalis in Alzheimer's disease brains: Evidence for disease causation and treatment with small-molecule inhibitors', *Sci Adv,* 5(1), pp. eaau3333.

Dong, T., Zhang, Q., Hamblin, M. R. and Wu, M. X. (2015) 'Low-level light in combination with metabolic modulators for effective therapy of injured brain', *Journal of Cerebral Blood Flow and Metabolism,* 35(9), pp. 1435-1444.

Dungel, P., Hartinger, J., Chaudary, S., Slezak, P., Hofmann, A., Hausner, T., Strassl, M., Wintner, E., Redl, H. and Mittermayr, R. (2014) 'Low level light therapy by LED of different wavelength induces angiogenesis and improves ischemic wound healing', *Lasers in Surgery and Medicine,* 46(10), pp. 773-780.

Elliott, C. L., Allport, V. C., Loudon, J. A. Z., Wu, G. D. and Bennett, P. R. (2001) 'Nuclear factor-kappa B is essential for up-regulation of interleukin-8 expression in human amnion and cervical epithelial cells', *Molecular Human Reproduction,* 7(8), pp. 787-790.

Ener, M. E., Lee, Y.-T., Winkler, J. R., Gray, H. B. and Cheruzel, L. (2010) 'Photooxidation of cytochrome P450-BM3', *Proceedings of the National Academy of Sciences of the United States of America,* 107(44), pp. 18783-18786.

Engel, K. W., Khan, I. and Arany, P. R. (2016) 'Cell lineage responses to photobiomodulation therapy', *Journal of Biophotonics,* 9(11-12), pp. 1148-1156.

Eriksson, L., Lif Holgerson, P. and Johansson, I. (2017) 'Saliva and tooth biofilm bacterial microbiota in adolescents in a low caries community', *Sci Rep,* 7(1), pp. 5861.

Erthal, V., Maria-Ferreira, D., Werner, M. F., Baggio, C. H. and Nohama, P. (2016) 'Anti-inflammatory effect of laser acupuncture in ST36 (Zusanli) acupoint in mouse paw edema', *Lasers Med Sci,* 31(2), pp. 315-22.

Eslami, H., Motahari, P., Safari, E. and Seyyedi, M. (2017) 'Evaluation effect of low level Helium-Neon laser and Iranian propolis extract on Collagen Type I gene expression by human gingival fibroblasts: an in vitro study', *Laser Ther,* 26(2), pp. 105-112.

Eslamipour, F., Motamedian, S. R. and Bagheri, F. (2017) 'Ibuprofen and low-level laser therapy for pain control during fixed orthodontic therapy: A systematic review of randomized controlled trials and meta-analysis', *Journal of Contemporary Dental Practice,* 18(6), pp. 527-533.

Ezzati, K., Fekrazad, R. and Raoufi, Z. (2019) 'The effects of photobiomodulation therapy on post-surgical pain', *Journal of Lasers in Medical Sciences,* 10(2), pp. 79-85.

Falcone, D., Uzunbajakava, N. E., van Abeelen, F., Oversluizen, G., Peppelman, M., van Erp, P. E. J. and van de Kerkhof, P. C. M. (2018) 'Effects of blue light on inflammation and skin barrier recovery following acute perturbation. Pilot study results in healthy human subjects', *Photodermatology Photoimmunology and Photomedicine,* 34(3), pp. 184-193.

Fang, Z., Cai, T., Li, K., Yu, J., Luo, Y., Qian, S., Xu, J., Xiao, G., Wu, N. and Zhao, H. (2013) 'Expression of messenger RNA for transforming growth factor-beta1 and for transforming growth factor-beta receptors in peripheral blood of immune thrombocytopenic purpura', *Platelets,* 24(3), pp. 250-2.

Fato, R., Bergamini, C., Bortolus, M., Maniero, A. L., Leoni, S., Ohnishi, T. and Lenaz, G. (2009) 'Differential effects of mitochondrial Complex I inhibitors on production of reactive oxygen species', *Biochim Biophys Acta,* 1787(5), pp. 384-92.

Fekrazad, R., Asefi, S., Eslaminejad, M. B., Taghiar, L., Bordbar, S. and Hamblin, M. R. (2018) 'Photobiomodulation with single and combination laser wavelengths on bone marrow mesenchymal stem cells: proliferation and differentiation to bone or cartilage', *Lasers in Medical Science*.

Fekrazad, R. and Chiniforush, N. (2014) 'Oral mucositis prevention and management by therapeutic laser in head and neck cancers', *Journal of Lasers in Medical Sciences,* 5(1), pp. 1-7.

Fekrazad, R., Mirmoezzi, A., Kalhori, K. A. and Arany, P. (2015) 'The effect of red, green and blue lasers on healing of oral wounds in diabetic rats', *J Photochem Photobiol B,* 148, pp. 242-245.

Fekrazad, R., Nikkerdar, A., Joharchi, K., Kalhori, K. A. M., Mashhadi Abbas, F. and Salimi Vahid, F. (2017) 'Evaluation of therapeutic laser influences on the healing of third-degree burns in rats according to different wavelengths', *Journal of Cosmetic and Laser Therapy,* 19(4), pp. 232-236.

Felix Gomez, G. G., Lippert, F., Ando, M., Zandona, A. F., Eckert, G. J. and Gregory, R. L. (2018) 'Effect of Violet-Blue Light on Streptococcus mutans-Induced Enamel Demineralization', *Dentistry journal,* 6(2), pp. 6.

Feng, R., Morine, Y., Ikemoto, T., Imura, S., Iwahashi, S., Saito, Y. and Shimada, M. (2018) 'Photobiomodulation with red light-emitting diodes accelerates hepatocyte proliferation through reactive oxygen species/extracellular signal-regulated kinase pathway', *Hepatology Research,* 48(11), pp. 926-936.

Ferraresi, C., de Sousa, M. V. P., Huang, Y. Y., Bagnato, V. S., Parizotto, N. A. and Hamblin, M. R. (2015a) 'Time response of increases in ATP and muscle resistance to fatigue after low-level laser (light) therapy (LLLT) in mice', *Lasers in Medical Science,* 30(4), pp. 1259-1267.

Ferraresi, C., Hamblin, M. R. and Parizotto, N. A. (2012) 'Low-level laser (light) therapy (LLLT) on muscle tissue: performance, fatigue and repair benefited by the power of light', *Photonics & lasers in medicine,* 1(4), pp. 267-286.

Ferraresi, C., Kaippert, B., Avci, P., Huang, Y. Y., De Sousa, M. V. P., Bagnato, V. S., Parizotto, N. A. and Hamblin, M. R. (2015b) 'Low-level laser (light) therapy increases mitochondrial membrane potential and ATP synthesis in C2C12 myotubes with a peak response at 3-6 h', *Photochemistry and Photobiology,* 91(2), pp. 411-416.

Ferrari, G., Cook, B. D., Terushkin, V., Pintucci, G. and Mignatti, P. (2009) 'Transforming growth factor-beta 1 (TGF-beta1) induces angiogenesis through vascular endothelial growth factor (VEGF)-mediated apoptosis', *J Cell Physiol,* 219(2), pp. 449-58.

Ferreira, M. C., Dias-Pereira, A. C., Branco-de-Almeida, L. S., Martins, C. C. and Paiva, S. M. (2017) 'Impact of periodontal disease on quality of life: a systematic review', *J Periodontal Res,* 52(4), pp. 651-665.

Figurová, M., Ledecký, V., Karasová, M., Hluchý, M., Trbolová, A., Capík, I., Horňák, S., Reichel, P., Bjordal, J. M. and Gál, P. (2016) 'Histological Assessment of a Combined Low-Level Laser/Light-Emitting Diode Therapy (685 nm/470 nm) for Sutured Skin Incisions in a Porcine Model: A Short Report', *Photomedicine and Laser Surgery,* 34(2), pp. 53-55.

Fleming, P. S., Strydom, H., Katsaros, C., Macdonald, L., Curatolo, M., Fudalej, P. and Pandis, N. (2016) 'Non-pharmacological interventions for alleviating pain during orthodontic treatment', *Cochrane Database of Systematic Reviews,* 2016(12).

Forkink, M., Smeitink, J. A., Brock, R., Willems, P. H. and Koopman, W. J. (2010) 'Detection and manipulation of mitochondrial reactive oxygen species in mammalian cells', *Biochim Biophys Acta,* 1797(6-7), pp. 1034-44.

Formentini, L., Santacatterina, F., Nunez de Arenas, C., Stamatakis, K., Lopez-Martinez, D., Logan, A., Fresno, M., Smits, R., Murphy, M. P. and Cuezva, J. M. (2017) 'Mitochondrial ROS Production Protects the Intestine from Inflammation through Functional M2 Macrophage Polarization', *Cell Rep,* 19(6), pp. 1202-1213.

Fornaini, C., Merigo, E., Vescovi, P., Lagori, G. and Rocca, J. P. (2013) 'Use of laser in orthodontics: Applications and perspectives', *Laser Therapy,* 22(2), pp. 115-124.

Frisard, M. I., Wu, Y., McMillan, R. P., Voelker, K. A., Wahlberg, K. A., Anderson, A. S., Boutagy, N., Resendes, K., Ravussin, E. and Hulver, M. W. (2015) 'Low levels of lipopolysaccharide modulate mitochondrial oxygen consumption in skeletal muscle', *Metabolism: Clinical and Experimental,* 64(3), pp. 416-427.

Frozanfar, A., Ramezani, M., Rahpeyma, A., Khajehahmadi, S. and Arbab, H. R. (2013) 'The effects of low level laser therapy on the expression of collagen type I gene and proliferation of human gingival fibroblasts (HGF3-PI 53): In vitro study', *Iranian Journal of Basic Medical Sciences,* 16(10), pp. 1071-1074.

Fuma, S., Murase, H., Kuse, Y., Tsuruma, K., Shimazawa, M. and Hara, H. (2015) 'Photobiomodulation with 670 nm light increased phagocytosis in human retinal pigment epithelial cells', *Molecular vision,* 21, pp. 883-892.

Fushimi, T., Inui, S., Nakajima, T., Ogasawara, M., Hosokawa, K. and Itami, S. (2012) 'Green light emitting diodes accelerate wound healing: characterization of the effect and its molecular basis in vitro and in vivo', *Wound Repair Regen,* 20(2), pp. 226-35.

Gao, X. and Xing, D. (2009) 'Molecular mechanisms of cell proliferation induced by low power laser irradiation', *Journal of Biomedical Science,* 16(1).

Garcia, V. G., Longo, M., Fernandes, L. A., Junior, E. C. G., Dos Santos Santinoni, C., Bosco, Á. F., Nagata, M. J. H. and Theodoro, L. H. (2013) 'Treatment of experimental periodontitis in rats using repeated adjunctive antimicrobial photodynamic therapy', *Lasers in Medical Science,* 28(1), pp. 143-150.

Garlet, G. P. (2010) 'Critical reviews in oral biology & medicine: Destructive and protective roles of cytokines in periodontitis: A re-appraisal from host defense and tissue destruction viewpoints', *Journal of Dental Research,* 89(12), pp. 1349-1363.

Ge, M. K., He, W. L., Chen, J., Wen, C., Yin, X., Hu, Z. A., Liu, Z. P. and Zou, S. J. (2015) 'Efficacy of low-level laser therapy for accelerating tooth movement during orthodontic treatment: a systematic review and meta-analysis', *Lasers in Medical Science,* 30(5), pp. 1609-1618.

George, S., Hamblin, M. R. and Abrahamse, H. (2018) 'Effect of red light and near infrared laser on the generation of reactive oxygen species in primary dermal fibroblasts', *Journal of Photochemistry and Photobiology B: Biology,* 188, pp. 60-68.

Gerits, E., Verstraeten, N. and Michiels, J. (2017) 'New approaches to combat Porphyromonas gingivalis biofilms', *J Oral Microbiol,* 9(1), pp. 1300366.

Giacci, M. K., Hart, N. S., Hartz, R. V., Harvey, A. R., Hodgetts, S. I. and Fitzgerald, M. (2015) 'Method for the assessment of effects of a range of wavelengths and intensities of red/near-infrared light therapy on oxidative stress in vitro', *Journal of Visualized Experiments,* 2015(97).

Gibellini, L., Bianchini, E., De Biasi, S., Nasi, M., Cossarizza, A. and Pinti, M. (2015) 'Natural Compounds Modulating Mitochondrial Functions', *Evidence-based complementary and alternative medicine : eCAM,* 2015, pp. 527209-527209.

Gkogkos, A. S., Karoussis, I. K., Prevezanos, I. D., Marcopoulou, K. E., Kyriakidou, K. and Vrotsos, I. A. (2015) 'Effect of Nd:YAG Low Level Laser Therapy on Human Gingival Fibroblasts', *International Journal of Dentistry,* 2015.

Gloire, G., Legrand-Poels, S. and Piette, J. (2006) 'NF-kappaB activation by reactive oxygen species: fifteen years later', *Biochem Pharmacol,* 72(11), pp. 1493-505.

GM., C. (2000) *The Cell: A Molecular Approach.* 2 edn.: Sunderland (MA): Sinauer Associates.

Gold, M. H., Biron, J. A. and Sensing, W. (2014) 'Clinical and usability study to determine the safety and efficacy of the Silk'n Blue Device for the treatment of mild to moderate inflammatory acne vulgaris', *J Cosmet Laser Ther,* 16(3), pp. 108-13.

Gomez-Florit, M., Monjo, M. and Ramis, J. M. (2014) 'Identification of quercitrin as a potential therapeutic agent for periodontal applications', *J Periodontol,* 85(7), pp. 966-74.

Graves, D. T., Jiang, Y. and Genco, C. (2000) 'Periodontal disease: bacterial virulence factors, host response and impact on systemic health', *Curr Opin Infect Dis,* 13(3), pp. 227-232.

Greenhough, A., Smartt, H. J., Moore, A. E., Roberts, H. R., Williams, A. C., Paraskeva, C. and Kaidi, A. (2009) 'The COX-2/PGE2 pathway: key roles in the hallmarks of cancer and adaptation to the tumour microenvironment', *Carcinogenesis,* 30(3), pp. 377-86.

Groeger, G., Doonan, F., Cotter, T. G. and Donovan, M. (2012) 'Reactive oxygen species regulate prosurvival ERK1/2 signaling and bFGF expression in gliosis within the retina', *Invest Ophthalmol Vis Sci,* 53(10), pp. 6645-54.

Gunduz, M., Unal, O., Kavurt, S., Turk, E. and Mungan, N. O. (2016) 'Clinical findings and effect of sodium hydrogen carbonate in patients with glutathione synthetase deficiency', *J Pediatr Endocrinol Metab,* 29(4), pp. 481-5.

Guo, Z. Y., Zhang, J., Dong, R. and Xu, J. (2017) 'Fasudil blocks muscle atrophy and C2C12 myoblasts respiratory dysfunction triggered by ROCK1', *Academic Journal of Second Military Medical University,* 38(6), pp. 734-738.

H. Bokhari, S. A., Khan, A. A., Butt, A. K., Azhar, M., Hanif, M., Izhar, M. and Tatakis, D. N. (2012) 'Non-surgical periodontal therapy reduces coronary heart disease risk markers: A randomized controlled trial', *Journal of Clinical Periodontology,* 39(11), pp. 1065-1074.

Hadis, M. A., Cooper, P. R., Milward, M. R., Gorecki, P., Tarte, E., Churm, J. and Palin, W. M. 'The effect of UV-Vis to near-infrared light on the biological response of human dental pulp cells'. *Progress in Biomedical Optics and Imaging - Proceedings of SPIE*.

Hadis, M. A., Cooper, P. R., Milward, M. R., Gorecki, P. C., Tarte, E., Churm, J. and Palin, W. M. (2017a) 'Development and application of LED arrays for use in phototherapy research', *J Biophotonics,* 10(11), pp. 1514-1525.

Hadis, M. A., Cooper, P. R., Milward, M. R., Gorecki, P. C., Tarte, E., Churm, J. and Palin, W. M. (2017b) 'Development and application of LED arrays for use in phototherapy research', *Journal of Biophotonics*.

Hadis, M. A., Zainal, S. A., Holder, M. J., Carroll, J. D., Cooper, P. R., Milward, M. R. and Palin, W. M. (2016a) 'The dark art of light measurement: accurate radiometry for low-level light therapy', *Lasers in Medical Science*, pp. 1-21.

Hadis, M. A., Zainal, S. A., Holder, M. J., Carroll, J. D., Cooper, P. R., Milward, M. R. and Palin, W. M. (2016b) 'The dark art of light measurement: accurate radiometry for low-level light therapy', *Lasers in Medical Science,* 31(4), pp. 789-809.

Haffajee, A. D., Socransky, S. S., Patel, M. R. and Song, X. (2008) 'Microbial complexes in supragingival plaque', *Oral Microbiol Immunol,* 23(3), pp. 196-205.

Hahnke, R. L., Meier-Kolthoff, J. P., Garcia-Lopez, M., Mukherjee, S., Huntemann, M., Ivanova, N. N., Woyke, T., Kyrpides, N. C., Klenk, H. P. and Goker, M. (2016) 'Genome-Based Taxonomic Classification of Bacteroidetes', *Front Microbiol,* 7, pp. 2003.

Hajishengallis, G. (2011) 'Immune evasion strategies of Porphyromonas gingivalis', *Journal of oral biosciences,* 53(3), pp. 233-240.

Hakki, S. S. and Bozkurt, S. B. (2012) 'Effects of different setting of diode laser on the mRNA expression of growth factors and type i collagen of human gingival fibroblasts', *Lasers in Medical Science,* 27(2), pp. 325-331.

Hamblin, M. R. 'The role of nitric oxide in low level light therapy'. *Progress in Biomedical Optics and Imaging - Proceedings of SPIE*.

Hamblin, M. R. (2017) 'Mechanisms and applications of the anti-inflammatory effects of photobiomodulation', *AIMS biophysics,* 4(3), pp. 337-361.

Hamblin, M. R. (2018a) 'Mechanisms and Mitochondrial Redox Signaling in Photobiomodulation', *Photochemistry and Photobiology,* 94(2), pp. 199-212.

Hamblin, M. R. (2018b) 'Photobiomodulation for traumatic brain injury and stroke', *Journal of Neuroscience Research,* 96(4), pp. 731-743.

Hamblin, M. R. and Demidova-Rice, T. N. 'Cellular chromophores and signaling in low level light therapy'. *Progress in Biomedical Optics and Imaging - Proceedings of SPIE*, SPIE.

Hamblin, M. R., Huang, Y. Y. and Heiskanen, V. (2019) 'Non-mammalian Hosts and Photobiomodulation: Do All Life-forms Respond to Light?', *Photochemistry and Photobiology,* 95(1), pp. 126-139.

Hamblin, M. R., Huang, Y. Y., Sharma, S. K. and Carroll, J. (2011) 'Biphasic dose response in low level light therapy - an update', *Dose-Response,* 9(4), pp. 602-618.

Hamilton, C., Hamilton, D., Nicklason, F., El Massri, N. and Mitrofanis, J. (2018) 'Exploring the use of transcranial photobiomodulation in Parkinson's disease patients', *Neural Regeneration Research,* 13(10), pp. 1738-1740.

Hammami, A., Amri, M. and Mokni, M. (2018) 'Low-level laser irradiation protects the chick embryo chorioallantoic membrane from UV cytotoxicity', *Archives of Biological Sciences,* 70(1), pp. 119-127.

Hannemann, F., Bichet, A., Ewen, K. M. and Bernhardt, R. (2007) 'Cytochrome P450 systems--biological variations of electron transport chains', *Biochim Biophys Acta,* 1770(3), pp. 330-44.

Hashmi, J. T., Huang, Y.-Y., Sharma, S. K., Kurup, D. B., De Taboada, L., Carroll, J. D. and Hamblin, M. R. (2010) 'Effect of Pulsing in Low-Level Light Therapy', *Lasers in surgery and medicine,* 42(6), pp. 450-466.

Hassell, T. M. (1993) 'Tissues and cells of the periodontium', *Periodontol 2000,* 3, pp. 9-38.
Hazeldine, J., Harris, P., Chapple, I. L., Grant, M., Greenwood, H., Livesey, A., Sapey, E. and Lord, J. M. (2014) 'Impaired neutrophil extracellular trap formation: A novel defect in the innate immune system of aged individuals', *Aging Cell,* 13(4), pp. 690-698.
He, G., Siddik, Z. H., Huang, Z., Wang, R., Koomen, J., Kobayashi, R., Khokhar, A. R. and Kuang, J. (2005) 'Induction of p21 by p53 following DNA damage inhibits both Cdk4 and Cdk2 activities', *Oncogene,* 24(18), pp. 2929-43.
He, H.-J., Stein, E. V., DeRose, P. and Cole, K. D. (2018a) 'Limitations of methods for measuring the concentration of human genomic DNA and oligonucleotide samples', *BioTechniques,* 64(2), pp. 59-68.
He, M., Zhang, B., Shen, N., Wu, N. and Sun, J. (2018b) 'A systematic review and meta-analysis of the effect of low-level laser therapy (LLLT) on chemotherapy-induced oral mucositis in pediatric and young patients', *European Journal of Pediatrics,* 177(1), pp. 7-17.
Heiskanen, V. and Hamblin, M. R. (2018a) 'Photobiomodulation: lasers vs. light emitting diodes?', *Photochem Photobiol Sci,* 17(8), pp. 1003-1017.
Heiskanen, V. and Hamblin, M. R. (2018b) 'Photobiomodulation: Lasers: vs. light emitting diodes?', *Photochemical and Photobiological Sciences,* 17(8), pp. 1003-1017.
Herbert, B. A., Novince, C. M. and Kirkwood, K. L. (2016) 'Aggregatibacter actinomycetemcomitans, a potent immunoregulator of the periodontal host defense system and alveolar bone homeostasis', *Molecular oral microbiology,* 31(3), pp. 207-227.
Hirata, S., Kitamura, C., Fukushima, H., Nakamichi, I., Abiko, Y., Terashita, M. and Jimi, E. (2010) 'Low-level laser irradiation enhances BMP-induced osteoblast differentiation by stimulating the BMP/Smad signaling pathway', *J Cell Biochem,* 111(6), pp. 1445-52.
Hirst, J. (2013) 'Mitochondrial complex I', *Annu Rev Biochem,* 82, pp. 551-75.
Hochman, B., Pinfildi, C. E., Nishioka, M. A., Furtado, F., Bonatti, S., Monteiro, P. K. P., Antunes, A. S., Quieregatto, P. R., Liebano, R. E., Chadi, G. and Ferreira, L. M. (2014) 'Low-level laser therapy and light-emitting diode effects in the secretion of neuropeptides SP and CGRP in rat skin', *Lasers in Medical Science,* 29(3), pp. 1203-1208.
Hode, T., Duncan, D., Kirkpatrick, S., Jenkins, P. and Hode, L. 'The importance of coherence in phototherapy'. *Progress in Biomedical Optics and Imaging - Proceedings of SPIE*.
Hoffmann, C., Höckele, S., Kappler, L., Hrabě de Angelis, M., Häring, H.-U. and Weigert, C. (2018) 'The effect of differentiation and TGFβ on mitochondrial respiration and mitochondrial enzyme abundance in cultured primary human skeletal muscle cells', *Scientific Reports,* 8, pp. 737.
Holder, M. J., Milward, M. R., Palin, W. M., Hadis, M. A. and Cooper, P. R. (2012) 'Effects of red light-emitting diode irradiation on dental pulp cells', *J Dent Res,* 91(10), pp. 961-6.
Holmstrom, K. M. and Finkel, T. (2014) 'Cellular mechanisms and physiological consequences of redox-dependent signalling', *Nat Rev Mol Cell Biol,* 15(6), pp. 411-21.
Horimoto, M., Kato, J., Takimoto, R., Terui, T., Mogi, Y. and Niitsu, Y. (1995) 'Identification of a transforming growth factor beta-1 activator derived from a human gastric cancer cell line', *Br J Cancer,* 72(3), pp. 676-82.
Houreld, N. N. (2014) 'Shedding Light on a New Treatment for Diabetic Wound Healing: A Review on Phototherapy', *The Scientific World Journal,* 2014, pp. 398412.
How, K. Y., Song, K. P. and Chan, K. G. (2016) 'Porphyromonas gingivalis: An Overview of Periodontopathic Pathogen below the Gum Line', *Frontiers in microbiology,* 7, pp. 53-53.
Huang, G. T., Kim, D., Lee, J. K., Kuramitsu, H. K. and Haake, S. K. (2001) 'Interleukin-8 and intercellular adhesion molecule 1 regulation in oral epithelial cells by selected periodontal bacteria: multiple effects of Porphyromonas gingivalis via antagonistic mechanisms', *Infect Immun,* 69(3), pp. 1364-72.
Huang, Y.-Y., Nagata, K., Tedford, C. E., McCarthy, T. and Hamblin, M. R. (2013) 'Low-level laser therapy (LLLT) reduces oxidative stress in primary cortical neurons in vitro', *Journal of biophotonics,* 6(10), pp. 829-838.

Huang, Y.-Y., Sharma, S. K., Carroll, J. and Hamblin, M. R. (2011) 'Biphasic Dose Response in Low Level Light Therapy – An Update', *Dose-Response,* 9(4), pp. 602-618.
Huang, Y. Y., Chen, A. C. H., Carroll, J. D. and Hamblin, M. R. (2009) 'Biphasic dose response in low level lightherapy', *Dose-Response,* 7(4), pp. 358-383.
Hunter, R. A., Storm, W. L., Coneski, P. N. and Schoenfisch, M. H. (2013) 'Inaccuracies of nitric oxide measurement methods in biological media', *Analytical chemistry,* 85(3), pp. 1957-1963.
Huttemann, M., Kadenbach, B. and Grossman, L. I. (2001) 'Mammalian subunit IV isoforms of cytochrome c oxidase', *Gene,* 267(1), pp. 111-23.
Hwang, N. L., Kang, Y. J., Sung, B., Hwang, S. Y., Jang, J. Y., Oh, H. J., Ahn, Y. R., Kim, D. H., Kim, S. J., Ullah, S., Hossain, M. A., Moon, H. R., Chung, H. Y. and Kim, N. D. (2017) 'MHY451 induces cell cycle arrest and apoptosis by ROS generation in HCT116 human colorectal cancer cells', *Oncol Rep,* 38(3), pp. 1783-1789.
Ibtisham, F., Zhao, Y., Nawab, A., Liguang, H., Wu, J., Xiao, M., Zhao, Z. and An, L. (2018) 'The effect of high temperature on viability, proliferation, apoptosis and anti-oxidant status of chicken embryonic fibroblast cells', *Revista Brasileira de Ciencia Avicola,* 20(3), pp. 463-470.
Imatani, T., Kato, T. and Okuda, K. (2001) 'Production of inflammatory cytokines by human gingival fibroblasts stimulated by cell-surface preparations of Porphyromonas gingivalis', *Oral Microbiol Immunol,* 16(2), pp. 65-72.
Ismaili, B. and Bokonjic, D. (2014) 'Short-term low-level laser therapy attenuates inflammation and production of interleukin-1, but elevates the level of matrix metalloproteinase 9 in chronic periodontitis', *Journal of International Dental and Medical Research,* 7(1), pp. 7-13.
Itoh, Y., Joh, T., Tanida, S., Sasaki, M., Kataoka, H., Itoh, K., Oshima, T., Ogasawara, N., Togawa, S., Wada, T., Kubota, H., Mori, Y., Ohara, H., Nomura, T., Higashiyama, S. and Itoh, M. (2005) 'IL-8 promotes cell proliferation and migration through metalloproteinase-cleavage proHB-EGF in human colon carcinoma cells', *Cytokine,* 29(6), pp. 275-82.
Jackson, M. S., Bagg, J., Kennedy, H. and Michie, J. (2000) 'Staphylococci in the oral flora of healthy children and those receiving treatment for malignant disease', *Microbial Ecology in Health and Disease,* 12(1), pp. 60-64.
Jain, M., Rivera, S., Monclus, E. A., Synenki, L., Zirk, A., Eisenbart, J., Feghali-Bostwick, C., Mutlu, G. M., Budinger, G. R. and Chandel, N. S. (2013) 'Mitochondrial reactive oxygen species regulate transforming growth factor-beta signaling', *J Biol Chem,* 288(2), pp. 770-7.
Jakubovics, N. S. and Kolenbrander, P. E. (2010) 'The road to ruin: the formation of disease-associated oral biofilms', *Oral Dis,* 16(8), pp. 729-39.
Janzadeh, A., Nasirinezhad, F., Masoumipoor, M., Jameie, S. B. and hayat, P. (2016) 'Photobiomodulation therapy reduces apoptotic factors and increases glutathione levels in a neuropathic pain model', *Lasers in Medical Science,* 31(9), pp. 1863-1869.
Jeffery Marano, R., Jane Wallace, H., Wijeratne, D., William Fear, M., San Wong, H. and O'Handley, R. (2015) 'Secreted biofilm factors adversely affect cellular wound healing responses in vitro', *Scientific reports,* 5, pp. 13296-13296.
Jenkins, P. A. and Carroll, J. D. (2011) 'How to report low-level laser therapy (LLLT)/photomedicine dose and beam parameters in clinical and laboratory studies', *Photomedicine and Laser Surgery,* 29(12), pp. 785-787.
Jobling, M. F., Mott, J. D., Finnegan, M. T., Jurukovski, V., Erickson, A. C., Walian, P. J., Taylor, S. E., Ledbetter, S., Lawrence, C. M., Rifkin, D. B. and Barcellos-Hoff, M. H. (2006) 'Isoform-specific activation of latent transforming growth factor beta (LTGF-beta) by reactive oxygen species', *Radiat Res,* 166(6), pp. 839-48.
Jones, K. J., Ekhlassi, S., Montufar-Solis, D., Klein, J. R. and Schaefer, J. S. (2010) 'Differential cytokine patterns in mouse macrophages and gingival fibroblasts after stimulation with porphyromonas gingivalis or Escherichia coli lipopolysaccharide', *J Periodontol,* 81(12), pp. 1850-7.

Jung, Y. R., Kim, S. J., Sohn, K. C., Lee, Y., Seo, Y. J., Lee, Y. H., Whang, K. U., Kim, C. D., Lee, J. H. and Im, M. (2015) 'Regulation of lipid production by light-emitting diodes in human sebocytes', *Archives of Dermatological Research,* 307(3), pp. 265-273.

Kacprzak, A. and Strzecki, A. (2018) 'Methods of accelerating orthodontic tooth movement: A review of contemporary literature', *Dental and Medical Problems,* 55(2), pp. 197-206.

Kalyanaraman, B., Darley-Usmar, V., Davies, K. J. A., Dennery, P. A., Forman, H. J., Grisham, M. B., Mann, G. E., Moore, K., Roberts, L. J., 2nd and Ischiropoulos, H. (2012) 'Measuring reactive oxygen and nitrogen species with fluorescent probes: challenges and limitations', *Free radical biology & medicine,* 52(1), pp. 1-6.

Kamel, M. S., Khosa, A., Tawse-Smith, A. and Leichter, J. (2014) 'The use of laser therapy for dental implant surface decontamination: a narrative review of in vitro studies', *Lasers in Medical Science,* 29(6), pp. 1977-1985.

Kang, M. S., Lim, H. S., Kim, S. M., Lee, H. C. and Oh, J. S. (2011) 'Effect of Weissella cibaria on Fusobacterium nucleatum-induced interleukin-6 and interleukin-8 production in KB cells', *Journal of Bacteriology and Virology,* 41(1), pp. 9-18.

Kang, W., Hu, Z. and Ge, S. (2016) 'Healthy and Inflamed Gingival Fibroblasts Differ in Their Inflammatory Response to Porphyromonas gingivalis Lipopolysaccharide', *Inflammation,* 39(5), pp. 1842-52.

Karu, T. I. (2008) 'Mitochondrial signaling in mammalian cells activated by red and near-IR radiation', *Photochemistry and Photobiology,* 84(5), pp. 1091-1099.

Karu, T. I. (2010) 'Multiple roles of cytochrome c oxidase in mammalian cells under action of red and IR-A radiation', *IUBMB Life,* 62(8), pp. 607-610.

Karu, T. I. and Kolyakov, S. F. (2005) 'Exact action spectra for cellular responses relevant to phototherapy', *Photomed Laser Surg,* 23(4), pp. 355-61.

Kasuga, Y., Ishihara, K. and Okuda, K. (2000) 'Significance of detection of Porphyromonas gingivalis, Bacteroides forsythus and Treponema denticola in periodontal pockets', *Bull Tokyo Dent Coll,* 41(3), pp. 109-17.

Kathuria, V., Dhillon, J. K. and Kalra, G. (2015) 'Low level laser therapy: A panacea for oral maladies', *Laser Therapy,* 24(3), pp. 215-223.

Kazemi Khoo, N., Iravani, A., Arjmand, M., Vahabi, F., Lajevardi, M., Akrami, S. M. and Zamani, Z. (2013) 'A metabolomic study on the effect of intravascular laser blood irradiation on type 2 diabetic patients', *Lasers Med Sci,* 28(6), pp. 1527-32.

KazemiKhoo, N. and Ansari, F. (2014) 'Blue or red: which intravascular laser light has more effects in diabetic patients?', *Lasers in Medical Science,* 30(1), pp. 363-366.

Kent, L. W., Dyken, R. A., Rahemtulla, F., Allison, A. C. and Michalek, S. M. (1996) 'Effect of in vitro passage of healthy human gingival fibroblasts on cellular morphology and cytokine expression', *Arch Oral Biol,* 41(3), pp. 263-70.

Kent, L. W., Rahemtulla, F., Hockett, R. D., Gilleland, R. C. and Michalek, S. M. (1998) 'Effect of Lipopolysaccharide and Inflammatory Cytokines on Interleukin-6 Production by Healthy Human Gingival Fibroblasts', *Infection and Immunity,* 66(2), pp. 608-614.

Keskiner, I., Lutfioğlu, M., Aydogdu, A., Saygun, N. I. and Serdar, M. A. (2016) 'Effect of Photobiomodulation on Transforming Growth Factor-β1, Platelet-Derived Growth Factor-BB, and Interleukin-8 Release in Palatal Wounds After Free Gingival Graft Harvesting: A Randomized Clinical Study', *Photomedicine and laser surgery,* 34(6), pp. 263-271.

Keszler, A., Lindemer, B., Hogg, N., Weihrauch, D. and Lohr, N. L. (2018) 'Wavelength-dependence of vasodilation and NO release from S-nitrosothiols and dinitrosyl iron complexes by far red/near infrared light', *Arch Biochem Biophys,* 649, pp. 47-52.

Khadra, M., Lyngstadaas, S. P., Haanæs, H. R. and Mustafa, K. (2005) 'Determining optimal dose of laser therapy for attachment and proliferation of human oral fibroblasts cultured on titanium implant material', *Journal of Biomedical Materials Research - Part A,* 73(1), pp. 55-62.

Khan, I., Tang, E. and Arany, P. (2015) 'Molecular pathway of near-infrared laser phototoxicity involves ATF-4 orchestrated ER stress', *Scientific Reports,* 5.

Kharkwal, G. B., Sharma, S. K., Huang, Y. Y., Taboada, L. D., McCarthy, T. and Hamblin, M. R. 'Effects of 810 nm laser on mouse primary cortical neurons'. *Progress in Biomedical Optics and Imaging - Proceedings of SPIE*.

Khori, V., Alizadeh, A. M., Gheisary, Z., Farsinejad, S., Najafi, F., Khalighfard, S., Ghafari, F., Hadji, M. and Khodayari, H. (2016) 'The effects of low-level laser irradiation on breast tumor in mice and the expression of Let-7a, miR-155, miR-21, miR125, and miR376b', *Lasers Med Sci,* 31(9), pp. 1775-1782.

Kianoush, N., Adler, C. J., Nguyen, K. A. T., Browne, G. V., Simonian, M. and Hunter, N. (2014) 'Bacterial profile of dentine caries and the impact of pH on bacterial population diversity', *PLoS ONE,* 9(3).

Kim, D.-L. and Kim, B.-T. (2016) 'Laser output power losses in ceramic Nd:YAG lasers due to thermal effects', *Optik - International Journal for Light and Electron Optics,* 127(20), pp. 9738-9742.

Kim, J. E., Woo, Y. J., Sohn, K. M., Jeong, K. H. and Kang, H. (2017a) 'Wnt/β-catenin and ERK pathway activation: A possible mechanism of photobiomodulation therapy with light-emitting diodes that regulate the proliferation of human outer root sheath cells', *Lasers in Surgery and Medicine,* 49(10), pp. 940-947.

Kim, O., Choi, H., Lim, W., Kim, I., Kim, J., Ko, Y., Kwon, H., Kim, S., Ahsan Kabir, K. M., Li, X., Kim, O., Lee, Y. J. and Kim, S. (2012) 'Inflammatory cytokines are suppressed by light-emitting diode irradiation of P. gingivalis LPS-treated human gingival fibroblasts', *Lasers in Medical Science,* 27(2), pp. 459-467.

Kim, S. K., Soh, B. W. and Kim, Y. C. (2017b) 'Low level light therapy using an 830-nm light emitting diode promotes wound healing via TGF-β/SMAD pathway activation', *Korean Journal of Dermatology,* 55(4), pp. 237-245.

Kiriakidis, S., Andreakos, E., Monaco, C., Foxwell, B., Feldmann, M. and Paleolog, E. (2003) 'VEGF expression in human macrophages is NF-kappaB-dependent: studies using adenoviruses expressing the endogenous NF-kappaB inhibitor IkappaBalpha and a kinase-defective form of the IkappaB kinase 2', *J Cell Sci,* 116(Pt 4), pp. 665-74.

Kiritoshi, S., Nishikawa, T., Sonoda, K., Kukidome, D., Senokuchi, T., Matsuo, T., Matsumura, T., Tokunaga, H., Brownlee, M. and Araki, E. (2003) 'Reactive oxygen species from mitochondria induce cyclooxygenase-2 gene expression in human mesangial cells: potential role in diabetic nephropathy', *Diabetes,* 52(10), pp. 2570-7.

Klug, B., Santigli, E., Westendorf, C., Tangl, S., Wimmer, G. and Grube, M. (2016a) 'From Mouth to Model: Combining in vivo and in vitro Oral Biofilm Growth', *Front Microbiol,* 7, pp. 1448.

Klug, B., Santigli, E., Westendorf, C., Tangl, S., Wimmer, G. and Grube, M. (2016b) 'From mouth to model: Combining in vivo and in vitro oral biofilm growth', *Frontiers in Microbiology,* 7(SEP).

Kolenbrander, P. E., Palmer, R. J., Periasamy, S. and Jakubovics, N. S. (2010) 'Oral multispecies biofilm development and the key role of cell-cell distance', *Nature Reviews Microbiology,* 8(7), pp. 471-480.

Koo, H., Xiao, J., Klein, M. I. and Jeon, J. G. (2010) 'Exopolysaccharides produced by Streptococcus mutans glucosyltransferases modulate the establishment of microcolonies within multispecies biofilms', *J Bacteriol,* 192(12), pp. 3024-32.

Koren, K., Borisov, S. M., Saf, R. and Klimant, I. (2011a) 'Strongly Phosphorescent Iridium(III)–Porphyrins – New Oxygen Indicators with Tuneable Photophysical Properties and Functionalities', *European Journal of Inorganic Chemistry,* 2011(10), pp. 1531-1534.

Koren, O., Spor, A., Felin, J., Fak, F., Stombaugh, J., Tremaroli, V., Behre, C. J., Knight, R., Fagerberg, B., Ley, R. E. and Backhed, F. (2011b) 'Human oral, gut, and plaque microbiota in patients with atherosclerosis', *Proc Natl Acad Sci U S A,* 108 Suppl 1, pp. 4592-8.

Koshy, B. S. and Mahendra, J. (2017) 'The Association between Periodontal Status, Serum Lipid Levels, Lipoprotein Associated Phosholipase A2 (Lp-PLA2) in Chronic Periodontitis Subjects

and Healthy Controls', *Journal of clinical and diagnostic research : JCDR,* 11(9), pp. ZC17-ZC21.
Koyanagi, M., Kawakabe, S. and Arimura, Y. (2016) 'A comparative study of colorimetric cell proliferation assays in immune cells', *Cytotechnology,* 68(4), pp. 1489-98.
Kraft, C. S., LeMoine, C. M., Lyons, C. N., Michaud, D., Mueller, C. R. and Moyes, C. D. (2006) 'Control of mitochondrial biogenesis during myogenesis', *Am J Physiol Cell Physiol,* 290(4), pp. C1119-27.
Krajcova, A., Ziak, J., Jiroutkova, K., Patkova, J., Elkalaf, M., Dzupa, V., Trnka, J. and Duska, F. (2015) 'Normalizing glutamine concentration causes mitochondrial uncoupling in an in vitro model of human skeletal muscle', *Journal of Parenteral and Enteral Nutrition,* 39(2), pp. 180-189.
Kreisler, M., Christoffers, A. B., Al-Haj, H., Willershausen, B. and D'Hoedt, B. (2002) 'Low level 809-nm diode laser-induced in vitro stimulation of the proliferation of human gingival fibroblasts', *Lasers in Surgery and Medicine,* 30(5), pp. 365-369.
Kreisler, M., Christoffers, A. B., Willershausen, B. and D'Hoedt, B. (2003) 'Effect of low-level GaAlAs laser irradiation on the proliferation rate of human periodontal ligament fibroblasts: An in vitro study', *Journal of Clinical Periodontology,* 30(4), pp. 353-358.
Kreisler, M., Daubländer, M., Willershausen-Zönnchen, B. and D'Hoedt, B. (2001) 'Effect of diode laser irradiation on the survival rate of gingival fibroblast cell cultures', *Lasers in Surgery and Medicine,* 28(5), pp. 445-450.
Kreisler, M., Kohnen, W., Christoffers, A. B., Götz, H., Jansen, B., Duschner, H. and D'Hoedt, B. (2005) 'In vitro evaluation of the biocompatibility of contaminated implant surfaces treated with an Er:YAG laser and an air powder system', *Clinical Oral Implants Research,* 16(1), pp. 36-43.
Kubo, Y. (1991) 'Comparison of initial stages of muscle differentiation in rat and mouse myoblastic and mouse mesodermal stem cell lines', *The Journal of physiology,* 442, pp. 743-759.
Kuffler, D. P. (2016) 'Photobiomodulation in promoting wound healing: A review', *Regenerative Medicine,* 11(1), pp. 107-122.
Kuluncsics, Z., Perdiz, D., Brulay, E., Muel, B. and Sage, E. (1999) 'Wavelength dependence of ultraviolet-induced DNA damage distribution: involvement of direct or indirect mechanisms and possible artefacts', *J Photochem Photobiol B,* 49(1), pp. 71-80.
Kurata, S. (2018) 'Light therapy (LLLT and LED) for the treatment of AGA', *Japanese Journal of Plastic Surgery,* 61(9), pp. 1110-1118.
Kushibiki, T., Hirasawa, T., Okawa, S. and Ishihara, M. (2013) 'Blue laser irradiation generates intracellular reactive oxygen species in various types of cells', *Photomedicine and Laser Surgery,* 31(3), pp. 95-104.
Kushibiki, T., Tajiri, T., Ninomiya, Y. and Awazu, K. (2010) 'Chondrogenic mRNA expression in prechondrogenic cells after blue laser irradiation', *J Photochem Photobiol B,* 98(3), pp. 211-5.
Kuznetsov, A. V. and Margreiter, R. (2009) 'Heterogeneity of mitochondria and mitochondrial function within cells as another level of mitochondrial complexity', *International journal of molecular sciences,* 10(4), pp. 1911-1929.
Lagdive, S. S., Marawar, P. P., Byakod, G. and Lagdive, S. B. (2013) 'Evaluation and comparison of interleukin-8 (IL-8) level in gingival crevicular fluid in health and severity of periodontal disease: a clinico-biochemical study', *Indian J Dent Res,* 24(2), pp. 188-92.
Lalla, R. V., Sonis, S. T. and Peterson, D. E. (2008) 'Management of oral mucositis in patients who have cancer', *Dental clinics of North America,* 52(1), pp. 61-viii.
Lamont RJ, B. R., Lantz MS, LeBlanc DJ (2006) *Oral Microbiology and Immunology.* American Society of Microbiology, p. 50-52.
Lamont, R. J. and Jenkinson, H. F. (1998) 'Life below the gum line: pathogenic mechanisms of Porphyromonas gingivalis', *Microbiology and molecular biology reviews : MMBR,* 62(4), pp. 1244-1263.

Lan, C. C. E., Wu, C. S., Chiou, M. H., Chiang, T. Y. and Yu, H. S. (2009) 'Low-energy helium-neon laser induces melanocyte proliferation via interaction with type IV collagen: Visible light as a therapeutic option for vitiligo', *British Journal of Dermatology,* 161(2), pp. 273-280.

Langfeldt, D., Neulinger, S. C., Heuer, W., Staufenbiel, I., Künzel, S., Baines, J. F., Eberhard, J. and Schmitz, R. A. (2014) 'Composition of microbial oral biofilms during maturation in young healthy adults', *PloS one,* 9(2), pp. e87449-e87449.

Larsen, S., Nielsen, J., Hansen, C. N., Nielsen, L. B., Wibrand, F., Stride, N., Schroder, H. D., Boushel, R., Helge, J. W., Dela, F. and Hey-Mogensen, M. (2012) 'Biomarkers of mitochondrial content in skeletal muscle of healthy young human subjects', *J Physiol,* 590(14), pp. 3349-60.

Lavi, R., Ankri, R., Sinyakov, M., Eichler, M., Friedmann, H., Shainberg, A., Breitbart, H. and Lubart, R. (2012) 'The plasma membrane is involved in the visible light-tissue interaction', *Photomed Laser Surg,* 30(1), pp. 14-9.

Lázaro, J. J., Jiménez, A., Camejo, D., Iglesias-Baena, I., Martí, M. D. C., Lázaro-Payo, A., Barranco-Medina, S. and Sevilla, F. (2013) 'Dissecting the integrative antioxidant and redox systems in plant mitochondria. Effect of stress and S-nitrosylation', *Frontiers in plant science,* 4, pp. 460-460.

Le, X., Laflamme, C. and Rouabhia, M. (2009) 'Porphyromonas gingivalis decreases osteoblast proliferation through IL-6-RANKL/OPG and MMP-9/TIMPs pathways', *Indian Journal of Dental Research,* 20(2), pp. 141-149.

Lee, G., Kim, B., Ko, Y., Park, M., Kim, D., Ryu, K. H., Jun, Y. C., Sohn, H. M. and Lim, W. (2017a) 'Regulation of RANKL-Induced Osteoclastogenesis by 635-nm Light-Emitting Diode Irradiation Via HSP27 in Bone Marrow-Derived Macrophages', *Photomedicine and Laser Surgery,* 35(2), pp. 78-86.

Lee, H. S., Jung, S. E., Kim, S. K., Kim, Y. S., Sohn, S. and Kim, Y. C. (2017b) 'Low-level light therapy with 410 nm light emitting diode suppresses collagen synthesis in human keloid fibroblasts: An in vitro study', *Annals of Dermatology,* 29(2), pp. 149-155.

Lee, S. H., Kim, K. K., Rhyu, I. C., Koh, S., Lee, D. S. and Choi, B. K. (2006) 'Phenol/water extract of Treponema socranskii subsp. socranskii as an antagonist of Toll-like receptor 4 signalling', *Microbiology,* 152(Pt 2), pp. 535-46.

Leggate, J., Allain, R., Isaac, L. and Blais, B. W. (2006) 'Microplate fluorescence assay for the quantification of double stranded DNA using SYBR Green I dye', *Biotechnol Lett,* 28(19), pp. 1587-94.

Lenaz, G., Fato, R., Genova, M. L., Bergamini, C., Bianchi, C. and Biondi, A. (2006) 'Mitochondrial Complex I: Structural and functional aspects', *Biochimica et Biophysica Acta (BBA) - Bioenergetics,* 1757(9–10), pp. 1406-1420.

Lev-Tov, H., Mamalis, A., Brody, N., Siegel, D. and Jagdeo, J. (2013) 'Inhibition of fibroblast proliferation in vitro using red light-emitting diodes', *Dermatol Surg,* 39(8), pp. 1167-70.

Li, F. J., Zhang, J. Y., Zeng, X. T. and Guo, Y. (2015) 'Low-level laser therapy for orthodontic pain: a systematic review', *Lasers in Medical Science,* 30(6), pp. 1789-1803.

Li, J., Chen, J. and Kirsner, R. (2007) 'Pathophysiology of acute wound healing', *Clin Dermatol,* 25(1), pp. 9-18.

Li, Y., Lee, M., Kim, N., Wu, G., Deng, D., Kim, J. M., Liu, X., Heo, W. D. and Zi, Z. (2018) 'Spatiotemporal Control of TGF-β Signaling with Light', *ACS synthetic biology,* 7(2), pp. 443-451.

Li, Y., Zhang, J., Xu, Y., Han, Y., Jiang, B., Huang, L., Zhu, H., Xu, Y., Yang, W. and Qin, C. (2016) 'The Histopathological Investigation of Red and Blue Light Emitting Diode on Treating Skin Wounds in Japanese Big-Ear White Rabbit', *PloS one,* 11(6), pp. e0157898-e0157898.

Liang, W. Z., Liu, P. F., Fu, E., Chung, H. S., Jan, C. R., Wu, C. H., Shu, C. W. and Hsieh, Y. D. (2015) 'Selective cytotoxic effects of low-power laser irradiation on human oral cancer cells', *Lasers in Surgery and Medicine,* 47(9), pp. 756-764.

Liebel, F., Kaur, S., Ruvolo, E., Kollias, N. and Southall, M. D. (2012) 'Irradiation of skin with visible light induces reactive oxygen species and matrix-degrading enzymes', *J Invest Dermatol,* 132(7), pp. 1901-7.

Liebmann, J., Born, M. and Kolb-Bachofen, V. (2010) 'Blue-light irradiation regulates proliferation and differentiation in human skin cells', *J Invest Dermatol,* 130(1), pp. 259-69.

Lim, W., Choi, H., Kim, J., Kim, S., Jeon, S., Zheng, H., Kim, D., Ko, Y., Kim, D., Sohn, H. and Kim, O. (2015) 'Anti-inflammatory effect of 635 nm irradiations on in vitro direct/indirect irradiation model', *Journal of Oral Pathology and Medicine,* 44(2), pp. 94-102.

Lim, W., Kim, J., Kim, S., Karna, S., Won, J., Jeon, S. M., Kim, S. Y., Choi, Y., Choi, H. and Kim, O. (2013) 'Modulation of lipopolysaccharide-induced NF-κB signaling pathway by 635 nm irradiation via heat shock protein 27 in human gingival fibroblast cells', *Photochemistry and Photobiology,* 89(1), pp. 199-207.

Lim, W., Lee, S., Kim, I., Chung, M., Kim, M., Lim, H., Park, J., Kim, O. and Choi, H. (2007) 'The anti-inflammatory mechanism of 635 nm light-emitting-diode irradiation compared with existing COX inhibitors', *Lasers in Surgery and Medicine,* 39(7), pp. 614-621.

Lima, A. F., Basso, F. G., Ribeiro, A. P. D., Bagnato, V. S., Hebling, J., Marchi, G. M. and De Souza Costa, C. A. (2014) 'Effects of laser irradiation on pulp cells exposed to bleaching agents', *Photochemistry and Photobiology,* 90(1), pp. 201-206.

Listgarten, M. A. (1988) 'The role of dental plaque in gingivitis and periodontitis', *J Clin Periodontol,* 15(8), pp. 485-7.

Listyarifah, D., Al-Samadi, A., Salem, A., Syaify, A., Salo, T., Tervahartiala, T., Grenier, D., Nordstrom, D. C., Sorsa, T. and Ainola, M. (2017) 'Infection and apoptosis associated with inflammation in periodontitis: An immunohistologic study', *Oral Dis,* 23(8), pp. 1144-1154.

Liu, R. M. and Desai, L. P. (2015) 'Reciprocal regulation of TGF-β and reactive oxygen species: A perverse cycle for fibrosis', *Redox Biology,* 6, pp. 565-577.

Liu, Y., Peterson, D. A., Kimura, H. and Schubert, D. (1997) 'Mechanism of cellular 3-(4,5-dimethylthiazol-2-yl)-2,5-diphenyltetrazolium bromide (MTT) reduction', *J Neurochem,* 69(2), pp. 581-93.

Loesche, W. J. (1986) 'Role of Streptococcus mutans in human dental decay', *Microbiol Rev,* 50(4), pp. 353-80.

Lohr, N. L., Keszler, A., Pratt, P., Bienengraber, M., Warltier, D. C. and Hogg, N. (2009) 'Enhancement of nitric oxide release from nitrosyl hemoglobin and nitrosyl myoglobin by red/near infrared radiation: potential role in cardioprotection', *J Mol Cell Cardiol,* 47(2), pp. 256-63.

López-Lluch, G., Irusta, P. M., Navas, P. and de Cabo, R. (2008) 'Mitochondrial biogenesis and healthy aging', *Experimental gerontology,* 43(9), pp. 813-819.

Luo, L., Sun, Z., Zhang, L., Li, X., Dong, Y. and Liu, T. C. Y. (2013) 'Effects of low-level laser therapy on ROS homeostasis and expression of IGF-1 and TGF-β1 in skeletal muscle during the repair process', *Lasers in Medical Science,* 28(3), pp. 725-734.

M, G. (1978) *Optical spectra and electronic structure of porphyrins and related rings. In: The Porphyrins* 3 edn. New York: New York: Academic Press, p. 1-16.

Madhavan, H. (2007) 'Simple Laboratory methods to measure cell proliferation using DNA synthesis property', *Journal of stem cells & regenerative medicine,* 3(1), pp. 12-14.

Madhumathi, D. and Santhosh Kumar, M. P. (2018) 'Low-level laser therapy in oral and maxillofacial surgery - A review', *Drug Invention Today,* 10(5), pp. 685-691.

Mah, W., Jiang, G., Olver, D., Cheung, G., Kim, B., Larjava, H. and Häkkinen, L. (2014) 'Human gingival fibroblasts display a non-fibrotic phenotype distinct from skin fibroblasts in three-dimensional cultures', *PloS one,* 9(3), pp. e90715-e90715.

Maldonado, E. Q., Morales, E. C. and Herrera, A. H. (2018) 'Use of low power laser as an adjuvant in the treatment of periapical lesions. Systematic review', *Salud Uninorte,* 34(3), pp. 797-805.

Mamalis, A., Garcha, M. and Jagdeo, J. (2015) 'Light emitting diode-generated blue light modulates fibrosis characteristics: fibroblast proliferation, migration speed, and reactive oxygen species generation', *Lasers Surg Med,* 47(2), pp. 210-5.
Mamalis, A., Koo, E., Garcha, M., Murphy, W. J., Isseroff, R. R. and Jagdeo, J. (2016) 'High fluence light emitting diode-generated red light modulates characteristics associated with skin fibrosis', *Journal of Biophotonics,* 9(11-12), pp. 1167-1179.
Marchesan, J. T., Scanlon, C. S., Soehren, S., Matsuo, M. and Kapila, Y. L. (2011) 'Implications of cultured periodontal ligament cells for the clinical and experimental setting: A review', *Archives of Oral Biology,* 56(10), pp. 933-943.
Marengo-Rowe, A. J. (2006) 'Structure-function relations of human hemoglobins', *Proceedings (Baylor University. Medical Center),* 19(3), pp. 239-245.
Marques, M. M., Pereira, A. N., Fujihara, N. A., Nogueira, F. N. and Eduardo, C. P. (2004) 'Effect of Low-Power Laser Irradiation on Protein Synthesis and Ultrastructure of Human Gingival Fibroblasts', *Lasers in Surgery and Medicine,* 34(3), pp. 260-265.
Marques, N. C. T., Neto, N. L., Prado, M. T. O., Vitor, L. L. R., Oliveira, R. C., Sakai, V. T., Santos, C. F., Machado, M. A. A. M. and Oliveira, T. M. (2017) 'Effects of PBM in different energy densities and irradiance on maintaining cell viability and proliferation of pulp fibroblasts from human primary teeth', *Lasers in Medical Science,* 32(7), pp. 1621-1628.
Marson, J. W. and Baldwin, H. E. (2019) 'New Concepts, Concerns, and Creations in Acne', *Dermatologic Clinics,* 37(1), pp. 1-9.
Masha, R. T., Houreld, N. N. and Abrahamse, H. (2013) 'Low-intensity laser irradiation at 660 nm stimulates transcription of genes involved in the electron transport chain', *Photomed Laser Surg,* 31(2), pp. 47-53.
Mashima, I., Theodorea, C. F., Thaweboon, B., Thaweboon, S. and Nakazawa, F. (2016) 'Identification of Veillonella Species in the Tongue Biofilm by Using a Novel One-Step Polymerase Chain Reaction Method', *PloS one,* 11(6), pp. e0157516-e0157516.
Masson-Meyers, D. S., Bumah, V. V., Biener, G., Raicu, V. and Enwemeka, C. S. (2015) 'The relative antimicrobial effect of blue 405 nm LED and blue 405 nm laser on methicillin-resistant Staphylococcus aureus in vitro', *Lasers in Medical Science,* 30(9), pp. 2265-2271.
Masson-Meyers, D. S., Bumah, V. V. and Enwemeka, C. S. (2016a) 'Blue light does not impair wound healing in vitro', *Journal of Photochemistry and Photobiology B: Biology,* 160, pp. 53-60.
Masson-Meyers, D. S., Bumah, V. V. and Enwemeka, C. S. (2016b) 'Blue light does not impair wound healing in vitro', *J Photochem Photobiol B,* 160, pp. 53-60.
Mathews, M. A., Pai, B. S. J. and Benedicenti, S. (2015) 'Effect of photobiomodulation on osseointegration and bone-A review', *Journal of Laser Applications,* 27(1).
Matsusaka, T., Fujikawa, K., Nishio, Y., Mukaida, N., Matsushima, K., Kishimoto, T. and Akira, S. (1993) 'Transcription factors NF-IL6 and NF-κB synergistically activate transcription of the inflammatory cytokines, interleukin 6 and interleukin 8', *Proceedings of the National Academy of Sciences of the United States of America,* 90(21), pp. 10193-10197.
McBain, A. J., Sissons, C., Ledder, R. G., Sreenivasan, P. K., De Vizio, W. and Gilbert, P. (2005) 'Development and characterization of a simple perfused oral microcosm', *J Appl Microbiol,* 98(3), pp. 624-34.
McGee, G. S., Davidson, J. M., Buckley, A., Sommer, A., Woodward, S. C., Aquino, A. M., Barbour, R. and Demetriou, A. A. (1988) 'Recombinant basic fibroblast growth factor accelerates wound healing', *J Surg Res,* 45(1), pp. 145-53.
Meng, M., Yang, M., Lv, C., Yang, Q., Yang, Z. and Chen, S. (2017) 'Effect of Low-Level Laser Therapy on Relapse of Rotated Teeth: A Systematic Review of Human and Animal Study', *Photomedicine and Laser Surgery,* 35(1), pp. 3-11.
Mengel-From, J., Thinggaard, M., Dalgård, C., Kyvik, K. O., Christensen, K. and Christiansen, L. (2014) 'Mitochondrial DNA copy number in peripheral blood cells declines with age and is associated with general health among elderly', *Human genetics,* 133(9), pp. 1149-1159.

Menshikova, E. V., Ritov, V. B., Fairfull, L., Ferrell, R. E., Kelley, D. E. and Goodpaster, B. H. (2006) 'Effects of exercise on mitochondrial content and function in aging human skeletal muscle', *The journals of gerontology. Series A, Biological sciences and medical sciences,* 61(6), pp. 534-540.

Merigo, E., Vescovi, P., Margalit, M., Ricotti, E., Stea, S., Meleti, M., Manfredi, M. and Fornaini, C. (2015) 'Efficacy of LLLT in swelling and pain control after the extraction of lower impacted third molars', *Laser Therapy,* 24(1), pp. 39-46.

Mesquita-Ferrari, R. A., Alves, A. N., de Oliveira Cardoso, V., Artilheiro, P. P., Bussadori, S. K., Rocha, L. A., Nunes, F. D. and Fernandes, K. P. S. (2015) 'Low-level laser irradiation modulates cell viability and creatine kinase activity in C2C12 muscle cells during the differentiation process', *Lasers in Medical Science,* 30(8), pp. 2209-2213.

Mesquita-Ferrari, R. A., Martins, M. D., Silva Jr, J. A., Da Silva, T. D., Piovesan, R. F., Pavesi, V. C. S., Bussadori, S. K. and Fernandes, K. P. S. (2011) 'Effects of low-level laser therapy on expression of TNF-α and TGF-β in skeletal muscle during the repair process', *Lasers in Medical Science,* 26(3), pp. 335-340.

Mester, E., Szende, B. and Gärtner, P. (1968) 'The effect of laser beams on the growth of hair in mice', *Radiobiologia Radiotherapia,* 9(5), pp. 621-626.

Migliario, M., Pittarella, P., Fanuli, M., Rizzi, M. and Renò, F. (2014) 'Laser-induced osteoblast proliferation is mediated by ROS production', *Lasers in Medical Science,* 29(4), pp. 1463-1467.

Migliario, M., Sabbatini, M., Mortellaro, C. and Renò, F. (2018a) 'Near infrared low-level laser therapy and cell proliferation: The emerging role of redox sensitive signal transduction pathways', *Journal of Biophotonics,* 11(11).

Migliario, M., Tonello, S., Rocchetti, V., Rizzi, M. and Renò, F. (2018b) 'Near infrared laser irradiation induces NETosis via oxidative stress and autophagy', *Lasers in Medical Science,* 33(9), pp. 1919-1924.

Mignon, C., Uzunbajakava, N. E., Castellano-Pellicena, I., Botchkareva, N. V. and Tobin, D. J. (2018) 'Differential response of human dermal fibroblast subpopulations to visible and near-infrared light: Potential of photobiomodulation for addressing cutaneous conditions', *Lasers in Surgery and Medicine,* 50(8), pp. 859-882.

Mignon, C., Uzunbajakava, N. E., Raafs, B., Botchkareva, N. V. and Tobin, D. J. (2017) 'Photobiomodulation of human dermal fibroblasts in vitro: decisive role of cell culture conditions and treatment protocols on experimental outcome', *Scientific Reports,* 7, pp. 2797.

Millhouse, E., Jose, A., Sherry, L., Lappin, D. F., Patel, N., Middleton, A. M., Pratten, J., Culshaw, S. and Ramage, G. (2014) 'Development of an in vitro periodontal biofilm model for assessing antimicrobial and host modulatory effects of bioactive molecules', *BMC Oral Health,* 14, pp. 80.

Milward, M. R., Hadis, M. A., Cooper, P. R., Gorecki, P., Carroll, J. D. and Palin, W. M. 'Biomodulatory effects of laser irradiation on dental pulp cells in vitro'. *Progress in Biomedical Optics and Imaging - Proceedings of SPIE*.

Milward, M. R., Holder, M. J., Palin, W. M., Hadis, M. A., Carroll, J. D. and Cooper, P. R. (2014) 'Low Level Light Therapy (LLLT) for the treatment and management of dental and oral diseases', *Dental Update,* 41(9), pp. 763-772.

Milward, M. T., Chapple, I. T. T., Wright, H. T., Millard, J. T., Matthews, J. T. and Cooper, P. R. (2007) 'Differential activation of NF-κB and gene expression in oral epithelial cells by periodontal pathogens', *Clinical and Experimental Immunology,* 148(2), pp. 307-324.

Mittermayr, R., Osipov, A., Piskernik, C., Haindl, S., Dungel, P., Weber, C., Vladimirov, Y. A., Redl, H. and Kozlov, A. V. (2007) 'Blue laser light increases perfusion of a skin flap via release of nitric oxide from hemoglobin', *Molecular Medicine,* 13(1-2), pp. 22-29.

Mize, T. W., Sundararaj, K. P., Leite, R. S. and Huang, Y. (2015) 'Increased and correlated expression of connective tissue growth factor and transforming growth factor beta 1 in surgically removed periodontal tissues with chronic periodontitis', *Journal of periodontal research,* 50(3), pp. 315-319.

Mok, S. F., Karuthan, C., Cheah, Y. K., Ngeow, W. C., Rosnah, Z., Yap, S. F. and Ong, H. K. A. (2017) 'The oral microbiome community variations associated with normal, potentially malignant disorders and malignant lesions of the oral cavity', *Malays J Pathol,* 39(1), pp. 1-15.

Montazeri, K., Mokmeli, S. and Barat, M. (2017) 'The Effect of Combination of Red, Infrared and Blue Wavelengths of Low-Level Laser on Reduction of Abdominal Girth: A Before-After Case Series', *J Lasers Med Sci,* 8(Suppl 1), pp. S22-s26.

Montoro, L. A., Turrioni, A. P. S., Basso, F. G., de Souza Costa, C. A. and Hebling, J. (2014) 'Infrared LED irradiation photobiomodulation of oxidative stress in human dental pulp cells', *International Endodontic Journal,* 47(8), pp. 747-755.

Mookerjee, S. A., Goncalves, R. L. S., Gerencser, A. A., Nicholls, D. G. and Brand, M. D. (2015) 'The contributions of respiration and glycolysis to extracellular acid production', *Biochimica et Biophysica Acta - Bioenergetics,* 1847(2), pp. 171-181.

Moraschini, V., da Costa, L. S. and dos Santos, G. O. (2018) 'Effectiveness for dentin hypersensitivity treatment of non-carious cervical lesions: a meta-analysis', *Clinical Oral Investigations,* 22(2), pp. 617-631.

Morgan, M. J. and Liu, Z.-g. (2011) 'Crosstalk of reactive oxygen species and NF-κB signaling', *Cell Research,* 21(1), pp. 103-115.

Moskvin, S. V. and Apolikhin, O. I. (2018) 'Effectiveness of low level laser therapy for treating male infertility', *BioMedicine (France),* 8(2), pp. 1-15.

Moskvin, S. V., Geynitz, A. V. and Askhadulin, E. V. (2017) 'Efficiency of a new combined laser therapy in patients with trophic ulcers of lower extremities and chronic venous insufficiency', *Journal of Lasers in Medical Sciences,* 8(3), pp. 132-135.

Mosmann, T. (1983) 'Rapid colorimetric assay for cellular growth and survival: application to proliferation and cytotoxicity assays', *J Immunol Methods,* 65(1-2), pp. 55-63.

Muller-Enoch, D. (1997) 'Blue light mediated photoreduction of the flavoprotein NADPH-cytochrome P450 reductase. A Forster-type energy transfer', *Z Naturforsch C,* 52(9-10), pp. 605-14.

Muller, F. L., Liu, Y. and Van Remmen, H. (2004) 'Complex III releases superoxide to both sides of the inner mitochondrial membrane', *J Biol Chem,* 279(47), pp. 49064-73.

Mun, S. E., Sim, B. W., Yoon, S. B., Jeong, P. S., Yang, H. J., Choi, S. A., Park, Y. H., Kim, Y. H., Kang, P., Jeong, K. J., Lee, Y., Jin, Y. B., Song, B. S., Kim, J. S., Huh, J. W., Lee, S. R., Choo, Y. K., Kim, S. U. and Chang, K. T. (2017) 'Dual effect of fetal bovine serum on early development depends on stage-specific reactive oxygen species demands in pigs', *PLoS One,* 12(4), pp. e0175427.

Murakami, S., Takayama, S., Ikezawa, K., Shimabukuro, Y., Kitamura, M., Nozaki, T., Terashima, A., Asano, T. and Okada, H. (1999) 'Regeneration of periodontal tissues by basic fibroblast growth factor', *J Periodontal Res,* 34(7), pp. 425-30.

Murphy, K. (2012) *Janeway's Immunobiology.* 8th edn., p. 86.

Murphy, Michael P. (2009) 'How mitochondria produce reactive oxygen species', *Biochemical Journal,* 417(Pt 1), pp. 1-13.

Mussttaf, R. A., Jenkins, D. F. L. and Jha, A. N. (2019) 'Assessing the impact of low level laser therapy (LLLT) on biological systems: a review', *International Journal of Radiation Biology,* 95(2), pp. 120-143.

Nagpal, R., Yamashiro, Y. and Izumi, Y. (2015) 'The Two-Way Association of Periodontal Infection with Systemic Disorders: An Overview', *Mediators Inflamm,* 2015, pp. 793898.

Najafipour, H., Malek Mohammadi, T., Rahim, F., Haghdoost, A. A., Shadkam, M. and Afshari, M. (2013) 'Association of oral health and cardiovascular disease risk factors "results from a community based study on 5900 adult subjects"', *ISRN cardiology,* 2013, pp. 782126-782126.

Najeeb, S., Zafar, M. S., Khurshid, Z., Zohaib, S. and Almas, K. (2016) 'The Role of Nutrition in Periodontal Health: An Update', *Nutrients,* 8(9), pp. 530.

Namkoong, S., Lee, S. J., Kim, C. K., Kim, Y. M., Chung, H. T., Lee, H., Han, J. A., Ha, K. S., Kwon, Y. G. and Kim, Y. M. (2005) 'Prostaglandin E2 stimulates angiogenesis by activating the nitric oxide/cGMP pathway in human umbilical vein endothelial cells', *Exp Mol Med,* 37(6), pp. 588-600.

Napa, K., Baeder, A. C., Witt, J. E., Rayburn, S. T., Miller, M. G., Dallon, B. W., Gibbs, J. L., Wilcox, S. H., Winden, D. R., Smith, J. H., Reynolds, P. R. and Bikman, B. T. (2017) 'LPS from P. gingivalis Negatively Alters Gingival Cell Mitochondrial Bioenergetics', *Int J Dent,* 2017, pp. 2697210.

Naylor, A. J., Filer, A. and Buckley, C. D. (2013) 'The role of stromal cells in the persistence of chronic inflammation', *Clin Exp Immunol,* 171(1), pp. 30-5.

Neutsch, L., Kroll, P., Brunner, M., Pansy, A., Kovar, M., Herwig, C. and Klein, T. (2018) 'Media photo-degradation in pharmaceutical biotechnology - impact of ambient light on media quality, cell physiology, and IgG production in CHO cultures', *Journal of chemical technology and biotechnology (Oxford, Oxfordshire : 1986),* 93(8), pp. 2141-2151.

Nguyen, L. M. D., Malamo, A. G., Larkin-Kaiser, K. A., Borsa, P. A. and Adhihetty, P. J. (2014) 'Effect of near-infrared light exposure on mitochondrial signaling in C<inf>2</inf>C<inf>12</inf> muscle cells', *Mitochondrion,* 14(1), pp. 42-48.

Nielsen, H. I. and Bertheussen, K. (1991) 'DEGRADING EFFECT OF LIGHT ON CELL CULTURE MEDIA', in Spier, R.E., Griffiths, J.B. & Meignier, B. (eds.) *Production of Biologicals from Animal Cells in Culture*: Butterworth-Heinemann, pp. 82-84.

Nielsen, O. S. and Overgaard, J. (1982) 'Influence of time and temperature on the kinetics of thermotolerance in L1A2 cells in vitro', *Cancer Res,* 42(10), pp. 4190-6.

Niu, T., Tian, Y., Cai, Q., Ren, Q. and Wei, L. (2015) 'Red light combined with blue light irradiation regulates proliferation and apoptosis in skin keratinocytes in combination with low concentrations of curcumin', *PLoS ONE,* 10(9).

Nobbs, A. H., Jenkinson, H. F. and Jakubovics, N. S. (2011) 'Stick to your gums: Mechanisms of oral microbial adherence', *Journal of Dental Research,* 90(11), pp. 1271-1278.

Nomura, K., Yamaguchi, M. and Abiko, Y. (2001) 'Inhibition of interleukin-1β production and gene expression in human gingival fibroblasts by low-energy laser irradiation', *Lasers in Medical Science,* 16(3), pp. 218-223.

Noursadeghi, M., Tsang, J., Haustein, T., Miller, R. F., Chain, B. M. and Katz, D. R. (2008) 'Quantitative imaging assay for NF-kappaB nuclear translocation in primary human macrophages', *Journal of immunological methods,* 329(1-2), pp. 194-200.

O'Toole, G., Kaplan, H. B. and Kolter, R. 2000. Biofilm formation as microbial development. *Annual Review of Microbiology.*

Ogita, M., Tsuchida, S., Aoki, A., Satoh, M., Kado, S., Sawabe, M., Nanbara, H., Kobayashi, H., Takeuchi, Y., Mizutani, K., Sasaki, Y., Nomura, F. and Izumi, Y. (2014) 'Increased cell proliferation and differential protein expression induced by low-level Er:YAG laser irradiation in human gingival fibroblasts: proteomic analysis', *Lasers in Medical Science,* 30(7), pp. 1855-1866.

Ohnishi, S. T., Ohnishi, T., Muranaka, S., Fujita, H., Kimura, H., Uemura, K., Yoshida, K. and Utsumi, K. (2005) 'A possible site of superoxide generation in the complex I segment of rat heart mitochondria', *J Bioenerg Biomembr,* 37(1), pp. 1-15.

Ohnishi, T. (1998) 'Iron–sulfur clusters/semiquinones in Complex I', *Biochimica et Biophysica Acta (BBA) - Bioenergetics,* 1364(2), pp. 186-206.

Omata, Y., Lewis, J. B., Rotenberg, S., Lockwood, P. E., Messer, R. L., Noda, M., Hsu, S. D., Sano, H. and Wataha, J. C. (2006) 'Intra- and extracellular reactive oxygen species generated by blue light', *J Biomed Mater Res A,* 77(3), pp. 470-7.

Onodera, Y., Teramura, T., Takehara, T., Shigi, K. and Fukuda, K. (2015) 'Reactive oxygen species induce Cox-2 expression via TAK1 activation in synovial fibroblast cells', *FEBS open bio,* 5, pp. 492-501.

Oplander, C., Deck, A., Volkmar, C. M., Kirsch, M., Liebmann, J., Born, M., van Abeelen, F., van Faassen, E. E., Kroncke, K. D., Windolf, J. and Suschek, C. V. (2013) 'Mechanism and biological relevance of blue-light (420-453 nm)-induced nonenzymatic nitric oxide generation from photolabile nitric oxide derivates in human skin in vitro and in vivo', *Free Radic Biol Med,* 65, pp. 1363-1377.

Osborne, N. N., Nunez-Alvarez, C. and Del Olmo-Aguado, S. (2014) 'The effect of visual blue light on mitochondrial function associated with retinal ganglions cells', *Exp Eye Res,* 128, pp. 8-14.

Oton-Leite, A. F., Silva, G. B. L., Morais, M. O., Silva, T. A., Leles, C. R., Valadares, M. C., Pinezi, J. C. D., Batista, A. C. and Mendonça, E. F. (2015) 'Effect of low-level laser therapy on chemoradiotherapy-induced oral mucositis and salivary inflammatory mediators in head and neck cancer patients', *Lasers in Surgery and Medicine,* 47(4), pp. 296-305.

Palaiologou, A. A., Yukna, R. A., Moses, R. and Lallier, T. E. (2001) 'Gingival, dermal, and periodontal ligament fibroblasts express different extracellular matrix receptors', *J Periodontol,* 72(6), pp. 798-807.

Palin, W. M., Hadis, M. A., Milward, M. R., Carroll, J. D. and Cooper, P. R. 'Beam profile measurements for dental phototherapy: The effect of distance, wavelength and tissue thickness'. *Progress in Biomedical Optics and Imaging - Proceedings of SPIE*.

Palm, E., Khalaf, H. and Bengtsson, T. (2013) 'Porphyromonas gingivalis downregulates the immune response of fibroblasts', *BMC Microbiol,* 13, pp. 155.

Palmer, R. J., Jr. (2014) 'Composition and development of oral bacterial communities', *Periodontology 2000,* 64(1), pp. 20-39.

Pamuk, F., Lutfioglu, M., Aydogdu, A., Koyuncuoglu, C. Z., Cifcibasi, E. and Badur, O. S. (2017) 'The effect of low-level laser therapy as an adjunct to non-surgical periodontal treatment on gingival crevicular fluid levels of transforming growth factor-beta 1, tissue plasminogen activator and plasminogen activator inhibitor 1 in smoking and non-smoking chronic periodontitis patients: A split-mouth, randomized control study', *J Periodontal Res,* 52(5), pp. 872-882.

Pandeshwar, P., Roa, M. D., Das, R., Shastry, S. P., Kaul, R. and Srinivasreddy, M. B. (2016) 'Photobiomodulation in oral medicine: a review', *Journal of investigative and clinical dentistry,* 7(2), pp. 114-126.

Pansani, T. N., Basso, F. G., Soares, D. G., Turrioni, A. P. S., Hebling, J. and de Souza Costa, C. A. (2018) 'Photobiomodulation in the Metabolism of Lipopolysaccharides-exposed Epithelial Cells and Gingival Fibroblasts', *Photochemistry and Photobiology,* 94(3), pp. 598-603.

Pansani, T. N., Basso, F. G., Turirioni, A. P. S., Kurachi, C., Hebling, J. and De Souza Costa, C. A. (2014) 'Effects of low-level laser therapy on the proliferation and apoptosis of gingival fibroblasts treated with zoledronic acid', *International Journal of Oral and Maxillofacial Surgery,* 43(8), pp. 1030-1034.

Pansani, T. N., Basso, F. G., Turrioni, A. P. S., Soares, D. G., Hebling, J. and de Souza Costa, C. A. (2017) 'Effects of low-level laser therapy and epidermal growth factor on the activities of gingival fibroblasts obtained from young or elderly individuals', *Lasers in Medical Science,* 32(1), pp. 45-52.

Park, J. T. and Hong, K. S. (2014) 'Effect of light-emitting-diode irradiation on the proliferation and migration in human gingival fibroblasts', *Tissue Engineering and Regenerative Medicine,* 12(1), pp. 37-42.

Pastore, D., Greco, M. and Passarella, S. (2000) 'Specific helium-neon laser sensitivity of the purified cytochrome c oxidase', *Int J Radiat Biol,* 76(6), pp. 863-70.

Patton, M. G., Gillum, T. L., Szymanski, M. C., Gould, L. M., Lauterbach, C. J., Vaughan, R. A. and Kuennen, M. R. (2018) 'Heat acclimation increases mitochondrial respiration capacity of

C2C12 myotubes and protects against LPS-mediated energy deficit', *Cell Stress and Chaperones,* 23(5), pp. 871-883.
Pegau, W. S., Gray, D. and Zaneveld, J. R. (1997) 'Absorption and attenuation of visible and near-infrared light in water: dependence on temperature and salinity', *Appl Opt,* 36(24), pp. 6035-46.
Penn, J. W., Grobbelaar, A. O. and Rolfe, K. J. (2012) 'The role of the TGF-β family in wound healing, burns and scarring: a review', *International journal of burns and trauma,* 2(1), pp. 18-28.
Peralta-Mamani, M., da Silva, B. M., da Silva Pinto, A. C., Rubira-Bullen, I. R. F., Honório, H. M., Rubira, C. M. F. and da Silva Santos, P. S. (2019) 'Low-level laser therapy dosimetry most used for oral mucositis due to radiotherapy for head and neck cancer: A systematic review', *Critical Reviews in Oncology/Hematology,* 138, pp. 14-23.
Persson, G. R. (2012) 'Rheumatoid arthritis and periodontitis - inflammatory and infectious connections. Review of the literature', *Journal of Oral Microbiology,* 4(2012).
Pfaff, S., Liebmann, J., Born, M., Merk, H. F. and Von Felbert, V. (2015) 'Prospective Randomized Long-Term Study on the Efficacy and Safety of UV-Free Blue Light for Treating Mild Psoriasis Vulgaris', *Dermatology,* 231(1), pp. 24-34.
Phipps, R. P., Borrello, M. A. and Blieden, T. M. (1997) 'Fibroblast heterogeneity in the periodontium and other tissues', *J Periodontal Res,* 32(1 Pt 2), pp. 159-65.
Picard, M., Taivassalo, T., Gouspillou, G. and Hepple, R. T. (2011) 'Mitochondria: isolation, structure and function', *J Physiol,* 589(Pt 18), pp. 4413-21.
Pizzorno, J. (2014) 'Mitochondria-Fundamental to Life and Health', *Integrative medicine (Encinitas, Calif.),* 13(2), pp. 8-15.
Pope, R. M. and Fry, E. S. (1997) 'Absorption spectrum (380-700 nm) of pure water. II. Integrating cavity measurements', *Appl Opt,* 36(33), pp. 8710-23.
Porteous, M. S. and Rowe, D. J. (2014) 'Adjunctive use of the diode laser in non-surgical periodontal therapy: exploring the controversy', *Journal of dental hygiene : JDH,* 88(2), pp. 78-86.
Pourzarandian, A., Watanabe, H., Ruwanpura, S. M. P. M., Aoki, A. and Ishikawa, I. (2005) 'Effect of low-level Er:YAG laser irradiation on cultured human gingival fibroblasts', *Journal of Periodontology,* 76(2), pp. 187-193.
Prados-Frutos, J. C., Rodríguez-Molinero, J., Prados-Privado, M., Torres, J. H. and Rojo, R. (2016) 'Lack of clinical evidence on low-level laser therapy (LLLT) on dental titanium implant: a systematic review', *Lasers in Medical Science,* 31(2), pp. 383-392.
Preshaw, P. M., Foster, N. and Taylor, J. J. (2007) 'Cross-susceptibility between periodontal disease and type 2 diabetes mellitus: An immunobiological perspective', *Periodontology 2000,* 45(1), pp. 138-157.
Prianti Jr, A. C. G., Silva Jr, J. A., Dos Santos, R. F., Rosseti, I. B. and Costa, M. S. (2014) 'Low-level laser therapy (LLLT) reduces the COX-2 mRNA expression in both subplantar and total brain tissues in the model of peripheral inflammation induced by administration of carrageenan', *Lasers in Medical Science,* 29(4), pp. 1397-1403.
Priglinger, E., Maier, J., Chaudary, S., Lindner, C., Wurzer, C., Rieger, S., Redl, H., Wolbank, S. and Dungel, P. (2018) 'Photobiomodulation of freshly isolated human adipose tissue-derived stromal vascular fraction cells by pulsed light-emitting diodes for direct clinical application', *Journal of Tissue Engineering and Regenerative Medicine,* 12(6), pp. 1352-1362.
Pyo, S. J., Song, W. W., Kim, I. R., Park, B. S., Kim, C. H., Shin, S. H., Chung, I. K. and Kim, Y. D. (2013) 'Low-level laser therapy induces the expressions of BMP-2, osteocalcin, and TGF-β1 in hypoxic-cultured human osteoblasts', *Lasers in Medical Science,* 28(2), pp. 543-550.
Qamruddin, I., Alam, M. K., Abdullah, H., Kamran, M. A., Jawaid, N. and Mahroof, V. (2018) 'Effects of single-dose, low-level laser therapy on pain associated with the initial stage of fixed orthodontic treatment: A randomized clinical trial', *Korean journal of orthodontics,* 48(2), pp. 90-97.

Quirk, B. J. and Whelan, H. T. (2016) 'Effect of Red-to-Near Infrared Light on the Reaction of Isolated Cytochrome c Oxidase with Cytochrome c', *Photomed Laser Surg,* 34(12), pp. 631-637.

Quoilin, C., Mouithys-Mickalad, A., Lecart, S., Fontaine-Aupart, M. P. and Hoebeke, M. (2014) 'Evidence of oxidative stress and mitochondrial respiratory chain dysfunction in an in vitro model of sepsis-induced kidney injury', *Biochim Biophys Acta,* 1837(10), pp. 1790-800.

Rafiei, M., Kiani, F., Sayehmiri, F., Sayehmiri, K., Sheikhi, A. and Zamanian Azodi, M. (2017) 'Study of Porphyromonas gingivalis in periodontal diseases: A systematic review and meta-analysis', *Medical journal of the Islamic Republic of Iran,* 31, pp. 62-62.

Rai, Y., Pathak, R., Kumari, N., Sah, D. K., Pandey, S., Kalra, N., Soni, R., Dwarakanath, B. S. and Bhatt, A. N. (2018) 'Mitochondrial biogenesis and metabolic hyperactivation limits the application of MTT assay in the estimation of radiation induced growth inhibition', *Sci Rep,* 8(1), pp. 1531.

Rashid, M. M., Runci, A., Polletta, L., Carnevale, I., Morgante, E., Foglio, E., Arcangeli, T., Sansone, L., Russo, M. A. and Tafani, M. (2015) 'Muscle LIM protein/CSRP3: a mechanosensor with a role in autophagy', *Cell Death Discov,* 1, pp. 15014.

Rastogi, R. P., Richa, Kumar, A., Tyagi, M. B. and Sinha, R. P. (2010) 'Molecular mechanisms of ultraviolet radiation-induced DNA damage and repair', *J Nucleic Acids,* 2010, pp. 592980.

Ren, C., McGrath, C., Jin, L., Zhang, C. and Yang, Y. (2016) 'Effect of diode low-level lasers on fibroblasts derived from human periodontal tissue: a systematic review of in vitro studies', *Lasers Med Sci,* 31(7), pp. 1493-510.

Ren, C., McGrath, C., Jin, L., Zhang, C. and Yang, Y. (2017) 'The effectiveness of low-level laser therapy as an adjunct to non-surgical periodontal treatment: a meta-analysis', *Journal of Periodontal Research,* 52(1), pp. 8-20.

Rhee, C., Chang, S.-Y., Ahn, J.-C., Suh, M.-W. and Jung, J. Y. (2014) *Effect of LLLT on the level of ATP and ROS from organ of corti cells. SPIE BiOS*: SPIE, p. PWB.

Ribeiro, B. G., Alves, A. N., Dos Santos, L. A., Cantero, T. M., Fernandes, K. P., Dias, D. a., Bernardes, N., De Angelis, K. and Mesquita-Ferrari, R. A. (2016) 'Red and Infrared Low-Level Laser Therapy Prior to Injury with or without Administration after Injury Modulate Oxidative Stress during the Muscle Repair Process', *PloS one,* 11(4), pp. e0153618.

Riss, T. L., Moravec, R. A., Niles, A. L., Duellman, S., Benink, H. A., Worzella, T. J. and Minor, L. (2004) 'Cell Viability Assays', in Sittampalam, G.S., Coussens, N.P., Brimacombe, K., Grossman, A., Arkin, M., Auld, D., Austin, C., Baell, J., Bejcek, B., Chung, T.D.Y., Dahlin, J.L., Devanaryan, V., Foley, T.L., Glicksman, M., Hall, M.D., Hass, J.V., Inglese, J., Iversen, P.W., Kahl, S.D., Kales, S.C., Lal-Nag, M., Li, Z., McGee, J., McManus, O., Riss, T., Trask, O.J., Jr., Weidner, J.R., Xia, M. & Xu, X. (eds.) *Assay Guidance Manual*. Bethesda (MD): Eli Lilly & Company and the National Center for Advancing Translational Sciences.

Robijns, J., Censabella, S., Bulens, P., Maes, A. and Mebis, J. (2017) 'The use of low-level light therapy in supportive care for patients with breast cancer: review of the literature', *Lasers in Medical Science,* 32(1), pp. 229-242.

Robin, E. D. and Wong, R. (1988) 'Mitochondrial DNA molecules and virtual number of mitochondria per cell in mammalian cells', *J Cell Physiol,* 136(3), pp. 507-13.

Rocca, J. P., Zhao, M., Fornaini, C., Tan, L., Zhao, Z. and Merigo, E. (2018) 'Effect of laser irradiation on aphthae pain management: A four different wavelengths comparison', *J Photochem Photobiol B,* 189, pp. 1-4.

Rocha, J. G., dos Santos, P., Paiva, W. S. and Teixeira, M. J. (2018) 'Transcranial light-emitting diode therapy for neuropsychological improvement after traumatic brain injury: A new perspective for diffuse axonal lesion management', *Medical Devices: Evidence and Research,* 11, pp. 139-146.

Rogers, J. E., Stogie, J. E., McLean, D. G., Sutherland, R. L., Sankaran, B., Kannan, R., Tan, L. S. and Fleitz, P. A. (2004) 'Understanding the one-photon photophysical properties of a two-photon absorbing chromophore', *Journal of Physical Chemistry A,* 108(26), pp. 5514-5520.

Rohringer, S., Holnthoner, W., Chaudary, S., Slezak, P., Priglinger, E., Strassl, M., Pill, K., Mühleder, S., Redl, H. and Dungel, P. (2017) 'The impact of wavelengths of LED light-therapy on endothelial cells', *Scientific Reports,* 7(1).

Rojas, A., Padidam, M., Cress, D. and Grady, W. M. (2009) 'TGF-beta receptor levels regulate the specificity of signaling pathway activation and biological effects of TGF-beta', *Biochim Biophys Acta,* 1793(7), pp. 1165-73.

Roncati, M., Lauritano, D., Cura, F. and Carinci, F. (2016) 'Evaluation of light-emitting diode (LED-835 NM) application over human gingival fibroblast: an in vitro study', *J Biol Regul Homeost Agents,* 30(2 Suppl 1), pp. 161-7.

Rubinov, A. N. and Afanas'ev, A. A. (2005) 'Nonresonance mechanisms of biological effects of coherent and incoherent light', *Optics and Spectroscopy (English translation of Optika i Spektroskopiya),* 98(6), pp. 943-948.

Rupel, K., Zupin, L., Colliva, A., Kamada, A., Poropat, A., Ottaviani, G., Gobbo, M., Fanfoni, L., Gratton, R., Santoro, M., Di Lenarda, R., Biasotto, M. and Zacchigna, S. (2018) 'Photobiomodulation at multiple wavelengths differentially modulates oxidative stress in vitro and in vivo', *Oxidative Medicine and Cellular Longevity,* 2018.

Sage, E., Girard, P. M. and Francesconi, S. (2012) 'Unravelling UVA-induced mutagenesis', *Photochem Photobiol Sci,* 11(1), pp. 74-80.

Sahingur, S. E. and Yeudall, W. A. (2015) 'Chemokine function in periodontal disease and oral cavity cancer', *Frontiers in Immunology,* 6(MAY).

Sakaki, H., Matsumiya, T., Kusumi, A., Imaizumi, T., Satoh, H., Yoshida, H., Satoh, K. and Kimura, H. (2004) 'Interleukin-1beta induces matrix metalloproteinase-1 expression in cultured human gingival fibroblasts: role of cyclooxygenase-2 and prostaglandin E2', *Oral Dis,* 10(2), pp. 87-93.

Sakurai, Y., Yamaguchi, M. and Abiko, Y. (2000) 'Inhibitory effect of low-level laser irradiation on LPS-stimulated prostaglandin E2 production and cyclooxygenase-2 in human gingival fibroblasts', *European Journal of Oral Sciences,* 108(1), pp. 29-34.

Salehpour, F., Ahmadian, N., Rasta, S. H., Farhoudi, M., Karimi, P. and Sadigh-Eteghad, S. (2017) 'Transcranial low-level laser therapy improves brain mitochondrial function and cognitive impairment in D-galactose–induced aging mice', *Neurobiology of Aging,* 58, pp. 140-150.

Salehpour, F., Farajdokht, F., Erfani, M., Sadigh-Eteghad, S., Shotorbani, S. S., Hamblin, M. R., Karimi, P., Rasta, S. H. and Mahmoudi, J. (2018a) 'Transcranial near-infrared photobiomodulation attenuates memory impairment and hippocampal oxidative stress in sleep-deprived mice', *Brain Research,* 1682, pp. 36-43.

Salehpour, F., Mahmoudi, J., Kamari, F., Sadigh-Eteghad, S., Rasta, S. H. and Hamblin, M. R. (2018b) 'Brain Photobiomodulation Therapy: a Narrative Review', *Molecular Neurobiology,* 55(8), pp. 6601-6636.

Sancar, A. (2004) 'Regulation of the mammalian circadian clock by cryptochrome', *J Biol Chem,* 279(33), pp. 34079-82.

Santos, A. S. D., Guimarães-Sousa, L., Costa, M. S., Zamuner, L. F., Sousa, N. C., Hyslop, S., Soares, A. M., Chavantes, M. C., Cogo, J. C. and Zamuner, S. R. (2018) 'Photobiomodulation of local alterations induced by BthTX-I, a phospholipase A2 myotoxin from Bothrops jararacussu snake venom: In vivo and in vitro evaluation', *International Journal of Biological Macromolecules,* 107, pp. 2020-2025.

Santos, L. A., Marcos, R. L., Tomazoni, S. S., Vanin, A. A., Antonialli, F. C., Grandinetti Vdos, S., Albuquerque-Pontes, G. M., de Paiva, P. R., Lopes-Martins, R. A., de Carvalho Pde, T., Bjordal, J. M. and Leal-Junior, E. C. (2014) 'Effects of pre-irradiation of low-level laser therapy with different doses and wavelengths in skeletal muscle performance, fatigue, and skeletal muscle damage induced by tetanic contractions in rats', *Lasers Med Sci,* 29(5), pp. 1617-26.

Santos, T., Ferreira, R., Quartin, E., Boto, C., Saraiva, C., Bragança, J., Peça, J., Rodrigues, C., Ferreira, L. and Bernardino, L. (2017) 'Blue light potentiates neurogenesis induced by retinoic acid-loaded responsive nanoparticles', *Acta Biomaterialia,* 59, pp. 293-302.

Saygun, I., Karacay, S., Serdar, M., Ural, A. U., Sencimen, M. and Kurtis, B. (2008) 'Effects of laser irradiation on the release of basic fibroblast growth factor (bFGF), insulin like growth factor-1 (IGF-1), and receptor of IGF-1 (IGFBP3) from gingival fibroblasts', *Lasers in Medical Science,* 23(2), pp. 211-215.

Sazanov, L. A. (2015) 'A giant molecular proton pump: Structure and mechanism of respiratory complex I', *Nature Reviews Molecular Cell Biology,* 16(6), pp. 375-388.

Schaefer, A. S., Richter, G. M., Nothnagel, M., Laine, M. L., Noack, B., Glas, J., Schrezenmeir, J., Groessner-Schreiber, B., Jepsen, S., Loos, B. G. and Schreiber, S. (2010) 'COX-2 is associated with periodontitis in Europeans', *J Dent Res,* 89(4), pp. 384-8.

Schafer, M. E. and McNeely, T. 'Coincident Light/ultrasound therapy to treat bacterial biofilms'. *2015 IEEE International Ultrasonics Symposium, IUS 2015*.

Schartinger, V. H., Galvan, O., Riechelmann, H. and Dudás, J. (2012) 'Differential responses of fibroblasts, non-neoplastic epithelial cells, and oral carcinoma cells to low-level laser therapy', *Supportive Care in Cancer,* 20(3), pp. 523-529.

Schnedeker, A. H., Cole, L. K., Lorch, G., Diaz, S. F., Bonagura, J. and Daniels, J. B. (2017) 'In vitro bactericidal activity of blue light (465 nm) phototherapy on meticillin-susceptible and meticillin-resistant Staphylococcus pseudintermedius', *Vet Dermatol,* 28(5), pp. 463-e106.

Schoenly, J. E., Seka, W. and Rechmann, P. (2014) 'Pulsed laser ablation of dental calculus in the near ultraviolet', *J Biomed Opt,* 19(2), pp. 028003.

Schoneich, C., Dremina, E., Galeva, N. and Sharov, V. (2014) 'Apoptosis in differentiating C2C12 muscle cells selectively targets Bcl-2-deficient myotubes', *Apoptosis : an international journal on programmed cell death,* 19(1), pp. 42-57.

Schwarz, H., Gornicec, J., Neuper, T., Parigiani, M. A., Wallner, M., Duschl, A. and Horejs-Hoeck, J. (2017) 'Biological Activity of Masked Endotoxin', *Scientific reports,* 7, pp. 44750-44750.

Scragg, M. A., Cannon, S. J., Rangarajan, M., Williams, D. M. and Curtis, M. A. (1999) 'Targeted disruption of fibronectin-integrin interactions in human gingival fibroblasts by the RI protease of Porphyromonas gingivalis W50', *Infect Immun,* 67(4), pp. 1837-43.

Sebbe, P. F., Villaverde, A. B., Moreira, L. M., Barbosa, A. M. and Veissid, N. (2009) 'Characterization of a novel LEDs device prototype for neonatal jaundice and its comparison with fluorescent lamps sources: Phototherapy treatment of hyperbilirubinemia in Wistar rats', *Spectroscopy,* 23(5-6), pp. 243-255.

Seifi, M. and Vahid-Dastjerdi, E. (2015) 'Tooth movement alterations by different low level laser protocols: A literature review', *Journal of Lasers in Medical Sciences,* 6(1), pp. 1-5.

Serrage, H., Joanisse, S., Cooper, P. R., Palin, W., Hadis, M., Darch, O., Philp, A. and Milward, M. R. (2019a) 'Differential Responses of Myoblasts and Myotubes to Photobiomodulation are associated with Mitochondrial Number', *J Biophotonics*, pp. e201800411.

Serrage, H. J., Joanisse, S., Cooper, P. R., Palin, W., Hadis, M., Darch, O., Philp, A. and Milward, M. R. (2019b) 'Differential responses of myoblasts and myotubes to photobiomodulation are associated with mitochondrial number', *J Biophotonics*, pp. e201800411.

Sexton, D. J., Muruganandam, A., McKenney, D. J. and Mutus, B. (1994) 'Visible light photochemical release of nitric oxide from S-nitrosoglutathione: potential photochemotherapeutic applications', *Photochem Photobiol,* 59(4), pp. 463-7.

Shaddox, L. M. and Walker, C. B. (2010) 'Treating chronic periodontitis: current status, challenges, and future directions', *Clinical, cosmetic and investigational dentistry,* 2, pp. 79-91.

Sharif, O., Bolshakov, V. N., Raines, S., Newham, P. and Perkins, N. D. (2007) 'Transcriptional profiling of the LPS induced NF-kappaB response in macrophages', *BMC immunology,* 8, pp. 1-1.

Sharma, S. K., Kharkwal, G. B., Sajo, M., Huang, Y.-Y., De Taboada, L., McCarthy, T. and Hamblin, M. R. (2011a) 'Dose response effects of 810 nm laser light on mouse primary cortical neurons', *Lasers in surgery and medicine,* 43(8), pp. 851-859.

Sharma, S. K., Kharkwal, G. B., Sajo, M., Huang, Y. Y., De Taboada, L., McCarthy, T. and Hamblin, M. R. (2011b) 'Dose response effects of 810 nm laser light on mouse primary cortical neurons', *Lasers Surg Med,* 43(8), pp. 851-9.

Sharma, S. K., Kharkwal, G. B., Sajo, M., Huang, Y. Y., De Taboada, L., McCarthy, T. and Hamblin, M. R. (2011c) 'Dose response effects of 810nm laser light on mouse primary cortical neurons', *Lasers in Surgery and Medicine,* 43(8), pp. 851-859.

Shearman, M. S., Hawtin, S. R. and Tailor, V. J. (1995) 'The Intracellular Component of Cellular 3-(4,5-Dimethylthiazol-2-yl)-2,5-Diphenyltetrazolium Bromide (MTT) Reduction Is Specifically Inhibited by β-Amyloid Peptides', *Journal of Neurochemistry,* 65(1), pp. 218-227.

Shelton, P. and Jaiswal, A. K. (2013) 'The transcription factor NF-E2-related factor 2 (Nrf2): a protooncogene?', *FASEB journal : official publication of the Federation of American Societies for Experimental Biology,* 27(2), pp. 414-423.

Shimono, M., Ishikawa, T., Enokiya, Y., Muramatsu, T., Matsuzaka, K., Inoue, T., Abiko, Y., Yamaza, T., Kido, M. A., Tanaka, T. and Hashimoto, S. (2003) 'Biological characteristics of the junctional epithelium', *J Electron Microsc (Tokyo),* 52(6), pp. 627-39.

Shu, C. W., Chang, H. T., Wu, C. S., Chen, C. H., Wu, S., Chang, H. W., Kuo, S. Y., Fu, E., Liu, P. F. and Hsieh, Y. D. (2016) 'RelA-mediated BECN1 expression is required for reactive oxygen species-induced autophagy in oral cancer cells exposed to low-power laser irradiation', *PLoS ONE,* 11(9).

Shuvaeva, V. N., Gorshkova, O. P., Kostylev, A. V. and Dvoretsky, D. P. (2011) 'Effect of laser irradiation on adrenoreactivity of pial arterial vessels in rats', *Bull Exp Biol Med,* 151(1), pp. 1-4.

Sieuwerts, A. M., Klijn, J. G., Peters, H. A. and Foekens, J. A. (1995) 'The MTT tetrazolium salt assay scrutinized: how to use this assay reliably to measure metabolic activity of cell cultures in vitro for the assessment of growth characteristics, IC50-values and cell survival', *Eur J Clin Chem Clin Biochem,* 33(11), pp. 813-23.

Silhavy, T. J., Kahne, D. and Walker, S. (2010) 'The bacterial cell envelope', *Cold Spring Harbor perspectives in biology,* 2(5), pp. a000414-a000414.

Silva, L. M. G., Da Silva, C. A. A., Da Silva, A., Vieira, R. P., Mesquita-Ferrari, R. A., Cogo, J. C. and Zamuner, S. R. (2016) 'Photobiomodulation protects and promotes differentiation of C2C12 myoblast cells exposed to Snake venom', *PLoS ONE,* 11(4).

Silveira, P. C., da Silva, L. A., Pinho, C. A., De Souza, P. S., Ronsani, M. M., Scheffer Dda, L. and Pinho, R. A. (2013) 'Effects of low-level laser therapy (GaAs) in an animal model of muscular damage induced by trauma', *Lasers Med Sci,* 28(2), pp. 431-6.

Sinclair, K. L., Ponsford, J. L., Taffe, J., Lockley, S. W. and Rajaratnam, S. M. W. (2014) 'Randomized controlled trial of light therapy for fatigue following traumatic brain injury', *Neurorehabilitation and Neural Repair,* 28(4), pp. 303-313.

Skaleric, U., Kramar, B., Petelin, M., Pavlica, Z. and Wahl, S. M. (1997) 'Changes in TGF-beta 1 levels in gingiva, crevicular fluid and serum associated with periodontal inflammation in humans and dogs', *Eur J Oral Sci,* 105(2), pp. 136-42.

Skondra, F. G., Koletsi, D., Eliades, T. and Farmakis, E. T. R. (2018) 'The Effect of Low-Level Laser Therapy on Bone Healing after Rapid Maxillary Expansion: A Systematic Review', *Photomedicine and Laser Surgery,* 36(2), pp. 61-71.

Slater, T. F., Sawyer, B. and Straeuli, U. (1963) 'STUDIES ON SUCCINATE-TETRAZOLIUM REDUCTASE SYSTEMS. III. POINTS OF COUPLING OF FOUR DIFFERENT TETRAZOLIUM SALTS', *Biochim Biophys Acta,* 77, pp. 383-93.

Smith, A. J., Jackson, M. S. and Bagg, J. (2001) 'The ecology of Staphylococcus species in the oral cavity', *J Med Microbiol,* 50(11), pp. 940-6.

Smith, P. C., Guerrero, J., Tobar, N., Caceres, M., Gonzalez, M. J. and Martinez, J. (2009) 'Tumor necrosis factor-alpha-stimulated membrane type 1-matrix metalloproteinase production is modulated by epidermal growth factor receptor signaling in human gingival fibroblasts', *J Periodontal Res,* 44(1), pp. 73-80.

Smith, P. C., Martínez, C., Martínez, J. and McCulloch, C. A. (2019) 'Role of Fibroblast Populations in Periodontal Wound Healing and Tissue Remodeling', *Frontiers in physiology,* 10, pp. 270-270.

Sobouti, F., Khatami, M., Heydari, M. and Barati, M. (2015) 'The role of low-level laser in periodontal surgeries', *Journal of Lasers in Medical Sciences,* 6(2), pp. 45-50.

Socransky, S. S., Haffajee, A. D., Cugini, M. A., Smith, C. and Kent, R. L., Jr. (1998) 'Microbial complexes in subgingival plaque', *J Clin Periodontol,* 25(2), pp. 134-44.

Sohn, H., Ko, Y., Park, M., Kim, D., Moon, Y. L., Jeong, Y. J., Lee, H., Moon, Y., Jeong, B. C., Kim, O. and Lim, W. (2015) 'Effects of light-emitting diode irradiation on RANKL-induced osteoclastogenesis', *Lasers in Surgery and Medicine,* 47(9), pp. 745-755.

Soleimani, M., Abbasnia, E., Fathi, M., Sahraei, H., Fathi, Y. and Kaka, G. (2012) 'The effects of low-level laser irradiation on differentiation and proliferation of human bone marrow mesenchymal stem cells into neurons and osteoblasts--an in vitro study', *Lasers Med Sci,* 27(2), pp. 423-30.

Song, H.-H., Lee, J.-K., Um, H.-S., Chang, B.-S., Lee, S.-Y. and Lee, M.-K. (2013) 'Phototoxic effect of blue light on the planktonic and biofilm state of anaerobic periodontal pathogens', *Journal of Periodontal & Implant Science,* 43(2), pp. 72-78.

Song, S., Zhou, F. and Chen, W. R. (2012) 'Low-level laser therapy regulates microglial function through Src-mediated signaling pathways: Implications for neurodegenerative diseases', *Journal of Neuroinflammation,* 9.

Sonis, S. T., Hashemi, S., Epstein, J. B., Nair, R. G. and Raber-Durlacher, J. E. (2016) 'Could the biological robustness of low level laser therapy (Photobiomodulation) impact its use in the management of mucositis in head and neck cancer patients', *Oral Oncology,* 54, pp. 7-14.

Spanemberg, J. C., de Figueiredo, M. A. Z., Cherubini, K. and Salum, F. G. (2016) 'Low-level laser therapy: A review of its applications in the management of oral mucosal disorders', *Alternative Therapies in Health and Medicine,* 22(6), pp. 24-31.

Spicer, P. P., Shah, S. R., Henslee, A. M., Watson, B. M., Kinard, L. A., Kretlow, J. D., Bevil, K., Kattchee, L., Bennett, G. N., Demian, N., Mende, K., Murray, C. K., Jansen, J. A., Wong, M. E., Mikos, A. G. and Kasper, F. K. (2013) 'Evaluation of antibiotic releasing porous polymethylmethacrylate space maintainers in an infected composite tissue defect model', *Acta Biomaterialia,* 9(11), pp. 8832-8839.

Spitler, R. and Berns, M. W. (2014) 'Comparison of laser and diode sources for acceleration of in vitro wound healing by low-level light therapy', *J Biomed Opt,* 19(3), pp. 38001.

Spitler, R., Ho, H., Norpetlian, F., Kong, X., Jiang, J., Yokomori, K., Andersen, B., Boss, G. R. and Berns, M. W. (2015) 'Combination of low level light therapy and nitrosyl-cobinamide accelerates wound healing', *Journal of Biomedical Optics,* 20(5).

Spolarics, Z. and Wu, J. X. (1997) 'Role of glutathione and catalase in H2O2 detoxification in LPS-activated hepatic endothelial and Kupffer cells', *Am J Physiol,* 273(6 Pt 1), pp. G1304-11.

Springer, J. E., Azbill, R. D. and Carlson, S. L. (1998) 'A rapid and sensitive assay for measuring mitochondrial metabolic activity in isolated neural tissue', *Brain Res Brain Res Protoc,* 2(4), pp. 259-63.

Srinivasan, R., Karaoz, U., Volegova, M., MacKichan, J., Kato-Maeda, M., Miller, S., Nadarajan, R., Brodie, E. L. and Lynch, S. V. (2015) 'Use of 16S rRNA Gene for Identification of a Broad Range of Clinically Relevant Bacterial Pathogens', *PLoS ONE,* 10(2), pp. e0117617.

Srivastava, V. K. and Mahajan, S. (2014) 'Diode lasers: A magical wand to an orthodontic practice', *Indian Journal of Dental Research,* 25(1), pp. 78-82.

Stack, E. and DuBois, R. N. (2001) 'Regulation of cyclo-oxygenase-2', *Best Practice and Research: Clinical Gastroenterology,* 15(5), pp. 787-800.

Suliman, H. B., Carraway, M. S., Welty-Wolf, K. E., Whorton, A. R. and Piantadosi, C. A. (2003) 'Lipopolysaccharide stimulates mitochondrial biogenesis via activation of nuclear respiratory factor-1', *J Biol Chem,* 278(42), pp. 41510-8.

Sullivan, L. B. and Chandel, N. S. (2014) 'Mitochondrial reactive oxygen species and cancer', *Cancer & Metabolism,* 2, pp. 17.

Sulyanto, R. M., Thompson, Z. A., Beall, C. J., Leys, E. J. and Griffen, A. L. (2019) 'The Predominant Oral Microbiota Is Acquired Early in an Organized Pattern', *Scientific Reports,* 9(1), pp. 10550.

Sun, X., Mao, Y., Dai, P., Li, X., Gu, W., Wang, H., Wu, G., Ma, J. and Huang, S. (2017) 'Mitochondrial dysfunction is involved in the aggravation of periodontitis by diabetes', *J Clin Periodontol,* 44(5), pp. 463-471.

Sung, L., Robinson, P., Treister, N., Baggott, T., Gibson, P., Tissing, W., Wiernikowski, J., Brinklow, J. and Dupuis, L. L. (2017) 'Guideline for the prevention of oral and oropharyngeal mucositis in children receiving treatment for cancer or undergoing haematopoietic stem cell transplantation', *BMJ Supportive and Palliative Care,* 7(1), pp. 7-16.

Swartz, T. E., Corchnoy, S. B., Christie, J. M., Lewis, J. W., Szundi, I., Briggs, W. R. and Bogomolni, R. A. (2001) 'The photocycle of a flavin-binding domain of the blue light photoreceptor phototropin', *J Biol Chem,* 276(39), pp. 36493-500.

Swidi, A. J., Taylor, R. W., Tadlock, L. P. and Buschang, P. H. (2018) 'Recent Advances in Orthodontic Dental Retention Methods: A Review article', *Journal of the World Federation of Orthodontists,* 7(1), pp. 6-12.

Taflinski, L., Demir, E., Kauczok, J., Fuchs, P. C., Born, M., Suschek, C. V. and Oplander, C. (2014) 'Blue light inhibits transforming growth factor-beta1-induced myofibroblast differentiation of human dermal fibroblasts', *Exp Dermatol,* 23(4), pp. 240-6.

Tafur, J. and Mills, P. J. (2008) 'Low-Intensity Light Therapy: Exploring the Role of Redox Mechanisms', *Photomedicine and Laser Surgery,* 26(4), pp. 323-328.

Takema, T., Yamaguchi, M. and Abiko, Y. (2000) 'Reduction of plasminogen activator activity stimulated by lipopolysaccharide from periodontal pathogen in human gingival fibroblasts by low-energy laser irradiation', *Lasers in Medical Science,* 15(1), pp. 35-42.

Takeshita, M., Haraguchi, A., Miura, M., Hamachi, T., Fukuda, T., Sanui, T., Takano, A. and Nishimura, F. (2017) 'Antibiotic effects against periodontal bacteria in organ cultured tissue', *Clinical and Experimental Dental Research,* 3(1), pp. 5-12.

Takhtfooladi, M. A., Shahzamani, M., Takhtfooladi, H. A., Moayer, F. and Allahverdi, A. (2014) 'Effects of light-emitting diode (LED) therapy on skeletal muscle ischemia reperfusion in rats', *Lasers in Medical Science,* 30(1), pp. 311-316.

Takhtfooladi, M. A. and Sharifi, D. (2015) 'A comparative study of red and blue light-emitting diodes and low-level laser in regeneration of the transected sciatic nerve after an end to end neurorrhaphy in rabbits', *Lasers in Medical Science,* 30(9), pp. 2319-2324.

Tamarova, Z. A., Limansky, Y. and Gulyar, S. A. (2009) 'Antinociceptive effects of color polarized light in animal with formalin test', *Fiziol Zh,* 55(3), pp. 81-93.

Tamura, M., Tokuda, M., Nagaoka, S. and Takada, H. (1992) 'Lipopolysaccharides of Bacteroides intermedius (Prevotella intermedia) and Bacteroides (Porphyromonas) gingivalis induce interleukin-8 gene expression in human gingival fibroblast cultures', *Infect Immun,* 60(11), pp. 4932-7.

Tan, B., Xiao, H., Xiong, X., Wang, J., Li, G., Yin, Y., Huang, B., Hou, Y. and Wu, G. (2015) 'L-arginine improves DNA synthesis in LPS-challenged enterocytes', *Front Biosci (Landmark Ed),* 20, pp. 989-1003.

Tang, B., Wang, K., Jia, Y. P., Zhu, P., Fang, Y., Zhang, Z. J., Mao, X. H., Li, Q. and Zeng, D. Z. (2016) 'Fusobacterium nucleatum-Induced Impairment of Autophagic Flux Enhances the Expression of Proinflammatory Cytokines via ROS in Caco-2 Cells', *PLoS One,* 11(11), pp. e0165701.

Tani, A., Chellini, F., Giannelli, M., Nosi, D., Zecchi-Orlandini, S. and Sassoli, C. (2018) 'Red (635 nm), Near-Infrared (808 nm) and Violet-Blue (405 nm) Photobiomodulation Potentiality on Human Osteoblasts and Mesenchymal Stromal Cells: A Morphological and Molecular In Vitro Study', *Int J Mol Sci,* 19(7).

Tania, S. D. M., Sathiasekar, C., Anison, J. J. and Reddy, B. V. S. (2015) 'The extended tentacles of laser - From diagnosis to treatment in orthodontics: An overview', *Journal of Pharmacy and Bioallied Sciences,* 7(6), pp. S387-S392.

Tatmatsu-Rocha, J. C., Ferraresi, C., Hamblin, M. R., Damasceno Maia, F., do Nascimento, N. R., Driusso, P. and Parizotto, N. A. (2016) 'Low-level laser therapy (904nm) can increase collagen and reduce oxidative and nitrosative stress in diabetic wounded mouse skin', *J Photochem Photobiol B,* 164, pp. 96-102.

Taubman, M. A. and Kawai, T. (2001) 'Involvement of T-lymphocytes in periodontal disease and in direct and indirect induction of bone resorption', *Crit Rev Oral Biol Med,* 12(2), pp. 125-35.

Taupin, P. (2007) 'BrdU immunohistochemistry for studying adult neurogenesis: paradigms, pitfalls, limitations, and validation', *Brain Res Rev,* 53(1), pp. 198-214.

Taylor, J. J., Preshaw, P. M. and Lalla, E. (2013) 'A review of the evidence for pathogenic mechanisms that may link periodontitis and diabetes', *Journal of Clinical Periodontology,* 40(SUPPL. 14), pp. S113-S134.

Tetz, L. M., Kamau, P. W., Cheng, A. A., Meeker, J. D. and Loch-Caruso, R. (2013) 'Troubleshooting the dichlorofluorescein assay to avoid artifacts in measurement of toxicant-stimulated cellular production of reactive oxidant species', *Journal of pharmacological and toxicological methods,* 67(2), pp. 56-60.

Teuschl, A., Balmayor, E. R., Redl, H., Van Griensven, M. and Dungel, P. (2015a) 'Phototherapy with LED light modulates healing processes in an in vitro scratch-wound model using 3 different cell types', *Dermatologic Surgery,* 41(2), pp. 261-268.

Teuschl, A., Balmayor, E. R., Redl, H., van Griensven, M. and Dungel, P. (2015b) 'Phototherapy with LED light modulates healing processes in an in vitro scratch-wound model using 3 different cell types', *Dermatol Surg,* 41(2), pp. 261-8.

Tim, C. R., Bossini, P. S., Kido, H. W., Malavazi, I., von Zeska Kress, M. R., Carazzolle, M. F., Parizotto, N. A. and Rennó, A. C. (2015) 'Effects of low-level laser therapy on the expression of osteogenic genes during the initial stages of bone healing in rats: a microarray analysis', *Lasers in Medical Science,* 30(9), pp. 2325-2333.

Tipton, D. A., Stricklin, G. P. and Dabbous, M. K. (1991) 'Fibroblast heterogeneity in collagenolytic response to cyclosporine', *J Cell Biochem,* 46(2), pp. 152-65.

Toomey, D. P., Murphy, J. F. and Conlon, K. C. (2009) 'COX-2, VEGF and tumour angiogenesis', *Surgeon,* 7(3), pp. 174-80.

Tóthová, L. u. and Celec, P. (2017) 'Oxidative Stress and Antioxidants in the Diagnosis and Therapy of Periodontitis', 8(1055).

Trotter, L. A., Patel, D., Dubin, S., Guerra, C., McCloud, V., Lockwood, P., Messer, R., Wataha, J. C. and Lewis, J. B. (2017) 'Violet/blue light activates Nrf2 signaling and modulates the inflammatory response of THP-1 monocytes', *Photochem Photobiol Sci,* 16(6), pp. 883-889.

Tsai, S.-R. and Hamblin, M. R. (2017) 'Biological effects and medical applications of infrared radiation', *Journal of photochemistry and photobiology. B, Biology,* 170, pp. 197-207.

Tunér, J. and Hode, L. (1998) 'It's all in the parameters: A critical analysis of some well-known negative studies on low-level laser therapy', *Journal of Clinical Laser Medicine and Surgery,* 16(5), pp. 245-248.

Turner, M. D., Nedjai, B., Hurst, T. and Pennington, D. J. (2014) 'Cytokines and chemokines: At the crossroads of cell signalling and inflammatory disease', *Biochimica et Biophysica Acta (BBA) - Molecular Cell Research,* 1843(11), pp. 2563-2582.

Turrioni, A. P., Alonso, J. R., Basso, F. G., Moriyama, L. T., Hebling, J., Bagnato, V. S. and De Souza, C. C. (2013) 'LED light attenuation through human dentin: a first step toward pulp photobiomodulation after cavity preparation', *Am J Dent,* 26(6), pp. 319-23.
Uehara, A. and Takada, H. (2007) 'Functional TLRs and NODs in human gingival fibroblasts', *J Dent Res,* 86(3), pp. 249-54.
Uitto, V.-J., Baillie, D., Wu, Q., Gendron, R., Grenier, D., Putnins, E. E., Kanervo, A. and Firth, J. D. (2005) 'Fusobacterium nucleatum increases collagenase 3 production and migration of epithelial cells', *Infection and immunity,* 73(2), pp. 1171-1179.
Urban, K., Hohling, H. J., Luttenberg, B., Szuwart, T. and Plate, U. (2012) 'An in vitro study of osteoblast vitality influenced by the vitamins C and E', *Head Face Med,* 8, pp. 25.
Usumez, A., Cengiz, B., Oztuzcu, S., Demir, T., Aras, M. H. and Gutknecht, N. (2014) 'Effects of laser irradiation at different wavelengths (660, 810, 980, and 1,064 nm) on mucositis in an animal model of wound healing', *Lasers in Medical Science,* 29(6), pp. 1807-1813.
Vale, F. A., Moreira, M. S., Almeida, F. C. S. D. and Ramalho, K. M. (2015) 'Low-level laser therapy in the treatment of recurrent aphthous ulcers: A systematic review', *Scientific World Journal,* 2015.
Veerman, E. C., Van Leeuwen, J. W., Van Buuren, K. J. and Van Gelder, B. F. (1982) 'The reaction of cytochrome aa3 with (porphyrin) cytochrome c as studied by pulse radiolysis', *Biochim Biophys Acta,* 680(2), pp. 134-41.
Veleska-Stevkoska, D. and Koneski, F. (2018) 'Haemostasis in oral surgery with blue-violet light', *Open Access Macedonian Journal of Medical Sciences,* 6(4), pp. 687-691.
Velikanov, A. N., Gostev, F. E., Suprunenko, E. A., Shelaev, I. V., Yusupov, V. I. and Nadtochenko, V. A. (2015) 'Stimulation of HaCaT keratinocyte and rat mesenchymal stromal cell proliferation by femtosecond laser pulses', *Cell and Tissue Biology,* 9(6), pp. 441-446.
Verma, S. K., Maheshwari, S., Singh, R. K. and Chaudhari, P. K. (2012) 'Laser in dentistry: An innovative tool in modern dental practice', *National journal of maxillofacial surgery,* 3(2), pp. 124-132.
Wagatsuma, A. and Sakuma, K. (2013) 'Mitochondria as a potential regulator of myogenesis', *TheScientificWorldJournal,* 2013, pp. 593267-593267.
Wahl, S. M., Costa, G. L., Mizel, D. E., Allen, J. B., Skaleric, U. and Mangan, D. F. (1993) 'Role of transforming growth factor beta in the pathophysiology of chronic inflammation', *J Periodontol,* 64(5 Suppl), pp. 450-5.
Walton, K. L., Johnson, K. E. and Harrison, C. A. (2017) 'Targeting TGF-beta Mediated SMAD Signaling for the Prevention of Fibrosis', *Front Pharmacol,* 8, pp. 461.
Wang, B.-y., Wu, J., Lamont, R. J., Lin, X. and Xie, H. (2009) 'Negative correlation of distributions of Streptococcus cristatus and Porphyromonas gingivalis in subgingival plaque', *Journal of clinical microbiology,* 47(12), pp. 3902-3906.
Wang, C. Y., Tsai, S. C., Yu, M. C., Lin, Y. F., Chen, C. C. and Chang, P. C. (2015) 'Light-emitting diode irradiation promotes donor site wound healing of the free gingival graft', *Journal of Periodontology,* 86(5), pp. 674-681.
Wang, H., Liu, W., Fang, X., Wang, H., Ma, W., Dong, H., Yin, H., Li, Y. X. and Sha, H. (2018) 'Effect of 405 nm low intensity irradiation on the absorption spectrum of in-vitro hyperlipidemia blood', *Technol Health Care,* 26(S1), pp. 135-143.
Wang, J., Hori, K., Ding, J., Huang, Y., Kwan, P., Ladak, A. and Tredget, E. E. (2011) 'Toll-like receptors expressed by dermal fibroblasts contribute to hypertrophic scarring', *J Cell Physiol,* 226(5), pp. 1265-73.
Wang, Y., Bai, X., Wang, Z., Cao, J., Dong, Y., Dong, Y. and Chen, Y. (2017a) 'Various LED Wavelengths Affected Myofiber Development and Satellite Cell Proliferation of Chick Embryos via the IGF-1 Signaling Pathway', *Photochemistry and Photobiology,* 93(6), pp. 1492-1501.
Wang, Y., He, X., Hao, D., Yu, D., Liang, J., Qu, Y., Sun, D., Yang, B., Yang, K., Wu, R. and Wang, J. (2014) 'Low-level laser therapy attenuates LPS-induced rats mastitis by inhibiting

polymorphonuclear neutrophil adhesion', *The Journal of veterinary medical science,* 76(11), pp. 1443-1450.
Wang, Y., Huang, Y. Y., Wang, Y., Lyu, P. and Hamblin, M. R. (2016) 'Photobiomodulation (blue and green light) encourages osteoblastic-differentiation of human adipose-derived stem cells: Role of intracellular calcium and light-gated ion channels', *Scientific Reports,* 6.
Wang, Y., Huang, Y. Y., Wang, Y., Lyu, P. and Hamblin, M. R. (2017b) 'Photobiomodulation of human adipose-derived stem cells using 810nm and 980nm lasers operates via different mechanisms of action', *Biochim Biophys Acta Gen Subj,* 1861(2), pp. 441-449.
Wang, Y., Huang, Y. Y., Wang, Y., Lyu, P. and Hamblin, M. R. (2017c) 'Red (660 nm) or near-infrared (810 nm) photobiomodulation stimulates, while blue (415 nm), green (540 nm) light inhibits proliferation in human adipose-derived stem cells', *Scientific Reports,* 7(1).
Wayne, J., Sielski, J., Rizvi, A., Georges, K. and Hutter, D. (2006) 'ERK regulation upon contact inhibition in fibroblasts', *Mol Cell Biochem,* 286(1-2), pp. 181-9.
Weinreb, M. and Nemcovsky, C. E. (2015) 'In vitro models for evaluation of periodontal wound healing/regeneration', *Periodontol 2000,* 68(1), pp. 41-54.
Weinrich, T. W., Coyne, A., Salt, T. E., Hogg, C. and Jeffery, G. (2017) 'Improving mitochondrial function significantly reduces metabolic, visual, motor and cognitive decline in aged Drosophila melanogaster', *Neurobiol Aging,* 60, pp. 34-43.
Werck-Reichhart, D. and Feyereisen, R. (2000) 'Cytochromes P450: a success story', *Genome Biology,* 1(6), pp. reviews3003.1-reviews3003.9.
White, D. A., Tsakos, G., Pitts, N. B., Fuller, E., Douglas, G. V. A., Murray, J. J. and Steele, J. G. (2012) 'Adult Dental Health Survey 2009: Common oral health conditions and their impact on the population', *British Dental Journal,* 213(11), pp. 567-572.
White, D. J. (1997) 'Dental calculus: recent insights into occurrence, formation, prevention, removal and oral health effects of supragingival and subgingival deposits', *Eur J Oral Sci,* 105(5 Pt 2), pp. 508-22.
Wigle, J. C. and Castellanos, C. C. 'In vitro measurements of oxygen consumption rates in hTERT-RPE cells exposed to low levels of red light'. *Progress in Biomedical Optics and Imaging - Proceedings of SPIE*.
Williams, R. C., Skelton, A. J., Todryk, S. M., Rowan, A. D., Preshaw, P. M. and Taylor, J. J. (2016) 'Leptin and Pro-Inflammatory Stimuli Synergistically Upregulate MMP-1 and MMP-3 Secretion in Human Gingival Fibroblasts', *PLoS One,* 11(2), pp. e0148024.
Wright Muelas, M., Ortega, F., Breitling, R., Bendtsen, C. and Westerhoff, H. V. (2018) 'Rational cell culture optimization enhances experimental reproducibility in cancer cells', *Sci Rep,* 8(1), pp. 3029.
Wu, J., Li, Q. and Fu, X. (2019) 'Fusobacterium nucleatum Contributes to the Carcinogenesis of Colorectal Cancer by Inducing Inflammation and Suppressing Host Immunity', *Translational oncology,* 12(6), pp. 846-851.
Xu, X., Zhao, X., Liu, T. C. Y. and Pan, H. (2008) 'Low-intensity laser irradiation improves the mitochondrial dysfunction of C2C12 induced by electrical stimulation', *Photomedicine and Laser Surgery,* 26(3), pp. 197-202.
Yamatake, K., Maeda, M., Kadowaki, T., Takii, R., Tsukuba, T., Ueno, T., Kominami, E., Yokota, S. and Yamamoto, K. (2007) 'Role for gingipains in Porphyromonas gingivalis traffic to phagolysosomes and survival in human aortic endothelial cells', *Infection and immunity,* 75(5), pp. 2090-2100.
Yamaura, M., Yao, M., Yaroslavsky, I., Cohen, R., Smotrich, M. and Kochevar, I. E. (2009) 'Low level light effects on inflammatory cytokine production by rheumatoid arthritis synoviocytes', *Lasers in Surgery and Medicine,* 41(4), pp. 282-290.
Yang, H., Bergmans, J. W. M., Schenk, T. C. W., Linnartz, J. P. M. G. and Rietman, R. (2008) 'An analytical model for the illuminance distribution of a power LED', *Optics Express,* 16(26), pp. 21641-21646.

Yang, H. Q., Wang, Y. H., Chen, J. X., Chen, X. G., Huang, Y. M., Li, H., Xie, S. S. and Zheng, L. Q. (2012) 'Efficacy of proliferation of hela cells under three different low-intensity red lasers irradiation', *International Journal of Photoenergy,* 2012.

Yang, J., Zhang, Q., Li, P., Dong, T. and Wu, M. X. (2016) 'Low-level light treatment ameliorates immune thrombocytopenia', *Scientific Reports,* 6.

Yang, J., Zhang, Q. and Wu, M. X. 'Low-level light treatment ameliorates immune thrombocytopenia'. *Progress in Biomedical Optics and Imaging - Proceedings of SPIE*.

Yang, M. Y., Chang, C. J. and Chen, L. Y. (2017b) 'Blue light induced reactive oxygen species from flavin mononucleotide and flavin adenine dinucleotide on lethality of HeLa cells', *J Photochem Photobiol B,* 173, pp. 325-332.

Yeh, M. C., Chen, K. K., Chiang, M. H., Chen, C. H., Chen, P. H., Lee, H. E. and Wang, Y. H. (2017) 'Low-power laser irradiation inhibits arecoline-induced fibrosis: an in vitro study', *Int J Oral Sci,* 9(1), pp. 38-42.

Yi, J., Xiao, J., Li, H., Li, Y., Li, X. and Zhao, Z. (2017) 'Effectiveness of adjunctive interventions for accelerating orthodontic tooth movement: a systematic review of systematic reviews', *Journal of Oral Rehabilitation,* 44(8), pp. 636-654.

Yin, K., Zhu, R., Wang, S. and Zhao, R. C. (2017) 'Low-Level Laser Effect on Proliferation, Migration, and Antiapoptosis of Mesenchymal Stem Cells', *Stem Cells and Development,* 26(10), pp. 762-775.

Yin, S. and Cao, W. (2015) 'Toll-Like Receptor Signaling Induces Nrf2 Pathway Activation through p62-Triggered Keap1 Degradation', *Mol Cell Biol,* 35(15), pp. 2673-83.

Yoshida, A., Yoshida, S., Khalil, A. K., Ishibashi, T. and Inomata, H. (1998) 'Role of NF-kappaB-mediated interleukin-8 expression in intraocular neovascularization', *Invest Ophthalmol Vis Sci,* 39(7), pp. 1097-106.

Yoshida, A., Yoshino, F., Makita, T., Maehata, Y., Higashi, K., Miyamoto, C., Wada-Takahashi, S., Takahashi, S. S., Takahashi, O. and Lee, M. C. (2013) 'Reactive oxygen species production in mitochondria of human gingival fibroblast induced by blue light irradiation', *J Photochem Photobiol B,* 129, pp. 1-5.

Yoshimoto, T., Morine, Y., Takasu, C., Feng, R., Ikemoto, T., Yoshikawa, K., Iwahashi, S., Saito, Y., Kashihara, H., Akutagawa, M., Emoto, T., Kinouchi, Y. and Shimada, M. (2018) 'Blue light-emitting diodes induce autophagy in colon cancer cells by Opsin 3', *Ann Gastroenterol Surg,* 2(2), pp. 154-161.

Yoshizaki, K. and Yamada, Y. (2013) 'Gene evolution and functions of extracellular matrix proteins in teeth', *Orthodontic waves (English ed.),* 72(1), pp. 1-10.

Yousefi-Nooraie, R., Schonstein, E., Heidari, K., Rashidian, A., Pennick, V., Akbari-Kamrani, M., Irani, S., Shakiba, B., Mortaz Hejri, S., Jonaidi, A. R. and et al. (2008) 'Low level laser therapy for nonspecific low-back pain', *Cochrane Database of Systematic Reviews,* (2).

Yu, S., Lan, C. C. E. and Yu, H. S. (2019) 'Mechanisms of repigmentation induced by photobiomodulation therapy in vitiligo', *Experimental Dermatology,* 28, pp. 10-14.

Yu, X., Liu, H., Klejnot, J. and Lin, C. (2010) 'The Cryptochrome Blue Light Receptors', *The Arabidopsis Book / American Society of Plant Biologists,* 8, pp. e0135.

Yuan, Y., Yan, G., Gong, R., Zhang, L., Liu, T., Feng, C., Du, W., Wang, Y., Yang, F., Li, Y., Guo, S., Ding, F., Ma, W., Idiiatullina, E., Pavlov, V., Han, Z., Cai, B. and Yang, L. (2017) 'Effects of Blue Light Emitting Diode Irradiation On the Proliferation, Apoptosis and Differentiation of Bone Marrow-Derived Mesenchymal Stem Cells', *Cell Physiol Biochem,* 43(1), pp. 237-246.

Zaccara, I. M., Mestieri, L. B., Moreira, M. S., Grecca, F. S., Martins, M. D. and Kopper, P. M. P. (2018) 'Photobiomodulation therapy improves multilineage differentiation of dental pulp stem cells in three-dimensional culture model', *Journal of Biomedical Optics,* 23(9).

Zecha, J. A. E. M., Raber-Durlacher, J. E., Nair, R. G., Epstein, J. B., Elad, S., Hamblin, M. R., Barasch, A., Migliorati, C. A., Milstein, D. M. J., Genot, M. T., Lansaat, L., van der Brink, R., Arnabat-Dominguez, J., van der Molen, L., Jacobi, I., van Diessen, J., de Lange, J., Smeele, L. E.,

Schubert, M. M. and Bensadoun, R. J. (2016a) 'Low-level laser therapy/photobiomodulation in the management of side effects of chemoradiation therapy in head and neck cancer: part 2: proposed applications and treatment protocols', *Supportive Care in Cancer,* 24(6), pp. 2793-2805.

Zecha, J. A. E. M., Raber-Durlacher, J. E., Nair, R. G., Epstein, J. B., Sonis, S. T., Elad, S., Hamblin, M. R., Barasch, A., Migliorati, C. A., Milstein, D. M. J., Genot, M. T., Lansaat, L., van der Brink, R., Arnabat-Dominguez, J., van der Molen, L., Jacobi, I., van Diessen, J., de Lange, J., Smeele, L. E., Schubert, M. M. and Bensadoun, R. J. (2016b) 'Low level laser therapy/photobiomodulation in the management of side effects of chemoradiation therapy in head and neck cancer: part 1: mechanisms of action, dosimetric, and safety considerations', *Supportive Care in Cancer,* 24(6), pp. 2781-2792.

Zhang, B., Elmabsout, A. A., Khalaf, H., Basic, V. T., Jayaprakash, K., Kruse, R., Bengtsson, T. and Sirsjo, A. (2013) 'The periodontal pathogen Porphyromonas gingivalis changes the gene expression in vascular smooth muscle cells involving the TGFbeta/Notch signalling pathway and increased cell proliferation', *BMC Genomics,* 14, pp. 770.

Zhang, H., Salo, D., Kim, D. M., Komarov, S., Tai, Y.-C. and Berezin, M. Y. (2016a) 'Penetration depth of photons in biological tissues from hyperspectral imaging in shortwave infrared in transmission and reflection geometries', *Journal of biomedical optics,* 21(12), pp. 126006-126006.

Zhang, N., Xu, Y., Zhang, B., Zhang, T., Yang, H., Zhang, B., Feng, Z. and Zhong, D. (2014) 'Analysis of Interleukin-8 Gene Variants Reveals Their Relative Importance as Genetic Susceptibility Factors for Chronic Periodontitis in the Han Population', *PLoS ONE,* 9(8), pp. e104436.

Zhang, Q., Dong, T., Li, P. and Wu, M. X. (2016b) 'Noninvasive low-level laser therapy for thrombocytopenia', *Science Translational Medicine,* 8(349).

Zhang, Y., Song, S., Fong, C. C., Tsang, C. H., Yang, Z. and Yang, M. (2003) 'cDNA microarray analysis of gene expression profiles in human fibroblast cells irradiated with red light', *J Invest Dermatol,* 120(5), pp. 849-57.

Zhang, Z., Huang, L., Shulmeister, V. M., Chi, Y. I., Kim, K. K., Hung, L. W., Crofts, A. R., Berry, E. A. and Kim, S. H. (1998) 'Electron transfer by domain movement in cytochrome bc1', *Nature,* 392(6677), pp. 677-84.

Zhao, Y. L., Zhang, F. Q., Ge, X. H., Yao, S. X. and Liang, E. J. (2004) '[The study of absorption spectrum for cell substrate]', *Guang Pu Xue Yu Guang Pu Fen Xi,* 24(8), pp. 907-10.

Zhou, Y., Yang, J., Zhang, L., Zhou, X., Cisar, J. O. and Palmer, R. J., Jr. (2016) 'Differential utilization of basic proline-rich glycoproteins during growth of oral bacteria in saliva', *Applied and Environmental Microbiology,* 82(17), pp. 5249-5258.

Zhu, J., Vinothkumar, K. R. and Hirst, J. (2016) 'Structure of mammalian respiratory complex I', *Nature,* 536(7616), pp. 354-358.

Zhu, W., George, J. K., Sorger, V. J. and Grace Zhang, L. (2017) '3D printing scaffold coupled with low level light therapy for neural tissue regeneration', *Biofabrication,* 9(2).

10 APPENDICES

10.1 Literature review tables and processes of systematic review

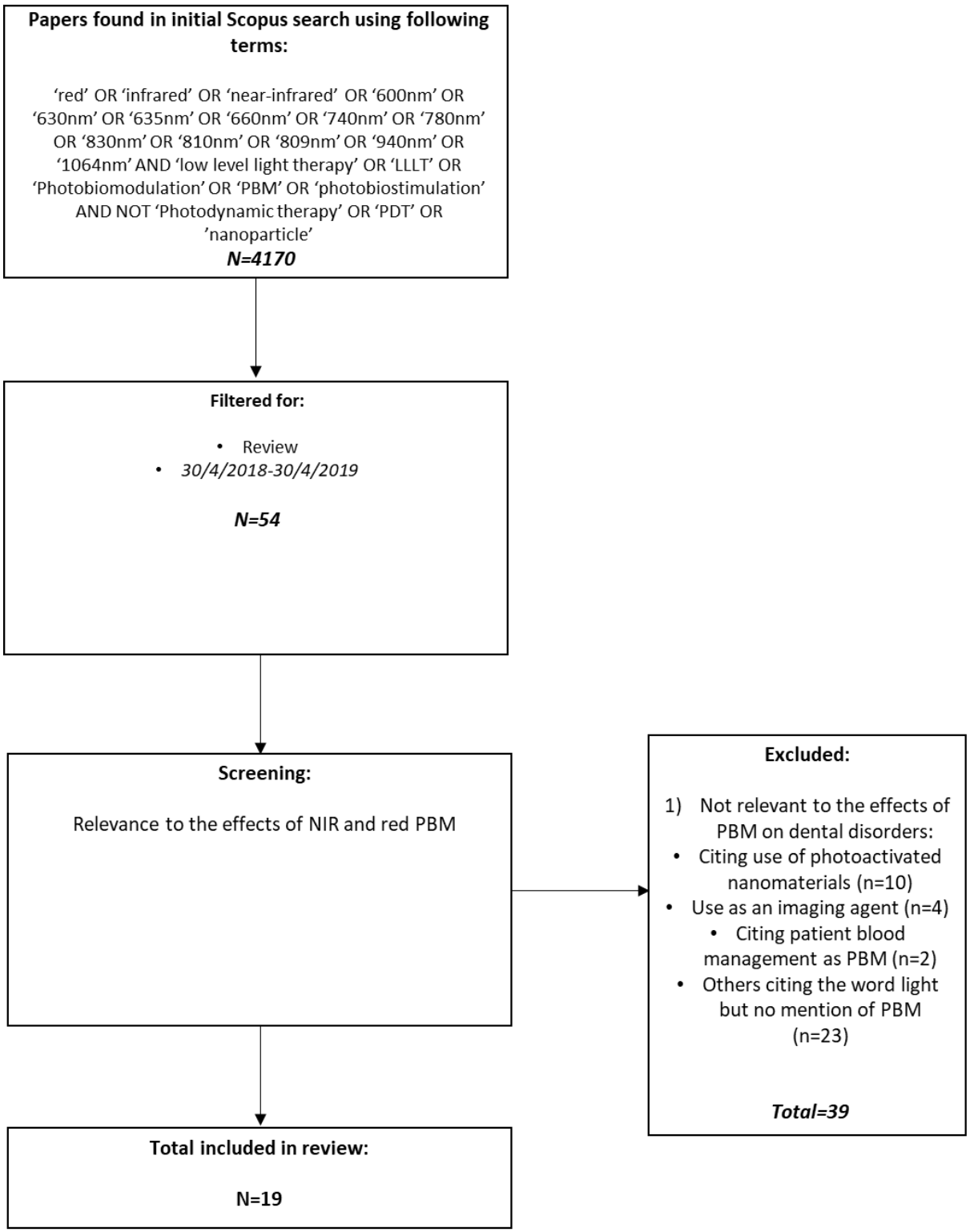

Figure 10.1: Flow chart indicating the strategy employed to identify relevant articles for review when evaluating the effects of red/NIR light.

Table 10.1: Publication identified from review to cite the following key words: 'red' OR 'infrared' OR 'near-infrared' OR '600 nm' OR '630 nm' OR '635 nm' OR '660 nm' OR '740 nm' OR '780 nm' OR '830 nm' OR '810 nm' OR '809 nm' OR '940 nm' OR '1064 nm' AND 'low level light therapy' OR 'PBM' OR 'Photobiomodulation' OR 'PBM' OR 'photobiostimulation' AND NOT 'Photodynamic therapy' OR 'PDT' OR 'nanoparticle'

Citation	Application	Outcome
1) Bath et al (Bath and Gupta, 2019)	Heart tissue	NIR light could be protective for patients after myocardial infarction or on ischemic heart conditions.
2) Yu et al (Yu et al., 2019)	Regimentation in Vitiligo	HeNe laser (632.8 nm) could be effective in inducing regimentation through modulation of mitochondrial activity.
3) Mussttaff et al (Mussttaf et al., 2019)	Increased cell proliferation and viability	Red and NIR promote cell viability, proliferation rates and DNA repair.
4) Chan et al (Chan et al., 2019)	Characteristics and management of Asian skin	NIR light could be useful in managing pigmentation and other ethnicity associated skin conditions.
5) Caldieraro et al (Caldieraro and Cassano, 2019)	Management of major depressive disorder	Red and NIR light could be useful in management of depression. Further studies required to elucidate possible beneficial parameters.
6) Hamblin et al (Hamblin et al., 2019)	The biological response of species across the animal kingdom to PBM.	Response to red and NIR light is not exclusive to Humans.
7) Marson et al (Marson and Baldwin, 2019)	Acne	Not only blue but red light could prove effective in management of acne vulagris.
8) Ezzati et al (Ezzati et al., 2019)	Post-surgical pain	Red light could prove effective in managing pain following surgeries such as tonsillectomy. However, further RCTs required to validate these findings.
9) Brassolatti et al (Brassolatti et al., 2018)	Bone defects	Red and NIR light could prove beneficial in the management of bone defects.
10) Migliario et al (Migliario et al., 2018a)	Cell proliferation and redox sensitive pathways induced by light.	NIR light could induce changes in cell proliferation through modulation of pathways including Nrf2 and NFκB.
11) Hamilton et al (Hamilton et al., 2018)	Parkinson's disease	Transcranial stimulation using NIR/red light could prove and effective modality in managing parkinson's disease symptoms.
12) Kurata et al (Kurata, 2018)	Androgenetic Alopecia (male-pattern baldness)	Red light could prove effective in promoting hair growth.
13) Salehpour et al (Salehpour et al., 2018b)	Brain disorders	Red/NIR light could be useful in management of depression, stroke and traumatic brain injury (TBI).
14) Ao et al (Ao et al., 2018)	Retinal pigment epithelium (RPE)	Red/NIR light could prove effective in the management of RPE through modulation of mitochondrial activity.
15) Moskvin et al (Moskvin and Apolikhin, 2018)	Male infertility	*'Local illumination of red (635 nm) and infrared (904 nm) spectra should be combined with intravenous laser blood illumination (ILBI) of red (635 nm) and ultraviolet (UV) (365 nm)'* to treat infertility.
16) Rocha et al (Rocha et al., 2018)	TBI	Red and NIR light penetrate scalp and skull thus may be able to modulate brain activity
17) Hamblin et al (Hamblin, 2018a)	Mitochondrial redox signalling	Red and NIR light induce their beneficial effects through modulation of mitochondrial activity, specifically through interaction with complex IV of the electron transport chain.
18) Hamblin et al (Hamblin, 2018b)	TBI	Red/NIR light application has been shown to improve executive function, working memory and sleep. Key side effects of TBI.
19) Heiskanen and Hamblin (Heiskanen and Hamblin, 2018b)	LEDs vs Lasers	There is no significant beneficial effects of the use of lasers or LEDs for application in PBM both *in vitro* and *in vivo*.

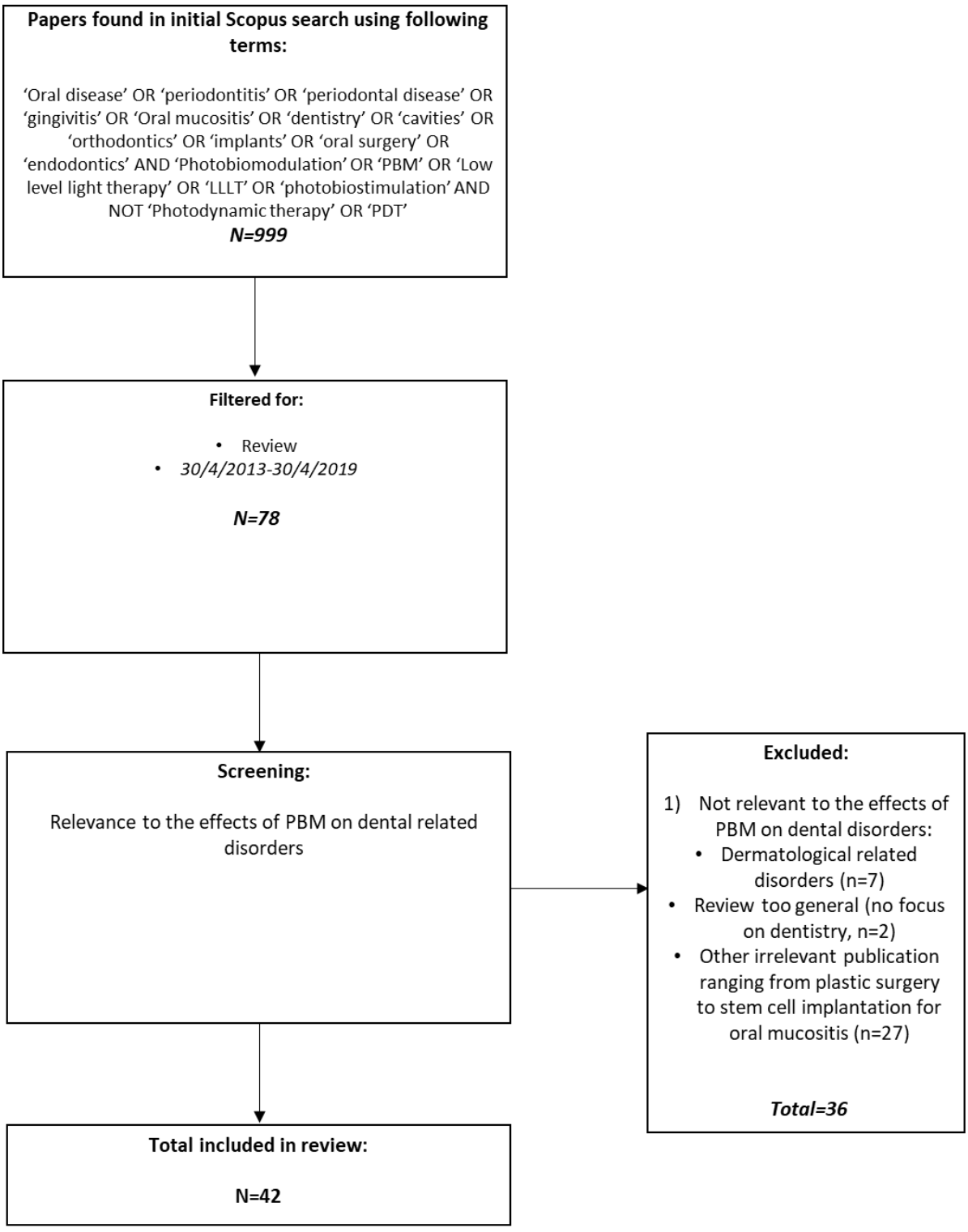

Figure 10.2: Flow chart providing evidence of strategy employed to select relevant articles for review

Table 10.2: Provides details of relevant articles including in this review citing the following key search terms: 'Oral disease' OR 'periodontitis' OR 'periodontal disease' OR 'gingivitis' OR 'Oral mucositis' OR 'dentistry' OR 'cavities' OR 'orthodontics' OR 'implants' OR 'oral surgery' OR 'endodontics' AND 'Photobiomodulation' OR 'PBM' OR 'Low level light therapy' OR 'PBM' OR 'photobiostimulation' AND NOT 'Photodynamic therapy' OR 'PDT'

Oral Speciality	Application	Conclusions	References
Orthodontics	• Orthodontic tooth movement *(n=7)* • Orthodontic related pain *(n=5)* • Rapid maxillary expansion *(n=2)* • Titanium implant *(n=3)*	• Could be effective but evidence is low quality, suggestion that dose between 5-8J/cm² could be most effective. Further RCTs required to validate • Could be effective but evidence is low quality. • Promising for stimulating bone regeneration, red-NIR light, 0.4-60J/cm². • Effective promotion of osseointegration but improved experimental design required. Also effective in Titanium surface decontamination.	(Carvalho-Lobato et al., 2014, Ge et al., 2015, Kacprzak and Strzecki, 2018, Meng et al., 2017, Seifi and Vahid-Dastjerdi, 2015, Swidi et al., 2018, Yi et al., 2017) (Eslamipour et al., 2017, Fleming et al., 2016, Li et al., 2015, Srivastava and Mahajan, 2014, Tania et al., 2015) (Amid et al., 2014, Skondra et al., 2018) (Kamel et al., 2014, Mathews et al., 2015, Prados-Frutos et al., 2016)
Maxillofacial	• Various *(n=2)*	• Treatment of oral mucositis, gingival healing, myofacial and dental pain but not temporal mandibular jaw disorder	(Doeuk et al., 2015, Madhumathi and Santhosh Kumar, 2018)
Oral Pathology	• Oral mucositis *(n=12)* • Various *(n=1)* • Herpes simplex virus (HSV, n=1) • Recurrent apthous ulcers *(n=1)*	• Red to NIR light could prove effective at low doses (<5J/cm²). However, outcomes variable possibly due to poor experimental design. Some authors suggest could act negatively in promoting cancer cell proliferation. • Promise in recurrent herpes simplex virus, OM and burning mouth syndrome. • Literature is lacking and provides no conclusive evidence of the benefits of PBM in managing recurrent HSV. • Useful but further research required with improved experimental design to ensure reproducibility.	(Anschau et al., 2019, Bensadoun, 2018, de Pauli Paglioni et al., 2019, Fekrazad and Chiniforush, 2014, He et al., 2018b, Peralta-Mamani et al., 2019, Robijns et al., 2017, Sonis et al., 2016, Spanemberg et al., 2016, Sung et al., 2017, Zecha et al., 2016a, Zecha et al., 2016b) (Pandeshwar et al., 2016)

				(Chi et al., 2015) (Vale et al., 2015)
Oral Surgery	•	Gingival recession defect surgery *(n=1)*	• Shown promise but further RCTs required to validate	(Akram et al., 2018)
Endodontics	•	Dentine hypersensivity *(n=1)*	• Relative to other treatments, PBM induced the greatest reduction in dentine hypersensitivity. • No sufficient evidence to draw conclusions	(Moraschini et al., 2018)
	•	Periapical lesions *(n=2)*		(Del Fabbro et al., 2016, Maldonado et al., 2018)
Periodontics	•	Periodontal therapy *(n=2)*	• Useful as an adjunct to scaling and root planning (SRP). However, further RCTs required to further elucidate possible beneficial treatment parameters.	(Ren et al., 2017, Porteous and Rowe, 2014)
General	•	Various dental applications *(n=2)*	• Effective in accelerating wound healing and pain management • Further RCTs required with greater experimental design required to validate positive results regarding the application of PBM to various oral diseases.	(Kathuria et al., 2015) (Carroll et al., 2014)

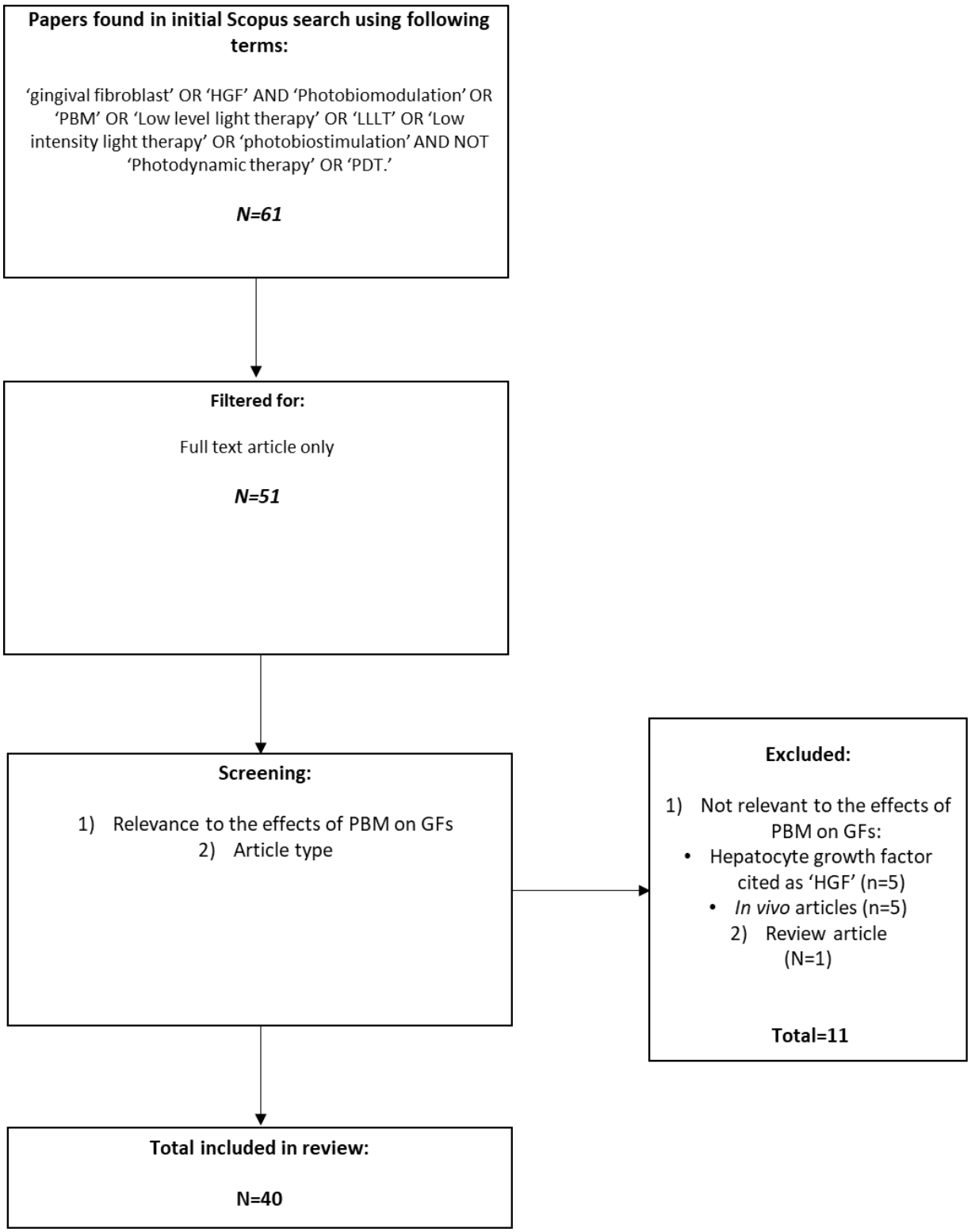

Figure 10.3: Indicates the systematic review process employed to evaluate the effects of PBM on GFs.

Table 10.3: Citations identified from a review of the literature evaluating the effects of PBM on gingival fibroblasts using the following key words: gingival fibroblast' OR 'HGF' AND 'Photobiomodulation' OR 'PBM' OR 'Low level light therapy' OR 'PBM' OR 'Low intensity light therapy' OR 'photobiostimulation' AND NOT 'Photodynamic therapy' OR 'PDT.'

	Citation	Parameters	Cell Type	Effects
(1)	**Almeida-Lopes et al 2001 (Almeida-Lopes et al., 2001b)**	**Wavelength:** 670 -786 nm **Light source type:** diode laser **Power (mW):** 10 – 50mW **Pulse frequency:** **Beam area (cm²):** 0.01cm² **Exposure time:** **Radiant energy (J)** **Fluence (J/cm²):** 2J/cm² **Irradiance (mW/cm²):**	Human gingival fibroblasts (HGFs), primary.	cells under stress proliferate more with light particularly light in the infra-red spectrum (5% FBS)
(2)	**Azevedo et al, 2006 (Azevedo et al., 2006)**	**Wavelength:** 660 nm **Light source type:** GaAlAs diode **Power (mW):** 10mW **Pulse frequency:** **Beam area (cm²):** 0.07 **Exposure time:** 4.8s and 14s (2 irradiations in 12h) **Radiant energy (J)** **Fluence (J/cm²):** 2J/cm² **Irradiance (mW/cm²):** 142.85mW/cm², 428.57mW/cm²	HGF cell line	greater number of cell numbers in irradiated groups compared to controls, all serum starved
(3)	**Basso et al, 2012 (Basso et al., 2012b)**	**Wavelength:** 780 nm **Light source type:** InGaAsP, LaserTABLE **Power (mW):** 0.04mW **Pulse frequency:** **Beam area (cm²):** **Exposure time:** 40 – 560s (every 24hrs, 3 days) **Radiant energy (J)** **Fluence (J/cm²):** 0.5 – 7J/cm² **Irradiance (mW/cm²):**	HGF cell line	increased number of viable cells and cell migration capacity
(4)	**Basso et al, 2013 (Basso et al., 2013a)**	**Wavelength:** 780 nm **Light source type:** InGaAsP, LaserTABLE **Power (mW):** 0.02mW **Pulse frequency:** **Beam area (cm²):** **Exposure time:** 40 – 560s **Radiant energy (J)** **Fluence (J/cm²):** 0.5 – 7J/cm² **Irradiance (mW/cm²):**	HGF cell line	at 5Jcm-2 increase total protein production, also improve attachement to surfaces (za usually renders this impossible)
(5)	**Basso et al, 2015 (Basso et al., 2015)**	**Wavelength:** 780 nm **Light source type:** InGaAsP, LaserTABLE **Power (mW):** 25mW **Pulse frequency:** **Beam area (cm²):** 2 **Exposure time:** 40 – 240s **Radiant energy (J)** **Fluence (J/cm²):** 0.5 – 3J/cm² **Irradiance (mW/cm²):**	Primary HGFs	at 1.5J/cm² and 3J/cm² biomodulation of the production of cytokines eg IL-6 and TNF-α compared to controls
(6)	**Chen et al, 2000 (Chen et al., 2000a)**	**Wavelength:** 1064 nm **Light source type:** Nd:YAG **Power (mW):** **Pulse frequency:** **Beam area (cm²):** 400µm (diameter) **Exposure time:** 10 – 30 pulse/second **Radiant energy (J):** 100 – 150mJ **Fluence (J/cm²):** **Irradiance (mW/cm²):**	Primary HGFs	severe damage to HGFs including cell death and loss of cellular vitality

(7)	**Choi et al, 2012 (Choi et al., 2012)**	**Wavelength:** 635 nm **Light source type:** LED **Power (mW):** **Pulse frequency:** **Beam area (cm²):** **Exposure time:** 1 hour **Radiant energy (J):** **Fluence (J/cm²):** **Irradiance (mW/cm²):** 5mW/cm²	Primary HGFs	decrease in COX-2, PGE-2, IL-6, IL-8 and p38 phosphorylation compared to non-irradiated LPS (from *P.gingivalis*) treated cells
(8)	**Damante et al, 2009 (Damante et al., 2009)**	**Wavelength:** 660 nm and 780 nm **Light source type:** InGaAlP and GaAlAs **Power (mW):** 40mW **Pulse frequency:** **Beam area (cm²):** 0.042cm² **Exposure time:** 3s and 5s (two sessions, 6hr intervals) **Radiant energy (J):** **Fluence (J/cm²):** 3 and 5J/cm² **Irradiance (mW/cm²):** 1000mW/cm²	HGF cell line	increased production of bFGF
(9)	**Frozanfar et al, 2013 (Frozanfar et al., 2013)**	**Wavelength:** 810 nm **Light source type:** GaAlAs **Power (mW):** 50mW **Pulse frequency:** **Beam area (cm²):** **Exposure time:** 32s **Radiant energy (J):** **Fluence (J/cm²):** 5J/cm² **Irradiance (mW/cm²):**	HGF	significant collagen type 1 expression, no sig diff in proliferation post irradiation but occurred after 24hrs - 72h
(10)	**Hakki et al, 2012 (Hakki and Bozkurt, 2012)**	**Wavelength:** 940 nm **Light source type:** InGaAsP **Power:** 0.3 – 2W **Pulse frequency:** **Beam area:** 20s/cm² **Exposure time:** pulsed 1ms or 20ms, CW: 20s/cm² **Radiant energy (J):** **Fluence (J/cm²):** 6 – 20J/cm² **Irradiance (mW/cm²):**	Primary HGFs	induction of collagen production at biostimulation setting, inducing growth factor mRNA expression including IGF, VEGF and TGFβ.
(11)	**Khadra et al, 2005 (Khadra et al., 2005)**	**Wavelength:** 830 nm **Light source type:** GaAlAs diode **Power:** 84mW **Pulse frequency:** **Beam area:** **Exposure time:** 90s – 360s (3 days) **Radiant energy (J):** **Fluence (J/cm²):** 0.75 – 3J/cm² **Irradiance (mW/cm²):**	Primary HGFs	1.5J/cm² and 3J/cm² multi exposure, significantly higher levels of proliferation and adhesion compared to control
(12)	**Kreisler et al, 2002 (Kreisler et al., 2002)**	**Wavelength:** 809 nm **Light source type:** GaAlAs diode **Power:** 10mW **Pulse frequency:** **Beam area:** **Exposure time:** 75 – 300s (2 -3 times in 24 hours) **Radiant energy (J):** **Fluence (J/cm²):** 1.96 – 7.84J/cm² **Irradiance (mW/cm²):**	Primary HGFs	significant increase in levels of HGF proliferation compared to control
(13)	**Kreisler et al, 2005 (Kreisler et al., 2005)**	**Wavelength:** 2940 nm **Light source type:** Er:YAG **Power:** **Pulse frequency:** 1 – 15Hz **Beam area:** **Exposure time:**60s **Radiant energy (J):** 60 – 250mJ **Fluence (J/cm²):** **Irradiance (mW/cm²):**	Primary HGFs	Increased HGF proliferation when treated with Er:YAG laser compared to cells treated only with *P.gingivalis*.
(14)	**Kriesler et al, 2001 (Kreisler et al., 2001)**	**Wavelength:** 810 nm **Light source type:** GaAlAs diode **Power:** 0.5 – 2.5W **Pulse frequency:** **Beam area:**	Primary HGFs	the higher the power output and time of exposure, the lower the survival rate, use of very high fluence values

		Exposure time: 60 -240s **Radiant energy (J):** **Fluence (J/cm²):** 24.64 – 492.8J/cm² **Irradiance (mW/cm²):**		
(15)	**Lim et al, 2007 (Lim et al., 2007)**	**Wavelength:** 635 nm **Light source type:** LED **Power:** **Pulse frequency:** **Beam area:** **Exposure time:** 1 hour per treatment **Radiant energy (J):** **Fluence (J/cm²):** **Irradiance (mW/cm²):** 1mW/cm²	Primary HGFs	compared to ibuprofen and indomethacin, caused decrease ROS, inhibition of PGE-2, COX-2 and PLA-2
(16)	**Lim et al, 2013 (Lim et al., 2013)**	**Wavelength:** 635 nm **Light source type:** LED **Power:** **Pulse frequency:** **Beam area:** **Exposure time:** 1 hour per treatment **Radiant energy (J):** **Fluence (J/cm²):** 18J/cm² **Irradiance (mW/cm²):** 5mW/cm²	Primary HGFs	decrease in PGE2, COX-1 and -2, decrease HSP27 activation, decrease ROS compared to P.gingivalis LPS treated cells without light treatment
(17)	**Lim et al, 2015 (Lim et al., 2015)**	**Wavelength:** 635 nm **Light source type:** LED **Power:** **Pulse frequency:** **Beam area:** **Exposure time:** 1 hour per treatment **Radiant energy (J):** **Fluence (J/cm²):** **Irradiance (mW/cm²):** 5mW/cm²	Immortalised HGFs	decrease in COX-2, PGE-2, leading to decrease in overall inflammatory state compared to non- irradiated LPS treated cells, greater effect by direct irradiation compared to indirect
(18)	**Marques et al, 2004 (Marques et al., 2004)**	**Wavelength:** 904 nm **Light source type:** GaAlAs diode **Power:** 120mW **Pulse frequency:** **Beam area:** 0.07cm² **Exposure time:** 24s **Radiant energy (J):** **Fluence (J/cm²):** 3J/cm² **Irradiance (mW/cm²):**	HGF cell line	no difference in procollagen synthesis, amount of type 1 collaged and protein lower compared to control, ultrastructural changes in mitochondria and RER
(19)	**Nomura et al, 2001 (Nomura et al., 2001)**	**Wavelength:** 830 nm **Light source type:** GaAlAs diode **Power:** 700mW **Pulse frequency:** **Beam area:** 130mm diameter **Exposure time:** 3 – 20 mins **Radiant energy (J):** **Fluence (J/cm²):** 7.9J/cm² **Irradiance (mW/cm²):**	Primary HGFs	low-energy laser irradiation inhibited LPS stimulated production of IL-1β
(20)	**Pansani et al, 2014 (Pansani et al., 2014)**	**Wavelength:** 780 nm **Light source type:** InGaAsP, LaserTABLE **Power:** 0.025W **Pulse frequency:** **Beam area:** 2cm² **Exposure time:** 40 – 240s **Radiant energy (J):** **Fluence (J/cm²):** 0.5 – 3J/cm² **Irradiance (mW/cm²):**	HGF cell line	PBM made no significant difference on proliferation rates.
(21)	**Park and Hong, 2015 (Park and Hong, 2014)**	**Wavelength:** 400 – 750 nm and 600 – 650 nm (mixed red and white light) **Light source type:** LED **Power:** **Pulse frequency:** **Beam area:** **Exposure time:** 9 mins for 3 days **Radiant energy (J):** **Fluence (J/cm²):** 1.26J/cm² (white) and 0.3J/cm² (red)	Primary HGFs	Increased cell proliferation, increased IGF-1 expression and COL1A1 (collagen type 1), decreased IGF-1R, ICAM-1 and SMAD-3 expression compared to control. Also, PBM promoted wound healing and cell migration.

		Irradiance (mW/cm²):		
(22)	**Pourzarandian et al, 2005 (Pourzarandian et al., 2005)**	**Wavelength:** 2940 nm **Light source type:** Pulsed Er:YAG **Power:** **Pulse frequency:** 30Hz **Beam area:** **Exposure time:** 200µs (pulse duration) **Radiant energy (J):** 30 – 350mJ **Fluence (J/cm²):** 1.68 – 5J/cm² **Irradiance (mW/cm²):**	Primary HGFs	Up to 3.37Jcm-2 greater number of cells after 3 days exposure compared to control, also increase metabolic activities.
(23)	**Sakurai et al, 2000 (Sakurai et al., 2000)**	**Wavelength:** 830 nm **Light source type:** GaAlAs diode **Power:** 700mW **Pulse frequency:** **Beam area:** 130mm diameter **Exposure time:** 3 – 20 minutes **Radiant energy (J):** **Fluence (J/cm²):** 0.95 – 6.32J/cm² **Irradiance (mW/cm²):**	Primary HGFs	inhibition of PGE2 production usually stimulated by LPS via a reduction of COX-2 produced by HGFs
(24)	**Saygun et al, 2008 (Saygun et al., 2008)**	**Wavelength:** 685 nm **Light source type:** Diode laser (BTL-2000) **Power:** 25mW **Pulse frequency:** **Beam area:** 1cm² **Exposure time:** 140s **Radiant energy (J):** **Fluence (J/cm²):** 3J/cm² **Irradiance (mW/cm²):**	Primary HGFs	increase HGF proliferation, viability and levels of bFGF, IGF-1 and IGFBP-3, compared to control
(25)	**Schartinger et al, 2012 (Schartinger et al., 2012)**	**Wavelength:** 600 nm **Light source type:** GaAlAs diode **Power:** **Pulse frequency:** **Beam area:** **Exposure time:** 15 mins per day for 3 days **Radiant energy (J):** **Fluence (J/cm²):** **Irradiance (mW/cm²):**	HGFs	Increased HGF proliferation compared to control
(26)	**Takema et al, 2000 (Takema et al., 2000)**	**Wavelength:** 830 nm **Light source type:** GaAlAs diode **Power:** 700mW **Pulse frequency:** **Beam area:** 130mm diameter **Exposure time:** 10 mins **Radiant energy (J):** **Fluence (J/cm²):** 7.9J/cm² **Irradiance (mW/cm²):** 0.39 – 63.7mW/cm²	Primary HGFs	PBM reduces levels of PA activity to control levels compared to LPS stimulated cells only
(27)	**Wang et al, 2015 (Wang et al., 2015)**	**Wavelength:** 660 nm **Light source type:** LED, red. **Power:** **Pulse frequency:** **Beam area:** **Exposure time:** 6 – 24 mins **Radiant energy (J):** **Fluence (J/cm²):** 0 – 20J/cm² **Irradiance (mW/cm²):** 3.5mW/cm²	Rat GFs	Accelerated rate of wound closure, increase GF proliferation, inhibit cytoxicity, decrease ROS, increase type 1 collagen.
(28)	**Basso et al, 2016 (Basso et al., 2016b)**	**Wavelength:** 780 nm **Light source type:** InGaAsP, 12 laser diodes **Power: 25mW** **Pulse frequency:** **Beam area:** **Exposure time:** 40, 120, 240s, 3 consecutive days, 24 hours apart. **Radiant energy (J):** **Fluence (J/cm²):** 0 – 3J/cm² **Irradiance (mW/cm²):**	Primary Gingival Fibroblasts	Stimulated fibroblasts with concentrations of IL-6, IL-8, IL-1B, TNF-α based on ability to induce the secretion of NO. The tested cell migration ability, cell proliferation, growth factor production and compared to results with PBM. PBM promoted acceleration of fibroblast migration and proliferation
(29)	**Basso et al, 2016 (Basso et al., 2016a)**	**Wavelength:** 780 nm **Light source type:** LaserTABLE **Power:** 70 **Pulse frequency:**	Primary gingival fibroblasts	Investigating PBM in 3D cell culture model. 3J/cm² induced significantly higher levels of cell viability compared to control.

		Beam area: **Exposure time:** 40, 120, 240s, 3 consecutive days, 24 hours apart. **Radiant energy (J):** **Fluence (J/cm²):** 0 – 3J/cm² **Irradiance (mW/cm²):** 25		Whilst 0.5J/cm² induced a significant increase in EGF and COL-1 expression
(30)	**Pansani et al, 2016 (Pansani et al., 2017)**	**Wavelength:** 780 nm **Light source type:** InGaAsP, 12 diodes **Power:** 25mW **Pulse frequency:** cw **Beam area:** **Exposure time:** 240s, 3 consecutive days, 24 hours apart. **Radiant energy (J):** **Fluence (J/cm²):** 3J/cm² **Irradiance (mW/cm²):**	Primary human gingival fibroblasts derived from both young (18-25) and elderly (>65) samples.	Increase in cell viability, collagen synthesis and increased expression of VEGF from laser irradiated samples.
(31)	**Ogita et al, 2015 (Ogita et al., 2014)**	**Wavelength:** 2940 nm **Light source type:** Er: YAG **Power:** 25mW **Pulse frequency:** 30-50mJ/pulse **Beam area:** **Exposure time:** 30s **Radiant energy (J):** **Fluence (J/cm²):** 1.65-2.61 **Irradiance (mW/cm²):**	pHGFs	Promote HGF proliferation, induce significant changes in protein expression and the upregulation of galectin-7. Grown in 0.5% FBS.
(32)	**Yoshida et al, 2013 (Yoshida et al., 2013)**	**Wavelength:** 460 nm **Light source type:** LED or quartz-tungsten halogen lamp (QTH) **Power:** 25mW **Pulse frequency:** **Beam area:** **Exposure time:** **Radiant energy (J):** **Fluence (J/cm²):** **Irradiance (mW/cm²):** 250	pHGFs	Increased mitochondrial ROS production and cytoxicity induced by blue light. Reduced cell proliferation following irradiation.
(33)	**Pansani et al, 2018 (Pansani et al., 2017)**	**Wavelength:** 780 nm **Light source type:** Laser **Power:** 25mW **Pulse frequency:** **Beam area:** 2cm² **Exposure time:** 240s **Radiant energy (J):** **Fluence (J/cm²):** 3 **Irradiance (mW/cm²):**	HGF cell line	Enhanced synthesis of CCL2 and increased proliferation following application of LPS
(34)	**Yeh et al, 2017 (Yeh et al., 2017)**	**Wavelength:** 660 **Light source type:** Laser **Power:** 70mW **Pulse frequency:** **Beam area:** **Exposure time:** **Radiant energy (J):** **Fluence (J/cm²):** 8 **Irradiance (mW/cm²):** 15.17	pHGFs	PBM induced reduction in acrecoline mediated fibrotic marker genes. However, application of an adenylyl cyclase inhibitor prevented this effect
(35)	**Eslami et al, 2017 (Eslami et al., 2017)**	**Wavelength:** 632.8 **Light source type:** Laser **Power:** 500mW **Pulse frequency:** **Beam area:** 9.6cm² **Exposure time:** **Radiant energy (J):** **Fluence (J/cm²):** 0.15-1.5 **Irradiance (mW/cm²):**	HGF3-PI 53	Irradiation induced increased collagen type I expression. Also evaluated combined effects of propalis and light.
(36)	**Roncati et al, 2016 (Roncati et al., 2016) (Roncati et al., 2016)**	**Wavelength:** 835 nm **Light source type:** LED **Power:** **Pulse frequency:** **Beam area:** **Exposure time:** 900 **Radiant energy (J):** **Fluence (J/cm²):** 155 **Irradiance (mW/cm²):**	pHGF	LED irradiation correlated to elastin gene expression. ELN expression inversely related to patient age where expression decreases with aging.

(37) Liang et al, 2015 (Liang et al., 2015)	**Wavelength:** 810 nm **Light source type:** Diode laser **Power:** **Pulse frequency:** **Beam area:** **Exposure time:** 10-60s **Radiant energy (J):** **Fluence (J/cm²):** 10-60 **Irradiance (mW/cm²):** 1000	HGFs and human oral cancer (OC2) cell	Reduced cell viability of oral cancer cells but had no significant effect on HGFs. ROS and MMP elevated in cancer cells but no significant effect on HGFs. Also induced caspase-3 dependent apoptosis in cancer cells but no significant effect from HGFs.
(38) Basso et al, 2013 (Basso et al., 2013b)	**Wavelength:** 780 nm **Light source type:** Laser **Power:** 25mW **Pulse frequency:** **Beam area:** **Exposure time:** **Radiant energy (J):** **Fluence (J/cm²):** 0.5-7 **Irradiance (mW/cm²):**	HGF cell line	Following Zoledronic acid (to induce cell death to mimic osteonecrosis), PBM at 5 and 7J/cm² induced significant increases in Col-I and VEGF expression. Key markers for tissue healing
(39) Khadra et al, 2005 (Khadra et al., 2005)	**Wavelength:** 830 nm **Light source type:** Laser **Power:** 84mW **Pulse frequency:** **Beam area:** **Exposure time:** **Radiant energy (J):** **Fluence (J/cm²):** 1.5-3 **Irradiance (mW/cm²):**	pHGFs	Laser irradiation promoted attachement to titanium implant material.
(40) Khadra at al, 2005 (Khadra et al., 2005)	**Wavelength:** 830 nm **Light source type:** GaAlAs laser **Power:** 84mW **Pulse frequency:** **Beam area:** **Exposure time:** **Radiant energy (J):** **Fluence (J/cm²):** 1.5-3 **Irradiance (mW/cm²):**	pHGFs and osteoblast like cells	Irradiation promoted attachment to titanium Application of light at 3J/cm² induced significant increases in Osteocalcin and TGFβ1.

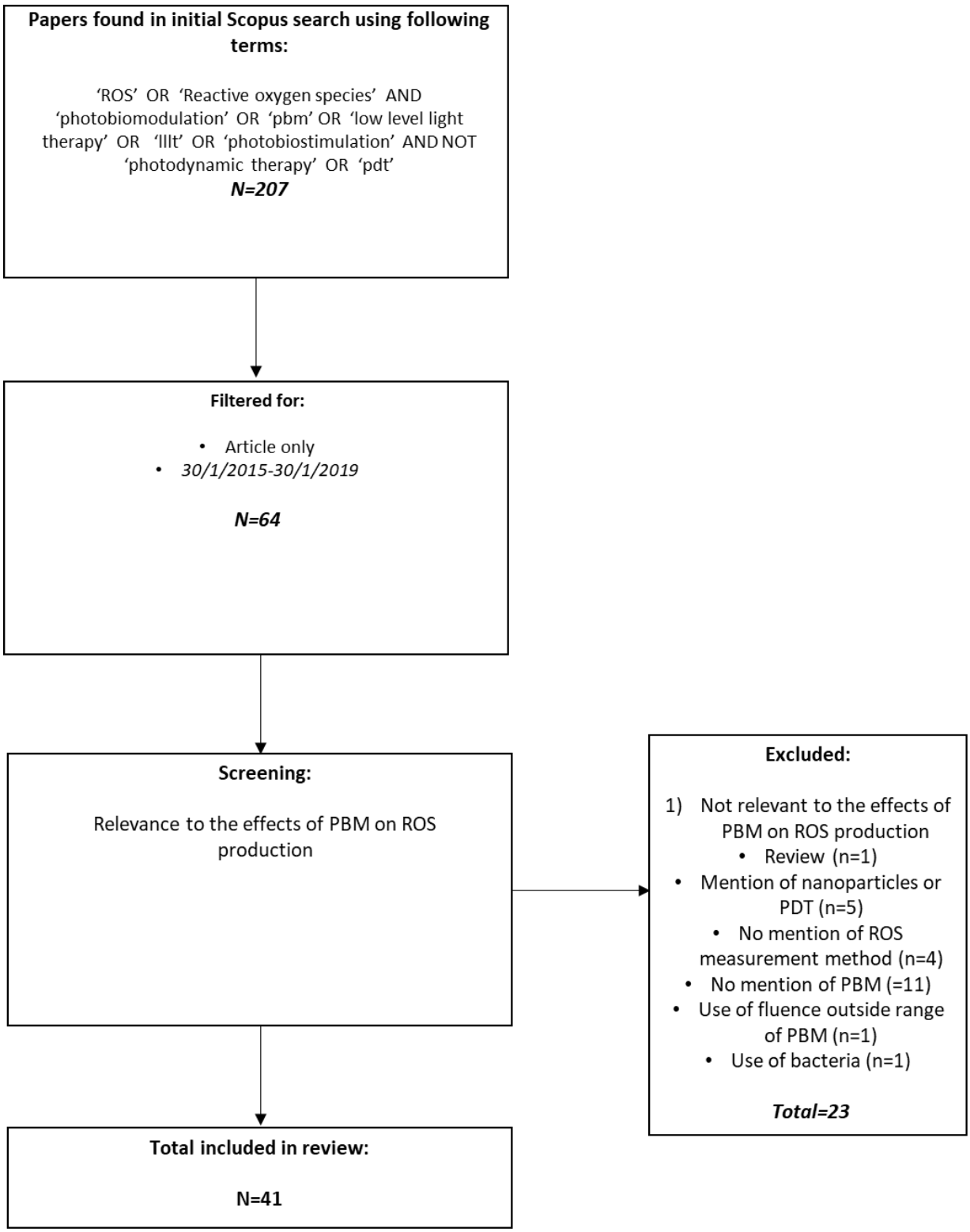

Figure 10.4: Indicates strategy employed to systematically evaluate the effects of PBM on ROS production.

Table 10.4: Citations identified from a review evaluating the effects of PBM on ROS production using the following key words: 'ROS' OR 'Reactive oxygen species' AND 'photobiomodulation' OR 'pbm' OR 'low level light therapy' OR 'PBM' OR 'photobiostimulation' AND NOT 'photodynamic therapy' OR 'pdt'

Citation	Light Parameters used	Subject/cell type	Effects	Probe Used
Lim et al, 2015 (Lim et al., 2015)	**Wavelength:**635 nm **Light source type:** LED **Power (mW):** **Pulse frequency:** N/A (continuous wave (cw)) **Beam area (cm^2):** **Exposure time:** 1 hour **Radiant energy (J)** **Fluence (J/cm^2):** **Irradiance (mW/cm^2):** 5	immortalized gingival fibroblasts	Light irradiation induced a decrease in ROS production compared to cells treated with LPS only. Indirect irradiation induced an initial increase in ROS production but then induced a decrease long term.	H_2DCFDA
Cavalcanti et al, 2015 (Cavalcanti et al., 2015)	**Wavelength:** 660 **Light source type:** laser **Power (mW):** 50 **Pulse frequency:** **Beam area (cm^2):** 0.38 **Exposure time (s):** 0-90 **Radiant energy (J)** **Fluence (J/cm^2):** 1-12 **Irradiance (mW/cm^2):**	dog bone marrow stem cell cultures	Irradiation induced no significant changes in ROS production.	Monoaldehyde formation assay (MDA)
Wang et al, 2015 (Wang et al., 2015)	**Wavelength:** 660 nm **Light source type:** LED **Power (mW):** **Pulse frequency:** **Beam area (cm^2): Exposure time (s):** **Radiant energy (J)** **Fluence (J/cm^2):** 0-20 **Irradiance (mW/cm^2):**	Sprague-Dawley male rats, with wound inflicted by incision	Application of 20J/cm^2 light induced increase in Heme oxygenase-1 (HO-1), thus thought to induce decreases in ROS production.	HO-1 gene expression as a marker for ROS
Liang et al, 2015 (Liang et al., 2015)	**Wavelength:** 810 nm **Light source type:** laser **Power (mW):** **Pulse frequency:** **Beam area (cm^2): Exposure time (s):** 0-60 **Radiant energy (J)** **Fluence (J/cm^2):** 10-60 **Irradiance (mW/cm^2):** 1000	Human oral cancer cell (OC2)	Increased ROS production induced by light.	H_2DCFDA
Fuma et al, 2015 (Fuma et al., 2015)	**Wavelength:** 670 nm **Light source type:** LED **Power (mW):** **Pulse frequency:** **Beam area (cm^2): Exposure time (s):** 250 (twice a day, for 4 days) **Radiant energy (J)** **Fluence (J/cm^2):** **Irradiance (mW/cm^2):** 3.89	ARPE-19 and human retinal pigment epithelium cells	PBM reduced ROS production.	CM-H2DCFDA
Denadai et al, 2015 (Denadai et al., 2015)	**Wavelength:** 660 nm **Light source type:** laser (InGaAlP) **Power (mW):** 100 **Pulse frequency:** **Beam area (cm^2):** 0.028 **Exposure time (s):** 60s per point **Radiant energy (J)** **Fluence (J/cm^2):** 6 **Irradiance (mW/cm^2):** 3570	Male Wistar rats, with diabetes induced by streptozotocin. Wounds also induced by incision.	Application of light reduced oxidative stress induced by wound incision.	TBARs (using MDA)
Giacci et al, 2015 (Giacci et al., 2015)	**Wavelength:** 440 nm, 550 nm, 670 nm, 810 nm **Light source type:** **Power (mW):** **Pulse frequency:** **Beam area (cm^2): Exposure time (s):** **Radiant energy (J)** **Fluence (J/cm^2):** 0.000234-0.38 **Irradiance (mW/cm^2):** 0.013-20.11	pheochromocytoma (PC12), Müller (rMC1) and primary mixed retinal cells.	PBM induced no significant effect on ROS production.	DCFH-DA and H_2O_2 detection assays

Spitler et al, 2015 (Spitler et al., 2015)	**Wavelength:** 652 nm, 806 nm, 637 nm and 901 nm **Light source type:** laser (652 nm and 901 nm), LED (637 nm and 901 nm) **Power (mW):** **Pulse frequency:** **Beam area (cm^2): Exposure time (s):** 1800 **Radiant energy (J)** **Fluence (J/cm^2):** 10.02(red), 2.334 (NIR) **Irradiance (mW/cm^2):** 5.57 (red), 1.3 (NIR)	Human osteosarcoma cells (U202)	Light application significantly reduced ROS production relative to the untreated control.	DCFDA
Khan et al, 2015 (Khan et al., 2015)	**Wavelength:** 810 **Light source type:** **Power (mW):** 3200-4500 (cells, 6 well plate), 1500-2100 (96-well plate) **Pulse frequency:** **Beam area (cm^2): Exposure time (s):** **Radiant energy (J)** **Fluence (J/cm^2):** 21 (mice), 20.7-28.2 **Irradiance (mW/cm^2):** 1000 (mice), 69-94 (cells)	HaCaT cells and normal oral keratinocyte cells (NOKSI). C57BL/6NCr male mice	Irradiation induced significant increases in ROS production from black plates, could be due to increase in temperature also. Laser also induced increases in ROS production from mice.	H_2DCFDA (cells), ROSstar 800CW probe, detects extracellular ROS (mice)
Velikanov et al, 2015 (Velikanov et al., 2015)	**Wavelength:** 590 **Light source type:** laser **Power (mW):** **Pulse frequency:** 2-60Hz **Beam area (cm^2): Exposure time (s):** 30fs **Radiant energy (J)** **Fluence (J/cm^2):** 6-4299 **Irradiance (mW/cm^2):** 1.07-$3.2x10^{13}$	rat mesenchymal stromal cells (MSCs)and human HaCaT keratinocytes	No increase in ROS generation was observed in analysis of culture medium.	Iodide-iodine method (measures H_2O_2).
Dong et al, 2015 (Dong et al., 2015)	**Wavelength:** 830 nm **Light source type:** **Power (mW):** **Pulse frequency:** **Beam area (cm^2): Exposure time (s):** **Radiant energy (J)** **Fluence (J/cm^2):** 0.1-10 **Irradiance (mW/cm^2):**	Human neuroblastoma SH-SY5Y and C57BL/6 mice with induced traumatic brain injury (TBI)	Decreased ROS production from Cobalt chloride treated cells	H_2DCFDA
Carvalho et al, 2016 (Costa Carvalho et al., 2016)	**Wavelength:**660 nm **Light source type:** GaAlAs diode laser **Power (mW):** 30 **Pulse frequency:** N/A (continuous wave (cw)) **Beam area (cm^2):** 0.8 **Exposure time:** 5 minutes **Radiant energy (J):** 9 **Fluence (J/cm^2):** 112.5 **Irradiance (mW/cm^2):** 375	BALF from Balb/c mice.	Light induced and increase in SOD activity of allergic mice but had no effect on healthy mice. Light also caused a reduction in ROS generation from allergic mice but had no effect on ROS generation from healthy mice.	ROS generation was assessed using ELISA. SOD activity was assessed using hypoxanthine.
Cedeira et al, 2016 (Cerdeira et al., 2016)	**Wavelength:**660 nm or 780 nm **Light source type:** **Power (mW):** 40 **Pulse frequency:** N/A (continuous wave (cw)) **Beam area (cm^2):** 0.04 **Exposure time (s):** 6-480 **Radiant energy (J):** 19.2 **Fluence (J/cm^2):** **Irradiance (mW/cm^2):** 1000	Neutrophils (healthy male)	Light induced an increase in generation of radicals including hydroxyl radical, hypochlorite anions and superoxide anions. PBM also induced generalised increase in ROS generation. 660 nm and 19.2J were most effective in inducing this increase.	Hydroxyl radical and hypocholite anion generation was assessed using hydroxyphenyl fluorescein and aminophenyl flourescein.
Bartos et al, 2016 (Bartos et al., 2016)	**Wavelength:**810 nm **Light source type:** **Power (mW):** **Pulse frequency:** N/A (continuous wave (cw)) **Beam area (cm^2):** **Exposure time (s):** 100 **Radiant energy (J):** 1 **Fluence (J/cm^2):** 3 **Irradiance (mW/cm^2):** 30	Cochlear hair cells (HEI-OCI, mouse)	PBM induced a decrease in gentamicin or LPS induced oxidative stress.	CellROX and DCF-DA were used to assess superoxide generation and generalised ROS generation.

Erthal et al, 2016 (Erthal et al., 2016)	**Wavelength:**830 nm **Light source type:** GaAlAs diode laser **Power (mW):** **Pulse frequency:** N/A (continuous wave (cw)) **Beam area (cm²):** 6 **Exposure time (s):** 10 **Radiant energy (J)** **Fluence (J/cm²):** 4 **Irradiance (mW/cm²):**	Paw tissue from Female swiss mice.	PBM induced a decrease in ROS generation by 55% caused by inflammation from edema induced by the drug carrageenan.	DCFH-DA
Alves et al, 2016 (Alves et al., 2016)	**Wavelength:**808 nm **Light source type:** GaAlAs diode laser **Power (mW):** 30 **Pulse frequency:** N/A (continuous wave (cw)) **Beam area (cm²):** **Exposure time:** **Radiant energy (J)** **Fluence (J/cm²):** 28 or 56 **Irradiance (mW/cm²):**	Sperm from rams diluted in TALP medium.	PBM had no significant effect on ROS generation from sperm.	CellROX
Tatmatsu-Rocha et al 2016 (Tatmatsu-Rocha et al., 2016)	**Wavelength:**904 nm **Light source type:** GaAlAs diode laser **Power (mW):** 40 **Pulse frequency:** pulsed, 20ms **Beam area (cm²):** 0.1309 **Exposure time (s):** 60 **Radiant energy (J)** **Fluence (J/cm²):** **Irradiance (mW/cm²):**	Male Swiss mice, skin supernatant	PBM induced a reduction in oxidative stress in diabetic mice compared to non-irradiated diabetic mice and non-irradiated control. However, light also induced an increase in oxidative stress in irradiated control mice compared to the control.	TBARs
Riberio et al, 2016 (Ribeiro et al., 2016)	**Wavelength:** 660 nm and 780 nm **Light source type:** AlGaInP (660 nm) or AlGaAs (780 nm) **Power (mW):** 40 **Pulse frequency:** **Beam area (cm²):** 0.04 **Exposure time (s):** 80 **Radiant energy (J):** 3.2 **Fluence (J/cm²):** 10 **Irradiance (mW/cm²):** 1000	Wisar rats with cryoinjury of tibialis anterior	Oxidative stress was modulated following application of 660 nm light	2,4-dinitrofenylhydrazyne, chemiluminecence assay, oxidative stress profile assessment
de Silva Neto Trajano et al, 2016 (Alexsandra da Silva Neto Trajano et al., 2016)	**Wavelength:** 808 nm **Light source type:** **Power (mW):** 100 **Pulse frequency:** **Beam area (cm²): Exposure time (s):** 2-19 **Radiant energy (J)** **Fluence (J/cm²):** 10-70 **Irradiance (mW/cm²):**	C2C12 myoblast cultures	No significant increase in ROS production detected.	Flow cytometry
Shu et al, 2016 (Shu et al., 2016)	**Wavelength:** 810 nm **Light source type:** laser **Power (mW):** **Pulse frequency:** **Beam area (cm²): Exposure time (s):** **Radiant energy (J)** **Fluence (J/cm²):** 60 **Irradiance (mW/cm²):** 1000	Oral cancer cells	Light application induced significant increases in ROS production	Hydrogen peroxide assay kit
Becker et al, 2016 (Becker et al., 2016b)	**Wavelength:** 453 **Light source type:** LED **Power (mW):** **Pulse frequency:** **Beam area (cm²): Exposure time (s):** **Radiant energy (J)** **Fluence (J/cm²):** 0-41.4 **Irradiance (mW/cm²):** 23	HaCaT cells	Initial increase in ROS production induced by PBM however levels resume to that of the control 2h post application.	Amplex UltraRed
Janzedeh et al, 2016 (Janzadeh et al., 2016)	**Wavelength:** 660 **Light source type:** diode laser **Power (mW):** 100 **Pulse frequency:** **Beam area (cm²):** 0.238 **Exposure time (s):** every day for 2 weeks **Radiant energy (J)** **Fluence (J/cm²):** 4 **Irradiance (mW/cm²):** 354	Adult male Wistar rats with chronic constriction injury (CCI) to mimic neuropathic injury.	Irradiation increased antioxidant levels.	GSH as a marker for changes in ROS levels

Mamalis et al, 2016 (Mamalis et al., 2016)	**Wavelength:** 633 **Light source type:** **Power (mW):** **Pulse frequency:** **Beam area (cm²): Exposure time (s):** **Radiant energy (J)** **Fluence (J/cm²):** 320-640 **Irradiance (mW/cm²):** 872.6	Human dermal fibroblast cells	Irradiation increased ROS production	Flow cytometry: 7-amino-actinomycin D, Annexin V and FlowJo.
Engel et al, 2016 (Engel et al., 2016)	**Wavelength:** 808 **Light source type:** GaAlAs laser diode **Power (mW):** 600-900 **Pulse frequency:** **Beam area (cm²):** **Exposure time (s):** **Radiant energy (J)** **Fluence (J/cm²):** 11.3-17 **Irradiance (mW/cm²):** 38-57	Oral keratinocytes and fibroblasts	Increased ROS production in keratinocytes compared to fibroblasts.	DCFDA
Lee et al, 2017 (Lee et al., 2017a)	**Wavelength:** 635 nm **Light source type:** **Power (mW):** **Pulse frequency:** **Beam area (cm²):** **Exposure time (s):** 300 **Radiant energy (J)** **Fluence (J/cm²):** **Irradiance (mW/cm²):** 5	Bone marrow derived macrophages (BMMs)	Light application decreased ROS production.	H_2DCFDA
Zhu et al, 2017 (Zhu et al., 2017)	**Wavelength:** 633 nm **Light source type:** laser diode **Power (mW):** 750 **Pulse frequency:** **Beam area (cm²):** **Exposure time (s):** 15 **Radiant energy (J):** 10.95 **Fluence (J/cm²):** **Irradiance (mW/cm²):**	Mouse neuronal stem cells (NSCs)	Light treatments induced ROS production.	DCFDA
Yin et al, 2017 (Yin et al., 2017)	**Wavelength:** 660 **Light source type:** **Power (mW):** 3-4.5 **Pulse frequency:** 50 **Beam area (cm²):** **Exposure time (s):** **Radiant energy (J)** **Fluence (J/cm²):** **Irradiance (mW/cm²):**	Mesenchymal stem cells	Increased intracellular ROS, to enhance stem cell survival	DCFH2-DA
Santos et al, 2017 (Santos et al., 2017)	**Wavelength:** 405 **Light source type:** LED **Power (mW):** **Pulse frequency:** **Beam area (cm²):** 0.27 **Exposure time (s):** 30-60 **Radiant energy (J)** **Fluence (J/cm²):** **Irradiance (mW/cm²):** 300	In vitro: Subventricular zone (SVZ) cell culture.	Blue light induced transient increases in ROS, causing increased neuronal differentiation and increases retinoic acid receptor levels.	DCFDA or MitoSOX red
Salehpour et al, 2017 (Salehpour et al., 2017)	**Wavelength:** 660 nm and 810 nm **Light source type:** laser **Power (mW):** 200 **Pulse frequency:** 10 **Beam area (cm²):** **Exposure time (s):** **Radiant energy (J)** **Fluence (J/cm²):** 4-8 **Irradiance (mW/cm²):** 4.75	Mitochondria isolated from adult male BALB/c mice	Application of light reduced D-galactose induced increases in ROS production.	DCFDA
Wang et al, 2017 (Wang et al., 2017c)	**Wavelength:** 415, 540, 660, 810 **Light source type:** LED array (415 nm), Filtered lamp (540 nm), Diode laser (660 nm and 810 nm) **Power (mW):** **Pulse frequency:** **Beam area (cm²):** 4 **Exposure time (s):** 188 **Radiant energy (J)** **Fluence (J/cm²):** 3 **Irradiance (mW/cm²):** 16	*In vitro:* human adipose-derived stem cells.	Blue and green light induce significant increases in intracellular calcium and ROS, reduce mitochondrial membrane potential, lower intracellular pH and reducing cellular proliferation. Red and NIR light have the opposite effect.	CM-H2DCFDA

Djavid et al, 2017 (Djavid et al., 2017)	**Wavelength:** 685 nm **Light source type:** **Power (mW):** 50 **Pulse frequency:** **Beam area (cm^2):** **Exposure time (s):** 300-1200 **Radiant energy (J)** **Fluence (J/cm^2):** 5-20 **Irradiance (mW/cm^2):** 16.6	HeLa cells	20J/cm^2 enhanced radio sensitivity to ionising radiation due to increased oxidative stress.	DCF-DA
Hammami et al, 2018 (Hammami et al., 2018)	**Wavelength:** 655 nm and 780 nm simultaneously **Light source type:** diode laser **Power (mW):** **Pulse frequency:** **Beam area (cm^2):** **Exposure time (s):** 3600 **Radiant energy (J)** **Fluence (J/cm^2):** 55.4 **Irradiance (mW/cm^2):** 15.43	*in vivo* model of the chick embryo chorioallantoic membrane	Irradiation inhibited UV induced ROS production and lipid peroxidation	Dihydroethidium (DHE)
Rupel et al, 2018 (Rupel et al., 2018)	**Wavelength:** 970 nm, 660 nm, 880 nm, 800 nm, combined (660 nm, 880 nm, 970 nm) **Light source type:** GaAs diode laser **Power (mW):** **Pulse frequency:** **Beam area (cm^2):** **Exposure time (s):** **Radiant energy (J)** **Fluence (J/cm^2):** 3-6 **Irradiance (mW/cm^2):** 50-200	10 patients affected by oral mucositis. Polymorphonuclear neutrophils (PMNs) were isolated from 5 healthy volunteers. HaCaT and keratinocyte cells.	Reduced ROS production significantly from OM patients. 970 nm light application induced reductions in ROS production from both LPS stimulated and unstimulated PMNs. Real time evaluation revealed 880 nm and 970 nm reduced H_2O_2 induced increases in ROS production.	Total antioxidant status (saliva). DCFDA for PMNs and keratinocyte cells. HaCaT cells transfected with roGFP2-Orp1 to establish real time effects of PBM on ROS production.
Salehpour et al, 2018 (Salehpour et al., 2018a)	**Wavelength:** 810 nm **Light source type:** GaAlAs **Power (mW):** 200 **Pulse frequency:** 10Hz (88% duty cycle) **Beam area (cm^2):** 0.03 **Exposure time (s):** 5 **Radiant energy (J)** **Fluence (J/cm^2):** 8 **Irradiance (mW/cm^2):** 4750	Adult male BALB/c mice	Reduced ROS production in sleep derived mice.	DCFDA
Diniz et al, 2018 (Diniz et al., 2018)	**Wavelength:** 660 **Light source type:** InGaAlP **Power (mW):** 20 **Pulse frequency:** **Beam area (cm^2):** **Exposure time (s):** 4-7 **Radiant energy (J)** **Fluence (J/cm^2):** 3-5 **Irradiance (mW/cm^2):** 710	DPSCs	ROS production is dose dependent, addition of recombinant human Bone Morphogenetic Protein 4 (rhBMP4) abrogates this effect.	Dihydrorhodamine 123 (DHR 123), flow cytometry.
Feng et al, 2018 (Feng et al., 2018)	**Wavelength:** 635 **Light source type:** LED **Power (mW):** **Pulse frequency:** **Beam area (cm^2):** **Exposure time (s):** 300 (0, 6, 24, 48h time points) **Radiant energy (J)** **Fluence (J/cm^2):** **Irradiance (mW/cm^2):** 15	Hepatocytes	Induced ROS production	ROS detection assay kit
Mignon et al, 2018 (Mignon et al., 2018)	**Wavelength:** 450, 490, 550, 590, 650, and 850 nm **Light source type:** LED **Power (mW):** **Pulse frequency:** **Beam area (cm^2):** **Exposure time (s):** **Radiant energy (J)** **Fluence (J/cm^2):** 0-250 **Irradiance (mW/cm^2):** 30 (450 nm, 500 nm, 530 nm), 7 (590 nm), 60 (655 nm), 80 (850 nm).	Primary human reticular and papillary dermal fibroblasts	Dose dependent increase in ROS production from blue light exposed cultures.	CellROX deep red
George et al, 2018 (George et al., 2018)	**Wavelength:** 636 nm and 825 nm **Light source type:** laser **Power (mW):** 75 (636 nm) and 104 (825 nm) **Pulse frequency:** **Beam area (cm^2):** 9.08 **Exposure time (s):** 605.28-3026.4 (636 nm), 436.5-2128.5 (825 nm) **Radiant energy (J)**	Human dermal fibroblasts	ROS production is both wavelength and dose dependent.	H_2DCFDA

	Fluence (J/cm²): 5-25 **Irradiance (mW/cm²):** 8.26 (636 nm), 11.45 (825 nm)			
Serrage et al, 2019 (Serrage et al., 2019b)	**Wavelength:** 400-830 nm **Light source type:** LED **Power (mW):** **Pulse frequency:** **Beam area (cm²):** 0.335-0.370 **Exposure time (s):** 30 **Radiant energy (J)** **Fluence (J/cm²):** 0.72 **Irradiance (mW/cm²):** 24	C2C12 myoblast cells	Significant increases in ROS production induced by blue light particularly 24h post irradiation	H_2DCFDA
Migliario et al, 2019 (Migliario et al., 2018b)	**Wavelength:** 980 **Light source type:** diode laser **Power (mW):** 1000 **Pulse frequency:** **Beam area (cm²):** 1.54 **Exposure time (s):** 0-75 **Radiant energy (J):** 0-75 **Fluence (J/cm²):** 0-48.7 **Irradiance (mW/cm²):**	Neutrophils (primary)	PBM induces NETosis through dose dependent increases in ROS production (>50J)	Application of ROS scavengers (e.g. vitamin C) to abrogate effects of PBM induced NETosis.
Amaroli et al, 2019 (Amaroli et al., 2019)	**Wavelength:** 808 **Light source type:** laser **Power (mW):** 950 **Pulse frequency:** **Beam area (cm²):** 1 **Exposure time (s):** 60 **Radiant energy (J):** 67 **Fluence (J/cm²):** 57 **Irradiance (mW/cm²):**	human endothelial cell line (HECV)	Induced significant increases in oxidative stress 30-60min post irradiation	TBARs

Figure 10.5: Flow chart describing the strategy employed to identify relevant articles illustrating the effects of blue light

Table 10.5: Citations identified from a review of the literature evaluating the effects of blue light PBM using the following search terms: 'Blue AND light' OR '400 nm' OR '405 nm' OR '420 nm' OR '450 nm' OR '475 nm' OR '480 nm' AND 'Photobiomodulation' OR 'PBM' OR 'LLLT' OR 'Low AND Level AND light AND therapy' OR 'LILT' OR 'Low AND Intensity AND Light AND therapy' OR 'Photobiostimulation' AND NOT 'Photodynamic AND therapy' OR 'PDT'

Citation	Light Source	Dose	Study type	Conclusion
1. **Mignon et al, 2018(Mignon et al., 2018)**	**Source: LED** **Wavelength (nm):** 450, 490, 550, 650 and 850 **Power (mW):** **Frequency (Hz):** **Spot area (cm^2):**	**Irradiance (mW/cm^2):** 30 (450 nm), 30 (490 nm), 30 (550 nm), 7 (590 nm), 60 (655 nm), 80 (850 nm) **Time (s):** **Energy (J):** **Radiant exposure (J/cm^2):** 0-250 **(dependent upon wavelength)**	*In Vitro:* Human reticular and papillary dermal fibroblasts	450 nm light at 30J/cm^2 induced 50% reductions in cell metabolic activity. 450 nm and 500 nm induced stronger inhibitory effects on reticular DFs vs papillary DFs. 450 nm light induced increases in intracellular ROS production. Blue and NIR light induced changes in some similar gene groups. However, more genes were downregulation following irradiation with blue light compared to NIR. Blue light also downregulated expression of genes associated with the TGF-β pathway.
2.Tani et al, 2018 (191)	**Source:** LED **Wavelength (nm):** 405, 635, 808 **Power (mW):** **Frequency (Hz):** **Spot area (cm^2):**	**Irradiance (mW/cm^2):** 12.59 **Time (s):** 30 **Energy (J):** **Radiant exposure (J/cm^2):** 0.378	*In Vitro:* human osteoblasts and human mesenchymal stromal cells.	Blue light had no significant effect on molecular signalling. 635 nm light could be effective in promoting or improving bone regeneration as shown through molecular analysis.
3.Priglinger et al, 2018 (Priglinger et al., 2018)	**Source:** LED **Wavelength (nm):** 475, 516, 635 **Power (mW):** **Frequency (Hz):** pulsed 2.5 (pulse rate 50%) **Spot area (cm^2):**	**Irradiance (mW/cm^2):** 40 **Time (s):** 600 **Energy (J):** **Radiant exposure (J/cm^2):** 24	*In Vitro:* Stromal Vascular fraction cells	Blue, green and red light did not have a cytotoxic effect on cells. Red and green light induced significant increases in vascular endothelial growth factor expression.
4.Falcone et al, 2018 (Falcone et al., 2018)	**Source:** LED **Wavelength (nm):** 453 **Power (mW):** **Frequency (Hz):** 5% duty cycle, 100Hz **Spot area (cm^2):**	**Irradiance (mW/cm^2):** 10 (cw), 200 (pulsed) **Time (s):** 1800 **Energy (J):** **Radiant exposure (J/cm^2):** 18	*In Vivo:* effects on inflammation and skin barrier recovery.	Reduced IL-1α following irradiation.
5.Veleska-Stevkoska and Koneski, 2018 (Veleska-Stevkoska and Koneski, 2018)	**Source:** LED **Wavelength (nm):** 410 and 470 **Power (mW):** **Frequency (Hz):** **Spot area (cm^2):** 1.25	**Irradiance (mW/cm^2):** 750 **Time (s):** 10-20 **Energy (J):** 50-100 **Radiant exposure (J/cm^2):** 7.5-15	*In Vivo:* Haemostasis in oral surgery (bleeding from tooth extractions).	Blue light shortens bleeding time from extraction socket.
6. Castellano-Pellicena et al, 2018 (Castellano-Pellicena et al., 2018)	**Source:** LED **Wavelength (nm):** 447, 505, 530, 655 and 850 (24 well) or 453, 656 (ex vivo) **Power (mW):** **Frequency (Hz):** **Spot area (cm^2):**	**Irradiance (mW/cm^2):** **Time (s):** 1200 (24 well) **Energy (J):** **Radiant exposure (J/cm^2):** 453 nm- 2, 656 nm- 30	*In vitro and ex vivo:* Keratinocytes and human skin epidermis	Blue light stimulated metabolic activity of cultured keratinocytes. Low levels of blue light reduced DNA synthesis and stimulated keratinocyte differentiation. Level of differentiation induced by blue light was reduced in opsin 3 (OPN3) knockdown,

				suggesting OPN3 may be Important in blue light induced restoration of barrier function.
7. Fekrazad et al, 2018(Fekrazad et al., 2018)	**Source:** Laser **Wavelength (nm):** 810, 660, 532, 485, *combinations:* 810-660, 810-485, 660-532, 660-485 **Power (mW):** 30-200 (dependent on wavelength) **Frequency (Hz):** **Spot area (cm^2):** 0.113-0.18	**Irradiance (mW/cm^2):** 266 (blue), 266 (green) 167 (red), 1333(NIR) **Time (s):** 3-24 (dependent upon wavelength) **Energy (J):** **Radiant exposure (J/cm^2):** 4 (8 for combination)	*In vitro:* Mesenchymal stem cells.	Cartilage markers were upregulated by 810 nm and 810-485 nm light. Red and blue-green irradiation induced expression of COL1. Blue, blue-green and green light irradiation reduced osteocalcin expression. Stimulatory effects on osteogenesis were seen for red and near infra-red lasers but green light had inhibitory effects. Blue light was not reported to induce inhibitory effects. Cons: Parameters differ considerably from one wavelength to the next, particularly when evaluating combination treatments. Making results of which wavelength is most effective questionable.
8. Rocca et al, 2018 ~~(183)~~ (Rocca et al., 2018)	**Source:** diode laser (450 nm, 635 nm, 808 nm, Er:YAG laser (2940 nm) **Wavelength (nm):** 2940, 808, 450, 635 **Power (mW):** 200 (635 nm), 1500 (808 nm), 500 (450 nm) **Frequency (Hz):** 20 (Er:YAG) **Spot area (cm^2):**	**Irradiance (mW/cm^2):** 280 (808 nm), 280 (450 nm), 1000 (63 5 nm) **Time (s):** 60 (2940 nm), 3x30 (635 nm), 60 (808 nm), 60 (450 nm) **Energy (J):** **Radiant exposure (J/cm^2):** 76.43 (Er:YAG), 36 (635 nm), 50 (808 nm), 17 (450 nm)	*In Vivo:* Human	The diode lasers proved more effective than the Er:YAG in reducing pain scores over a 7 day period. 635 nm had the most immediate effect, but there was no significant difference pain score using the 3 diode lasers after 7 days.
9. Wang et al, 2018 (Wang et al., 2018)	**Source:** LEDs **Wavelength (nm):** 405 **Power (mW):** 200 **Frequency (Hz):** **Spot area (cm^2):**	**Irradiance (mW/cm^2):** 20 **Time (s):** 900 **Energy (J):** **Radiant exposure (J/cm^2):** 12	*In Vitro:* Whole blood samples (human)	No significant change in the absorption spectra exhibited by blood following irradiation.
10. Kim et al, 2017(Kim et al., 2017b)	**Source:** LEDs **Wavelength (nm):** 410, 630, 830 **Power (mW):** **Frequency (Hz):** **Spot area (cm^2):**	**Irradiance (mW/cm^2):** **Time (s):** **Energy (J):** **Radiant exposure (J/cm^2):**	*In Vivo:* Mouse model	Wound closure percentage over 10 days was greatest when an 830 nm LED used. Increased TGF-β and collagen 1 but downregulated SMAD7.
11.Rohringer et al, 2017 (Rohringer et al., 2017)	**Source:** LED **Wavelength (nm):** 475, 516, 635 **Power (mW):** **Frequency (Hz):** 50% pulse rate, 2.5Hz **Spot area (cm^2):**	**Irradiance (mW/cm^2):** 80 **Time (s):** 600 **Energy (J):** **Radiant exposure (J/cm^2):** 24	*In Vitro:* Human umbilical vein endothelial cells	Red and green light induced proliferation and migration of endothelial cells whilst blue light had no significant impact. Blue light only induced significant increases in ROS production. NOTE: irradiance and irradiation time values do not correlate with fluency. Cells irradiated at 20% confluency – may explain negative effects of blue light.

12.Wang et al, 2017 (Wang et al., 2017c)	**Source:** LED array (415 nm), Filtered lamp (540 nm), Diode laser (660 nm and 810 nm) **Wavelength (nm):** 415, 540, 660, 810 **Power (mW):** **Frequency (Hz):** **Spot area (cm^2):** 4	**Irradiance (mW/cm^2):** 16 **Time (s):** 188 **Energy (J):** **Radiant exposure (J/cm^2):** 3	*In vitro:* human adipose-derived stem cells.	Blue and green light induce significant increases in intracellular calcium and ROS, reduce mitochondrial membrane potential, lower intracellular pH and reducing cellular proliferation. Red and NIR light have the opposite effect. Labelled fluency as irradiance. Different delivery systems may alter light delivery (coherent vs non-coherent light sources).
13.Wang et al, 2017(Wang et al., 2017a)	**Source:** LED **Wavelength (nm):** 480, 560, 660 and white (400-750) **Power (mW):** 3000 **Frequency (Hz):** **Spot area (cm^2):**	**Irradiance (mW/cm^2):** 250 **Time (s):** **Energy (J):** **Radiant exposure (J/cm^2):**	*In vitro and in vivo:* Irradiated fertile broiler eggs and isolated skeletal muscle and satellite cells.	Green PBM promoted muscle growth and satellite cell proliferation through insulin growth factor-1 signalling in late embryogenesis.
14.Choe et al, 2017 (Choe et al., 2017)	**Source:** LED **Wavelength (nm):** 622, 535, 462 **Power (mW):** 24000 **Frequency (Hz):** **Spot area (cm^2):**	**Irradiance (mW/cm^2):** 16 **Time (s):** 600-1800 (daily) **Energy (J):** **Radiant exposure (J/cm^2):**	*In Vitro*: HeLa cells (cancer cell line).	Blue light and high frequency ultrasound induced significant reductions in cell density when compared to red and green light combined with ultrasound. This could be beneficial in alleviating cancer cell proliferation.
15.Buscone et al, 2017 (Buscone et al., 2017)	**Source:** LED **Wavelength (nm):** 453, 689 **Power (mW):** **Frequency (Hz):** **Spot area (cm^2):**	**Irradiance (mW/cm^2):** **Time (s):** **Energy (J):** **Radiant exposure (J/cm^2):** 3.2	*In vitro and ex vivo:* hair growth and outer root sheath cells.	Blue light at low radiant exposure stimulate hair growth ex vivo.
16. Santos et al, 2017 (Santos et al., 2017)	**Source:** LED **Wavelength (nm):** 405 **Power (mW):** **Frequency (Hz):** **Spot area (cm^2):** 0.27	**Irradiance (mW/cm^2):** 300 **Time (s):** 30-60 **Energy (J):** **Radiant exposure (J/cm^2):**	*In vitro:* Subventricular zone (SVZ) cell culture.	Blue light induced transient increases in ROS, causing increased neuronal differentiation and increases retinoic acid receptor levels. The effects are heightened with the addition of light reactive nanoparticles.
17. Fekrazad et al, 2017(Fekrazad et al., 2017)	**Source:** laser: GaAs (405 nm, 532 nm), InGaAlP (660 nm) and GaAlAs (810 nm) **Wavelength (nm):** 405, 532, 660, 810 **Power (mW):** **Frequency (Hz):** **Spot area (cm^2):** 1	**Irradiance (mW/cm^2):** 200 **Time (s):** **Energy (J):** **Radiant exposure (J/cm^2):** 1.5	*In Vivo:* Male Wistar rats (n=60)	Green, blue, red and infrared light irradiation may accelerate healing process.
18.Lee et al, 2017(Lee et al., 2017b)	**Source:** LED **Wavelength (nm):** 410, 630, 830 **Power (mW):** **Frequency (Hz):** **Spot area (cm^2):**	**Irradiance (mW/cm^2):** 205 (405 nm), 172 (630), 50 (830) **Time (s):** **Energy (J):** **Radiant exposure (J/cm^2):** 10	*In Vitro:* Keloid fibroblasts	Blue did not affect cell viability. COL1 gene and protein expression decreased significantly after irradiation with blue light and may be effective in preventing keloid formation.
19. Alba et al, 2017 (Alba et al., 2017)	**Source:** LED (470) and laser (660) **Wavelength (nm):** 470 and 660 **Power (mW):** **Frequency (Hz):** **Spot area (cm^2):**	**Irradiance (mW/cm^2):** **Time (s):** 180 (470), 60 (660) **Energy (J):** 6-8 **Radiant exposure (J/cm^2):**	*In Vivo:* treatment of acne vulgaris	The combined use of red and blue light proved beneficial in reducing inflammation and enhancing wound healing when

				compared to the use of salicylic acid for treatment.
20. Mignon et al, 2017(Mignon et al., 2017)	**Source:** LED **Wavelength (nm):** 400, 500, 530, 590, 655, 850 **Power (mW):** **Frequency (Hz):** **Spot area (cm²):**	**Irradiance (mW/cm²):** 3-80 **Time (s):** **Energy (J):** **Radiant exposure (J/cm²):** 2-30	*In Vitro:* Human dermal fibroblasts	The effects of blue light on cell metabolism were dramatically influenced by FBS concentration, confluency level of cells and the fluency values applied to cells.
21. Yoshimoto et al, 2017(Yoshimoto et al., 2018)	**Source:** LED **Wavelength (nm):** 465 **Power (mW):** **Frequency (Hz):** **Spot area (cm²):**	**Irradiance (mW/cm²):** 30 **Time (s):** 1800 **Energy (J):** **Radiant exposure (J/cm²):** 54	*In Vitro:* Human colon cancer cells (HT-29 or HCT-116)	Blue light irradiation reduced cancer cell viability. However, this effect was reversed in an Opsin 3 (Opn3) knockdown.
22. Yuan et al, 2017(Yuan et al., 2017)	**Source:** LED **Wavelength (nm):** 470 **Power (mW):** **Frequency (Hz):** **Spot area (cm²):**	**Irradiance (mW/cm²):** 20 **Time (s):** 60-3600 **Energy (J):** **Radiant exposure (J/cm²):**	*In Vitro:* Bone marrow-derived mesenchymal stem cells (BMSCs)	Blue light inhibited osteogenic differentiation, induced apoptosis as a result of increased ROS production and DNA damage.
23. Monrazeri et al, 2017 (Montazeri et al., 2017)	**Source:** LED **Wavelength (nm):** 630, 808, 450 **Power (mW):**100 (630 nm and 808 nm), 3000 (450 nm) **Frequency (Hz):** **Spot area (cm²):** 1	**Irradiance (mW/cm²):** 100 (630 nm) **Time (s):** **Energy (J):** 48J per point **Radiant exposure (J/cm²):**	*In vivo:* Human	Combining all three wavelengths reduced abdominal girth significantly.
24. Li et al, 2016(Li et al., 2016)	**Source:** LED **Wavelength (nm):** 630, 460 **Power (mW):**100 (630 nm and 808 nm), 3000 (450 nm) **Frequency (Hz):** **Spot area (cm²):** 300	**Irradiance (mW/cm²):** 50 **Time (s):** 900-1800 **Energy (J):** **Radiant exposure (J/cm²):** 45-90	*In vivo:* Japanese big ear white rabbits, induced wound model (incisions in back)	Red light was more effective in promoting wound healing than blue light.
25. Khori et al, 2016 (Khori et al., 2016)	**Source:** Laser **Wavelength (nm):** 405, 532, 632 **Power (mW):** 1-3 **Frequency (Hz):** **Spot area (cm²):**	**Irradiance (mW/cm²):** **Time (s):** 600 (10 treatments, 3 times a week) **Energy (J):** **Radiant exposure (J/cm²):**	*In vivo and in vitro:* BALB/c inbred female mice and mouse mammary carcinoma cell line (4T1).	Blue light reduced tumour volume and gene expression markers for tumorigenesis.
26. AlGhamdi et al, 2016 (AlGhamdi et al., 2016)	**Source:** laser **Wavelength (nm):** 457, 635, 355 **Power (mW):** **Frequency (Hz):** **Spot area (cm²):**	**Irradiance (mW/cm²):** 25 **Time (s):** 80 **Energy (J):** **Radiant exposure (J/cm²):** 2	*In Vitro:* Melanocytes from normal human melanocytes.	PBM at all wavelengths induced the production of stage I melanosomes to the highest levels relative to control cells. In particular, red and blue laser PBM induced the highest increase in % level of stage I melanosomes. This indicates significant stimulation of melanogenesis.
27. Wang et al, 2016 (Wang et al., 2016)	**Source:** LED array (420), Filtered lamp (540), Diode laser (660, 810). **Wavelength (nm):** 420, 540, 660, 810 **Power (mW):** **Frequency (Hz):** **Spot area (cm²):** 4	**Irradiance (mW/cm²):** 16 **Time (s):** 188 (five times, every 2 days). **Energy (J):** **Radiant exposure (J/cm²):** 3	*In Vitro:* Human adipose-derived stem cells.	Blue and green light were effective in stimulating osteoblast differentiation and increasing intracellular calcium levels than red and near infra-red light. Blue and green light could activate light-gated calcium ion channels.
28. Masson-Meyers et al, 2016(Masson-Meyers et al., 2016a)	**Source:** LED **Wavelength (nm):** 470 **Power (mW):** 150 **Frequency (Hz):** **Spot area (cm²):**	**Irradiance (mW/cm²):** 30 **Time (s):** **Energy (J):** **Radiant exposure (J/cm²):** 3, 5, 10, 55	*In Vitro:* Human Dermal Fibroblasts	Blue light and radiant exposure of 5J/cm² improved wound healing, increased protein concentration and reduced IL-6 secretion significantly. There was no effect of

				irradiation on cell viability.
29. Ashworth et al, 2016 (Ashworth et al., 2016)	**Source:** LED **Wavelength (nm):** 450, 510, 660, 860 **Power (mW):** **Frequency (Hz):** **Spot area (cm²):**	**Irradiance (mW/cm²):** **Time (s):** **Energy (J):** **Radiant exposure (J/cm²):** **Other:** photons/cm²/s	*Ex Vivo*: Rat or mouse spinal cord slices	All four wavelengths at the highest intensity output reduced immunoreactivity.
30. Figurova et al, 2016 (Figurová et al., 2016)	**Source:** LED **Wavelength (nm):** 685/470 combined **Power (mW):** **Frequency (Hz):** **Spot area (cm²):**	**Irradiance (mW/cm²):** 8 **Time (s):** **Energy (J):** **Radiant exposure (J/cm²):** 3.36	*In Vivo*: Minipigs	Combined red and blue light therapy induced improved tissue healing relative to control groups.
31. Becker et al, 2016 (Becker et al., 2016a)	**Source:** LED **Wavelength (nm):** 453 **Power (mW):** **Frequency (Hz):** **Spot area (cm²):**	**Irradiance (mW/cm²):** 23 **Time (s):** 1800 **Energy (J):** **Radiant exposure (J/cm²):**	*In Vitro*: Melanoma cells	The effects of blue light on cell viability were dose dependent and blue light down regulated anti-inflammatory genes but upregulated genes associated with apoptosis. Significant decreases in viability were witnessed after irradiation times of 1800s.
32. Dereci et al, 2016 (Dereci et al., 2016)	**Source:** LED (blue, 400-490), GaAlAs diode laser (NIR, 980 nm) **Wavelength (nm):** 400-490, 980 **Power (mW):** **Frequency (Hz):** **Spot area (cm²):**	**Irradiance (mW/cm²):** 12 (400-490), 200 (980) **Time (s):** **Energy (J):** **Radiant exposure (J/cm²):** 13 (400-490, 20 (980)	*In Vivo*: Wistar rats	Whilst high doses of blue light were inhibitory, low doses proved efficacious in promoting bone regeneration to similar levels to NIR light.
33. Takhtfooladi and Sharifi, 2015 (Takhtfooladi and Sharifi, 2015)	**Source:** GaAlAs (680), LED (650, 450) **Wavelength (nm):** 680, 650, 450 **Power (mW):** 10 (680) **Frequency (Hz):** Pulsed (no info, 680 only) **Spot area (cm²):** 0.4 (680), 1.5 (650, 450)	**Irradiance (mW/cm²):** **Time (s):** 200s (680), 600s (450, 650) 14 days **Energy (J):** **Radiant exposure (J/cm²):** 10 (680), 650 (2.4), 450 (2.4)	*In Vivo*: New Zealand rabbits	Blue and red LEDs had no significant effect on cell proliferation or myelination. Conversely, laser red light had a significant effect. This may be due to the pulsed modality of the laser light source.
34. Fekrazad et al, 2015 (Fekrazad et al., 2015)	**Source:** laser **Wavelength (nm):** 630, 532, 425 **Power (mW): Frequency (Hz):** **Spot area (cm²):**	**Irradiance (mW/cm²):** 50 (630 nm and 532 nm), 55 (425 nm) **Time (s):** **Energy (J):** **Radiant exposure (J/cm²):** 2	*In Vivo:* Diabetes induced male Wistar rats	All three wavelengths induced significant increases in wound healing, where red light was most effective.
35. Masson-Meyers et al, 2015 (Masson-Meyers et al., 2015)	**Source:** LED or Laser **Wavelength (nm):** 405 **Power (mW):** **Frequency (Hz):** **Spot area (cm²):**	**Irradiance (mW/cm²):** **Time (s):** 900, 1800, 14400 **Energy (J):** **Radiant exposure (J/cm²):** 40, 54, 81, 121	*In Vitro*: Methicillin Resistant Staphylococcus Aureus (MRSA)	Both LED and laser proved efficacious in supressing bacterial growth to significant levels at all four radiant exposure values evaluated.
36. Schafer and McNeely, 2015 (Schafer and McNeely, 2015)	**Source:** LED **Wavelength (nm):** 405 **Power (mW):** **Frequency (Hz):** **Spot area (cm²):**	**Irradiance (mW/cm²):** 30 **Time (s):** **Energy (J):** **Radiant exposure (J/cm²):**	*In Vitro:* *Staphylococcus Epidermis*, *Staphylococcus Aureus* and *Propionibacterium Acnes*	The effects of blue light combined with ultrasound were dose dependent where it is proposed that bacterial cells become more susceptible to the antimicrobial effects of blue light following ultrasound application.
37. Niu et al, 2015 (Niu et al., 2015)	**Source:** LED **Wavelength (nm):** 405, 630, 660 **Power (mW):** **Frequency (Hz):** **Spot area (cm²):**	**Irradiance (mW/cm²):** 161μW/cm² nm (405 nm), 300μW/cm² nm (630 nm), 545μW/cm² nm (660 nm) **Time (s):** 600 **Energy (J):** **Radiant exposure (J/cm²):** 1.604 (405 nm), 3.409 (630 nm), 6.538 (660 nm)	*In Vitro*: Keratinocytes	The combination of blue light, red light and curcumin was able to regulate proliferation and apoptosis of keratinocytes. Without curcumin, light did not influence cell viability.

38. AlGhamdi et al, 2015 (AlGhamdi et al., 2015)	**Source:** diode laser **Wavelength (nm):** 355, 457, 635 **Power (mW):** **Frequency (Hz):** **Spot area (cm²):**	**Irradiance (mW/cm²):** 25 **Time (s):** 20-200 **Energy (J):** **Radiant exposure (J/cm²):** 0.5-5	*In Vitro*: Melanocytes	Blue laser proved most efficacious in promoting cell proliferation and migration.
39. Pfaff et al, 2015 (Pfaff et al., 2015)	**Source:** LED **Wavelength (nm):** 453 **Power (mW):** **Frequency (Hz):** High (200mW/cm²) and low (100mW/cm²) duty cycles employed **Spot area (cm²):**	**Irradiance (mW/cm²):** 100 (low), 200 (high) **Time (s):** 1800 **Energy (J):** **Radiant exposure (J/cm²):** 90	*In Vivo*: Treatment of patients with mild Psoriasis Vulgaris (Pv).	Blue light proved to significantly reduce Pv severity at both irradiance outputs.
40. Bumah et al, 2015(Bumah et al., 2015)	**Source:** LED **Wavelength (nm):** 470 **Power (mW):** 150 (18 delivered to cultures) **Frequency (Hz):** **Spot area (cm²):**	**Irradiance (mW/cm²):** 30 **Time (s):** **Energy (J):** **Radiant exposure (J/cm²):** 55	*In Vitro*: MRSA	Blue light alone is effective in supressing MRSA growth, where there was no significant difference in the effect of blue light and the combination of blue light and hyperbaric oxygen.
41. Jung et al, 2015 (Jung et al., 2015)	**Source:** LED **Wavelength (nm):** 415, 630 **Power (mW):** **Frequency (Hz):** **Spot area (cm²):**	**Irradiance (mW/cm²):** **Time (s):** 76-615 **Energy (J):** **Radiant exposure (J/cm²):** 5-40	*In Vitro*: Human Sebocytes	Blue and red light influence lipid production and may have beneficial effects on acne through the suppression of sebum production.
42. Teuschl et al, 2015 (Teuschl et al., 2015a)	**Source:** LED **Wavelength (nm):** 470, 630 **Power (mW):** 1000 **Frequency (Hz):** **Spot area (cm²):**	**Irradiance (mW/cm²):** 50 **Time (s):** 600 (5 times, once per day) **Energy (J):** **Radiant exposure (J/cm²):** 30	*In Vitro*: C2C12 (myoblast), NIH/3T3 (fibroblast), BICR10 (keratinocytes)	Blue light reduced cell proliferation and promoted necrosis. Red light promoted cell proliferation and increased rate of wound healing.
43. Hadis et al, 2015(Hadis et al., 2015)	**Source:** LED **Wavelength (nm):** 400-900 **Power (mW):** **Frequency (Hz):** **Spot area (cm²):**	**Irradiance (mW/cm²):** 3.5 **Time (s):** 15-120 **Energy (J):** **Radiant exposure (J/cm²):** 0.05-0.42	*In Vitro:* Dental Pulp cells (DPCs)	Blue light had no significant effect on DPCs whilst wavelengths of 625 nm, 660 nm, 789 nm and 800 nm induced significant increases in mitochondrial activity. Particularly after 24hrs and irradiation periods of 30s.
44. De Sousa et al, 2015 (De Sousa et al., 2015)	**Source:** LED **Wavelength (nm):** 450 **Power (mW):** 70 **Frequency (Hz):** **Spot area (cm²):** 0.00785	**Irradiance (mW/cm²):** **Time (s):** 0-343 **Energy (J):** **Radiant exposure (J/cm²):** 3-24	*In Vitro: Staphylococcus aureus, Pseudomonas aeruginosa*	Blue light inhibited bacterial growth at fluency values greater than 6J/cm².
45. Gold et al, 2014 (Gold et al., 2014)	**Source:** LEDs **Wavelength (nm):** 405-460 **Power (mW):** **Frequency (Hz):** **Spot area (cm²):**	**Irradiance (mW/cm²):** **Time (s):** **Energy (J):** **Radiant exposure (J/cm²):**	*In Vivo:* Human	Induced a reduction in acne vulgaris inflammatory lesions. Did induce increases in skin temperature up to 41°C.
46. Schoenly et al, 2014(Schoenly et al., 2014)	**Source:** laser **Wavelength (nm):** 400 **Power (mW):** **Frequency (Hz):** 60ns laser pulse **Spot area (cm²):**	**Irradiance (mW/cm²):** **Time (s):** **Energy (J):** **Radiant exposure (J/cm²):** <8	*In Vitro:* Human teeth	Removal of calculus is thickness dependent and can occur at radiant exposure <5J/cm²
47. Buravlev et al, 2014 (Buravlev et al., 2014b)	**Source:** LED **Wavelength (nm):** 442 **Power (mW):** 70 **Frequency (Hz):** **Spot area (cm²):** 0.00785	**Irradiance (mW/cm²):** **Time (s):** 30-300 **Energy (J):** **Radiant exposure (J/cm²):** 30	*In Vitro:* Mitochondria isolated from male albino rat livers.	Blue light restored nitric oxide inhibited rates of respiration to normal. It is hypothesised blue light irradiation induces photolytic destruction of nitrosyl complexes that inhibit the activities of complex I and III of the electron transport chain.

48. Sinclair et al, 2014 (Sinclair et al., 2014)	**Source:** LED **Wavelength (nm):** 465, 574 **Power (mW):** **Frequency (Hz):** **Spot area (cm^2):**	**Irradiance (mW/cm^2):** 0.0848 (blue), 0.0185 (yellow) **Time (s):** 2700 **Energy (J):** **Radiant exposure (J/cm^2):** **Other:** 68 lux, 1.21xphotons/cm^2/s	*In Vivo:* Patients with traumatic brain injury (TBI)	Blue light is effective in alleviating fatigue and daytime sleeping following TBI
49. Hochman et al, 2014 (Hochman et al., 2014)	**Source:** LED (470 nm and 660 nm) and Laser (660 nm and 808 nm, no details of laser source) **Wavelength (nm):** 470, 660, 808 **Power (mW):** 100 (808 nm, 660 nm Laser) and 350 (470 nm and 660 nm LED). **Frequency (Hz):** **Spot area (cm^2):** 0.5 (LED), 0.028 (laser)	**Irradiance (mW/cm^2):** **Time (s):** 114 (LED), 396 (laser) **Energy (J):** 40 (both) **Radiant exposure (J/cm^2):** 80 (LED), 1429 (laser)	*In Vivo:* Skin of adult male Wistar rats.	Infrared (808 nm) laser irradiation enhances neuropeptide secretion in healthy rat skin, whilst other sources of light and wavelengths had no significant impact.
50. Dungel et al, 2014(Dungel et al., 2014)	**Source:** LED **Wavelength (nm):** 470, 629 **Power (mW):** **Frequency (Hz):** **Spot area (cm^2):**	**Irradiance (mW/cm^2):** 50 **Time (s):** 600 **Energy (J):** **Radiant exposure (J/cm^2):** 30	*In Vivo*: Sprague-Dawley rats	Both wavelengths promoted angiogenesis, improved tissue perfusion, reduced tissue necrosis and therefore promoted wound healing.
51. KazemiKhoo and Ansari et al, 2014 (KazemiKhoo and Ansari, 2014)	**Source:** Optical fiber **Wavelength (nm):** 405, 632.8 **Power (mW):** 1.5 **Frequency (Hz):** **Spot area (cm^2):** 0.01	**Irradiance (mW/cm^2):** **Time (s):** 1800 (every other day, 14 sessions) **Energy (J):** **Radiant exposure (J/cm^2):**	*In Vivo*: Intravascular laser irradiation of blood in type 2 diabetic patients and measurements of changes in blood sugar.	Both wavelengths induced significant decreases in blood sugar levels.
52. Burvalev et al, 2014 (Buravlev et al., 2014a)	**Source:** Laser (442 nm, 532 nm) and LED (650 nm) **Wavelength (nm):** 442, 532, 650 **Power (mW):** 20 **Frequency (Hz):** **Spot area (cm^2):** 1.57	**Irradiance (mW/cm^2):** 30 **Time (s):** 30-300 **Energy (J):** **Radiant exposure (J/cm^2):** 3-31	*In Vitro*: Mitochondria isolated from rat liver.	Laser of mitochondria at 442 nm restored mitochondrial respiration inhibited by NO. Blue light also restored complex IV activity but not complexes I-III. Other wavelengths had no significant effect.
53. Turrioni et al, 2013(Turrioni et al., 2013)	**Source:** **Wavelength (nm):** 450, 630, 850 **Power (mW):** **Frequency (Hz):** **Spot area (cm^2):**	**Irradiance (mW/cm^2):** **Time (s):** **Energy (J):** **Radiant exposure (J/cm^2):**	*In Vitro:* Human dentin	All three wavelengths passed through the dentin barrier. LED power loss and transmittance varied dependent upon dentin thickness and wavelength.
54. Kazemi Khoo et al, 2013(Kazemi Khoo et al., 2013)	**Source:** laser **Wavelength (nm):** 405 **Power (mW):** 1.5 **Frequency (Hz):** **Spot area (cm^2):**	**Irradiance (mW/cm^2):** **Time (s):** 1800 **Energy (J):** **Radiant exposure (J/cm^2):**	*In Vivo:* Human diabetic patients	Resulted in modulation of metabolites associated with type 2 diabetes following intravenous PBM.
55. Cheon et al, 2013 (Cheon et al., 2013)	**Source:** LED **Wavelength (nm):** 470, 525, 633 **Power (mW):** **Frequency (Hz):** **Spot area (cm^2):**	**Irradiance (mW/cm^2):** 3.55 (470 nm), 4.02 (525 nm) and 6.78 (633 nm) **Time (s):** 3600 (9 days) **Energy (J):** **Radiant exposure (J/cm^2):**	*In Vivo*: Sprague Dawley rats and histological analysis	Blue and green light promoted wound healing significantly. Red light promoted collagen production.
56. Burvalev et al, 2013 (Buravlev et al., 2013)	**Source:** HeCd laser (442 nm) diode pumped solid state laser (532 nm) and LED (650 nm) **Wavelength (nm):** 442, 532, 650 **Power (mW):** 20 **Frequency (Hz):** **Spot area (cm^2):** 1.57	**Irradiance (mW/cm^2):** **Time (s):** 30-300 (1 treatment) **Energy (J):** **Radiant exposure (J/cm^2):**	*In Vivo*: Lipopolysaccharide B was applied through intraperitoneal injection to outbred albino rats. Mitochondria were then isolated from rat liver.	Blue light induced a 40% increase in mitochondrial respiration from LPS treated animals at a dose of 6J/cm^2
57. Kushibiki et al, 2013 (Kushibiki et al., 2013)	**Source:** Laser **Wavelength (nm):** 405, 664, 808 **Power (mW):** **Frequency (Hz):** **Spot area (cm^2):**	**Irradiance (mW/cm^2):** 100 **Time (s):** 60-120 **Energy (J):** **Radiant exposure (J/cm^2):**	*In Vitro*: mouse preadipocytes (3T3-L1), prechondrocytes (ATDC5), myoblasts (C2C12), mesenchymal stromal cells (KUSA-	After blue light irradiation, intracellular ROS production was significantly increased in all cell types whilst

			A1), lung cancer cells (LLC), insulinoma cells (MIN6), fibroblasts (NIH-3T3), human cervix adenocarcinoma cells (HeLa), macrophages differentiated from lymphocytes (THP-1) after treatment with phorbol ester, and rat basophilic leukemia cells (RBL-2H3)	red and near infra-red light had no significant effect.
58. Fushimi et al, 2012(Fushimi et al., 2012)	**Source:** LED **Wavelength (nm):** 456, 518, 638 **Power (mW):** 7560 (63 8 nm), 6930 (456 nm) and 6840 (518 nm) **Frequency (Hz):** **Spot area (cm²):** 30	**Irradiance (mW/cm²):** 0.75 (638 nm), 0.25 (456 nm) and 0.17 (518 nm) **Time (s):** 1200 **Energy (J):** **Radiant exposure (J/cm²):** 0.6 (638 nm), 0.3 (456 nm), 0.2 (518 nm)	*In Vivo and in vitro:* Induced wound model in ob/ob mice	LED irradiation induced significant increases in growth factor and cytokine secretion. Green LEDs promote wound healing by inducing migratory and proliferative mediators.
59. Lavi et al, 2012(Lavi et al., 2012)	**Source:** LED **Wavelength (nm):** 400-505, 600-800 **Power (mW):** **Frequency (Hz):** **Spot area (cm²):**	**Irradiance (mW/cm²):** 30 (600-800 nm), 10 (400-505 nm) **Time (s):** **Energy (J):** **Radiant exposure (J/cm²):**	*In Vitro:* Sperm membranes	Visible (especially blue) light induce increase in ROS production in isolate sperm isolated plasma membranes
60. Adamskaya N et al, 2011(Adamskaya et al., 2011)	**Source:** LED **Wavelength (nm):** 470, 630 **Power (mW):** 1000 **Frequency (Hz):** **Spot area (cm²):**	**Irradiance (mW/cm²):** 50 **Time (s):** 600 **Energy (J):** **Radiant exposure (J/cm²):**	*In Vivo:* Induced wound model (excision wound on dorsum), Sprague Dawley rats	Blue light was effective in inducing wound healing and promoting keratin expression.
61. Shuvaeva et al, 2011(Shuvaeva et al., 2011)	**Source:** laser **Wavelength (nm):** 473, 650 **Power (mW):** 20 **Frequency (Hz):** **Spot area (cm²):**	**Irradiance (mW/cm²):** 20 **Time (s):** **Energy (J):** **Radiant exposure (J/cm²):**	*In vivo:* WKY and SHR rats	Irradiation with red light proved more effective than blue light in augmenting the constrictive effects of Norepinephrine on pial arteries. However both exerted a significant difference relative to the control.
62. Bonatti et al, 2011(Bonatti et al., 2011)	**Source:** LED **Wavelength (nm):** 470 **Power (mW):** 100 **Frequency (Hz):** **Spot area (cm²):** 0.8	**Irradiance (mW/cm²):** 125 **Time (s):** 60-180 **Energy (J):** 6, 12, 18 **Radiant exposure (J/cm²):** 59.87, 122.3, 183.43	*In vitro:* Keloid and skin fibroblasts, human	Reduced skin fibroblasts following irradiation at 183.43J/cm² but induced no significant effect on keloid fibroblast number.
63. Ankri et al, 2010(Ankri et al., 2010b)	**Source:** LED **Wavelength (nm):** 400-830 **Power (mW):** **Frequency (Hz):** **Spot area (cm²):**	**Irradiance (mW/cm²):** **Time (s):** **Energy (J):** **Radiant exposure (J/cm²):**	Computational model of human dermis: photon migration model	480 nm may be useful for treating infected wounds whilst 780 nm has a higher penetration depth and therefore may be useful for wound healing.
64. De Sousa et al, 2010(de Sousa et al., 2010)	**Source:** LED **Wavelength (nm):** 700, 530, 460 **Power (mW):** 15 (700 nm), 8 (530 nm), 22 (460 nm) **Frequency (Hz):** **Spot area (cm²):** 2.01	**Irradiance (mW/cm²):** 7.46 (700 nm), 3.98 (530 nm), 10.94 (460 nm) **Time (s):** 668 (700 nm), 1250 (530 nm), 456 (460 nm) **Energy (J):** **Radiant exposure (J/cm²):** 10	*In Vivo and In vitro:* Male Wistar rats with excisional wound, followed by histological analysis.	Green and red LEDs induced increases in fibroblast number relative to the control.
65. Ankri et al, 2010(Ankri et al., 2010a)	**Source:** LED **Wavelength (nm):** 400-800 **Power (mW):** **Frequency (Hz):** **Spot area (cm²):**	**Irradiance (mW/cm²):** 130 **Time (s):** 300 **Energy (J):** **Radiant exposure (J/cm²):**	*In vitro:* Sperm and endothelial cells	Illumination induced increase in NO concentration, particularly blue light.
66. Kushibiki et al, 2010(Kushibiki et al., 2010)	**Source:** LED **Wavelength (nm):** 405 **Power (mW):**	**Irradiance (mW/cm²):** 100 **Time (s):** 180 **Energy (J):**	*In vitro:* Prechondrogenic cells	Intracellular ROS increased and mRNA levels relating to

	Frequency (Hz): **Spot area (cm^2):**	**Radiant exposure (J/cm^2):**		chondrogenesis were elevated.
67. Sebbe et al, 2009(Sebbe et al., 2009)	**Source:** LED **Wavelength (nm):** 472 **Power (mW):** **Frequency (Hz):** **Spot area (cm^2):**	**Irradiance (mW/cm^2):** 1.26-4.73 **Time (s):** 8-24h **Energy (J):** **Radiant exposure (J/cm^2):**	*In vivo:* Male Wistar rats.	Increased bilirubin degradation, important for neonatal jaundice.
68. Tamarova et al, 2009 (Tamarova et al., 2009)	**Source:** LED **Wavelength (nm):** 480-3400 (range of source, evaluated 'red, orange, yellow, blue, green, violet') **Power (mW):** **Frequency (Hz):** **Spot area (cm^2):**	**Irradiance (mW/cm^2):** 40 **Time (s):** 600 **Energy (J):** **Radiant exposure (J/cm^2):** 2.4 (per minute)	*In vivo:* Male albino rats with area of pain induced by saline injection	Red light was more effective in inducing an analgesic effect. However, all colours induced significant increases in analgesia relative to control.

10.2 Conference abstracts

Photobiomodulatory Effect of Low Level Light on Oral Fibroblasts: H. Serrage, P. Cooper, W. Palin, O. Darch, M. Milward, M Hadis, BSODR-IADR17/ British Society for Oral and Dental Research.

The Photobiomodulatory Effect of Blue Light on Oral Fibroblasts: H. Serrage, P. Cooper, W. Palin, O. Darch, M. Milward, M Hadis IADR, IADR18/ International Association for dental research.

The Differential Responses of Myoblasts and Myotubes to Photobiomodulation is associated with Mitochondrial Number: H. Serrage, S. Joanisse, P. R. Cooper, W. Palin, M Hadis, O. Darch, A. Philp, M. R. Milward, WALT 18/World Association for Light Therapy.

Photobiomodulatory Effect of Blue Light on Oral Fibroblasts: H. Serrage, P. Cooper, W. Palin, O. Darch, S. Kuehne, M Hadis, M. Milward, OMIG19/ Oral Microbiology and Immunology group PGR prize symposium.

The use of Photobiomodulation in the management of oral disease: H. Serrage, P. Cooper, W. Palin, O. Darch, P. Horstman, M Hadis, M. Milward, BSP19/British Society for Periodontology

10.3 Awards, grants and prizes

2018: IADR 3MT® (3 minute thesis): 1st Place

(www.youtube.com/watch?v=wHCMqwTY8fo)

2019: OMIG PGR Prize Symposium, 15-minute presentation: 1st Place

2019: Finalist for 3MT® competition (University of Birmingham, UK).

2019: Last round Finalist for the Sir Wilfred Fish Prize (BSP, Brighton, UK).

10.4 Publications

Published: (Major contributor and first author)

Serrage H, Joanisse S, Cooper PR, Palin W, Hadis M, Darch O, Philp A, Milward M. *Differential Responses of Myoblasts and Myotubes to Photobiomodulation are associated with Mitochondrial Number*. J Biophotonics. 2019:e201800411.

Published: (Major contributor and first author)

Serrage H, Heiskanen V, Palin W, Cooper P, Milward M, Hadis M, Hamblin M. *Under the spotlight: mechanisms of photobiomodulation concentrating on blue and green light*. Photochemistry and Photobiology Sciences. doi: 10.1039/c9pp00089

Received: 6 November 2018 | Revised: 22 January 2019 | Accepted: 29 January 2019

DOI: 10.1002/jbio.201800411

Journal of BIOPHOTONICS

FULL ARTICLE

Differential responses of myoblasts and myotubes to photobiomodulation are associated with mitochondrial number

Hannah J. Serrage[1,2,3]* | Sophie Joanisse[2] | Paul R. Cooper[1] | William Palin[1] | Mohammed Hadis[1] | Owen Darch[3] | Andrew Philp[2,4] | Mike R. Milward[1]

[1]School of Dentistry, College of Medical and Dental Sciences, Institute of Clinical Sciences, University of Birmingham, Birmingham, UK

[2]School of Sport, Exercise and Rehabilitation Sciences, University of Birmingham, Birmingham, UK

[3]Philips Research, Eindhoven, The Netherlands

[4]Garvan Institute of Medical Research, Darlinghurst, New South Wales, Australia

*Correspondence
Hannah J. Serrage, Birmingham Dental Hospital, 5 Mill Pool Way, Birmingham B5 7EG, UK.
Email: hjs535@student.bham.ac.uk

Funding information
Engineering and Physical Sciences Research Council

Objective: Photobiomodulation (PBM) is the application of light to promote tissue healing. Current indications suggest PBM induces its beneficial effects in vivo through upregulation of mitochondrial activity. However, how mitochondrial content influences such PBM responses have yet to be evaluated. Hence, the current study assessed the biological response of cells to PBM with varying mitochondrial contents.

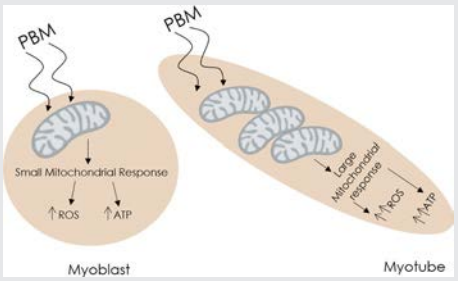

Methods: DNA was isolated from myoblasts and myotubes (differentiated myoblasts), and mitochondrial DNA (mtDNA) was amplified and quantified using a microplate assay. Cells were seeded in 96-wellplates, incubated overnight and subsequently irradiated using a light-emitting diode array (400, 450, 525, 660, 740, 810, 830 and white light, 24 mW/cm^2, 30-240 seconds, 0.72-5.76J/cm^2). The effects of PBM on markers of mitochondrial activity including reactive-oxygen-species and real-time mitochondrial respiration (Seahorse XFe96) assays were assessed 8 hours post-irradiation. Datasets were analysed using general linear model followed by one-way analysis of variance (and post hoc-Tukey tests); $P = 0.05$).

Results: Myotubes exhibited mtDNA levels 86% greater than myoblasts ($P < 0.001$). Irradiation of myotubes at 400, 450 or 810 nm induced 53%, 29% and 47% increases (relative to non-irradiated control) in maximal respiratory rates, respectively ($P < 0.001$). Conversely, irradiation of myoblasts at 400 or 450 nm had no significant effect on maximal respiratory rates.

Conclusion: This study suggests that mitochondrial content may influence cellular responses to PBM and as such explain the variability of PBM responses seen in the literature.

KEYWORDS

low-level laser therapy, low-level light therapy, mitochondria, myogenesis, photobiomodulation

1 | INTRODUCTION

Photobiomodulation (PBM) is a non-invasive treatment that utilises light at a power output less than 500 mW at wavelengths from 400 to 1100 nm to promote tissue healing, reduce inflammation and induce analgesia [1]. Over 800 publications have reported the efficacy of PBM in treating an array of musculoskeletal conditions including subacute and chronic low back pain [2] and exercise induced muscle fatigue [3]. Musculoskeletal disorders relate to an array of conditions that affect movement and are a significant burden, not only to the affected individual but also to healthcare systems due to the costs associated with management. Indeed, a report by the World Health Organization concluded that up to 33% of the population are affected by lower back pain at any given time [4].

Despite the positive evidence surrounding the use of PBM in treating musculoskeletal conditions, controversy still surrounds its application in practice due to a lack of consistency in the recording of treatment parameters. Notably, a number of key irradiation parameters should be reported including wavelength (nm) and irradiance (mW/cm^2), amongst others [5]. These parameters are often either misreported or not reported at all making it difficult to compare literature currently published.

Another key caveat in the use of PBM is the lack of knowledge as to how light energy elicits its beneficial molecular effects. Current literature indicates light acts directly upon the mitochondrial electron transport chain (ETC), specifically complex IV [6]. The ETC is formed of five complexes, and its main purpose is to produce adenosine triphosphate (ATP), the cells energy source. It is understood that photons of light at wavelengths including 810 nm excite complex IV, causing the dissociation of nitric oxide (NO) from its binding site, allowing oxygen to bind in its place and therefore allowing the progression of the ETC [6, 7]. As the ETC progresses, complexes I and III of the chain also produce reactive oxygen species (ROS). The production of ROS and ATP then induce the activation of transcription factors and subsequent gene expression changes including increased nuclear factor E2-related factor 2 (Nrf2) [8], a gene whose expression is commonly associated with increased mitochondrial biogenesis [9].

Many studies report the effect of PBM on mitochondrial activity through the use of surrogate assays including ROS [10] and ATP [11] generation. However, despite wide evidence supporting this ideology, no studies to date report the effects of PBM on mitochondrial respiration or whether mitochondrial number can influence response to PBM. In fact, the number of mitochondria per cell can vary from 80 to 2000 dependent upon the cell type explored [12]. Robin and Wong reported that there are approximately 1000 mitochondria per liver cell, whilst there are around 300 mitochondria per human lung fibroblast cell [13].

This study aimed to first characterise a system that could be employed to evaluate the effects of PBM on changes in mitochondrial respiration in real time and second to determine the optimal treatment parameters that elicit a molecular response in muscle-derived cells in which mitochondrial activity is key to their behaviour. C2C12 myoblasts have been suggested to be an appropriate model for mimicking the process of skeletal muscle cell differentiation in vitro [14]. When exposed to appropriate conditions myoblasts differentiate into myotubes in vitro [15]. Mature myotubes are cited to have a higher population of mitochondria than myoblasts [16, 17]. Hence, myoblasts and myotubes were employed to determine whether cells with a higher mitochondrial population responded differently to PBM.

2 | METHODS

2.1 | Light-emitting diode array characterisation

2.1.1 | Spectral characterisation

A UV–Vis spectrometer (USB4000; Ocean Optics, Largo, Florida) coupled to a 200-μm optical fibre and 3.9-mm cosine corrector and calibrated to the National Institute of Standards and Technology (NIST) standards was employed to assess the spectral irradiance and wavelength delivered at the base of each individual culture well (n = 6). Absolute irradiance was determined from the integral of the spectral irradiance (380-880 nm). Further detail outlining spectral characterisation methods, light-emitting diode (LED) array design and selection of wavelengths are described by Hadis et al [18].

2.1.2 | Beam profile

A charge coupled device beam profile camera (SP620; Ophir, Spiricon, Israel) was employed to measure spatial distribution of power emitted from each LED in the array. A 50-mm closed-circuit television lens (Ophir) was attached to the camera and focused on the base of each well. Following linear, optical and ambient light correction, images were recorded using BeamGage software (Ophir). Detailed experimental procedure has previously been reported by Hadis et al [18].

2.2 | Biological responses

2.2.1 | Myoblasts culture

A mouse myoblast cell line (C2C12 [American Type Culture Collection (ATCC) CRL-1722], ATCC, LGC standards, UK, passage 8-11) [14] was cultured in monolayers in Dulbecco's modified eagle medium (DMEM, Gibco, ThermoFischer Scientific, Waltham, Massachusetts) supplemented with 10% v/v fetal calf serum, 1% v/v penicillin/streptomycin (P/S) and 1% v/v L-glutamine (Sigma-Aldrich, St Louis, Missouri). Cells were seeded into 96-well black clear bottom plates (7000 cells/well; Sigma-Aldrich) and Seahorse XFe96 plates (10,000 cells/well; Agilent, Santa Clara, California), incubated overnight (37°C, 5% CO_2>), irradiated as

described in Section 2.2.3 and changes in mitochondrial activity were assessed 8 or 24 hours post-irradiation.

2.2.2 | Myotube differentiation

Myoblast cultures were seeded into Seahorse XFe96 plates as described in Section 2.2.1 and approximately 70% confluency was reached, cultures were washed with phosphate buffered saline (PBS) and differentiation media was subsequently applied which contained phenol red free DMEM containing 2% v/v horse serum and 1% v/v sodium pyruvate (Sigma-Aldrich) to induce differentiation for 6 days. Myotubes were then irradiated as described above, and changes in mitochondrial activity were assessed 8 hours post-irradiation.

2.2.3 | Array characterisation for Seahorse XF cell mitochondrial stress assay [Agilent]

A Seahorse XFe96 Analyser (Agilent) was employed to measure the cells' oxygen consumption rate (OCR) as a marker of mitochondrial respiration. One hour prior to undertaking the assay, culture media was aspirated, cells washed with PBS three times and Seahorse XF assay media (25-mM glucose, 1-mM pyruvate and 2-mM glutamine; Agilent) was applied and equilibrated in a CO_2 free incubator (INCU-line; VWR, Radnor, Pennsylvania). Compounds altering mitochondrial activity were then applied to the system including: Oligomycin (inhibits complex V of the ETC, 1 μM), carbonyl cyanide-4(trifluoromethoxy)phenylhydrazone (FCCP, uncoupling agent induces respiration to be undergone at maximal rates, 2 μM), antimycin and rotenone A (inhibit complexes I and III, inhibiting ETC activity, 0.5 μM). Subsequently, the plate was placed in a Seahorse XFe96 analyser (Agilent) and compounds were sequentially injected into the system to induce changes in ETC activity. The Seahorse analyser then measured changes via assessment of OCR in real time (OCR, pmol/min). OCR values were subsequently normalised for protein content in individual wells. Protein concentration was determined using detergent compatible protein assay (Bio-rad, Hercules, California). This enabled calculation of individual parameters including basal respiration, maximal respiration, ATP production, spare respiratory capacity and non-mitochondrial respiration [8]. During analysis, values for non-mitochondrial activity were subtracted from values evaluating the effects of PBM directly on the mitochondrial activity. This provided a further control step ensuring results would reflect the effects of PBM on mitochondrial activity only.

An opaque dental silicone impression material (3 M; Impregum Penta Soft, Maplewood, Minnesota) mask (Figure 1B) was created to ensure uniform irradiation of in vitro cultures and to eliminate light bleed at the base of wells where cells adhere (Figure 1C and D). The distance between the LEDs and specimen surface was fixed at 3 mm in each well. The spectral irradiance and beam profile of each diode were evaluated with the mask fitted to a Seahorse microplate (Figure 1D). Characterisation was then undergone as described in Section 2.1. The effects of PBM were evaluated at wavelengths spanning the visible and near infrared spectra (400-830 nm) at irradiation periods between 30 and 240 seconds and an irradiance output of 24 mW/cm^2 to achieve radiant exposures of 0.72 to 5.76 J/cm^2.

2.2.4 | Mitochondrial DNA quantification

A REPLI-g mitochondrial DNA kit (Qiagen, Hilden, Germany) was used to amplify mtDNA in whole DNA samples isolated from cell cultures. Sample DNA concentrations were measured spectrophotometrically (Eppendorf Biophotometer, Eppendorf, UK) and diluted accordingly to contain 10 ng/μl of DNA. Amplification of mtDNA was then undertaken according to the manufacturer's protocol.

To assess mtDNA quantities in cell supernatants, initially a standard curve was generated using calf thymus DNA at a maximal concentration of 10 ng/μl. SYBR Safe DNA gel stain (10 000× concentrate; Invitrogen, Carlsbad, California) was diluted in Tris-acetate-EDTA buffer at 1:1250. Samples and standards were then combined at 2% v/v with the dilute SYBR Safe dye and incubated for 10 minutes [19]. Fluorescence was measured using a fluorimeter (Twinkle LB 970, 485 nm/535 nm, excitation/emission, respectively; Berthold Industries Ltd., Bad Wildbad, Germany).

2.2.5 | 3-(4, 5-dimethylthiazol-2-yl)-2,5-diphenyltetrazolium bromide assay

To assess cell metabolic activity, a 3-(4, 5-dimethylthiazol-2-yl)-2,5-diphenyltetrazolium bromide (MTT) assay (Sigma-Aldrich) was utilised [20]. MTT was dissolved in PBS at 0.05 g/mL and aliquoted at 15 μL/well 8/24 hours post-irradiation and incubated for 4 hours at 37°C. MTT solution was aspirated and replaced with 50 μL/well of dimethyl sulphoxide (Sigma-Aldrich). Absorbance was read at 570 nm using a microplate reader (ELx800 Universal Microplate reader; Bio-Tek Instruments, Winooski, Vermont).

2.2.6 | ROS assay

ROS formation was assessed using 2′, 7′-dichlorodihydrofluorescein diacetate (H_2DCFDA) fluorescent probe (Thermo-Fischer Scientific, Waltham, Massachusetts). Free radicals catalyse the conversion of H_2DCFDA to its fluorescent bi-marker 2′,7′-dichlorofluorescein, enabling quantification of ROS production. At 8 hours post-irradiation media was aspirated, cells were washed with PBS and were treated with 10-μm H_2DCFDA and incubated for 1 hour at 37°C [21]. Fluorescence was read using a fluorimeter as described in Section 2.2.3.

2.3 | Statistical analysis

Data were processed utilising Excel software (Microsoft Redmond, Washington), and analysis was performed using

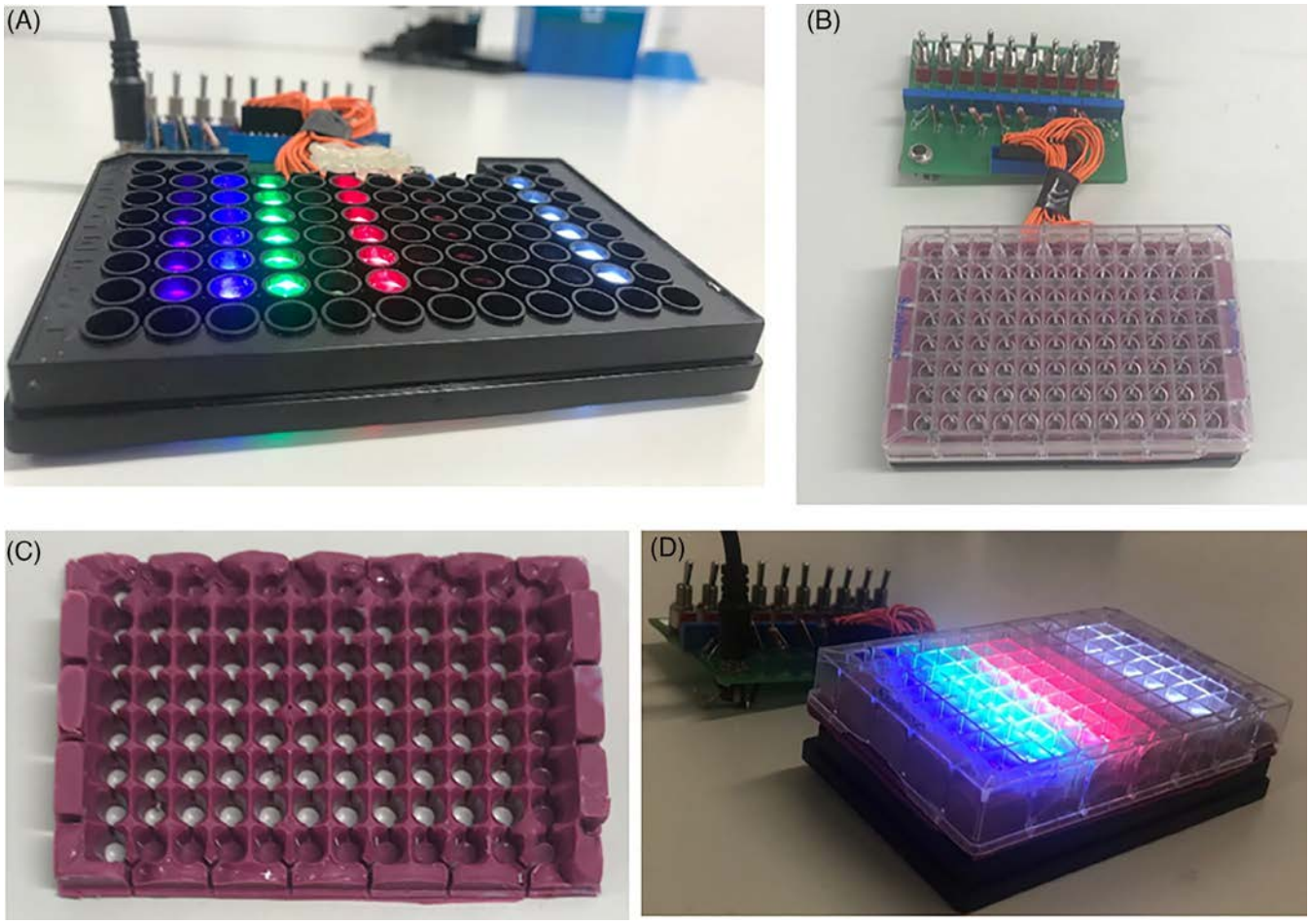

FIGURE 1 Indicates design and experimental setup of the LED array in 96 well format in which shows (A) LED array without plate-overlaid (B) array overlaid with 96 well black clear bottom plate (no wavelengths on) (C) mask constructed from opaque dental silicone impression material and (D) seahorse XFe96 plate fitted with mask and placed upon LED array when on (all wavelengths). All spectral characterisation experiments were undertaken with the Seahorse plate fitted mask placed directly above the LED array ensuring concentric alignment with LEDs beneath

SigmaPlot software (Systat Software Inc, San Jose, California). All data were analysed using a general linear model followed by one-way analysis of variance test followed by a Tukey test to determine significant differences between non-irradiated controls and light treated groups ($P < 0.05$).

3 | RESULTS AND DISCUSSION

3.1 | Characterisation of LED arrays for use in seahorse assays

LED arrays provide a high-throughput approach for analysis of multiple parameters and their effects in vitro. The current study first aimed to characterise a system that could be employed for use with the Seahorse XFe96 analyser system.

A mask constructed from silicon was designed to surround each well of the plate, preventing bleed between wells to ensure only a single wavelength of light would impact the biological response in each well-culture. Spectral characterisation undertaken to confirm wavelength and spectral irradiance values were consistent with those used in previous studies employing different plate formats [18]. Data indicated the array employed for in vitro studies emitted wavelengths ranging from 400 to 830 nm (Figure 2A) and an average irradiance of 23.05 mW/cm^2 (Figure 2B). These data also confirmed there was no bleed of light between LED columns where Figure 2A indicates LEDs exhibited only a single peak of the expected wavelength and Figure 2B shows there was no significant difference in irradiance output from one wavelength to the next. Similar irradiance values have also been used in studies exploring the effect of PBM on myoblast function (see Table S3 in Appendix S1, for examples, [22, 23]). Table 1 indicates radiant exposure values in which there is no significant difference from one wavelength to the next (irradiation parameters and the effects of PBM on media temperature are further elucidated in Figure S1, Figure 2 and Table 1). Hence, the data confirm the accurate delivery of key radiometric parameters without confounding effects such as temperature.

Another key parameter to be considered was that of the beam profiles of each LED utilised in this array. LEDs employed in this array exhibit a typical Gaussian distribution of light (Figure 3A, indicates a single representative from each wavelength channel) in which spectral irradiance is

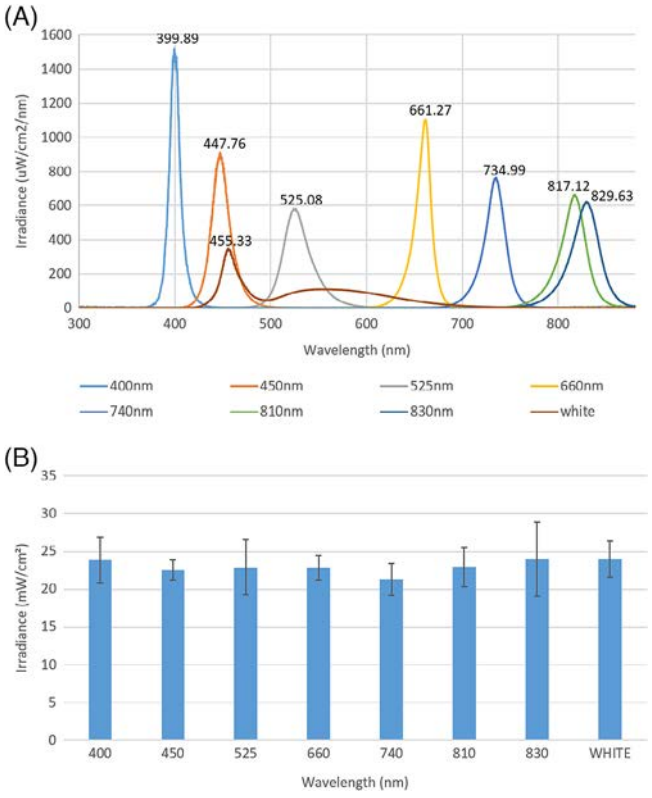

FIGURE 2 Array spectral characterisation data where (A) Spectral irradiance values of LED channels in the array (n = 6) and (B) average absolute irradiance in each channel (n = 6)

most intense in the central area and becomes more diffuse towards the edges of the beam area [24]. Table 2 indicates LEDs emitting a wavelength of 525 nm exhibited a significantly smaller ($P < 0.05$) beam area and power output than LEDs emitting wavelengths of 400 and 660 nm, whilst there was no significant difference at all other wavelengths. In this particular experimental setup, the LED array was designed to enable alignment of LEDs with the plate directly above at a specific irradiance value. As described by Hadis et al [18] that whilst there is variability in the homogeneity of each LED, the effects of this have been minimised through ensuring there is no significant difference in the output of a series of parameters including irradiance (mW/cm^2) and radiant exposure (J/cm^2). However, despite this it will be important to take into account the effects this may have on the biological output of our experiment. These data indicate the importance of evaluation of beam area.

The data obtained for array characterisation indicate its suitability for use in subsequent in vitro assay application.

3.2 | The effects of PBM on mitochondrial activity

The second objective of this study was to evaluate the effects of PBM on mitochondrial activity of myoblasts and myotubes. Myotubes are reported to possess higher quantities of mitochondrial proteins and enzymes [25] and hence greater numbers of mitochondria. Whilst it is not feasible to directly measure the number of mitochondria per cell due to the dynamic nature of mitochondria, mtDNA copy number has been correlated to mitochondrial content in previous studies [26]. Hence, mtDNA was isolated from both myoblasts and myotubes and quantified. Figure 4 provides evidence that myotubes possessed a greater ratio of mtDNA:nDNA compared with myoblasts ($P < 0.05$). Therefore, an MTT assay was employed as a high-throughput method to examine the effects of a series of wavelengths (400-830 nm) and irradiation times (30-240 seconds) on the cell metabolic activity of myoblasts 24 hours post-irradiation. Irradiation for 30 seconds at wavelengths of 400 and 810 nm induced 18.46%, and 16.38% increases in cell proliferation, respectively (Figure 5, $P < 0.05$). Interestingly, white light induced a significant increase in cell proliferative capacity following irradiation for 240 seconds, whilst all other wavelengths proved to induce the greatest affect following a 30-second irradiation period. This may be reflective of the differential biphasic dose response from one wavelength to the next where longer or shorter periods of irradiation could cause the most significant effects dependent upon the wavelength used. Also, white light is a combination of multiple visible light wavelengths and therefore the contribution of a single wavelength for any potential therapeutic effect within the white light band must be substantially reduced compared to the use of narrower wavebands at similar irradiance. It can also be noted that whilst wavelengths within the red spectra are commonly used in PBM research (620-750 nm) [27], no

TABLE 1 Indicates values of emitted wavelengths, spectral irradiance and radiant exposure after irradiation periods ranging between 30 and 240 seconds

	Radiant exposure (J/cm^2)			
Wavelength (nm)	**30 seconds**	**60 seconds**	**120 seconds**	**240 seconds**
399.89 ± 1.55	0.72	1.43	2.86	5.73
447.76 ± 1.69	0.68	1.35	2.70	5.41
525.08 ± 1.25	0.69	1.37	2.75	5.50
661.27 ± 0.56	0.68	1.37	2.74	5.48
734.99 ± 1.21	0.64	1.28	2.55	5.11
817.12 ± 0.64	0.69	1.37	2.75	5.50
829.63 ± 2.64	0.72	1.44	2.88	5.76
455.33 ± 0.11	0.72	1.44	2.87	5.75
Average	0.69 ± 0.03	1.38 ± 0.05	2.76 ± 0.10	5.53 ± 0.21

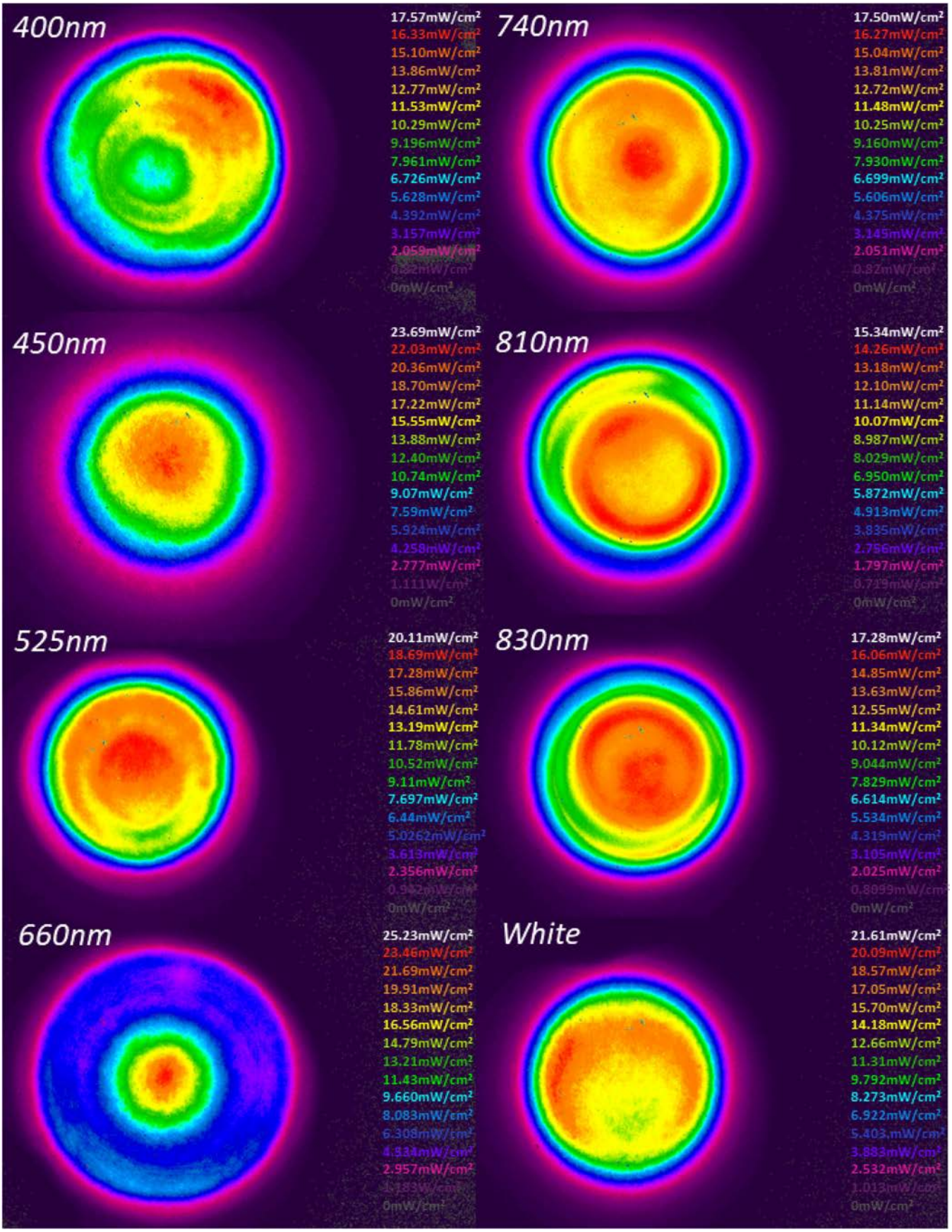

FIGURE 3 Demonstrates spatial distribution of irradiance of LEDs emitting each wavelength on the array. Images were taken in the plane of a target screen placed over the array surface to enable accurate measurement of beam diameter using BeamGage software. The target screen was placed at the same distance away from the array as a Seahorse XFe96 plate. Whilst the target screen could not be incorporated with the plate in place Figure S3 and Table S1 indicate beam profiles, average beam areas and power output with the plate in place

TABLE 2 Indicates differences in average beam area and power output emitted from one wavelength to the next

Wavelength (nm)	Average Beam area (cm^2)	Power (mW)
400	0.370 ± 0.008^{A}	8.931 ± 0.184^{A}
450	0.337 ± 0.003^{AB}	8.484 ± 0.063^{AB}
525	0.257 ± 0.007^{B}	6.039 ± 0.157^{B}
660	0.364 ± 0.003^{A}	9.01 ± 0.068^{A}
740	0.298 ± 0.007^{AB}	6.834 ± 0.159^{AB}
810	0.335 ± 0.007^{AB}	7.688 ± 0.158^{AB}
830	0.307 ± 0.01^{AB}	7.453 ± 0.233^{AB}
White	0.291 ± 0.009^{AB}	7.721 ± 0.242^{AB}

Means that do not share the same letter are significantly different, in which LEDs emitting wavelengths of 400 and 660 nm (A) exhibit significantly larger beam areas and power outputs than LEDs emitting 525-nm light (B, $P = <0.05$). Average beam area was calculated from diameters provided from the use of BeamGage software.

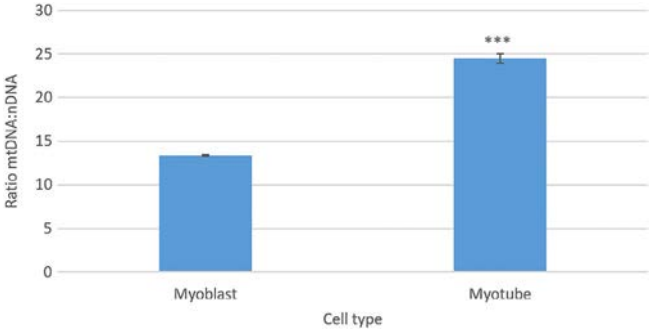

FIGURE 4 Shows relative differences in the ratio of mtDNA:nDNA between myoblasts and myotubes (n = 4, p8). Significance was assessed using a *t* test (*** = $P < 0.001$)

effect on cell metabolic activity was measured here. This may be due to the homogeneity of the beam profile at 660 nm (Figure 3) or indeed as discussed above, the optimal range for red light to induce an effect was not reached in this experimental setup. Hence, further study will be required to determine whether irradiation at 660 nm and with a more homogenous beam profile will influence biological output in vitro. Whilst other wavelengths and irradiation periods proved effective in inducing a significant response from myoblasts, wavelengths of 400, 450 and 810 nm and an irradiation period of 30 seconds were selected to compare the response of myoblasts and myotubes to PBM due to their efficacy in inducing a response from an array of other cell types previously studied (data not shown).

Once parameters were identified for further study, a series of key markers for mitochondrial activity were explored 8 hours post-irradiation. A period of 8 hours post-irradiation was selected as a previous study indicated this time point post-irradiation induced the most significant and reliable changes in real-time mitochondrial activity (Figure S4, [1, 8 and 24 hours post-irradiation were evaluated]). Figure 6 indicates that whilst a wavelength of 400 nm and irradiation period of 30 seconds induced significant increases in markers for mitochondrial activity from myoblasts and myotubes, increases in the activities of these mitochondrial markers at all wavelengths were only observed in myotube cultures ($P < 0.05$). This may indicate that cells with higher mitochondrial content have increased responsivity to light. Interestingly, Kushibiki et al investigated the effect of PBM at wavelengths of 405 and 808 nm at 100 mW/cm^2 on ROS production from C2C12 cells. They found that only violet-blue light upregulated ROS production whilst near infrared light had no effect. Our data provide similar findings, with a wavelength of 400 nm inducing significant increases in ROS production from myoblasts [28]. Some authors have also reported the effects of PBM in inducing myogenic differentiation from myoblasts to myotubes [29, 30]. Hence, future work may involve evaluation of the effects of parameters illustrated in this study on markers for myogenic differentiation.

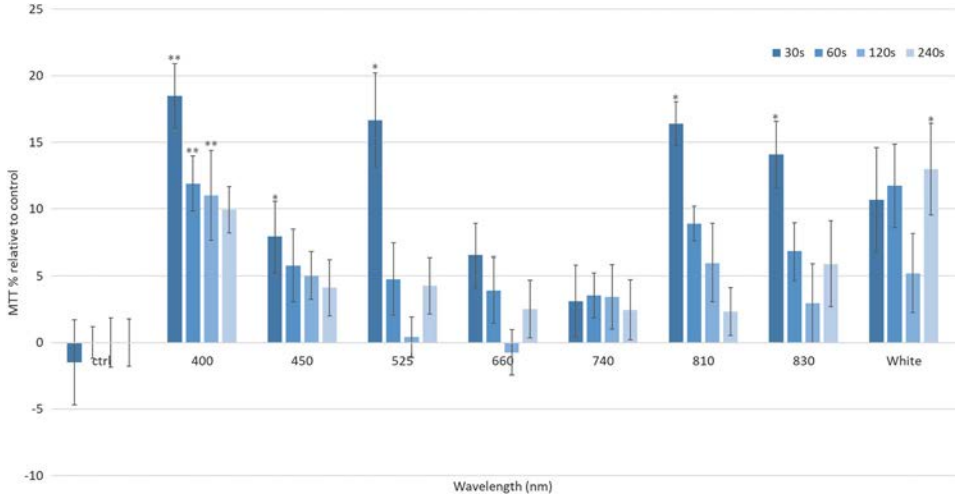

FIGURE 5 Indicates high-throughput analysis of wavelengths (400-830 nm) and irradiation periods (30-240 seconds) on cell metabolic activity of mouse myoblast cells (C2C12, n = 12 replicates, three plates irradiated) (24 mW/cm^2, 0.72-5.76J/cm^2, 30-240 seconds). Significance is indicated by ** = $P < 0.01$, * = $P < 0.05$ relative to the non-irradiated control, where all data are shown as a percentage of the non-irradiated control, where the non-irradiated control was normalised to 0%

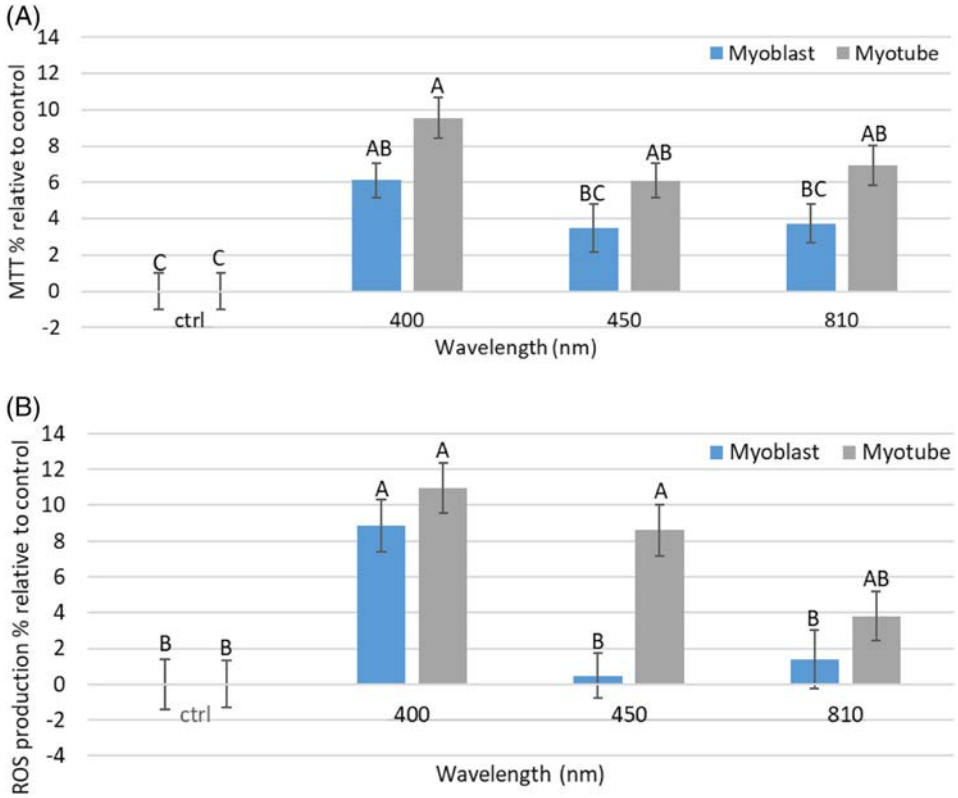

FIGURE 6 (A) Effect of PBM on cell metabolic activity from myoblasts and myotubes (30 seconds, 0.72 J/cm^2, n = 18, three plates irradiated) to wavelengths of 400, 450 and 810 nm. (B) Indicates the effects of PBM on ROS production from myoblasts and myotubes (30 seconds, 0.72 J/cm^2, n = 18, three plates irradiated). The effects of PBM were evaluated 8 hours post-irradiation. Means that do not share the same letter are significantly different ($P < 0.05$)

Subsequently, Seahorse assay technology was utilised to explore the effect of a series of wavelengths on real-time mitochondrial respiration. Whilst several studies have explored the effect of specific PBM parameters utilising Seahorse technology [31, 32], ours is the first that has explored an array of wavelengths and in particular the use of blue light in PBM. Our data showed that PBM at all wavelengths upregulated both maximal and basal respiratory rates, ATP production and spare respiratory capacity (the amount of extra ATP produced through oxidative phosphorylation available in the case of an increase in energy demand [33]) in myotubes (Figure 7, $P < 0.05$), whilst these were only upregulated at a wavelength of 810 nm from myoblasts ($P < 0.05$). Comparatively, previous studies exploring the effects of PBM using a Seahorse analyser only explored the effects of red light (635-700 nm) and only Chu-Tan et al found PBM modulated real-time mitochondrial activity [31]. Data from this study suggest that mitochondrial content may influence cellular response to PBM. However, further investigations are required to confirm this finding. Furthermore, our data indicate that blue light promoted greater increases in mitochondrial activity from myotubes compared with near infra-red (NIR) irradiation. Interestingly, PBM research does not often employ light within the blue range. However, recently, the application of blue light has gathered considerable interest and several authors have provided evidence that blue light not only could be beneficial in reducing inflammation by reducing circulating levels of cytokines [34] and promoting cell proliferation [35]. Hence, in future studies, it will be important to explore the response of other cell types to low doses of blue light. However, whilst we have reported blue light induces a greater response compared to NIR light in vitro, it may be wise to consider the possible limitations of blue light in terms of tissue penetration depth. Hence, future studies may aim to evaluate the effects of combining both blue and NIR light to ensure light penetrates target tissue in vivo. The use of blue light may also be considered for superficial injuries including applications for wound healing, which have proven beneficial both in vitro [34] and in vivo [36, 37].

In summary, we demonstrate for the first time that PBM promotes greater increases in mitochondrial respiration in myotubes compared with myoblasts, a cell type with higher levels of mitochondrial content. These data may prove useful in understanding why some patients are more responsive to PBM in vivo as it is well reported there is a great deal of variability in the mitochondrial genome from one individual to the next [38]. We also provide novel evidence that blue light could also be effective in promoting mitochondrial respiration. These data provide further evidence supporting the premise that response to PBM in vitro is induced by changes in mitochondrial activity and provide evidence that PBM could

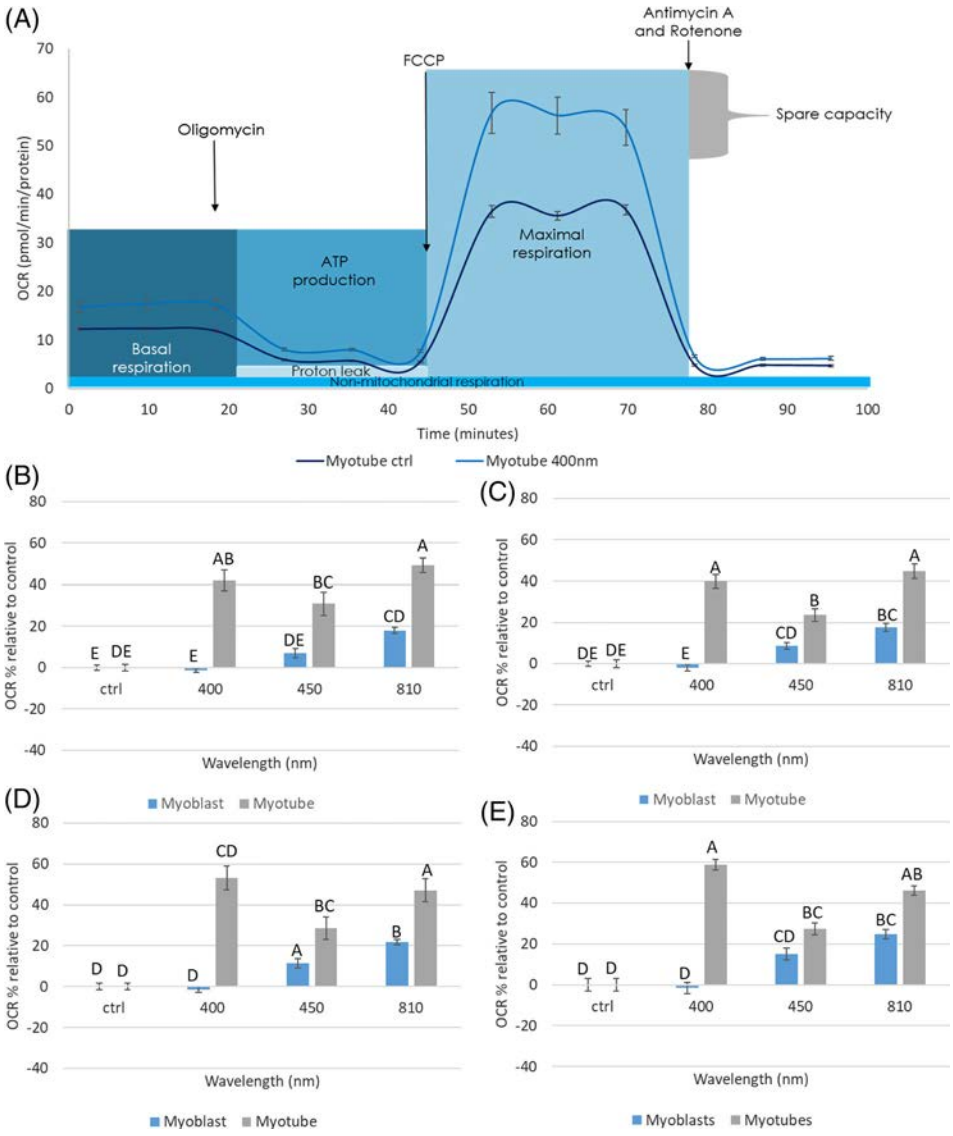

FIGURE 7 Shows the effects of PBM on markers for changes in real-time mitochondrial activity utilising the Seahorse mitochondrial stress assay from myoblasts and myotubes (myotubes, p7, myoblasts p13, n = 6, effects evaluated 8 hours post-irradiation). Markers are denoted by (A) indicates trace comparing response of untreated myotubes and myotubes treated with 400-nm light in which compounds were sequentially applied to the system to alter elements of oxidative phosphorylation. This then enabled calculation of specific parameters of oxidative phosphorylation including (B) basal respiration, (C) maximal respiration, (D) ATP production and (E) Spare respiratory capacity. Means that do not share the same letter are significantly different ($P < 0.05$)

be employed to promote increased muscle cell activity. Hence, these data support current findings that indicate the potential effectiveness of PBM in sport performance and rehabilitation following muscle injury [39].

ACKNOWLEDGMENTS

The research in this report is funded as part of an iCASE PHD studentship funded by Engineering and Physical Sciences Research Council and Philips.

CONFLICTS OF INTEREST

The authors declare no potential conflicts of interest with respect to the authorship and/or publication of this article.

AUTHOR BIOGRAPHIES

Please see Supporting Information online.

ORCID

Hannah J. Serrage https://orcid.org/0000-0002-4995-6076

REFERENCES

[1] M. R. Hamblin, T. N. Demidova, Eds. Mechanisms of low level light therapy. *Progress in Biomedical Optics and Imaging – Proc. SPIE*, **2006**.
[2] R. Yousefi-Nooraie, E. Schonstein, K. Heidari, A. Rashidian, V. Pennick, M. Akbari-Kamrani, S. Irani, B. Shakiba, S. Mortaz Hejri, A. R. Jonaidi, S. Mortaz-Hedjri, Cochrane Back and Neck Group, *Cochrane Database Syst. Rev.* **2008**.
[3] C. Ferraresi, Y.-Y. Huang, M. R. Hamblin, *J. Biophotonics* **2016**, *9*, 1273.
[4] A. D. Woolf, B. Pfleger, *Bull. World Health Organ.* **2003**, *81*, 646.
[5] P. A. Jenkins, J. D. Carroll, *Photomed. Laser Surg.* **2011**, *29*, 785.

[6] T. I. Karu, S. F. Kolyakov, *Photomed. Laser Surg.* **2005**, *23*, 355.
[7] M. R. Hamblin, T. N. Demidova-Rice, Eds. Cellular chromophores and signaling in low level light therapy. *Progress in Biomedical Optics and Imaging – Proc. SPIE*, **2007**.
[8] B. Tan, H. Xiao, X. Xiong, J. Wang, G. Li, Y. Yin, B. Huang, Y. Hou, G. Wu, *Front. Biosci.* **2015**, *20*, 989.
[9] C. A. Piantadosi, M. S. Carraway, A. Babiker, H. B. Suliman, *Circ. Res.* **2008**, *103*, 1232.
[10] M. Migliario, P. Pittarella, M. Fanuli, M. Rizzi, F. Renò, *Lasers Med. Sci.* **2014**, *29*, 1463.
[11] C. K. Rhee, S. Y. Chang, J. C. Ahn, M. W. Suh, J. Y. Jung, Eds. Effect of LLLT on the level of ATP and ROS from organ of corti cells. *Progress in Biomedical Optics and Imaging - Proc. SPIE*, **2014**.
[12] L. W. Cole, *Front. Cell Dev. Biol.* **2016**, *4*, 85.
[13] E. D. Robin, R. Wong, *J. Cell. Physiol.* **1988**, *136*, 507.
[14] M. M. Rashid, A. Runci, L. Polletta, I. Carnevale, E. Morgante, E. Foglio, T. Arcangeli, L. Sansone, M. A. Russo, M. Tafani, *Cell Death Dis.* **2015**, *1*, 15014.
[15] C. F. Bentzinger, Y. X. Wang, M. A. Rudnicki, *Cold Spring Harb. Perspect. Biol.* **2012**, *4*, a008342.
[16] C. Schoneich, E. Dremina, N. Galeva, V. Sharov, *Apoptosis* **2014**, *19*, 42.
[17] C. S. Kraft, C. M. LeMoine, C. N. Lyons, D. Michaud, C. R. Mueller, C. D. Moyes, *Am. J. Physiol. Cell Physiol.* **2006**, *290*, C1119.
[18] M. A. Hadis, P. R. Cooper, M. R. Milward, P. C. Gorecki, E. Tarte, J. Churm, W. M. Palin, *J. Biophotonics* **2017**, *10*, 1514.
[19] J. Leggate, R. Allain, L. Isaac, B. W. Blais, *Biotechnol. Lett.* **2006**, *28*, 1587.
[20] A. M. Sieuwerts, J. G. Klijn, H. A. Peters, J. A. Foekens, *Eur J Clin Chem Clin Biochem* **1995**, *33*, 813.
[21] M. Gomez-Florit, M. Monjo, J. M. Ramis, *J. Periodontol.* **2014**, *85*, 966.
[22] L. M. Nguyen, A. G. Malamo, K. A. Larkin-Kaiser, P. A. Borsa, P. J. Adhihetty, *Mitochondrion* **2014**, *14*, 42.
[23] C. Ferraresi, M. V. P. de Sousa, Y. Y. Huang, V. S. Bagnato, N. A. Parizotto, M. R. Hamblin, *Lasers Med. Sci.* **2015**, *30*, 1259.
[24] H. Yang, J. W. M. Bergmans, T. C. W. Schenk, J. P. M. G. Linnartz, R. Rietman, *Opt. Express* **2008**, *16*, 21641.
[25] A. H. Remels, R. C. Langen, P. Schrauwen, G. Schaart, A. M. Schols, H. R. Gosker, *Mol. Cell. Endocrinol.* **2010**, *315*, 113.
[26] S. Larsen, J. Nielsen, C. N. Hansen, L. B. Nielsen, F. Wibrand, N. Stride, H. D. Schroder, R. Boushel, J. W. Helge, F. dela, M. Hey-Mogensen, *J. Physiol.* **2012**, *590*, 3349.
[27] A. Teuschl, E. R. Balmayor, H. Redl, M. van Griensven, P. Dungel, *Dermatol. Surg.* **2015**, *41*, 261.
[28] T. Kushibiki, T. Hirasawa, S. Okawa, M. Ishihara, *Photomed. Laser Surg.* **2013**, *31*, 95.
[29] L. M. G. Silva, C. A. A. Da Silva, A. Da Silva, R. P. Vieira, R. A. Mesquita-Ferrari, J. C. Cogo, S. R. Zamuner, *PLoS One* **2016**, *11*, 16.
[30] G. Shefer, N. Ben-Dov, O. Halevy, U. Oron, *Lasers Surg. Med.* **2008**, *40*, 38.
[31] J. A. Chu-Tan, M. Rutar, K. Saxena, Y. Wu, L. Howitt, K. Valter, J. Provis, R. Natoli, *Int J Photoenergy* **2016**, *2016*, 1.
[32] J. C. Wigle, C. C. Castellanos, Eds. in vitro measurements of oxygen consumption rates in hTERT-RPE cells exposed to low levels of red light. *Progress in Biomedical Optics and Imaging – Proc. SPIE*, **2016**.
[33] C. Desler, T. L. Hansen, J. B. Frederiksen, M. L. Marcker, K. K. Singh, L. Juel Rasmussen, *J Aging Res* **2012**, *2012*, 192503.
[34] D. S. Masson-Meyers, V. V. Bumah, C. S. Enwemeka, *J. Photochem. Photobiol. B* **2016**, *160*, 53.
[35] M. W. Cheon, T. G. Kim, Y. S. Lee, S. H. Kim, *Pers. Ubiquit. Comput.* **2013**, *17*, 1421.
[36] M. N. Alba, M. Gerenutti, V. M. H. Yoshida, D. Grotto, *J. Cosmet. Laser Ther.* **2017**, *19*, 49.
[37] M. Figurová, V. Ledecký, M. Karasová, M. Hluchý, A. Trbolová, I. Capík, S. Horňák, P. Reichel, J. M. Bjordal, P. Gál, *Photomed. Laser Surg.* **2016**, *34*, 53.
[38] R. W. Carter, *Nucleic Acids Res.* **2007**, *35*, 3039.
[39] P. A. Borsa, K. A. Larkin, J. M. True, *J. Athl. Train.* **2013**, *48*, 57.

SUPPORTING INFORMATION

Additional supporting information may be found online in the Supporting Information section at the end of the article.

How to cite this article: Serrage HJ, Joanisse S, Cooper PR, et al. Differential responses of myoblasts and myotubes to photobiomodulation are associated with mitochondrial number. *J. Biophotonics*. 2019;12: e201800411. https://doi.org/10.1002/jbio.201800411

Photochemical & Photobiological Sciences

PERSPECTIVE

View Article Online
View Journal | View Issue

Cite this: *Photochem. Photobiol. Sci.*, 2019, **18**, 1877

Under the spotlight: mechanisms of photobiomodulation concentrating on blue and green light

Hannah Serrage, *[a] Vladimir Heiskanen,*[b] William M. Palin, [a] Paul R. Cooper, [a] Michael R. Milward, [a] Mohammed Hadis [a] and Michael R. Hamblin [c]

Photobiomodulation (PBM) describes the application of light at wavelengths ranging from 400–1100 nm to promote tissue healing, reduce inflammation and promote analgesia. Traditionally, red and near-infra red (NIR) light have been used therapeutically, however recent studies indicate that other wavelengths within the visible spectrum could prove beneficial including blue and green light. This review aims to evaluate the literature surrounding the potential therapeutic effects of PBM with particular emphasis on the effects of blue and green light. In particular focus is on the possible primary and secondary molecular mechanisms of PBM and also evaluation of the potential effective parameters for application both *in vitro* and *in vivo*. Studies have reported that PBM affects an array of molecular targets, including chromophores such as signalling molecules containing flavins and porphyrins as well as components of the electron transport chain. However, secondary mechanisms tend to converge on pathways induced by increases in reactive oxygen species (ROS) production. Systematic evaluation of the literature indicated 72% of publications reported beneficial effects of blue light and 75% reported therapeutic effects of green light. However, of the publications evaluating the effects of green light, reporting of treatment parameters was uneven with 41% failing to report irradiance (mW cm^{-2}) and 44% failing to report radiant exposure (J cm^{-2}). This review highlights the potential of PBM to exert broad effects on a range of different chromophores within the body, dependent upon the wavelength of light applied. Emphasis still remains on the need to report exposure and treatment parameters, as this will enable direct comparison between different studies and hence enable the determination of the full potential of PBM.

Received 21st February 2019,
Accepted 30th May 2019

DOI: 10.1039/c9pp00089e

rsc.li/pps

1. Introduction

The potential application of what is now known as Photobiomodulation (PBM) was first reported by Endre Mester in 1967 at Semmelweiss University, Budapest.[1] Mester shaved the backs of mice and shone a ruby red laser emitting a wavelength of 694 nm on the backs of a group of mice in order to investigate carcinogenicity. To his surprise, the hair on the backs of the irradiated mice grew back faster compared with that of the non-irradiated control group. He called this phenomenon 'photobiostimulation' and to date (January 2019), over 6000 papers have been published regarding the efficacy of PBM in treating a number of ailments by inducing analgesia,[2] promoting wound healing[3] and reducing inflammation.[4]

PBM encompasses a broad range of different terminologies including low level laser/light therapy (LLLT), cold laser therapy and phototherapy. Whilst the term PBM is the most recent addition to this list, and is currently the preferred Medical Subject Heading Term (MeSH) which encompasses both the stimulatory and inhibitory mechanisms involved, PBM is also often called photobiomodulation therapy (PBMT) which further adds to the list of terms for the same therapy. Fig. 1 gives an overview of PBM publications so far.

Nonetheless, a growing number of observations suggests that specific wavelengths of electromagnetic radiation spanning the visible to near infra-red spectrum (400–1100 nm) could lead to photo-physical and photochemical effects that can modulate major biological processes to achieve therapeutic goals such as cellular proliferation, mitochondrial function and inflammatory signalling[5] in various eukaryotic organisms, including humans. The majority of the literature reports the beneficial therapeutic effects of red and near infrared light (red: ~600–750, NIR: ~750–1100 nm) in promoting tissue

[a]*College of Medical and Dental Sciences, University of Birmingham, UK. E-mail: hannah.serrage@bristol.ac.uk*
[b]*Oral and Maxillofacial Diseases, University of Helsinki, Finland. E-mail: valtsu.heiskanen@gmail.com*
[c]*Wellman Center for Photomedicine, Massachussetts General Hospital, Harvard Medical School, Boston, MA, USA*

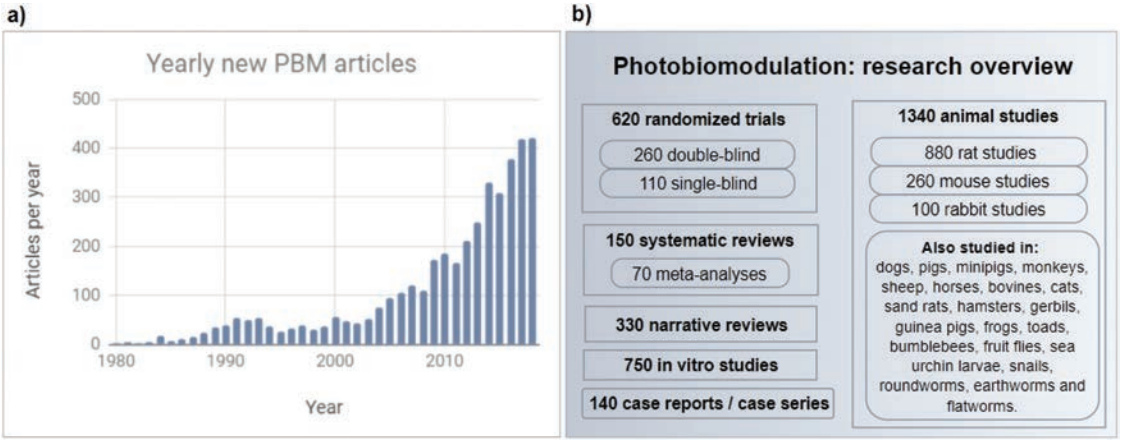

Fig. 1 Preliminary PBM research overview based on a personal database of approximately 4000 scientific articles related to PBM, compiled by manual PubMed and Google Scholar literature search using more than 80 different keywords (http://www.bitly.com/PBM-database). (a) The amount of newly published PBM-related scientific articles has been increasing steadily during the 21st century, recently reaching a level of approximately 400 new articles per year. (b) The published research includes experimental *in vitro* studies and animal research. Also, a variety of randomized human trials and systematic reviews have been published so far.

healing and reducing inflammation.[6–14] Nevertheless, controversy still surrounds the application of PBM in practice, due to the lack of knowledge concerning how PBM elicits its molecular effects and also a poor understanding of photophysics and radiometric parameters which affect repeatability and reliability.[15] The importance of reporting treatment parameters in a more consistent and reliable way has been emphasised in several articles and guidance for reporting radiometric properties has previously been published[15,16] to little or no general avail.[17–21] Indeed, those articles that have provided guidance for reporting radiometric parameters have commonly recommended the consistent reporting of up to ten key radiometric parameters (wavelength, power, irradiation time, beam area (at the skin or culture surface; this is not necessarily the same size as the aperture), radiant energy, radiant exposure, pulse parameters, number of treatments, interval between treatments and anatomical location).[22]

Whilst the majority of the literature supports the application of PBM using wavelengths between 600–1100 nm, wavelengths <600 nm are less commonly researched or reported. The use of blue light in particular (400–500 nm) is additionally surrounded by significant controversy relating to the premise that the margin between 'safe' blue light and potentially damaging ultraviolet (UV) light is not well defined.

UV light is divided into three discrete categories: UV-C (~100–280 nm), UV-B (~280–315 nm) and UV-A (~315–400 nm).[23] A common misconception is that all UV radiation is associated with DNA damage and mutagenesis.[24] In fact, DNA damage is reportedly more efficient at UV-C and UV-B wavelengths with a peak absorption at 254 nm which corresponds to absorption by one of the nucleotide bases of DNA known as thymine, resulting in the formation of thymine dimers and rendering the DNA molecule inactive and unable to replicate. UV-A radiation on the other hand has a poor efficiency in inducing DNA damage, because it is not absorbed by native DNA or any of its bases. However, like red and NIR wavelengths, UV-A wavelengths are able to generate singlet oxygen (reactive oxygen species, ROS), and if the concentration of these radicals is in sufficient quantity, they can damage DNA.[25] However, ROS in small quantities can be beneficial to cells and is commonly associated with proposed mechanisms of PBM.[26] Indeed, the production of ROS is likely to be influenced by radiometric parameters, namely, wavelength, irradiance, dose and the number of photons delivered and again highlighting the importance of these parameters. Nonetheless, the use of wavelengths in PBM at 400 nm or lower should be utilised in practice with extreme caution.

In addition, another key caveat regarding the use of blue light for PBM is the low penetration depth of blue light through tissue compared with that of red or NIR light.[27] Whilst blue light is cited to possess a penetration depth corresponding to an intensity decrease by 1/e (or approximately 63%) at 1 mm, NIR light has a penetration depth of up to 5 mm through tissue.[28] However, there is a body of growing evidence supporting the use of PBM using blue light to reduce inflammation in superficial tissues[29] and promote wound healing,[30] as well as being able to limit bacterial growth.[31] Similarly, wavelengths within the green section of the visible spectrum (495–570 nm) have also gathered considerable interest. Published reports have indicated PBM effects for green light ranging from improved cellulite appearance[32] to reduced tissue swelling.[33]

This review aims to evaluate the main primary and secondary mechanisms involved in light transduction in particular with blue and green wavelength of light. Secondly we focus on evaluation of current literature regarding the therapeutic efficacy of blue and green PBM.

2. Primary mechanisms of PBM

According to the Grotthuss–Draper law, commonly termed "the First Law of Photochemistry", photochemical reactions

are dependent on the absorption of light by a system. Subsequently in this section, we provide a review of the literature of the most often proposed cellular photoacceptors (chromophores) that are reported to mediate the biological effects in PBM. We cover in particular the possible photoacceptors responsible for the transduction of blue and green wavelengths of light.

2.1. Cytochrome c oxidase

It has been proposed that PBM acts directly on the electron transport chain located in the mitochondrial membrane, specifically on the enzyme cytochrome c oxidase (CCO), also known as complex IV.[34] The electron transport chain is comprised of five complexes: complex I (NADH-CoQ reductase), complex II (succinate dehydrogenase), complex III (cytochrome c reductase), cytochrome c oxidase and complex V (ATP synthase). Electrons are passed systematically down the chain of these complexes in order to generate a proton gradient to provide the activation energy for ATP synthase to catalyse the production of ATP.[35] CCO is responsible for the conversion of molecular oxygen (O_2) to two molecules of water (H_2O). CCO contains two copper centres (Cu_A, Cu_B) and two hemes (cytochrome a, cytochrome a_3), which are involved in redox reactions within the enzyme.

The most widely accepted explanation for the beneficial photobiological effects of red and near-infrared light has been the "CCO theory" largely established by Tiina Karu in the 1990s. It posits that the light-cell interaction responsible for the observed PBM effects occurs initially at the redox-active copper atoms of CCO complex in the mitochondrial electron transport chain.[36–39] The CCO theory was based on Karu's earlier findings in the 1980s, which showed that the position of peaks in the action spectrum measured for a variety of light-induced cellular changes (including DNA synthesis, RNA synthesis and cell attachment) were practically identical. These findings suggested that a universal cellular photoacceptor could be capable of absorbing those specific wavelengths and producing cellular changes affecting multiple cellular compartments. The observed peaks in the action spectrum were located within the blue (404 nm), red (620 and 680 nm) and near-infrared (760 and 820 nm) parts of the electromagnetic spectrum.[36]

Various *in vitro* and *in vivo* studies have observed effects related to increased mitochondrial activity, including increased ATP levels, ROS levels, and mitochondrial membrane potential following irradiation. Interestingly, the time it takes for these effects to become evident varies from minutes to hours depending upon the experimental settings.[40–42] Effects on mitochondrial function have also been demonstrated in animals.[43,44]

Interestingly there remains no clear understanding, however, of the exact events that occur within the electron transport chain or the enzyme CCO during light absorption to produce these effects. A multitude of hypotheses have been proposed, including photodissociation of nitric oxide (NO), changes in CCO redox properties with acceleration of electron transfer, superoxide generation and biochemical changes related to transient heating of irradiated photoacceptors.[45] It has also been suggested that cytochrome c oxidation by CCO might be catalysed by red light irradiation.[46] However, a later replication study failed to confirm this effect, and also raised doubts indicating that the initial positive results could have been experimental artefacts due to lack of detergent used for the CCO solubilization.[47] An alternative explanation for the observed mitochondrial effects could also be an increased efficiency of CCO proton pumping.[48] Regardless, the very limited amount of observations allows no firm conclusions to be made on the subject.

The hypothesis of NO photodissociation from CCO is relatively popular, and based on the understanding of the reversible inhibitory effects of NO on CCO.[49,50] There is some evidence suggesting that light can attenuate the mitochondrial inhibitory effects of NO[51] and some suggesting that NO can also inhibit the cellular effects of light.[52] Light has been shown to increase NO levels in cells and blood.[53] However, the evidence is not completely consistent. One experiment failed to demonstrate the protective effect of red light against NO-induced inhibition of mitochondrial respiration, but demonstrated partial protective effects with blue light (442 nm).[54] Another experiment with blue light (430 nm) recovered the mitochondrial function that had been inhibited by nitric oxide at the levels generated under septic conditions.[55] Hence, these data demonstrate that wavelengths outside the red and NIR range could be effective in modulating mitochondrial activity.

2.2. Opsins

Opsins are G-protein coupled receptors that have gained considerable interest in phototherapy research due to their excitation by blue or green light[56] (see Fig. 2). Opsins can be divided into subcategories dependent upon the location they are expressed.

Opsin 1 (OPN1) and 2 (OPN2) expression is localised to the retina in the eye. OPN1 is expressed by cone cells, photoreceptors within the eye that recognise coloured light and can be subdivided into three types: OPN1 short wavelength (OPN1-SW), OPN1 medium wavelength (OPN1-MW) and OPN1 long wavelength (OPN1-LW). Conversely, OPN2 (rhodopsin) is expressed by rod photoreceptors, cells that recognise dim light and are important in peripheral vision.[17] Three further opsins are expressed within the human body including OPN3 (encephalopsin), OPN4 (melanopsin) and OPN5 (neuropsin) all of which exhibit an absorption spectrum ranging between 380–496 nm. Notably, OPN expression has been detected throughout the body with the expression of OPN2, OPN3 and OPN5 being found in epidermal skin[58] and the expression of OPN3 in the brain.[59]

A number of publications have explored the role of OPNs in blue light mediated PBM signalling both *in vitro* and *in vivo*. For example, Regazzetti *et al.*[44] explored the effects of irradiation at 415 nm (50 J cm^{-2}) or 465 nm (62.5 J cm^{-2}) on the regulation of pigmentation through OPN signalling. The authors concluded that OPN3 could provide a novel target for

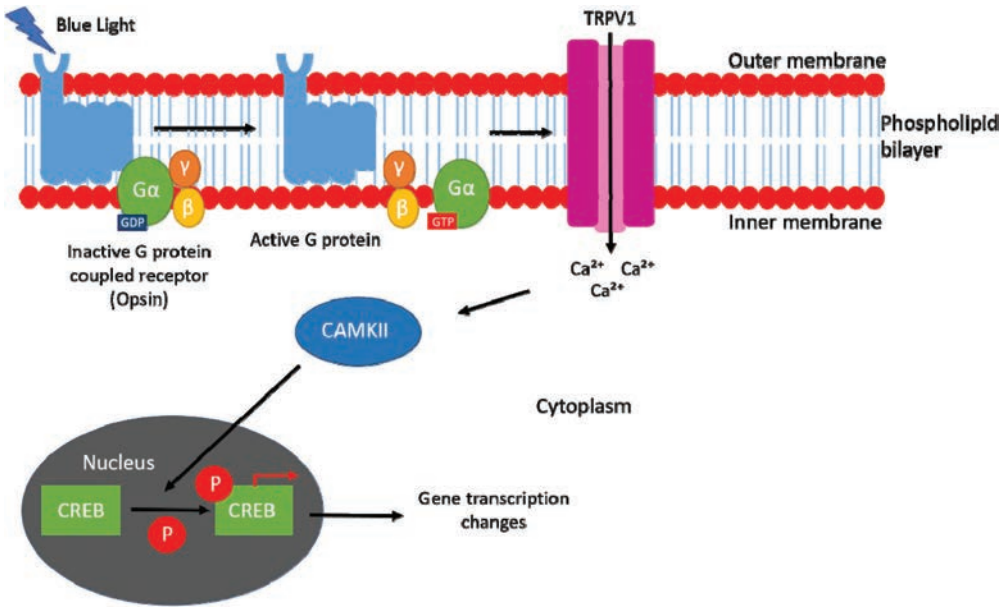

Fig. 2 Possible molecular mechanism of blue light PBM in which an opsin receptor is activated by blue light, which induces a conformational change in the *cis*-retinaldehyde cofactor, allowing it to act as a guanine nucleotide exchange factor. This then enables the dissociation of guanosine diphosphate (GDP) from subunit Gα of the associated G protein and the binding of guanosine triphosphate (GTP). In turn this provides the activation energy to enable Gα to dissociate from Gβ and Gγ (the other subunits of the G protein) and enables signalling of Gα through a series of pathways including the cAMP and phosphatidylinositol pathways. In turn, signalling through these pathways is understood to induce the downstream activity of transient receptor protein (TRP) channels including the capsaicin receptor (TRPV1), which causes a flood of calcium ions into the intracellular space, resulting in the activation of calcium/calmodulin dependent protein kinase-II (CAMKII) and thus the phosphorylation of CREB (a transcription factor). CREB then induces a series of transcriptional events.

regulating melanogenesis.[60] Oritz *et al.*[45] also explored the effects of irradiation at 400 nm or 460 nm on the influence of signalling through OPN3 and OPN4 on pulmonary vaso-relaxation.[61] The authors concluded that blue light induced vaso-relaxation and reduced arterial relaxation, through OPN3 and OPN4 signalling. A series of further publications have also evaluated the role of blue light in influencing opsin signalling to regenerate visual pigments[62] and promote hair regrowth.[56] Notably, whilst there is a wealth of literature supporting the idea that opsin signalling influences responses both *in vitro* and *in vivo*, the molecular and cellular mechanisms of this signalling pathway are yet to be fully elucidated.

Current literature indicates that different opsins are coupled to different subtypes of G-proteins and hence induce different signalling pathways. For example OPN4 is coupled to Gq (activates the phospholipase C pathway) whilst other opsins (OPN1, OPN2, OPN3 and OPN5) are coupled to Go (inhibits adenylate cyclase), Gi (inhibits adenylate cyclase), Gt (transducing, activates phosphodiesterase 6) and Gs (activates adenylate cyclase).[57,63,64]

It is proposed that one downstream target of opsins is transient receptor potential (TRP) channels, particularly the TRPV1 subtype (capsaicin receptor), which has been cited to be activated by light.[65] TRP channels are ligand-gated ion channels. When a stimulus is applied, the TRP channel opens and this enables a flood of calcium (Ca^{2+}) ions into the cytoplasm of the cell. In turn, Ca^{2+} then induces the activity of calcium/calmodulin dependent kinase II (CAMKII), which in turn induces the phosphorylation of the transcription factor, cAMP response element-binding protein (CREB) located in the nucleus. In turn, CREB induces a series of changes in gene transcription ultimately proposed to lead to some of the beneficial effects of PBM, seen both *in vitro* and *in vivo*.[60,66] Fig. 2 highlights the current proposed molecular mechanisms relating to how blue and green light PBM triggers opsin signalling. It has also been shown that increased activity of TRP channels induces ROS generation[67] and thus the activation of the Ras pathway, a key pathway involved in the modulation of the activity of small GTPases, ultimately leading to the modulation of calcium signalling and apoptosis.[68] Hence, these mechanisms may explain current findings which indicate that blue light induces significant increases in ROS production.[19,69–73] However, evidence also suggests this may be due to the effects of blue light on mitochondrial activity, inducing increases in ROS production as a result of the stimulation of the electron transport chain.[74] Therefore, whilst there is a wealth of literature suggesting that blue light induces the activity of opsins and TRP channels, the pathway that links these two complexes is yet to be elucidated. Therefore, further work is required to determine the molecular mechanisms involved.

2.3. Flavins and flavoproteins

Blue light (400–500 nm) is known to excite flavins and flavoproteins including flavin mononucleotide (FMN) and flavin

adenine dinucleotide (FAD).[75] A well-characterised family of flavin containing complexes is called "cryptochromes".[76] Notably, cryptochromes have been widely documented to absorb blue light[77] and are proposed to be involved in the regulation of the circadian rhythm in mammals.[78] Notably, FMN is also found within complex I of the electron transport chain and it is proposed that blue light provides the activation energy for FMN to catalyse the reduction of oxygen (O_2) to superoxide ($O_2^{\bullet-}$).[79] Hence, blue light is understood to induce increases in the levels of circulating ROS.[80] Complex II is also a flavin (contains $FADH_2$) containing cytochrome,[81] and also absorbs blue light.[82] Hence, it is plausible that like red and NIR light, blue light could affect mitochondrial activity. Indeed, Serrage *et al.* demonstrated that blue light (400–450 nm, 5.76 J cm^{-2}) was as effective in inducing increases in mitochondrial activity as NIR light (810 nm, 5.76 J cm^{-2} (ref. 83)). However, further work is required to validate this hypothesis to determine whether blue light can modulate the activity of flavin containing complexes of the ETC.

2.4. Porphyrins

Porphyrins, a group of heterocyclic organic compounds found complexed to proteins ranging from haemoglobin,[84] to cytochrome p450 enzymes,[85] to complex IV of the electron transport chain (CCO)[86] are known to possess a typical Soret band at 400–420 m and hence possess the ability to absorb blue light.[87] Blue light of wavelengths between 400–415 nm induces the π to π^* transition in porphyrin rings.[88] Wavelengths between 400–420 nm could oxidise porphyrin containing heme groups (found within complex IV), whilst a wavelength of 450 nm could induce CuB (a component of complex IV) reduction hence inducing complex IV oxidation or reduction respectively.[89]

When evaluating the influence of PBM on mitochondrial electron transport chain activity, Evgeny *et al.* concluded that blue light application (442 nm, 30 mW cm^{-2}, 3 J cm^{-2}) induced significant increases in complex IV activity and cell metabolic activity, compared to NO which inhibited cell responses.[54] Also, Ankiri *et al.* reported that complex IV possesses a maximal absorption at 410 nm and hence this could be due to porphyrins contained within the complex.[90] Similarly, Del Olmo-Aguado *et al.* evaluated the effects of blue light on retinal ganglion cell mitochondrial activity. The authors concluded that blue light upregulated the activities of complexes III, IV and V of the electron transport chain, but also induced significant reduction in cell viability, and induced apoptosis.[91] These data indicated a possible role of blue light in affecting porphyrin-containing complexes of the electron transport chain.

Cytochrome p450s (CYPs) are also porphyrin-containing complexes that have gained interest in phototherapy research, as their activation by blue light has been cited.[92] CYPs are a family of proteins that contain heme and are vital for drug metabolism. The p450 element of the cytochrome refers to the protein absorption spectra, since CYPs exhibit a maximal absorption peak at 450 nm when bound to carbon monoxide.[93] CYPs are membrane bound proteins and can be located either in the endoplasmic reticulum or the inner mitochondrial membrane. Mitochondrially-located CYPs including cytochrome P450 reductase, transfer electrons from nicotinamide adenine dinucleotide phosphate (NAPDH) and thus could play a role in ETC activity.[94]

Interestingly, Becker *et al.* evaluated the effects of blue LED irradiation (453 nm, 23 mW cm^{-2}, 41.4 J cm^{-2}) on the proliferation and gene expression of keratinocytes, and found that irradiation induced a decrease in cell proliferation. However, the authors also reported that blue light induced significant increases in the transcription of electron transport chain-related genes, cytochrome P450-related genes and also genes relevant to steroid hormone synthesis.[95] Becker and colleagues also reported that genes relevant to inflammation were significantly down-regulated due to this exposure, and proposed that this may be due to the induction of steroid hormone biosynthesis *via* the CYPs pathway. Hence, these data provide an additional hypothesis as to how blue light PBM could affect cellular signalling.

2.5. Nitric oxide (NO)-containing compounds and nitrite reductases

In addition to the NO photodissociation hypothesis (see section 2.1), there is some literature suggesting that light-mediated effects are related to the synthesis combined with, or without, the release of NO due to light exposure.

Firstly, CCO has also been shown to function as a nitrite reductase, thus being able to produce NO locally in the mitochondria. This nitrite-dependent NO synthesis in isolated mitochondria has been demonstrated to increase by yellow light (590 nm), without any concomitant increase in mitochondrial oxygen consumption.[96] These data suggest that light-induced cellular effects do not necessarily have to be coupled with changes in mitochondrial respiration.

Secondly, there is also evidence that certain wavelengths of light can induce the release of NO from photolabile sources of stored NO, such as nitrosyl hemoglobin (HbNO), nitrosyl myoglobin (MbNO), S-nitrosothiols (RSNO) or dinitrosyl iron complexes (DNIC). This effect is reportedly much greater with red light (670 nm) compared with some longer wavelengths that have been examined, including 740 nm and 830 nm.[97,98] NO release from some S-nitrosothiols (RSNOs) has also been demonstrated with ultraviolet (340 nm) and green (545 nm) wavelengths of light.[99] Blue light (420–453 nm) has been shown to be capable of eliciting NO release from S-nitrosoalbumin (SNO-Alb), HbNO and aqueous nitrite solutions.[100,101]

3. Secondary mechanisms of PBM

From evaluation of the possible hypotheses of the primary mechanisms of PBM, it is apparent that several pathways converge on the induction of the same signalling molecules; *i.e.* ROS. Therefore, this section of the review evaluates the poss-

ible effects of PBM on ROS-related pathways. It is important to point out that this review evaluates the effects of PBM on a number of downstream targets. PBM may modulate a different number of these targets, dependent upon the dose of light used, the wavelength employed and also the *in vitro*/*in vivo* model that the light is applied to. The same is true for the primary mechanisms of PBM, illustrated in section 2.

3.1. Nuclear factor kappa-light-chain-enhancer of activated B cells (NFκB)

ROS production instigates a signalling cascade ultimately leading to the phosphorylation of IκB, an inhibitor of the pro-inflammatory transcription factor NFκB. In its inactive state IκB is bound to NFκB in the cytoplasm, however, once phosphorylated, IκB dissociates from NFκB and is targeted to the proteasome for degradation. This then allows the translocation of free NFκB to the nucleus binding to DNA, and initiation of a series of gene transcription changes, mRNA production and potential downstream expression of key cytokines, chemokines and growth factors including interlukin-8 (IL-8), IL-6 and vascular endothelial growth factor (VEGF[102–105]).

A number of authors report the modulation of NFκB by light. For example, Chen *et al.* reported that irradiation at 810 nm and radiant exposure of 0.003 J cm^{-2} induced the activation of NFκB through increased ROS production induced by light.[40] Similarly, Curra *et al.* evaluated the effects of a 660 nm diode laser on NFκB protein levels using an *in vivo* hamster model of oral mucositis.[106] The authors concluded that PBM reduced disease severity through the activation of the NFκB pathway. Conversely, PBM reportedly may reduce NFκB activation and subsequently reduce the expression of pro-inflammatory mediators in several diseases.[107] Interestingly, de Farias Gabriel also reported that application of 660 nm (4 J cm^{-2}) modulated NFκB activation leading to keratinocyte migration, resulting in improved wound healing in a rat model for oral epithelial wound healing.[108] Hence, modulation of NFκB not only affects pathways related to inflammation but also those influencing wound healing.

Another gene directly regulated by NFκB activation is cyclooxygenase-2 (COX-2). Its main role is to catalyse the conversion of arachidonic acid to prostaglandins including PGE2.[109] PGE2 has then been reported to be involved in the activation of a variety of pathways including cyclic adenosine monophosphate/protein kinase A (cAMP/PKA) signalling.[110,111]

To stimulate activity of the cAMP pathway, PGE2 binds to prostaglandin E_2 receptor 4 (EP4). EP4 is a GPCR coupled to a stimulatory G protein (Gs). On binding, PGE_2 induces a conformational change activating Gs, which then activate adenylyl cyclase to catalyse the conversion of ATP (a second molecule whose production is increased by PBM) to cAMP.[112] cAMP then induces the activation of protein kinase A (PKA) leading to the phosphorylation of transcription factors including CREB.[113] Several authors have reported the effects of PBM on NFκB induced signalling. Lim *et al.* reported that irradiation at 635 nm modulated both COX2 and PGE_2 protein expression.[114] Current literature also indicates the effects of PBM on a series of signalling proteins/molecules implicated in this pathway, including CREB.[115]

Another key molecule modulated by NFκB signalling is VEGF, a growth factor central to the promotion of angiogenic events.[116,117] Literature reports indicate that activation of EP4 induces the upregulation of the expression of VEGF and several authors have reported the effects of PBM on VEGF expression and activity. Tim *et al.* concluded that 830 nm irradiation of male Wistar rats with induced bone defects induced significant increases in COX2 and VEGF expression,[118] and das Neves *et al.* also reported an increase in VEGF expression following irradiation of male Wistar rats with transverse *rectus abdominis* musculocutaneous flap at 660 nm or 830 nm.[103] Cheng *et al.* also reported application of 450 nm light induced significant increases in COX2 and VEGF in a dose dependent manner (0.001–0.1 J cm^{-2}) relative to lipopolysaccharide treated microglial cells.[119] Hence, the effects of blue, red and NIR light on NFκB associated pathways have been reported in a handful of studies. However, none to date have evaluated the effects of green light on these pathways. Hence, it will be prudent in the future to evaluate the wavelength and dose dependent effects of light on downstream targets of PBM.

3.2. Transforming growth factor-β (TGFβ) signalling

Transforming growth factor-β (TGF-β) molecules represent a family of growth factors in which there are three mammalian isoforms: TGF-β1, TGF-β2 and TGF-β3. They have been extensively documented for their crucial role in wound healing processes[120] and in promoting angiogenesis and fibrosis.[121] They are secreted by a variety of cell types in inactive form as latent-TGF-β in which a TGF-β dimer held together by disulphide bonds is non-covalently bound to a pro-domain known as latency associated peptide (LAP). This complex is also commonly referred to as small latent complex (SLC). The dissociation of this complex to enable activation of free TGF-β can be induced by a range of activation stimuli including heat and pH changes.[122,123] Notably, one mechanism of particular interest here is that PBM could induce activation of TGF-β signalling.[124–126] In a recent study Arany *et al.* employed a laser emitting a wavelength of 904 nm with radiant exposure outputs ranging from 0.1–6 J cm^{-2} and concluded that PBM was able to activate latent-TGFβ1.[127] It has subsequently been hypothesised that light induces an increase in levels of ROS including superoxide ($O_2^{\bullet-}$)[128] which interacts with the methionine 253 amino acid residue on LAP.[129] This, in turn, then induces a conformational change in LAP, enabling its dissociation from TGF-β enabling it to bind with high affinity to its cell-surface receptors, including TGF-β receptors (TGFβRI, TGFβRII and TGFβRIII). Notably, TGFβRIII binds TGF-β1 and then transfers it to TGFβRI and TGFβRII, which are both serine/threonine kinases. In turn, these receptors phosphorylate transcription factors including "small mothers against decentaplegic" (Smad). Once phosphorylated Smad2 and Smad3 bind Smad4, the complex then translocates to the nucleus and interacts with transcriptional coactivators includ-

ing p300, a nuclear scaffolding protein. This signalling then enables the binding of the complex with the Smad binding element, leading to the transcription of multiple target genes.[130]

Interestingly, several authors have also provided evidence for an increase in the activity of Smad proteins following irradiation. The Smad family is comprised of the receptor Smads (Smad-1, -2, -3, -5 and -8/-9), the inhibitory Smads (Smad-6 and -7) and the co-Smad, Smad-4. Hirata *et al.* found that irradiation at 805 nm induced increases in phosphorylation of Smad-1/-5/-8.[131] Interestingly, Dang *et al.* also found an increase in phosphorylated Smad proteins, specifically Smad-2 and Smad-4 following irradiation at 800 nm.[132] Similarly, Yuchao *et al.* reported application of 475 nm light induced significant increases in Smad2 phosphorylation, providing evidence that blue light may also show efficacy in modulating TGFβ signalling.[133] Hence, these data indicate the possible involvement of TGF-β signalling through Smad proteins during the transduction of the molecular effects of PBM. However, other pathways are also induced by TGF-β signalling including the mitogen associated protein kinase pathway (MAPK[134]). Therefore, it will be interesting to determine how PBM, modulates TGF-β signalling through these interlinked pathways, and which wavelengths of light can induce which pathway.

3.3. Nuclear factor erythroid 2-related factor 2 (Nrf2) signalling

Nrf2 is a protein in the "basic leucine zipper protein" (bZIP) family and is implicated in regulation of the expression of antioxidant proteins.[135] Increases in ROS production lead to the dissociation of Nrf2 from its inhibitor, Keap1, targeting it for degradation. This enables Nrf2 to translocate into the nucleus and induce the transcription of antioxidant genes, due to the binding of Nrf2 to antioxidant response elements (AREs). To date, only a handful of studies have evaluated the effects of PBM on Nrf2 expression and activity. Interestingly, Sohn *et al.* reported an increase in Nrf2 gene expression following irradiation at 635 nm.[136] Similarly, Trotter *et al.* also found that application of blue light induced significant increases in Nrf2 expression *in vitro.*[137] This acts as a feedback mechanism following NFkB activation so the interaction of these two pathways may be important in PBM modulation of chronic inflammatory diseases. Indeed a differential upregulation of Nrf2 may be important in such diseases. However, further work will be required to fully dissect the effects of blue and green light on Nrf2 signalling.

3.4. Mitogen activated protein kinase (MAPK) signalling

Mitogen activated protein kinases (MAPKs) are a family of serine/threonine protein kinases that play an essential role in the regulation of a diverse number of cellular activities ranging from cell signalling to cell death. There are three subgroups of MAPKs including extracellular signal regulated kinases (ERKs including ERK-1 and ERK-2), p38 MAPKs (p38α, p38β, p38γ and p38δ) and c-Jun-N-terminal kinases (JNKs including JNK-1, JNK-2 and JNK-3). The three subgroups of MAPKs are finely regulated by a series of different kinases. Their activation is initiated by first the induction of MAPK kinase kinase (MAP3K) which in turn phosphorylates MAPK kinase (MAP2K). This then finally leads to the phosphorylation and activation of the MAPKs. Each MAPK is regulated by specific kinases as described below:

3.4.1. Extracellular-regulated kinase (ERK) signalling. The activity of the ERK pathway can initially be induced by receptor tyrosine kinases including TGFβR1, a member of the TGFβ signalling pathway previously proposed to play a role in transducing the effects of PBM.[127] The activation of TGFβR1 enables the downstream activation of Ras-activating protein, which catalyses the phosphorylation of inactive Ras bound to guanosine diphosphate (Ras-GDP) to form active Ras guanosine triphosphate (Ras-GTP). Ras then phosphorylates Raf, which in turn phosphorylates MEK, which ultimately induces phosphorylation of ERK, culminating in gene transcription changes that lead to proliferation, differentiation or apoptosis. Interestingly, several authors have reported the effects of PBM on signalling molecules involved in this pathway. In their study, Kim *et al.* evaluated the response of human outer root sheath cells to PBM at wavelengths of 415 nm, 525 nm, 660 nm or 830 nm.[138] Notably they found that PBM induced an increase in ERK phosphorylation.

3.4.2. p38 MAPKs. The p38 MAPK pathway is activated by an array of stimuli including inflammatory cytokines, heat shock or ligands for G-protein coupled receptors (GPCRs). These stimuli induce the activation of an array of MAP3Ks including TGFβ activated kinase-1 (TAK1). Activation of MAP3Ks enables the phosphorylation of MEK3 or MEK6. In turn, these kinases phosphorylate members of the p38 family, inducing their activation and hence a series of downstream effects including modulation of cytokine production and apoptosis.[139]

Several authors have reported the effects of PBM on p38 MAPK signalling. Interestingly, both Kim *et al.* and Chu *et al.* concluded that red light PBM induced increased p38 phosphorylation and therefore increases in the activity of this pathway.[138,140] However, a further study concluded that following application of red light, there was a decrease in p38 phosphorylation.[141] The difference in response may be due to the difference in radiant exposures employed in the different studies. For example, the authors reporting an increase in p38 phosphorylation when using a light source with a radiant exposure output of less than 12 J cm^{-2}, whilst, a radiant exposure of 18 J cm^{-2} induced a decrease in p38 phosphorylation. Hence, this may show a biphasic dose response in which lower doses of light induce stimulatory effects whilst higher doses cause inhibitory effects. However, further work will be required to evaluate this hypothesis, particularly with reference to blue and green light.

3.4.3. c-Jun N-terminal kinase (JNK). The JNK pathway is activated by an array of stimuli including cytokines, growth factors and the ligation of specific receptors. In turn these stimuli activate some of the same MAP3Ks induced in the p38

MAPK pathway including apoptosis signal-regulating kinase 1 (ASK1), mitogen-activated protein kinase kinase kinase (MEKK1) and mitogen-activated protein kinase kinase kinase 3 (MEKK3). In turn, these MAP3Ks can phosphorylate either MKK4 or MKK7, Mitogen-activated protein kinase kinases (MAP2Ks) specific to the JNK pathway. MKK4 and MKK7 can also activate MKK3 and 6, enabling the activation of the p38 MAPK pathway.[142]

Interestingly, Silva *et al.* explored the effects of 780 nm light at a radiant exposure of 10 J cm^{-2} on JNK phosphorylation of mice with diet-induced obesity. They concluded that PBM induced a significant reduction in JNK phosphorylation and hence could prove useful in treating effects induced by a high fat diet.[143] Similarly, in a mouse model for depression, Salehpour *et al.* evaluated the effects of 810 nm light at a radiant exposure of 33.3 J cm^{-2} and found that PBM induced reductions in JNK phosphorylation and other members of the MAPK signalling pathway including p38.[144] The authors also reported that treatment induced decreases in the serum levels of key pro-inflammatory cytokines, including Tumour necrosis factor-α (TNF-α). Hence, these data provide evidence that PBM could modulate JNK signalling and therefore downstream effects, including the production of pro-inflammatory cytokines. However, the effects of blue and green light on JNK signalling are yet to be explored, hence future work should evaluate the wavelength dependent effects of PBM on the JNK pathway.

4. *In vitro* and *in vivo* application of blue and green light PBM therapy

4.1. Introduction

Whilst a number of reviews have been published detailing the possible therapeutic efficacy of red and NIR PBM,[128,145] none to date have extensively explored the effects of blue or green light either *in vitro* or *in vivo*. Hence, this section investigates the potential of blue and green light PBM in therapeutic application to determine whether these short wavelengths of light could be efficacious.

4.2. Methods

To assess literature surrounding the effects of green and blue light PBM, a systematic review of relevant literature was performed using Scopus. The Scopus database was employed as a means to undergo key word searches to provide an overview of literature regarding the effects of blue and green light PBM. Future work may endeavour to use a broader range of databases including MEDLINE and PubMed to evaluate the effects of blue and green light PBM.

The two searches outlined in Fig. 3 were performed separately and a series of key terms and wavelengths were included to refine the search. Following literature searches, the results were filtered for 'articles only' and for articles published within the past ten years (25/1/2008–25/1/2019). This timeline was selected to ensure a manageable sample of articles were included in the review, where key MeSH accepted terms were relevant to articles (including LLLT and PBM) investigated. Key words described in Fig. 3 were input into the Scopus database and systematic evaluation ensured irrelevant articles were excluded from the review. For example, those reporting the use of PBM but using biological assays including 'Alamar blue' (cell metabolic activity assay) or 'trypan blue' (a vital stain used to differentiate between live and dead cells *in vitro*) were not included as they did not specifically report the effects of blue light *in vitro* or *in vivo*. Other exclusion criteria included elimination of articles that reported the effects of lasers on remodelling tissue at a high power. For example, photoselective vaporisation commonly uses lasers emitting green light and the procedure involves the burning away of excess tissue to enable normal urine flow through the prostate.[146] As PBM is commonly defined as modulation of tissue response rather than removal of tissue, these articles were excluded. Review articles were also excluded from analysis. Articles selected for review were then assessed in terms of the reporting of light properties (including wavelength, irradiance, radiant exposure, exposure time and beam area), the application of the light source (*i.e. in vitro*, *in vivo* or *ex vivo*) and the outcome of each study (therapeutically beneficial or harmful).

4.3. Results

A Scopus search was undergone to identify publications citing key words illustrated in Fig. 3 and published within the following time frame: 25/1/2008–25/1/2019. This would then enable identification of key parameters that may induce beneficial effects *in vivo*.

4.3.1 Blue light PBM. An initial search employing the Scopus database resulted in 317 articles citing the search terms described in Fig. 3a, articles were then subsequently filtered and screened, and it was concluded that 68 articles were suitable for further review.[17–21,29–31,57,66,69–74,80,90,147–198]

Of the articles reviewed, 72% (49/68) reported a positive effect following the application of blue light, with 7% (5/68) reporting negative effects and 21% (14/68) reporting no significant effect. Whilst, the majority of articles within this review reported the effects of PBM on tissue, a handful also evaluated the bactericidal effect of blue light PBM (3/68[154,179,186]). Although, the mechanism of blue light in inducing bacterial cell death is not a focus of this current review, we felt it important to highlight this as a further application of PBM which has therapeutic application.[199] Notably however, the parameters required to induce a bactericidal effect (>55 J cm^{-2}) are much higher than those applied to induce tissue effects (<55 J cm^{-2}). Hence, when exploring possible beneficial parameters for tissular applications, articles evaluating the antimicrobial properties of blue light were excluded.

When evaluating the recording and reporting of treatment parameters, it was found that 68% (46/68) of articles failed to report any information regarding light characterisation procedures and relied entirely on the manufacturers reported values. Of the other 22 articles, the light characterisation procedures reported were minimal, where the majority reported either analysis of power or irradiance output of a light source

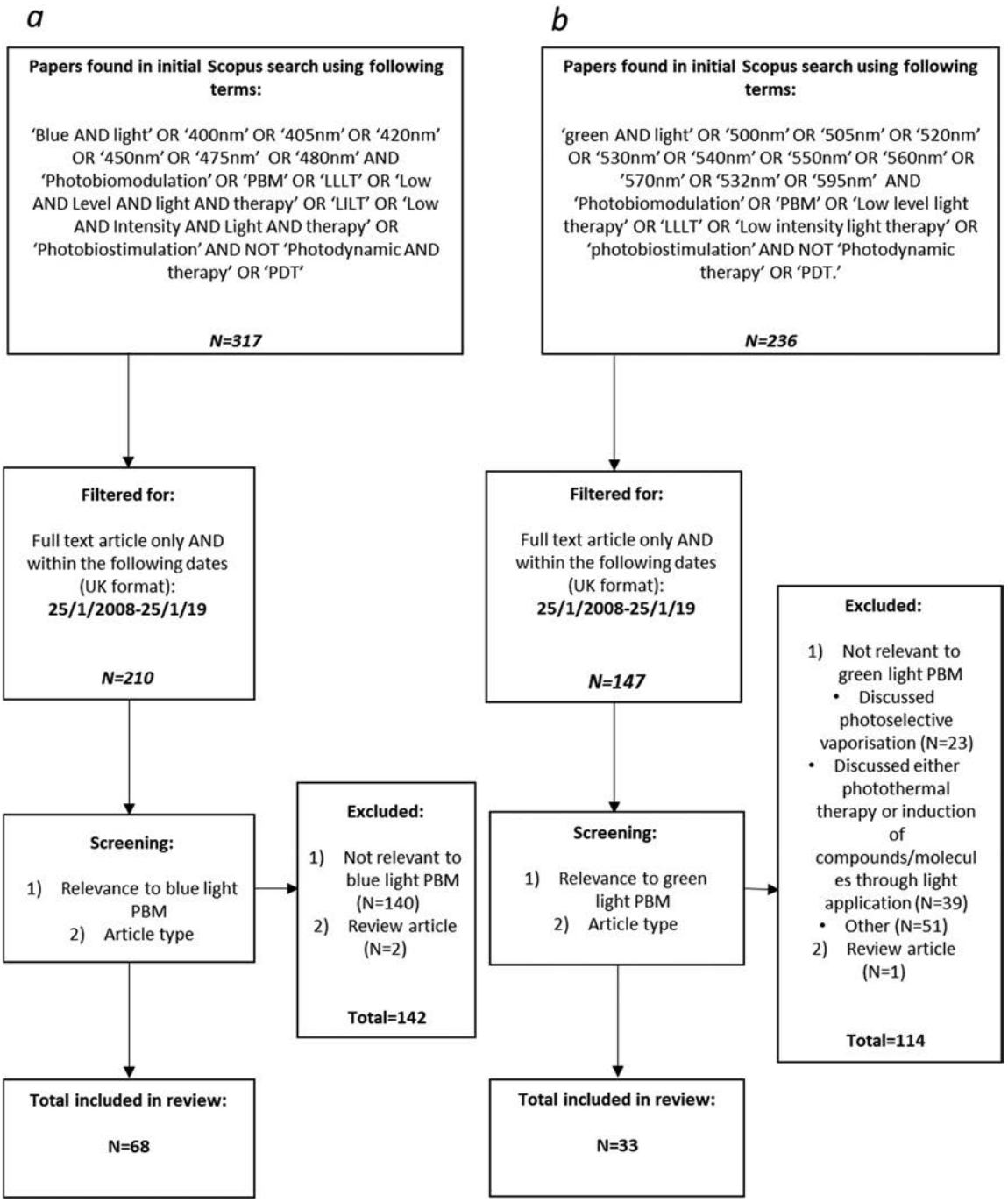

Fig. 3 Flow chart describing the strategy employed to identify relevant articles illustrating the effects of (a) blue light and (b) green light PBM.

(12/22[69,74,147,151,155,156,161,166,182,184,191,193]). Interestingly, these figures are similar to those reported by Hadis *et al.* in which 76% of articles evaluated failed to report the use of any light characterisation techniques.[15] A series of other key parameters were also not reported in full by authors including irradiance (29%, 20/68), exposure time (34%, 23/68), radiant exposure (38%, 26/68) and beam area (82%, 56/68).

From those articles reporting parameters, median values could be calculated. For example, for those articles reporting a positive effect of PBM, a median value of radiant exposure of 7.8 J cm^{-2} (range: 1.5–90 J cm^{-2}) was determined. In fact, 63% (17/27) of articles reporting both positive effects of PBM used radiant exposure values <10 J cm^{-2}. Interestingly, only one article reported a beneficial effect of PBM on tissue at a radiant exposure >55 J cm^{-2}.[183] For articles reporting negative effects of PBM, a median radiant exposure of 7.5 J cm^{-2} (range: 3–183.43 J cm^{-2}) was calculated. However, of the 5 articles reporting a negative effect of PBM only 4 reported

Table 1 Citations identified from a review of the literature evaluating the effects of blue light PBM using the following search terms: 'Blue AND light' OR '400 nm' OR '405 nm' OR '420 nm' OR '450 nm' OR '475 nm' OR '480 nm' AND 'Photobiomodulation' OR 'PBM' OR 'LLLT' OR 'Low AND Level AND light AND therapy' OR 'LILT' OR 'Low AND Intensity AND Light AND therapy' OR 'Photobiostimulation' AND NOT 'Photodynamic AND therapy' OR 'PDT'

Citation	Light source	Dose	Study type	Conclusion
1. Mignon *et al.*, 2018[19]	Source: LED Wavelength (nm): 450, 490, 550, 650 and 850 Power (mW): Frequency (Hz): Spot area (cm^2):	Irradiance (mW cm^{-2}): 30 (450 nm), 30 (490 nm), 30 (550 nm), 7 (590 nm), 60 (655 nm), 80 (850 nm) Time (s): Energy (J): Radiant exposure (J cm^{-2}): 0–250 (dependent upon wavelength)	*In vitro*: human reticular and papillary dermal fibroblasts	450 nm light at 30 J cm^{-2} induced 50% reductions in cell metabolic activity. 450 nm and 500 nm induced stronger inhibitory effects on reticular DFs *vs.* papillary DFs. 450 nm light induced increases in intracellular ROS production. Blue and NIR light induced changes in some similar gene groups. However, more genes were downregulation following irradiation with blue light compared to NIR. Blue light also downregulated expression of genes associated with the TGF-β pathway
2. Tani *et al.*, 2018[178]	Source: LED Wavelength (nm): 405, 635, 808 Power (mW): Frequency (Hz): Spot area (cm^2):	Irradiance (mW cm^{-2}): 12.59 Time (s): 30 Energy (J): Radiant exposure (J cm^{-2}): 0.378	*In vitro*: human osteoblasts and human mesenchymal stromal cells	Blue light had no significant effect on molecular signalling. 635 nm light could be effective in promoting or improving bone regeneration as shown through molecular analysis
3. Priglinger *et al.*, 2018[184]	Source: LED Wavelength (nm): 475, 516, 635 Power (mW): Frequency (Hz): pulsed 2.5 (pulse rate 50%) Spot area (cm^2):	Irradiance (mW cm^{-2}): 40 Time (s): 600 Energy (J): Radiant exposure (J cm^{-2}): 24	*In vitro*: stromal Vascular fraction cells	Blue, green and red light did not have a cytotoxic effect on cells. Red and green light induced significant increases in vascular endothelial growth factor expression
4. Falcone *et al.*, 2018[162]	Source: LED Wavelength (nm): 453 Power (mW): Frequency (Hz): 5% duty cycle, 100 Hz Spot area (cm^2):	Irradiance (mW cm^{-2}): 10 (cw), 200 (pulsed) Time (s): 1800 Energy (J): Radiant exposure (J cm^{-2}): 18	*In vivo*: effects on inflammation and skin barrier recovery	Reduced IL-1α following irradiation
5. Veleska-Stevkoska and Koneski, 2018[21]	Source: LED Wavelength (nm): 410 and 470 Power (mW): Frequency (Hz): Spot area (cm^2): 1.25	Irradiance (mW cm^{-2}): 750 Time (s): 10–20 Energy (J): 50–100 Radiant exposure (J cm^{-2}): 7.5–15	*In vivo*: haemostasis in oral surgery (bleeding from tooth extractions)	Blue light shortens bleeding time from extraction socket
6. Castellano-Pellicena *et al.*, 2018[17]	Source: LED Wavelength (nm): 447, 505, 530, 655 and 850 (24 well) or 453, 656 (*ex vivo*) Power (mW): Frequency (Hz): Spot area (cm^2):	Irradiance (mW cm^{-2}): Time (s): 1200 (24 well) Energy (J): Radiant exposure (J cm^{-2}): 453 nm – 2, 656 nm – 30	*In vitro* and *ex vivo*: keratinocytes and human skin epidermis	Blue light stimulated metabolic activity of cultured keratinocytes. Low levels of blue light reduced DNA synthesis and stimulated keratinocyte differentiation. Level of differentiation induced by blue light was reduced in opsin 3 (OPN3) knockdown, suggesting OPN3 may be Important in blue light induced restoration of barrier function

Table 1 *(Contd.)*

Citation	Light source	Dose	Study type	Conclusion
7. Fekrazad *et al.*, 2018[163]	Source: laser	Irradiance (mW cm^{-2}): 266 (blue), 266 (green) 167 (red), 1333 (NIR)	*In vitro*: mesenchymal stem cells	Cartilage markers were upregulated by 810 nm and 810–485 nm light. Red and blue-green irradiation induced expression of COL1. Blue, blue-green and green light irradiation reduced osteocalcin expression. Stimulatory effects on osteogenesis were seen for red and near infra-red lasers but green light had inhibitory effects. Blue light was not reported to induce inhibitory effects
	Wavelength (nm): 810, 660, 532, 485, combinations: 810–660, 810–485, 660–532, 660–485	Time (s): 3–24 (dependent upon wavelength)		Cons: parameters differ considerably from one wavelength to the next, particularly when evaluating combination treatments. Making results of which wavelength is most effective questionable
	Power (mW): 30–200 (dependent on wavelength)	Energy (J):		
	Frequency (Hz):	Radiant exposure (J cm^{-2}):		
	Spot area (cm^2): 0.113–0.18	4 (8 for combination)		
8. Rocca *et al.*, 2018[185]	Source: diode laser (450 nm, 635 nm, 808 nm, Er:YAG laser (2940 nm)	Irradiance (mW cm^{-2}): 280 (808 nm), 280 (450 nm), 1000 (63 5 nm)	*In vivo*: human	The diode lasers proved more effective than the Er:YAG in reducing pain scores over a 7 day period. 635 nm had the most immediate effect, but there was no significant difference pain score using the 3 diode lasers after 7 days
	Wavelength (nm): 2940, 808, 450, 635	Time (s): 60 (2940 nm), 3 × 30 (635 nm), 60 (808 nm), 60 (450 nm)		
	Power (mW): 200 (635 nm), 1500 (808 nm), 500 (450 nm)	Energy (J):		
	Frequency (Hz): 20 (Er:YAG)	Radiant exposure (J cm^{-2}): 76.43 (Er:YAG), 36 (635 nm), 50 (808 nm), 17 (450 nm)		
	Spot area (cm^2):			
9. Wang *et al.*, 2018[195]	Source: LEDs	Irradiance (mW cm^{-2}): 20	*In vitro*: whole blood samples (human)	No significant change in the absorption spectra exhibited by blood following irradiation
	Wavelength (nm): 405	Time (s): 900		
	Power (mW): 200	Energy (J):		
	Frequency (Hz):	Radiant exposure (J cm^{-2}): 12		
	Spot area (cm^2):			
10. Kim *et al.*, 2017[174]	Source: LEDs	Irradiance (mW cm^{-2}):	*In vivo*: mouse model	Wound closure percentage over 10 days was greatest when an 830 nm LED used. Increased TGF-β and collagen 1 but downregulated SMAD7
	Wavelength (nm): 410, 630, 830	Time (s):		
	Power (mW):	Energy (J):		
	Frequency (Hz):	Radiant exposure (J cm^{-2}):		
	Spot area (cm^2):			
11. Rohringer *et al.*, 2017[69]	Source: LED	Irradiance (mW cm^{-2}): 80	*In vitro*: human umbilical vein endothelial cells	Red and green light induced proliferation and migration of endothelial cells whilst blue light had no significant impact. Blue light only induced significant increases in ROS production
	Wavelength (nm): 475, 516, 635	Time (s): 600		NOTE: irradiance and irradiation time values do not correlate with fluency. Cells irradiated at 20% confluency – may explain negative effects of blue light
	Power (mW):	Energy (J):		
	Frequency (Hz): 50% pulse rate, 2.5 Hz	Radiant exposure (J cm^{-2}): 24		
	Spot area (cm^2):			

Table 1 *(Contd.)*

Citation	Light source	Dose	Study type	Conclusion
12. Wang *et al.*, 2017[66]	Source: LED array (415 nm), filtered lamp (540 nm), diode laser (660 nm and 810 nm) Wavelength (nm): 415, 540, 660, 810 Power (mW): Frequency (Hz): Spot area (cm^2): 4	Irradiance (mW cm^{-2}): 16 Time (s): 188 Energy (J): Radiant exposure (J cm^{-2}): 3	*In vitro*: human adipose-derived stem cells	Blue and green light induce significant increases in intracellular calcium and ROS, reduce mitochondrial membrane potential, lower intracellular pH and reducing cellular proliferation. Red and NIR light have the opposite effect Labelled fluency as irradiance. Different delivery systems may alter light delivery (coherent *vs.* non-coherent light sources)
13. Wang *et al.*, 2017[70]	Source: LED Wavelength (nm): 480, 560, 660 and white (400–750) Power (mW): 3000 Frequency (Hz): Spot area (cm^2):	Irradiance (mW cm^{-2}): 250 Time (s): Energy (J): Radiant exposure (J cm^{-2}):	*In vitro* and *in vivo*: irradiated fertile broiler eggs and isolated skeletal muscle and satellite cells	Green PBM promoted muscle growth and satellite cell proliferation through insulin growth factor-1 signalling in late embryogenesis
14. Choe *et al.*, 2017[158]	Source: LED Wavelength (nm): 622, 535, 462 Power (mW): 24 000 Frequency (Hz): Spot area (cm^2):	Irradiance (mW cm^{-2}): 16 Time (s): 600–1800 (daily) Energy (J): Radiant exposure (J cm^{-2}):	*In vitro*: HeLa cells (cancer cell line)	Blue light and high frequency ultrasound induced significant reductions in cell density when compared to red and green light combined with ultrasound. This could be beneficial in alleviating cancer cell proliferation
15. Buscone *et al.*, 2017[157]	Source: LED Wavelength (nm): 453, 689 Power (mW): Frequency (Hz): Spot area (cm^2):	Irradiance (mW cm^{-2}): Time (s): Energy (J): Radiant exposure (J cm^{-2}): 3.2	*In vitro* and *ex vivo*: hair growth and outer root sheath cells	Blue light at low radiant exposure stimulate hair growth *ex vivo*
16. Santos *et al.*, 2017[71]	Source: LED Wavelength (nm): 405 Power (mW): Frequency (Hz): Spot area (cm^2): 0.27	Irradiance (mW cm^{-2}): 300 Time (s): 30–60 Energy (J): Radiant exposure (J cm^{-2}):	*In vitro*: subventricular zone (SVZ) cell culture	Blue light induced transient increases in ROS, causing increased neuronal differentiation and increases retinoic acid receptor levels. The effects are heightened with the addition of light reactive nanoparticles
17. Fekrazad *et al.*, 2017[18]	Source: laser: GaAs (405 nm, 532 nm), InGaAlP (660 nm) and GaAlAs (810 nm) Wavelength (nm): 405, 532, 660, 810 Power (mW): Frequency (Hz): Spot area (cm^2): 1	Irradiance (mW cm^{-2}): 200 Time (s): Energy (J): Radiant exposure (J cm^{-2}): 1.5	*In vivo*: male Wistar rats (n = 60)	Green, blue, red and infrared light irradiation may accelerate healing process
18. Lee *et al.*, 2017[177]	Source: LED Wavelength (nm): 410, 630, 830 Power (mW): Frequency (Hz): Spot area (cm^2):	Irradiance (mW cm^{-2}): 205 (405 nm), 172 (630), 50 (830) Time (s): Energy (J): Radiant exposure (J cm^{-2}): 10	*In vitro*: keloid fibroblasts	Blue did not affect cell viability. COL1 gene and protein expression decreased significantly after irradiation with blue light and may be effective in preventing keloid formation
19. Alba *et al.*, 2017[29]	Source: LED (470) and laser (660) Wavelength (nm): 470 and 660 Power (mW): Frequency (Hz): Spot area (cm^2):	Irradiance (mW cm^{-2}): Time (s): 180 (470), 60 (660) Energy (J): 6–8 Radiant exposure (J cm^{-2}):	*In vivo*: treatment of acne vulgaris	The combined use of red and blue light proved beneficial in reducing inflammation and enhancing wound healing when compared to the use of salicylic acid for treatment

Table 1 *(Contd.)*

Citation	Light source	Dose	Study type	Conclusion
20. Mignon *et al.*, 2017[180]	Source: LED Wavelength (nm): 400, 500, 530, 590, 655, 850 Power (mW): Frequency (Hz): Spot area (cm^2):	Irradiance (mW cm^{-2}): 3–80 Time (s): Energy (J): Radiant exposure (J cm^{-2}): 2–30	*In vitro*: human dermal fibroblasts	The effects of blue light on cell metabolism were dramatically influenced by FBS concentration, confluency level of cells and the fluency values applied to cells
21. Yoshimoto *et al.*, 2017[197]	Source: LED Wavelength (nm): 465 Power (mW): Frequency (Hz): Spot area (cm^2):	Irradiance (mW cm^{-2}): 30 Time (s): 1800 Energy (J): Radiant exposure (J cm^{-2}): 54	*In vitro*: human colon cancer cells (HT-29 or HCT-116)	Blue light irradiation reduced cancer cell viability. However, this effect was reversed in an Opsin 3 (Opn3) knockdown
22. Yuan *et al.*, 2017[72]	Source: LED Wavelength (nm): 470 Power (mW): Frequency (Hz): Spot area (cm^2):	Irradiance (mW cm^{-2}): 20 Time (s): 60–3600 Energy (J): Radiant exposure (J cm^{-2}):	*In vitro*: bone marrow-derived mesenchymal stem cells (BMSCs)	Blue light inhibited osteogenic differentiation, induced apoptosis as a result of increased ROS production and DNA damage
23. Monrazeri *et al.*, 2017[181]	Source: LED Wavelength (nm): 630, 808, 450 Power (mW): 100 (630 nm and 808 nm), 3000 (450 nm) Frequency (Hz): Spot area (cm^2): 1	Irradiance (mW cm^{-2}): 100 (630 nm) Time (s): Energy (J): 48 J per point Radiant exposure (J cm^{-2}):	*In vivo*: human	Combining all three wavelengths reduced abdominal girth significantly
24. Li *et al.*, 2016[178]	Source: LED Wavelength (nm): 630, 460 Power (mW): 100 (630 nm and 808 nm), 3000 (450 nm) Frequency (Hz): Spot area (cm^2): 300	Irradiance (mW cm^{-2}): 50 Time (s): 900–1800 Energy (J): Radiant exposure (J cm^{-2}): 45–90	*In vivo*: Japanese big ear white rabbits, induced wound model (incisions in back)	Red light was more effective in promoting wound healing than blue light
25. Khori *et al.*, 2016[173]	Source: laser Wavelength (nm): 405, 532, 632 Power (mW): 1–3 Frequency (Hz): Spot area (cm^2):	Irradiance (mW cm^{-2}): Time (s): 600 (10 treatments, 3 times a week) Energy (J): Radiant exposure (J cm^{-2}):	*In vivo* and *in vitro*: BALB/c inbred female mice and mouse mammary carcinoma cell line (4T1)	Blue light reduced tumour volume and gene expression markers for tumorigenesis
26. AlGhamdi *et al.*, 2016[148]	Source: laser Wavelength (nm): 457, 635, 355 Power (mW): Frequency (Hz): Spot area (cm^2):	Irradiance (mW cm^{-2}): 25 Time (s): 80 Energy (J): Radiant exposure (J cm^{-2}): 2	*In vitro*: melanocytes from normal human melanocytes	PBM at all wavelengths induced the production of stage I melanosomes to the highest levels relative to control cells. In particular, red and blue laser PBM induced the highest increase in % level of stage I melanosomes. This indicates significant stimulation of melanogenesis
27. Wang *et al.*, 2016[196]	Source: LED array (420), filtered lamp (540), diode laser (660, 810) Wavelength (nm): 420, 540, 660, 810 Power (mW): Frequency (Hz): Spot area (cm^2): 4	Irradiance (mW cm^{-2}): 16 Time (s): 188 (five times, every 2 days) Energy (J): Radiant exposure (J cm^{-2}): 3	*In vitro*: human adipose-derived stem cells	Blue and green light were effective in stimulating osteoblast differentiation and increasing intracellular calcium levels than red and near infra-red light. Blue and green light could activate light-gated calcium ion channels
28. Masson-Meyers *et al.*, 2016[30]	Source: LED Wavelength (nm): 470 Power (mW): 150 Frequency (Hz): Spot area (cm^2):	Irradiance (mW cm^{-2}): 30 Time (s): Energy (J): Radiant exposure (J cm^{-2}): 3, 5, 10, 55	*In vitro*: human dermal fibroblasts	Blue light and radiant exposure of 5 J cm^{-2} improved wound healing, increased protein concentration and reduced IL-6 secretion significantly. There was no effect of irradiation on cell viability

Table 1 *(Contd.)*

Citation	Light source	Dose	Study type	Conclusion
29. Ashworth *et al.*, 2016[151]	Source: LED Wavelength (nm): 450, 510, 660, 860 Power (mW): Frequency (Hz): Spot area (cm^2):	Irradiance (mW cm^{-2}): Time (s): Energy (J): Radiant exposure (J cm^{-2}): Other: photons per cm^2 per s	*Ex vivo*: rat or mouse spinal cord slices	All four wavelengths at the highest intensity output reduced immunoreactivity
30. Figurova *et al.*, 2016[165]	Source: LED Wavelength (nm): 685/470 combined Power (mW): Frequency (Hz): Spot area (cm^2):	Irradiance (mW cm^{-2}): 8 Time (s): Energy (J): Radiant exposure (J cm^{-2}): 3.36	*In vivo*: minipigs	Combined red and blue light therapy induced improved tissue healing relative to control groups
31. Becker *et al.*, 2016[152]	Source: LED Wavelength (nm): 453 Power (mW): Frequency (Hz): Spot area (cm^2):	Irradiance (mW cm^{-2}): 23 Time (s): 1800 Energy (J): Radiant exposure (J cm^{-2}):	*In vitro*: melanoma cells	The effects of blue light on cell viability were dose dependent and blue light down regulated anti-inflammatory genes but upregulated genes associated with apoptosis. Significant decreases in viability were witnessed after irradiation times of 1800 s
32. Dereci *et al.*, 2016[160]	Source: LED (blue, 400–490), GaAlAs diode laser (NIR, 980 nm) Wavelength (nm): 400–490, 980 Power (mW): Frequency (Hz): Spot area (cm^2):	Irradiance (mW cm^{-2}): 12 (400–490), 200 (980) Time (s): Energy (J): Radiant exposure (J cm^{-2}): 13 (400–490, 20 (980)	*In vivo*: Wistar rats	Whilst high doses of blue light were inhibitory, low doses proved efficacious in promoting bone regeneration to similar levels to NIR light
33. Takhtfooladi and Sharifi, 2015[191]	Source: GaAlAs (680), LED (650, 450) Wavelength (nm): 680, 650, 450 Power (mW): 10 (680) Frequency (Hz): pulsed (no info, 680 only) Spot area (cm^2): 0.4 (680), 1.5 (650, 450)	Irradiance (mW cm^{-2}): Time (s): 200 s (680), 600 s (450, 650) 14 days Energy (J): Radiant exposure (J cm^{-2}): 10 (680), 650 (2.4), 450 (2.4)	*In vivo*: New Zealand rabbits	Blue and red LEDs had no significant effect on cell proliferation or myelination. Conversely, laser red light had a significant effect. This may be due to the pulsed modality of the laser light source
34. Fekrazad *et al.*, 2015[164]	Source: laser Wavelength (nm): 630, 532, 425 Power (mW): Frequency (Hz): Spot area (cm^2):	Irradiance (mW cm^{-2}): 50 (630 nm and 532 nm), 55 (425 nm) Time (s): Energy (J): Radiant exposure (J cm^{-2}): 2	*In vivo*: diabetes induced male Wistar rats	All three wavelengths induced significant increases in wound healing, where red light was most effective
35. Masson-Meyers *et al.*, 2015[179]	Source: LED or Laser Wavelength (nm): 405 Power (mW): Frequency (Hz): Spot area (cm^2):	Irradiance (mW cm^{-2}): Time (s): 900, 1800, 14 400 Energy (J): Radiant exposure (J cm^{-2}): 40, 54, 81, 121	*In vitro*: methicillin resistant Staphylococcus aureus (MRSA)	Both LED and laser proved efficacious in supressing bacterial growth to significant levels at all four radiant exposure values evaluated
36. Schafer and McNeely, 2015[186]	Source: LED Wavelength (nm): 405 Power (mW): Frequency (Hz): Spot area (cm^2):	Irradiance (mW cm^{-2}): 30 Time (s): Energy (J): Radiant exposure (J cm^{-2}):	*In vitro: Staphylococcus Epidermis*, *Staphylococcus Aureus* and *Propionibacterium Acnes*	The effects of blue light combined with ultrasound were dose dependent where it is proposed that bacterial cells become more susceptible to the antimicrobial effects of blue light following ultrasound application
37. Niu *et al.*, 2015[182]	Source: LED Wavelength (nm): 405, 630, 660 Power (mW): Frequency (Hz): Spot area (cm^2):	Irradiance (mW cm^{-2}): 161 μW cm^{-2} nm (405 nm), 300 μW cm^{-2} nm (630 nm), 545 μW cm^{-2} nm (660 nm) Time (s): 600 Energy (J): Radiant exposure (J cm^{-2}): 1.604 (405 nm), 3.409 (630 nm), 6.538 (660 nm)	*In vitro*: keratinocytes	The combination of blue light, red light and curcumin was able to regulate proliferation and apoptosis of keratinocytes. Without curcumin, light did not influence cell viability

Table 1 *(Contd.)*

Citation	Light source	Dose	Study type	Conclusion
38. AlGhamdi *et al.*, 2015[149]	Source: diode laser Wavelength (nm): 355, 457, 635 Power (mW): Frequency (Hz): Spot area (cm^2):	Irradiance (mW cm^{-2}): 25 Time (s): 20–200 Energy (J): Radiant exposure (J cm^{-2}): 0.5–5	*In vitro*: melanocytes	Blue laser proved most efficacious in promoting cell proliferation and migration
39. Pfaff *et al.*, 2015[183]	Source: LED Wavelength (nm): 453 Power (mW): Frequency (Hz): high (200 mW cm^{-2}) and low (100 mW cm^{-2}) duty cycles employed Spot area (cm^2):	Irradiance (mW cm^{-2}): 100 (low), 200 (high) Time (s): 1800 Energy (J): Radiant exposure (J cm^{-2}): 90	*In vivo*: treatment of patients with mild Psoriasis Vulgaris (Pv)	Blue light proved to significantly reduce Pv severity at both irradiance outputs
40. Bumah *et al.*, 2015[154]	Source: LED Wavelength (nm): 470 Power (mW): 150 (18 delivered to cultures) Frequency (Hz): Spot area (cm^2):	Irradiance (mW cm^{-2}): 30 Time (s): Energy (J): Radiant exposure (J cm^{-2}): 55	*In vitro*: MRSA	Blue light alone is effective in supressing MRSA growth, where there was no significant difference in the effect of blue light and the combination of blue light and hyperbaric oxygen
41. Jung *et al.*, 2015[170]	Source: LED Wavelength (nm): 415, 630 Power (mW): Frequency (Hz): Spot area (cm^2):	Irradiance (mW cm^{-2}): Time (s): 76–615 Energy (J): Radiant exposure (J cm^{-2}): 5–40	*In vitro*: human sebocytes	Blue and red light influence lipid production and may have beneficial effects on acne through the suppression of sebum production
42. Teuschl *et al.*, 2015[193]	Source: LED Wavelength (nm): 470, 630 Power (mW): 1000 Frequency (Hz): Spot area (cm^2):	Irradiance (mW cm^{-2}): 50 Time (s): 600 (5 times, once per day) Energy (J): Radiant exposure (J cm^{-2}): 30	*In vitro*: C2C12 (myoblast), NIH/3T3 (fibroblast), BICR10 (keratinocytes)	Blue light reduced cell proliferation and promoted necrosis. Red light promoted cell proliferation and increased rate of wound healing
43. Hadis *et al.*, 2015[168]	Source: LED Wavelength (nm): 400–900 Power (mW): Frequency (Hz): Spot area (cm^2):	Irradiance (mW cm^{-2}): 3.5 Time (s): 15–120 Energy (J): Radiant exposure (J cm^{-2}): 0.05–0.42	*In vitro*: dental pulp cells (DPCs)	Blue light had no significant effect on DPCs whilst wavelengths of 625 nm, 660 nm, 789 nm and 800 nm induced significant increases in mitochondrial activity. Particularly after 24 h and irradiation periods of 30 s
44. De Sousa *et al.*, 2015[31]	Source: LED Wavelength (nm): 450 Power (mW): 70 Frequency (Hz): Spot area (cm^2): 0.00785	Irradiance (mW cm^{-2}): Time (s): 0–343 Energy (J): Radiant exposure (J cm^{-2}): 3–24	*In vitro: Staphylococcus aureus, Pseudomonas aeruginosa*	Blue light inhibited bacterial growth at fluency values greater than 6 J cm^{-2}
45. Gold *et al.*, 2014[167]	Source: LEDs Wavelength (nm): 405–460 Power (mW): Frequency (Hz): Spot area (cm^2):	Irradiance (mW cm^{-2}): Time (s): Energy (J): Radiant exposure (J cm^{-2}):	*In vivo*: human	Induced a reduction in acne vulgaris inflammatory lesions. Did induce increases in skin temperature up to 41 °C
46. Schoenly *et al.*, 2014[187]	Source: laser Wavelength (nm): 400 Power (mW): Frequency (Hz): 60 ns laser pulse Spot area (cm^2):	Irradiance (mW cm^{-2}): Time (s): Energy (J): Radiant exposure (J cm^{-2}): <8	*In vitro*: human teeth	Removal of calculus is thickness dependent and can occur at radiant exposure <5 J cm^{-2}
47. Buravlev *et al.*, 2014[74]	Source: LED Wavelength (nm): 442 Power (mW): 70 Frequency (Hz): Spot area (cm^2): 0.00785	Irradiance (mW cm^{-2}): Time (s): 30–300 Energy (J): Radiant exposure (J cm^{-2}): 30	*In vitro*: mitochondria isolated from male albino rat livers	Blue light restored nitric oxide inhibited rates of respiration to normal. It is hypothesised blue light irradiation induces photolytic destruction of nitrosyl complexes that inhibit the activities of complex I and III of the electron transport chain

Table 1 *(Contd.)*

Citation	Light source	Dose	Study type	Conclusion
48. Sinclair *et al.*, 2014[190]	Source: LED	Irradiance (mW cm^{-2}): 0.0848 (blue), 0.0185 (yellow)	*In vivo*: patients with traumatic brain injury (TBI)	Blue light is effective in alleviating fatigue and daytime sleeping following TBI
	Wavelength (nm): 465, 574	Time (s): 2700		
	Power (mW):	Energy (J):		
	Frequency (Hz):	Radiant exposure (J cm^{-2}):		
	Spot area (cm^2):	Other: 68 lux, 1.21× photons per cm^2 per s		
49. Hochman *et al.*, 2014[169]	Source: LED (470 nm and 660 nm) and Laser (660 nm and 808 nm, no details of laser source)	Irradiance (mW cm^{-2}):	*In vivo*: skin of adult male Wistar rats	Infrared (808 nm) laser irradiation enhances neuropeptide secretion in healthy rat skin, whilst other sources of light and wavelengths had no significant impact
	Wavelength (nm): 470, 660, 808	Time (s): 114 (LED), 396 (laser)		
	Power (mW): 100 (808 nm, 660 nm Laser) and 350 (470 nm and 660 nm LED)	Energy (J): 40 (both)		
	Frequency (Hz):	Radiant exposure (J cm^{-2}):		
	Spot area (cm^2): 0.5 (LED), 0.028 (laser)	80 (LED), 1429 (laser)		
50. Dungel *et al.*, 2014[161]	Source: LED	Irradiance (mW cm^{-2}): 50	*In vivo*: Sprague-Dawley rats	Both wavelengths promoted angiogenesis, improved tissue perfusion, reduced tissue necrosis and therefore promoted wound healing
	Wavelength (nm): 470, 629	Time (s): 600		
	Power (mW):	Energy (J):		
	Frequency (Hz):	Radiant exposure (J cm^{-2}):		
	Spot area (cm^2):	30		
51. KazemiKhoo and Ansari *et al.*, 2014[172]	Source: optical fiber	Irradiance (mW cm^{-2}):	*In vivo*: intravascular laser irradiation of blood in type 2 diabetic patients and measurements of changes in blood sugar	Both wavelengths induced significant decreases in blood sugar levels
	Wavelength (nm): 405, 632.8	Time (s): 1800 (every other day, 14 sessions)		
	Power (mW): 1.5	Energy (J):		
	Frequency (Hz):	Radiant exposure (J cm^{-2}):		
	Spot area (cm^2): 0.01			
52. Burvalev *et al.*, 2014[155]	Source: laser (442 nm, 532 nm) and LED (650 nm)	Irradiance (mW cm^{-2}): 30	*In vitro*: mitochondria isolated from rat liver	Laser of mitochondria at 442 nm restored mitochondrial respiration inhibited by NO. Blue light also restored complex IV activity but not complexes I–III. Other wavelengths had no significant effect
	Wavelength (nm): 442, 532, 650	Time (s): 30–300		
	Power (mW): 20	Energy (J):		
	Frequency (Hz):	Radiant exposure (J cm^{-2}):		
	Spot area (cm^2): 1.57	3–31		
53. Turrioni *et al.*, 2013[194]	Source:	Irradiance (mW cm^{-2}):	*In vitro*: human dentin	All three wavelengths passed through the dentin barrier. LED power loss and transmittance varied dependent upon dentin thickness and wavelength
	Wavelength (nm): 450, 630, 850	Time (s):		
	Power (mW):	Energy (J):		
	Frequency (Hz):	Radiant exposure (J cm^{-2}):		
	Spot area (cm^2):			
54. Kazemi Khoo *et al.*, 2013[171]	Source: laser	Irradiance (mW cm^{-2}):	*In vivo*: human diabetic patients	Resulted in modulation of metabolites associated with type 2 diabetes following intravenous PBM
	Wavelength (nm): 405	Time (s): 1800		
	Power (mW): 1.5	Energy (J):		
	Frequency (Hz):	Radiant exposure (J cm^{-2}):		
	Spot area (cm^2):			
55. Cheon *et al.*, 2013[80]	Source: LED	Irradiance (mW cm^{-2}): 3.55 (470 nm), 4.02 (525 nm) and 6.78 (633 nm)	*In vivo*: Sprague Dawley rats and histological analysis	Blue and green light promoted wound healing significantly. Red light promoted collagen production
	Wavelength (nm): 470, 525, 633	Time (s): 3600 (9 days)		
	Power (mW):	Energy (J):		
	Frequency (Hz):	Radiant exposure (J cm^{-2}):		
	Spot area (cm^2):			

Table 1 *(Contd.)*

Citation	Light source	Dose	Study type	Conclusion
56. Burvalev *et al.*, 2013[156]	Source: HeCd laser (442 nm) diode pumped solid state laser (532 nm) and LED (650 nm) Wavelength (nm): 442, 532, 650 Power (mW): 20 Frequency (Hz): Spot area (cm^2): 1.57	Irradiance (mW cm^{-2}): Time (s): 30–300 (1 treatment) Energy (J): Radiant exposure (J cm^{-2}):	*In vivo*: lipopolysaccharide B was applied through intraperitoneal injection to outbred albino rats. Mitochondria were then isolated from rat liver	Blue light induced a 40% increase in mitochondrial respiration from LPS treated animals at a dose of 6 J cm^{-2}
57. Kushibiki *et al.*, 2013[73]	Source: laser Wavelength (nm): 405, 664, 808 Power (mW): Frequency (Hz): Spot area (cm^2):	Irradiance (mW cm^{-2}): 100 Time (s): 60–120 Energy (J): Radiant exposure (J cm^{-2}):	*In vitro*: mouse preadipocytes (3T3-L1), prechondrocytes (ATDC5), myoblasts (C2C12), mesenchymal stromal cells (KUSA-A1), lung cancer cells (LLC), insulinoma cells (MIN6), fibroblasts (NIH-3T3), human cervix adenocarcinoma cells (HeLa), macrophages differentiated from lymphocytes (THP-1) after treatment with phorbol ester, and rat basophilic leukemia cells (RBL-2H3)	After blue light irradiation, intracellular ROS production was significantly increased in all cell types whilst red and near infra-red light had no significant effect
58. Fushimi *et al.*, 2012[166]	Source: LED Wavelength (nm): 456, 518, 638 Power (mW): 7560 (638 nm), 6930 (456 nm) and 6840 (518 nm) Frequency (Hz): Spot area (cm^2): 30	Irradiance (mW cm^{-2}): 0.75 (638 nm), 0.25 (456 nm) and 0.17 (518 nm) Time (s): 1200 Energy (J): Radiant exposure (J cm^{-2}): 0.6 (638 nm), 0.3 (456 nm), 0.2 (518 nm)	*In vivo* and *in vitro*: induced wound model in ob/ob mice	LED irradiation induced significant increases in growth factor and cytokine secretion. Green LEDs promote wound healing by inducing migratory and proliferative mediators
59. Lavi *et al.*, 2012[176]	Source: LED Wavelength (nm): 400–505, 600–800 Power (mW): Frequency (Hz): Spot area (cm^2):	Irradiance (mW cm^{-2}): 30 (600–800 nm), 10 (400–505 nm) Time (s): Energy (J): Radiant exposure (J cm^{-2}):	*In vitro*: sperm membranes	Visible (especially blue) light induce increase in ROS production in isolate sperm isolated plasma membranes
60. Adamskaya N *et al.*, 2011[147]	Source: LED Wavelength (nm): 470, 630 Power (mW): 1000 Frequency (Hz): Spot area (cm^2):	Irradiance (mW cm^{-2}): 50 Time (s): 600 Energy (J): Radiant exposure (J cm^{-2}):	*In vivo*: induced wound model (excision wound on dorsum), Sprague Dawley rats	Blue light was effective in inducing wound healing and promoting keratin expression
61. Shuvaeva *et al.*, 2011[189]	Source: laser Wavelength (nm): 473, 650 Power (mW): 20 Frequency (Hz): Spot area (cm^2):	Irradiance (mW cm^{-2}): 20 Time (s): Energy (J): Radiant exposure (J cm^{-2}):	*In vivo*: WKY and SHR rats	Irradiation with red light proved more effective than blue light in augmenting the constrictive effects of Norepinephrine on pial arteries. However both exerted a significant difference relative to the control
62. Bonatti *et al.*, 2011[153]	Source: LED Wavelength (nm): 470 Power (mW): 100 Frequency (Hz): Spot area (cm^2): 0.8	Irradiance (mW cm^{-2}): 125 Time (s): 60–180 Energy (J): 6, 12, 18 Radiant exposure (J cm^{-2}): 59.87, 122.3, 183.43	*In vitro*: keloid and skin fibroblasts, human	Reduced skin fibroblasts following irradiation at 183.43 J cm^{-2} but induced no significant effect on keloid fibroblast number
63. Ankri *et al.*, 2010[90]	Source: LED Wavelength (nm): 400–830 Power (mW): Frequency (Hz): Spot area (cm^2):	Irradiance (mW cm^{-2}): Time (s): Energy (J): Radiant exposure (J cm^{-2}):	Computational model of human dermis: photon migration model	480 nm may be useful for treating infected wounds whilst 780 nm has a higher penetration depth and therefore may be useful for wound healing

Table 1 *(Contd.)*

Citation	Light source	Dose	Study type	Conclusion
64. De Sousa *et al.*, 2010[159]	Source: LED Wavelength (nm): 700, 530, 460 Power (mW): 15 (700 nm), 8 (530 nm), 22 (460 nm) Frequency (Hz): Spot area (cm^2): 2.01	Irradiance (mW cm^{-2}): 7.46 (700 nm), 3.98 (530 nm), 10.94 (460 nm) Time (s): 668 (700 nm), 1250 (530 nm), 456 (460 nm) Energy (J): Radiant exposure (J cm^{-2}): 10	*In vivo* and *in vitro*: male Wistar rats with excisional wound, followed by histological analysis	Green and red LEDs induced increases in fibroblast number relative to the control
65. Ankri *et al.*, 2010[150]	Source: LED Wavelength (nm): 400–800 Power (mW): Frequency (Hz): Spot area (cm^2):	Irradiance (mW cm^{-2}): 130 Time (s): 300 Energy (J): Radiant exposure (J cm^{-2}):	*In vitro*: sperm and endothelial cells	Illumination induced increase in NO concentration, particularly blue light
66. Kushibiki *et al.*, 2010[175]	Source: LED Wavelength (nm): 405 Power (mW): Frequency (Hz): Spot area (cm^2):	Irradiance (mW cm^{-2}): 100 Time (s): 180 Energy (J): Radiant exposure (J cm^{-2}):	*In vitro*: prechondrogenic cells	Intracellular ROS increased and mRNA levels relating to chondrogenesis were elevated
67. Sebbe *et al.*, 2009[188]	Source: LED Wavelength (nm): 472 Power (mW): Frequency (Hz): Spot area (cm^2):	Irradiance (mW cm^{-2}): 1.26–4.73 Time (s): 8–24 h Energy (J): Radiant exposure (J cm^{-2}):	*In vivo*: male Wistar rats	Increased bilirubin degradation, important for neonatal jaundice
68. Tamarova *et al.*, 2009[192]	Source: LED Wavelength (nm): 480–3400 (range of source, evaluated 'red, orange, yellow, blue, green, violet') Power (mW): Frequency (Hz): Spot area (cm^2):	Irradiance (mW cm^{-2}): 40 Time (s): 600 Energy (J): Radiant exposure (J cm^{-2}): 2.4 (per minute)	*In vivo*: male albino rats with area of pain induced by saline injection	Red light was more effective in inducing an analgesic effect. However, all colours induced significant increases in analgesia relative to control

radiant exposure values, 3 of which were >30 J cm^{-2}. Interestingly of those reporting no significant effect of blue light, an average radiant exposure of 8 J cm^{-2} was reported (range: 0.378–80 J cm^{-2}). In which, 4/7 of those articles studied reported the radiant exposure utilised in experimentation. Hence, it is apparent from these findings that further work is required to gain a better understanding of the biphasic effect of blue light and also to demonstrate the importance of recording and reporting treatment parameters. Table 1 summarises the studies evaluated in this review including the study type, reported parameters and outcomes.

4.3.2 Green light PBM. A second Scopus database search was undertaken to evaluate the effects of green light PBM using the terms described in Fig. 3b. An initial search resulted in 236 articles being identified and these articles were subsequently screened for suitability, which then identified 32 relevant articles for further review.[18,32,33,66,70,80,151,155,158,163,164,173,184,192,196,200–216]

When evaluating the outcomes of studies reporting the effects of PBM it was found that 75% (24/32) reported a beneficial effect of green light, whilst 9% (3/32) reported negative effects and 16% (5/32) reported no significant response. Interestingly, this review also included an article evaluating the effect of green light PBM on microbial cell death[207] with high radiant exposures also being used (≤172.8 J cm^{-2}). These findings further support the use of other visible wavelengths of light in applications other than modulation of tissue response. As described previously this article was also excluded from evaluation of parameters for suitable application to tissue PBM.

Exploration of treatment parameters revealed that 72% (23/32) articles failed to report any characterisation protocols or relied entirely upon the parameters stated by the manufacturer. In fact, only one article reported the use of beam profiling to accurately calculate beam area and to provide representative images of the distribution of spectral irradiance.[202] Similar to reports in section 4.3.1, a series of key parameters were also not always reported including irradiance (41%, 13/32), radiant exposure (44%, 14/32) and beam area (66%, 21/32). In the articles reporting treatment parameters, median treatment values were also determined. In the articles reporting a positive effect of green light PBM, there was a median radiant exposure output of 4 J cm^{-2} (range: 0.00362–30 J cm^{-2}).

Table 2 Citations identified from a review of the literature evaluating the effects of green and yellow light PBM using the following search terms: 'green AND light' OR '500 nm' OR '505 nm' OR '520 nm' OR '530 nm' OR '540 nm' OR '550 nm' OR '560 nm' OR '570 nm' OR '532 nm' OR '595 nm' AND 'Photobiomodulation' OR 'PBM' OR 'Low level light therapy' OR 'LLLT' OR 'Low intensity light therapy' OR 'photobiostimulation' AND NOT 'Photodynamic therapy' OR 'PDT'

Citation	Light source	Dose	Study type	Conclusion
1. Priglinger *et al.*, 2018[184]	Source: LED cluster lamp Wavelength (nm): 475, 516, 635 Power (mW): Frequency (Hz): 2.5 (pulsed, 50% rate) Spot area (cm^2):	Irradiance (mW cm^{-2}): 40 Time (s): 120–300 Energy (J): Radiant exposure (J cm^{-2}): 24	*In vitro*: adipose tissue derived stromal vascular fraction cells	Green and red light resulted in increased vascular tube formation and increased concentration vascular endothelial growth factor (VEGF) concentration. Blue light had no significant effect
2. Askhadulin *et al.*, 2018[201]	Source: laser Wavelength (nm): 365, 525, 635 Power (mW): 1–2 Frequency (Hz): 80 (635 nm) Spot area (cm^2): 8 (635 nm)	Irradiance (mW cm^{-2}): 5000 (635 nm) Time (s): 120 (365 nm, 635 nm) 300 (525 nm), 6 sessions of each Energy (J): Radiant exposure (J cm^{-2}):	*In vivo*: human	Reduced ulcer healing time and adapted physiological responses ultimately preventing relapse
3. Fekrazad *et al.*, 2018[163]	Source: laser Wavelength (nm): 810, 660, 532, 485, combinations: 810–660, 810–485, 660–532, 660–485 Power (mW): 30–200 (dependent on wavelength) Frequency (Hz): Spot area (cm^2): 0.113–0.18	Irradiance (mW cm^{-2}): 266 (blue), 266 (green) 167 (red), 1333 (NIR) Time (s): 3–24 (dependent upon wavelength) Energy (J): Radiant exposure (J cm^{-2}): 4 (8 for combination)	*In vitro*: mesenchymal stem cells	Cartilage markers were upregulated by 810 nm and 810–485 nm light. Red and blue-green irradiation induced expression of COL1. Blue, blue-green and green light irradiation reduced osteocalcin expression. Stimulatory effects on osteogenesis were seen for red and near infra-red lasers but green light had inhibitory effects. Blue light was not reported to induce inhibitory effects
4. Oh *et al.*, 2018[213]	Source: LED Wavelength (nm): 630, 595, 480, 410 Power (mW): Frequency (Hz): Spot area (cm^2):	Irradiance (mW cm^{-2}): 5.47 (410 nm), 13.2 (480 nm), 5.8 (595 nm), 8.63 (630 nm) Time (s): 410 nm: 181.2–1816.8 480 nm: 69.6–742.2 595 nm: 151.2–1706.4 630 nm: 93–1146 Energy (J): Radiant exposure (J cm^{-2}): 1–10	*In vitro*: human umbilical vein endothelial cells (HUVEC)	Irradiation at 630 nm induced increases in cell proliferation, NO secretion and eNOS expression from HUVECs. Only evaluated effects on proliferation using other wavelengths where no significant change was witnessed
5. Rohringer *et al.*, 2017[215]	Source: LED Wavelength (nm): 475, 516, 635 Power (mW): Frequency (Hz): 50% pulse rate, 2.5 Hz Spot area (cm^2):	Irradiance (mW cm^{-2}): 80 Time (s): 600 Energy (J): Radiant exposure (J cm^{-2}): 24	*In vitro*: human umbilical vein endothelial cells	Red and green light induced proliferation and migration of endothelial cells whilst blue light had no significant impact. Blue light only induced significant increases in ROS production
6. Wang *et al.*, 2017[66]	Source: LED array (415 nm), filtered lamp (540 nm), diode laser (660 nm and 810 nm) Wavelength (nm): 415, 540, 660, 810 Power (mW): Frequency (Hz): Spot area (cm^2): 4	Irradiance (mW cm^{-2}): 16 Time (s): 188 Energy (J): Radiant exposure (J cm^{-2}): 3	*In vitro*: human adipose-derived stem cells	Blue and green light induce significant increases in intracellular calcium and ROS, reduce mitochondrial membrane potential, lower intracellular pH and reducing cellular proliferation. Red and NIR light have the opposite effect. Blue and green light inhibit proliferation through activation of TRPV1
7. Baek *et al.*, 2017[202]	Source: laser Wavelength (nm): 532 Power (mW): 300 Frequency (Hz): 0.2 (1 s) Spot area (cm^2): diameter 1 mm	Irradiance (mW cm^{-2}): Time (s): 10–300 Energy (J): Radiant exposure (J cm^{-2}):	*In vitro*: vascular smooth muscle cells	Inhibited platelet derived growth factor-BB induced proliferation and migration. Also induced apoptosis *via* the p38 MAPK pathway

Table 2 *(Contd.)*

Citation	Light source	Dose	Study type	Conclusion
8. Wang *et al.*, 2017[70]	Source: LED Wavelength (nm): 480, 560, 660 and white (400–750) Power (mW): 3000 Frequency (Hz): Spot area (cm^2):	Irradiance (mW cm^{-2}): 250 Time (s): Energy (J): Radiant exposure (J cm^{-2}):	*In vitro* and *in vivo*: fertile broiler eggs were irradiated and satellite cells were isolated	Green light promoted muscle growth and satellite cell proliferation which may be due to an increase in signalling through the insulin growth factor (IGF-1) pathway
9. Choe *et al.*, 2017[158]	Source: LED Wavelength (nm): 622, 535, 462 Power (mW): 24 000 Frequency (Hz): Spot area (cm^2):	Irradiance (mW cm^{-2}): 16 Time (s): 600–1800 (daily) Energy (J): Radiant exposure (J cm^{-2}):	*In vitro*: HeLa cells (cancer cell line)	Blue light and high frequency ultrasound induced significant reductions in cell density when compared to red and green light combined with ultrasound. This could be beneficial in alleviating cancer cell proliferation. Green light also drove decreases in cell density but not significantly
10. Fekrazad *et al.*, 2017[18]	Source: laser: GaAs (405 nm, 532 nm), InGaAlP (660 nm) and GaAlAs (810 nm) Wavelength (nm): 405, 532, 660, 810 Power (mW): Frequency (Hz): Spot area (cm^2): 1	Irradiance (mW cm^{-2}): 200 Time (s): Energy (J): Radiant exposure (J cm^{-2}): 1.5	*In vivo*: male Wistar rats (n = 60)	Green, blue, red and infrared light irradiation may accelerate healing process
11. Moskvin *et al.*, 2017[210]	Source: LAMSIK® device, external pulsed laser (635), intravenous laser blood illumination (ILBI, 365–405 nm and 520–525 nm) Wavelength (nm): 635, 365–405, 520–525 Power (mW): 40 000 (635 nm) Frequency (Hz): pulsed 635 nm Spot area (cm^2): 8 (635 nm)	Irradiance (mW cm^{-2}): Time (s): 12 sessions, 120 s (per point, 635 nm), 120 s (365–405 nm), 300 s (520–525 nm) 6 sessions each alternate Energy (J): Radiant exposure (J cm^{-2}):	*In vivo*: treatment of patients with chronic venous diseases	Reduced time for wound cleansing, stimulates proliferation and epithelialisation processes
12. Khori *et al.*, 2016[173]	Source: laser Wavelength (nm): 405, 532, 632 Power (mW): 1–3 Frequency (Hz): Spot area (cm^2):	Irradiance (mW cm^{-2}): Time (s): 600 (10 treatments, 3 times a week) Energy (J): Radiant exposure (J cm^{-2}):	*In vivo* and *in vitro*: BALB/c inbred female mice and mouse mammary carcinoma cell line (4T1)	Blue light reduced tumour volume and gene expression markers for tumorigenesis
13. Roche *et al.*, 2017[214]	Source: laser diodes Wavelength (nm): 532 Power (mW): 17 (per diode, 170 total) Frequency (Hz): Spot area (cm^2):	Irradiance (mW cm^{-2}): 0.03 Time (s): 1800 (3 times weekly) Energy (J): Radiant exposure (J cm^{-2}): 0.03 (per treatment), 0.36 (in total) calculations appear wrong	*In vivo*: obese but otherwise healthy individuals, RCT	Reduced circumference of hips, waist and upper abdomen when applied to individuals with a body mass index (BMI) between 30–40 kg m^{-2}
14. Khurana *et al.*, 2017[206]	Source: Qs Nd:YAG laser Wavelength (nm): 1064, 532 Power (mW): Frequency (Hz): Spot area (cm^2):	Irradiance (mW cm^{-2}): Time (s): Energy (J): Radiant exposure (J cm^{-2}): 9.3 (1064 nm), 5 (532 nm)	*In vivo*: case study, patient with Fusarium solani infection on toe nail	Application of PBM with sequential use of either wavelength cured infection and promoted healthy toe nail growth
15. Wang *et al.*, 2016[196]	Source: LED array (420), filtered lamp (540), diode laser (660, 810) Wavelength (nm): 420, 540, 660, 810 Power (mW): Frequency (Hz): Spot area (cm^2): 4	Irradiance (mW cm^{-2}): 16 Time (s): 188 (five times, every 2 days) Energy (J): Radiant exposure (J cm^{-2}): 3	*In vitro*: human adipose-derived stem cells	Blue and green light were effective in stimulating osteoblast differentiation and increasing intracellular calcium levels than red and near infra-red light. Blue and green light could activate light-gated calcium ion channels

Table 2 *(Contd.)*

Citation	Light source	Dose	Study type	Conclusion
16. Ashworth *et al.*, 2016[151]	Source: Wavelength (nm): 450, 510, 660, 860 Power (mW): Frequency (Hz): Spot area (cm^2):	Irradiance (mW cm^{-2}): Time (s): Energy (J): Radiant exposure (J cm^{-2}): Other: 1.93×, 3.85×, 7.70× photons per cm^2 per s	*Ex vivo*: adapted mouse spinal cord organotypic culture model	Red and near infra-red light are effective antioxidant therapies for spinal cord injury
17. Merigo *et al.*, 2016[209]	Source: KTP laser Wavelength (nm): 532 Power (mW): 780 Frequency (Hz): Spot area (cm^2): 2.4	Irradiance (mW cm^{-2}): Time (s): Energy (J): Radiant exposure (J cm^{-2}): 4 Other:	*In vitro*: primary bone marrow stromal cells	Green light induces osteogenic differentiation of bone marrow stromal cells
18. O'Connor *et al.*, 2016[212]	Source: diode laser Wavelength (nm): 405, 532, 635 Power (mW): 17.5 Frequency (Hz): Spot area (cm^2): 1.413	Irradiance (mW cm^{-2}): 12.2 Time (s): 300 Energy (J): 0.0051748 Radiant exposure (J cm^{-2}): 0.003662 Other: calculations wrong should be 3.66 J cm^{-2} and 5.1748 J	*In vivo*: C57BL6 mice treated with light and/or Mesenchymal Stem cells	405, 532, and 635 induced increases in mitochondrial activity and reduced apoptosis. Endothelial proliferation increased in response to 635 nm light and combined effects of MSC and the 405 nm wavelength. Reduced TGF-β levels were induced by 532 nm alone and when combined with MSC
19. Fekrazad *et al.*, 2015[164]	Source: laser Wavelength (nm): 630, 532, 425 Power (mW): Frequency (Hz): Spot area (cm^2):	Irradiance (mW cm^{-2}): 50 (630 nm and 532 nm), 55 (425 nm) Time (s): Energy (J): Radiant exposure (J cm^{-2}): 2	*In vivo*: diabetes induced male Wistar rats	All three wavelengths induced significant increases in wound healing, where red light was most effective
20. Na, C–S *et al.*, 2015[211]	Source: laser diodes Wavelength (nm): 532, 658 Power (mW): 30 (532 nm), 60 (658 nm) Frequency (Hz): 20 Spot area (cm^2):	Irradiance (mW cm^{-2}): Time (s): 180 Energy (J): Radiant exposure (J cm^{-2}): Other:	*In vivo*: rat model with induced middle cerebral artery occlusion (MCAO)	Decrease in Bax and cytochrome c levels in hippocampus, increase in hemoglobin, haematocrit, total white blood cell, neutrophil, lymphocyte, monocyte and erythrocyte counts
21. Burvalev *et al.*, 2014[155]	Source: laser (442 nm, 532 nm) and LED (650 nm) Wavelength (nm): 442, 532, 650 Power (mW): 20 Frequency (Hz): Spot area (cm^2): 1.57	Irradiance (mW cm^{-2}): 30 Time (s): 30–300 Energy (J): Radiant exposure (J cm^{-2}): 3–31	*In vitro*: mitochondria isolated from rat liver	Laser of mitochondria at 442 nm restored mitochondrial respiration inhibited by NO. Blue light also restored complex IV activity but not complexes I–III. Other wavelengths had no significant effect
22. Kuboyama *et al.*, 2014[33]	Source: LED Wavelength (nm): 570 and 940 Power (mW): Frequency (Hz): Spot area (cm^2):	Irradiance (mW cm^{-2}): Time (s): Energy (J): Radiant exposure (J cm^{-2}): 5 (24 sessions) Other:	*In vivo*: DBA/1 LacJ male mice with collagen induced arthritis	Reducing swelling induced by both wavelengths. 940 nm irradiation induced significant reduction in circulating levels of IL-1β, IL-6 and MMP-3.
23. Cheon *et al.*, 2013[80]	Source: LED Wavelength (nm): 470, 525, 633 Power (mW): Frequency (Hz): Spot area (cm^2):	Irradiance (mW cm^{-2}): 3.55 (470 nm), 4.02 (525 nm) and 6.78 (633 nm) Time (s): 3600 (9 days) Energy (J): Radiant exposure (J cm^{-2}):	*In vivo*: Sprague Dawley rats and histological analysis	Blue and green light promoted wound healing significantly. Red light promoted collagen production

Table 2 *(Contd.)*

Citation	Light source	Dose	Study type	Conclusion
24. De Sousa *et al.*, 2013[203]	Source: laser (660 nm, and 790 nm), LED (700 nm, 530 nm and 460 nm) Wavelength (nm): 660, 790, 700, 530, 460 Power (mW): 60 (660 nm), 50 (790 nm), 15 (700 nm), 8 (530 nm), 22 (460 nm) Frequency (Hz): Spot area (cm^2): 0.03	Irradiance (mW cm^{-2}): 1911 (660 nm), 1592 (790 nm), 7.46 (700 nm), 8 (530 nm), 22 (460 nm) Time (s): 168 (660 nm), 200 (790 nm), 668 (700 nm), 1250 (530 nm), 456 (460 nm) (every other day, 7 days) Energy (J): Radiant exposure (J cm^{-2}): 10 Other:	*In vivo*: male Wistar rats wound model and stained for histological evaluation	530 nm, 700 nm, 790 nm and 660 nm induced significant increases in angiogenesis
25. Tamarova *et al.*, 2009[192]	Source: LED Wavelength (nm): 480–3400 (range of source, evaluated 'red, orange, yellow, blue, green, violet') Power (mW): Frequency (Hz): Spot area (cm^2):	Irradiance (mW cm^{-2}): 40 Time (s): 600 Energy (J): Radiant exposure (J cm^{-2}): 2.4 (per minute)	*In vivo*: male albino rats with area of pain induced by saline injection	Red light was more effective in inducing an analgesic effect. However, all colours induced significant increases in analgesia relative to control
26. Jackson *et al.*, 2013[32]	Source: laser diodes (Erchonia GL scanner) Wavelength (nm): 532 nm (6 diodes) Power (mW): 17 per diode, 125 total (sham 1.25) Frequency (Hz): Spot area (cm^2): 516 (target area)	Irradiance (mW cm^{-2}): Time (s): 900 (two weeks once every 2–3 days) Energy (J): Radiant exposure (J cm^{-2}): Other:	*In vivo*: human laser irradiation to improve cellulite appearance	532 nm improved cellulite appearance on thighs and buttocks
27. Kim *et al.*, 2013[207]	Source: Wavelength (nm): 425, 525, 625 Power (mW): Frequency (Hz): Spot area (cm^2):	Irradiance (mW cm^{-2}): 6 Time (s): 3600–28 800 Energy (J): Radiant exposure (J cm^{-2}): 21.6–172.8 Other:	*In vitro: Staphylococcus. Aureus, Escherichia. Coli, Porphyromonas. gingivalis*	No bactericidal effect induced by red light. Blue and green light were bactericidal where green light also killed *S. aureus*
28. Fushimi *et al.*, 2012[205]	Source: LED Wavelength (nm): 63 8 nm, 456 nm, 518 nm Power (mW): 2520 (638 nm), 2310 (456 nm), 2500 (518 nm): *in vivo* 7560 (638 nm), 6930 (456 nm), 6840 (518 nm): *in vitro* Frequency (Hz): Spot area (cm^2):	Irradiance (mW cm^{-2}): 0.25: *in vivo* 0.75 (638 nm), 0.25 (456 nm), 0.17 (518 nm): *in vitro* Time (s): 1200 Energy (J): Radiant exposure (J cm^{-2}): 0.3: *in vivo* 0.6 (638 nm), 0.3 (456 nm), 0.2 (518 nm) Other:	*In vivo*: mice *In vitro*: fibroblasts and HaCat keratinocytes	Green light decreased wound size. Green and red light accelerated reepithelialisation. Green light induced increases in leptin, IL-8 and VEGF. Keratinocyte migration enhanced by red and green light
29. Li *et al.*, 2011[208]	Source: laser (Nd:YAG) Wavelength (nm): 532 nm Power (mW): 40 Frequency (Hz): pulsed at 'double frequency' Spot area (cm^2): 0.32	Irradiance (mW cm^{-2}): Time (s): 300 Energy (J): Radiant exposure (J cm^{-2}): Other:	*In vitro*: vascular smooth muscle cells (VMSCs)	Low intensity laser can prevent VMSC proliferation through induction of increases in markers for apoptosis
30. De Sousa *et al.*, 2010[204]	Source: LED Wavelength (nm): 700, 530, 460 Power (mW): 15 (700 nm), 8 (530 nm), 22 (460 nm) Frequency (Hz): Spot area (cm^2):	Irradiance (mW cm^{-2}): Time (s): every other day 7 days Energy (J): Radiant exposure (J cm^{-2}): 10 Other:	*In vivo*: Wistar rats and fibroblasts grown from biopsy	Green and red light induced significant increases in fibroblast number

Table 2 *(Contd.)*

Citation	Light source	Dose	Study type	Conclusion
31. Al-Watban *et al.*, 2009[200]	Source: laser diode Wavelength (nm): 532, 633, 670, 810, 980 Power (mW): 143 (532 nm), 140 (633 nm), 120 (670 nm), 200 (810 nm), 200 (980 nm) Frequency (Hz): Spot area (cm^2): 7 (532 nm), 9 (633 nm), 5.25 (670 nm), 9 (810 nm), 9 (980 nm)	Irradiance (mW cm^{-2}): 20.4 (532 nm), 15.56 (633 nm), 22.86 (670 nm), 22.22 (810 nm and 980 nm) Time (s): 532 nm: 246–1470 633 nm: 324–1926 670 nm: 216–1314 810 nm: 228–1350 980 nm: 450–1350 Three times per week Energy (J): Radiant exposure (J cm^{-2}): 5, 10, 20, 30 (532 nm, 633 nm, 670 nm, 810) 10, 20, 30 (980 nm) Other:	*In vivo*: wound healing in diabetic Sprague-Dawley rats	PBM accelerated burn healing, particularly visible lasers. Response was dose dependent where highest increase in healing was induced at 30 J cm^{-2} by green light but 20 J cm^{-2} by red light
32. Tierney and Hanke, 2009[216]	Source: diode laser Wavelength (nm): 532 and 940 Power (mW): Frequency (Hz): pulse duration: 60 ms (532 nm) and 21 ms (940 nm) Spot area (cm^2): spot size: 1 mm	Irradiance (mW cm^{-2}): Time (s): Energy (J): Radiant exposure (J cm^{-2}): 15 (532 nm) and 100 (940 nm) Other:	*In vivo*: RCT, humans with facial telangiectasias	Both wavelengths proved effective in treating facial telangiectasias, but 940 nm proved more effective as well as inducing fewer/milder side effects

Interestingly, it was also found that the most commonly employed wavelength used in these studies was 532 nm, and 35% (11/32) of studies reported the use of this wavelength. Further information detailing parameters and study types employed by authors reviewing the effects of green light PBM are provided in Table 2.

4.4. Discussion

It is apparent from this literature review, that whilst the majority of articles reported a positive effect of blue (72%) and green (75%) light PBM, further work is required to demonstrate the importance of the correct recording and reporting of treatment parameters. In fact, in this review 69% of all articles failed to report any means of measuring the output of their light source. While a number of studies have highlighted the importance of proper and thorough reporting and recording of treatment parameters,[15,217,218] it appears these guidelines are yet to be fully implemented in practice. Future efforts are therefore required to ensure the correct reporting of parameters, to enable comparison PBM studies and therefore enable identification of beneficial parameters for therapeutic application.

Furthermore this literature review has revealed that for articles reporting the beneficial effects of both, green or blue light application, the majority of publications employed radiant exposures <10 J cm^{-2} (66%, 26/39, excluding articles that did not report radiant exposure values). Interestingly, the beneficial effects of blue and green light included the promotion of wound healing,[29] reduced inflammation,[162] reduction of symptoms of acne[29,170] and reduced bleeding time following tooth extraction[21] to name only a few. The full range of applications of blue and green light discussed in this review are summarized in Tables 1 and 2 respectively. A handful of authors also reported on the biphasic dose response of light.[19,219] For example, Masson-Meyers *et al.* investigated the effect of blue light on wound healing *in vitro* using human dermal fibroblast.[219] The authors utilised a scratch assay to inflict a 'wound' on cell cultures and following this irradiated cells at 470 nm (30 mW cm^{-2}, 3–55 J cm^{-2}) and evaluated the effect of irradiation on a series of markers for wound healing. The authors reported that at fluence values of 3, 5 and 10 J cm^{-2}, irradiation significantly reduced the secretion of IL-6, a key pro-inflammatory cytokine, increased overall protein production (as a marker for transcription and translational activity) and had no significant impact on wound healing. They also found that irradiation induced mean increases in basic fibroblast growth factor (bFGF) levels, however, this was not significant. Conversely, when utilising a fluency value of 55 J cm^{-2}, the authors found that irradiation did significantly reduce rate of wound healing. These data suggest that lower doses of blue light could prove beneficial in inducing decreases in inflammation and promoting gene expression. This theory is in agreement with the 'Arndt-Schulz law' in which the application of a stimulus is only beneficial within a relatively narrow therapeutic window. Outside this window a stimulus can either have no effect or induce bioinhibition.[220] Interestingly, previous articles have also suggested that 453 nm light is non-toxic up to 500 J cm^{-2}, when applied to human skin cells.[221] Hence, future work may prioritise the study of the biphasic effect of various wavelengths of blue and green light on cells isolated from different sources in the human body.

This review, has also provided evidence for alternative applications of PBM, in which visible light could not only modulate tissue response but also exert antimicrobial properties. Notably the majority of articles citing the antibacterial properties of light use high radiant exposures (>55 J cm^{-2} (ref. 154, 179 and 207)) and these levels could potentially be toxic to eukaryotic cells. Comparatively, de Sousa *et al.* reported that 450 nm light inhibited bacterial growth (*Staphylococcus aureus* and *Pseudomonas aeruginosa*) at doses as low as 6 J cm^{-2}.[31] Hence, future work may endeavour to determine parameters of visible light required to modulate tissue response whilst also inhibiting bacterial growth.

However, it is prudent to highlight one limitation of this review where radiant exposure values were used to compare literature currently published. Radiant exposure is an important parameter as it takes into consideration a number of other key parameters including irradiance and enables initial establishment of a possible therapeutic window in which blue and green light could induce beneficial effects *in vivo*. However, it is also unreliable as it assumes there is an inverse correlation between both irradiance and exposure time.[15] Hence, it is important that authors report all treatment parameters values utilised in studies. This will therefore ensure reliable comparison of current literature and provide further detail as to the parameters that may induce beneficial effects clinically. Future work may also endeavour to evaluate the possible parameter combinations that may induce a beneficial effect within this therapeutic window.

5. Conclusions

This review has provided examples of the wide range of possible targets for various wavelengths of light employed in PBM. These ranged from the application of blue and green light to modulate opsin signalling[17] to the application of red and NIR light to induce cytochrome c oxidase activity.[220] We provide evidence for the idea that the majority of these primary mechanisms converge on their ability to modulate ROS production. It has been proposed that small increases in ROS production can induce beneficial effects including increases in cell proliferation, whilst large increases can induce apoptosis signalling pathways.[26] Literature currently suggests that light application to 'healthy' cells and tissue induces small increases in ROS production,[71] whilst PBM can induce decreases in ROS production in inflamed tissue.[107,222] Hence, PBM could plausibly be applied both as a preventive measure, as well as a means to modulate inflammation in disease. However, further work is required to validate this hypothesis.

We also report how PBM induces the activity of downstream signalling pathways, which are modulated by this ROS production. Current literature also demonstrates the wavelength dependent effects of PBM on downstream signalling pathways, where red and NIR light have been proposed to increase the activity of TGF-β signalling,[127] whilst blue light has been shown to inhibit the same pathway.[223] It will therefore be important in the future to evaluate the wavelength dependent effects of PBM on downstream signalling pathways to provide further indications as to which wavelengths are beneficial for the resolution of different diseases and disorders.

This review is also the first report, to our knowledge, which systematically reviews the current literature evaluating the effects of green and blue light PBM both *in vitro* and *in vivo*. We provide evidence that application of blue or green light PBM could have beneficial effects. However, it is apparent that to date, the majority of authors have not appropriately recorded and reported their parameters, meaning that firm conclusions cannot be drawn regarding the optimum parameters to be applied therapeutically.

Overall we conclude that PBM exhibits the ability to modulate the activity of an array of signalling pathways, ultimately inducing the beneficial effects seen *in vitro* and *in vivo*. However, further work is required to ensure that experimental studies carry out rigorous spectral characterisation to enable improved reproducibility.

Funding

The research in this report was funded as part of an iCASE PHD studentship to HS funded by EPSRC. MRH was supported by US NIH Grants R01AI050875 and R21AI121700.

Conflicts of interest

MRH declares the following potential conflicts of interest: Dr Hamblin is on the following Scientific Advisory Boards; Transdermal Cap Inc., Cleveland, OH; BeWell Global Inc., Wan Chai, Hong Kong; Hologenix Inc., Santa Monica, CA; LumiThera Inc., Poulsbo, WA; Vielight, Toronto, Canada; Bright Photomedicine, Sao Paulo, Brazil; Quantum Dynamics LLC, Cambridge, MA; Global Photon Inc., Bee Cave, TX; Medical Coherence, Boston MA; NeuroThera, Newark DE; JOOVV Inc., Minneapolis-St Paul MN; AIRx Medical, Pleasanton CA; FIR Industries, Inc., Ramsey, NJ; UVLRx Therapeutics, Oldsmar, FL; Ultralux UV Inc., Lansing MI; Illumiheal & Petthera, Shoreline, WA; MB Lasertherapy, Houston, TX; ARRC LED, San Clemente, CA; Varuna Biomedical Corp. Incline Village, NV; Niraxx Light Therapeutics, Inc., Boston, MA. Dr Hamblin has been a consultant for Lexington Int, Boca Raton, FL; USHIO Corp, Japan; Merck KGaA, Darmstadt, Germany; Philips Electronics Nederland B.V.; Johnson & Johnson Inc., Philadelphia, PA; Sanofi-Aventis Deutschland GmbH, Frankfurt am Main, Germany. Dr Hamblin is a stockholder in Global Photon Inc., Bee Cave, TX and Mitonix, Newark, DE.

References

1 E. Mester, B. Szende and P. Gärtner, The effect of laser beams on the growth of hair in mice, *Radiobiol., Radiother.*, 1968, **9**(5), 621–626.

2 E. Merigo, P. Vescovi, M. Margalit, E. Ricotti, S. Stea, M. Meleti, M. Manfredi and C. Fornaini, Efficacy of LLLT in swelling and pain control after the extraction of lower impacted third molars, *Laser Ther.*, 2015, **24**(1), 39–46.
3 D. P. Kuffler, Photobiomodulation in promoting wound healing: A review, *Regener. Med.*, 2016, **11**(1), 107–122.
4 R. M. da Silveira Campos, A. R. Dâmaso, D. C. L. Masquio, A. E. Aquino Jr., M. Sene-Fiorese, F. O. Duarte, L. Tock, N. A. Parizotto and V. S. Bagnato, Low-level laser therapy (LLLT) associated with aerobic plus resistance training to improve inflammatory biomarkers in obese adults, *Lasers Med. Sci.*, 2015, **30**(5), 1553–1563.
5 *Mechanisms of low level light therapy. Progress in Biomedical Optics and Imaging - Proceedings of SPIE*, ed. M. R. Hamblin and T. N. Demidova, 2006.
6 R. T. Chow, M. I. Johnson, R. A. Lopes-Martins and J. M. Bjordal, Efficacy of low-level laser therapy in the management of neck pain: a systematic review and meta-analysis of randomised placebo or active-treatment controlled trials, *Lancet*, 2009, **374**(9705), 1897–1908.
7 F. G. Basso, T. N. Pansani, D. G. Soares, D. L. Scheffel, V. S. Bagnato, C. A. De Souza Costa and J. Hebling, Biomodulation of Inflammatory Cytokines Related to Oral Mucositis by Low-Level Laser Therapy, *Photochem. Photobiol.*, 2015, **91**(4), 952–956.
8 J. Foley, D. B. Vasily, J. Bradle, C. Rudio and R. G. Calderhead, 830 nm light-emitting diode (LED) phototherapy significantly reduced return-to-play in injured university athletes: A pilot study, *Laser Ther.*, 2016, **25**(1), 35–42.
9 R. D. Furquim, R. C. Pascotto, J. R. Neto, J. R. Cardoso and A. L. Ramos, Low-level laser therapy effects on pain perception related to the use of orthodontic elastomeric separators, *Dental Press J. Orthod.*, 2015, **20**(3), 37–42.
10 M. R. Milward, M. J. Holder, W. M. Palin, M. A. Hadis, J. D. Carroll and P. R. Cooper, Low Level Light Therapy (LLLT) for the treatment and management of dental and oral diseases, *Dent. Update*, 2014, **41**(9), 763–772.
11 H. Morita, J. Kohno, S. Tanaka, Y. Kitano and S. Sagami, Clinical application of GaAlAs 830 nm diode laser for atopic dermatitis, *Laser Ther.*, 1993, **5**(2), 75–78.
12 S. E. Sahingur and W. A. Yeudall, Chemokine function in periodontal disease and oral cavity cancer, *Front. Immunol.*, 2015, **6**(MAY).
13 J. B. B. Weber, L. Mayer, R. A. Cenci, C. E. Baraldi, D. Ponzoni and M. G. De Oliveira, Effect of three different protocols of low-level laser therapy on thyroid hormone production after dental implant placement in an experimental rabbit model, *Photomed. Laser Surg.*, 2014, **32**(11), 612–617.
14 J. Yi, J. Xiao, H. Li, Y. Li, X. Li and Z. Zhao, Effectiveness of adjunctive interventions for accelerating orthodontic tooth movement: a systematic review of systematic reviews, *J. Oral Rehabil.*, 2017, **44**(8), 636–654.
15 M. A. Hadis, S. A. Zainal, M. J. Holder, J. D. Carroll, P. R. Cooper, M. R. Milward and W. M. Palin, The dark art of light measurement: accurate radiometry for low-level light therapy, *Lasers Med. Sci.*, 2016, 1–21.
16 P. A. Jenkins and J. D. Carroll, How to report low-level laser therapy (LLLT)/photomedicine dose and beam parameters in clinical and laboratory studies, *Photomed. Laser Surg.*, 2011, **29**(12), 785–787.
17 I. Castellano-Pellicena, N. E. Uzunbajakava, C. Mignon, B. Raafs, V. A. Botchkarev and M. J. Thornton, Does blue light restore human epidermal barrier function via activation of Opsin during cutaneous wound healing?, *Lasers Surg. Med.*, 2019, **51**(4), 370–382.
18 R. Fekrazad, A. Nikkerdar, K. Joharchi, K. A. M. Kalhori, F. Mashhadi Abbas and F. Salimi Vahid, Evaluation of therapeutic laser influences on the healing of third-degree burns in rats according to different wavelengths, *J. Cosmet. Laser Ther.*, 2017, **19**(4), 232–236.
19 C. Mignon, N. E. Uzunbajakava, I. Castellano-Pellicena, N. V. Botchkareva and D. J. Tobin, Differential response of human dermal fibroblast subpopulations to visible and near-infrared light: Potential of photobiomodulation for addressing cutaneous conditions, *Lasers Surg. Med.*, 2018, **50**(8), 859–882.
20 A. Tani, F. Chellini, M. Giannelli, D. Nosi, S. Zecchi-Orlandini and C. Sassoli, Red (635 nm), Near-Infrared (808 nm) and Violet-Blue (405 nm) Photobiomodulation Potentiality on Human Osteoblasts and Mesenchymal Stromal Cells: A Morphological and Molecular In Vitro Study, *Int. J. Mol. Sci.*, 2018, **19**(7), 1946.
21 D. Veleska-Stevkoska and F. Koneski, Haemostasis in oral surgery with blue-violet light, *Open Access Maced. J. Med. Sci.*, 2018, **6**(4), 687–691.
22 M. A. Hadis, S. A. Zainal, M. J. Holder, J. D. Carroll, P. R. Cooper, M. R. Milward and W. M. Palin, The dark art of light measurement: accurate radiometry for low-level light therapy, *Lasers Med. Sci.*, 2016, **31**(4), 789–809.
23 Y. Izumizawa, S. J. Yang, T. Negishi and K. Negishi, DNA lesion and mutagenesis induced in phageM13mp2 by UVA, UVB and UVC irradiation, *Nucleic Acids Symp. Ser.*, 2000, (44), 73–74.
24 E. Sage, P. M. Girard and S. Francesconi, Unravelling UVA-induced mutagenesis, *Photochem. Photobiol. Sci.*, 2012, **11**(1), 74–80.
25 R. Rastogi RP, A. Kumar, M. B. Tyagi and R. P. Sinha, Molecular mechanisms of ultraviolet radiation-induced DNA damage and repair, *J. Nucleic Acids*, 2010, **2010**, 592980.
26 R. M. Day and Y. J. Suzuki, Cell proliferation, reactive oxygen and cellular glutathione, *Dose-Response*, 2006, **3**(3), 425–442.
27 D. Barolet, Light-Emitting Diodes (LEDs) in Dermatology, *Semin. Cutaneous Med. Surg.*, 2008, **27**(4), 227–238.
28 C. Ash, M. Dubec, K. Donne and T. Bashford, Effect of wavelength and beam width on penetration in light-tissue interaction using computational methods, *Lasers Med. Sci.*, 2017, **32**(8), 1909–1918.
29 M. N. Alba, M. Gerenutti, V. M. H. Yoshida and D. Grotto, Clinical comparison of salicylic acid peel and LED-Laser

phototherapy for the treatment of Acne vulgaris in teenagers, *J. Cosmet. Laser Ther.*, 2017, **19**(1), 49–53.

30 D. S. Masson-Meyers, V. V. Bumah and C. S. Enwemeka, Blue light does not impair wound healing in vitro, *J. Photochem. Photobiol., B*, 2016, **160**, 53–60.

31 D. Sousa NTA, M. F. Santos, R. C. Gomes, H. E. Brandino, R. Martinez and R. R. De Jesus Guirro, Blue laser inhibits bacterial growth of staphylococcus aureus, escherichia coli, and pseudomonas aeruginosa, *Photomed. Laser Surg.*, 2015, **33**(5), 278–282.

32 R. F. Jackson, G. C. Roche and S. C. Shanks, A double-blind, placebo-controlled randomized trial evaluating the ability of low-level laser therapy to improve the appearance of cellulite, *Lasers Surg. Med.*, 2013, **45**(3), 141–147.

33 N. Kuboyama, M. Ohta, Y. Sato and Y. Abiko, Anti-inflammatory activities of light emitting diode irradiation on collagen-induced arthritis in mice (a secondary publication), *Laser Ther.*, 2014, **23**(3), 191–199.

34 *To begin at the beginning: The science of bio-stimulation in cells and tissues. Progress in Biomedical Optics and Imaging - Proceedings of SPIE*, ed. S. K. Bisland and B. C. Wilson, 2006.

35 L. A. Sazanov, A giant molecular proton pump: Structure and mechanism of respiratory complex I, *Nat. Rev. Mol. Cell Biol.*, 2015, **16**(6), 375–388.

36 T. Karu, Primary and secondary mechanisms of action of visible to near-IR radiation on cells, *J. Photochem. Photobiol., B*, 1999, **49**(1), 1–17.

37 M. T. Wong-Riley, H. L. Liang, J. T. Eells, B. Chance, M. M. Henry, E. Buchmann, M. Kane and H. T. Whelan, Photobiomodulation directly benefits primary neurons functionally inactivated by toxins: role of cytochrome c oxidase, *J. Biol. Chem.*, 2005, **280**(6), 4761–4771.

38 M. R. Hamblin, Mechanisms and Mitochondrial Redox Signaling in Photobiomodulation, *Photochem. Photobiol.*, 2018, **94**(2), 199–212.

39 T. H. Sanderson, J. M. Wider, I. Lee, C. A. Reynolds, J. Liu, B. Lepore, R. Tousignant, M. J. Bukowski, H. Johnston, A. Fite, S. Raghunayakula, J. Kamholz, L. I. Grossman, K. Przyklenk and M. Huttemann, Inhibitory modulation of cytochrome c oxidase activity with specific near-infrared light wavelengths attenuates brain ischemia/reperfusion injury, *Sci. Rep.*, 2018, **8**(1), 3481.

40 A. C. Chen, P. R. Arany, Y. Y. Huang, E. M. Tomkinson, S. K. Sharma, G. B. Kharkwal, T. Saleem, D. Mooney, F. E. Yull, T. S. Blackwell and M. R. Hamblin, Low-level laser therapy activates NF-kB via generation of reactive oxygen species in mouse embryonic fibroblasts, *PLoS One*, 2011, **6**(7), e22453.

41 N. N. Houreld, Shedding Light on a New Treatment for Diabetic Wound Healing: A Review on Phototherapy, *Sci. World J.*, 2014, **2014**, 398412.

42 C. Ferraresi, B. Kaippert, P. Avci, Y. Y. Huang, M. V. P. De Sousa, V. S. Bagnato, N. A. Parizotto and M. R. Hamblin, Low-level laser (light) therapy increases mitochondrial membrane potential and ATP synthesis in C2C12 myotubes with a peak response at 3–6 h, *Photochem. Photobiol.*, 2015, **91**(2), 411–416.

43 T. W. Weinrich, A. Coyne, T. E. Salt, C. Hogg and G. Jeffery, Improving mitochondrial function significantly reduces metabolic, visual, motor and cognitive decline in aged Drosophila melanogaster, *Neurobiol. Aging*, 2017, **60**, 34–43.

44 C. Regazzetti, L. Sormani, D. Debayle, F. Bernerd, M. K. Tulic, G. M. De Donatis, *et al.*, Melanocytes Sense Blue Light and Regulate Pigmentation through Opsin-3, *J. Invest. Dermatol.*, 2018, **138**(1), 171–178.

45 T. I. Karu, Cellular and Molecular Mechanisms of Photobiomodulation (Low-Power Laser Therapy), *IEEE J. Sel. Top. Quantum Electron.*, 2014, **20**(2), 143–148.

46 D. Pastore, M. Greco and S. Passarella, Specific helium-neon laser sensitivity of the purified cytochrome c oxidase, *Int. J. Radiat. Biol.*, 2000, **76**(6), 863–870.

47 B. J. Quirk and H. T. Whelan, Effect of Red-to-Near Infrared Light on the Reaction of Isolated Cytochrome c Oxidase with Cytochrome c, *Photomed. Laser Surg.*, 2016, **34**(12), 631–637.

48 D. Pastore, M. Greco, V. A. Petragallo and S. Passarella, Increase in <–H+/e- ratio of the cytochrome c oxidase reaction in mitochondria irradiated with helium-neon laser, *Biochem. Mol. Biol. Int.*, 1994, **34**(4), 817–826.

49 G. C. Brown, Nitric oxide and mitochondria, *Front. Biosci.*, 2007, **12**, 1024–1033.

50 H. Chung, T. Dai, S. K. Sharma, Y. Y. Huang, J. D. Carroll and M. R. Hamblin, The nuts and bolts of low-level laser (light) therapy, *Ann. Biomed. Eng.*, 2012, **40**(2), 516–533.

51 R. Zhang, Y. Mio, P. F. Pratt, N. Lohr, D. C. Warltier, H. T. Whelan, D. Zhu, E. R. Jacobs, M. Medhora and M. Bienengraeber, Near infrared light protects cardiomyocytes from hypoxia and reoxygenation injury by a nitric oxide dependent mechanism, *J. Mol. Cell. Cardiol.*, 2009, **46**(1), 4–14.

52 T. I. Karu, L. V. Pyatibrat and N. I. Afanasyeva, Cellular effects of low power laser therapy can be mediated by nitric oxide, *Lasers Surg. Med.*, 2005, **36**(4), 307–314.

53 U. H. Mitchell and G. L. Mack, Low-level laser treatment with near-infrared light increases venous nitric oxide levels acutely: a single-blind, randomized clinical trial of efficacy, *Am. J. Phys. Med. Rehabil.*, 2013, **92**(2), 151–156.

54 E. A. Buravlev, T. V. Zhidkova, A. N. Osipov and Y. A. Vladimirov, Are the mitochondrial respiratory complexes blocked by NO the targets for the laser and LED therapy?, *Lasers Med. Sci.*, 2015, **30**(1), 173–180.

55 P. Dungel, R. Mittermayr, S. Haindl, A. Osipov, C. Wagner, H. Redl and A. V. Kozlov, Illumination with blue light reactivates respiratory activity of mitochondria inhibited by nitric oxide, but not by glycerol trinitrate, *Arch. Biochem. Biophys.*, 2008, **471**(2), 109–115.

56 S. Buscone, A. N. Mardaryev, B. Raafs, J. W. Bikker, C. Sticht, N. Gretz, N. Farjo, N. E. Uzunbajakava and N. V. Botchkareva, A new path in defining light parameters for hair growth: Discovery and modulation of

photoreceptors in human hair follicle, *Lasers Surg. Med.*, 2017, **49**(7), 705–718.

57 I. Castellano-Pellicena, N. E. Uzunbajakava, C. Mignon, B. Raafs, V. A. Botchkarev and M. J. Thornton, Does blue light restore human epidermal barrier function via activation of Opsin during cutaneous wound healing?, *Lasers Surg. Med.*, 2019, **51**(4), 370–382.

58 K. Haltaufderhyde, R. N. Ozdeslik, N. L. Wicks, J. A. Najera and E. Oancea, Opsin expression in human epidermal skin, *Photochem. Photobiol.*, 2015, **91**(1), 117–123.

59 S. Blackshaw and S. H. Snyder, Encephalopsin: a novel mammalian extraretinal opsin discretely localized in the brain, *J. Neurosci.*, 1999, **19**(10), 3681–3690.

60 C. Regazzetti, L. Sormani, D. Debayle, F. Bernerd, M. K. Tulic, G. M. De Donatis, B. Chignon-Sicard, S. Rocchi and T. Passeron, Melanocytes Sense Blue Light and Regulate Pigmentation through Opsin-3, *J. Invest. Dermatol.*, 2018, **138**(1), 171–178.

61 S. Barreto Ortiz, D. Hori, Y. Nomura, X. Yun, H. Jiang, H. Yong, J. Chen, S. Paek, D. Pandey, G. Sikka, A. Bhatta, A. Gillard, J. Steppan, J. H. Kim, H. Adachi, V. M. Barodka, L. Romer, S. S. An, L. A. Shimoda, L. Santhanam and D. E. Berkowitz, Opsin 3 and 4 mediate light-induced pulmonary vasorelaxation that is potentiated by G protein-coupled receptor kinase 2 inhibition, *Am. J. Physiol. Lung Cell Mol. Physiol.*, 2018, **314**(1), L93–L106.

62 J. J. Kaylor, T. Xu, N. T. Ingram, A. Tsan, H. Hakobyan, G. L. Fain and G. H. Travis, Blue light regenerates functional visual pigments in mammals through a retinyl-phospholipid intermediate, *Nat. Commun.*, 2017, **8**(1), DOI: 10.1038/s41467-017-00018-4.

63 I. Castellano-Pellicena, N. E. Uzunbajakava, C. Mignon, B. Raafs, V. A. Botchkarev and M. J. Thornton, Does blue light restore human epidermal barrier function via activation of Opsin during cutaneous wound healing?, *Lasers Surg. Med.*, 2019, **51**(4), 370–382.

64 B. Alberts, A. Johnson, J. Lewis, M. Raff, K. Roberts and P. Walter, *Molecular biology of the cell*, Garland Science, 5th edn, 2008, 1 p.

65 Q. Gu, L. Wang, F. Huang and W. Schwarz, Stimulation of TRPV1 by Green Laser Light, *Evidence-Based Complementary Altern. Med.*, 2012, **2012**, 857123.

66 Y. Wang, Y. Y. Huang, Y. Wang, P. Lyu and M. R. Hamblin, Red (660 nm) or near-infrared (810 nm) photobiomodulation stimulates, while blue (415 nm), green (540 nm) light inhibits proliferation in human adipose-derived stem cells, *Sci. Rep.*, 2017, **7**(1), 7781.

67 C. Kim, Transient receptor potential ion channels and animal sensation: lessons from Drosophila functional research, *Clin. Infect. Dis*, 2004, **37**(1), 114–121.

68 W. Xu, J. Trepel and L. Neckers, Ras, ROS and proteotoxic stress: A delicate balance, *Cancer Cell*, 2011, **20**(3), 281–282.

69 S. Rohringer, W. Holnthoner, S. Chaudary, P. Slezak, E. Priglinger, M. Strassl, K. Pill, S. Mühleder, H. Redl and P. Dungel, The impact of wavelengths of LED light-therapy on endothelial cells, *Sci. Rep.*, 2017, **7**(1), 10700.

70 Y. Wang, X. Bai, Z. Wang, J. Cao, Y. Dong, Y. Dong and Y. Chen, Various LED Wavelengths Affected Myofiber Development and Satellite Cell Proliferation of Chick Embryos via the IGF-1 Signaling Pathway, *Photochem. Photobiol.*, 2017, **93**(6), 1492–1501.

71 T. Santos, R. Ferreira, E. Quartin, C. Boto, C. Saraiva, J. Bragança, J. Peça, C. Rodrigues, L. Ferreira and L. Bernardino, Blue light potentiates neurogenesis induced by retinoic acid-loaded responsive nanoparticles, *Acta Biomater.*, 2017, **59**, 293–302.

72 Y. Yuan, G. Yan, R. Gong, L. Zhang, T. Liu, C. Feng, W. Du, Y. Wang, F. Yang, Y. Li, S. Guo, F. Ding, W. Ma, E. Idiiatullina, V. Pavlov, Z. Han, B. Cai and L. Yang, Effects of Blue Light Emitting Diode Irradiation On the Proliferation, Apoptosis and Differentiation of Bone Marrow-Derived Mesenchymal Stem Cells, *Cell. Physiol. Biochem.*, 2017, **43**(1), 237–246.

73 T. Kushibiki, T. Hirasawa, S. Okawa and M. Ishihara, Blue laser irradiation generates intracellular reactive oxygen species in various types of cells, *Photomed. Laser Surg.*, 2013, **31**(3), 95–104.

74 E. A. Buravlev, T. V. Zhidkova, Y. A. Vladimirov and A. N. Osipov, Effects of low-level laser therapy on mitochondrial respiration and nitrosyl complex content, *Lasers Med. Sci.*, 2014, **29**(6), 1861–1866.

75 T. E. Swartz, S. B. Corchnoy, J. M. Christie, J. W. Lewis, I. Szundi, W. R. Briggs and R. A. Bogomolni, The photocycle of a flavin-binding domain of the blue light photoreceptor phototropin, *J. Biol. Chem.*, 2001, **276**(39), 36493–36500.

76 X. Yu, H. Liu, J. Klejnot and C. Lin, The Cryptochrome Blue Light Receptors, *Arabidopsis Book/Am. Soc. Plant Biol.*, 2010, **8**, e0135.

77 J. P. Bouly, E. Schleicher, M. Dionisio-Sese, F. Vandenbussche, D. Van Der Straeten, N. Bakrim, S. Meier, A. Batschauer, P. Galland, R. Bittl and M. Ahmad, Cryptochrome blue light photoreceptors are activated through interconversion of flavin redox states, *J. Biol. Chem.*, 2007, **282**(13), 9383–9391.

78 A. Sancar, Regulation of the mammalian circadian clock by cryptochrome, *J. Biol. Chem.*, 2004, **279**(33), 34079–34082.

79 M. Y. Yang, C. J. Chang and L. Y. Chen, Blue light induced reactive oxygen species from flavin mononucleotide and flavin adenine dinucleotide on lethality of HeLa cells, *J. Photochem. Photobiol., B*, 2017, **173**, 325–332.

80 M. W. Cheon, T. G. Kim, Y. S. Lee and S. H. Kim, Low level light therapy by Red-Green-Blue LEDs improves healing in an excision model of Sprague-Dawley rats, *Pers. Ubiquit. Comput.*, 2013, **17**(7), 1421–1428.

81 G. M. Cooper, *The Cell: A Molecular Approach*, Sinauer Associates, Sunderland (MA), 2nd edn, 2000, 1 p.

82 N. N. Osborne, C. Nunez-Alvarez and S. Del Olmo-Aguado, The effect of visual blue light on mitochondrial function

associated with retinal ganglions cells, *Exp. Eye Res.*, 2014, **128**, 8–14.

83 H. Serrage, S. Joanisse, P. R. Cooper, W. Palin, M. Hadis, O. Darch, A. Philp and M. R. Milward, Differential Responses of Myoblasts and Myotubes to Photobiomodulation are associated with Mitochondrial Number, *J. Biophotonics*, 2019, e201800411.

84 A. J. Marengo-Rowe, Structure-function relations of human hemoglobins, *Proceedings*, 2006, **19**(3), 239–245.

85 M. E. Ener, Y.-T. Lee, J. R. Winkler, H. B. Gray and L. Cheruzel, Photooxidation of cytochrome P450-BM3, *Proc. Natl. Acad. Sci. U. S. A.*, 2010, **107**(44), 18783–18786.

86 E. C. Veerman, J. W. Van Leeuwen, K. J. Van Buuren and B. F. Van Gelder, The reaction of cytochrome aa3 with (porphyrin) cytochrome c as studied by pulse radiolysis, *Biochim. Biophys. Acta*, 1982, **680**(2), 134–141.

87 K. Koren, S. M. Borisov, R. Saf and I. Klimant, Strongly Phosphorescent Iridium(III)–Porphyrins – New Oxygen Indicators with Tuneable Photophysical Properties and Functionalities, *Eur. J. Inorg. Chem.*, 2011, **2011**(10), 1531–1534.

88 M. Gouterman, *Optical spectra and electronic structure of porphyrins and related rings*, Academic Press, New York, 3rd edn, 1978, 16 p.

89 T. I. Karu, Multiple roles of cytochrome c oxidase in mammalian cells under action of red and IR-A radiation, *IUBMB Life*, 2010, **62**(8), 607–610.

90 R. Ankri, R. Lubart and H. Taitelbaum, Estimation of the optimal wavelengths for laser-induced wound healing, *Lasers Surg. Med.*, 2010, **42**(8), 760–764.

91 S. del Olmo-Aguado, A. G. Manso and N. N. Osborne, Light might directly affect retinal ganglion cell mitochondria to potentially influence function, *Photochem. Photobiol.*, 2012, **88**(6), 1346–1355.

92 D. Muller-Enoch, Blue light mediated photoreduction of the flavoprotein NADPH-cytochrome P450 reductase. A Forster-type energy transfer, *Z. Naturforsch., C: J. Biosci.*, 1997, **52**(9–10), 605–614.

93 D. Werck-Reichhart and R. Feyereisen, Cytochromes P450: a success story, *Genome Biol.*, 2000, **1**(6), 9.

94 F. Hannemann, A. Bichet, K. M. Ewen and R. Bernhardt, Cytochrome P450 systems–biological variations of electron transport chains, *Biochim. Biophys. Acta*, 2007, **1770**(3), 330–344.

95 *Impact of blue LED irradiation on proliferation and gene expression of cultured human keratinocytes. Progress in Biomedical Optics and Imaging - Proceedings of SPIE*, ed. A. Becker, C. Sticht, H. Dweep, F. A. Van Abeelen, N. Gretz and G. Oversluizen, 2015.

96 K. A. Ball, P. R. Castello and R. O. Poyton, Low intensity light stimulates nitrite-dependent nitric oxide synthesis but not oxygen consumption by cytochrome c oxidase: Implications for phototherapy, *J. Photochem. Photobiol., B*, 2011, **102**(3), 182–191.

97 N. L. Lohr, A. Keszler, P. Pratt, M. Bienengraber, D. C. Warltier and N. Hogg, Enhancement of nitric oxide release from nitrosyl hemoglobin and nitrosyl myoglobin by red/near infrared radiation: potential role in cardioprotection, *J. Mol. Cell. Cardiol.*, 2009, **47**(2), 256–263.

98 A. Keszler, B. Lindemer, N. Hogg, D. Weihrauch and N. L. Lohr, Wavelength-dependence of vasodilation and NO release from S-nitrosothiols and dinitrosyl iron complexes by far red/near infrared light, *Arch. Biochem. Biophys.*, 2018, **649**, 47–52.

99 D. J. Sexton, A. Muruganandam, D. J. McKenney and B. Mutus, Visible light photochemical release of nitric oxide from S-nitrosoglutathione: potential photochemotherapeutic applications, *Photochem. Photobiol.*, 1994, **59**(4), 463–467.

100 C. Oplander, A. Deck, C. M. Volkmar, M. Kirsch, J. Liebmann, M. Born, F. van Abeelen, E. E. van Faassen, K. D. Kroncke, J. Windolf and C. V. Suschek, Mechanism and biological relevance of blue-light (420–453 nm)-induced nonenzymatic nitric oxide generation from photolabile nitric oxide derivates in human skin in vitro and in vivo, *Free Radical Biol. Med.*, 2013, **65**, 1363–1377.

101 Y. Vladimirov, G. Borisenko, N. Boriskina, K. Kazarinov and A. Osipov, NO-hemoglobin may be a light-sensitive source of nitric oxide both in solution and in red blood cells, *J. Photochem. Photobiol., B*, 2000, **59**(1–3), 115–122.

102 C. L. Elliott, V. C. Allport, J. A. Z. Loudon, G. D. Wu and P. R. Bennett, Nuclear factor-kappa B is essential for up-regulation of interleukin-8 expression in human amnion and cervical epithelial cells, *Mol. Hum. Reprod.*, 2001, **7**(8), 787–790.

103 L. M. S. das Neves, G. P. M. F. Leite, A. M. Marcolino, C. E. Pinfildi, S. B. Garcia, J. E. de Araújo and E. C. O. Guirro, Laser photobiomodulation (830 and 660 nm) in mast cells, VEGF, FGF, and CD34 of the musculocutaneous flap in rats submitted to nicotine, *Lasers Med. Sci.*, 2017, **32**(2), 335–341.

104 V. Cury, A. I. S. Moretti, L. Assis, P. Bossini, J. De Souza Crusca, C. B. Neto, R. Fangel, H. P. De Souza, M. R. Hamblin and N. A. Parizotto, Low level laser therapy increases angiogenesis in a model of ischemic skin flap in rats mediated by VEGF, HIF-1α and MMP-2, *J. Photochem. Photobiol., B*, 2013, **125**, 164–170.

105 H. Choi, W. Lim, I. Kim, J. Kim, Y. Ko, H. Kwon, S. Kim, K. M. Kabir, X. Li, O. Kim, Y. Lee, S. Kim and O. Kim, Inflammatory cytokines are suppressed by light-emitting diode irradiation of P. gingivalis LPS-treated human gingival fibroblasts: inflammatory cytokine changes by LED irradiation, *Lasers Med. Sci.*, 2012, **27**(2), 459–467.

106 M. Curra, A. C. Pellicioli, N. A. Filho, G. Ochs, U. Matte, M. S. Filho, M. A. Martins and M. D. Martins, Photobiomodulation reduces oral mucositis by modulating NF-kB, *J. Biomed. Opt.*, 2015, **20**(12), 125008.

107 M. R. Hamblin, Mechanisms and applications of the anti-inflammatory effects of photobiomodulation, *AIMS Biophys.*, 2017, **4**(3), 337–361.

108 A. de Farias Gabriel, V. P. Wagner, C. Correa, L. P. Webber, E. F. S. Pilar, M. Curra, V. C. Carrard, M. A. T. Martins and M. D. Martins, Photobiomodulation therapy modulates

epigenetic events and NF-κB expression in oral epithelial wound healing, *Lasers Med. Sci.*, 2019, DOI: 10.1007/s10103-019-02745-0.

109 E. Stack and R. N. DuBois, Regulation of cyclo-oxygenase-2, *Best Pract. Res. Clin. Gastroenterol.*, 2001, **15**(5), 787–800.

110 A. Greenhough, H. J. Smartt, A. E. Moore, H. R. Roberts, A. C. Williams, C. Paraskeva and A. Kaidi, The COX-2/PGE2 pathway: key roles in the hallmarks of cancer and adaptation to the tumour microenvironment, *Carcinogenesis*, 2009, **30**(3), 377–386.

111 S. Namkoong, S. J. Lee, C. K. Kim, Y. M. Kim, H. T. Chung, H. Lee, J. A. Han, K. S. Ha, Y. G. Kwon and Y. M. Kim, Prostaglandin E2 stimulates angiogenesis by activating the nitric oxide/cGMP pathway in human umbilical vein endothelial cells, *Exp. Mol. Med.*, 2005, **37**(6), 588–600.

112 M. D. Diaz-Munoz, I. C. Osma-Garcia, M. Fresno and M. A. Iniguez, Involvement of PGE2 and the cAMP signalling pathway in the up-regulation of COX-2 and mPGES-1 expression in LPS-activated macrophages, *Biochem. J.*, 2012, **443**(2), 451–461.

113 M. P. Delghandi, M. Johannessen and U. Moens, The cAMP signalling pathway activates CREB through PKA, p38 and MSK1 in NIH 3T3 cells, *Cell. Signalling*, 2005, **17**(11), 1343–1351.

114 W. Lim, H. Choi, J. Kim, S. Kim, S. Jeon, H. Zheng, D. Kim, Y. Ko, D. Kim, H. Sohn and O. Kim, Anti-inflammatory effect of 635 nm irradiations on in vitro direct/indirect irradiation model, *J. Oral Pathol. Med.*, 2015, **44**(2), 94–102.

115 C. C. E. Lan, C. S. Wu, M. H. Chiou, T. Y. Chiang and H. S. Yu, Low-energy helium-neon laser induces melanocyte proliferation via interaction with type IV collagen: Visible light as a therapeutic option for vitiligo, *Br. J. Dermatol.*, 2009, **161**(2), 273–280.

116 D. P. Toomey, J. F. Murphy and K. C. Conlon, COX-2, VEGF and tumour angiogenesis, *Surgeon*, 2009, **7**(3), 174–180.

117 S. Kiriakidis, E. Andreakos, C. Monaco, B. Foxwell, M. Feldmann and E. Paleolog, VEGF expression in human macrophages is NF-kappaB-dependent: studies using adenoviruses expressing the endogenous NF-kappaB inhibitor IkappaBalpha and a kinase-defective form of the IkappaB kinase 2, *J. Cell Sci.*, 2003, **116**(Pt 4), 665–674.

118 C. R. Tim, P. S. Bossini, H. W. Kido, I. Malavazi, M. R. von Zeska Kress, M. F. Carazzolle, N. A. Parizotto and A. C. Rennó, Effects of low-level laser therapy on the expression of osteogenic genes during the initial stages of bone healing in rats: a microarray analysis, *Lasers Med. Sci.*, 2015, **30**(9), 2325–2333.

119 K. P. Cheng, E. A. Kiernan, K. W. Eliceiri, J. C. Williams and J. J. Watters, Blue Light Modulates Murine Microglial Gene Expression in the Absence of Optogenetic Protein Expression, *Sci. Rep.*, 2016, **6**, 21172.

120 J. W. Penn, A. O. Grobbelaar and K. J. Rolfe, The role of the TGF-β family in wound healing, burns and scarring: a review, *Int. J. Burns Trauma*, 2012, **2**(1), 18–28.

121 G. Ferrari, B. D. Cook, V. Terushkin, G. Pintucci and P. Mignatti, Transforming growth factor-beta 1 (TGF-beta1) induces angiogenesis through vascular endothelial growth factor (VEGF)-mediated apoptosis, *J. Cell. Physiol.*, 2009, **219**(2), 449–458.

122 R. M. Liu and L. P. Desai, Reciprocal regulation of TGF-β and reactive oxygen species: A perverse cycle for fibrosis, *Redox Biol.*, 2015, **6**, 565–577.

123 M. Horimoto, J. Kato, R. Takimoto, T. Terui, Y. Mogi and Y. Niitsu, Identification of a transforming growth factor beta-1 activator derived from a human gastric cancer cell line, *Br. J. Cancer*, 1995, **72**(3), 676–682.

124 L. Luo, Z. Sun, L. Zhang, X. Li, Y. Dong and T. C. Y. Liu, Effects of low-level laser therapy on ROS homeostasis and expression of IGF-1 and TGF-β1 in skeletal muscle during the repair process, *Lasers Med. Sci.*, 2013, **28**(3), 725–734.

125 F. Pamuk, M. Lutfioglu, A. Aydogdu, C. Z. Koyuncuoglu, E. Cifcibasi and O. S. Badur, The effect of low-level laser therapy as an adjunct to non-surgical periodontal treatment on gingival crevicular fluid levels of transforming growth factor-beta 1, tissue plasminogen activator and plasminogen activator inhibitor 1 in smoking and non-smoking chronic periodontitis patients: A split-mouth, randomized control study, *J. Periodontal Res.*, 2017, **52**(5), 872–882.

126 S. J. Pyo, W. W. Song, I. R. Kim, B. S. Park, C. H. Kim, S. H. Shin, I. K. Chung and Y. D. Kim, Low-level laser therapy induces the expressions of BMP-2, osteocalcin, and TGF-β1 in hypoxic-cultured human osteoblasts, *Lasers Med. Sci.*, 2013, **28**(2), 543–550.

127 P. R. Arany, R. S. Nayak, S. Hallikerimath, A. M. Limaye, A. D. Kale and P. Kondaiah, Activation of latent TGF-beta1 by low-power laser in vitro correlates with increased TGF-beta1 levels in laser-enhanced oral wound healing, *Wound Repair Regen.*, 2007, **15**(6), 866–874.

128 L. F. de Freitas and M. R. Hamblin, Proposed Mechanisms of Photobiomodulation or Low-Level Light Therapy, *IEEE J. Sel. Top. Quantum Electron.*, 2016, **22**(3), 7000417.

129 M. F. Jobling, J. D. Mott, M. T. Finnegan, V. Jurukovski, A. C. Erickson, P. J. Walian, S. E. Taylor, S. Ledbetter, C. M. Lawrence, D. B. Rifkin and M. H. Barcellos-Hoff, Isoform-specific activation of latent transforming growth factor beta (LTGF-beta) by reactive oxygen species, *Radiat. Res.*, 2006, **166**(6), 839–848.

130 M. Jain, S. Rivera, E. A. Monclus, L. Synenki, A. Zirk, J. Eisenbart, C. Feghali-Bostwick, G. M. Mutlu, G. R. Budinger and N. S. Chandel, Mitochondrial reactive oxygen species regulate transforming growth factor-beta signaling, *J. Biol. Chem.*, 2013, **288**(2), 770–777.

131 S. Hirata, C. Kitamura, H. Fukushima, I. Nakamichi, Y. Abiko, M. Terashita and E. Jimi, Low-level laser irradiation enhances BMP-induced osteoblast differentiation by stimulating the BMP/Smad signaling pathway, *J. Cell. Biochem.*, 2010, **111**(6), 1445–1452.

132 Y. Dang, B. Liu, L. Liu, X. Ye, X. Bi, Y. Zhang and J. Gu, The 800 nm diode laser irradiation induces skin collagen synthesis by stimulating TGF-beta/Smad signaling pathway, *Lasers Med. Sci.*, 2011, **26**(6), 837–843.

133 Y. Li, M. Lee, N. Kim, G. Wu, D. Deng, J. M. Kim, X. Liu, W. D. Heo and Z. Zi, Spatiotemporal Control of TGF-β Signaling with Light, *ACS Synth. Biol.*, 2018, **7**(2), 443–451.

134 R. Derynck, B. P. Muthusamy and K. Y. Saeteurn, Signaling pathway cooperation in TGF-β-induced epithelial-mesenchymal transition, *Curr. Opin. Cell Biol.*, 2014, **31**, 56–66.

135 P. Shelton and A. K. Jaiswal, The transcription factor NF-E2-related factor 2 (Nrf2): a protooncogene?, *FASEB J.*, 2013, **27**(2), 414–423.

136 H. Sohn, Y. Ko, M. Park, D. Kim, Y. L. Moon, Y. J. Jeong, H. Lee, Y. Moon, B. C. Jeong, O. Kim and W. Lim, Effects of light-emitting diode irradiation on RANKL-induced osteoclastogenesis, *Lasers Surg. Med.*, 2015, **47**(9), 745–755.

137 L. A. Trotter, D. Patel, S. Dubin, C. Guerra, V. McCloud, P. Lockwood, R. Messer, J. C. Wataha and J. B. Lewis, Violet/blue light activates Nrf2 signaling and modulates the inflammatory response of THP-1 monocytes, *Photochem. Photobiol. Sci.*, 2017, **16**(6), 883–889.

138 J. E. Kim, Y. J. Woo, K. M. Sohn, K. H. Jeong and H. Kang, Wnt/β-catenin and ERK pathway activation: A possible mechanism of photobiomodulation therapy with light-emitting diodes that regulate the proliferation of human outer root sheath cells, *Lasers Surg. Med.*, 2017, **49**(10), 940–947.

139 T. Zarubin and J. Han, Activation and signaling of the p38 MAP kinase pathway, *Cell Res.*, 2005, **15**, 11.

140 Y. H. Chu, S. Y. Chen, Y. L. Hsieh, Y. H. Teng and Y. J. Cheng, Low-level laser therapy prevents endothelial cells from TNF-alpha/cycloheximide-induced apoptosis, *Lasers Med. Sci.*, 2018, **33**(2), 279–286.

141 O. Kim, H. Choi, W. Lim, I. Kim, J. Kim, Y. Ko, H. Kwon, S. Kim, K. M. Ahsan Kabir, X. Li, O. Kim, Y. J. Lee and S. Kim, Inflammatory cytokines are suppressed by light-emitting diode irradiation of P. gingivalis LPS-treated human gingival fibroblasts, *Lasers Med. Sci.*, 2012, **27**(2), 459–467.

142 F. Verrecchia, C. Tacheau, E. F. Wagner and A. Mauviel, A central role for the JNK pathway in mediating the antagonistic activity of pro-inflammatory cytokines against transforming growth factor-beta-driven SMAD3/4-specific gene expression, *J. Biol. Chem.*, 2003, **278**(3), 1585–1593.

143 G. Silva, C. Ferraresi, R. T. de Almeida, M. L. Motta, T. Paixao, V. O. Ottone, I. A. Fonseca, M. X. Oliveira, E. Rocha-Vieira, M. F. Dias-Peixoto, E. A. Esteves, C. C. Coimbra, F. T. Amorim and F. de Castro Magalhaes, Infrared photobiomodulation (PBM) therapy improves glucose metabolism and intracellular insulin pathway in adipose tissue of high-fat fed mice, *Lasers Med. Sci.*, 2018, **33**(3), 559–571.

144 F. Salehpour, F. Farajdokht, P. Cassano, S. Sadigh-Eteghad, M. Erfani, M. R. Hamblin, M. M. Salimi, P. Karimi, S. H. Rasta and J. Mahmoudi, Near-infrared photobiomodulation combined with coenzyme Q10 for depression in a mouse model of restraint stress: reduction in oxidative stress, neuroinflammation, and apoptosis, *Brain Res. Bull.*, 2019, **144**, 213–222.

145 C. Ferraresi, Y.-Y. Huang and M. R. Hamblin, Photobiomodulation in human muscle tissue: an advantage in sports performance?, *J. Biophotonics*, 2016, **9**(11–12), 1273–1299.

146 T. Stafinski, D. Menon, K. Harris, G. G. Md and G. Jhangri, Photoselective vaporization of the prostate for the treatment of benign prostatic hyperplasia, *Can. Urol. Assoc. J.*, 2008, **2**(2), 124–134.

147 N. Adamskaya, P. Dungel, R. Mittermayr, J. Hartinger, G. Feichtinger, K. Wassermann, H. Redl and M. van Griensven, Light therapy by blue LED improves wound healing in an excision model in rats, *Injury*, 2011, **42**(9), 917–921.

148 K. M. AlGhamdi, A. Kumar, A. Al-ghamdi A, A. C. Al-Rikabi, M. Mubarek and A. E. Ashour, Ultra-structural effects of different low-level lasers on normal cultured human melanocytes: an in vitro comparative study, *Lasers Med. Sci.*, 2016, **31**(9), 1819–1825.

149 K. M. AlGhamdi, A. Kumar, A. E. Ashour and A. A. AlGhamdi, A comparative study of the effects of different low-level lasers on the proliferation, viability, and migration of human melanocytes in vitro, *Lasers Med. Sci.*, 2015, **30**(5), 1541–1551.

150 R. Ankri, H. Friedman, N. Savion, S. Kotev-Emeth, H. Breitbart and R. Lubart, Visible light induces nitric oxide (NO) formation in sperm and endothelial cells, *Lasers Surg. Med.*, 2010, **42**(4), 348–352.

151 B. E. Ashworth, E. Stephens, C. A. Bartlett, S. Serghiou, M. K. Giacci, A. Williams, N. S. Hart and M. Fitzgerald, Comparative assessment of phototherapy protocols for reduction of oxidative stress in partially transected spinal cord slices undergoing secondary degeneration, *BMC Neurosci.*, 2016, **17**(1), DOI: 10.1186/s12868-016-0259-6.

152 *Blue light inhibits proliferation of melanoma cells. Progress in Biomedical Optics and Imaging - Proceedings of SPIE*, ed. A. Becker, E. Distler, A. Klapczynski, F. Arpino, N. Kuch, K. Simon-Keller, C. Sticht, F. A. Van Abeelen, N. Gretz and G. Oversluizen, 2016.

153 S. Bonatti, B. Hochman, V. M. Tucci-Viegas, F. Furtado, C. E. Pinfildi, A. C. Pedro and L. M. Ferreira, In vitro effect of 470 nm LED (Light Emitting Diode) in keloid fibroblasts, *Acta Cir. Bras.*, 2011, **26**(1), 25–30.

154 V. V. Bumah, H. T. Whelan, D. S. Masson-Meyers, B. Quirk, E. Buchmann and C. S. Enwemeka, The bactericidal effect of 470 nm light and hyperbaric oxygen on methicillin-resistant Staphylococcus aureus (MRSA), *Lasers Med. Sci.*, 2015, **30**(3), 1153–1159.

155 E. A. Buravlev, T. V. Zhidkova, A. N. Osipov and Y. A. Vladimirov, Are the mitochondrial respiratory

complexes blocked by NO the targets for the laser and LED therapy?, *Lasers Med. Sci.*, 2014, **30**(1), 173–180.

156 E. A. Buravlev, T. V. Zhidkova, Y. A. Vladimirov and A. N. Osipov, Effects of laser and LED radiation on mitochondrial respiration in experimental endotoxic shock, *Lasers Med. Sci.*, 2013, **28**(3), 785–790.

157 S. Buscone, A. N. Mardaryev, B. Raafs, J. W. Bikker, C. Sticht, N. Gretz, N. Farjo, N. E. Uzunbajakava and N. V. Botchkareva, A new path in defining light parameters for hair growth: Discovery and modulation of photoreceptors in human hair follicle, *Lasers Surg. Med.*, 2017, **49**(7), 705–718.

158 S. W. Choe, K. Park, C. Park, J. Ryu and H. Choi, Combinational light emitting diode-high frequency focused ultrasound treatment for HeLa cell, *Comput. Assist. Surg.*, 2017, **22**, 79–85.

159 A. P. de Sousa, J. N. Santos, J. A. Dos Reis Jr., T. A. Ramos, J. de Souza, M. C. Cangussu and A. L. Pinheiro, Effect of LED phototherapy of three distinct wavelengths on fibroblasts on wound healing: a histological study in a rodent model, *Photomed. Laser Surg.*, 2010, **28**(4), 547–552.

160 Ö. Dereci, A. Sindel, H. Serap, E. Yüce, S. Ay and S. Tozoglu, The Comparison of the Efficacy of Blue Light-Emitting Diode Light and 980 nm Low-Level Laser Light on Bone Regeneration, *J. Craniofac. Surg.*, 2016, **27**(8), 2185–2189.

161 P. Dungel, J. Hartinger, S. Chaudary, P. Slezak, A. Hofmann, T. Hausner, M. Strassl, E. Wintner, H. Redl and R. Mittermayr, Low level light therapy by LED of different wavelength induces angiogenesis and improves ischemic wound healing, *Lasers Surg. Med.*, 2014, **46**(10), 773–780.

162 D. Falcone, N. E. Uzunbajakava, F. van Abeelen, G. Oversluizen, M. Peppelman, P. E. J. van Erp and P. C. M. van de Kerkhof, Effects of blue light on inflammation and skin barrier recovery following acute perturbation. Pilot study results in healthy human subjects, *Photodermatol., Photoimmunol. Photomed.*, 2018, **34**(3), 184–193.

163 R. Fekrazad, S. Asefi, M. B. Eslaminejad, L. Taghiar, S. Bordbar and M. R. Hamblin, Photobiomodulation with single and combination laser wavelengths on bone marrow mesenchymal stem cells: proliferation and differentiation to bone or cartilage, *Lasers Med. Sci.*, 2018, **34**(1), 115–126.

164 R. Fekrazad, A. Mirmoezzi, K. A. Kalhori and P. Arany, The effect of red, green and blue lasers on healing of oral wounds in diabetic rats, *J. Photochem. Photobiol., B*, 2015, **148**, 242–245.

165 M. Figurová, V. Ledecký, M. Karasová, M. Hluchý, A. Trbolová, I. Capík, S. Horňák, P. Reichel, J. M. Bjordal and P. Gál, Histological Assessment of a Combined Low-Level Laser/Light-Emitting Diode Therapy (685 nm/470 nm) for Sutured Skin Incisions in a Porcine Model: A Short Report, *Photomed. Laser Surg.*, 2016, **34**(2), 53–55.

166 T. Fushimi, S. Inui, T. Nakajima, M. Ogasawara, K. Hosokawa and S. Itami, Green light emitting diodes accelerate wound healing: characterization of the effect and its molecular basis in vitro and in vivo, *Wound Repair Regen.*, 2012, **20**(2), 226–235.

167 M. H. Gold, J. A. Biron and W. Sensing, Clinical and usability study to determine the safety and efficacy of the Silk'n Blue Device for the treatment of mild to moderate inflammatory acne vulgaris, *J. Cosmet. Laser Ther.*, 2014, **16**(3), 108–113.

168 *The effect of UV-Vis to near-infrared light on the biological response of human dental pulp cells. Progress in Biomedical Optics and Imaging - Proceedings of SPIE*, ed. M. A. Hadis, P. R. Cooper, M. R. Milward, P. Gorecki, E. Tarte, J. Churm and W. M. Palin, 2015.

169 B. Hochman, C. E. Pinfildi, M. A. Nishioka, F. Furtado, S. Bonatti, P. K. P. Monteiro, A. S. Antunes, P. R. Quieregatto, R. E. Liebano, G. Chadi and L. M. Ferreira, Low-level laser therapy and light-emitting diode effects in the secretion of neuropeptides SP and CGRP in rat skin, *Lasers Med. Sci.*, 2014, **29**(3), 1203–1208.

170 Y. R. Jung, S. J. Kim, K. C. Sohn, Y. Lee, Y. J. Seo, Y. H. Lee, K. U. Whang, C. D. Kim, J. H. Lee and M. Im, Regulation of lipid production by light-emitting diodes in human sebocytes, *Arch. Dermatol. Res.*, 2015, **307**(3), 265–273.

171 K. Khoo N, A. Iravani, M. Arjmand, F. Vahabi, M. Lajevardi, S. M. Akrami and Z. Zamani, A metabolomic study on the effect of intravascular laser blood irradiation on type 2 diabetic patients, *Lasers Med. Sci.*, 2013, **28**(6), 1527–1532.

172 N. KazemiKhoo and F. Ansari, Blue or red: which intravascular laser light has more effects in diabetic patients?, *Lasers Med. Sci.*, 2014, **30**(1), 363–366.

173 V. Khori, A. M. Alizadeh, Z. Gheisary, S. Farsinejad, F. Najafi, S. Khalighfard, F. Ghafari, M. Hadji and H. Khodayari, The effects of low-level laser irradiation on breast tumor in mice and the expression of Let-7a, miR-155, miR-21, miR125, and miR376b, *Lasers Med. Sci.*, 2016, **31**(9), 1775–1782.

174 S. K. Kim, B. W. Soh and Y. C. Kim, Low level light therapy using an 830 nm light emitting diode promotes wound healing via TGF-β/SMAD pathway activation, *Korean J. Ophthalmol.*, 2017, **55**(4), 237–245.

175 T. Kushibiki, T. Tajiri, Y. Ninomiya and K. Awazu, Chondrogenic mRNA expression in prechondrogenic cells after blue laser irradiation, *J. Photochem. Photobiol., B*, 2010, **98**(3), 211–215.

176 R. Lavi, R. Ankri, M. Sinyakov, M. Eichler, H. Friedmann, A. Shainberg, H. Breitbart and R. Lubart, The plasma membrane is involved in the visible light-tissue interaction, *Photomed. Laser Surg.*, 2012, **30**(1), 14–19.

177 H. S. Lee, S. E. Jung, S. K. Kim, Y. S. Kim, S. Sohn and Y. C. Kim, Low-level light therapy with 410 nm light emitting diode suppresses collagen synthesis in human keloid fibroblasts: An in vitro study, *Ann. Dermatol.*, 2017, **29**(2), 149–155.

178 Y. Li, J. Zhang, Y. Xu, Y. Han, B. Jiang, L. Huang, H. Zhu, Y. Xu, W. Yang and C. Qin, The Histopathological

Investigation of Red and Blue Light Emitting Diode on Treating Skin Wounds in Japanese Big-Ear White Rabbit, *PLoS One*, 2016, **11**(6), 157898.

179 D. S. Masson-Meyers, V. V. Bumah, G. Biener, V. Raicu and C. S. Enwemeka, The relative antimicrobial effect of blue 405 nm LED and blue 405 nm laser on methicillin-resistant Staphylococcus aureus in vitro, *Lasers Med. Sci.*, 2015, **30**(9), 2265–2271.

180 C. Mignon, N. E. Uzunbajakava, B. Raafs, N. V. Botchkareva and D. J. Tobin, Photobiomodulation of human dermal fibroblasts *in vitro*: decisive role of cell culture conditions and treatment protocols on experimental outcome, *Sci. Rep.*, 2017, **7**, 2797.

181 K. Montazeri, S. Mokmeli and M. Barat, The Effect of Combination of Red, Infrared and Blue Wavelengths of Low-Level Laser on Reduction of Abdominal Girth: A Before-After Case Series, *J. Lasers Med. Sci.*, 2017, **8**(Suppl 1), S22–Ss6.

182 T. Niu, Y. Tian, Q. Cai, Q. Ren and L. Wei, Red light combined with blue light irradiation regulates proliferation and apoptosis in skin keratinocytes in combination with low concentrations of curcumin, *PLoS One*, 2015, **10**(9), DOI: 10.1371/journal.pone.0138754.

183 S. Pfaff, J. Liebmann, M. Born, H. F. Merk and V. Von Felbert, Prospective Randomized Long-Term Study on the Efficacy and Safety of UV-Free Blue Light for Treating Mild Psoriasis Vulgaris, *Dermatology*, 2015, **231**(1), 24–34.

184 E. Priglinger, J. Maier, S. Chaudary, C. Lindner, C. Wurzer, S. Rieger, H. Redl, S. Wolbank and P. Dungel, Photobiomodulation of freshly isolated human adipose tissue-derived stromal vascular fraction cells by pulsed light-emitting diodes for direct clinical application, *J. Tissue Eng. Regen. Med.*, 2018, **12**(6), 1352–1362.

185 J. P. Rocca, M. Zhao, C. Fornaini, L. Tan, Z. Zhao and E. Merigo, Effect of laser irradiation on aphthae pain management: A four different wavelengths comparison, *J. Photochem. Photobiol., B*, 2018, **189**, 1–4.

186 *Coincident Light/ultrasound therapy to treat bacterial biofilms. 2015 IEEE International Ultrasonics Symposium, IUS, 2015*, ed. M. E. Schafer and T. McNeely, 2015.

187 J. E. Schoenly, W. Seka and P. Rechmann, Pulsed laser ablation of dental calculus in the near ultraviolet, *J. Biomed. Opt.*, 2014, **19**(2), 028003.

188 P. F. Sebbe, A. B. Villaverde, L. M. Moreira, A. M. Barbosa and N. Veissid, Characterization of a novel LEDs device prototype for neonatal jaundice and its comparison with fluorescent lamps sources: Phototherapy treatment of hyperbilirubinemia in Wistar rats, *Spectroscopy*, 2009, **23**(5–6), 243–255.

189 V. N. Shuvaeva, O. P. Gorshkova, A. V. Kostylev and D. P. Dvoretsky, Effect of laser irradiation on adrenoreactivity of pial arterial vessels in rats, *Bull. Exp. Biol. Med.*, 2011, **151**(1), 1–4.

190 K. L. Sinclair, J. L. Ponsford, J. Taffe, S. W. Lockley and S. M. W. Rajaratnam, Randomized controlled trial of light therapy for fatigue following traumatic brain injury, *Neurorehabil. Neural Repair*, 2014, **28**(4), 303–313.

191 M. A. Takhtfooladi and D. Sharifi, A comparative study of red and blue light-emitting diodes and low-level laser in regeneration of the transected sciatic nerve after an end to end neurorrhaphy in rabbits, *Lasers Med. Sci.*, 2015, **30**(9), 2319–2324.

192 Z. A. Tamarova, Y. Limansky and S. A. Gulyar, Antinociceptive effects of color polarized light in animal with formalin test, *Fiziol. Zh.*, 2009, **55**(3), 81–93.

193 A. Teuschl, E. R. Balmayor, H. Redl, M. Van Griensven and P. Dungel, Phototherapy with LED light modulates healing processes in an in vitro scratch-wound model using 3 different cell types, *Dermatol. Surg.*, 2015, **41**(2), 261–268.

194 A. P. Turrioni, J. R. Alonso, F. G. Basso, L. T. Moriyama, J. Hebling, V. S. Bagnato and C. C. De Souza, LED light attenuation through human dentin: a first step toward pulp photobiomodulation after cavity preparation, *Am. J. Dent.*, 2013, **26**(6), 319–323.

195 H. Wang, W. Liu, X. Fang, H. Wang, W. Ma, H. Dong, H. Yin, Y. X. Li and H. Sha, Effect of 405 nm low intensity irradiation on the absorption spectrum of *in vitro* hyperlipidemia blood, *Technol. Health Care*, 2018, **26**(S1), 135–143.

196 Y. Wang, Y. Y. Huang, Y. Wang, P. Lyu and M. R. Hamblin, Photobiomodulation (blue and green light) encourages osteoblastic-differentiation of human adipose-derived stem cells: Role of intracellular calcium and light-gated ion channels, *Sci. Rep.*, 2016, **6**, DOI: 10.1038/srep33719.

197 T. Yoshimoto, Y. Morine, C. Takasu, R. Feng, T. Ikemoto, K. Yoshikawa, S. Iwahashi, Y. Saito, H. Kashihara, M. Akutagawa, T. Emoto, Y. Kinouchi and M. Shimada, Blue light-emitting diodes induce autophagy in colon cancer cells by Opsin 3, *Ann. Gastroenterol. Surg.*, 2018, **2**(2), 154–161.

198 A. Tani, F. Chellini, M. Giannelli, D. Nosi, S. Zecchi-Orlandini and C. Sassoli, Red (635 nm), Near-Infrared (808 nm) and Violet-Blue (405 nm) Photobiomodulation Potentiality on Human Osteoblasts and Mesenchymal Stromal Cells: A Morphological and Molecular In Vitro Study, *Int. J. Mol. Sci.*, 2018, **19**(7), 1946.

199 Z. Malik, J. Hanania and Y. Nitzan, Bactericidal effects of photoactivated porphyrins–an alternative approach to antimicrobial drugs, *J. Photochem. Photobiol., B*, 1990, **5**(3–4), 281–293.

200 F. A. H. Al-Watban, X. Y. Zhang, B. L. Andres and A. Al-Anize, Visible lasers were better than invisible lasers in accelerating burn healing on diabetic rats, *Photomed. Laser Surg.*, 2009, **27**(2), 269–272.

201 E. V. Askhadulin, T. V. Konchugova and S. V. Moskvin, The application of combined low-intensity laser therapy for the treatment of the patients presenting with trophic ulcers associated with chronic venous insufficiency of the lower extremities, *Vopr. Kurortol. Fizioter. Lech. Fiz. Kult.*, 2018, **95**(6), 27–33.

202 S. Baek, K. P. Lee, L. Cui, Y. Ryu, J. M. Hong, J. Kim, S. H. Jung, Y. M. Bae, K. J. Won and B. Kim, Low-power laser irradiation inhibits PDGF-BB-induced migration and proliferation via apoptotic cell death in vascular smooth muscle cells, *Lasers Med. Sci.*, 2017, **32**(9), 2121–2127.

203 D. Sousa APC, G. M. Paraguassú, N. T. T. Silveira, J. De Souza, M. C. T. Cangussú, J. N. Dos Santos and A. L. B. Pinheiro, Laser and LED phototherapies on angiogenesis, *Lasers Med. Sci.*, 2013, **28**(3), 981–987.

204 D. Sousa APC, J. N. Santos, J. A. Dos Reis, T. A. Ramos, J. De Souza, M. C. T. Cangussú and A. L. B. Pinheiro, Effect of LED phototherapy of three distinct wavelengths on fibroblasts on wound healing: A histological study in a rodent model, *Photomed. Laser Surg.*, 2010, **28**(4), 547–552.

205 T. Fushimi, S. Inui, T. Nakajima, M. Ogasawara, K. Hosokawa and S. Itami, Green light emitting diodes accelerate wound healing: Characterization of the effect and its molecular basis in vitro and in vivo, *Wound Repair Regen.*, 2012, **20**(2), 226–235.

206 A. Khurana, A. Chowdhary, K. Sardana, R. K. Gautam and P. K. Sharma, Complete cure of Fusarium solani sp. complex onychomycosis with Qs NdYAG treatment, *Dermatol. Ther.*, 2018, **31**(2), e12580.

207 S. Kim, J. Kim, W. Lim, S. Jeon, O. Kim, J. T. Koh, C. S. Kim, H. Choi and O. Kim, In vitro bactericidal effects of 625, 525, and 425 nm wavelength (red, green, and blue) light-emitting diode irradiation, *Photomed. Laser Surg.*, 2013, **31**(11), 554–562.

208 S. D. Li, P. Chen, C. P. Zhang, J. X. Wen, J. Liang, H. X. Kang, R. L. Gao and X. B. Fu, Effects of low-intensity laser irradiation on the apoptosis of rabbit vascular smooth muscle cells in culture, *Laser Phys.*, 2011, **21**(11), 1989–1994.

209 E. Merigo, S. Bouvet-Gerbettaz, F. Boukhechba, J. P. Rocca, C. Fornaini and N. Rochet, Green laser light irradiation enhances differentiation and matrix mineralization of osteogenic cells, *J. Photochem. Photobiol., B*, 2016, **155**, 130–136.

210 S. V. Moskvin, A. V. Geynitz and E. V. Askhadulin, Efficiency of a new combined laser therapy in patients with trophic ulcers of lower extremities and chronic venous insufficiency, *J. Lasers Med. Sci.*, 2017, **8**(3), 132–135.

211 C. S. Na, W. I. Kim, H. S. Jang, D. H. Youn, Y. M. Moon, S. H. Jeong and M. W. Cheon, Low-level green and red laser treatment of Shaochong (HT9)·Dadun (LR1) and Shaohai (HT3)·Yingu (KI10) acupoints in a rat model of focal cerebral ischemia, *Trans. Electr. Electr. Mater.*, 2015, **16**(2), 65–69.

212 M. O'Connor, R. Patil, J. Yu, R. Hickey, K. Premanand, A. Kajdacsy-Balla, E. Benedetti and A. Bartholomew, Mesenchymal Stem Cells Synergize with 635, 532, and 405 nm Laser Wavelengths in Renal Fibrosis: A Pilot Study, *Photomed. Laser Surg.*, 2016, **34**(11), 556–563.

213 K. J. Oh, J. Park, H. S. Lee and K. Park, Effects of light-emitting diodes irradiation on human vascular endothelial cells, *Int. J. Impot. Res.*, 2018, **30**(6), 312–317.

214 G. C. Roche, S. Shanks, R. F. Jackson and L. J. Holsey, Low-Level Laser Therapy for Reducing the Hip, Waist, and Upper Abdomen Circumference of Individuals with Obesity, *Photomed. Laser Surg.*, 2017, **35**(3), 142–149.

215 S. Rohringer, W. Holnthoner, S. Chaudary, P. Slezak, E. Priglinger, M. Strassl, K. Pill, S. Mühleder, H. Redl and P. Dungel, The impact of wavelengths of LED light-therapy on endothelial cells, *Sci. Rep.*, 2017, **7**(1), 10700.

216 E. Tierney and C. W. Hanke, Randomized controlled trial: Comparative efficacy for the treatment of facial telangiectasias with 532 nm versus 940 nm diode laser, *Lasers Surg. Med.*, 2009, **41**(8), 555–562.

217 D. H. Sliney, Radiometric quantities and units used in photobiology and photochemistry: recommendations of the Commission Internationale de L'Eclairage (International Commission on Illumination), *Photochem. Photobiol.*, 2007, **83**(2), 425–432.

218 P. A. Jenkins and J. D. Carroll, How to report low-level laser therapy (LLLT)/photomedicine dose and beam parameters in clinical and laboratory studies, *Photomed. Laser Surg.*, 2011, **29**(12), 785–787.

219 D. S. Masson-Meyers, V. V. Bumah and C. S. Enwemeka, Blue light does not impair wound healing in vitro, *J. Photochem. Photobiol., B*, 2016, **160**, 53–60.

220 M. R. Hamblin, Y. Y. Huang, S. K. Sharma and J. Carroll, Biphasic dose response in low level light therapy - an update, *Dose-Response*, 2011, **9**(4), 602–618.

221 J. Liebmann, M. Born and V. Kolb-Bachofen, Blue-light irradiation regulates proliferation and differentiation in human skin cells, *J. Invest. Dermatol.*, 2010, **130**(1), 259–269.

222 Y.-Y. Huang, K. Nagata, C. E. Tedford, T. McCarthy and M. R. Hamblin, Low-level laser therapy (LLLT) reduces oxidative stress in primary cortical neurons in vitro, *J. Biophotonics*, 2013, **6**(10), 829–838.

223 L. Taflinski, E. Demir, J. Kauczok, P. C. Fuchs, M. Born, C. V. Suschek and C. Oplander, Blue light inhibits transforming growth factor-beta1-induced myofibroblast differentiation of human dermal fibroblasts, *Exp. Dermatol.*, 2014, **23**(4), 240–246.